frontiers | Research Topics

Expression and variation in non-coding RNAs for diagnosis, prevention and cure

Edited by
Deepanjan Paul, Rajesh Pandey and William C. Cho

Published in
Frontiers in Genetics

ISSN 1664-8714
ISBN 978-2-83251-142-8
DOI 10.3389/978-2-83251-142-8

About Frontiers

Frontiers is more than just an open access publisher of scholarly articles: it is a pioneering approach to the world of academia, radically improving the way scholarly research is managed. The grand vision of Frontiers is a world where all people have an equal opportunity to seek, share and generate knowledge. Frontiers provides immediate and permanent online open access to all its publications, but this alone is not enough to realize our grand goals.

Frontiers journal series

The Frontiers journal series is a multi-tier and interdisciplinary set of open-access, online journals, promising a paradigm shift from the current review, selection and dissemination processes in academic publishing. All Frontiers journals are driven by researchers for researchers; therefore, they constitute a service to the scholarly community. At the same time, the *Frontiers journal series* operates on a revolutionary invention, the tiered publishing system, initially addressing specific communities of scholars, and gradually climbing up to broader public understanding, thus serving the interests of the lay society, too.

Dedication to quality

Each Frontiers article is a landmark of the highest quality, thanks to genuinely collaborative interactions between authors and review editors, who include some of the world's best academicians. Research must be certified by peers before entering a stream of knowledge that may eventually reach the public - and shape society; therefore, Frontiers only applies the most rigorous and unbiased reviews. Frontiers revolutionizes research publishing by freely delivering the most outstanding research, evaluated with no bias from both the academic and social point of view. By applying the most advanced information technologies, Frontiers is catapulting scholarly publishing into a new generation.

What are Frontiers Research Topics?

Frontiers Research Topics are very popular trademarks of the *Frontiers journals series*: they are collections of at least ten articles, all centered on a particular subject. With their unique mix of varied contributions from Original Research to Review Articles, Frontiers Research Topics unify the most influential researchers, the latest key findings and historical advances in a hot research area.

Find out more on how to host your own Frontiers Research Topic or contribute to one as an author by contacting the Frontiers editorial office: frontiersin.org/about/contact

Expression and variation in non-coding RNAs for diagnosis, prevention and cure

Topic editors

Deepanjan Paul — Children's Hospital of Philadelphia, United States

Rajesh Pandey — CSIR-Institute of Genomics and Integrative Biology (CSIR-IGIB), India

William C. Cho — QEH, Hong Kong, SAR China

Citation

Paul, D., Pandey, R., Cho, W. C., eds. (2023). *Expression and variation in non-coding RNAs for diagnosis, prevention and cure*. Lausanne: Frontiers Media SA. doi: 10.3389/978-2-83251-142-8

Table of contents

frontiers in Genetics

ORIGINAL RESEARCH
published: 18 November 2021
doi: 10.3389/fgene.2021.780431

Identification of Two Long Non-Coding RNAs AC010082.1 and AC011443.1 as Biomarkers of Coronary Heart Disease Based on Logistic Stepwise Regression Prediction Model

Chao Liu[1,2†], *Lanchun Liu*[1,2†], *Jialiang Gao*[1], *Jie Wang*[1,3*] and *Yongmei Liu*[1,3*]

[1]Guang'anmen Hospital, China Academy of Chinese Medical Sciences, Beijing, China, [2]Graduate School, Beijing University of Chinese Medicine, Beijing, China, [3]Key Technology Laboratory of Cardiovascular Disease-Syndrome Combination, Guang'anmen Hospital, China Academy of Chinese Medical Sciences, Beijing, China

OPEN ACCESS

Edited by:
Arijit Mukhopadhyay,
University of Salford Manchester,
United Kingdom

Reviewed by:
Bharati Mehani,
National Cancer Institute,
United States
Mirka Rabajdova,
University of Pavol Jozef Šafárik,
Slovakia

***Correspondence:**
Jie Wang
wangjie0103@126.com
Yongmei Liu
lymsd@163.com

[†]These authors have contributed equally to this work and share first authorship

Specialty section:
This article was submitted to RNA, a section of the journal Frontiers in Genetics

Received: 21 September 2021
Accepted: 01 November 2021
Published: 18 November 2021

Citation:
Liu C, Liu L, Gao J, Wang J and Liu Y (2021) Identification of Two Long Non-Coding RNAs AC010082.1 and AC011443.1 as Biomarkers of Coronary Heart Disease Based on Logistic Stepwise Regression Prediction Model. Front. Genet. 12:780431. doi: 10.3389/fgene.2021.780431

Coronary heart disease (CHD) is a global health concern with high morbidity and mortality rates. This study aimed to identify the possible long non-coding RNA (lncRNA) biomarkers of CHD. The lncRNA- and mRNA-related data of patients with CHD were downloaded from the Gene Expression Omnibus database (GSE113079). The limma package was used to identify differentially expressed lncRNAs and mRNAs (DElncRNAs and DEmRNAs, respectively). Then, miRcode, TargetScan, miRDB, and miRTarBase databases were used to form the competing endogenous RNA (ceRNA) network. Furthermore, SPSS Modeler 18.0 was used to construct a logistic stepwise regression prediction model for CHD diagnosis based on DElncRNAs. Of the microarray data, 70% was used as a training set and 30% as a test set. Moreover, a validation cohort including 30 patients with CHD and 30 healthy controls was used to verify the hub lncRNA expression through real-time reverse transcription-quantitative PCR (RT-qPCR). A total of 185 DElncRNAs (114 upregulated and 71 downregulated) and 382 DEmRNAs (162 upregulated and 220 downregulated) between CHD and healthy controls were identified from the microarray data. Furthermore, through bioinformatics prediction, a 38 lncRNA-21miRNA-40 mRNA ceRNA network was constructed. Next, by constructing a logistic stepwise regression prediction model for 38 DElncRNAs, we screened two hub lncRNAs AC010082.1 and AC011443.1 ($p < 0.05$). The sensitivity, specificity, and area under the curve were 98.41%, 100%, and 0.995, respectively, for the training set and 93.33%, 91.67%, and 0.983, respectively, for the test set. We further verified the significant upregulation of AC010082.1 ($p < 0.01$) and AC011443.1 ($p < 0.05$) in patients with CHD using RT-qPCR in the validation cohort. Our results suggest that lncRNA AC010082.1 and AC011443.1 are potential biomarkers of CHD. Their pathological mechanism in CHD requires further validation.

Keywords: long non-coding RNAs, biomarkers, competing endogenous RNA, logistic stepwise regression, RT-qPCR

INTRODUCTION

Globally, coronary heart disease (CHD) is a major disease with high morbidity and mortality, which seriously threatens human health (Collet et al., 2021), killing approximately 8 million people annually worldwide (Mortality and Causes of Death, 2015). Reportedly, > 700,000 people die from CHD annually in China, and the overall mortality rate has been increasing each year (Wang et al., 2011). CHD is a complex multifactorial disease with many risk factors, such as age, hypertension, diabetes, dyslipidemia, and smoking status (Knuuti et al., 2020). The definitive diagnosis of CHD primarily depends on invasive coronary angiography, which is relatively costly, time-consuming, and uncomfortable for the patient (Novak et al., 2021). However, CHD in its early stage is not easily detected by routine examinations, such as electrocardiography and cardiac ultrasound, resulting in a high mortality rate of CHD (Miao et al., 2019). Therefore, it is necessary to identify a novel non-invasive biomarker in the early stages of CHD, to enable early diagnosis and prevention of CHD.

Evidence in recent years has showed that long non-coding RNAs (lncRNAs) have a key role in the gene regulation and widely concerned (Statello et al., 2020; Zhang et al., 2020; Hongkuan et al., 2021). LncRNAs are non-coding RNAs with a transcription length >200 bp and lack protein-coding potential. A variety of cellular functions within the nucleus and cytoplasm could be regulated by lncRNAs, which are important for normal development and disease progression (Lu and Thum, 2019). Due to their tissue-specific and condition-specific expression patterns, lncRNAs can be used as biomarkers and therapeutic targets for multiple diseases in blood, plasma, and urine (Beermann et al., 2016). A variety of lncRNAs, such as lncRNA OTTHUMT00000387022 (Cai et al., 2016), AC100865.1 (Yang et al., 2015), and uc010yfd.1 (Li et al., 2018), are abnormally expressed in CHD and therefore, can be used as potential biomarkers of CHD. LncRNAs play key roles in specific physiological and pathological processes of CHD, including the induction of vascular smooth muscle cell proliferation, apoptosis, lipid metabolism, and inflammation (Li et al., 2020; Li et al., 2021a). LncRNAs have been considered promising regulatory genes or biomarkers for CHD (Lu and Thum, 2019).

Recently, the proposed competing endogenous RNAs (ceRNAs) hypothesis has provided the possibility for further study of molecular mechanisms underlying several diseased conditions (Cheng et al., 2015; Ouyang et al., 2020; Wang et al., 2020). CeRNAs can act as miRNA sponges and regulate mRNA expression through their miRNA response elements (MREs) (Salmena et al., 2011). A number of studies have shown that lncRNA can regulate the progression of CHD through the ceRNA mechanism. For instance, lncRNA HCG11 affects the expression of FOXF1 by targeting miR-144-3p, thereby regulating the proliferation and apoptosis of vascular smooth muscle cells in atherosclerosis (Liu et al., 2020). The lncRNA HOTAIR can protect myocardial infraction and hypoxia-induced cardiomyocyte apoptosis by interacting with miR-519d-3p (Zhang et al., 2019). In the present study, we aimed to construct the ceRNA regulatory network of CHD using the Gene Expression Omnibus (GEO) database and screen the possible lncRNAs as biomarkers of CHD.

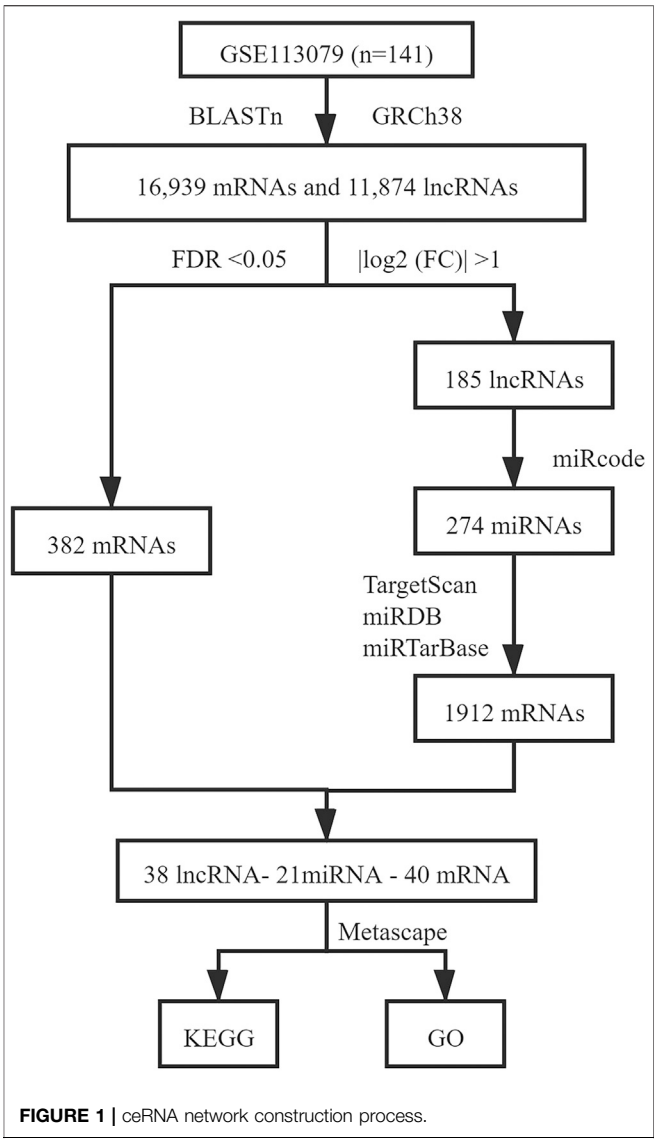

FIGURE 1 | ceRNA network construction process.

MATERIALS AND METHODS

Data Acquisition and Preprocessing

The gene expression profile of human CHD was obtained from the GEO (https://www.ncbi.nlm.nih.gov/geo) with accession number GSE113079. This dataset included 93 patients with CHD and 48 healthy controls using the GPL20115 platform (Agilent-067406 Human CBC lncRNA + mRNA microarray V4.0). LncRNA and mRNA expression data from the GPL20115 platform were obtained by reannotating microarray probes according to the probe set sequences and the annotations of protein-coding genes and lncRNA records in GENCODE (GRCh38, release 35, http://www.gencodegenes.org/). The BLASTn (https://ftp.ncbi.nlm.nih.gov/blast/executables/

LATEST/) was used to align the probe sequences with those of non-coding and coding transcript sequences from GENCODE. The transformed data (lincRNA, antisense, sense_overlapping, processed_transcript, 3prime_overlapping_ncrna, ncrna_host, bidirectional_promoter_lncrna, ambiguous_orf, retained_intron and sense_intronic) were considered as lncRNAs.

Screening Differentially Expressed lncRNAs (DElncRNAs) and mRNAs (DEmRNAs)

The identification of DElncRNAs and DEmRNAs between patients with CHD and healthy controls were performed by using the "limma" package of R software (version 4.0.1) (R Core Team, 2018). An independent two-sample *t*-test and the false discovery rate (FDR) adjusted using the Benjamini–Hochberg method were used to analyze the DElncRNAs and DEmRNAs (Long et al., 2019). $p < 0.05$, FDR <0.05, and $|\log_2$ fold change (FC)$| > 1$ were considered as the cut-off criteria.

Target Genes Prediction and Construction of the ceRNA Network

The prediction of lncRNAs to target miRNAs was conducted using the miRcode database (Jeggari et al., 2012). DEmRNAs targeted by differentially expressed miRNAs (DEmiRNAs) were retrieved based on the TargetScan, miRDB, and mirtarbase databases, and only those recognized by these three databases were considered candidate DEmRNAs (Agarwal et al., 2015; Wong and Wang, 2015; Chou et al., 2016). Next, the predicted target DEmRNAs and previous identified DEmRNAs were intersected. Based on the above lncRNA-miRNA and miRNA-mRNA interactions, the lncRNA-miRNA-mRNA network was visualized using Cytoscape 3.8.0 software (Shannon et al., 2003). The R package "pheatmap" was used to draw heatmaps for DElncRNAs and DEmRNAs. **Figure 1** shows the process used for ceRNA network construction.

Functional and Pathway Enrichment Analysis of DEmRNAs

To clarify the potential biological processes of DEmRNAs associated with the ceRNA network, we used Metascape (http://metascape.org) to analyze the Gene Ontology (GO) and Kyoto Encyclopedia of Genes and Genomes (KEGG) functional enrichment of the DEmRNAs (Zhou et al., 2019). $p < 0.05$, min overlap mRNAs≥2, and enrichment factor >1.5 were considered to be statistically significant (Gao et al., 2020).

Constructing a Logistic Stepwise Regression Prediction Model and Screening Hub lncRNAs

The 141 samples from the GSE113079 dataset were randomly divided into training (70% of the samples, 63 patients with CHD and 36 healthy controls) and test (30%, 30 patients with CHD and 12 healthy controls) sets, and they maintained the similar ratio for patients with CHD and healthy controls ($p = 0.372$). SPSS Modeler 18.0 (IBM Canada Ltd., Markham, Ontario, Canada) was used to construct a logistic stepwise regression prediction model for CHD diagnosis based on DElncRNAs. Further, the sensitivity and specificity of the model were calculated using SPSS Modeler. The receiver operating characteristic (ROC) curve was used to evaluate the effectiveness of the classification model, and the area under the curve (AUC) value was calculated from the ROC curve. ROC curves were calculated using the R package "pROC." Principal component analysis (PCA) using the R package "ggplot2" was performed on the screened hub lncRNAs, and their expression levels in patients with CHD and healthy controls were analyzed. The selection process for screening hub lncRNAs is shown in **Figure 2**.

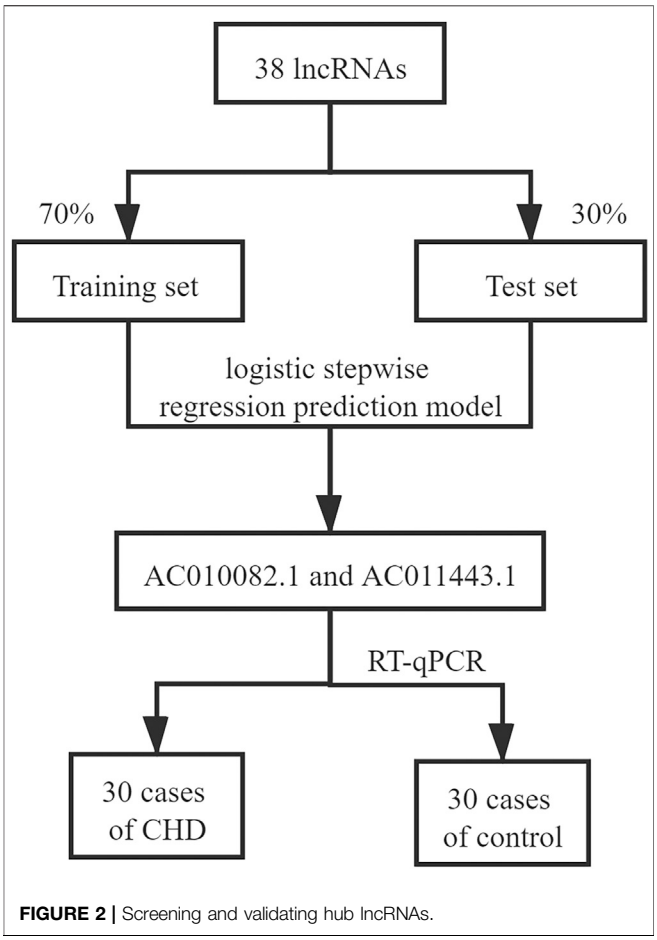

FIGURE 2 | Screening and validating hub lncRNAs.

Study Population

A total of 30 patients with CHD (17 males) and 30 healthy controls (6 males) were recruited in Guang'anmen Hospital, Beijing, China, as the validation cohort. This study complied with the Declaration of Helsinki and was approved by the Ethics Committee of Guang'anmen Hospital, China Academy of Chinese Medical Sciences (no. 2019–224-KY). All subjects were aged between 42 and 77 years. CHD diagnosis was based on the European Society of Cardiology criteria, which specifies at least one vessel lesion (>50% narrowing of luminal diameter) using coronary angiography (Task

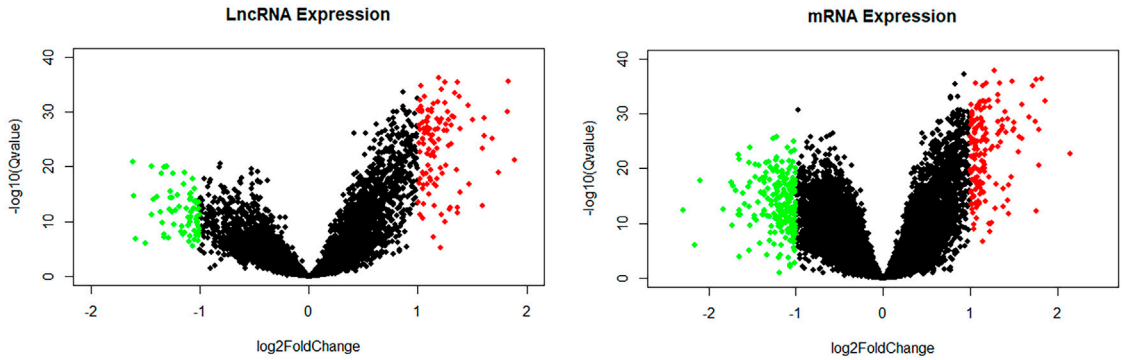

FIGURE 3 | Volcano map of lncRNAs and mRNAs. Green spots represent downregulated DElncRNAs or DEmRNAs; red spots represent upregulated DElncRNAs or DEmRNAs.

Force et al., 2013). Healthy controls without chronic disease or acute infection in the last 2 weeks were recruited from the medical examination center of Guang'anmen Hospital. All participants signed an informed consent upon receiving a complete explanation of the study.

Total RNA Isolation and Reverse Transcription

Peripheral blood samples (4–8 ml) were collected in the early morning from patients with CHD and healthy controls using EDTA vacuum anticoagulant blood vessels. Peripheral blood mononuclear cells (PBMCs) were isolated using the Red Blood Cell Lysis kit (TIANGEN, Beijing, China) and total RNA was extracted from PBMCs using TRIzol reagent (Invitrogen, Carlsbad, CA, United States) according to the manufacturers' instructions. RNA quality and quantity were evaluated using a NanoDrop 2000 spectrophotometer (Thermo Fisher Scientific, MA, United States). LncRNA reverse transcription was performed using the lncRcute lncRNA First-Strand cDNA Kit (TIANGEN) from 1 μg total RNA according to the manufacturer's instructions.

Validation of Hub lncRNAs Using RT-qPCR

Reverse transcription-quantitative PCR (RT-qPCR) was performed using the lncRcute lncRNA qPCR kit (TIANGEN) to detect relative expression using the standard protocols on the ABI7900HT Fast Real-Time PCR system (Applied Biosystems, MA, United States). *ACTB* was used as an internal reference. The cycling PCR conditions were: 95°C for 3 min; 40 cycles of 95°C for 5 s, 55°C for 10 s, and 72°C for 15 s; 95°C for 15 s, 65°C for 15 s, and 95°C for 15 s. The primer sequences are as follows: AC010082.1 forward primer, 5′-TTTGGT CTAGGCGCTAGGAAT-3′; AC010082.1 reverse primer, 5′-CTT TTCCCCTTACCCTGCTTT-3′; AC011443.1 forward primer, 5′-TGTTCCAAGGTCAACCAAAAA-3′; AC011443.1 reverse primer, 5′-CCAAGGTGGTCAAATCTGTGT-3′; *ß*-actin forward primer, 5′-GAGACCTTCAACACCCCAGCC-3′; *ß*-actin reverse primer, 5′-AATGTCACGCACGATTTCCC-3′. Relative expression data were analyzed using the $2^{-\Delta\Delta CT}$ method (Livak and Schmittgen, 2001). R 4.0.1 software was used to analyze differences in expression.

RESULTS

DElncRNAs and DEmRNAs

In all, 16,939 mRNAs and 11,874 lncRNAs were derived from the microarray data by conducting the GENCODE probe reannotation. Using $p < 0.05$, FDR <0.05, and $|\log2(FC)| > 1$ as screening criteria, 185 DElncRNAs (114 upregulated and 71 downregulated) and 382 DEmRNAs (162 upregulated and 220 downregulated) between CHD and healthy controls were identified. The volcano maps of DElncRNAs and DEmRNAs are shown in **Figure 3**.

Construction of the ceRNA Network

We used the miRcode database to predict miRNA-targeted lncRNAs. The constructed ceRNA network only included interactions between the DEmiRNAs and DElncRNAs; thus, 1794 interactions between 47 DElncRNAs (including AC011443.1, AC010082.1, and LIN00283) and 274 DEmiRNAs (including hsa-mir-27a-3p, hsa-mir-206, and hsa-mir-1244) were identified. We mapped the abovementioned 274 DEmiRNAs against TargetScan, miRDB, and miRTarBase to search for target DEmRNAs. A total of 1912 DEmRNAs that interacted with 40 of the 274 DEmiRNAs in all three datasets were selected. After intersecting the predicted 1912 DEmRNAs and previous 382 DEmRNAs, a 38 lncRNA-21 miRNA-40 mRNA ceRNA network was constructed (**Figures 4**, **5**).

Functional Enrichment Analysis

To determine the biological functions and pathways of the 40 DEmRNAs in the constructed ceRNA network, we used the Metascape database to analyze the GO functional enrichment and KEGG pathway enrichment (**Figure 6**). The top terms of biological processes were "BMP signaling pathway," "protein polyubiquitination," and "cellular response to transforming growth factor beta stimulus"; the top cellular component terms were "spindle pole," "mitotic spindle pole," and "catenin complex"; the top molecular function terms were "activin binding," "ubiquitin-protein transferase activity," and "transforming growth factor beta receptor binding." According to KEGG pathway analyses, the most significant pathways included "TGF-beta signaling pathway," "TNF signaling pathway," and "leukocyte transendothelial migration."

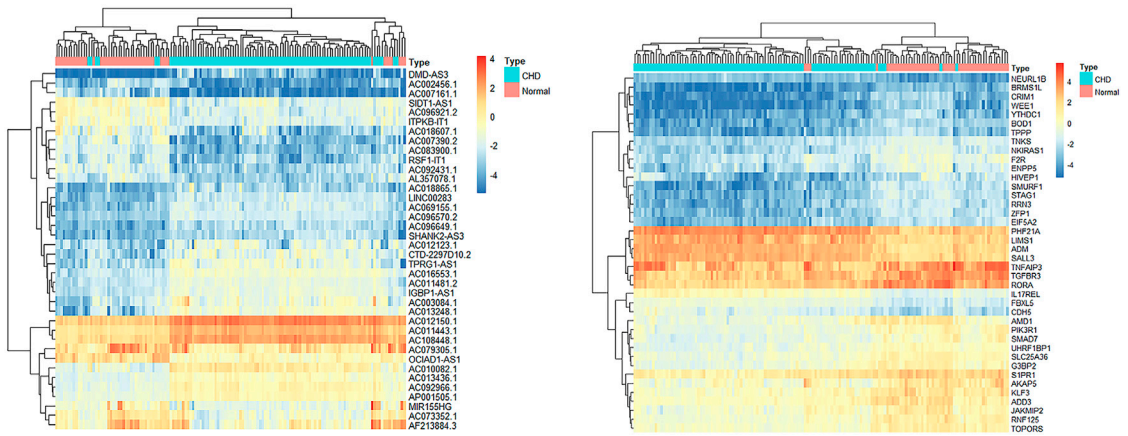

FIGURE 4 | Heatmaps of DElncRNAs and DEmRNAs.

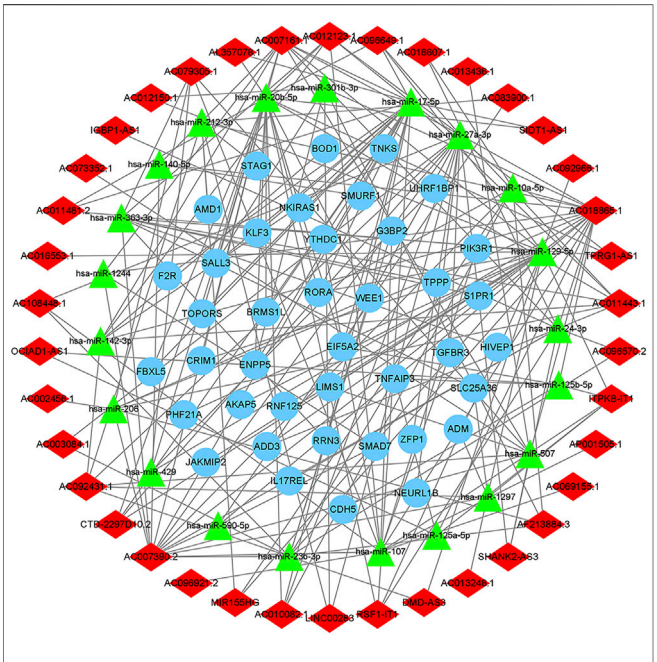

FIGURE 5 | The ceRNA network of lncRNA-miRNA-mRNA. The light blue round nodes, red diamond nodes, and green triangle nodes indicate mRNA, lncRNA, and miRNA, respectively.

Logistic Stepwise Regression Prediction Model Based on DElncRNAs

By setting 38 DElncRNAs as independent variables, we constructed a logistic stepwise regression prediction model for CHD. The analysis reveals that AC010082.1 and AC011443.1 ($p < 0.05$) as lncRNAs were statistically significant for model construction among the 38 independent variables. The prediction model formula is:

Logit(P) = −13.718 + AC010082.1*8.099 + AC011443.1*3.825.

The sensitivity, specificity, and AUC were 98.41%, 100%, and 0.995, respectively, for the training set, and 93.33%, 91.67%, and 0.983, respectively, for the test set (**Figure 7**). These two lncRNAs can be regarded as important signatures for the prediction of CHD. PCA of these two lncRNAs can distinguish patients with CHD from healthy controls (**Figure 8**). At the same time, the results show that AC010082.1 and AC011443.1 are upregulated in patients with CHD ($p < 0.05$), and that AC010082.1 and AC011443.1 have a significant positive correlation (r = 0.7, $p < 0.01$, **Figure 9**).

According to the database targeted prediction analysis, AC010082.1 could bind to hsa-miR-10a-5p, hsa-miR-17-5p, hsa-miR-20b-5p and hsa-miR-27a-3p, and then regulate the expression of 16 mRNAs through MREs. The AC011443.1 could target to hsa-miR-142-3p, hsa-miR-17-5p, hsa-miR-206, hsa-miR-20b-5p, hsa-miR-24-3p, hsa-miR-27a-3p and hsa-miR-363-3p, and regulate the expression of 25 mRNAs (**Table 1**). These two DElncRNAs could jointly bind to hsa-miR-17-5p, hsa-miR-20b-5p and hsa-miR-27a-3p, thus regulating the expression of 25 mRNAs through MREs and forming the 2lncRNA-8miRNA-25 mRNA -related ceRNA networks (**Figure 10**).

External Validation of AC010082.1 and AC011443.1 Using RT-qPCR

RT-qPCR was used to verify the relative expression of AC010082.1 and AC011443.1 in the validation cohort. The results show that AC010082.1 ($p = 0.009 < 0.01$) and AC011443.1 ($p = 0.02 < 0.05$) were significantly higher in the CHD group than in the healthy control group, and the AC010082.1 and AC011443.1 expression levels were significantly positively correlated (r = 0.5, $p < 0.01$, **Figure11**). Simultaneously, the relative expression levels of AC010082.1 and AC011443.1 were inserted in the prediction model formula Logit(P) = −13.718 + AC010082.1*8.099 + AC011443.1*3.825. The sensitivity, specificity, and AUC of the prediction model were 63.3%, 60.0%, and 0.691, respectively, implying that the model can effectively identify CHD (**Figure 12**).

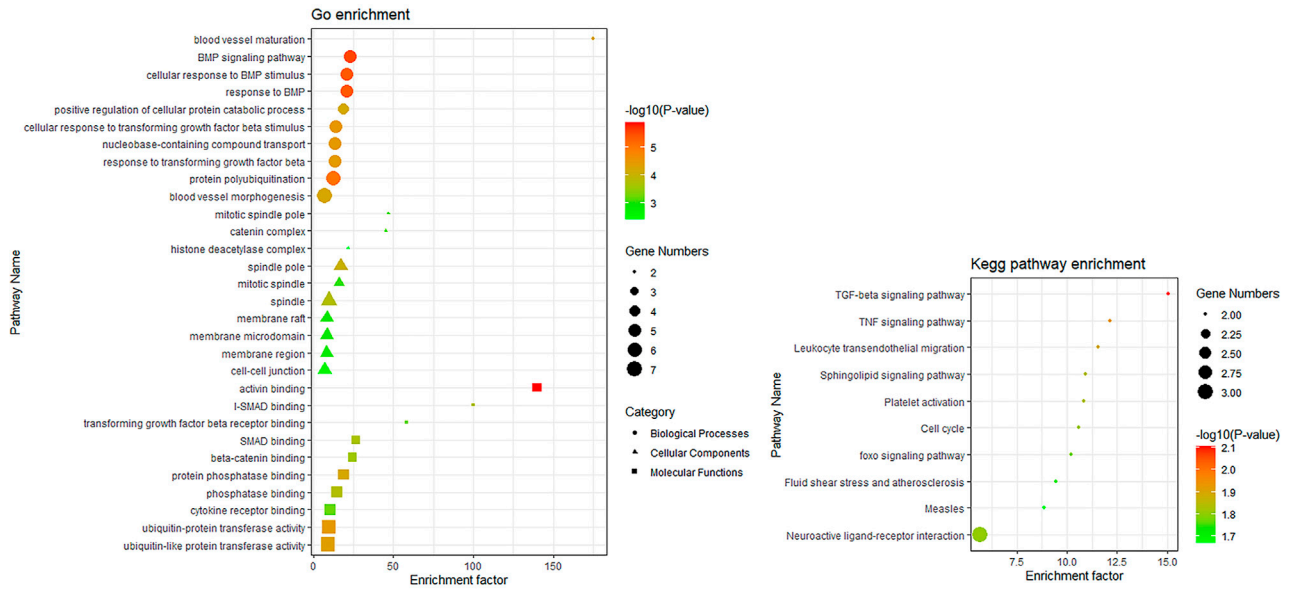

FIGURE 6 | Top 10 terms obtained using GO functional and KEGG pathway enrichment analyses.

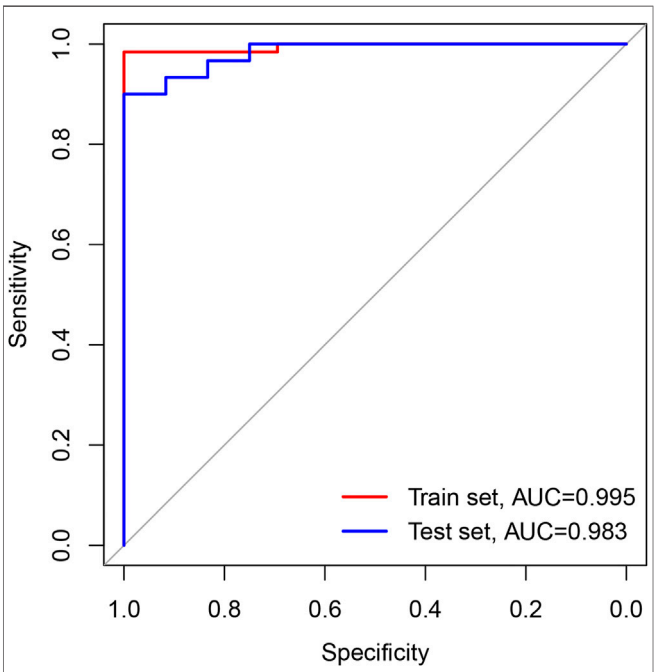

FIGURE 7 | ROC curve based on GEO database. The red line represents train set and the blue line represents test set.

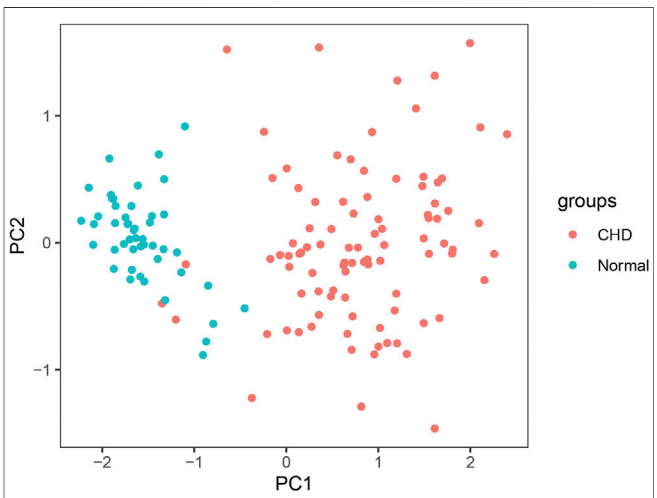

FIGURE 8 | PCA of AC010082.1 and AC011443.1. Red dots represent patients with CHD and light blue dots represent healthy controls.

DISCUSSION

Despite considerable advances in modern medicine, CHD diagnosis remains difficult, particularly in the early stages. LncRNA is an important regulator of gene expression, and one of its regulatory mechanisms is ceRNA. MiRNAs can bind to mRNA through MREs, resulting in mRNA degradation or translation inhibition. When lncRNAs and mRNAs have the same MREs, lncRNAs can compete with mRNA for binding to miRNA to prevent mRNA degradation and achieve indirect regulation of mRNA expression level (Wang et al., 2021). The ceRNA mechanism provides a new method for studying the biological functions of lncRNAs and has garnered extensive attention to date (Li et al., 2021b; Lin et al., 2021; Ma et al., 2021).

In this study, a ceRNA network consisting of 38 lncRNAs, 21 miRNAs, and 40 mRNAs was constructed using bioinformatics analysis. KEGG function enrichment in this network was mainly

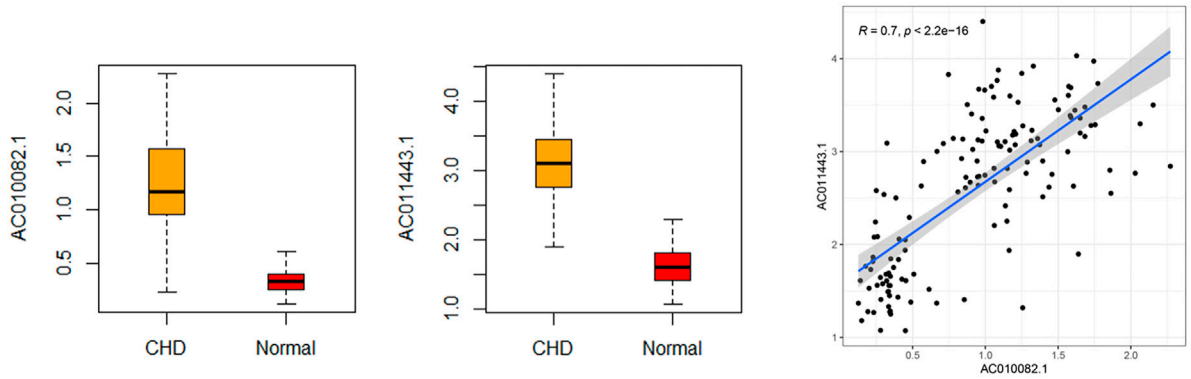

FIGURE 9 | Relative expression level and correlation of AC010082.1 and AC011443.1 based on GEO database.

TABLE 1 | AC010082.1- and AC011443.1-related target miRNA and target mRNA.

lncRNA	miRNA	mRNA
AC010082.1	hsa-miR-10a-5p	RORA
AC011443.1	hsa-miR-142-3p	BOD1/TNKS
	hsa-miR-206	WEE1
	hsa-miR-24-3p	ADD3/IL17REL
	hsa-miR-363-3p	HIVEP1/RRN3/S1PR1/SLC25A36/TPPP
AC010082.1 and AC011443.1	hsa-miR-17-5p	BRMS1L/EIF5A2/ENPP5/F2R/FBXL5/KLF3/NKIRAS1/RORA/SALL3/TOPORS/WEE1/YTHDC1
	hsa-miR-20b-5p	BRMS1L/CRIM1/EIF5A2/ENPP5/FBXL5/KLF3/NKIRAS1/RORA/SALL3/TOPORS/WEE1
	hsa-miR-27a-3p	EIF5A2/NEURL1B/TGFBR3/WEE1/ZFP1

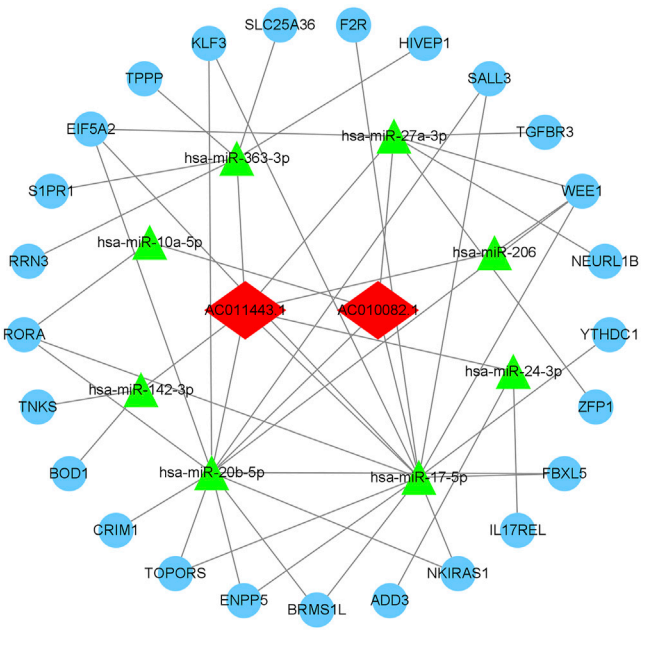

FIGURE 10 | AC010082.1- and AC011443.1-related ceRNA network. The light blue round nodes, red diamond nodes, and green triangle nodes indicate mRNA, lncRNA, and miRNA, respectively.

concentrated in the TGF-β signaling pathway, TNF signaling pathway, and leukocyte transendothelial migration. These signaling pathways have been previously shown to be closely related to the pathological mechanisms of CHD (Shen et al., 2020; Guo et al., 2021; Sluiter et al., 2021). The TGF-β signaling pathway can regulate the proliferation and migration of vascular smooth muscle and endothelial cells, and affect the stability of plaque, which plays an important role in CHD pathogenesis (Zeng et al., 2016). The TNF signaling pathway is involved in myocardial I/R injury and cardiomyocyte apoptosis (Tan et al., 2018). Leukocyte transmigration is critical to the inflammatory response and accelerates the progression of atherosclerosis (Muller, 2011; Bhui and Hayenga, 2017). These DElncRNAs can interfere with pathological changes in CHD through various signaling pathways.

However, further lncRNA analysis using the logistic stepwise regression prediction model revealed that AC010082.1 and AC011443.1 might be important biomarkers of CHD, which was confirmed using RT-qPCR. AC010082.1 is an antisense molecule with a length of 546 bp and is located on chr7: 18,429,062–18,430,738, whereas AC011443.1 is also an antisense molecule with a length of 365 bp and is located on chr19:39,134,882–39,136,463. Unfortunately, no relevant studies have been conducted on these two lncRNAs, and their direct mechanism of action remains unclear. Through bioinformatics

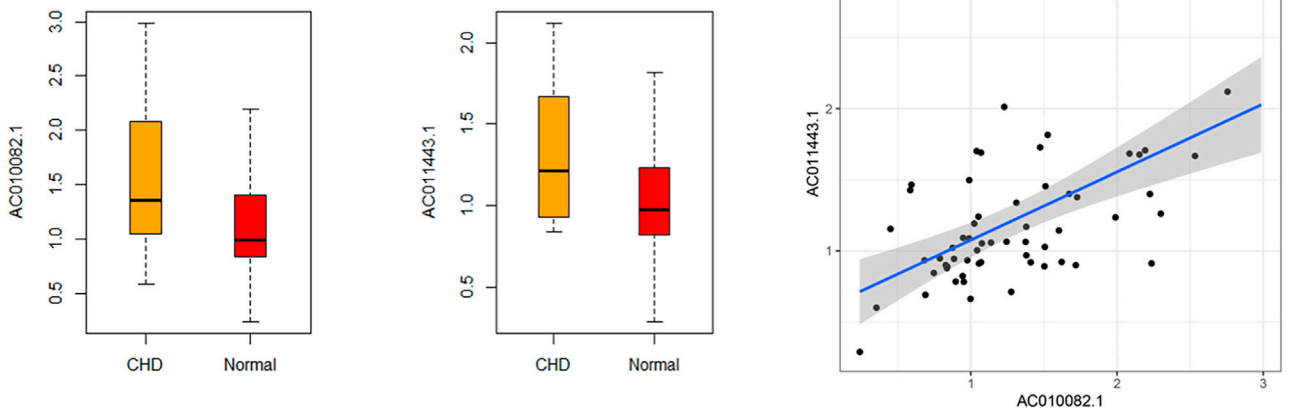

FIGURE 11 | Relative expression level and correlation of AC010082.1 and AC011443.1 in the validation cohort.

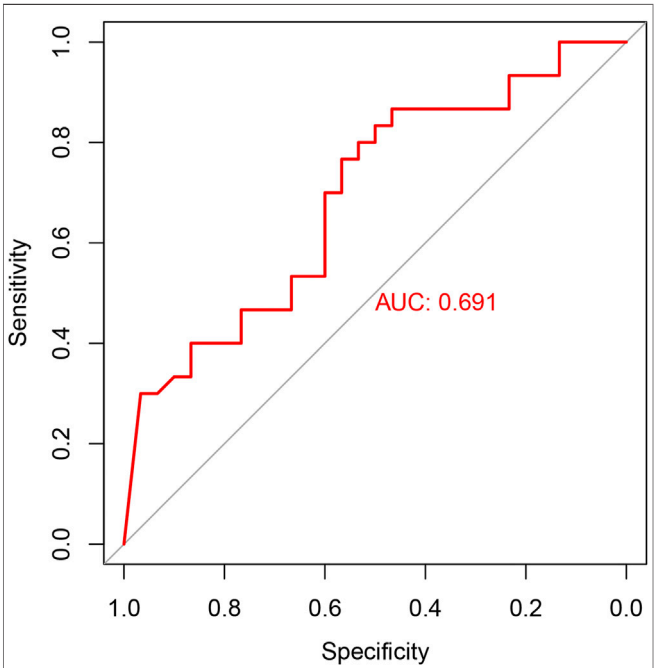

FIGURE 12 | ROC curve in the validation cohort.

analysis, it was found that these two DElncRNAs affect the expression of 25 mRNAs by regulating eight miRNAs. The hsa-miR-17-5p, hsa-miR-20b-5p and hsa-miR-27a-3p were jointly regulated by these two DElncRNAs, which may contain a common MRE and have a regulatory relationship through ceRNA mechanism. We found that AC010082.1 and AC011443.1 were overexpressed in patients with CHD and showed a significant positive correlation. The mechanism may be that when lncRNA AC010082.1 is highly expressed in patients with CHD, it will bind more miRNAs, so as to release the inhibition of miRNA on the other lncRNA AC011443.1, thus leading to its high expression (Salmena et al., 2011). AC010082.1 and AC011443.1 bind to miRNA through MREs, thus affecting mRNA expression and biological functions.

Interestingly, we found that hsa-miR-17-5p, hsa-miR-20b-5p and hsa-miR-27a-3p co-regulated by these two DElncRNAs have important biological roles in CHD. The expression of hsa-miR-17-5p is down-regulation in patients with CHD, which could be as a biomarker of CHD (Zhelankin et al., 2021) and a good predictor of the severity of coronary atherosclerosis (Chen et al., 2015). In addition, lncRNA SNHG16 could regulate NF-κB signaling pathway by binding hsa-miR-17-5p, and then affect proliferation and inflammatory response in atherosclerosis patients, which provide a potential target for treating AS (An et al., 2019). Furthermore, miR-20b-5p plays an important role in mediating cardiomyocytes apoptosis via the HIF-1 α/NF- κ B pathway (Zhou et al., 2020). And circHIPK3 acting as miR-20b-5p sponge could accelerate cardiomyocyte autophagy and apoptosis during myocardial I/R injury (Qiu et al., 2021). Reportedly, miR-27a expression is upregulated in patients with CHD, and its expression level is remarkable correlated with the severity of coronary artery stenosis, which can be used as a biomarker of CHD (Babaee et al., 2020). Meanwhile, miR-27a may lead to the progression of atherosclerotic plaques by downregulating *ABCA1* and *ABCG1* gene expression (Rafiei et al., 2021).

Besides, these two DElncRNAs affected TGFBR3 expression by co-regulating the miR-27a-3p sponge via bioinformatics prediction. TGFBR3 expression is significantly upregulated in patients after myocardial infarction and may serve as a therapeutic target and biomarker for myocardial damage by activating p38 MAPK to induce cardiomyocyte apoptosis (Chu et al., 2011; Chen et al., 2019). Moreover, it has been found that lncRNA SOX2-OT exacerbates hypoxia-induced cardiomyocyte injury by regulating the miR-27a-3p/TGFβR1 axis (Yang and Lin, 2020). Therefore, we speculated that AC010082.1 and

AC011443.1 play important roles in the pathological progression of CHD through the ceRNA mechanism and are potential biomarkers of CHD.

The present study had some limitations. First, we only verified the possibility of using AC010082.1 and AC011443.1 as biomarkers through RT-qPCR, and the clinical samples were obtained from only one research center. In future, larger sample sizes and data from multiple centers countrywide are required to verify our findings. In addition, *in vitro* and *in vivo* experiments to further explore the functions of AC010082.1 and AC011443.1, and the related pathological mechanisms, are warranted.

In summary, our study identified AC010082.1 and AC011443.1 as possible biomarkers of CHD through bioinformatics analysis and RT-qPCR. The ceRNA network associated with these lncRNAs possibly plays a key role in the pathological process of CHD.

DATA AVAILABILITY STATEMENT

The datasets presented in this study can be found in online repositories. The names of the repository/repositories and accession number(s) can be found in the article/ **Supplementary Material**.

ETHICS STATEMENT

The studies involving human participants were reviewed and approved by The Ethics Committee of Guang'anmen Hospital, China Academy of Chinese Medical Sciences (no. 2019-224-KY). The patients/participants provided their written informed consent to participate in this study.

AUTHOR CONTRIBUTIONS

CL and JW contributed to the study design. CL and LL searched for and downloaded the gene expression profiles from the Gene Expression Omnibus database. JG was the clinician involved in enrolling the patients and in diagnosing the coronary heart disease cases. CL, LL, and YL performed the RT-qPCR. CL and YL prepared the draft of the manuscript. All authors revised and approved the final manuscript.

FUNDING

This work was supported by the Programs Foundation for Leading Talents in State Administration of Traditional Chinese Medicine of China, "Qihuang Chief Scientists" and Project and National Natural Science Foundation of China (No. 81974556).

SUPPLEMENTARY MATERIAL

The Supplementary Material for this article can be found online at: https://www.frontiersin.org/articles/10.3389/fgene.2021.780431/full#supplementary-material

REFERENCES

Agarwal, V., Bell, G. W., Nam, J.-W., and Bartel, D. P. (2015). Predicting Effective microRNA Target Sites in Mammalian mRNAs. *eLife* 4. doi:10.7554/eLife.05005

An, J. H., Chen, Z. Y., Ma, Q. L., Wang, H. J., Zhang, J. Q., and Shi, F. W. (2019). LncRNA SNHG16 Promoted Proliferation and Inflammatory Response of Macrophages through miR-17-5p/NF-Kb Signaling Pathway in Patients with Atherosclerosis. *Eur. Rev. Med. Pharmacol. Sci.* 23, 8665–8677. doi:10.26355/eurrev_201910_19184

Babaee, M., Chamani, E., Ahmadi, R., Bahreini, E., Balouchnejadmojarad, T., Nahrkhalaji, A. S., et al. (2020). The Expression Levels of miRNAs- 27a and 23a in the Peripheral Blood Mononuclear Cells (PBMCs) and Their Correlation with FOXO1 and Some Inflammatory and Anti-inflammatory Cytokines in the Patients with Coronary Artery Disease (CAD). *Life Sci.* 256, 117898. doi:10.1016/j.lfs.2020.117898

Beermann, J., Piccoli, M.-T., Viereck, J., and Thum, T. (2016). Non-coding RNAs in Development and Disease: Background, Mechanisms, and Therapeutic Approaches. *Physiol. Rev.* 96, 1297–1325. doi:10.1152/physrev.00041.2015

Bhui, R., and Hayenga, H. N. (2017). An Agent-Based Model of Leukocyte Transendothelial Migration during Atherogenesis. *Plos Comput. Biol.* 13, e1005523. doi:10.1371/journal.pcbi.1005523

Cai, Y., Yang, Y., Chen, X., Wu, G., Zhang, X., Liu, Y., et al. (2016). Circulating 'lncRNA OTTHUMT00000387022' from Monocytes as a Novel Biomarker for Coronary Artery Disease. *Cardiovasc. Res.* 112, 714–724. doi:10.1093/cvr/cvw022

Chen, C.-Y., Choong, O. K., Liu, L.-W., Cheng, Y.-C., Li, S.-C., Yen, C. Y. T., et al. (2019). MicroRNA Let-7-TGFBR3 Signalling Regulates Cardiomyocyte Apoptosis after Infarction. *EBioMedicine* 46, 236–247. doi:10.1016/j.ebiom.2019.08.001

Chen, J., Xu, L., Hu, Q., Yang, S., Zhang, B., and Jiang, H. (2015). MiR-17-5p as Circulating Biomarkers for the Severity of Coronary Atherosclerosis in Coronary Artery Disease. *Int. J. Cardiol.* 197, 123–124. doi:10.1016/j.ijcard.2015.06.037

Cheng, D.-L., Xiang, Y.-Y., Ji, L.-j., and Lu, X.-J. (2015). Competing Endogenous RNA Interplay in Cancer: Mechanism, Methodology, and Perspectives. *Tumor Biol.* 36, 479–488. doi:10.1007/s13277-015-3093-z

Chou, C.-H., Chang, N.-W., Shrestha, S., Hsu, S.-D., Lin, Y.-L., Lee, W.-H., et al. (2016). miRTarBase 2016: Updates to the Experimentally Validated miRNA-Target Interactions Database. *Nucleic Acids Res.* 44, D239–D247. doi:10.1093/nar/gkv1258

Chu, W., Li, X., Li, C., Wan, L., Shi, H., Song, X., et al. (2011). TGFBR3, a Potential Negative Regulator of TGF-β Signaling, Protects Cardiac Fibroblasts from Hypoxia-Induced Apoptosis. *J. Cel. Physiol.* 226, 2586–2594. doi:10.1002/jcp.22604

Collet, J. P., Thiele, H., Barbato, E., Barthélémy, O., Bauersachs, J., Bhatt, D. L., et al. (2021). 2020 ESC Guidelines for the Management of Acute Coronary Syndromes in Patients Presenting without Persistent ST-Segment Elevation. *Eur. Heart J.* 42, 1289–1367. doi:10.1093/eurheartj/ehaa575

Gao, L., Nie, X., Zhang, W., Gou, R., Hu, Y., Qi, Y., et al. (2020). Identification of Long Noncoding RNA RP11-89K21.1 and RP11-357H14.17 as Prognostic Signature of Endometrial Carcinoma via Integrated Bioinformatics Analysis. *Cancer Cel Int* 20, 268. doi:10.1186/s12935-020-01359-9

Guo, F., Sha, Y., Hu, B., and Li, G. (2021). Correlation of Long Non-coding RNA LncRNA-Fa2h-2 with Inflammatory Markers in the Peripheral Blood of Patients with Coronary Heart Disease. *Front. Cardiovasc. Med.* 8, 682959. doi:10.3389/fcvm.2021.682959

Hongkuan, Z., Karsoon, T., Shengkang, L., Hongyu, M., and Huaiping, Z. (2021). The Functional Roles of the Non-coding RNAs in Molluscs. *Gene* 768, 145300. doi:10.1016/j.gene.2020.145300

Jeggari, A., Marks, D. S., and Larsson, E. (2012). miRcode: a Map of Putative microRNA Target Sites in the Long Non-coding Transcriptome. *Bioinformatics (Oxford, England)* 28, 2062–2063. doi:10.1093/bioinformatics/bts344

Knuuti, J., Wijns, W., Saraste, A., Capodanno, D., Barbato, E., Funck-Brentano, C., et al. (2020). 2019 ESC Guidelines for the Diagnosis and Management of Chronic Coronary Syndromes. *Eur. Heart J.* 41, 407–477. doi:10.1093/eurheartj/ehz425

Li, J., Chen, J., Zhang, F., Li, J., An, S., Cheng, M., et al. (2021a). LncRNA CDKN2B-AS1 Hinders the Proliferation and Facilitates Apoptosis of Ox-LDL-Induced Vascular Smooth Muscle Cells via the ceRNA Network of CDKN2B-AS1/miR-126-5p/PTPN7. *Int. J. Cardiol.* 340, 79–87. doi:10.1016/j.ijcard.2021.08.009

Li, L., Wang, L., Li, H., Han, X., Chen, S., Yang, B., et al. (2018). Characterization of LncRNA Expression Profile and Identification of Novel LncRNA Biomarkers to Diagnose Coronary Artery Disease. *Atherosclerosis* 275, 359–367. doi:10.1016/j.atherosclerosis.2018.06.866

Li, P., Yan, X., Xu, G., Pang, Z., Weng, J., Yin, J., et al. (2020). A Novel Plasma lncRNA ENST00000416361 Is Upregulated in Coronary Artery Disease and Is Related to Inflammation and Lipid Metabolism. *Mol. Med. Rep.* 21, 2375–2384. doi:10.3892/mmr.2020.11067

Li, S., Cao, Y., Zhang, H., Lu, X., Wang, T., Xu, S., et al. (2021b). Construction of lncRNA-Mediated ceRNA Network for Investigating Immune Pathogenesis of Ischemic Stroke. *Mol. Neurobiol.* 58, 4758–4769. doi:10.1007/s12035-021-02426-6

Lin, X., Zhuang, S., Chen, X., Du, J., Zhong, L., Ding, J., et al. (2021). LncRNA ITGB8-AS1 Functions as a ceRNA to Promote Colorectal Cancer Growth and Migration through Integrin-Mediated Focal Adhesion Signaling. *Mol. Ther.* doi:10.1016/j.ymthe.2021.08.011

Liu, Y., Cui, X., Wang, C., and Zhao, S. (2020). RETRACTED ARTICLE: LncRNA HCG11 Regulates Proliferation and Apoptosis of Vascular Smooth Muscle Cell through Targeting miR-144-3p/FOXF1 axis in Atherosclerosis. *Biol. Res.* 53, 44. doi:10.1186/s40659-020-00306-2

Livak, K. J., and Schmittgen, T. D. (2001). Analysis of Relative Gene Expression Data Using Real-Time Quantitative PCR and the 2−ΔΔCT Method. *Methods* 25, 402–408. doi:10.1006/meth.2001.1262

Long, J., Xiong, J., Bai, Y., Mao, J., Lin, J., Xu, W., et al. (2019). Construction and Investigation of a lncRNA-Associated ceRNA Regulatory Network in Cholangiocarcinoma. *Front. Oncol.* 9, 649. doi:10.3389/fonc.2019.00649

Lu, D., and Thum, T. (2019). RNA-based Diagnostic and Therapeutic Strategies for Cardiovascular Disease. *Nat. Rev. Cardiol.* 16, 661–674. doi:10.1038/s41569-019-0218-x

Ma, Y., Ma, L., Cao, Y., and Zhai, J. (2021). Construction of a ceRNA-Based lncRNA-mRNA Network to Identify Functional lncRNAs in Polycystic Ovarian Syndrome. *Aging* 13, 8481–8496. doi:10.18632/aging.202659

Miao, L., Yin, R.-X., Zhang, Q.-H., Hu, X.-J., Huang, F., Chen, W.-X., et al. (2019). A Novel lncRNA-miRNA-mRNA Triple Network Identifies lncRNA TWF1 as an Important Regulator of miRNA and Gene Expression in Coronary Artery Disease. *Nutr. Metab. (Lond)* 16, 39. doi:10.1186/s12986-019-0366-3

Mortality, G. B. D., and Causes of Death, C. (2015). Global, Regional, and National Age-Sex Specific All-Cause and Cause-specific Mortality for 240 Causes of Death, 1990-2013: a Systematic Analysis for the Global Burden of Disease Study 2013. *Lancet* 385, 117–171. doi:10.1016/S0140-6736(14)61682-2

Muller, W. A. (2011). Mechanisms of Leukocyte Transendothelial Migration. *Annu. Rev. Pathol. Mech. Dis.* 6, 323–344. doi:10.1146/annurev-pathol-011110-130224

Novák, J., Macháčková, T., Krejčí, J., Bienertová-Vašků, J., and Slabý, O. (2021). MicroRNAs as Theranostic Markers in Cardiac Allograft Transplantation: from Murine Models to Clinical Practice. *Theranostics* 11, 6058–6073. doi:10.7150/thno.56327

Ouyang, M., Lu, J., Ding, Q., Qin, T., Peng, C., and Guo, Q. (2020). Knockdown of Long Non-coding RNA PVT1 Protects Human AC16 Cardiomyocytes from Hypoxia/reoxygenation-Induced Apoptosis and Autophagy by Regulating miR-186/Beclin-1 axis. *Gene* 754, 144775. doi:10.1016/j.gene.2020.144775

Qiu, Z., Wang, Y., Liu, W., Li, C., Zhao, R., Long, X., et al. (2021). CircHIPK3 Regulates the Autophagy and Apoptosis of Hypoxia/reoxygenation-Stimulated Cardiomyocytes via the miR-20b-5p/ATG7 axis. *Cell Death Discov.* 7, 64. doi:10.1038/s41420-021-00448-6

R Core Team (2018). *R: A Language and Environment for Statistical Computing*. Vienna, Austria: R Foundation for Statistical Computing. Available online at: https://www.R-project.org/.

Rafiei, A., Ferns, G. A., Ahmadi, R., Khaledifar, A., Rahimzadeh-Fallah, T., Mohmmad-Rezaei, M., et al. (2021). Expression Levels of miR -27a, miR -329, ABCA1 , and ABCG1 Genes in Peripheral Blood Mononuclear Cells and Their Correlation with Serum Levels of Oxidative Stress and hs-CRP in the Patients with Coronary Artery Disease. *IUBMB life* 73, 223–237. doi:10.1002/iub.2421

Salmena, L., Poliseno, L., Tay, Y., Kats, L., and Pandolfi, P. P. (2011). A ceRNA Hypothesis: the Rosetta Stone of a Hidden RNA Language? *Cell* 146, 353–358. doi:10.1016/j.cell.2011.07.014

Shannon, P., Markiel, A., Ozier, O., Baliga, N., Wang, J., Ramage, D., et al. (2003). Cytoscape: a Software Environment for Integrated Models of Biomolecular Interaction Networks. *Genome Res.* 13, 2498–2504. doi:10.1101/gr.1239303

Shen, Z., Shen, A., Chen, X., Wu, X., Chu, J., Cheng, Y., et al. (2020). Huoxin Pill Attenuates Myocardial Infarction-Induced Apoptosis and Fibrosis via Suppression of P53 and TGF-β1/Smad2/3 Pathways. *Biomed. Pharmacother.* 130, 110618. doi:10.1016/j.biopha.2020.110618

Sluiter, T. J., Van Buul, J. D., Huveneers, S., Quax, P. H. A., and De Vries, M. R. (2021). Endothelial Barrier Function and Leukocyte Transmigration in Atherosclerosis. *Biomedicines* 9, 328. doi:10.3390/biomedicines9040328

Statello, L., Guo, C.-J., Chen, L.-L., and Huarte, M. (2020). Gene Regulation by Long Non-coding RNAs and its Biological Functions. *Nat. Rev. Mol. Cel Biol* 22, 96–118. doi:10.1038/s41580-020-00315-9

Tan, H., Qi, J., Fan, B.-Y., Zhang, J., Su, F.-F., and Wang, H.-T. (2018). MicroRNA-24-3p Attenuates Myocardial Ischemia/Reperfusion Injury by Suppressing RIPK1 Expression in Mice. *Cell Physiol Biochem* 51, 46–62. doi:10.1159/000495161

Task Force, M., Montalescot, G., Sechtem, U., Achenbach, S., Andreotti, F., Arden, C., et al. (2013). 2013 ESC Guidelines on the Management of Stable Coronary Artery Disease. *Eur. Heart J.* 34, 2949–3003. doi:10.1093/eurheartj/eht296

Wang, F., Xu, C.-Q., He, Q., Cai, J.-P., Li, X.-C., Wang, D., et al. (2011). Genome-wide Association Identifies a Susceptibility Locus for Coronary Artery Disease in the Chinese Han Population. *Nat. Genet.* 43, 345–349. doi:10.1038/ng.783

Wang, W., Hu, W., Wang, Y., An, Y., Song, L., Shang, P., et al. (2020). Long Non-coding RNA UCA1 Promotes Malignant Phenotypes of Renal Cancer Cells by Modulating the miR-182-5p/DLL4 axis as a ceRNA. *Mol. Cancer* 19, 18. doi:10.1186/s12943-020-1132-x

Wang, W., Min, L., Qiu, X., Wu, X., Liu, C., Ma, J., et al. (2021). Biological Function of Long Non-coding RNA (LncRNA) Xist. *Front. Cel Dev. Biol.* 9, 645647. doi:10.3389/fcell.2021.645647

Wong, N., and Wang, X. (2015). miRDB: an Online Resource for microRNA Target Prediction and Functional Annotations. *Nucleic Acids Res.* 43, D146–D152. doi:10.1093/nar/gku1104

Yang, G., and Lin, C. (2020). Long Noncoding RNA SOX2-OT Exacerbates Hypoxia-Induced Cardiomyocytes Injury by Regulating miR-27a-3p/TGFβR1 Axis. *Cardiovasc. Ther.* 2020, 1–11. doi:10.1155/2020/2016259

Yang, Y., Cai, Y., Wu, G., Chen, X., Liu, Y., Wang, X., et al. (2015). Plasma Long Non-coding RNA, CoroMarker, a Novel Biomarker for Diagnosis of Coronary Artery Disease. *Clin. Sci. (Lond)* 129, 675–685. doi:10.1042/CS20150121

Zeng, L., Dang, T. A., and Schunkert, H. (2016). Genetics Links between Transforming Growth Factor β Pathway and Coronary Disease. *Atherosclerosis* 253, 237–246. doi:10.1016/j.atherosclerosis.2016.08.029

Zhang, D., Wang, B., Ma, M., Yu, K., Zhang, Q., and Zhang, X. (2019). lncRNA HOTAIR Protects Myocardial Infarction Rat by Sponging miR-519d-3p. *J. Cardiovasc. Trans. Res.* 12, 171–183. doi:10.1007/s12265-018-9839-4

Zhang, X., Chen, M., Liu, X., Zhang, L., Ding, X., Guo, Y., et al. (2020). A Novel lncRNA, Lnc403, Involved in Bovine Skeletal Muscle Myogenesis by Mediating KRAS/Myf6. *Gene* 751, 144706. doi:10.1016/j.gene.2020.144706

Zhelankin, A. V., Stonogina, D. A., Vasiliev, S. V., Babalyan, K. A., Sharova, E. I., Doludin, Y. V., et al. (2021). Circulating Extracellular miRNA Analysis in

Patients with Stable CAD and Acute Coronary Syndromes. *Biomolecules* 11, 962. doi:10.3390/biom11070962

Zhou, Y., Zhou, B., Pache, L., Chang, M., Khodabakhshi, A. H., Tanaseichuk, O., et al. (2019). Metascape Provides a Biologist-Oriented Resource for the Analysis of Systems-Level Datasets. *Nat. Commun.* 10, 1523. doi:10.1038/s41467-019-09234-6

Zhou, Z., Chen, S., Tian, Z., Deng, S., Yi, X., Yang, S., et al. (2020). miR-20b-5p Attenuates Hypoxia-Induced Apoptosis in Cardiomyocytes via the HIF-1α/nf-Kb Pathway. *Acta Biochim. Biophys. Sinica* 52, 927–934. doi:10.1093/abbs/gmaa056

Conflict of Interest: The authors declare that the research was conducted in the absence of any commercial or financial relationships that could be construed as a potential conflict of interest.

Publisher's Note: All claims expressed in this article are solely those of the authors and do not necessarily represent those of their affiliated organizations, or those of the publisher, the editors and the reviewers. Any product that may be evaluated in this article, or claim that may be made by its manufacturer, is not guaranteed or endorsed by the publisher.

frontiers in Genetics

ORIGINAL RESEARCH
published: 13 January 2022
doi: 10.3389/fgene.2021.796776

Comprehensive Assessment of Serum hsa_circ_0070354 as a Novel Diagnostic and Predictive Biomarker in Non-small Cell Lung Cancer

Yuejiao Huang[1,2†], Shiyi Qin[2,3†], Xinliang Gu[2,3], Ming Zheng[2,3], Qi Zhang[2,3], Yupeng Liu[4], Chun Cheng[4], Kaibin Huang[5], Chunlei Peng[6] and Shaoqing Ju[2,3]**

[1]Department of Medical Oncology, Affiliated Hospital of Nantong University, Nantong, China, [2]Medical School of Nantong University, Nantong, China, [3]Department of Laboratory Medicine, Affiliated Hospital of Nantong University, Nantong, China, [4]Department of Thoracic Surgery, Affiliated Tumor Hospital of Nantong University, Nantong, China, [5]Department of General Surgery, Nantong Haimen People's Hospital, Nantong, China, [6]Department of Medical Oncology, Affiliated Tumor Hospital of Nantong University, Nantong, China

OPEN ACCESS

Edited by:
Deepanjan Paul,
Children's Hospital of Philadelphia,
United States

Reviewed by:
Marco Bono,
University of Palermo, Italy
Yuan Zhou,
Peking University, China
Disha Sharma,
Stanford Healthcare, United States

***Correspondence:**
Chunlei Peng
sword226@163.com
Shaoqing Ju
jsq814@hotmail.com

[†]These authors have contributed equally to this work

Specialty section:
This article was submitted to RNA,
a section of the journal
Frontiers in Genetics

Received: 17 October 2021
Accepted: 24 November 2021
Published: 13 January 2022

Citation:
Huang Y, Qin S, Gu X, Zheng M, Zhang Q, Liu Y, Cheng C, Huang K, Peng C and Ju S (2022) Comprehensive Assessment of Serum hsa_circ_0070354 as a Novel Diagnostic and Predictive Biomarker in Non-small Cell Lung Cancer. Front. Genet. 12:796776. doi: 10.3389/fgene.2021.796776

Background: More and more studies have shown that circular RNAs (circRNAs) play an essential role in the occurrence and development of tumors. Hence, they can be used as biomarkers to assist in diagnosing tumors. This study focuses on exploring the role of circular RNA (hsa_circ_0070354) in the diagnosis and prognosis of non-small cell lung cancer (NSCLC).

Materials and Methods: First of all, high-throughput sequencing was used to find the difference in the expression of circular RNA between NSCLC and adjacent tissues. The circRNAs with higher differences in expression were selected to verify their expressions in tissues, cells, and serum using qRT-PCR. Secondly, the hsa_circ_0070354 with a significant difference was chosen as the research goal, and the molecular properties were verified by agarose gel electrophoresis and Sanger sequencing, etc. Then, actinomycin D and repeated freeze-thaw were used to explore the stability and repeatability of hsa_circ_0070354. Finally, the expression of hsa_circ_0070354 in serum of 133 patients with NSCLC and 97 normal donors was detected, and its sensitivity, specificity, and prognosis as tumor markers were statistically analyzed.

Results: Hsa_circ_0070354 was highly expressed in tissues, cells, and serum of NSCLC, and it has the characteristics of sensitivity, stability, and repeatability. The ROC curve indicates that hsa_circ_0070354 is superior to conventional tumor markers in detecting NSCLC, and the combined diagnosis is of more significance in the diagnosis. The high expression of hsa_circ_0070354 is closely related to the late-stage, poor differentiation of the tumor and the short survival time of the patients, which is an independent indicator of poor prognosis.

Abbreviations: ACCU, overall accuracy; AUC, area under the curve; cDNA, complementary DNA; ceRNA, competitive endogenous RNA; circRNAs, circular RNAs; COPD, chronic obstructive pulmonary disease; GO, Gene Ontology; gDNA, genomic DNA; KEGG, Kyoto Encyclopedia of Genes and Genomes; NPV, negative predictive value; NSCLC, non-small cell lung cancer; OS, overall survival; PD-1, programmed cell death protein-1; PPV, positive predictive value; ROC, receiver operating characteristic; SEN, sensitivity; SPE, specificity.

Conclusion: Hsa_circ_0070354 is not only a novel sensitive index for the diagnosis of NSCLC but also a crucial marker for bad biological behavior.

Keywords: circular RNA, non-small cell lung cancer, diagnosis, prognosis, biomarker

INTRODUCTION

Previously, lung cancer has been the leading malignant tumor with the highest morbidity and mortality globally. Although the global cancer data in 2020 showed that the incidence rate of lung cancer has changed from the first place, the mortality rate was still the highest (Ma et al., 2021). In Asia, the incidence and mortality of lung cancer occupy the first place in the global data, and China is at the top of the list compared to other countries. Even though risk factors such as smoking are under control, the incidence rises in both sexes (Zukotynski et al., 2021). In all lung cancer cases, non-small cell lung cancer (NSCLC) accounts for more than 80%, with a 5-year survival rate of only about 15% (Ferlay et al., 2010; Hang et al., 2018) and a recurrence rate after radical treatment of more than 40% (Zheng et al., 2013). In the past 2 decades, an endless stream of treatments has been widely applied to NSCLC to reduce mortality and improve quality of life. Compared with conventional radiotherapy and chemotherapy, molecular targeting and immunotherapy have been preferred for patients with advanced, recurrent, and metastatic NSCLC (Ma et al., 2021). However, radical surgery for early NSCLC is still the key to curing the disease (Chaft et al., 2021). The reason for the high mortality rate of NSCLC is that patients were diagnosed at an advanced stage or local late-stage, missing the possibility of early cure. The leading causes include lack of routine physical examination, lack of biomarkers for early diagnosis, and disease surveillance methods (Qian et al., 2021). Therefore, with the progress of imaging, more sensitive and specific tumor biomarkers are needed to screen and diagnose NSCLC.

Circular RNAs (CircRNAs) are a class of non-coding RNAs derived from single or multiple exons (ENCODE Project Consortium, 2012; Zhao et al., 2019), a unique subtype of non-coding RNAs, with a covalently, closed continuous loop structure and no polarized or polyadenylated tail (Memczak et al., 2013; Rybak-Wolf et al., 2015). Unlike the traditional linear RNAs, circRNA has a high tolerance to exonuclease and is widely and stably expressed in the cytoplasm of various eukaryotic cells (Glažar et al., 2014; Zhao et al., 2019; Pei et al., 2020).

CircRNAs have always been regarded as by-products of low abundance splicing or splicing errors (Nigro et al., 1991; Cocquerelle et al., 1993). With the rapid development of high-throughput sequencing and bioinformatics technology, plenty of circRNAs have sprung up and been studied (Jeck et al., 2013; Memczak et al., 2013; Jeck and Sharpless, 2014). CircRNAs are generally considered the primary regulators of cellular processes because of their unique properties, such as richness, stability, and specific expression in cells and tissues (Di et al., 2019; Yu et al., 2020). CircRNAs can regulate gene expression at the transcriptional and post-transcriptional level by interacting with microRNAs (miRNAs) or other competing endogenous RNAs and participate in various biological activities (Hansen et al., 2013; Peng et al., 2015; Wang et al., 2018). Growing evidence showed that abnormal expression of circRNA may lead to the occurrence and development of cancers, including NSCLC (Wan et al., 2016; Zhu et al., 2017). Besides, numerous researches have identified that circRNAs are related to the clinical characteristics of patients and play a regulatory role in NSCLC (Zhang et al., 2019).

Tumor biomarkers are essential methods for tumor screening and early diagnosis due to their multiple sampling, dynamic monitoring, economic efficiency, as well as the advantages of high sensitivity and specificity. At present, the most commonly used serum tumor biomarkers for the diagnosis of NSCLC are embryonic antigen (CEA), squamous cell carcinoma antigen (SCC), and cytokeratin 19 fragment (Cyfra21-1) (Ye et al., 2020). However, the sensitivity and specificity of the above three markers for diagnosing NSCLC are not satisfactory, especially in the early stage of the disease (Kamel et al., 2019). CircRNAs play a vital role in the occurrence and development of NSCLC and can stably exist in patients' body fluids. Combined with their high sensitivity and specificity, they are ideal choices for liquid biopsy. Therefore, circRNAs can be considered as new specific diagnostic biomarkers of NSCLC (Huang et al., 2021a). Existing studies have successively verified the feasibility of circRNAs as a biomarker for the early diagnosis of NSCLC. For example, the differential expression of circ_0047921, circ_0056285, and circ_0007761 in exosomes can distinguish early NSCLC from healthy people, chronic obstructive pulmonary disease (COPD), or pulmonary tuberculosis (Xian et al., 2020). The high expression of hsa_circ_0102533 in peripheral blood indicated the occurrence of NSCLC (Zhou et al., 2018). Nevertheless, hsa_circ_0046264 was highly expressed in serum of patients with NSCLC, and it was closely related to clinical factors such as the age of onset, tumor size, disease stage, and lymph node metastasis (Liu et al., 2020). Moreover, circRNAs can also be regarded as predictors of adverse biological behaviors of lung cancer. For instance, a statistical difference between the high expression of hsa_circ_0060937 in serum and the occurrence of bone metastasis occurred in NSCLC (Zhang et al., 2020). The increased expression of circFARSA in plasma of patients was closely related to the migration and invasion of tumor cells as well (Hang et al., 2018). What's more, circRNAs could be used as biological indicators to guide treatment. Specifically, the high expression of circPVT1 often indicates that patients are not sensitive to chemotherapy (Lu et al., 2021). Likewise, the expressions of hsa_circ_0134501 and hsa_circ_0109320 were low in NSCLCs' plasma, and the combination of them can be used as a predictor of response to gefitinib (Liu et al., 2019a). Similarly, in the immunotherapy of NSCLC, circ-CPA4 participated in the regulation of $CD8^+$T cell response (Hong et al., 2020), while the overexpression of circFGFR1 led to drug

resistance to programmed cell death protein-1 (PD-1) (Zhang et al., 2019).

In this study, through high-throughput sequencing, it was found that a dramatic difference in the expression of hsa_circ_0070354 between NSCLC and adjacent tissues. Our team demonstrated the expression of hsa_circ_0070354 in serum of patients with NSCLC for the first time, analyzed its correlation with clinical features, evaluated its diagnostic efficacy, and explored its possibility as a novel biomarker for diagnosing NSCLC.

TABLE 1 | Primer sequences for Real-Time qPCR.

Gene	Primer sequences
has_circ_0070354	Forward: 5′-TCTGGGAAATCTTTCTGGGTAA-3′
	Reverse: 5′- CTACCAGATGGCAGCAACAG-3′
PTPN13	Forward: 5′-TTGCTGCCATCTGGTAGTGTG-3′
	Reverse: 5′-TGGTGCAGTGAATGCTCGAAG-3′
GAPDH	Forward: 5′-AGAAGGCTGGGGCTCATTTG-3′
	Reverse: 5′-GCAGGAGGCATTGCTGATGAT-3′
U6	Forward: 5′-GACTATCATATGCTTACCGT-3′
	Reverse: 5′-GGGCAGGAAGAGGGCCTAT-3′
18S	Forward: 5′-AGAAGGCTGGGGCTCATTTG-3′
	Reverse: 5′-GCAGGAGGCATTGCTGATGAT-3′

MATERIALS AND METHODS

Serum and Tissue Samples

The serum samples of 133 patients with NSCLC (I-IV stage) and 97 healthy donors were collected from the affiliated Hospital of Nantong University from 2015 to 2016 for follow-up experimental analysis. The sera collected by us were those after the initial diagnosis without any treatment. The preoperative and postoperative sera were the samples within 1 week before and after the operation. A flowchart showing the inclusion/exclusion criteria and analysis pipeline of this investigation were provided in **Supplementary Figure S1**. The tissue samples of NSCLC came from the thoracic surgery of the Affiliated Hospital of Nantong University and the Affiliated Tumor Hospital of Nantong University. Special thanks to Yupeng Liu, Guanjun Ju, Chun Cheng, and others of thoracic surgery for their strict control over the quality inspection of tissue samples, collecting tumor tissues, and paracancerous tissues (>5 cm tumor margin) with a diameter greater than 0.5 cm. More than two pathologists diagnosed all the samples, and TNM staging was performed according to the 8th edition of WHO. Every patient signed the informed consent form for collecting and preserving specimens and documenting details. All the samples were immediately kept in enzyme-free aseptic cryopreservation tubes at −80°C for a long time.

High Throughput Sequencing

Relying on Hipure Total RNA Minikit (Magen, Guangzhou, China), we extracted total RNA from 3 pairs of cancer and paracancerous tissues. Then, the concentration and purity of the total RNAs were evaluated by Qubit 3.0 Fluorometer (Invitrogen, California, CA, United States) and Agilent 2100 Bioanalyzer (Applied Biosystems, California, CA, United States). Ribosomal RNAs were fractionated from total RNA samples, meanwhile linear RNAs were removed (Geneseed, Guangzhou, China), and RNA-seq libraries were orderly constructed by TruSeq RNA sample preparation kits (Illumina, California, CA, United States). The purified cDNA library was sequenced on the Illumina HiSeq Xten platform via the PE150 sequencing model.

Cell Culture

Four human NSCLC cell lines, A549, H1299, HUT226, SPCA, and normal bronchial epithelial cell line HBE1 were purchased from Shanghai Institutes for Biological Sciences, China Academy of Science (Shanghai, China) and conserved in our laboratory. All cells were cultured in RPMI 1640 medium (Corning, Virginia, VA, United States) containing 10% fetal bovine serum (FBS, Gibco, South Dakota, SD, United States), 100 U/ml penicillin-streptomycin mixture (Gibco, South Dakota, SD, United StatesA) in a humidified incubator (Thermo, Massachusetts, MA, United States) with 5% CO_2 at 37°C.

Total RNA Extraction and qRT-PCR

Serum, tissue, and cell total RNAs were extracted by TRIzol reagent (Invitrogen, Karlsruhe, Germany). According to the manufacturer's instruction, complementary DNAs (cDNAs) were reverse transcribed by Revert Aid RT Reverse Transcription Kit (Thermo Fisher Scientific, Massachusetts, MA, United States). The specific divergent primers involved in this paper were designed and synthesized by Ribobio Corporation (Suzhou, China), with the forward and reverse primer as shown in **Table 1**. RT-qPCR was performed as described in previous studies (Huang et al., 2021b). In brief, the reaction was initiated at 95°C (10 min), followed by 40 cycles at 95°C (10s) and 62°C (34s) in the 20 ul system. PCR products were identified by Sanger sequencing.

RNase R and Agarose Gel Electrophoresis

RNase R treatment was executed at 37°C with 4 U/μg of RNase R (Epicentre Biotechnologies, Wisconsin, WI, United States) for 3 min and then inactivated at 70°C for 10 min to deactivate the enzyme, after which the mixture was reversely transcribed into cDNA for qRT-PCR. 2.5% agarose gel was prepared, and then the electrophoresis bands of PCR products were observed under UV conditions after about 20 min electrophoretic at 100 V.

Actinomycin D

The actinomycin D of 1,000 mg/ml was diluted to 2.5 μg/ml using RPMI-1640 complete medium and replaced the ordinary medium for 24 h. After treatment, total RNA was extracted from the cells for subsequent determination at 0, 2, 4, 8, 12, 24 h, respectively.

Nuclear and Cytoplasmic RNA Separation Assay

Up to 5×10^6 cells were digested by trypsin and collected in a small centrifuge tube for backup use. According to the

manufacturer's protocol, RNA fractions from the nucleus and cytoplasm of cells were separated by the Ambion®PARIS™Kit (Thermo Fisher Scientific, Massachusetts, MA, United States). Nuclear and cytoplasmic RNAs were then converted to cDNAs and detected by qRT-PCR or stored in the refrigerator at −80°C.

Statistical Analysis

Statistical analyses in this study were mainly conducted by SPSS 20.0 (IBM SPSS Statistics, Chicago, USA) and GraphPad Prism v8.0 (Graphpad Software Inc., California, USA). The differences between groups were analyzed using Student's t-test and one-way ANOVA. The correlation of hsa_circ_0070354 to clinical characteristics was analyzed by chi-square test. The receiver operating characteristic (ROC) curve and area under the curve (AUC) were determined to evaluate the diagnostic performance of hsa_circ_0070354 in NSCLC. Before plotting the ROC curve, we performed binomial logistic regression. Univariate and multivariate Cox proportional hazards regression models were carried out to assess the clinical variables' impacts on the overall survival (OS) of NSCLC patients. Survival curves were estimated by the Kaplan-Meier method, while the log-rank test evaluated statistical significance. Data are denoted by mean value ± standard deviation (SD) from at least three biological replicates independently. p values < 0.05 were indicated statistical significant.

RESULTS

Screening and Detecting the Expression of hsa_circ_0070354 in NSCLC Tissues, Cells, and Sera

High-throughput sequencing was implemented in 3 pairs of cancerous and adjacent noncancerous tissues from NSCLC patients to determine and characterize the differential expression of circRNAs in NSCLC. A total of 2319 circRNAs were identified, of which 56 were significantly up-regulated and 50 were down-regulated when we set the filter criteria as fold-change ≥ 2 and $p < 0.05$ (**Figures 1A,B**). **Figure 1C** showed the top 9 up-regulated circRNAs with remarkable differences, among which our study object hsa_circ_0070354 is included. Then the expression of hsa_circ_0070354 in 16 pairs of NSCLC tissue samples was verified by qRT-PCR (**Figure 1E**, small sample verification). Notably, 11 cases of adenocarcinoma and 5 cases of squamous cell carcinoma were concluded among the collected cases of NSCLC (**Supplementary Table S1**). Compared with the corresponding adjacent tissue adjacent tissues, hsa_circ_0070354 showed high expression in tumors. This result also corresponded to the presentation of cell lines. Similarly, compared with normal bronchial epithelial cells, the expression of hsa_circ_0070354 was also increased meaningfully in NSCLC cell lines (**Figure 1D** above), which indicated that hsa_circ_0070354 might be related to the presence of lung cancer. At the same time, we also detected the expression levels of hsa_circ_0070354 in cell lines of gastric cancer (AGS and BGC-823), hepatocellular carcinoma (Hep-G2), cervical cancer (Hela), and NSCLC (A549), respectively (**Figure 4D** below). Compared with A549, their CT value was significantly higher (**Figure 1D** below). Under the verification of large numbers of serum samples, the expression of hsa_circ_0070354 was detected in the serum of 133 patients with NSCLC and 97 normal donors and verified the conclusion of its high expression (**Figure 1F**).

Molecular Properties and Methodological Evaluation of hsa_circ_0070354 in NSCLC

The high expression of hsa_circ_0070354 has a clear relationship with cancer, providing the possibility of hsa_circ_0070354 as a tumor biomarker. Due to the lack of previous studies, to further clarify the properties of hsa_circ_0070354, we have completed the following explorations. Initially, the Ensembl genome database (GRCh37/hg19) was applied to verify hsa_circ_0070354 located on chr4_87593517_87610343_+, with a predicted length of 431 bp (**Figure 2A**). In order to ensure that hsa_circ_0070354 was not *trans*-splicing or genomic rearrangement, we designed divergent and convergent primers to amplify the circRNA 0070354 and its source gene PTPN13 linear mRNA, respectively. The results of PCR amplification pointed out hsa_circ_0070354 was amplified from cDNA, excluding the existence of genomic DNA (gDNA), while convergent primers amplified PTPN13 from both cDNA and gDNA (**Figure 2B**). Consistently, agarose gel electrophoresis presented a single electrophoretic band, which was about the same size as the primer amplification product about 70 bp (**Figure 2B**). In addition, the presence of hsa_circ_0070354 was proved by RT-PCR (**Figure 2C**), and the back splicing junction of hsa_circ_0070354 in PCR products was confirmed by Sanger sequencing (**Figure 2D**).

Since circRNA is more stable than linear RNA and is not easily degraded by exonuclease, the expression of hsa_circ_0070354 and linear PTPN13 were detected by qRT-PCR after being treated with RNase R. The results presented that compared with linear PTPN13, the degradation of hsa_circ_0070354 was not significant (**Figures 3A,B**). The serum samples from 20 healthy controls were randomly mixed with equal volume, placed at room temperature for 24 h (**Figure 3C**), frozen, and thawed 0, 1, 3, 5, 10 times repeatedly (**Figure 3D**). Interestingly, the results showed no significant difference in cycle threshold (CT) value of hsa_circ_0070354 after these operations. As we are known, actinomycin D could inhibit the synthesis of new RNAs. To further evaluate the stability, the expression of hsa_circ_0070354 and linear PTPN13 was detected at the indicated time points after treatment with actinomycin D. The results signified that hsa_circ_0070354 had a longer half-life after treatment with actinomycin D (**Figure 3E**). All these results illustrated that hsa_circ_0070354 is a circRNA and the stability met the requirement of tumor biomarker. It is known that the circular RNA in the nucleus mainly regulates the transcription of parental genes, while the circular RNA in the cytoplasm primarily acts as a competitive endogenous RNA (ceRNA) (Rong et al., 2017; Xu et al., 2020). Through the nuclear-cytoplasmic separation experiment, we found that hsa_circ_0070354 is mainly located in the cytoplasm

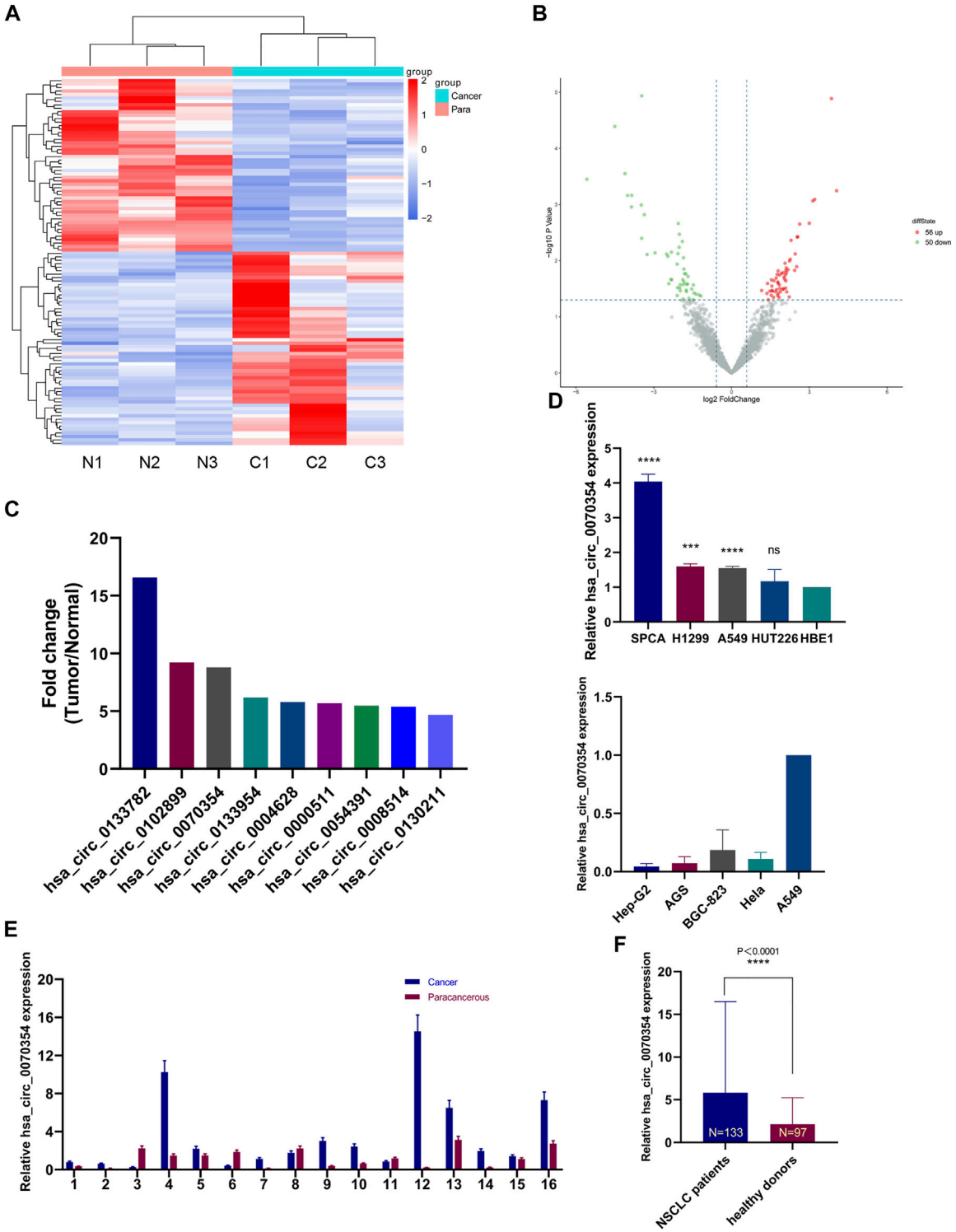

FIGURE 1 | circRNAs microarray sequencing of lung cancer tissues and adjacent tissues. **(A)** The clustered heatmap showed the differentially expressed circRNAs in 3 pairs of human NSCLC tissues and adjacent normal tissues. **(B)** The volcano plots of circRNAs expressions. The red and green strips indicate up-regulated and down-regulated circRNAs, respectively. **(C)** The nine predominantly up-regulated circRNAs between the two groups were shown (>2.0-fold change, $p < 0.05$). **(D–F)** The expression of hsa_circ_0070354 in NSCLC tissues, cells, and serums. Paracancerous tissues, normal lung epithelial cells (HBE1), and healthy donor sera served as controls.

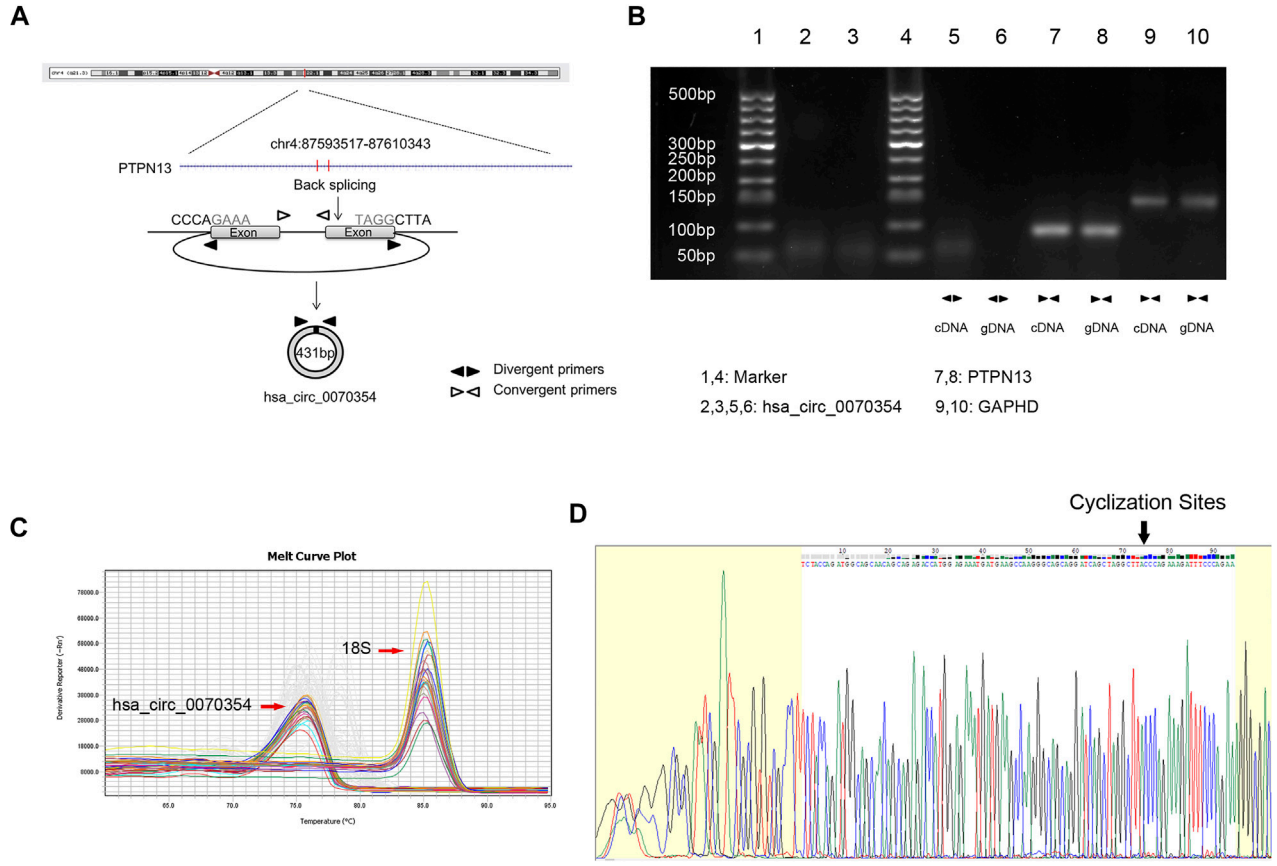

FIGURE 2 | Identification of the molecular properties of hsa_circ_0070354. **(A)** Genomic location and splicing mode of hsa_circ_0070354. **(B)** Agarose gel electrophoresis was performed to detect the existence of hsa_circ_0070354 and PTPN13 from cDNA and gDNA in A549 cells using the divergent and convergent primers, respectively. Glyceraldehyde 3-phosphate dehydrogenase (GAPDH) as the negative control. **(C)** The PCR melting curve of hsa_circ_0070354. **(D)** Identification of hsa_circ_0070354 qPCR amplification products and the back-splice junction site by Sanger sequencing.

(**Figure 3F**) may be involved in post-transcriptional gene regulation, which is a new potential way for the treatment of NSCLC.

Correlation Between High Expression of hsa_circ_0070354 and Clinicopathological Features

For the purpose of analyzing the expression and clinical value of hsa_circ_0070354, we evaluated the relationship between the expression of hsa_circ_0070354 and clinicopathological features. The results illustrated that the expression of hsa_circ_0070354 was positively correlated with differentiation degree ($p = 0.002$), tumor size ($p < 0.001$), lymph node metastasis ($p = 0.001$), distant metastasis ($p = 0.028$), TNM stage ($p < 0.001$), Ki-67 expression ($p = 0.005$), the value of CEA ($p = 0.038$) and Cyfra21-1 ($p = 0.007$) by Chi-square test, but not with other clinicopathological parameters such as age, sex, smoking status, pathological type and so forth (**Table 2**). Secondly, the increase of hsa_circ_0070354 expression in serum of NSCLC patients was significantly different from that of TNM and differentiation in different stages (**Figures 4A–C**), which was basically consistent with the results in **Table 2**. Unfortunately, the difference between the actual expression of hsa_circ_0070354 and the N stage decreased statistically. When the tumor load decreased after the operation, the expression of hsa_circ_0070354 was conspicuous lower than that before the operation (**Figure 4D**). Univariate and multivariate Cox proportional hazards regression models were performed to assess the impacts of the clinical variables on the OS of NSCLC patients (**Table 3**). The multivariate Cox analysis results indicated that the high expression of hsa_circ_0070354 was an independent predictor of poor prognosis in patients with NSCLC (HR = 5.087, 95% CI: 2.442–10.600, $p < 0.001$). Importantly, the Kaplan-Meier survival curve showed that the patients with hsa_circ_0070354 high expression had a significantly worse prognosis than those with hsa_circ_0070354 low ($p < 0.001$, log-rank test; **Figure 4E**). Through the qRT-PCR, we found that there was no statistically significant difference between the patients with gastric cancer ($N = 20$, $p = 0.1403$), hepatocellular carcinoma ($N = 20$, $p = 0.3788$), cervical cancer ($N = 20$, $p = 0.9301$), and healthy donors (**Figures 4F–H**). Given its overexpression in NSCLC, it would be appropriate to suggest that hsa_circ_0070354 was NSCLC-specific through serum

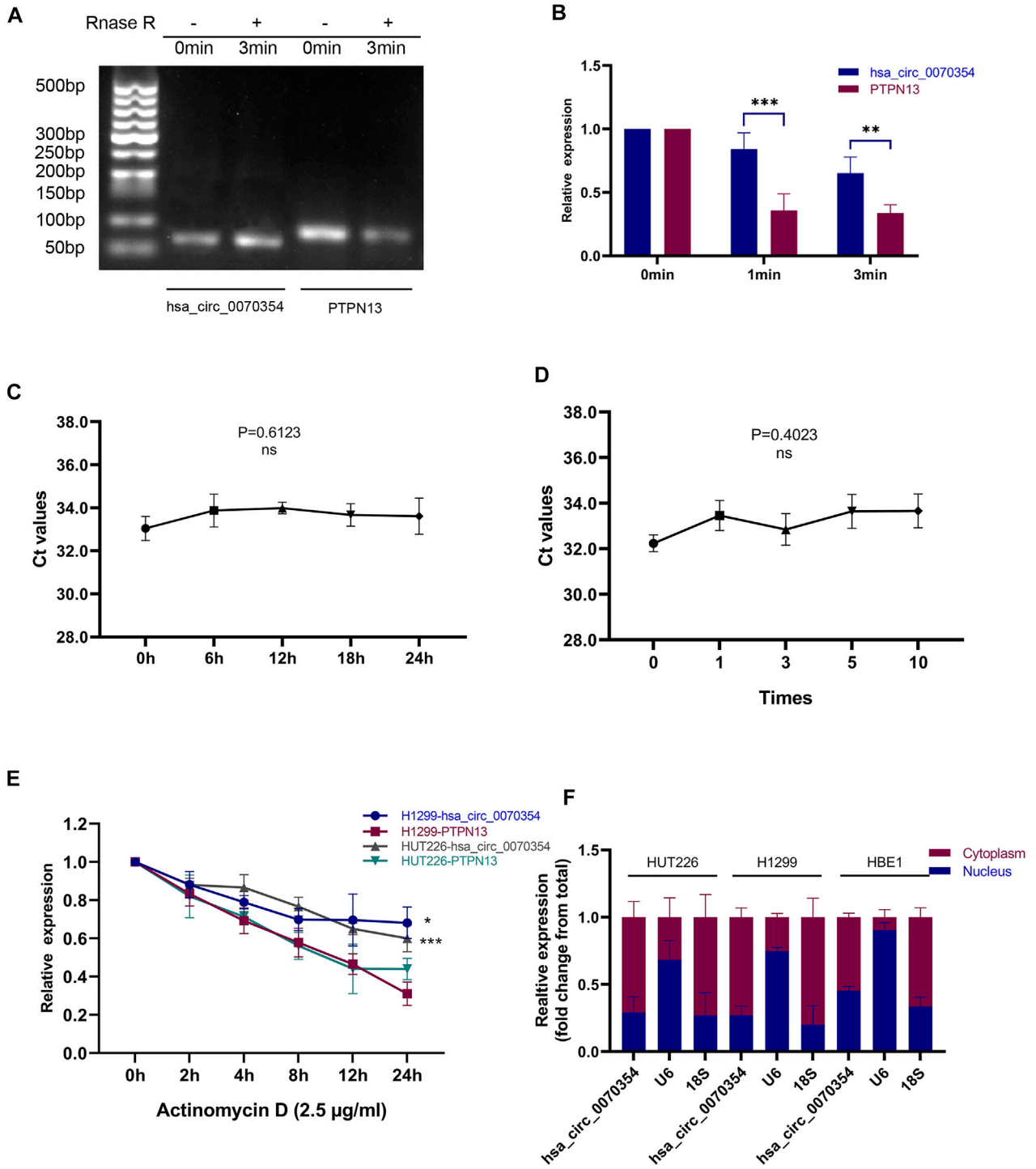

FIGURE 3 | Characteristics of hsa_circ_0070354 as a serum tumor biomarker. **(A,B)** qRT-PCR analyses were conducted to determine the abundances of hsa_circ_0070354 and linear PTPN13 mRNA in A549 cells after treatment with RNase R at the indicated time points. **(C,D)** The expressions of hsa_circ_0070354 in mix serum which placed at room temperature at the indicated time points **(C)** or frozen and thawed 0, 1, 3, 5, 10 times **(D)**. **(E)** The RNA expressions of hsa_circ_0070354 and linear PTPN13 mRNA in A549 cells were analyzed by qRT-PCR after treatment with 2.5 μg/ml actinomycin D for 2, 4, 8, 12, 24 h. **(F)** Nuclear-cytoplasmic RNA fractionation assay showed that hsa_circ_0070354 was mainly localized in the cytoplasm of A549 cells.18S was used as a cytoplasmic protein control while U6 was considered as a nuclear control. *$p < 0.05$, **$p < 0.01$, ***$p < 0.001$.

TABLE 2 | The association between hsa_circ_0070354 expression and clinicopathologic parameters in 133 NSCLC specimens.

Parameters	Total	hsa_circ_0070354 expression		*p* Value
		Low (≤median)	High (≥median)	
Age				0.850
< 55	39	20	19	
≥ 55	94	46	48	
Gender				1.000
Male	63	31	32	
Female	70	35	35	
Smoking status				0.581
Non-smoker	89	46	43	
Smoker	44	20	24	
Pathological Type				0.179
Suqamous	38	15	23	
Adenocarcinoma	95	51	44	
Differentiation grade				0.002**
Well-moderate	64	41	23	
Poor-undifferentiation	69	25	44	
Tumor size				0.000***
<5 cm	91	57	34	
≥5 cm	42	9	33	
Lymph node metastasis				0.001**
Negative	90	54	36	
Positive	43	12	31	
Distant metastasis				0.028*
Negative	99	55	44	
Positive	34	11	23	
TNM stage				0.000***
I–II	70	54	16	
III–IV	63	12	51	
Ki-67 expression				0.005**
< 30%	78	47	31	
≥ 30%	55	19	36	
Pleural invasion				0.186
Negative	93	50	43	
Positive	40	16	24	
Nerve invasion				0.244
Negative	131	64	67	
Positive	2	2	0	
Vascular invasion				0.682
Negative	102	52	50	
Positive	31	14	17	
Spread through Air Spaces				0.858
Negative	83	42	41	
Positive	50	24	26	
CEA				0.038*
Negative(<5 ng/ml)	66	39	27	
Positive(≥5 ng/ml)	67	27	40	
SCC				0.469
Negative(<1.5 μg/L)	86	45	41	
Positive(≥1.5 μg/L)	47	21	26	
Cyfra21-1				0.007**
Negative(<2.08 ng/ml)	94	54	40	
Positive(≥2.08 ng/ml)	39	12	27	
CA199				0.115
Negative(<37 U/ml)	126	65	61	
Positive(≥37 U/ml)	7	1	6	
Serum ferritsn				0.483
Negative(<204 μg/L)	78	41	37	
Positive(≥204 μg/L)	55	25	30	

*Statistical analyses were performed by the Pearson χ^2 test. *p < 0.05, **p < 0.01, ***p < 0.001 was considered significant.*

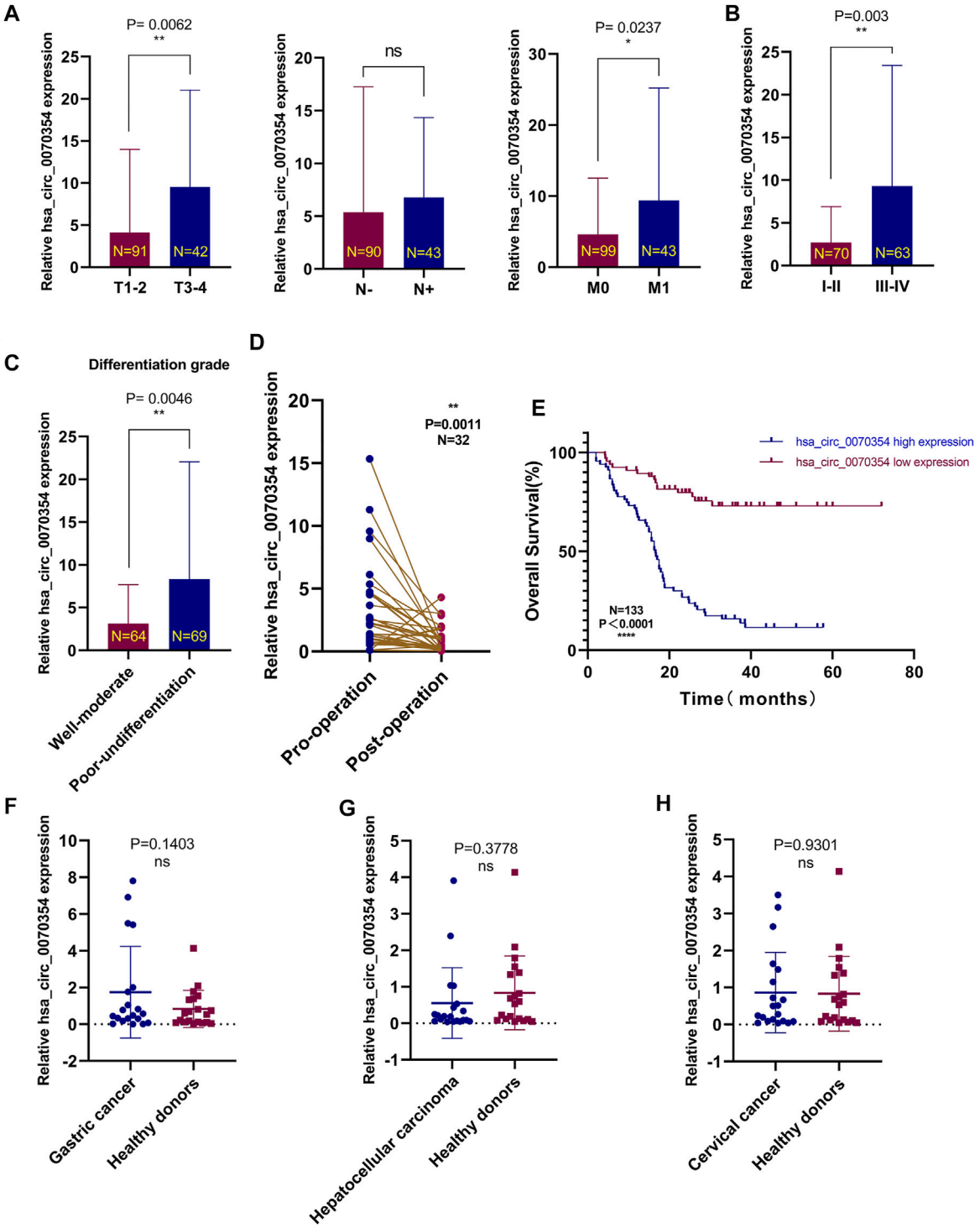

FIGURE 4 | High hsa_circ_0070354 expression in the NSCLC serums and prognostic significance. **(A)** The expression levels of hsa_circ_0070354 in serum specimens of NSCLC at different stages of tumor size, lymph node metastasis, and distant metastasis. **(B,C)** The expression levels of hsa_circ_0070354 in serum specimens of NSCLC at different stages of TNM stage **(B)** and differentiation degree **(C)**. **(D)** The expression of hsa_circ_0070354 in patients with NSCLC before and after operation. **(E)** Prognostic analysis of hsa_circ_0070354 expression in 133 NSCLC patients. **(F–H)** The expression level of hsa_circ_0070354 in 20 cases of patients with gastric cancer, hepatocellular carcinoma, cervical cancer, and healthy donors, respectively. $^{*}p < 0.05$, $^{**}p < 0.01$, $^{***}p < 0.001$, $^{****}p < 0.0001$, NS $p > 0.05$.

TABLE 3 | Univariate and multivariate Cox regression analysis of has_circ_0070354 and clinical variables predicting survival from 133 NSCLC specimens.

Parameter	Univariate analysis			Multivariate analysis		
	HR	95% CI	*p* Value	HR	95% CI	*p* Value
Age (<55 vs ≥55)	1.252	0.742–2.113	0.401	—	—	—
Gender (Male vs. Female)	0.800	0.505–1.268	0.343	—	—	—
Smoking status (Non-smoker vs. Smoker)	0.524	0.304–0.903	0.020*	1.571	0.720–3.426	0.256
Pathological Type (Suqamous vs. Adenocarcinoma)	1.423	0.835–2.423	0.194	-	—	—
Differentiation grade (Well-moderate vs. Poor-undifferentiation)	2.445	1.498–3.990	<0.001***	1.054	0.477–2.328	0.896
Tumor size (<5 cm vs. ≥5 cm)	2.526	1.592–4.007	<0.001***	1.336	0.717–2.487	0.361
Lymph node metastasis (Negative vs. Positive)	2.935	1.846–4.666	<0.001***	0.664	0.339–1.303	0.234
Distant metastasis (Negative vs. Positive)	2.611	1.622–4.201	<0.001***	1.575	0.578–4.287	0.347
TNM stage (I–II vs. III–IV)	5.666	3.309–9.700	<0.001***	0.317	0.112–0.892	0.029*
Ki-67 expression (<30% vs. ≥30%)	2.459	1.541–3.924	<0.001***	0.977	0.453–2.108	0.953
Pleural invasion (Negative vs. Positive)	1.335	0.827–2.156	0.237	—	—	—
Nerve invasion (Negative vs. Positive)	0.854	0.119–6.156	0.876	—	—	—
Vascular invasion (Negative vs. Positive)	2.526	1.549–4.118	<0.001***	0.462	0.140–1.519	0.203
Spread through Air Spaces (Negative vs. Positive)	1.752	1.103–2.781	0.017*	0.793	0.324–1.940	0.611
CEA (<5 ng/ml vs. ≥5 ng/ml)	2.147	1.328–3.473	0.002**	1.260	0.641–2.478	0.502
SCC (<1.5 μg/L vs. ≥1.5 μg/L)	1.070	0.665–1.721	0.781	—	—	—
Cyfra21-1 (<2.08 ng/ml vs. ≥2.08 ng/ml)	1.668	1.031–2.697	0.037*	1.103	0.592–2.057	0.757
CA199 (<37 U/ml vs. ≥37 U/ml)	2.435	1.050–5.646	0.038*	0.715	0.235–2.169	0.553
Serum ferritsn (<204 μg/L vs. ≥204 μg/L)	1.381	0.872–2.186	0.169	—	—	—
has_circ_0070354 (Negative vs. Positive)	5.641	3.222–9.876	<0.001***	5.087	2.442–10.600	<0.001***

*p < *0.05*, **p < *0.01*, ***p < *0.001 was considered significant.*

screening of other small tumor samples. In conclusion, hsa_circ_0070354 likely participates in the progression of NSCLC, and the high expression of hsa_circ_0070354 can be used as a poor prognostic factor.

Evaluation of the Diagnostic Accuracy of Serum hsa_circ_0070354 Independent and Combined Diagnostic Model in NSCLC

In previous essays, hsa_circ_0070354 has been confirmed to have the molecular properties of tumor biomarkers and was related to poor tumor prognosis. And yet, its efficacy in the diagnosis of NSCLC needs to be further explored. Compared with the mature lung cancer markers such as CEA and SCC, the diagnostic efficiency of hsa_circ_0070354 is the key factor in evaluating it as a novel diagnostic and predictive biomarker. The ROC curve showed that the AUC of hsa_circ_0070354 was 0.660 (95% CI: 0.589–0.730), which was higher than 0.631 of CEA (95% CI: 0.559–0.703), 0.638 of SCC (95% CI: 0.557–0.709), and 0.568 of Cyfra21-1 (95% CI: 0.495–0.642) (**Figure 5A**). **Figures 5B,C** demonstrated the AUC of hsa_circ_0070354 combined with the other three tumor markers, respectively. Compared with the single diagnosis, the AUC of the combined diagnosis of hsa_circ_0070354 and CEA increased to 0.691 (95% CI: 0.623–0.758), as well as the AUC of combined diagnosis with SCC and Cyfra21-1 increased to 0.711 (95% CI: 0.644–0.779) and 0.669 (95% CI: 0.599–0.733) respectively, which were both higher than the single diagnosis (**Figure 5B**). Similarly, the three-combination diagnosis of AUC was remarkably higher than that of a single diagnosis (**Figure 5C**). What is particularly striking is that in **Figure 5D**, the AUC of the combination of hsa_circ_0070354 and the other three mature tumor markers reached 0.730 (95% CI: 0.663–0.796), which was significantly higher than that of the single diagnosis of hsa_circ_0070354, and also higher than the combined diagnosis of the two or three. Subsequently, we also analyzed the sensitivity (SEN), specificity (SPE), overall accuracy (ACCU), positive predictive value (PPV), as well as negative predictive value (NPV) of single and combined diagnostic models (**Table 4**). According to our statistics, the SEN, SPE, ACCU, PPV and NPV of hsa_circ_0070354 were 52.63, 76.29, 62.61, 75.27 and 54.01%, respectively, while the combined diagnosis of the four tumor markers were 63.91, 84.54, 72.61, 85.00 and 63.08%. Therefore, hsa_circ_0070354 is superior to traditional tumor markers in diagnosis, and the combined diagnosis has higher sensitivity and specificity for the diagnosis of NSCLC.

Exploration of the Downstream and Function Prediction of hsa_circ_0070354

Previous studies have implied that circRNAs have four main functions: acting as a miRNA sponge, interacting with RNA binding proteins, regulating gene transcription, and encoding peptides. circRNAs contain a massive number of miRNA binding sites, which act as miRNA sponges and adjust gene expression indirectly (Huang et al., 2021a). Hsa_circ_0070354 was mainly located in the cytoplasm and may participate in the competitive inhibition of endogenous RNA as a microRNA sponge. Yet, its participation in the occurrence and development of NSCLC is a very complex process, which is worth our further in-depth study. Here, we analyze its potential function and regulation mechanism through the prediction of the relevant database. The Gene Ontology (GO) functional enrichment analysis of the target gene shows that 354 may play a potential role in RNA binding, splicing, and processing (**Figure 6A**). The enrichment analysis of the Kyoto Encyclopedia of Genes and Genomes

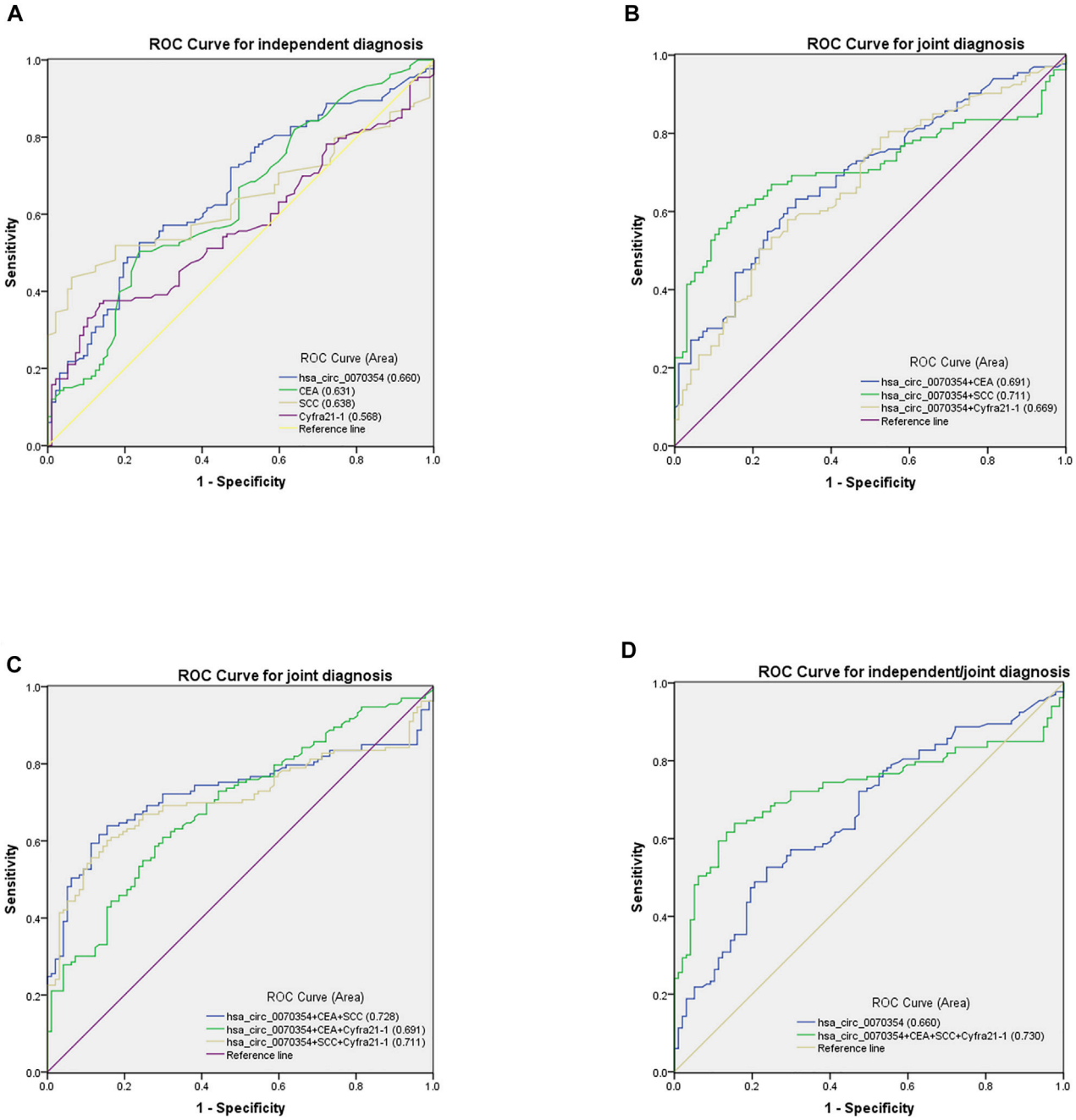

FIGURE 5 | ROC curve evaluated the diagnostic value of hsa_circ_0070354 in NSCLC. **(A)** ROC curves for diagnosis using serum hsa_circ_0070354, CEA, SCC, and Cyfra21-1 between NSCLC patients (*N* = 133) and healthy controls (*N* = 97) independently. **(B–D)** ROC curves for combined diagnostic efficacy of serum hsa_circ_0070354, CEA, SCC, and Cyfra21-1 in distinguishing NSCLC patients with healthy donors.

(KEGG) signal pathway showed that hsa_circ_0070354 was significantly enriched in a variety of tumors, and the ErbB and MAPK signal pathway was also the focus of our subsequent attention (**Figure 6B**). The Venny diagram shows our prediction of downstream miRNAs in four common databases. The three miRNAs obtained by repeated intersection are miR-1257, miR-1272, and miR-1305 (**Figure 6C**). According to the results of databases and bioinformatics analysis, we predict the possible circRNA-miRNA-mRNA axis. As shown in **Figures 5A,D** total of 7 miRNAs (3 above, also including miR-922, miR-4322, miR-4632-5p, and miR-6879-5p) and their corresponding mRNAs are presented, which may provide a research direction for the progress of NSCLC regulation by hsa_circ_0070354. In any case, based on the above results, more experimental work is needed to confirm the regulation mechanism of hsa_circ_0070354.

TABLE 4 | Use the expression levels of has_circ_0070354, CEA, SCC and Cyfra21-1 to distinguish NSCLC patients from healthy donors.

	SEN (%)	SPE (%)	ACCU (%)	PPV (%)	NPV (%)
has_circ_0070354	52.63 (70/133)	76.29 (74/97)	62.61 (144/230)	75.27 (70/93)	54.01 (74/137)
CEA	50.38 (67/133)	77.32 (75/97)	61.74 (142/230)	75.28 (67/89)	53.19 (75/141)
SCC	35.34 (47/133)	94.85 (92/97)	60.43 (139/230)	90.38 (47/52)	51.69 (92/178)
Cyfra21-1	29.32 (39/133)	90.72 (88/97)	55.22 (127/230)	81.25 (39/48)	48.35 (88/182)
has_circ_0070354 + CEA	63.16 (84/133)	69.07 (67/97)	65.65 (151/230)	73.68 (84/114)	57.76 (67/116)
has_circ_0070354 + SCC	60.15 (80/133)	74.23 (72/97)	66.09 (152/230)	84.21 (80/95)	57.60 (72/125)
has_circ_0070354 + Cyfra21-1	57.89 (77/133)	71.13 (69/97)	63.48 (146/230)	73.33 (77/105)	55.20 (69/125)
has_circ_0070354 + CEA + SCC	63.91 (85/133)	84.54 (82/97)	72.61 (167/230)	85.00 (85/100)	63.08 (82/130)
has_circ_0070354 + CEA + Cyfra21-1	60.90 (81/133)	70.10 (68/97)	64.78 (149/230)	73.64 (81/110)	56.67 (68/120)
has_circ_0070354 + SCC + Cyfra21-1	60.15 (80/133)	84.54 (82/97)	70.43 (162/230)	84.21 (80/95)	60.74 (82/135)
has_circ_0070354 + CEA + SCC + Cyfra21-1	63.91 (85/133)	84.54 (82/97)	72.61 (167/230)	85.00 (85/100)	63.08 (82/130)

SEN, sensitivity; SPE, specificity; ACCU, overall accuracy; PPV, positive predictive value; NPV, negative predictive value.

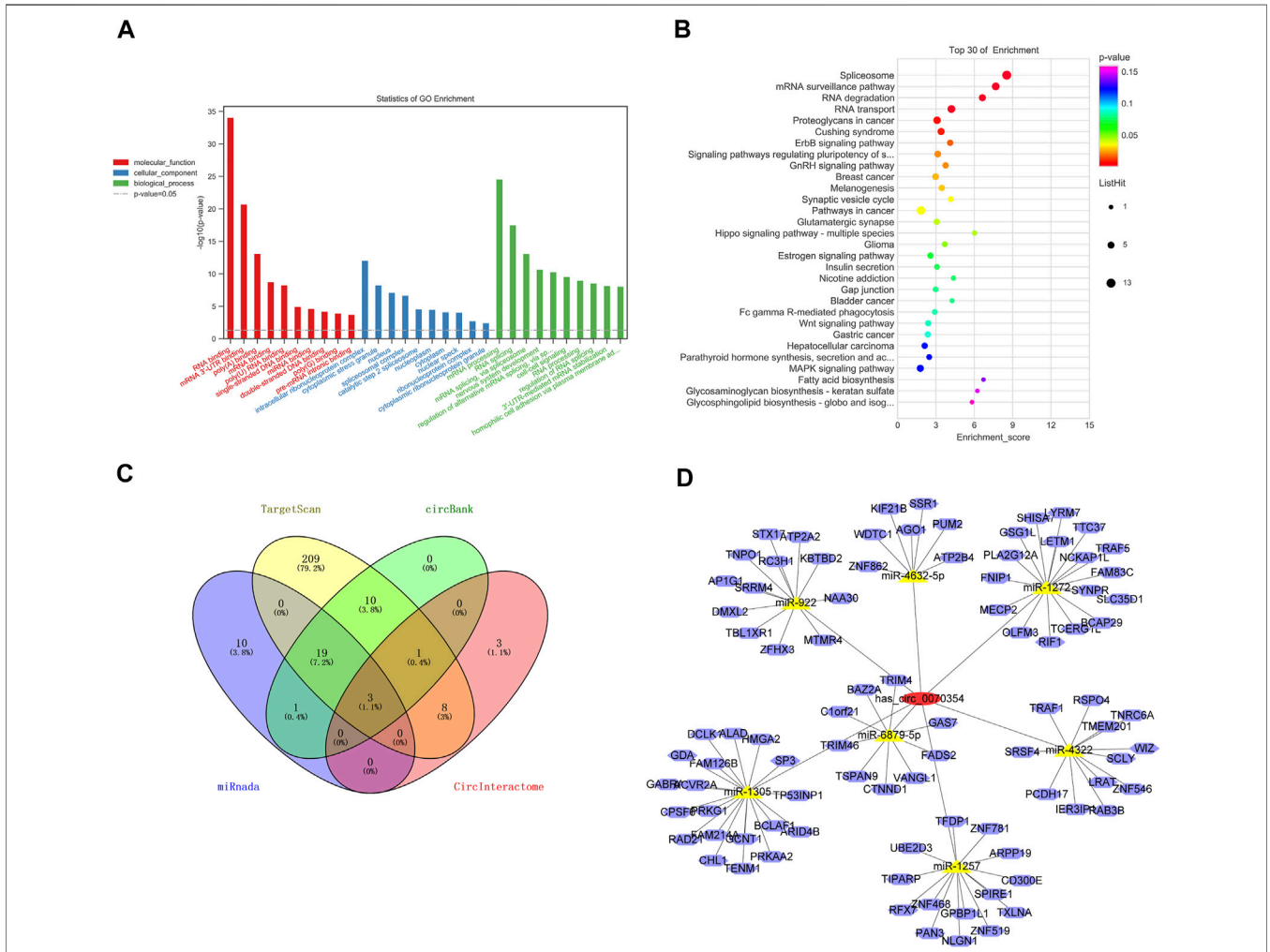

FIGURE 6 | Exploration of the downstream regulatory network of hsa_circ_0070354 in NSCLC. **(A)** GO analysis of the hsa_circ_0070354 target genes enriched in molecular function (red), cellular component (blue), and biological process (green). **(B)** Bubble chart of KEGG analysis of candidate hsa_circ_0070354 different target genes expressed of enriched pathways. **(C)** Venny diagram evaluated the overlapped genes between TargetScan, circBank, miRandan, and CircInteractome predictions. **(D)** Prediction of the circRNA-miRNA-mRNA network map of hsa_circ_0070354 by Cytoscape analysis. The red oval represents hsa_circ_0070354, and the yellow triangle represents seven miRNAs that could interact with hsa_circ_0070354, while the purple oval represents the target mRNA of the corresponding miRNA.

DISCUSSION

Generally, the incidence and malignancy of NSCLC are high, and the 5-year survival rate is lower than other malignant tumors, which is mainly due to the enormous heterogeneity of NSCLC and the insufficient understanding of the biological of NSCLC, leading to the lack of effective biomarkers for diagnosis and targeted therapies (Fu et al., 2020). Besides, the survival of NSCLC is closely related to staging. Studies have shown that as patients develop from stage I to IV, the 5-year survival rate of NSCLC decreases from 82 to 6% (Goldstraw et al., 2016). Most of the patients have been in the advanced or locally advanced stage at the time of diagnosis and have missed the best opportunity for surgical treatment, mainly conservative palliative treatment. Despite that, the research on targeted therapy and immunotherapy for advanced patients is advancing by leaps and bounds. The lack of targets and low mutation rate is still the treatment dilemma. The high cost of immunotherapy and unpredictable side effects also deter many patients. Even so, the increased drug resistance of targeted therapy and immunotherapy is also the limitation of treatment, and tumors develop irreversible outcomes (Hong et al., 2020). For these reasons, early detection and improving the accuracy of diagnosis are conducive to improve the prognosis and survival rate of patients, which not only depends on the popularization of physical examination and computerized tomography (CT) but also requires the exploration and research of humoral tumor biomarkers which are non-radiation, dynamic monitoring, simple and easy to popularize. It is an urgent issue to identify new specific biomarkers for NSCLC to aid in diagnosis and clinical decision.

CircRNA was first observed in the 1970s (Hsu and Coca-Prados, 1979), but its biological function was considered unclear for a long time (Cocquerelle et al., 1993; Zaphiropoulos, 1997). Until 2012, with the advancement of high-throughput sequencing and bioinformatics analysis, the distribution and function of circRNAs in different cells and tissues were progressively discovered, not just an idle by-product of mRNA splicing (Djebali et al., 2012; Salzman et al., 2012). Since then, the researchers focused on circRNAs have shifted attention to clarifying their associations with human diseases, including cancers. Some kinds of literature have reported that the abnormal expressions of circRNAs were associated with the clinical characteristics of tumors and might become biomarkers of NSCLC (Kristensen et al., 2018; Qu et al., 2018; Di et al., 2019). In this study, we determined for the first time that hsa_circ_0070354 was higher in tumor tissues, cells, and serum than in adjacent normal tissues, cell lines, or healthy human sera. At the same time, we found that the high expression of hsa_circ_0070354 was significantly positively correlated with the late TNM stage and poor differentiation of NSCLC, indicating a poor prognosis and survival time. Combined with the biological characteristics of sensitivity, stability, and ease to be detected in body fluids, hsa_circ_0070354 would be a promising biomarker of NSCLC and has a bright prospect for early diagnosis and treatment of lung cancer in the future. The relevant information at the beginning of our research came from some circRNA databases, such as circBank, circBase and circular RNA Interactome. Through circBase, we found that hsa_circ_0070354 studies included Rybak2015 and Salzman2013. Except for A549 cell line, which was consistent with our experimental results, it was only expressed in the brain parenchyma, such as the cerebellum, occipital_lobe and frontal_cortex, but no evidence was found in other cancers. In the exosomes database, such as ExoRbase, we have not queried the relevant included information. The existing information supports the specific expression of hsa_circ_0070354 in NSCLCs. In addition, the transition from a single biomarker to the joint diagnosis of multiple biomarkers is the development direction of tumor markers. Our results revealed that the combined diagnosis of multiple tumor markers has significantly higher sensitivity and specificity than a single biomarker. The combination of hsa_circ_0070354 with other tumor markers is expected to improve further the accuracy of hsa_circ_0070354 in the diagnosis, prognosis, and prediction of NSCLC. Generally, circRNAs are formed by reverse splicing of pre-mRNAs through several acknowledged mechanisms, namely lariat-driven circularization (Eger et al., 2018), intron pairing-driven circularization (Liu et al., 2019b), RBP-mediated circularization (Conn et al., 2015), and intronic circularization (Zhang et al., 2013). The relationship between host gene and circRNA is complex and diverse. However, the expression levels of circRNAs and the abundance of mRNA produced by the parental gene were not significantly related (Barrett and Salzman, 2016; Chen et al., 2019). By querying TCGA resource, it can be easily noted that the host gene of hsa_circ_0070354 (PTPN13) show negative association with cancer prognosis (HR<1), which is contrary to hsa_circ_0070354 (HR>1). Due to the limitations of database speculation and the incidence characteristics of NSCLC in Asia, the expression of PTPN13 in Chinese population needs further large sample study. This different expression trend inspired us to explore the further regulatory axis between hsa_circ_0070354 and its host gene PTPN13 in depth.

In the study of the mechanisms of circRNAs, the ceRNA hypothesis proposes that RNA transcripts share the same miRNA response elements, leading to the competition with miRNA combinations and then regulating the expressions (Salmena et al., 2011). In our study, we combined the results of bioinformatics analysis and sequencing to screen the miRNA and mRNA binding to hsa_circ_0070354. Unfortunately, the high expression of hsa_circ_0070354 in the biological, behavioral regulation of NSCLC remains unclear. The analysis between hsa_circ_0070354 and clinicopathological features suggested it was related to tumor size and metastasis, corresponding to biological behaviors such as cell proliferation and invasion, which provides a direction for further exploration. Whether the hsa_circ_0070354-miRNA-mRNA axis is involved in regulating NSCLC cell proliferation, migration and invasion will be the direction of our next exploration and study. Although no study has confirmed that circRNA would be a new therapeutic target for tumors, the effects of circRNAs on the proliferation,

metastasis, and drug resistance of lung cancer indicate that they may become a target of therapeutic, which is worthy of our profound understanding. CircRNAs are expected to make significant contributions to cancer prevention, diagnosis, and treatment in the future.

DATA AVAILABILITY STATEMENT

The data presented in the study are deposited in the NCBI SRA repository, accession number PRJNA 781220.

ETHICS STATEMENT

The studies involving human participants were reviewed and approved by the Ethics Committee of the Affiliated Hospital of Nantong University. The patients/participants provided their written informed consent to participate in this study.

AUTHOR CONTRIBUTIONS

YL, CC and KH control over the quality inspection of tissue samples and collect tissues. All authors have read and approved the final submitted version.

FUNDING

This study was supported by grants from the National Natural Science Foundation of China (No. 81600158, No. 81871720, 82072363).

SUPPLEMENTARY MATERIAL

The Supplementary Material for this article can be found online at: https://www.frontiersin.org/articles/10.3389/fgene.2021.796776/full#supplementary-material

REFERENCES

Barrett, S. P., and Salzman, J. (2016). Circular RNAs: Analysis, Expression and Potential Functions. *Development* 143 (11), 1838–1847. doi:10.1242/dev.128074

Chaft, J. E., Rimner, A., Weder, W., Azzoli, C. G., Kris, M. G., and Cascone, T. (2021). Evolution of Systemic Therapy for Stages I-III Non-metastatic Non-small-cell Lung Cancer. *Nat. Rev. Clin. Oncol.* 18 (9), 547–557. doi:10.1038/s41571-021-00501-4

Chen, S., Huang, V., Xu, X., Livingstone, J., Soares, F., Jeon, J., et al. (2019). Widespread and Functional RNA Circularization in Localized Prostate Cancer. *Cell* 176 (4), 831–843. doi:10.1016/j.cell.2019.01.025

Cocquerelle, C., Mascrez, B., Hétuin, D., and Bailleul, B. (1993). Mis-splicing Yields Circular RNA Molecules. *FASEB J.* 7 (1), 155–160. doi:10.1096/fasebj.7.1.7678559

Conn, S. J., Pillman, K. A., Toubia, J., Conn, V. M., Salmanidis, M., Phillips, C. A., et al. (2015). The RNA Binding Protein Quaking Regulates Formation of circRNAs. *Cell* 160 (6), 1125–1134. doi:10.1016/j.cell.2015.02.014

Di, X., Jin, X., Li, R., Zhao, M., and Wang, K. (2019). CircRNAs and Lung Cancer: Biomarkers and Master Regulators. *Life Sci.* 220, 177–185. doi:10.1016/j.lfs.2019.01.055

Djebali, S., Davis, C. A., Merkel, A., Dobin, A., Lassmann, T., Mortazavi, A., et al. (2012). Landscape of Transcription in Human Cells. *Nature* 489 (7414), 101–108. doi:10.1038/nature11233

Eger, N., Schoppe, L., Schuster, S., Laufs, U., and Boeckel, J.-N. (2018). Circular RNA Splicing. *Adv. Exp. Med. Biol.* 1087, 41–52. doi:10.1007/978-981-13-1426-1_4

ENCODE Project Consortium (2012). An Integrated Encyclopedia of DNA Elements in the Human Genome. *Nature* 489 (7414), 57–74. doi:10.1038/nature11247

Ferlay, J., Shin, H.-R., Bray, F., Forman, D., Mathers, C., and Parkin, D. M. (2010). Estimates of Worldwide burden of Cancer in 2008: GLOBOCAN 2008. *Int. J. Cancer* 127 (12), 2893–2917. doi:10.1002/ijc.25516

Fu, Y., Huang, L., Tang, H., and Huang, R. (2020). Hsa_circRNA_012515 Is Highly Expressed in NSCLC Patients and Affects its Prognosis. *Cancer Manag. Res.* 12, 1877–1886. doi:10.2147/CMAR.S245525

Glažar, P., Papavasileiou, P., and Rajewsky, N. (2014). circBase: a Database for Circular RNAs. *RNA* 20 (11), 1666–1670. doi:10.1261/rna.043687.113

Goldstraw, P., Chansky, K., Crowley, J., Rami-Porta, R., Asamura, H., Eberhardt, W. E., et al. (2016). The IASLC Lung Cancer Staging Project: Proposals for Revision of the TNM Stage Groupings in the Forthcoming (Eighth) Edition of the TNM Classification for Lung Cancer. *J. Thorac. Oncol.* 11 (1), 39–51. doi:10.1016/j.jtho.2015.09.009

Hang, D., Zhou, J., Qin, N., Zhou, W., Ma, H., Jin, G., et al. (2018). A Novel Plasma Circular RNA circFARSA Is a Potential Biomarker for Non-small Cell Lung Cancer. *Cancer Med.* 7 (6), 2783–2791. doi:10.1002/cam4.1514

Hansen, T. B., Jensen, T. I., Clausen, B. H., Bramsen, J. B., Finsen, B., Damgaard, C. K., et al. (2013). Natural RNA Circles Function as Efficient microRNA Sponges. *Nature* 495 (7441), 384–388. doi:10.1038/nature11993

Hong, W., Xue, M., Jiang, J., Zhang, Y., and Gao, X. (2020). Circular RNA Circ-CPA4/Let-7 miRNA/PD-L1 axis Regulates Cell Growth, Stemness, Drug Resistance and Immune Evasion in Non-small Cell Lung Cancer (NSCLC). *J. Exp. Clin. Cancer Res.* 39 (1), 149. doi:10.1186/s13046-020-01648-1

Hsu, M.-T., and Coca-Prados, M. (1979). Electron Microscopic Evidence for the Circular Form of RNA in the Cytoplasm of Eukaryotic Cells. *Nature* 280 (5720), 339–340. doi:10.1038/280339a0

Huang, L., Rong, Y., Tang, X., Yi, K., Wu, J., and Wang, F. (2021). Circular RNAs Are Promising Biomarkers in Liquid Biopsy for the Diagnosis of Non-small Cell Lung Cancer. *Front. Mol. Biosci.* 8, 625722. doi:10.3389/fmolb.2021.625722

Huang, Y., Zhang, H., Gu, X., Qin, S., Zheng, M., Shi, X., et al. (2021). Elucidating the Role of Serum tRF-31-U5YKFN8DYDZDD as a Novel Diagnostic Biomarker in Gastric Cancer (GC). *Front. Oncol.* 11, 723753. doi:10.3389/fonc.2021.723753

Jeck, W. R., and Sharpless, N. E. (2014). Detecting and Characterizing Circular RNAs. *Nat. Biotechnol.* 32 (5), 453–461. doi:10.1038/nbt.2890

Jeck, W. R., Sorrentino, J. A., Wang, K., Slevin, M. K., Burd, C. E., Liu, J., et al. (2013). Circular RNAs Are Abundant, Conserved, and Associated with ALU Repeats. *RNA* 19 (2), 141–157. doi:10.1261/rna.035667.112

Kamel, L. M., Atef, D. M., Mackawy, A. M. H., Shalaby, S. M., and Abdelraheim, N. (2019). Circulating Long Non-coding RNA GAS5 and SOX2OT as Potential Biomarkers for Diagnosis and Prognosis of Non-small Cell Lung Cancer. *Biotechnol. Appl. Biochem.* 66 (4), 634–642. doi:10.1002/bab.1764

Kristensen, L. S., Hansen, T. B., Venø, M. T., and Kjems, J. (2018). Circular RNAs in Cancer: Opportunities and Challenges in the Field. *Oncogene* 37 (5), 555–565. doi:10.1038/onc.2017.361

Liu, Y.-T., Han, X.-H., Xing, P.-Y., Hu, X.-S., Hao, X.-Z., Wang, Y., et al. (2019). Circular RNA Profiling Identified as a Biomarker for Predicting the Efficacy of Gefitinib Therapy for Non-small Cell Lung Cancer. *J. Thorac. Dis.* 11 (5), 1779–1787. doi:10.21037/jtd.2019.05.22

Liu, K. S., Pan, F., Mao, X. D., Liu, C., and Chen, Y. J. (2019). Biological Functions of Circular RNAs and Their Roles in Occurrence of Reproduction and Gynecological Diseases. *Am. J. Transl. Res.* 11 (1), 1–15.

Liu, Z. H., Yang, S. Z., Chen, X. T., Shao, M. R., Dong, S. Y., Zhou, S. Y., et al. (2020). Correlations of Hsa_circ_0046264 Expression with Onset, Pathological Stage and Chemotherapy Resistance of Lung Cancer. *Eur. Rev. Med. Pharmacol. Sci.* 24 (18), 9511–9521. doi:10.26355/eurrev_202009_23036

Lu, H., Xie, X., Chen, Q., Cai, S., Liu, S., Bao, C., et al. (2021). Clinical Significance of circPVT1 in Patients with Non-small Cell Lung Cancer Who Received Cisplatin Combined with Gemcitabine Chemotherapy. *Tumori* 107 (3), 030089162094194. doi:10.1177/0300891620941940

Ma, L.-R., Li, J.-X., Tang, L., Li, R.-Z., Yang, J.-S., Sun, A., et al. (2021). Immune Checkpoints and Immunotherapy in Non-Small Cell Lung Cancer: Novel Study Progression, Challenges and Solutions (Review). *Oncol. Lett.* 22 (5), 787. doi:10.3892/ol.2021.13048

Memczak, S., Jens, M., Elefsinioti, A., Torti, F., Krueger, J., Rybak, A., et al. (2013). Circular RNAs Are a Large Class of Animal RNAs with Regulatory Potency. *Nature* 495 (7441), 333–338. doi:10.1038/nature11928

Nigro, J. M., Cho, K. R., Fearon, E. R., Kern, S. E., Ruppert, J. M., Oliner, J. D., et al. (1991). Scrambled Exons. *Cell* 64 (3), 607–613. doi:10.1016/0092-8674(91)90244-s

Pei, X., Chen, S.-W., Long, X., Zhu, S.-Q., Qiu, B.-Q., Lin, K., et al. (2020). circMET Promotes NSCLC Cell Proliferation, Metastasis, and Immune Evasion by Regulating the miR-145-5p/CXCL3 axis. *Aging* 12 (13), 13038–13058. doi:10.18632/aging.103392

Peng, L., Yuan, X. Q., and Li, G. C. (2015). The Emerging Landscape of Circular RNA ciRS-7 in Cancer (Review). *Oncol. Rep.* 33 (6), 2669–2674. doi:10.3892/or.2015.3904

Qian, H., Zhang, Y., Xu, J., He, J., and Gao, W. (2021). Progress and Application of Circulating Tumor Cells in Non-small Cell Lung Cancer. *Mol. Ther. Oncol.* 22, 72–84. doi:10.1016/j.omto.2021.05.005

Qu, S., Liu, Z., Yang, X., Zhou, J., Yu, H., Zhang, R., et al. (2018). The Emerging Functions and Roles of Circular RNAs in Cancer. *Cancer Lett.* 414, 301–309. doi:10.1016/j.canlet.2017.11.022

Rong, D., Sun, H., Li, Z., Liu, S., Dong, C., Fu, K., et al. (2017). An Emerging Function of circRNA-miRNAs-mRNA axis in Human Diseases. *Oncotarget* 8 (42), 73271–73281. doi:10.18632/oncotarget.19154

Rybak-Wolf, A., Stottmeister, C., Glažar, P., Jens, M., Pino, N., Giusti, S., et al. (2015). Circular RNAs in the Mammalian Brain Are Highly Abundant, Conserved, and Dynamically Expressed. *Mol. Cel* 58 (5), 870–885. doi:10.1016/j.molcel.2015.03.027

Salmena, L., Poliseno, L., Tay, Y., Kats, L., and Pandolfi, P. P. (2011). A ceRNA Hypothesis: the Rosetta Stone of a Hidden RNA Language? *Cell* 146 (3), 353–358. doi:10.1016/j.cell.2011.07.014

Salzman, J., Gawad, C., Wang, P. L., Lacayo, N., and Brown, P. O. (2012). Circular RNAs Are the Predominant Transcript Isoform from Hundreds of Human Genes in Diverse Cell Types. *PLoS One* 7 (2), e30733. doi:10.1371/journal.pone.0030733

Wan, L., Zhang, L., Fan, K., Cheng, Z.-X., Sun, Q.-C., and Wang, J.-J. (2016). Circular RNA-ITCH Suppresses Lung Cancer Proliferation via Inhibiting the Wnt/β-Catenin Pathway. *Biomed. Res. Int.* 2016, 1–11. doi:10.1155/2016/1579490

Wang, L., Tong, X., Zhou, Z., Wang, S., Lei, Z., Zhang, T., et al. (2018). Circular RNA Hsa_circ_0008305 (circPTK2) Inhibits TGF-β-Induced Epithelial-Mesenchymal Transition and Metastasis by Controlling TIF1γ in Non-small Cell Lung Cancer. *Mol. Cancer* 17 (1), 140. doi:10.1186/s12943-018-0889-7

Xian, J., Su, W., Liu, L., Rao, B., Lin, M., Feng, Y., et al. (2020). Identification of Three Circular RNA Cargoes in Serum Exosomes as Diagnostic Biomarkers of Non-small-cell Lung Cancer in the Chinese Population. *J. Mol. Diagn.* 22 (8), 1096–1108. doi:10.1016/j.jmoldx.2020.05.011

Xu, Y., Kong, S., Qin, X., and Ju, S. (2020). Comprehensive Assessment of Plasma Circ_0004771 as a Novel Diagnostic and Dynamic Monitoring Biomarker in Gastric Cancer. *Onco. Targets Ther.* 13, 10063–10074. doi:10.2147/OTT.S263536

Ye, R., Tang, R., Gan, S., Li, R., Cheng, Y., Guo, L., et al. (2020). New Insights into Long Non-coding RNAs in Non-small Cell Lung Cancer. *Biomed. Pharmacother.* 131, 110775. doi:10.1016/j.biopha.2020.110775

Yu, C., Cheng, Z., Cui, S., Mao, X., Li, B., Fu, Y., et al. (2020). circFOXM1 Promotes Proliferation of Non-small Cell Lung Carcinoma Cells by Acting as a ceRNA to Upregulate FAM83D. *J. Exp. Clin. Cancer Res.* 39 (1), 55. doi:10.1186/s13046-020-01555-5

Zaphiropoulos, P. G. (1997). Exon Skipping and Circular RNA Formation in Transcripts of the Human Cytochrome P-450 2C18 Gene in Epidermis and of the Rat Androgen Binding Protein Gene in Testis. *Mol. Cel Biol.* 17 (6), 2985–2993. doi:10.1128/MCB.17.6.2985

Zhang, Y., Zhang, X.-O., Chen, T., Xiang, J.-F., Yin, Q.-F., Xing, Y.-H., et al. (2013). Circular Intronic Long Noncoding RNAs. *Mol. Cel* 51 (6), 792–806. doi:10.1016/j.molcel.2013.08.017

Zhang, P.-F., Pei, X., Li, K.-S., Jin, L.-N., Wang, F., Wu, J., et al. (2019). Circular RNA circFGFR1 Promotes Progression and Anti-PD-1 Resistance by Sponging miR-381-3p in Non-small Cell Lung Cancer Cells. *Mol. Cancer* 18 (1), 179. doi:10.1186/s12943-019-1111-2

Zhang, J., Mao, W., Chen, Z., Gu, H., and Lian, C. (2020). Clinical Significance of Has_circ_0060937 in Bone Metastasis of NSCLC. *Int. J. Gen. Med.* 13, 1115–1121. doi:10.2147/IJGM.S279023

Zhao, J., Lee, E. E., Kim, J., Yang, R., Chamseddin, B., Ni, C., et al. (2019). Transforming Activity of an Oncoprotein-Encoding Circular RNA from Human Papillomavirus. *Nat. Commun.* 10 (1), 2300. doi:10.1038/s41467-019-10246-5

Zheng, Y.-W., Li, R.-M., Zhang, X.-W., and Ren, X.-B. (2013). Current Adoptive Immunotherapy in Non-small Cell Lung Cancer and Potential Influence of Therapy Outcome. *Cancer Invest.* 31 (3), 197–205. doi:10.3109/07357907.2013.775294

Zhou, X., Liu, H. Y., Wang, W. Y., Zhao, H., and Wang, T. (2018). Hsa_circ_0102533 Serves as a Blood-Based Biomarker for Non-small-cell Lung Cancer Diagnosis and Regulates Apoptosis *In Vitro*. *Int. J. Clin. Exp. Pathol.* 11 (9), 4395–4404.

Zhu, X., Wang, X., Wei, S., Chen, Y., Chen, Y., Fan, X., et al. (2017). hsa_circ_0013958: a Circular RNA and Potential Novel Biomarker for Lung Adenocarcinoma. *FEBS J.* 284 (14), 2170–2182. doi:10.1111/febs.14132

Zukotynski, K. A., Hasan, O. K., Lubanovic, M., and Gerbaudo, V. H. (2021). Update on Molecular Imaging and Precision Medicine in Lung Cancer. *Radiol. Clin. North Am.* 59 (5), 693–703. doi:10.1016/j.rcl.2021.05.002

Conflict of Interest: The authors declare that the research was conducted in the absence of any commercial or financial relationships that could be construed as a potential conflict of interest.

frontiers in Genetics

ORIGINAL RESEARCH
published: 23 February 2022
doi: 10.3389/fgene.2022.784089

CircATRNL1 and circZNF608 Inhibit Ovarian Cancer by Sequestering miR-152-5p and Encoding Protein

Mengmeng Lyu[1†], Xiujuan Li[2†], Yang Shen[1], Jin Lu[1], Lihua Zhang[1], Shanliang Zhong[3] and Jinhua Wang[1]**

[1]*Department of Gynecologic Oncology, The Affiliated Cancer Hospital of Nanjing Medical University and Jiangsu Cancer Hospital and Jiangsu Institute of Cancer Research, Nanjing, China,* [2]*Department of General Surgery, The Affiliated Cancer Hospital of Nanjing Medical University and Jiangsu Cancer Hospital and Jiangsu Institute of Cancer Research, Nanjing, China,* [3]*Center of Clinical Laboratory Science, The Affiliated Cancer Hospital of Nanjing Medical University and Jiangsu Cancer Hospital and Jiangsu Institute of Cancer Research, Nanjing, China*

Background: CircRNAs have been found to be involved in the pathogenesis of various diseases. We aimed to explore the roles of circRNAs in ovarian cancer.

Methods: The expression levels of circRNAs in ovarian cancer and normal ovarian tissues were analyzed using RNA sequencing. Fluorescent *in situ* hybridization (FISH), proliferation assays and transwell assays were used to assess the effects of circRNAs on ovarian cancer.

Results: CircATRNL1 and circZNF608 were downregulated in 20 ovarian cancer tissues compared to normal tissues. CircATRNL1 and circZNF608 are mainly located in the cytoplasm of ovarian cancer cells, and circATRNL1 is a highly conserved circRNA. The overexpression of circATRNL1 and circZNF608 inhibits the proliferation and invasion of ovarian cancer cells. We predicted miRNA–circRNA interactions for circZNF608 and circATRNL1 and obtained 63 interactions. However, a luciferase reporter assay showed that only miR-152-5p was sequestered by circZNF608. Bioinformatics analysis and experiments indicated that circATRNL1 contains an internal ribosome entry site and an open reading frame encoding a 131 aa protein.

Conclusion: In conclusion, circATRNL1 and circZNF608 are two downregulated circRNAs in ovarian cancer and work as tumor suppressors. CircZNF608 may exert antitumor activity in ovarian cancer by binding miR-152-5p, and circATRNL1 may encode a 131 aa protein.

Keywords: circular RNA, protein, ovarian cancer, translation, peptide

Edited by:
Deepanjan Paul,
Children's Hospital of Philadelphia, United States

Reviewed by:
Nana Jin,
Codex Genetics Limited, Hong Kong SAR, China
Disha Sharma,
Stanford Healthcare, United States

****Correspondence:***
Shanliang Zhong
slzhong@njmu.edu.cn
Jinhua Wang
wangjinhua588@163.com

[†]These authors have contributed equally to this work

Specialty section:
This article was submitted to RNA, a section of the journal Frontiers in Genetics

Received: *27 September 2021*
Accepted: *31 January 2022*
Published: *23 February 2022*

Citation:
Lyu M, Li X, Shen Y, Lu J, Zhang L, Zhong S and Wang J (2022) CircATRNL1 and circZNF608 Inhibit Ovarian Cancer by Sequestering miR-152-5p and Encoding Protein. Front. Genet. 13:784089. doi: 10.3389/fgene.2022.784089

INTRODUCTION

Ovarian cancer is the seventh most prevalent female cancer worldwide (Vafadar et al., 2020). Ovarian cancer is usually associated with silent and unclear symptoms, which makes it a difficult disease to diagnose, and it is usually diagnosed in advanced stages (Jayson et al., 2014). Standard treatment options for ovarian cancer include surgery and chemotherapy (Stewart et al., 2019). However, current treatments are unable to cure advanced ovarian cancer. Therefore, early diagnosis represents the best hope for mortality reduction and long-term disease control (Rauh-Hain et al., 2011). The

lack of a powerful biomarker for early diagnosis is the main obstacle. New biomarkers and new mechanisms are needed to help manage patients with ovarian cancer.

Recently, circular RNAs (circRNAs) have been shown to exhibit biomarker potential due to their abundance, specificity and stability (Shafabakhsh et al., 2019). Compared to linear RNAs, which feature terminal 5′ caps and 3′ tails, circRNAs have a covalently closed loop structure without 5′ to 3′ polarity and a polyadenylated tail (Zhong et al., 2018a). Therefore, on account of the unique structure, circRNAs were initially underestimated. With the emergence of advanced technology, an increasing number of circRNAs have been identified from different cell lines and species (Zhong et al., 2019). CircRNAs have been found to be involved in the pathogenesis of various diseases, including diabetes (Xu et al., 2015), cardiovascular diseases (Wang et al., 2016), Alzheimer's disease (Dube et al., 2019) and cancers (Zhong et al., 2018a; Zhang et al., 2019b; Wang et al., 2019; Zhou et al., 2019; Verduci et al., 2021). For example, FECR1, a circRNA derived from exons 2, 3, and 4 of the FLI1 gene, could bind to the promoter of FLI1 and then activate FLI1 by inducing DNA hypomethylation in CpG islands of the promoter, thus promoting the metastasis of breast cancer (Chen et al., 2018). Several studies have explored the roles of circRNA in ovarian cancer (Yang et al., 2020). Gan et al. found that circMUC16 had a higher expression level in ovarian cancer tissues than in healthy ovarian tissues, and its expression level was correlated with the stage and grade of ovarian cancer; the authors further demonstrated that circMUC16 promotes autophagy of epithelial ovarian cancer *via* interaction with ATG13 and miR-199a (Gan et al., 2020). In the present study, we profiled circRNA expression in 3 paired ovarian cancer tissues and normal ovarian tissues and identified two anticancer circRNAs.

MATERIALS AND METHODS

Specimens

We recruited 20 patients with stage III-IV high-grade serous ovarian cancer from the Affiliated Cancer Hospital of Nanjing Medical University. The patients were aged from 50 to 65, born in China, lived in the province of Jiangsu and did not receive any anticancer treatment before surgery. Ovarian cancer tissues and paired normal ovarian tissues were collected, flash frozen in liquid nitrogen, and stored at −80°C. The ethics committee of The Affiliated Cancer Hospital of Nanjing Medical University approved the study protocol, and informed consent was obtained from all the patients.

Cell Culture

Ovarian cancer cell lines (A2780, SKOV3, and SW626) and a normal ovarian epithelial cell line (IOSE80) were purchased from Shanghai Guan & Dao Biological Engineering Co., Ltd. The identities of the cell lines were authenticated by short-tandem-repeat (STR) profiling. All four cell lines were cultured in DMEM (Keygen Biotech, Nanjing, China) with 10% fetal bovine serum, 100 units/ml penicillin, and 100 μg/ml streptomycin.

Profiling of circRNAs

We randomly selected 3 paired ovarian cancer tissues and normal ovarian tissues from the 20 paired samples for circRNA profiling. CircRNAs were profiled using the RNA-seq technique by Gene Denovo Biotechnology Co. (Guangzhou, China). Briefly, total RNA was extracted and then treated with Ribonuclease R (RNase R) to degrade linear RNAs. A strand-specific library was constructed using a VAHTS Total RNAseq (H/M/R) Library Prep Kit (Vazyme, Nanjing, China). After removing ribosomal RNAs, the enriched circRNAs were fragmented into short fragments and reverse transcribed into cDNA. Second-strand cDNA was synthesized. The cDNA fragments were purified, end repaired, poly(A) added, and ligated to Illumina sequencing adapters. The second-strand cDNA was digested with uracil-N-glycosylase (UNG). The digested products were purified, PCR amplified, and sequenced using an Illumina Novaseq60000. The raw RNA-seq data have been submitted to the Gene Expression Omnibus (GEO) database (accession number GSE192410).

After obtaining clean reads and removing ribosome RNA (rRNA)-mapped reads, the remaining reads were mapped to the reference genome. Then, the unmapped reads were collected for circRNA identification using find_circ (version 1) (Memczak et al., 2013). Finally, we filtered raw read counts of circRNAs and kept only the genes with a nonzero read count in 3 or more samples and then used DESeq2 (version 1.32) (Love et al., 2014) in the statistical program R (version 4.0.1) to normalize the read counts. Differentially expressed circRNAs were identified based on a fold change of at least 2 and an adjusted p value <0.05.

Real-Time Quantitative PCR

CircPrimer (Zhong et al., 2018b) was used to annotate circRNAs and design primers for circRNAs. We performed reverse transcription and RT–qPCR as in our previous study (Zhong et al., 2018a; Zhou et al., 2020). The expression levels of genes were detected as described in our previous report (Wang et al., 2020b). β-action was used as a reference gene. All samples were analyzed in duplicate for each circRNA.

Transfection Experiment

Plasmids expressing circATRNL1 (p-circATRNL1) and circZNF608 (p-circZNF608) as well as control plasmids (p-control) were purchased from HanBio Biotechnology (Hanbio, Shanghai, China). Cells in logarithmic phase were harvested and seeded at 4×10^5 cells per well into a 6-well plate. After incubation for 24 h, the cells were transfected using Lipofectamine 3000 (Invitrogen, Carlsbad, CA, USA) following the manufacturer's instructions.

Fluorescent *In Situ* Hybridization

The FISH probes and Ribo™ fluorescent *in situ* hybridization Kit were purchased from Guangzhou RiboBio Co., Ltd. (RiboBio, Guangzhou, China). *In situ* hybridization was conducted as described previously (Zhong et al., 2018a; Zhou et al., 2020).

CCK8 Proliferation Assay

After transfection for 24 h, 4,000 cells were seeded per well (96-well plate) in the presence of 200 μL of complete medium. The

cells were divided into four groups. After cell attachment, the medium of the first group was removed, 100 μL CCK8 was added, the cells were incubated at 37°C for 1 h. Then, the absorbance was measured at 450 nm. The other three groups were detected at 24, 48 and 72 h, respectively.

Transwell Migration and Invasion Assays

Transwell migration and invasion assays were conducted as described previously (Zhou et al., 2020). For cell migration, 4×10^4 cells were seeded into the upper chamber of transwell assay inserts (pore size of 8 mm; Corning) containing 200 μL DMEM medium without serum. We added 600 μL DMEM with 20% fetal bovine serum to the lower chamber of 24-well culture plates. After incubation for 48 h, the cells on the filter surface were fixed with 4% paraformaldehyde, stained with crystal violet and imaged using a microscope (Carl Zeiss). For cell invasion, serum-free DMEM containing 100 μL mixture (1:8) of Matrigel (Corning, NY, USA) was coated on the upper transwell chamber before seeding cells. After allowing 4 h for the Matrigel to solidify, the subsequent experimental steps were similar to those in the migration assay.

circRNA-miRNA Interaction Prediction

We used circMir (www.bio-inf.cn/circmir) to predict miRNA–circRNA interactions. CircMir is a homemade software that runs miRanda (August 2010 release) and RNAhybrid (version 2.1.2) to obtain miRNA–circRNA interactions. Miranda software was set using the following default parameters: gap extend penalty, −4.0; gap open penalty, −9.0; energy threshold, 1.0 kcal/mol; score threshold, 140.0; and scaling parameter, 4.0. The following parameters were used for RNAhybrid: perfect miRNA seed complementarity with circRNA sequence, miRNA:circRNA binding energy < −26 kcal/mol and p value <0.05. Only the circRNA–miRNA interactions predicted by both miRanda and RNAhybrid were kept for further study.

Luciferase Reporter Assay

MiR mimics and negative control mimics (mimics-NC) were purchased from Guangzhou RiboBio Co., Ltd. (RiboBio, Guangzhou, China). The entire sequences of circZNF608 and circATRNL1 were cloned into the downstream region of the humanized form of Renilla luciferase (hRLuc) of the pmiR-RB-REPORT vector (RiboBio, Guangzhou, China), denoted circZNF608/vector-wd and circATRNL1/vector-wd.

To screen the miRNAs binding to the two circRNAs, miR mimics or negative control mimics (mimics-NC) were cotransfected with the vectors into cells. After 24 h, the luciferase activity was assessed using a dual-luciferase reporter gene assay kit (Beyotime Biotechnology, Shanghai, China). Because we found that only miR-152-5p inhibited the luciferase activity of circZNF608/vector-wd by more than 50%, we further mutated the miR-152-5p binding site from circZNF608/vector-wd to construct circZNF608/vector-mut. Then, mimics-NC or miR-152-5p mimics were cotransfected with circZNF608/vector-wd or circZNF608/vector-mut into cells, and luciferase activity was assessed.

Statistical Analysis

R software (version 4.0.1) was used to perform all statistical analyses. RT–qPCR results were assessed using the Wilcoxon rank test, paired test for patients and unpaired test for cells. Other data were evaluated using Student's t test and one-way analysis of variance. A p value <0.05 was considered statistically significant.

RESULTS

Identification and Characteristics of circZNF608 and circATRNL1

We profiled 3 paired ovarian cancer tissues and normal ovarian tissues using RNA-seq, and the raw read counts are presented in **Supplementary Table S1**. We identified 844 differentially expressed circRNAs in ovarian cancer tissues compared to normal ovarian tissues, including 45 upregulated circRNAs and 799 downregulated circRNAs (**Supplementary Table S2**, **Figures 1A–C**).

According to the fold change and normalized read counts, we selected 10 upregulated circRNAs and 10 downregulated circRNAs for RT–qPCR validation using cell lines. The 20 circRNAs can be found in **Supplementary Table S2** and are labeled in bold font. Among the 20 circRNAs, 3 circRNAs [circZNF608 (hsa_circ_0001523), circATRNL1 (hsa_circ_0020093) and circATXN10 (hsa_circ_0001246)] were differentially expressed in cell lines. Two (circATRNL1 and circATXN10) of the three circRNAs showed the same trend as RNA-seq, and one (circZNF608) showed the reverse trend. We further validated these three circRNAs in 20 paired tissues. All three circRNAs were downregulated in ovarian cancer tissues compared with normal ovarian tissues (**Figure 1D** for circZNF608 and **Figure 1E** for circATRNL1). Because we failed to overexpress hsa_circ_0001246 using plasmids, we focused on the other two circRNAs in the following studies.

We analyzed circZNF608 and circATRNL1 using circPrimer 2.0. CircZNF608 is located at chr5:124701013-124701269- and is derived from exon 2 of the ZNF608 gene with a spliced length of 256 nt (**Figure 1F**). CircATRNL1 is derived from exons 2–5 of the ATRNL1 gene with a spliced length of 536 nt (**Figure 1G**). CircATRNL1 is a highly conserved circRNA located at chr10: 115120184–115129535+ in the human genome and chr19: 57703574–57717118+ in the mouse genome (mmu_circ_0007920) (**Supplementary Figure S1**). The existence of circZNF608 and circATRNL1 was confirmed by Sanger sequencing (**Figures 1F,G**). FISH showed that circZNF608 and circATRNL1 are mainly located in the cytoplasm of ovarian cancer cells (**Figure 1H**).

Overexpression of circZNF608 and circATRNL1 Inhibits Proliferation, Migration and Invasion

We explored the effects of circZNF608 and circATRNL1 on ovarian cancer cells. We transfected p-control, p-circATRNL1, and p-circZNF608 into ovarian cancer cell lines, detected the expression of circATRNL1 and circZNF608, and found that the

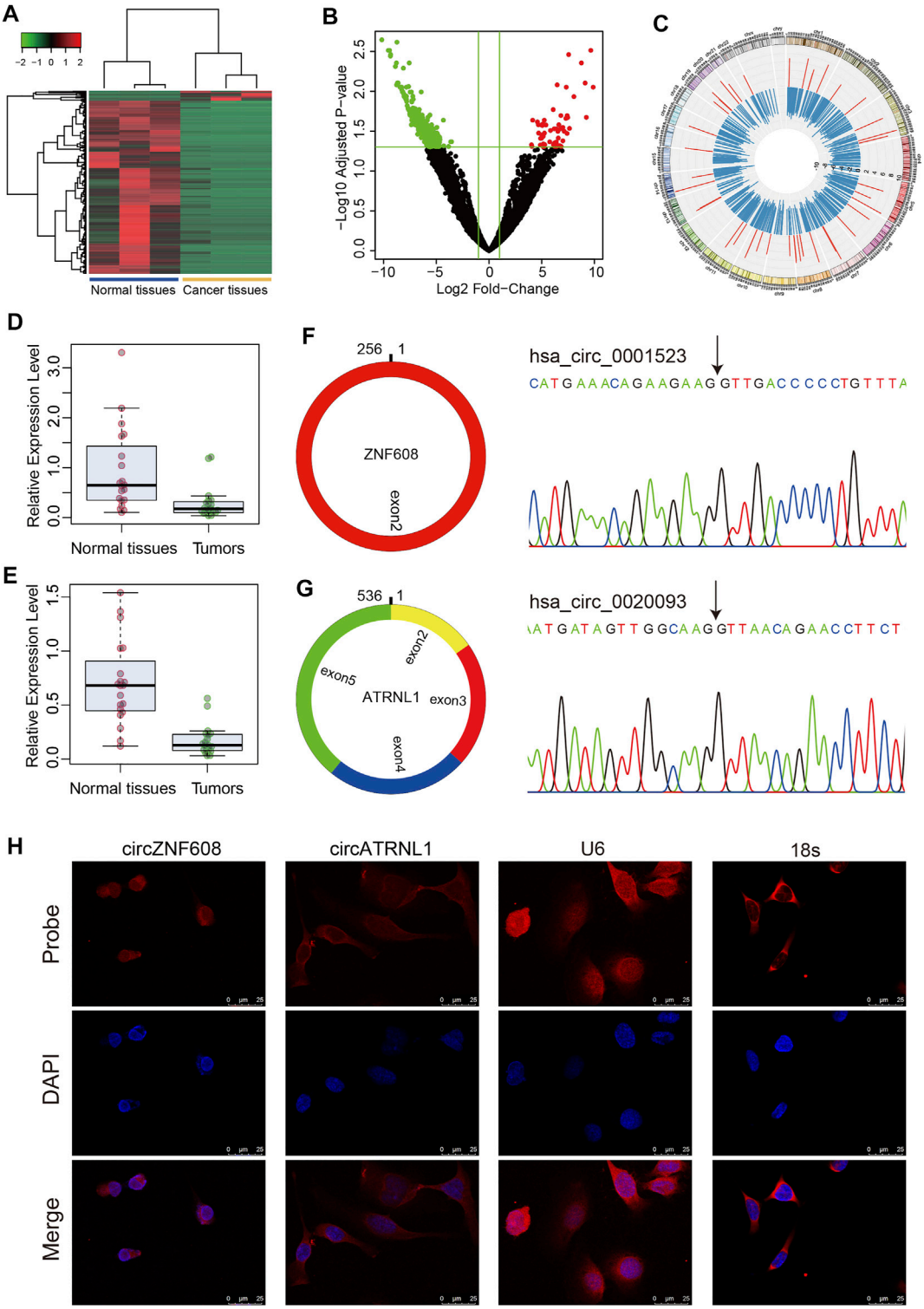

FIGURE 1 | Characteristics of circZNF608 and circATRNL1. **(A)** Heatmap of differentially expressed circRNAs in ovarian cancer tissues compared with normal ovarian tissues. **(B)** Volcano plot of circRNAs in RNA-seq data. Green dots: downregulated circRNAs; red dots: upregulated circRNAs. **(C)** Circos diagram illustrating the fold change of differentially expressed circRNAs in RNA-seq data. The red bar indicates log2 (fold change) of upregulated circRNAs, and the blue bar indicates downregulated circRNAs. **(D)** circZNF608 and **(E)** circATRNL1 were downregulated in ovarian cancer tissues compared with normal ovarian tissues ($p < 0.001$). **(F)** and **(G)** The back-splice junction of circZNF608 and circATRNL1 was confirmed by sequencing the PCR products from the RNase R-treated RNA. **(H)** RNA fluorescence *in situ* hybridization for circZNF608 and circATRNL1. Nuclei were stained with 4,6-DAPI.

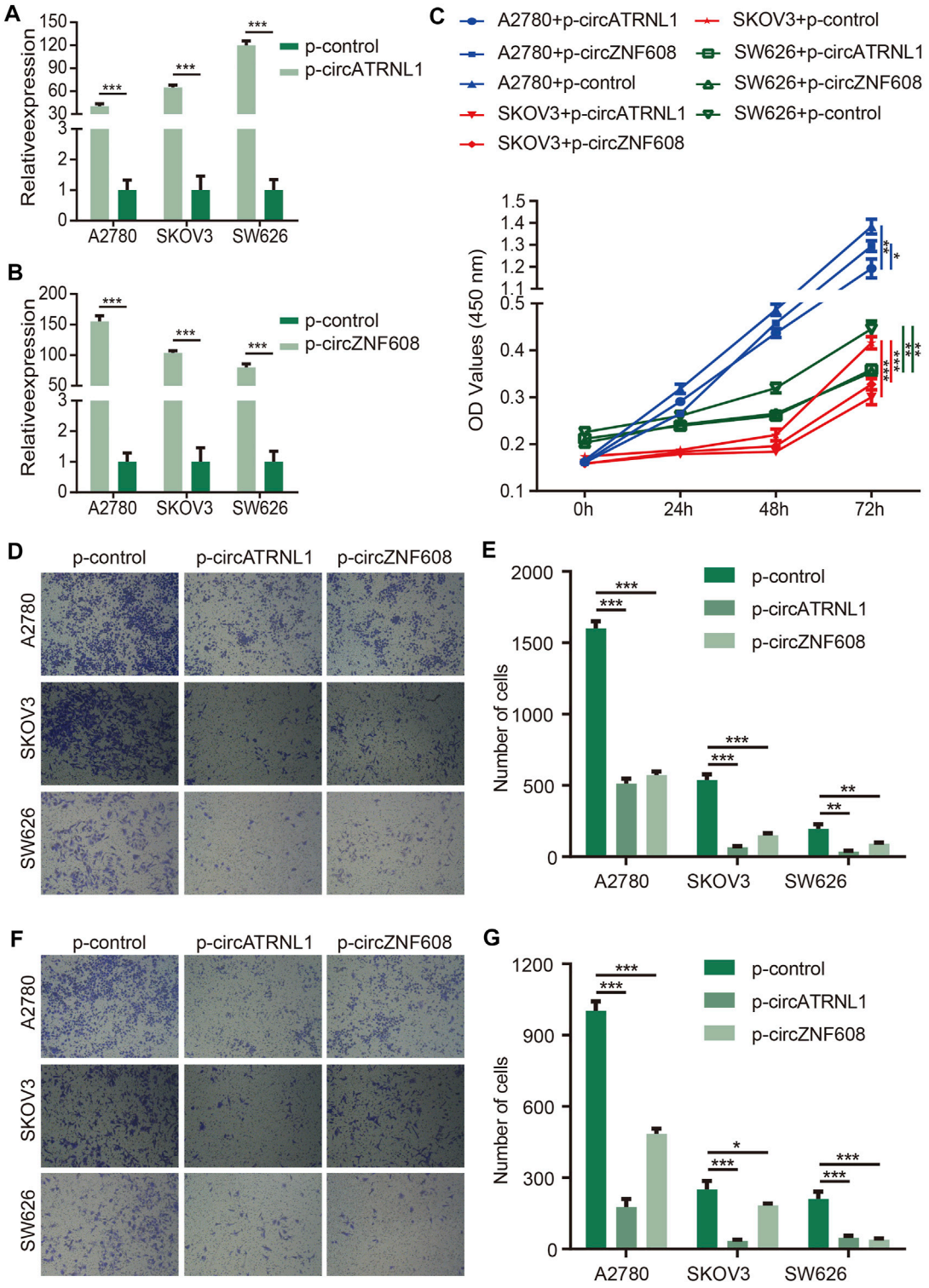

FIGURE 2 | circATRNL1 and circZNF608 overexpression inhibited ovarian cancer cell proliferation and invasion. **(A)** circATRNL1 was overexpressed after transfecting p-circATRNL1. **(B)** circZNF608 was overexpressed after transfecting p-circZNF608. **(C)** circATRNL1 and circZNF608 inhibited the proliferation of ovarian cancer cells. **(D)** Representative pictures of the transwell migration assay. **(E)** circATRNL1 and circZNF608 decreased the migration of ovarian cancer cells. **(F)** Representative pictures of the transwell invasion assay. **(G)** circATRNL1 and circZNF608 decreased the invasion of ovarian cancer cells. p-circATRNL1, plasmids expressing circATRNL1; p-circZNF608, plasmids expressing circZNF608, p-control, control plasmids; $*p < 0.05$; $**p < 0.01$; and $***p < 0.001$.

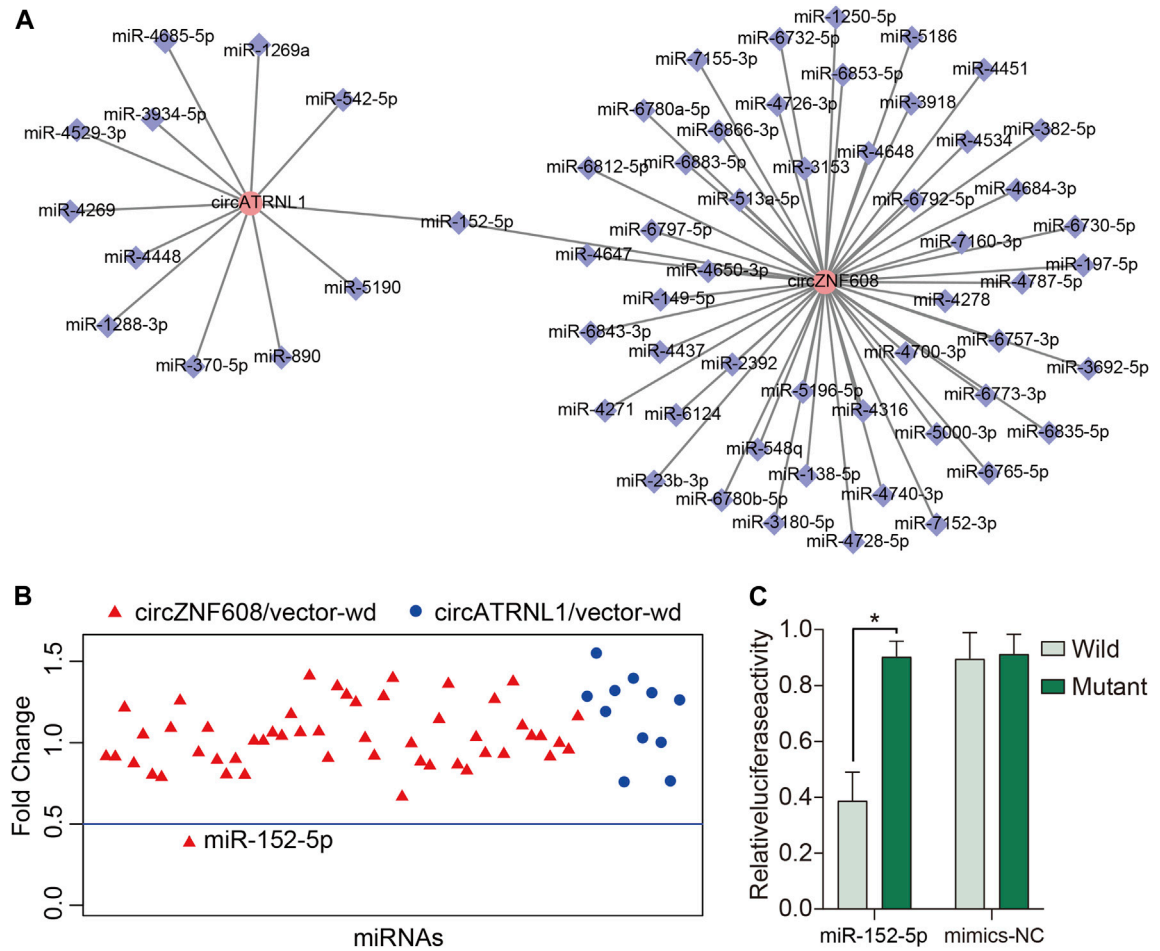

FIGURE 3 | circZNF608 serves as a sponge for miR-152-5p in ovarian cancer cells. **(A)** The 63 predicted miRNA–circRNA interactions for circZNF608 and circATRNL1. **(B)** Luciferase reporter assay of the 63 miRNA–circRNA interactions to identify miRNAs that were able to bind to the circZNF608 or circATRNL1 sequence. Only miR-152-5p inhibited luciferase activity by more than 50%. **(C)** Luciferase reporter assay for the luciferase activity of wild-type and mutant circATRNL1 vectors cotransfected with miR-152-5p mimics or mimic-NC (negative control of mimics).

cells transfected with p-circATRNL1 and p-circZNF608 had higher expression levels of circATRNL1 and circZNF608 than control cells (**Figures 2A,B**). The CCK8 proliferation assay showed that both circATRNL1 and circZNF608 could inhibit the proliferation of all three ovarian cancer cell lines (**Figure 2C**). The transwell migration assay indicated that higher expression of circATRNL1 and circZNF608 was associated with lower migration rates (**Figures 2D,E**). We further explored circATRNL1 and circZNF608 on invasion and found that the overexpression of circATRNL1 and circZNF608 inhibited the invasion of ovarian cancer cell lines (**Figures 2F,G**).

CircZNF608 Acts as a miRNA Sponge for miR-152-5p

Studies have reported that the subcellular localization of a circRNA is closely correlated with its function (Panda et al., 2017; Qu et al., 2018). CircRNAs that are mainly located in the cytoplasm may act as miRNA sponges to bind miRNAs (Qu et al., 2018). Because circZNF608 and circATRNL1 are predominantly located in the cytoplasm of ovarian cancer cells, we predicted miRNA–circRNA interactions for circZNF608 and circATRNL1 and obtained 63 interactions (**Figure 3A**). We screened the miRNAs that bind to circZNF608 and circATRNL1 using a luciferase reporter assay and found that only miR-152-5p inhibited the luciferase activity of circZNF608/vector-wd by more than 50% (**Figure 3B**). We further mutated the miR-152-5p binding site from circZNF608/vector-wd and constructed circZNF608/vector-mut. CircZNF608/vector-wd or circZNF608/vector-mut was cotransfected with miR-152-5p mimics or mimics-NC, and a luciferase reporter assay showed that miR-152-5p could inhibit the luciferase activity of circZNF608/vector-wd significantly compared to circZNF608/vector-Mut, and mimics-NC had no effect on luciferase activity, suggesting that circZNF608 may exert its anticancer effects by sequestering miR-152-5p (**Figure 3C**). We further detected the expression of miR-152-5p in the 20 paired ovarian cancer tissues and normal ovarian tissues and failed to

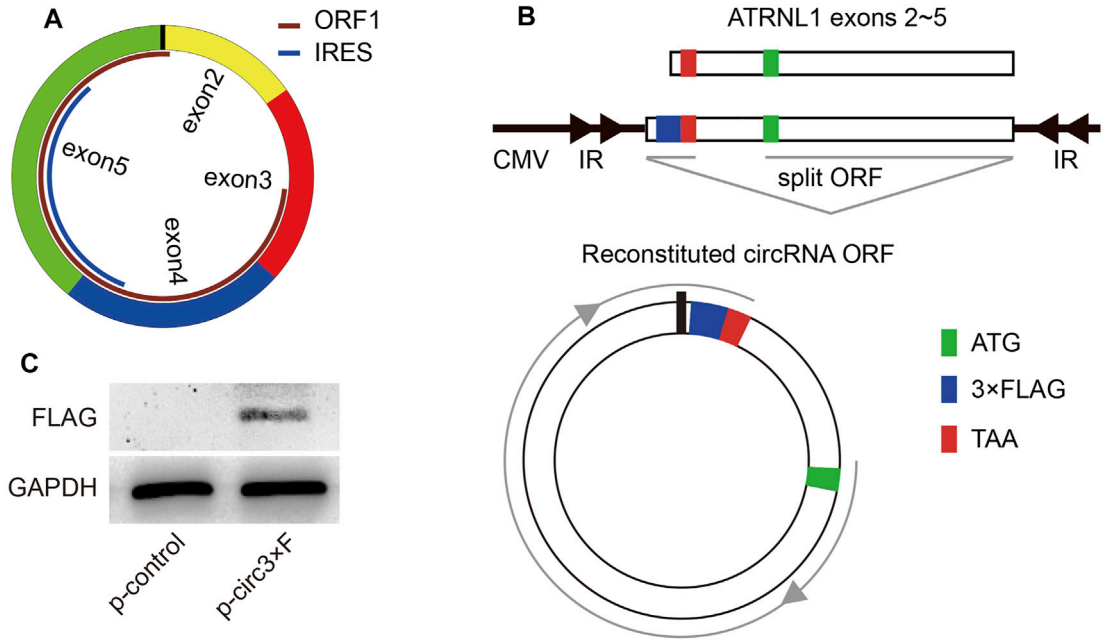

FIGURE 4 | circATRNL1 encodes a protein. **(A)** circPrimer 2.0 indicates that circATRNL1 contains an open reading frame (ORF) and an internal ribosome entry site (IRES). **(B)** Schematic representation of the p-circ3×F construct. IR, inverted repeats. **(C)** Western blot analysis with an anti-FLAG antibody on proteins from cells transfected with p-circ3×F or p-control (control plasmids).

find a difference between the two groups (**Supplementary Figure S2**), suggesting that circZNF608 binds miR-152-5p but does not influence its expression.

CircATRNL1 Encodes a Protein

To further uncover the underlying mechanisms of circATRNL1, we explored circATRNL1 using circPrimer 2.0, which shows that circATRNL1 may encode a 131 aa protein (**Figure 4A**). The open reading frame (ORF) of this protein spans the splice junction of circATRNL1. An internal ribosome entry site (IRES) overlaps with the ORF and may initiate ORF translation. To test the protein-coding ability of circATRNL1, we constructed a plasmid from p-circATRNL1, named p-circ3×F, which contained a 3×FLAG-coding sequence immediately upstream of the stop codon of the ORF (**Figure 4B**). If the ORF has protein-coding ability, a flagged peptide will be produced. After transfecting p-circ3×F and p-control into the HEK-293 cell line for 48 h, western blotting showed that p-circ3×F produced one flagged protein (**Figure 4C**).

DISCUSSION

CircRNAs have been shown to play important roles in cancers, including ovarian cancer. However, most studies have shown that circRNAs are sponges for miRNAs. For example, hsa_circ_0015326 facilitated the progression of ovarian cancer by regulating the miR-127-3p/MYB axis (Zhang et al., 2021a). CircRAB11FIP1-induced autophagy accelerated the proliferation and invasion of epithelial ovarian cancer by binding miR-129 (Zhang et al., 2021d). Other mechanisms of circRNAs include binding proteins (Du et al., 2016; Zhang et al., 2021b), modulating the transcriptional activity of RNA Pol II (Zhang et al., 2013), coding proteins (Legnini et al., 2017; Yang et al., 2017), and competing with linear splicing (Ashwal-Fluss et al., 2014).

In the present study, we profiled the expression of circRNAs in 3 paired ovarian cancer tissues and normal ovarian tissues, and then the differentially expressed circRNAs were validated in 20 paired tissues; two circRNAs were downregulated in ovarian cancer tissues. CircZNF608 was an upregulated circRNA in RNA-seq data; however, RT–qPCR showed that it was a downregulated circRNA. The conflicting results may be due to the small sample size (n = 3) and intrinsic bias of RNA-Seq (Rodriguez-Esteban et al., 2015). After searching exoRBase 2.0 (www.exorbase.org) (Lai et al., 2021), we found that circZNF608 but not circATRNL1 was also expressed in exosomes from blood, urine, cerebrospinal fluid and bile. We investigated the effects of the two circRNAs on ovarian cancer cell lines and found that circATRNL1 and circZNF608 inhibited the proliferation, migration and invasion of ovarian cancer cells. These results suggested that circATRNL1 and circZNF608 may exert anticancer effects in ovarian cancer.

We investigated the underlying mechanisms by which circATRNL1 and circZNF608 exert their effects. As mentioned above, the subcellular localization of a circRNA is closely correlated with its function (Panda et al., 2017; Qu et al., 2018). CircRNAs that are mainly located in the cytoplasm may act as miRNA sponges to bind miRNAs (Qu et al., 2018). CircZNF608 and circATRNL1 are predominantly located in the cytoplasm of ovarian cancer cells, suggesting that they may exert

their effects by sequestering miRNAs. Therefore, we predicted miRNA–circRNA interactions for circZNF608 and circATRNL1 and obtained 63 interactions. We validated all the interactions using a luciferase reporter assay and only obtained one positive interaction, i.e., circZNF608-miR-152-5p. A study reported that miR-152-5p was significantly downregulated in the serum/plasma of ovarian cancer patients (Langhe et al., 2015). However, we failed to find a difference in the expression level of miR-152-5p between ovarian cancer and normal ovarian tissues, suggesting that circZNF608 may competitively bind miR-152-5p but not influence its expression.

Because we failed to find an interaction for circATRNL1, we further explored the underlying mechanisms of circATRNL1 and found that circATRNL1 may exert its effects by encoding a 131 aa protein. Studies have shown that some circRNAs can be translated into functional peptides by small ORFs in a 5′ cap-independent manner (Pamudurti et al., 2017). In 2007, Legnini et al. first demonstrated that a eukaryotic endogenous circRNA encodes a protein in a splicing-dependent and cap-independent manner (Legnini et al., 2017). Yang et al. found that circ-FBXW7 contains a spanning junction ORF and encodes a novel 21-kDa protein that is driven by IRES, and circ-FBXW7 and its encoded protein have potential prognostic implications in brain cancer (Yang et al., 2018). Yang et al. reported that SHPRH-146aa encoded by circ-SHPRH is a tumor suppressor in human glioblastoma (Zhang et al., 2018a). Other coding circRNAs were also found in breast cancer (Li et al., 2020), glioblastoma (Zhang et al., 2018b; Xia et al., 2019), bladder cancer (Gu et al., 2018), colorectal cancer (Zheng et al., 2019; Zhi et al., 2019; Pan et al., 2020) and liver cancer (Liang et al., 2019). CircATRNL1 is the first reported coding circRNA in ovarian cancer. At present, seven studies have explored the roles of circATRNL1 (Zhang et al., 2019a; Wang et al., 2020a; Chen et al., 2020; Wang et al., 2021a; Wang et al., 2021b; Zhang et al., 2021c; Zheng et al., 2021), but three did not include has_circ_0020093 (Chen et al., 2020; Wang et al., 2021b; Zhang et al., 2021c). In a study by Wang et al., circATRNL1 activated Smad4 signaling and suppressed angiogenesis and ovarian cancer metastasis by binding miR-378 (Wang et al., 2021a). Zhang et al. found that circATRNL1 was downregulated in women with polycystic ovary syndrome (Zhang et al., 2019a). Zheng et al. showed that circATRNL1 is beneficial to bone marrow mesenchymal stem cell differentiation into cartilage by regulating miR-338-3p (Zheng et al., 2021). However, circATRNL1 contributes to the progression of endometriosis by promoting epithelial–mesenchymal transition (Wang et al., 2020a). Combining the findings in our study, circATRNL1 has beneficial effects on ovarian cancer and ovarian disease.

There are several limitations to our study. First, the sample size is relatively small and is therefore of limited power, which may weaken the conclusion of the present study. Second, we did not confirm the downstream effects of these two circRNAs, which may also inhibit ovarian cancer by other mechanisms. Third, circPrimer2.0 shows that circZNF608 contains an ORF and an IRES, supporting its encoding potential. However, we did not verify this finding using experiments. Fourth, SW626 may be a cell line of colonic origin (Furlong et al., 1999); thus, circATRNL1 and circZNF608 may not enact their roles specific to ovarian cancer. At least, they may also have an effect on colon cancer. Taken together, further studies based on large samples are needed to assess the expression of the 2 circRNAs, miR-152-5p and the 131 aa protein in ovarian cancer. Further studies with a functional analysis to highlight the molecular mechanisms underlying the encoded protein are proposed.

In conclusion, circATRNL1 and circZNF608 are two downregulated circRNAs in ovarian cancer and work as tumor suppressors. CircZNF608 may exert antitumor activity in ovarian cancer by binding miR-152-5p, and circATRNL1 may encode a 131 aa protein.

DATA AVAILABILITY STATEMENT

The datasets presented in this study can be found in online repositories. The names of the repository/repositories and accession number(s) can be found below: GEO with accession GSE192410.

ETHICS STATEMENT

The studies involving human participants were reviewed and approved by the ethics committee of The Affiliated Cancer Hospital of Nanjing Medical University. The patients/participants provided their written informed consent to participate in this study.

AUTHOR CONTRIBUTIONS

SZ and JW contributed to conception and design of the study. ML, XL, and YS performed the experiments. JL and LZ performed the statistical analysis. SZ and ML wrote the first draft of the manuscript. All authors contributed to manuscript revision, read, and approved the submitted version.

FUNDING

This study was funded by the National Natural Science Foundation of China (grant number 81702895).

SUPPLEMENTARY MATERIAL

The Supplementary Material for this article can be found online at: https://www.frontiersin.org/articles/10.3389/fgene.2022.784089/full#supplementary-material

REFERENCES

Ashwal-Fluss, R., Meyer, M., Pamudurti, N. R., Ivanov, A., Bartok, O., Hanan, M., et al. (2014). circRNA Biogenesis Competes with Pre-mRNA Splicing. *Mol. Cel* 56 (1), 55–66. doi:10.1016/j.molcel.2014.08.019

Chen, G., Li, Y., He, Y., Zeng, B., Yi, C., Wang, C., et al. (2020). Upregulation of Circular RNA circATRNL1 to Sensitize Oral Squamous Cell Carcinoma to Irradiation. *Mol. Ther. - Nucleic Acids* 19, 961–973. doi:10.1016/j.omtn.2019.12.031

Chen, N., Zhao, G., Yan, X., Lv, Z., Yin, H., Zhang, S., et al. (2018). A Novel FLI1 Exonic Circular RNA Promotes Metastasis in Breast Cancer by Coordinately Regulating TET1 and DNMT1. *Genome Biol.* 19 (1), 218. doi:10.1186/s13059-018-1594-y

Du, W. W., Yang, W., Liu, E., Yang, Z., Dhaliwal, P., and Yang, B. B. (2016). Foxo3 Circular RNA Retards Cell Cycle Progression *via* Forming Ternary Complexes with P21 and CDK2. *Nucleic Acids Res.* 44 (6), 2846–2858. doi:10.1093/nar/gkw027

Dube, U., Del-Aguila, J. L., Del-Aguila, J. L., Li, Z., Budde, J. P., Jiang, S., et al. (2019). An Atlas of Cortical Circular RNA Expression in Alzheimer Disease Brains Demonstrates Clinical and Pathological Associations. *Nat. Neurosci.* 22 (11), 1903–1912. doi:10.1038/s41593-019-0501-5

Furlong, M. T., Hough, C. D., Sherman-Baust, C. A., Pizer, E. S., and Morin, P. J. (1999). Evidence for the Colonic Origin of Ovarian Cancer Cell Line SW626. *JNCI J. Natl. Cancer Inst.* 91 (15), 1327–1328. doi:10.1093/jnci/91.15.1327

Gan, X., Zhu, H., Jiang, X., Obiegbusi, S. C., Yong, M., Long, X., et al. (2020). CircMUC16 Promotes Autophagy of Epithelial Ovarian Cancer *via* Interaction with ATG13 and miR-199a. *Mol. Cancer* 19 (1), 45. doi:10.1186/s12943-020-01163-z

Gu, C., Zhou, N., Wang, Z., Li, G., Kou, Y., Yu, S., et al. (2018). circGprc5a Promoted Bladder Oncogenesis and Metastasis through Gprc5a-Targeting Peptide. *Mol. Ther. - Nucleic Acids* 13, 633–641. doi:10.1016/j.omtn.2018.10.008

Jayson, G. C., Kohn, E. C., Kitchener, H. C., and Ledermann, J. A. (2014). Ovarian Cancer. *The Lancet* 384 (9951), 1376–1388. doi:10.1016/S0140-6736(13)62146-7

Lai, H., Li, Y., Zhang, H., Hu, J., Liao, J., Su, Y., et al. (2021). exoRBase 2.0: an Atlas of mRNA, lncRNA and circRNA in Extracellular Vesicles from Human Biofluids. *Nucleic Acids Res.* 50, D118–D128. doi:10.1093/nar/gkab1085

Langhe, R., Norris, L., Saadeh, F. A., Blackshields, G., Varley, R., Harrison, A., et al. (2015). A Novel Serum microRNA Panel to Discriminate Benign from Malignant Ovarian Disease. *Cancer Lett.* 356 (2 Pt B), 628–636. doi:10.1016/j.canlet.2014.10.010

Legnini, I., Di Timoteo, G., Rossi, F., Morlando, M., Briganti, F., Sthandier, O., et al. (2017). Circ-ZNF609 Is a Circular RNA that Can Be Translated and Functions in Myogenesis. *Mol. Cel* 66 (1), 22–37. e29. doi:10.1016/j.molcel.2017.02.017

Li, J., Ma, M., Yang, X., Zhang, M., Luo, J., Zhou, H., et al. (2020). Circular HER2 RNA Positive Triple Negative Breast Cancer Is Sensitive to Pertuzumab. *Mol. Cancer* 19 (1), 142. doi:10.1186/s12943-020-01259-6

Liang, W.-C., Wong, C.-W., Liang, P.-P., Shi, M., Cao, Y., Rao, S.-T., et al. (2019). Translation of the Circular RNA Circβ-Catenin Promotes Liver Cancer Cell Growth through Activation of the Wnt Pathway. *Genome Biol.* 20 (1), 84. doi:10.1186/s13059-019-1685-4

Love, M. I., Huber, W., and Anders, S. (2014). Moderated Estimation of Fold Change and Dispersion for RNA-Seq Data with DESeq2. *Genome Biol.* 15 (12), 550. doi:10.1186/s13059-014-0550-8

Memczak, S., Jens, M., Elefsinioti, A., Torti, F., Krueger, J., Rybak, A., et al. (2013). Circular RNAs Are a Large Class of Animal RNAs with Regulatory Potency. *Nature* 495 (7441), 333–338. doi:10.1038/nature11928

Pamudurti, N. R., Bartok, O., Jens, M., Ashwal-Fluss, R., Stottmeister, C., Ruhe, L., et al. (2017). Translation of CircRNAs. *Mol. Cel* 66 (1), 9–21. e27. doi:10.1016/j.molcel.2017.02.021

Pan, Z., Cai, J., Lin, J., Zhou, H., Peng, J., Liang, J., et al. (2020). A Novel Protein Encoded by circFNDC3B Inhibits Tumor Progression and EMT through Regulating Snail in colon Cancer. *Mol. Cancer* 19 (1), 71. doi:10.1186/s12943-020-01179-5

Panda, A. C., Grammatikakis, I., Munk, R., Gorospe, M., and Abdelmohsen, K. (2017). Emerging Roles and Context of Circular RNAs. *WIREs RNA* 8 (2), e1386. doi:10.1002/wrna.1386

Qu, S., Liu, Z., Yang, X., Zhou, J., Yu, H., Zhang, R., et al. (2018). The Emerging Functions and Roles of Circular RNAs in Cancer. *Cancer Lett.* 414, 301–309. doi:10.1016/j.canlet.2017.11.022

Rauh-Hain, J. A., Krivak, T. C., Del Carmen, M. G., and Olawaiye, A. B. (2011). Ovarian Cancer Screening and Early Detection in the General Population. *Rev. Obstet. Gynecol.* 4 (1), 15–21.

Rodríguez-Esteban, G., González-Sastre, A., Rojo-Laguna, J. I., Saló, E., and Abril, J. F. (2015). Digital Gene Expression Approach over Multiple RNA-Seq Data Sets to Detect Neoblast Transcriptional Changes in Schmidtea Mediterranea. *BMC Genomics* 16, 361. doi:10.1186/s12864-015-1533-1

Shafabakhsh, R., Mirhosseini, N., Chaichian, S., Moazzami, B., Mahdizadeh, Z., and Asemi, Z. (2019). Could circRNA Be a New Biomarker for Pre-eclampsia. *Mol. Reprod. Dev.* 86 (12), 1773–1780. doi:10.1002/mrd.23262

Stewart, C., Ralyea, C., and Lockwood, S. (2019). Ovarian Cancer: An Integrated Review. *Semin. Oncol. Nurs.* 35 (2), 151–156. doi:10.1016/j.soncn.2019.02.001

Vafadar, A., Shabaninejad, Z., Movahedpour, A., Fallahi, F., Taghavipour, M., Ghasemi, Y., et al. (2020). Quercetin and Cancer: New Insights into its Therapeutic Effects on Ovarian Cancer Cells. *Cell Biosci* 10, 32. doi:10.1186/s13578-020-00397-0

Verduci, L., Tarcitano, E., Strano, S., Yarden, Y., and Blandino, G. (2021). CircRNAs: Role in Human Diseases and Potential Use as Biomarkers. *Cell Death Dis* 12 (5), 468. doi:10.1038/s41419-021-03743-3

Wang, D., Luo, Y., Wang, G., and Yang, Q. (2020). CircATRNL1 Promotes Epithelial-Mesenchymal Transition in Endometriosis by Upregulating Yes-Associated Protein 1 *In Vitro*. *Cel Death Dis* 11 (7), 594. doi:10.1038/s41419-020-02784-4

Wang, J., Zhang, Q., Wang, D., Yang, S., Zhou, S., Xu, H., et al. (2020). Microenvironment-induced TIMP2 Loss by Cancer-secreted Exosomal miR-4443 Promotes Liver Metastasis of Breast Cancer. *J. Cel Physiol* 235 (7-8), 5722–5735. doi:10.1002/jcp.29507

Wang, J., Zhang, Q., Zhou, S., Xu, H., Wang, D., Feng, J., et al. (2019). Circular RNA Expression in Exosomes Derived from Breast Cancer Cells and Patients. *Epigenomics* 11 (4), 411–421. doi:10.2217/epi-2018-0111

Wang, J., Li, Y., Zhou, J. H., Shen, F. R., Shi, X., and Chen, Y. G. (2021). CircATRNL1 Activates Smad4 Signaling to Inhibit Angiogenesis and Ovarian Cancer Metastasis *via* miR-378. *Mol. Oncol.* 15 (4), 1217–1233. doi:10.1002/1878-0261.12893

Wang, K.-F., Shi, Z.-W., and Dong, D.-M. (2021). CircATRNL1 Protects against Osteoarthritis by Targeting miR-153-3p and KLF5. *Int. Immunopharmacology* 96, 107704. doi:10.1016/j.intimp.2021.107704

Wang, K., Long, B., Liu, F., Wang, J.-X., Liu, C.-Y., Zhao, B., et al. (2016). A Circular RNA Protects the Heart from Pathological Hypertrophy and Heart Failure by Targeting miR-223. *Eur. Heart J.* 37 (33), 2602–2611. doi:10.1093/eurheartj/ehv713

Xia, X., Li, X., Li, F., Wu, X., Zhang, M., Zhou, H., et al. (2019). A Novel Tumor Suppressor Protein Encoded by Circular AKT3 RNA Inhibits Glioblastoma Tumorigenicity by Competing with Active Phosphoinositide-dependent Kinase-1. *Mol. Cancer* 18 (1), 131. doi:10.1186/s12943-019-1056-5

Xu, H., Guo, S., Li, W., and Yu, P. (2015). The Circular RNA Cdr1as, *via* miR-7 and its Targets, Regulates Insulin Transcription and Secretion in Islet Cells. *Sci. Rep.* 5 (1), 12453. doi:10.1038/srep12453

Yang, X., Mei, J., Wang, H., Gu, D., Ding, J., and Liu, C. (2020). The Emerging Roles of Circular RNAs in Ovarian Cancer. *Cancer Cel Int* 20, 265. doi:10.1186/s12935-020-01367-9

Yang, Y., Fan, X., Mao, M., Song, X., Wu, P., Zhang, Y., et al. (2017). Extensive Translation of Circular RNAs Driven by N6-Methyladenosine. *Cell Res* 27 (5), 626–641. doi:10.1038/cr.2017.31

Yang, Y., Gao, X., Zhang, M., Yan, S., Sun, C., Xiao, F., et al. (2018). Novel Role of FBXW7 Circular RNA in Repressing Glioma Tumorigenesis. *J. Natl. Cancer Inst.* 110 (3), 304–315. doi:10.1093/jnci/djx166

Zhang, C., Liu, J., Lai, M., Li, J., Zhan, J., Wen, Q., et al. (2019). Circular RNA Expression Profiling of Granulosa Cells in Women of Reproductive Age with Polycystic Ovary Syndrome. *Arch. Gynecol. Obstet.* 300 (2), 431–440. doi:10.1007/s00404-019-05129-5

Zhang, C., Liu, W., Li, F., Feng, Y., Li, Y., and Wang, J. (2021). Hsa_circ_0015326 Promotes the Proliferation, Invasion and Migration of Ovarian Cancer through miR-127-3p/MYB. *Cmar* Vol. 13, 2265–2277. doi:10.2147/cmar.S291218

Zhang, M., Huang, N., Yang, X., Luo, J., Yan, S., Xiao, F., et al. (2018a). A Novel Protein Encoded by the Circular Form of the SHPRH Gene Suppresses Glioma Tumorigenesis. *Oncogene* 37 (13), 1805–1814. doi:10.1038/s41388-017-0019-9

Zhang, M., Zhao, K., Xu, X., Yang, Y., Yan, S., Wei, P., et al. (2018b). A Peptide Encoded by Circular Form of LINC-PINT Suppresses Oncogenic Transcriptional Elongation in Glioblastoma. *Nat. Commun.* 9 (1), 4475. doi:10.1038/s41467-018-06862-2

Zhang, M., Xu, Y., Zhang, Y., Li, B., and Lou, G. (2021). Circular RNA circE2F2 Promotes Malignant Progression of Ovarian Cancer Cells by Upregulating the Expression of E2F2 Protein *via* Binding to HuR Protein. *Cell Signal.* 84, 110014. doi:10.1016/j.cellsig.2021.110014

Zhang, Q., Wang, J., Zhou, S., Yang, S., and Zhong, S. (2019). Circular RNA Expression in Pancreatic Ductal Adenocarcinoma. *Oncol. Lett.* 18 (3), 2923–2930. doi:10.3892/ol.2019.10624

Zhang, Q., Wang, L., Cao, L., and Wei, T. (2021). Novel Circular RNA circATRNL1 Accelerates the Osteosarcoma Aerobic Glycolysis through Targeting miR-409-3p/LDHA. *Bioengineered* 12 (2), 9965–9975. doi:10.1080/21655979.2021.1985343

Zhang, Y., Zhang, X.-O., Chen, T., Xiang, J.-F., Yin, Q.-F., Xing, Y.-H., et al. (2013). Circular Intronic Long Noncoding RNAs. *Mol. Cel* 51 (6), 792–806. doi:10.1016/j.molcel.2013.08.017

Zhang, Z., Zhu, H., and Hu, J. (2021). CircRAB11FIP1 Promoted Autophagy Flux of Ovarian Cancer through DSC1 and miR-129. *Cel Death Dis* 12 (2), 219. doi:10.1038/s41419-021-03486-1

Zheng, J., Lin, Y., Tang, F., Guo, H., Yan, L., Hu, S., et al. (2021). Promotive Role of CircATRNL1 on Chondrogenic Differentiation of BMSCs Mediated by miR-338-3p. *Arch. Med. Res.* 52 (5), 514–522. doi:10.1016/j.arcmed.2021.02.003

Zheng, X., Chen, L., Zhou, Y., Wang, Q., Zheng, Z., Xu, B., et al. (2019). A Novel Protein Encoded by a Circular RNA circPPP1R12A Promotes Tumor Pathogenesis and Metastasis of colon Cancer *via* Hippo-YAP Signaling. *Mol. Cancer* 18 (1), 47. doi:10.1186/s12943-019-1010-6

Zhi, X., Zhang, J., Cheng, Z., Bian, L., and Qin, J. (2022). Withdrawn: circLgr4 Drives Colorectal Tumorigenesis and Invasion through Lgr4-targeting Peptide. *Intl J. Cancer* 150. doi:10.1002/ijc.32549

Zhong, S., Wang, J., Hou, J., Zhang, Q., Xu, H., Hu, J., et al. (2018a). Circular RNA Hsa_circ_0000993 Inhibits Metastasis of Gastric Cancer Cells. *Epigenomics* 10 (10), 1301–1313. doi:10.2217/epi-2017-0173

Zhong, S., Wang, J., Zhang, Q., Xu, H., and Feng, J. (2018b). CircPrimer: a Software for Annotating circRNAs and Determining the Specificity of circRNA Primers. *BMC Bioinformatics* 19 (1), 292. doi:10.1186/s12859-018-2304-1

Zhong, S., Zhou, S., Yang, S., Yu, X., Xu, H., Wang, J., et al. (2019). Identification of Internal Control Genes for Circular RNAs. *Biotechnol. Lett.* 41 (10), 1111–1119. doi:10.1007/s10529-019-02723-0

Zhou, S.-y., Chen, W., Yang, S.-j., Li, J., Zhang, J.-y., Zhang, H.-d., et al. (2020). Circular RNA circVAPA Regulates Breast Cancer Cell Migration and Invasion *via* Sponging miR-130a-5p. *Epigenomics* 12 (4), 303–317. doi:10.2217/epi-2019-0124

Zhou, S.-y., Chen, W., Yang, S.-j., Xu, Z.-h., Hu, J.-h., Zhang, H.-d., et al. (2019). The Emerging Role of Circular RNAs in Breast Cancer. *Biosci. Rep.* 39 (6), BSR20190621. doi:10.1042/BSR20190621

Conflict of Interest: The authors declare that the research was conducted in the absence of any commercial or financial relationships that could be construed as a potential conflict of interest.

Publisher's Note: All claims expressed in this article are solely those of the authors and do not necessarily represent those of their affiliated organizations, or those of the publisher, the editors, and the reviewers. Any product that may be evaluated in this article, or claim that may be made by its manufacturer, is not guaranteed or endorsed by the publisher.

frontiers in Genetics

ORIGINAL RESEARCH
published: 07 March 2022
doi: 10.3389/fgene.2022.786689

A Novel Ferroptosis-Related lncRNAs Signature Predicts Clinical Prognosis and Is Associated With Immune Landscape in Pancreatic Cancer

Haiqin Ping[1], *Xingqing Jia*[2] *and Hengning Ke*[1,3,4]*

[1]Department of Infectious Disease, Hubei AIDS Clinical Training Center, Zhongnan Hospital of Wuhan University, Wuhan, China, [2]Jinan City People's Hospital, Jinan, China, [3]Wuhan Research Center for Infectious Diseases and Cancer, Chinese Academy of Medical Sciences, Wuhan, China, [4]Cancer Research Institute, General Hospital, Ningxia Medical University, Yinchuan, China

Pancreatic cancer is one of the most lethal malignancies and currently therapies are severely lacking. In this study, we aimed to establish a novel ferroptosis-related lncRNAs signature to predict the prognosis of patients with pancreatic cancer and evaluate the predictive abilities of candidate lncRNAs. According to The Cancer Genome Atlas (TCGA) database, a total of 182 patients with pancreatic cancer were included in our study. Ferroptosis-related lncRNAs were screened by Pearson correlation analysis with 60 reported ferroptosis-related genes. Through univariate, least absolute shrinkage and selection operator (LASSO) regression and multivariate regression analyses, a novel signature based on five ferroptosis-related lncRNAs(*ZNF236-DT, CASC8, PAN3-AS1, SH3PXD2A-AS1, LINP1*) was constructed. Risk-related differentially expressed genes (DEGs) were subjected to enrichment analyses for Gene Ontology (GO), Kyoto Encyclopedia of Genes and Genomes (KEGG) pathway enrichment analysis. The results revealed that immune cell infiltration, immune-related functions and checkpoints were factors to affect prognoisis of pancreatic cancer. In summary, we identified the prognostic ferroptosis-related lncRNAs(*ZNF236-DT, CASC8, PAN3-AS1, SH3PXD2A-AS1, LINP1*) in pancreatic cancer and these lncRNAs may serve as therapeutic targets for pancreatic cancer.

Keywords: pancreatic cancer, ferroptosis, lncRNAs, clinical prognosis, immune landscape

OPEN ACCESS

Edited by:
Arijit Mukhopadhyay,
University of Salford, United Kingdom

Reviewed by:
Daiwei Wan,
The First Affiliated Hospital of Soochow University, China
Yuting He,
First Affiliated Hospital of Zhengzhou University, China
Gang Yang,
Peking Union Medical College Hospital (CAMS), China

***Correspondence:**
Hengning Ke
kehengning@znhospital.cn

Specialty section:
This article was submitted to RNA, a section of the journal Frontiers in Genetics

Received: *30 September 2021*
Accepted: *31 January 2022*
Published: *07 March 2022*

Citation:
Ping H, Jia X and Ke H (2022) A Novel Ferroptosis-Related lncRNAs Signature Predicts Clinical Prognosis and Is Associated With Immune Landscape in Pancreatic Cancer. Front. Genet. 13:786689. doi: 10.3389/fgene.2022.786689

INTRODUCTION

Pancreatic cancer is one of the most lethal malignancies with a high mortality rate, and the incidence has steadily increased in the past few years. A family history of pancreatic cancer has been considered as an important risk factor for the disease (Raimondi et al., 2009), other risk factors include cigarette smoking, gender, advancing age, diabetes and so on. Early-stage pancreatic cancer is often asymptomatic. Symptoms usually occur after the surrounding tissues has been invaded or tumours metastasized to distant organs. As a result, the disease has already progressed to an advanced stage at the time of diagnosis (Gillen et al., 2010; Kamisawa et al., 2016). So far, surgery is considered the only potentially curative therapy for patients with pancreatic cancer. Unfortunately, many patients eventually experience recurrence after surgery and the impact of pancreatectomy on the quality of life and long-term outcomes is

uncertain (Siegel et al., 2014). Therefore, identifying biomarkers for prognosis are of great clinical significance for patients.

Ferroptosis is a novel form of regulated cell death driven by iron-dependent lipid peroxidation (Xie et al., 2016a). Intracellular iron accumulation and lipid peroxidation are two central events in ferroptosis. Ferroptosis induced by small-molecule compounds or chemical drugs can suppress the growth of many types of tumors and improve the efficacy of chemotherapy, radiotherapy, or immunotherapy. In recent years, it has become a new strategy for treating many types of tumors including those from iron-rich tissues such as pancreas (Eling et al., 2015; Xie et al., 2016b). Research showed that the deletion of a system X_C-subunit, SLC7A11, induced tumor-selective ferroptosis and inhibited pancreatic ductal adenocarcinoma growth (Badgley et al., 2020).

The long non-coding RNAs(lncRNAs) are a class of RNAs with a minimum length of about 200 nucleotides and with non-protein-coding ability (Guttman and Rinn, 2012). The function of lncRNAs is not fully understood. It may be involved in the regulation of genes by affecting translational regulation, histone modifications, or post-transcriptional processes (Huang et al., 2018). Studies have shown that lncRNAs play an important role in the regulation of cell cycle and cell differentiation in, and thus affect the development of tumors (Ramilowski et al., 2020). Research on lncRNAs has become a hot topic, but there are few studies on ferroptosis related lncRNA, especially in pancreatic cancer. In this article, we aimed to establish a novel ferroptosis-related lncRNAs (FRlncRNAs) signature to predict the prognosis of patients with pancreatic cancer and evaluate the predictive abilities of candidate lncRNAs. This study identified multiple ferroptosis-related lncRNAs as potential biomarkers for pancreatic cancer prognosis and further studies will improve current diagnosis, treatment, follow-up and prevention strategies of this disease.

MATERIALS AND METHODS

Dataset

The public RNA sequencing of 182 patients and full clinical information were obtained from the GDC data portal using gdc-client (https://gdc-portal.nci.nih.gov/). The clinical characteristics including (age, gender, clinical grade and clinical stage) and survival overall survival (OS) information. Patients without survival information were excluded from further evaluation. In addition, the expression level of 60 ferroptosis-related genes (ACSL4, AKR1C1, AKR1C2, AKR1C3, ALOX15, ALOX5, ALOX12, ATP5MC3, CARS1, CBS, CD44, CHAC1, CISD1, CS, DPP4, FANCD2, GCLC, GCLM, GLS2, GPX4, GSS, HMGCR, HSPB1, CRYAB, LPCAT3, MT1G, NCOA4, PTGS2, RPL8, SAT1, SLC7A11, FDFT1, TFRC, TP53, EMC2, AIFM2, PHKG2, HSBP1, ACO1, FTH1, STEAP3, NFS1, ACSL3, ACACA, PEBP1, ZEB1, SQLE, FADS2, NFE2L2, KEAP1, NQO1, NOX1, ABCC1, SLC1A5, GOT1, G6PD, PGD, IREB2, HMOX1, ACSF2) were constructed from the dataset.

Identification of Prognostic Ferroptosis-Related lncRNAs

Based on the lncRNA annotation file downloaded from the GENCODE (https://www.gencodegenes.org/human/) website and Ensemble IDs, we annotated 14,086 lncRNAs and 19,604 mRNAs according in the TCGA datdset. Pearson correlation analysis was used to evaluate the ferroptosis-related lncRNA. LncRNAs with p value <0.01 and an absolute Pearson correlation coeffcient≥ 0.4 or ≤0.4 were selected as ferroptosis-related lncRNAs. Then, the univariate cox regression analysis was used to screen out the prognostic lncRNAs($p < 0.05$).

Prognostic Score Risk Model Based on Independent Prognostic Ferroptosis-Related LncRNAs

The risk model was constructed through the Least Absolute Shrinkage and Selection operator (LASSO) and multivariate Cox regression analysis. To improve the accuracy of the statistical model, Lasso Cox regression analysis was carried out by using the R package "glmnet". There are 10 ferroptosis-related lncRNAs were screened to construct the best prognostic model through the multivariate Cox regression analysis. The risk score was generated using the following formula:

$$\textbf{risk score} = \sum \textbf{CoeflncRNAs} \times \textbf{ExplncRNAs}$$

All patients were divided into high-risk and low-risk groups according to the median cutoff of risk score.

Survival Analysis

The Kaplan-Meier survival method was applied to evaluate the availability of the prognostic model and all the statistical analyses were conducted using R language (version 4.0). In addition, the area under the ROC curve (AUC) was calculated to evaluate the prognostic accuracy and sensitivity of the model. Survival analysis was also performed for the five crucial lncRNAs(*ZNF236-DT, CASC8, PAN3-AS1, SH3PXD2A-AS1, LINP1*) respectively in the model. We divided pancreatic cancer patients into different subgroups and compared whether there were differences in risk scores among the groups.

Establishment a Nomogram

Nomogram is a tool that can personally calculate the survival rate of patients with specific tumors and has great value in clinical application (Park, 2018). So, we constructed a nomogram to help clinicians conveniently use our model to predict the overall survival at 1, 3, and 5 years of patients with pancreatic cancer. The nomogram is completed by use the R package "rms", "Hmisc", it includes risk score, age, gender, grade and stage.

Functional Enrichment Analysis

We identified differentially expressed genes (DEGs) between low-risk and high-risk subgroups in the TCGA cohort in order to investigate potential biological functions and pathways between the two groups. All the DEGs in the study were performed for Gene Ontology (GO) and Kyoto Encyclopedia of Genes and

Genomes (KEGG) pathway enrichment analysis by using the clusterProfile R package, which the results with $p < 0.05$ were considered significant.

Evaluation of the Immune Landscape

The proportion of tumor-infiltrating immune cells between two risk groups were calculated by CIBERSORT, ESTIMATE, single-sample gene set enrichment analysis (ssGSEA) algorithms based on FRlncRNAs signature. The results were filtered with p value < 0.05.

Immune checkpoints are the immunosuppressive pathways that immune cells possess to regulate and control the persistence of the immune responses (Abril-Rodriguez and Ribas, 2017). The up-regulation of immune checkpoint protein is also one of the mechanisms by which tumor cells evade immune responses (Pardoll, 2012). In recent years, checkpoint blockade therapies have become a new type of cancer treatment. Thus, we investigated whether there were differences in the expression of immune checkpoint genes between the two risk groups, which aimed to investigate the potential role of FRlncRNAs signature in immune checkpoint blockade therapy.

Finally, we used a variety of currently acknowledged methods to analyze the relationship between risk and immune-cell characteristics, including XCELL, TIMER, QUANTISEQ, MCPOUNTER, EPIC, CIBERSORT-ABS and CIBERSORT. The relationship between the risk score and the immune infiltrated cells was performed by Spearmen correlation analysis. The correlation coefficient is bounded by 0 and the results were shown in a lollipop diagram.

Cell Culture and Knockdown of SH3PXD2A-AS1 and LINP1

Human pancreatic cancer cells PANC-1 were used in our experiment. Cells were cultured in high-glucose Dulbecco's Modified Eagle's Medium (supplemented with 10% fetal bovine serum and 1% penicillin/streptomycin) at 37°C and 5% CO2 in a cell incubator. The siRNA against SH3PXD2A-AS1 (siSH3PXD2A-AS1), the LINP1(siLINP1) and the control siRNA (siNC) were purchased from RiboBio Corporation (Guangzhou, China). The siRNAs transfection were performed using Lipofectamine 2000 transfection reagent. The sequence of siLINP1 and siSH3PXD2A-AS1 were showed below:

siLINP1

5′-CCAACTGCGGGACTTCAGA dTdT-3′(sense), 5′-TCT GAAGTCCCGCAGTTGG dTdT- 3′(antisense).

siSH3PXD2A-AS1

5′-CCCTAAGGACAGAATGCAA dTdT-3′(sense), 5′- TTG CATTCTGTCCTTAGGG dTdT- 3′(antisense).

Wound Healing Assay

PANC-1 cells were grown in six-well plates until they formed a tight cell monolayer. A 200ul sterile tip was used to form a wound in the middle of the cell. Cells were then cultured in medium supplemented with 2% FBS. The width of wounds were photographed using a microscope at 0 and 24 h. The percentage of wound healing was generated using the following formula: average of ([gap area: 0 h]–[gap area: 24 h])/[gap area: 0 h]).

Transwell Assay

Firstly, PANC-1 cells in 200 μl of serum-free DMEM were incubated to the upper chamber which is coated with Matrigel, 500 μl of complete medium was placed in the lower chamber. The upper chambers containing non-invasive cells were removed with cottons swabs after 48 h. Then, the lower chamber was fixed with 4% paraformaldehyde and stained in crystal violet. The chambers were observed under microscope.

Cell Proliferation Assay

For Cell Counting Kit-8 (CCK-8) assays, cells transfected for 48 h were collected and seeded into a 96-well plate. According to the instructions, the optical density (OD) values were measured at a 450-nm wavelength after the cells were incubated for 2 h at 37°C.

RESULTS

Identification of Ferroptosis-Related lncRNAs in Pancreatic Cancer

There are a total of 182 patients from the TCGA dataset who were identified and included in this study. 14,086 lncRNAs in the TCGA datasets were obtained by matching the lnRNA annotation with the ENSEMBL ID downloaded from the "GENCODE" website. 60 ferroptosis-related genes were collected from the published literature for subsequent analysis. LncRNAs with p value < 0.01 and an absolute Pearson correlation coeffcient ≥ 0.4 or ≤ 0.4 were selected as ferroptosis-related lncRNAs. Among 246 ferroptosis-related lncRNAs, 89 lncRNAs were identified as prognostic ferroptosis-related lncRNAs through the univariate cox regression analysis ($p < 0.05$). The research process is shown in **Figure 1A** and the forest map of these 89 lncRNAs is shown in **Figure 1B**.

Construction of the Ferroptosis-Related lncRNAs Signature (FRLS) in the TCGA Dataset

To build the FRLS for the patients of pancreatic cancer in TCGA dataset, the above 89 prognostic ferroptosis-related lncRNAs were incorporated into the least absolute shrinkage and selection operator (LASSO) regression firstly (**Figures 1C,D**). 10 ferroptosis-related lncRNAs including *ZNF236-DT, AC005332.6, AC019186.1, AC087501.4, CASC8, PAN3-AS1, LINC01133, SH3PXD2A-AS1, LINP1, AC090114.2* were generated. To further optimize the results, we performed the multivariate Cox regression analysis to construct a prognostic model for OS using the expression level of the 10 ferroptosis-related lncRNAs. An optimal 5 lncRNAs (*ZNF236-DT, CASC8, PAN3-AS1, SH3PXD2A-AS1, LINP1*) signature and coefficient of each were identified (**Figures 1E,F**). The forest plot shows that *ZNF236-DT* and *PAN3-AS1* are protective factors with HR (Hazard Ratio) < 1, while *CASC8, SH3PXD2A-AS1* and *LINP1* are risk factors with HR > 1 (**Figure 1E**). The patients were

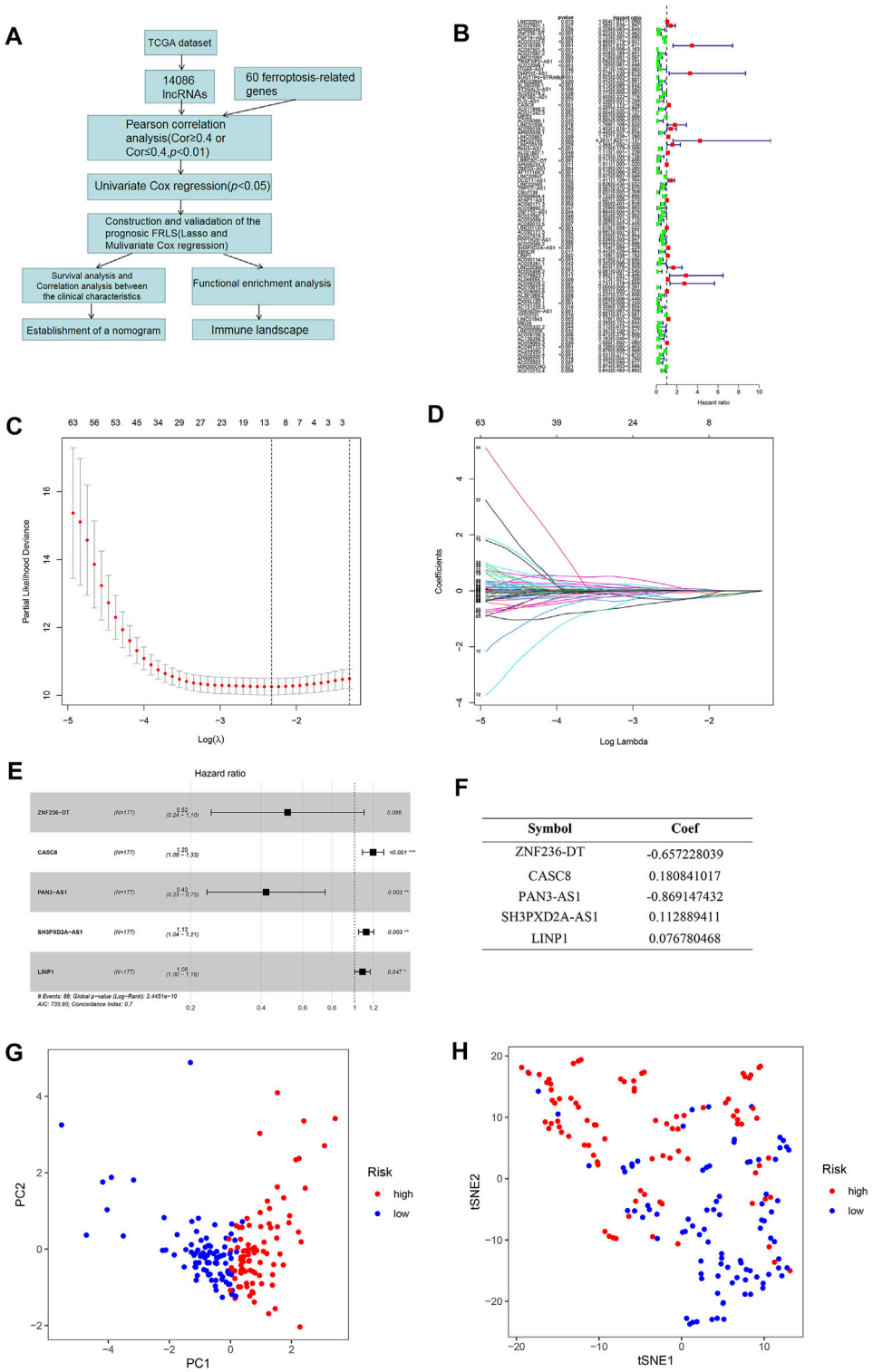

FIGURE 1 | (A) The flow diagram of the research process. **(B)** Forest plots revealed prognosis-related ferroptosis-related lncRNAs based on the results of univariate Cox regression. **(C,D)** The least absolute shrinkage and selection operator (LASSO) regression was performed with the minimum criteria. An optimal log λ value is indicated by the vertical black line in the plot. **(E)** The forest plot of the multivariate Cox regression analysis. **(F)** The coefficients of five selected ferroptosis-related lncRNAs measured by the multivariate Cox. **(G)** PCA plot showing the distribution of the established FRLS expression in different risk groups. **(H)** t-SNE plot showing the distribution of the patients in different risk groups.

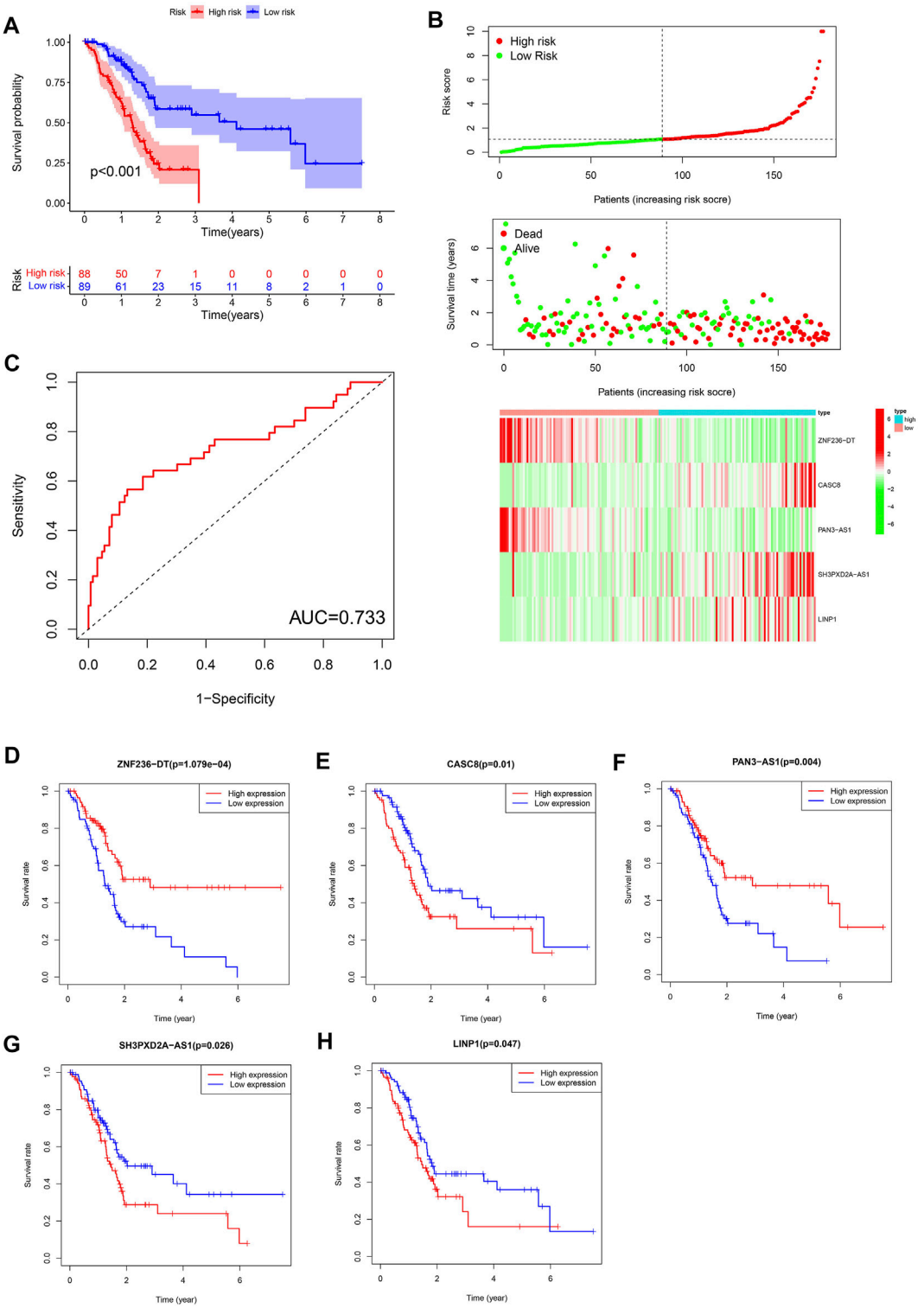

FIGURE 2 | (A) Kaplan-Meier curves for the overall survival of patients in the high- and low-risk groups in the TCGA cohort. **(B)** Distributions of risk scores, survival status and expression of five ferroptosis-related lncRNAs in the TCGA dataset. **(C)** The receiver operating characteristic (ROC) curve analyses of the prognostic FRLS in the TCGA cohorts. **(D–H)** Kaplan-Meier curves analyzed on the correlation between the expression of the five crucial lncRNAs and the prognosis of pancreatic cancer.

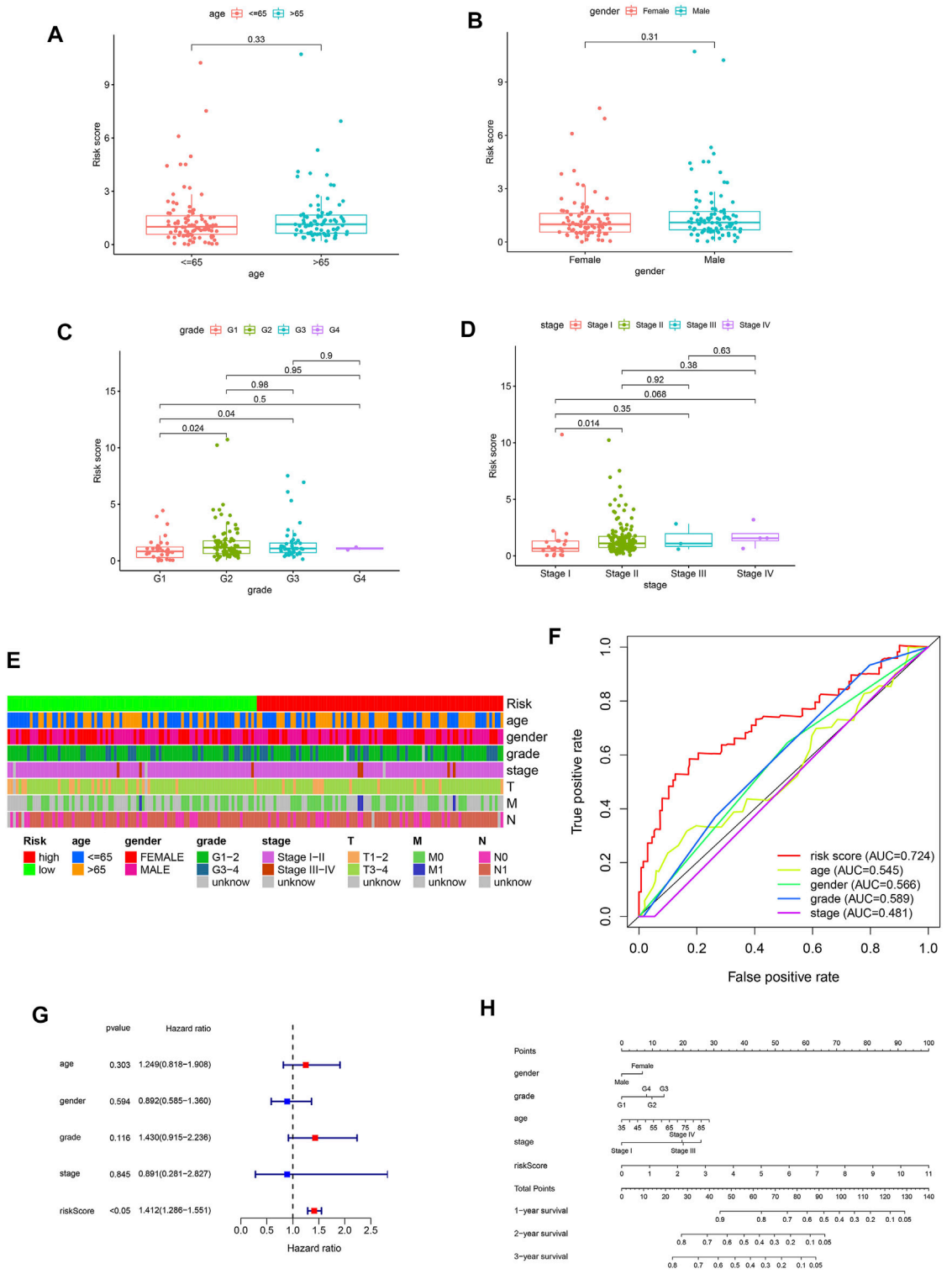

FIGURE 3 | (A–D) Different levels of risk scores in pantients with pancreatic cancer stratified by age,gender, grade and stage. **(E)** A strip chart of the associations between risk score and clinicopathological features in the TCGA dataset. **(F)** The receiver operating characteristic (ROC) curves for the risk score, age, gender, grade and stage in the TCGA dataset. **(G)** Results of the univariate Cox regression analysis regarding OS in the TCGA cohort. Risk score was the only independent prognostic parameter. **(H)** Nomogram based on risk score, age, gender, grade and stage.

further divided into high-risk group (n = 88) and low-risk group (n = 89). The groups were generated by the formula mentioned in section "*Materials and Methods*". Principal Component Analyses (PCA) showed a significant distribution difference between high- and low-risk subgroups (**Figures 1G,H**).

The Kaplan-Meier survival analysis showed that the high-risk group (n = 88) had a lower probability of survival and a shorter overall survival (OS) time than patients in the low-risk group (n = 89) (**Figure 2A**). The area under ROC curve (AUC) reached 0.733, which demonstrated that the FRLS could be used to predict OS in the TCGA cohort (**Figure 2C**). Risk score, survival status and heatmap are plotted in **Figure 2B**. Then, the 5 crucial lncRNAs(*ZNF236-DT, CASC8, PAN3-AS1, SH3PXD2A-AS1, LINP1*) of the FRLS were evaluated by survival analysis. The Kaplan–Meier survival curves confirmed the forest plot shown in **Figure 1E**, which means higher expressions of *ZNF236-DT, PAN3-AS1* and lower expressions of *CASC8, SH3PXD2A-AS1* and *LINP1* were associated with better overall survival (OS) (**Figures 2D–H**).

Correlation Analysis Between the FRLS and Clinicopathological Features

To further assess the prognostic efficacy of FRLS, we divided patients into various subgroups based on clinicopathological features and compared the levels of risk score between different groups. No risk score differences were observed between patients satisfied by gender and age (age was divided by 65 years old) (**Figures 3A,B**). But the results suggested that patients with the clinicopathological characteristics of grade 2 and 3, stage II have higher levels of risk score compared with other corresponding subgroups (**Figures 3C,D**). Thus, FRLS may have certain predictive value for clinicopathological features. The heatmap in **Figure 3E** further shows the distribution of clinicopathological characteristics and the risk groups.

Afterward, we have used univariate and multivariate Cox analyses to identify independent prognostic factors indicator. The results of univariate Cox and multivariate Cox regression analysis showed that only the risk score was significantly associated with OS in TCGA dataset (univariate Cox analyses: HR = 1.412, 95% CI = 1.286–1.551, $p < 0.05$) (**Figure 3G**). As shown in **Figure 3F**, the AUC value of the risk score was 0.724, higher than the AUC values of other clinicopathological factors. These results confirmed the FRLS is an independent and reliable prognostic indicators for pancreatic cancer.

In summary, we constructed a nomogram using the risk score (based on FRLS) and clinicopathological features, including age, gender, WHO grade and stage in the TCGA dataset (**Figure 3H**).

Functional Enrichment Analysis

To investigate potential biological functions and pathways between the two risk subgroups, we performed functional enrichment analysis of the differentially expressed genes (DEGs) between the two groups. There are 973 DEGs [|log2 (fold change)| > 1 and $p < 0.05$] between the low- and high-risk subgroups. Interestingly, the GO analysis revealed that the DEGs were highly enriched in several immune-related biological processes, including immune response-activating cell surface receptor signaling pathway, immune response-activating signal transduction, humoral immune response, lymphocyte mediated immunity, complement activation, B cell receptor signaling pathway (**Figure 4A**). Similarly, the KEGG analysis also showed significant enrichment of DEGs in immune-related pathways, for instance, cytokine-cytokine receptor interaction, chemokine signaling pathway, T cell receptor signaling pathway, B cell receptor signaling pathway (**Figure 4B**).

Correlation of the Prognostic FRLS With the Immune Landscape

Since the KEGG and GO analysis suggested that DEGs were enriched in immune-related functions and pathways, we further investigated the immune landscape in TCGA dataset. The ESTIMATE algorithm showed that the immune score, stromal score and ESTIMATE score were all higher in the low-risk group than in the high-risk group (**Figures 5A–C**). These results also suggest that tumor purity was lower in the low-risk group than in the high-risk group.

Moreover, the CIBERSORT algorithm was used to analyze the 22 different immune cell types among the two risk group. As shown in **Figures 5B,D** cell naive, T cell CD8 and T cells regulatory (Tregs) were up-regulated in the low risk subgroup of the TCGA cohort, while NK cells activated and mast cell resting were significantly down-regulated ($p < 0.05$). Next,we further analyzed the correlation between FRLS and immune cells. The results indicated that this signature was most significantly positive correlation with immune infiltration of Macrophages M0(Cor = 0.25, p = 0.004), Macrophages M1(Cor = 0.2, p = 0.022), Macrophages M2(Cor = 0.22, p = 0.012) and Mast cells resting (Cor = 0.2, p = 0.02), but negatively correlated with B cells naive (Cor = −0.35, p = 4.5e-05), Plasma cells (Cor = −0.2, p = 0.023), T cells CD4 memory activated (Cor = −0.2, p = 0.022), T cells CD8 (Cor = −0.3, p = 0.00059) and T cells regulatory (Tregs, Cor = −0.27, p = 0.0014) (**Figures 5F–N**). These findings again confirmed that this FRlncRNAs signature was associated to immune cell infiltration in pancreatic cancer.

By using the ssGSEA analysis, we quantified the enrichment scores of immune-related functions in the two risk groups. The results showed that the high-risk group was significantly correlated with most immune-related functions, such as CCR, Check-point, Cytolytic-activity, HLA, Inflammation-promoting, T cell co-inhibition, T cell co-stimulation and Type II IFN Response (**Figure 5E**). Moreover, the expression of immune checkpoint molecules also differed significantly between the two risk groups, such as HHLA2, CD44 and TNFSF9 in the high-risk group were higher than those in the low-risk group, while other molecules were higher in the low-risk group (**Figure 6A**).

Finally, detailed Spearman correlation analysis was conducted. The risk score was positively correlated with common lymphoid progenitor, $CD4^+$ T cells, Macrophage M1, Macrophage M0, Neutrophil, NK cells, Eosinophil and Monocyte. It was inversely associated with most other tumor-infiltrating immune cells (**Figure 6B**).

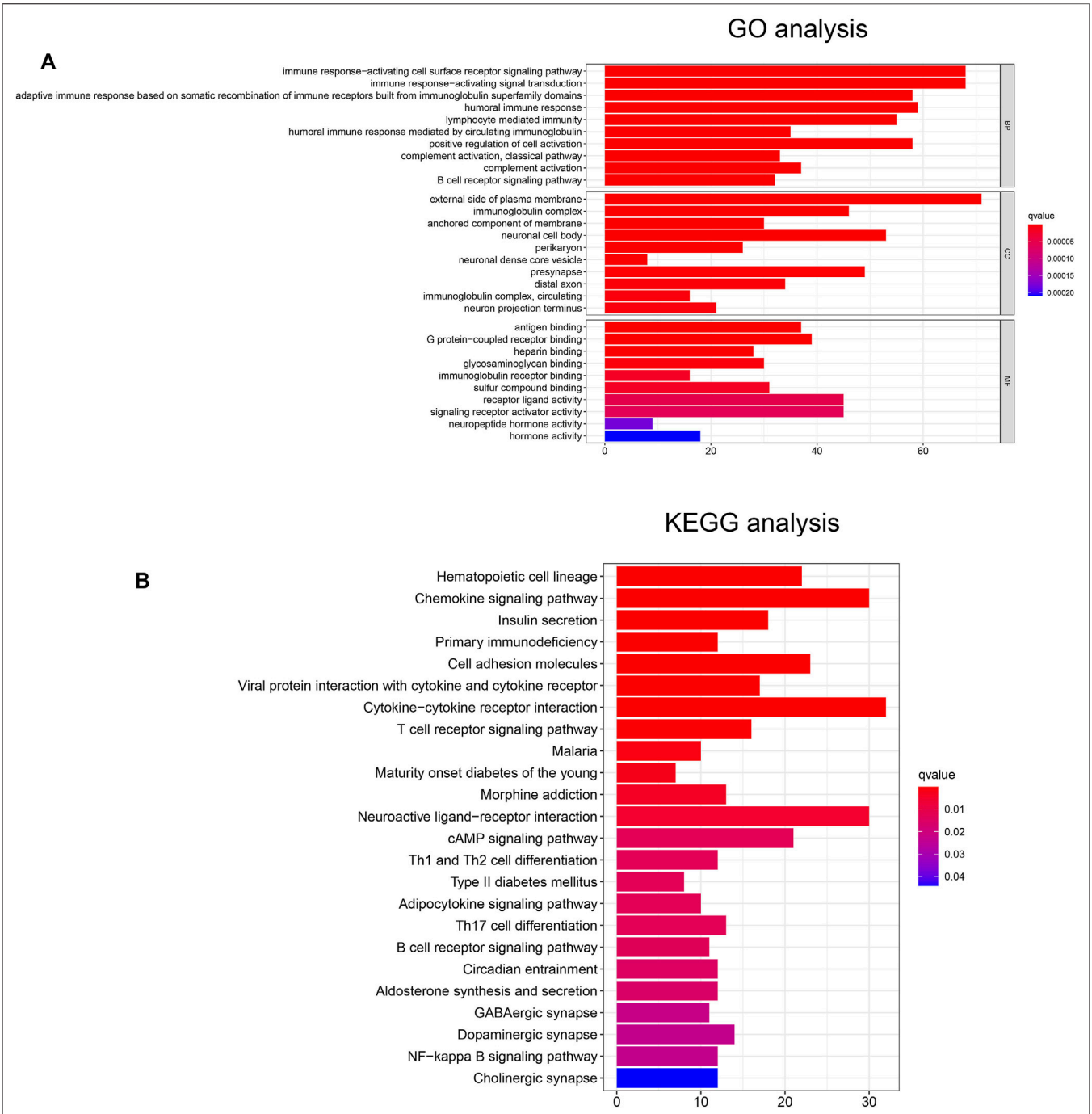

FIGURE 4 | (A) The GO analysis of DEGs between the high- and low-risk groups. **(B)** The KEGG analysis of DEGs between the high- and low-risk groups.

Knockdown of Both LINP1 and SH3PXD2A-AS1 Suppressed Pancreatic Cancer Cell Proliferation, Invasion and Migration

Wound healing assay, transwell assay and cell proliferation assay were performed in order to investigate the effect of LINP1 and SH3PXD2A-AS1 on invasion, migration, and proliferation of pancreatic cancer cells. As shown in **Supplementary Figures S3A,B**, LINP1 and SH3PXD2A-AS1 knockdown in PANC-1 inhibited the wound closure compared to the control cells. Similarly, LINP1 and SH3PXD2A-AS1 knockdown resulted in the decreased of invasive cells and cell viability (**Supplementary Figures S3C–E**) compared to the control group. These results indicated that downregulation of LINP1 and SH3PXD2A-AS1 can inhibit the proliferation, invasion and migration of pancreatic cancer cells.

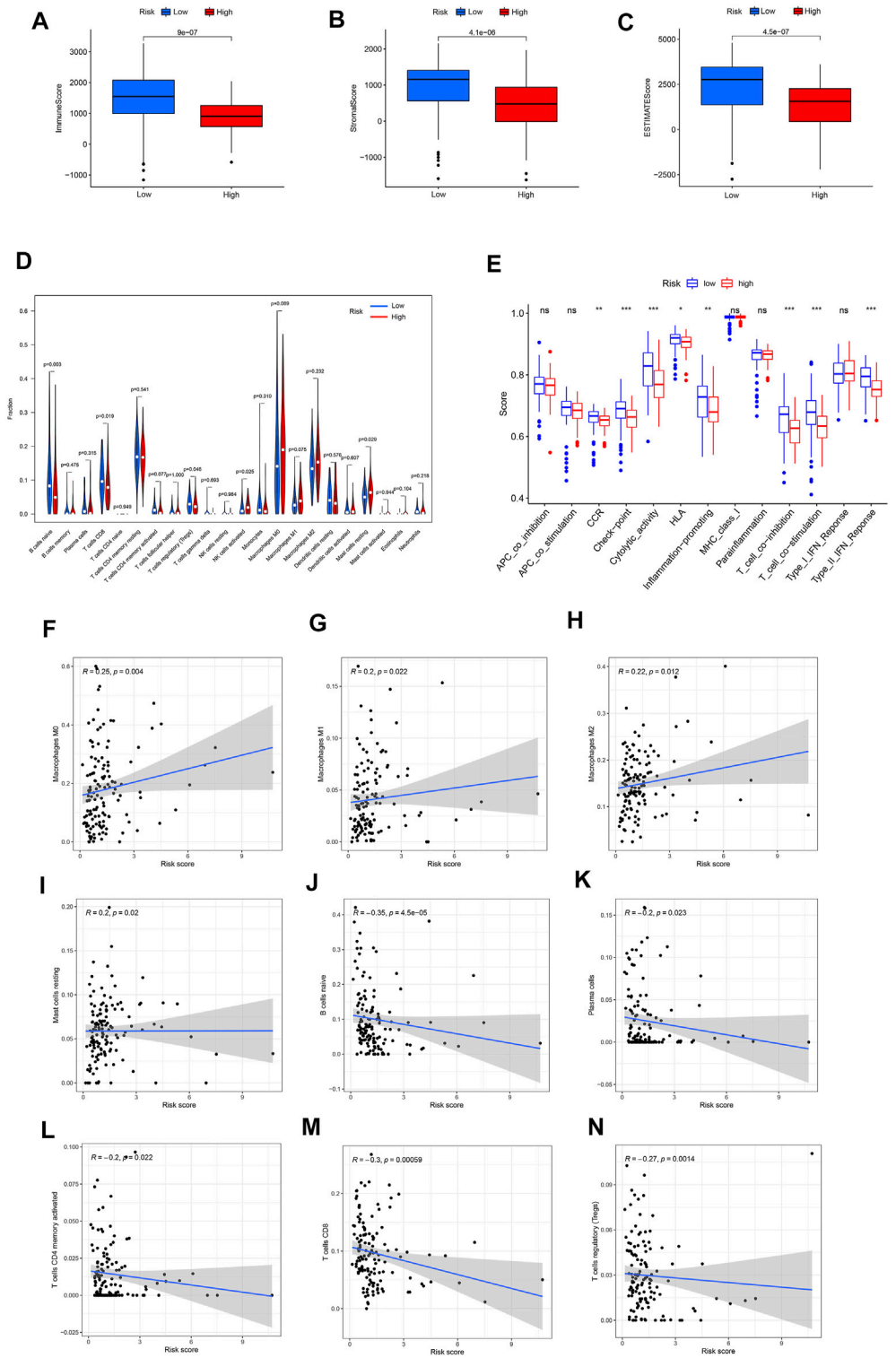

FIGURE 5 | (A–C) Different expression of immune score, stromal score and ESTIMATE score in the high- and low-risk groups. **(D)** Violin plot visualizing the differentially infiltrated immune cells. **(E)** The ssGSEA scores of 13 immune-related functions between different risk groups in the TCGA cohort. **(F–N)** Relationships between the FRLS and infiltration abundances of nine types of immune cells. The correlation was performed by Pearson correlation analysis. **(F)** Macrophages M0; **(G)** Macrophages M1; **(H)** Macrophages M2; **(I)** Mast cells resting; **(J)** B cells naive; **(K)** Plasma cells; **(L)** T cells CD4 memory activated; **(M)** T cells CD8; **(N)** T cells regulatory. Treg, regulatory T cell; APC,antigen presenting cell; CCR, cytokine-cytokine receptor; HLA, human leukocyte antigen; MHC, major histocompatibility complex; IFN, immune interferon; ns, not significant; ***$p < 0.001$; **$p < 0.01$; *$p < 0.05$.

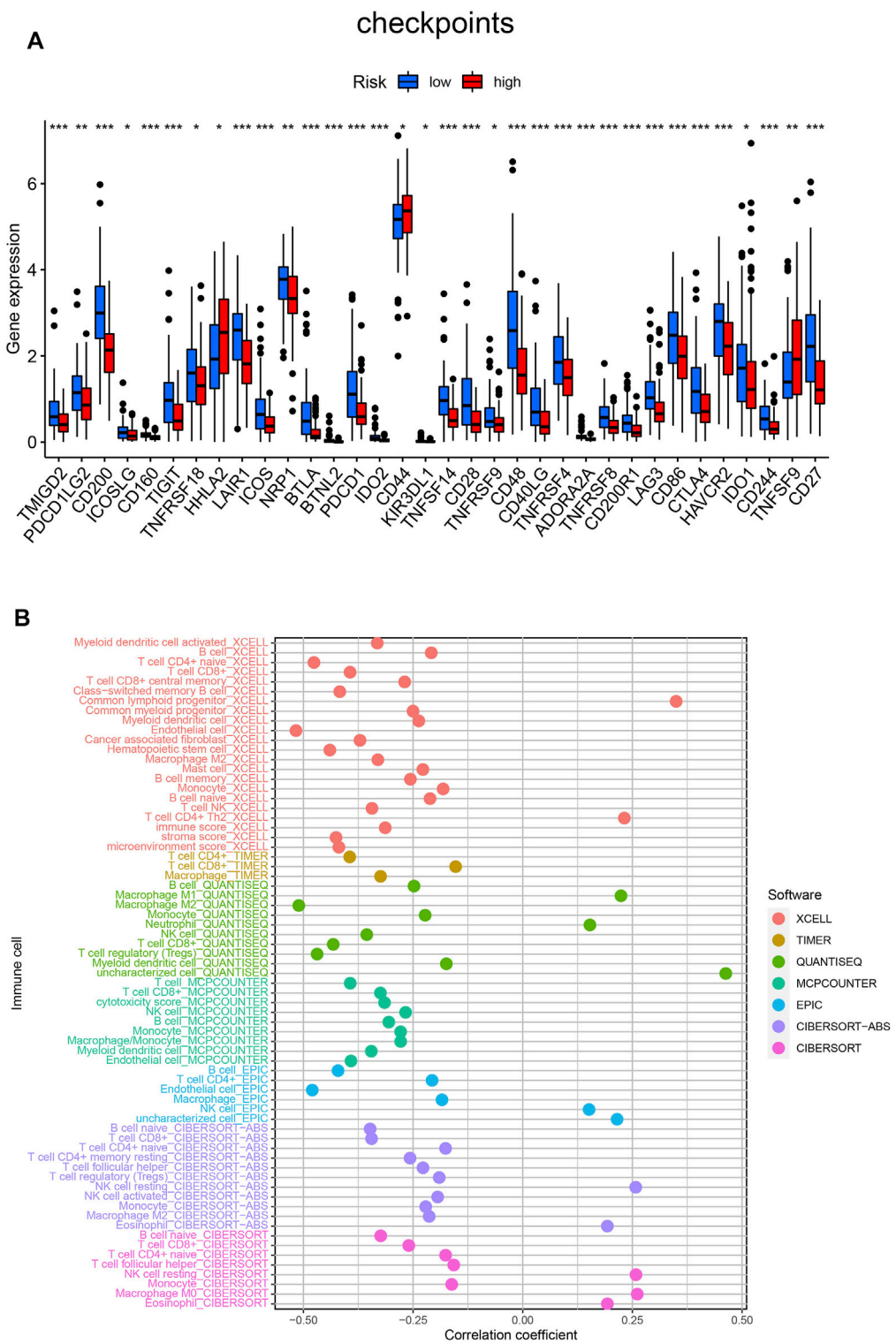

FIGURE 6 | (A) Differences expression of thirty-four immune checkpoints in the two risk groups. **(B)** Estimation of tumor-infiltrating immune cells based on XCELL, TIMER, QUANTISEQ, MCPOUNTER, EPIC, CIBERSORT-ABS and CIBERSORT algorithms. ***$p < 0.001$; **$p < 0.01$; *$p < 0.05$.

DISCUSSION

In this study, a total of 182 patients with pancreatic cancer from the TCGA dataset were included to exploit the prognostic significance of ferrotosis-related lncRNAs. Firstly, we identified 89 prognostic ferroptosis-related lncRNAs through the univariate Cox regression analysis. Under the LASSO regression and multivariate Cox regression analysis, five lncRNAs(*ZNF236-DT, CASC8, PAN3-AS1, SH3PXD2A-AS1, LINP1*) of them were selected to establish the novel prognostic FRLS for predicting the OS of patients with pancreatic cancer. Among the five lncRNAs, *ZNF236-DT* and *PAN3-AS1* are protective factors, while *CASC8*, *SH3PXD2A-AS1* and *LINP1* are risk factors. Secondly, based on the median risk score, patients were divided into the low- and high-risk subgroups and the high-risk group had worse clinical outcomes than patients in the low-risk group. Functional enrichment analysis showed that the DEGs between the two subgroups were highly enriched in several immune-related biological processes and pathways. Finally, we compared the immune and stromal scores, the infiltration of different immune cells and expression levels of immune checkpoint molecules. These results confirmed differences in the immune landscape between the two risk subgroups.

Pancreatic cancer is a malignant tumor with a high mortality rate. So far, the underlying mechanism of pancreatic cancer is not completely understood. A number of studies have revealed the functions and regulatory roles of lncRNAs in pancreatic cancer behaviors. Hisashi Yoshimura revealed that *H19* has important roles in pancreatic cancer metastasis, and that inhibition of *H19* represents a novel candidate for pancreatic cancer therapy (Yoshimura et al., 2018). *SNHG15* could act as an oncogene in pancreatic cancer, further research found that *SNHG15* knockdown inhibited proliferative capacities and suppressed apoptotic rate of pancreatic cancer cells *in vitro*, and impaired *in vivo* tumorigenicity (Ma et al., 2017). In addition, the correlation between immune-related lncRNAs and pancreatic cancer has also been reported in some studies. Zhang et al. (2021) reported that 3 immune-related lncRNA pairs (AC244035.1_vs._AC063926.1, AC066612.1_vs._AC090124.1 and AC244035.1_vs._LINC01885) exhibit effective prognostic prediction performance in pancreatic cancer. However, there are few studies about ferroptosis-related lncRNAs, especially in pancreatic cancer.

In ferroptotic cells, cytological changes mainly include increased mitochondrial membrane density, decrease or disappearance of mitochondrial crest (Yagoda et al., 2007). Ferroptosis is a novel method for the destruction of cancer cells and it can be triggered by some exogenic small molecules, e.g., erastin, Ras-selective lethal small molecule 3, certain clinical drugs and even nano ferroptosis inducers. Notably, ferroptosis has also been shown to be associated with tumor immunotherapy (Wang et al., 2019a). Yu et al. (2021) constructed six ferroptosis-related gene signature prognostic model and this model was proven to be stable and effective in predicting the prognosis of pancreatic cancer.

lncRNAs are part of the noncoding RNAs family and several new studies have suggested that lncRNAs play an important role in ferroptosis of tumors. For instance, long noncoding RNA *LINC00336* was found to inhibit ferroptosis in lung cancer by functioning as a competing endogenous RNA via sponging *miR-6852* (Wang et al., 2019b). In addition, Mao et al. (2018) found that lncRNA *P53RRA* can bind to Ras GTPase-activating protein-binding protein 1 (*G3BP1*) and promote ferroptosis in breast cancer and lung cancer. Among the established 5 ferroptosis-related lncRNAs in this study, three have been found to be associated with tumor development. Silencing *CASC8* inhibited the proliferation, migration, and invasion of non-small cell lung cancer cells and promoted their sensitivity to osimertinib (Jiang et al., 2021). *LINP1* may be involved in the regulation of cell proliferation, cell adhesion and cell cycle-related biological processes in early stage pancreatic ductal adenocarcinoma (Shang et al., 2020). Consistent with the findings of A-Y Chen (Chen et al., 2020), we found that the proliferation, invasion, and migration ability of Pancreatic cancer cells decreased remarkably in LINP1 knockdown group, compared to the si-NC group. These results suggested that LINP1 is important in cancer cell proliferation and invasin. Mechanism studies have found that *SH3PXD2A-AS1* can directly interact with *p53* protein and regulate p53-mediated gene transcription in colorectal cancer, and eventually lead to increased cell proliferation, angiogenesis, and metastasis (Hou et al., 2021). Whatsmore, it has been reported that ferroptosis-related lncRNAs were prognostic risk factors in different types of tumors. Three ferroptosis-related lncRNAs (DUXAP8, LINC02609, and LUCAT1) (Xing et al., 2021) were reported to significantly correlate with the overall survival and clinicopathological features of kidney renal clear cell carcinoma. In another study (Fei et al., 2021), a ferroptosis-related lncRNA prognostic signature (FLPS), which included six ferroptosis-related lncRNAs, provided a new strategy for the prediction of prognosis in lung adenocarcinoma.

The DEGs between the two subgroups of the FRLS were highly enriched in several immune-related biological processes and pathways and the immune score, stromal score were significantly different between the two groups. B cells, $CD8^+$ T cells, Tregs were significantly enriched in the low risk group, NK cells and mast cells were enriched in the high risk group. Among these types of cell, mast cells, B cells and Tregs are antigen presenting cell (APCs) that are capable of presenting processed antigens to T cells and activating the immune response. Besides, it is interesting that the immune-related functions also differed significantly between the two risk groups. These functions are related to the development and treatment of tumors. For instance, Hiraoka et al. (2020) found that the higher expression of HLA-I, HLA-E and HLA-G on pancreatic ductal adenocarcinoma cells is an unfavorable prognosticator. High cytolytic activity was confirmed to associate with increased expression of genes involved in multiple immune checkpoints (with the notable exception of PD-L1) in pancreatic cancer (Balli et al., 2017). Therefore, we assume that ferroptosis is closely related to the immune landscape of microenvironment in pancreatic cancer. However, the potential molecular mechanisms remain to be explored by in-depth experimental researches.

In addition, further analysis found that the low-risk group exhibited higher expression levels of immune checkpoints.

Among these immune checkpoints, therapy that targets programmed death 1 or programmed death 1 ligand 1 (*PD-1/PD-L1*) has been rapidly developing as oncotherapy for various carcinomas, including pancreatic cancer. Whatsmore, *CD200* has been shown to promote immunosuppression in the pancreatic tumor microenvironment and targeting *CD200* may enhance activity of checkpoint immunotherapy (Choueiry et al., 2020). Although immunotherapies such as checkpoint inhibition monotherapy have yet to demonstrate efficacy, a growing body of evidence suggests that combination regimens including chemotherapy could unlock immunotherapy in pancreatic cancer. Our analysis offered the possibility of several potential checkpoint targets for pancreatic cancer, but the mechanism and efficacy remained to be validated in the future.

However, there are several limitations in our study. Firstly, our study is only based on the TCGA public database and the sample size was relatively small. Secondly, our study lacks a validation cohort set and prospective, multicenter, real-world data to be further verified.

CONCLUSION

The present study implicates that several ferroptosis-related lncRNAs(*ZNF236-DT, CASC8, PAN3-AS1, SH3PXD2A-AS1, LINP1*) may serve as independent prognostic biomarkers for pancreatic cancer. And this research provides a theoretical basis for therapeutic targets.

DATA AVAILABILITY STATEMENT

Publicly available datasets were analyzed in this study. This data can be found here: https://portal.gdc.cancer.gov/.

AUTHOR CONTRIBUTIONS

PHQ collected the data and designed the research. JXQ conducted statistical analyses. PHQ drafted the manuscript, KHN revised the manuscript. All authors collected patient data and read and approved the fnal manuscript.

FUNDING

This work was supported by the Natural Science Foundation of China (31760263) and the Non-profit Central Research Institute Fund of the Chinese Academy of Medical Sciences (2020-PT320-004).

SUPPLEMENTARY MATERIAL

The Supplementary Material for this article can be found online at: https://www.frontiersin.org/articles/10.3389/fgene.2022.786689/full#supplementary-material

Supplementary Figure S1 | (A) The characteristics of the external validation cohorts in GEO and ICGC. **(B)** The validation results in the Canadian Pancreatic Cancer dataset of ICGC

Supplementary Figure S2 | The results of internal validation in TCGA database. **(A,B)** The Kaplan-Meier curves for survival in the training cohort and validation cohort. **(C–F)** The distribution plots of the risk score and survival status in the training cohort and validation cohort. **(G–H)** The ROC curve analyses of the prognostic FRLS in the training cohort and validation cohort.

Supplementary Figure S3 | (A,B) Wound healing assay was performed to measure the effect of LINP1 and SH3PXD2A-AS1 downregulation on PANC-1 cell migration. **(C,D)** Transwell assay was performed to measure the effect of LINP1 and SH3PXD2A-AS1 downregulation on PANC-1 cell invasion. **(E)** Cell proliferation assay was performed to measure the effect of LINP1 and SH3PXD2A-AS1 downregulation on PANC-1 cell proliferation. $^{***}P < 0.001$; $^{**}P < 0.01$; $^{*}P < 0.05$.

REFERENCES

Abril-Rodriguez, G., and Ribas, A. (2017). SnapShot: Immune Checkpoint Inhibitors. *Cancer Cell* 31 (6), 848. e1. doi:10.1016/j.ccell.2017.05.010

Badgley, M. A., Kremer, D. M., Maurer, H. C., DelGiorno, K. E., Lee, H.-J., Purohit, V., et al. (2020). Cysteine Depletion Induces Pancreatic Tumor Ferroptosis in Mice. *Science* 368 (6486), 85–89. doi:10.1126/science.aaw9872

Balli, D., Rech, A. J., Stanger, B. Z., and Vonderheide, R. H. (2017). Immune Cytolytic Activity Stratifies Molecular Subsets of Human Pancreatic Cancer. *Clin. Cancer Res.* 23 (12), 3129–3138. doi:10.1158/1078-0432.CCR-16-2128

Chen, A. Y., Zhang, K., and Liu, G. Q. (2020). LncRNA LINP1 Promotes Malignant Progression of Pancreatic Cancer by Adsorbing microRNA-491-3p. *Eur. Rev. Med. Pharmacol. Sci.* 24 (18), 9315–9324. doi:10.26355/eurrev_202009_23013

Choueiry, F., Torok, M., Shakya, R., Agrawal, K., Deems, A., Benner, B., et al. (2020). CD200 Promotes Immunosuppression in the Pancreatic Tumor Microenvironment. *J. Immunother. Cancer* 8 (1), e000189. doi:10.1136/jitc-2019-000189

Eling, N., Reuter, L., Hazin, J., Hamacher-Brady, A., and Brady, N. R. (2015). Identification of Artesunate as a Specific Activator of Ferroptosis in Pancreatic Cancer Cells. *Oncoscience* 2 (5), 517–532. doi:10.18632/oncoscience.160

Fei, X., Hu, C., Wang, X., Lu, C., Chen, H., Sun, B., et al. (2021). Construction of a Ferroptosis-Related Long Non-coding RNA Prognostic Signature and Competing Endogenous RNA Network in Lung Adenocarcinoma. *Front. Cel Dev. Biol.* 9, 751490. doi:10.3389/fcell.2021.751490

Gillen, S., Schuster, T., Meyer zum BüschenfeldeBüschenfelde, C. C., Friess, H., and Kleeff, J. (2010). Preoperative/neoadjuvant Therapy in Pancreatic Cancer: a Systematic Review and Meta-Analysis of Response and Resection Percentages. *Plos Med.* 7 (4), e1000267. doi:10.1371/journal.pmed.1000267

Guttman, M., and Rinn, J. L. (2012). Modular Regulatory Principles of Large Non-coding RNAs. *Nature* 482 (7385), 339–346. doi:10.1038/nature10887

Hiraoka, N., Ino, Y., Hori, S., Yamazaki-Itoh, R., Naito, C., Shimasaki, M., et al. (2020). Expression of Classical Human Leukocyte Antigen Class I Antigens, HLA-E and HLA-G, Is Adversely Prognostic in Pancreatic Cancer Patients. *Cancer Sci.* 111 (8), 3057–3070. doi:10.1111/cas.14514

Hou, P., Lin, T., Meng, S., Shi, M., Chen, F., Jiang, T., et al. (2021). Long Noncoding RNA SH3PXD2A-AS1 Promotes Colorectal Cancer Progression by Regulating P53-Mediated Gene Transcription. *Int. J. Biol. Sci.* 17 (8), 1979–1994. doi:10.7150/ijbs.58422

Huang, Q., Yan, J., and Agami, R. (2018). Long Non-coding RNAs in Metastasis. *Cancer Metastasis Rev.* 37 (1), 75–81. doi:10.1007/s10555-017-9713-x

Jiang, X., Guan, J., Xu, Y., Ren, H., Jiang, J., Wudu, M., et al. (2021). Silencing of CASC8 Inhibits Non-small Cell Lung Cancer Cells Function and Promotes Sensitivity to Osimertinib via FOXM1. *J. Cancer* 12 (2), 387–396. doi:10.7150/jca.47863

Kamisawa, T., Wood, L. D., Itoi, T., and Takaori, K. (2016). Pancreatic Cancer. *The Lancet* 388 (10039), 73–85. doi:10.1016/S0140-6736(16)00141-0

Ma, Z., Huang, H., Wang, J., Zhou, Y., Pu, F., Zhao, Q., et al. (2017). Long Non-coding RNA SNHG15 Inhibits P15 and KLF2 Expression to Promote

Pancreatic Cancer Proliferation through EZH2-Mediated H3K27me3. *Oncotarget* 8 (48), 84153–84167. doi:10.18632/oncotarget.20359

Mao, C., Wang, X., Liu, Y., Wang, M., Yan, B., Jiang, Y., et al. (2018). A G3BP1-Interacting lncRNA Promotes Ferroptosis and Apoptosis in Cancer via Nuclear Sequestration of P53. *Cancer Res.* 78 (13), 3484–3496. doi:10.1158/0008-5472.CAN-17-3454

Pardoll, D. M. (2012). The Blockade of Immune Checkpoints in Cancer Immunotherapy. *Nat. Rev. Cancer* 12 (4), 252–264. doi:10.1038/nrc3239

Park, S. Y. (2018). Nomogram: An Analogue Tool to Deliver Digital Knowledge. *J. Thorac. Cardiovasc. Surg.* 155 (4), 1793. doi:10.1016/j.jtcvs.2017.12.107

Raimondi, S., Maisonneuve, P., and Lowenfels, A. B. (2009). Epidemiology of Pancreatic Cancer: an Overview. *Nat. Rev. Gastroenterol. Hepatol.* 6 (12), 699–708. doi:10.1038/nrgastro.2009.177

Ramilowski, J. A., Yip, C. W., Agrawal, S., Chang, J. C., Ciani, Y., Kulakovskiy, I. V., et al. (2020). Functional Annotation of Human Long Noncoding RNAs via Molecular Phenotyping. *Genome Res.* 30 (7), 1060–1072. doi:10.1101/gr.254219.119

Shang, L.-M., Liao, X.-W., Zhu, G.-Z., Huang, K.-T., Han, C.-Y., Yang, C.-K., et al. (2020). Genome-wide RNA-Sequencing Dataset Reveals the Prognostic Value and Potential Molecular Mechanisms of lncRNA in Non-homologous End Joining Pathway 1 in Early Stage Pancreatic Ductal Adenocarcinoma. *J. Cancer* 11 (19), 5556–5567. doi:10.7150/jca.39888

Siegel, R., Ma, J., Zou, Z., and Jemal, A. (2014). Cancer Statistics, 2014. *CA A Cancer J. Clinicians* 64 (1), 9–29. doi:10.3322/caac.21208

Wang, M., Mao, C., Ouyang, L., Liu, Y., Lai, W., Liu, N., et al. (2019). Long Noncoding RNA LINC00336 Inhibits Ferroptosis in Lung Cancer by Functioning as a Competing Endogenous RNA. *Cell Death Differ* 26 (11), 2329–2343. doi:10.1038/s41418-019-0304-y

Wang, W., Green, M., Choi, J. E., Gijón, M., Kennedy, P. D., Johnson, J. K., et al. (2019). CD8+ T Cells Regulate Tumour Ferroptosis during Cancer Immunotherapy. *Nature* 569 (7755), 270–274. doi:10.1038/s41586-019-1170-y

Xie, Y., Hou, W., Song, X., Yu, Y., Huang, J., Sun, X., et al. (2016a). Ferroptosis: Process and Function. *Cel Death Differ* 23 (3), 369–379. doi:10.1038/cdd.2015.158

Xie, Y., Song, X., Sun, X., Huang, J., Zhong, M., Lotze, M. T., et al. (2016b). Identification of Baicalein as a Ferroptosis Inhibitor by Natural Product Library Screening. *Biochem. Biophysical Res. Commun.* 473 (4), 775–780. doi:10.1016/j.bbrc.2016.03.052

Xing, X.-L., Yao, Z.-Y., Ou, J., Xing, C., and Li, F. (2021). Development and Validation of Ferroptosis-Related lncRNAs Prognosis Signatures in Kidney Renal clear Cell Carcinoma. *Cancer Cel Int* 21 (1), 591. doi:10.1186/s12935-021-02284-1

Yagoda, N., von Rechenberg, M., Zaganjor, E., Bauer, A. J., Yang, W. S., Fridman, D. J., et al. (2007). RAS-RAF-MEK-dependent Oxidative Cell Death Involving Voltage-dependent Anion Channels. *Nature* 447 (7146), 865–869. doi:10.1038/nature05859

Yoshimura, H., Matsuda, Y., Yamamoto, M., Michishita, M., Takahashi, K., Sasaki, N., et al. (2018). Reduced Expression of the H19 Long Non-coding RNA Inhibits Pancreatic Cancer Metastasis. *Lab. Invest.* 98 (6), 814–824. doi:10.1038/s41374-018-0048-1

Yu, X., Zheng, Q., Zhang, M., Zhang, Q., Zhang, S., He, Y., et al. (2021). A Prognostic Model of Pancreatic Cancer Based on Ferroptosis-Related Genes to Determine its Immune Landscape and Underlying Mechanisms. *Front. Cel Dev. Biol.* 9, 746696. doi:10.3389/fcell.2021.746696

Zhang, Q., Wang, Z., Yu, X., Zhang, M., Zheng, Q., He, Y., et al. (2021). Immune Subtypes Based on Immune-Related lncRNA: Differential Prognostic Mechanism of Pancreatic Cancer. *Front. Cel Dev. Biol.* 9, 698296. doi:10.3389/fcell.2021.698296

Conflict of Interest: The authors declare that the research was conducted in the absence of any commercial or financial relationships that could be construed as a potential conflict of interest.

Publisher's Note: All claims expressed in this article are solely those of the authors and do not necessarily represent those of their affiliated organizations, or those of the publisher, the editors and the reviewers. Any product that may be evaluated in this article, or claim that may be made by its manufacturer, is not guaranteed or endorsed by the publisher.

frontiers in Genetics

ORIGINAL RESEARCH
published: 09 March 2022
doi: 10.3389/fgene.2022.790621

miR-145-5p Inhibits Neuroendocrine Differentiation and Tumor Growth by Regulating the SOX11/MYCN Axis in Prostate cancer

Shuya Ji[1], *Yi Shi*[1], *Lin Yang*[1], *Feng Zhang*[2], *Yong Li*[1]* *and Feng Xu*[1]*

[1]Department of Oncology, Shanghai Pudong New Area Gongli Hospital, Shanghai, China, [2]Department of General Practice, Shanghai Gonghexin Road Community Health Care Service Center, Shanghai, China

Recent studies have shown that the downregulation of miR-145-5p in prostate cancer (PCa) is significantly associated with poor differentiation and prognosis. We aimed to investigate the biological role of miR-145-5p in the neuroendocrine differentiation (NED) of PCa. In this study, TheCancer Genome Atlas was used to identify the association of miR-145-5p with PCa. The functions of miR-145-5p were evaluated using the Cell Counting Kit-8 (CCK-8) assay and cell cycle analysis. We validated changes in cell cycle control by testing the expression of cyclin-related genes by western blot. The luciferase reporter assay was performed to test miR-145-5p-targeting genes and direct transcriptional targets of *SOX11*. The expression of miR-145-5p was found to be significantly downregulated in castration-resistant PCa, and this was correlated with higher Gleason score and prostate-specific antigen. We confirmed these results using PC3 and LNCaP cell lines depicted a gradual decline of miR-145-5p while the cells were cultured under androgen depletion conditions. Moreover, the knockdown of miR-145-5p significantly promoted NED and proliferation of LNCaP cells, whereas overexpression of miR-145-5p significantly inhibited NED and proliferation of LNCaP cells. Mechanistically, we found that *SOX11* was a direct target of miR-145-5p, which regulates *MYCN* might mediate induction of NED and proliferation of LNCaP cells. Furthermore, knockdown of miR-145-5p promoted tumor growth *in vivo*. Our findings suggest that miR-145-5p can inhibit NED and tumor growth by targeting *SOX11*, which regulates the expression of *MYCN*, and that this could be a novel therapeutic strategy for preventing the progression of PCa.

Keywords: castration-resistant prostate cancer, neuroendocrine differentiation, miR-145-5p, SOX11, MYCN

OPEN ACCESS

Edited by:
Deepanjan Paul,
Children's Hospital of Philadelphia, United States

Reviewed by:
Nagalakshmi Nadiminty, University of Toledo, United States
Claus Jürgen Scholz, Laboratory Dr. Wisplinghoff, Germany
Subhashree Nayak, National Institute of Arthritis and Musculoskeletal and Skin Diseases (NIH), United States

***Correspondence:**
Yong Li
xlliyong@sina.com
Feng Xu
finnxu@foxmail.com

Specialty section:
This article was submitted to RNA, a section of the journal Frontiers in Genetics

Received: *07 October 2021*
Accepted: *24 February 2022*
Published: *09 March 2022*

Citation:
Ji S, Shi Y, Yang L, Zhang F, Li Y and Xu F (2022) miR-145-5p Inhibits Neuroendocrine Differentiation and Tumor Growth by Regulating the SOX11/MYCN Axis in Prostate cancer. Front. Genet. 13:790621. doi: 10.3389/fgene.2022.790621

INTRODUCTION

Prostate cancer (PCa) is the world's second most common malignancy among men (Ferlay et al., 2019). In the development and progression of PCa, the androgen receptor (AR) pathway plays a key role (Giguere, 2020). For many decades, androgen deprivation therapy (ADT) has been the standard of care for patients with advanced and metastatic PCa. However, the majority of these patients develop castration-resistant PCa (CRPC) (Bishop et al., 2017). Enzalutamide (Enz) and abiraterone, two novel AR signaling inhibitors, have been approved as first-line treatments for CRPC. However,

the treatment's benefits are short-lived, and resistance develops quickly. Treatment-induced neuroendocrine PCa (NEPC) has been identified as an AR-independent resistance mechanism (Scher et al., 2012; Mu et al., 2017). Several studies have shown that neuroendocrine differentiation (NED) is correlated with tumor progression, poor prognosis, and hormone-refractory stage (Yuan et al., 2007). NEPC is associated with genomic, epigenomic, neuronal and stem cell pathway dysregulation, and epithelial-mesenchymal transition (Yamada and Beltran, 2021). However, to date, the mechanisms leading to NED in PCa progression have not been fully understood.

MicroRNAs (miRNAs) are essential epigenetic modulators in the progression of PCa. MiRNAs bind to specific sequences in the 3′-untranslated region (3′UTR) of mRNAs, causing mRNA degradation, translation, or post-transcriptional suppression, which inhibits transcript expression. Previous research has shown that miR-145-5p has a tumor-suppressing effect and is significantly downregulated in many cancers, including PCa (Avgeris et al., 2013; Xu et al., 2019; Xu et al., 2020). Several studies have used small RNA sequencing to investigate the dysregulated expression of miRNAs in CRPC and found that miR-145-5p contributes to the development of CRPC, suggesting that miR-145-5p may play a role in the NED of PCa progression (Zhu et al., 2015; Goto et al., 2017).

In this study, reduced expression of miR-145-5p was found to be strongly correlated with a higher Gleason score, N stage, and p53 mutation in PCa. In PCa cell lines, miR-145-5p levels were significantly decreased. While LNCaP cells was cultured under androgen depletion conditions, we observed a time-dependent gradual decline in the expression of miR-145-5p. According to gain- and loss-of-function studies, miR-145-5p is involved in NED and the growth of PCa cells. Mechanistically, we found that *SOX11* is a direct target of miR-145-5p, which might mediate miR-145-5p's tumor-suppressive functions by regulating *MYCN* during NED of PCa cells.

MATERIALS AND METHODS

Cell Lines

LNCaP and PC3 cells (Sigma-Aldrich, Hamburg, Germany) were grown in RPMI-1640 media and supplemented with 10% fetal bovine serum (FBS) or 5% charcoal-dextran-stripped FBS and penicillin-streptomycin (100 IU/ml and 100 μg/ml, respectively). All cell lines were cultured at 37°C in a humidified 5% carbon dioxide (CO2) atmosphere. Unless stated otherwise, cells were treated with 10 μM Enz (Selleck, China) for 24 h (Nguyen et al., 2014).

Cell Transfection

Negative control (NC), miR-145-5p mimics, and inhibitor were purchased from GenePharma (Shanghai, China). Small interfering RNAs (siRNA) that specifically target human *SOX11 (si-SOX11)* and nonspecific NC oligonucleotides (si-NC) were purchased from GenePharma (Shanghai, China). According to the manufacturer's instructions, LNCaP cells were transfected with siRNA using Lipofectamine 3000 (Invitrogen; Thermo Fisher Scientific, Inc.,, United States). **Supplementary Table S1** shows the oligonucleotide sequences.

RNA Extraction and Quantitative Real-Time Polymerase Chain Reaction

Trizol reagent (Invitrogen, Carlsbad, CA, United States) was used to extract total RNA from the cell lines according to the manufacturer's protocol. The miRNA First-Strand cDNA Synthesis (Tailing Reaction, Sangon, China) and the PrimeScript RT Reagent Kit (Takara, Japan) were used to reverse transcribe miRNAs and mRNAs into complementary DNA (cDNA).

The ABI Prism 7500 Sequence Detection System (Applied Biosystems, Foster City, CA, United States) was used to perform quantitative PCR (qPCR) amplification using the KAPA SYBR FAST qPCR Kit. **Supplementary Table S1** lists the primer sequences. For miRNAs and mRNAs, target gene expression was normalized to total U6 and actin, respectively.

Target Prediction

The target genes of miR-145-5p were predicted using the miRSystem database (http://mirsystem.cgm.ntu.edu.tw). The miRSystem is a database that integrates DIANA, miRanda, miRBridge, PicTar, PITA, rna22, and TargetScan, which are all well-known miRNA target gene prediction programs (Lu et al., 2012). The MatInspector and JASPAR datasets were used to predict the target genes of transcription factors (Cartharius et al., 2005; Mathelier et al., 2016).

Dual-Luciferase Assay

We constructed the *SOX11*-wild type (*SOX11*-WT) and *SOX11*-mutant (*SOX11*-Mut) 3′-UTR pmirGLO luciferase reporter vectors. HEK293T cells were seeded in 24-well plates and allowed to grow overnight before being transfected. The *SOX11*-WT or *SOX11*-Mut luciferase reporter and miRNA mimic or nonspecific NC were co-transfected into cells. Using Lipofectamine 2000 (Invitrogen; Thermo Fisher Scientific, Inc.,, MA, United States), cells were co-transfected with 0.4 μg pGL4.27-MYCN-promoter reporter plasmid and 0.3 μg pcDNA3.1-hSOX11 effector plasmid. A dual-luciferase reporter assay system was used to measure luciferase activity after incubation for 48 h according to the manufacturer's protocol (Promega, Madison, WI, United States).

Western Blot Analysis

Total protein was lysed from cells using radioimmunoprecipitation assay buffer (RIPA buffer; Beyotime, Shanghai, China) supplemented with protease inhibitors. SDS/PAGE was used to separate 30 μg of total proteins, which were then transferred to a nitrocellulose membrane. The membranes were blocked with 5% non-fat milk and then incubated overnight at 4°C with specific primary antibodies. The membranes were washed and incubated with secondary antibodies at room temperature for 1 h. Electro chemiluminescent detection was used to visualize the protein bands. The expressions of GAPDH and β-actin were used

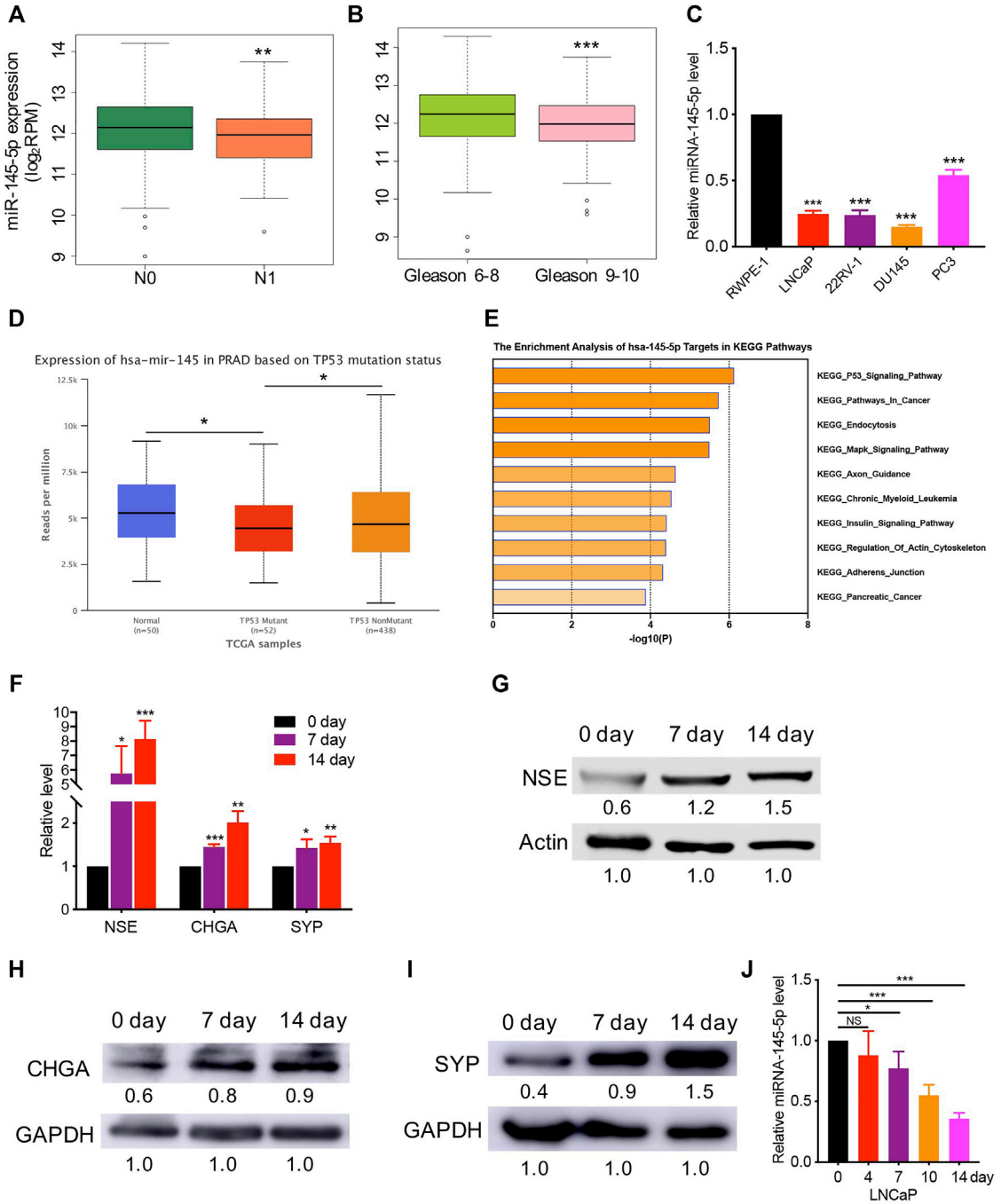

FIGURE 1 | Decreased expression of miR-145-5p has correlated with prostate cancer(PCa) neuroendocrine transdifferentiation. **(A, B)** The decreased expression of miR-145-5p is correlated with lymph node metastasis and a higher Gleason score. **(C)** Quantitative real-time polymerase chain reaction (qRT-PCR) analysis of miR-145-5p expression in PCa cells compared with those in normal cells. **(D)**. Expression level of miR-145-5p in p53 mutation tissues compared to that in p53 nonmutation PCa and normal samples. **(E)** Gene set enrichment analysis of miR-145-5p targets in Kyoto Encyclopedia of Genes and Genomics pathways. **(F–I)** qRT-PCR and western blot analysis of neuroendocrine markers, including NSE, CHGA, and SYP. **(J)** Expression level of miR-145-5p during the neuroendocrine differentiation of LNCaP. The analysis was performed on PCa tumor data extracted from The Cancer Genome Atlas **(A–D)**. $^{*}p < 0.05$, $^{**}p < 0.01$, $^{***}p < 0.001$.

as internal controls. The primary antibodies were used in this study: anti-SOX11 (Santa Cruz, CA, United States), anti-MYCN (#84406, Cell Signaling Technology, United States), anti-p21 (ab109199, Abcam, United States), anti-p27 (ab32034, Abcam, United States), anti-Cyclin D1 (ab134175, Abcam, United States), anti-NSE (ab180943, Abcam, United States), anti-CHGA

(ab68271, Abcam, United States), and anti-SYP (ab32127, Abcam, United States). Quantification of the western blots was performed using ImageJ.

Cell Cycle Analysis

LNCaP-vector, LNCaP-has-miR-145-5p-mimic, and LNCaP-has-miR-145-5p-inhibitor cells transfected with *SOX11* siRNA (GenePharma, Shanghai, China) or NC were treated with Enz for 72 h. Cells were trypsinized, washed, and fixed in 70% ethanol overnight at 4°C. The following day, cells were washed, centrifuged, and stained with propidium iodide (PI) containing RNase in the dark at 37°C for 15 min. The cell cycle distribution was assessed using flow cytometry.

Cell Proliferation Assay

According to the manufacturer's instructions, the CCK-8 assay was used to evaluate cell proliferation (Yeasen, Shanghai, China). The experiment was performed as described previously (Mao et al., 2020).

Mouse Xenograft Studies

Twelve 5 week-old male nude BALB/c mice were obtained from the Shanghai Sipper-BK Laboratory Animal Company (Shanghai, China). The testicles of the mice were surgically removed and split into two groups at random. At 6-weeks after cell inoculation, both groups were subcutaneously inoculated with 3×10^6 PC3 cells (co-suspended with 50% matrigel) stably expressed with sh-miR-145-5p or sh-NC. Mice were sacrificed after 8 weeks, and all tumor xenografts were collected.

Statistical Methods

Statistical analyses were performed using Prism 8 software (GraphPad Software, Inc., La Jolla, CA), and the results are presented as mean ± standard deviation. Error bars represent the normalized standard of the mean for at least three experiments. The analysis of variance was performed using the Student's *t*-test. $p < 0.05$ was considered statistically significant.

RESULTS

Decreased miR-145-5p Expression Is Associated With PCa Neuroendocrine Transdifferentiation

Using The Cancer Genome Atlas (TCGA) data, we discovered that lower miR-145-5p expression was linked to a higher N stage and Gleason score, which is a grading system for determining the aggressiveness of PCa (**Figures 1A,B**). When compared to normal prostatic epithelial cell lines such as RWPE-1, the expression of miR-145-5p is significantly downregulated in PCa cells (**Figure 1C**). The expression of miR-145-5p was significantly downregulated in p53 mutation than in p53 nonmutation PCa, and normal tissues (**Figure 1D**). Gene set enrichment analysis of miR-145-5p targets in Kyoto Encyclopedia of Genes and Genomics pathways showed that starBase online enriched the p53 signal pathway (**Figure 1E**). Moreover, miR-145 is important in the differentiation of human embryonic stem cells (Xu et al., 2009). This research suggests a link between decreased expression of miR-145-5p and NEPC, which could explain the biological behavior of prostatic NED. LNCaP cells, which are androgen-sensitive prostate adenocarcinoma cells, were used to test this hypothesis. After 14 days of androgen depletion, LNCaP cells displayed morphological changes, including neurite-like outgrowths and decreased cell growth (**Supplementary Figure S1A**). RT-qPCR and western blot analysis revealed that the neuroendocrine (NE) markers NSE, CHGA, and SYP were gradually upregulated at both the mRNA and protein levels (**Figures 1F–I**). However, during the NED of LNCaP cells, miR-145-5p gradually decreased (**Figure 1J**). These results suggest that miR-145-5p may be involved in the induction of NEPC.

The Downregulation of miR-145-5p Expression Promotes the NED and Proliferation of PCa Cells

Using miRNA transfection of LNCaP cells, we performed gain- and loss-of-function studies to investigate the role of miR-145-5p on NED of PCa. Indeed, RT-qPCR revealed that downregulation of miR-145-5p promoted the upregulation of NE markers expression compared to cells transfected with NC (**Figures 2A,B**). In comparison to control cells, overexpression of miR-145-5p downregulated the expression of NE markers (**Figures 2C,D**). There was no obvious change in AR protein in LNCaP cells with the knockdown or overexpression of miR-145-5p (**Supplementary Figure S1B**). Furthermore, when miR-145-5p was knocked down, the proliferation of LNCaP cells increased compared to controls (**Figure 2E**). The proliferation assay revealed that the overexpression of miR-145-5p markedly inhibited the proliferation of LNCaP cells compared to NC (**Figure 2F**). To learn more about how miRNA knockdown enhances cell proliferation, we used PI staining and fluorescence-activated cell sorting analysis to look at the cell cycle distribution of transfected LNCaP cells. The proportion of cells in the S phase was significantly higher in miR-145-5p knockdown cells (**Figures 2G,H**), indicating that the knockdown of miR-145-5p resulted in increased cell cycle progression. Using western analysis, we discovered that overexpression of miR-145-5p decreased the expression of Cyclin D1 but increased the expressions of p21 and p27 (**Figure 2I**; **Supplementary Figure S1C**). Moreover, knocking down miR-145-5p increased the expression of Cyclin D1 while decreasing the expressions of p21 and p27 in PCa cells (**Figure 2J**; **Supplementary Figure S1D**). These findings suggested that miR-145-5p inhibited the proliferation of LNCaP cells by regulating the cell cycle progression. We constructed a stable knockdown of miR-145-5p and control cells with shRNA to further determine the effect of miR-145-5p *in vivo* (**Supplementary Figure S1E**). We chose PC3 with NE characteristics for the subcutaneous tumorigenesis experiment because LNCaP cells are difficult to develop into xenograft tumors, *in vivo,* under androgen depletion conditions. The results showed that the knockdown of miR-145-5p in PCa cells promoted tumor growth *in vivo* (**Figures 2K,L**).

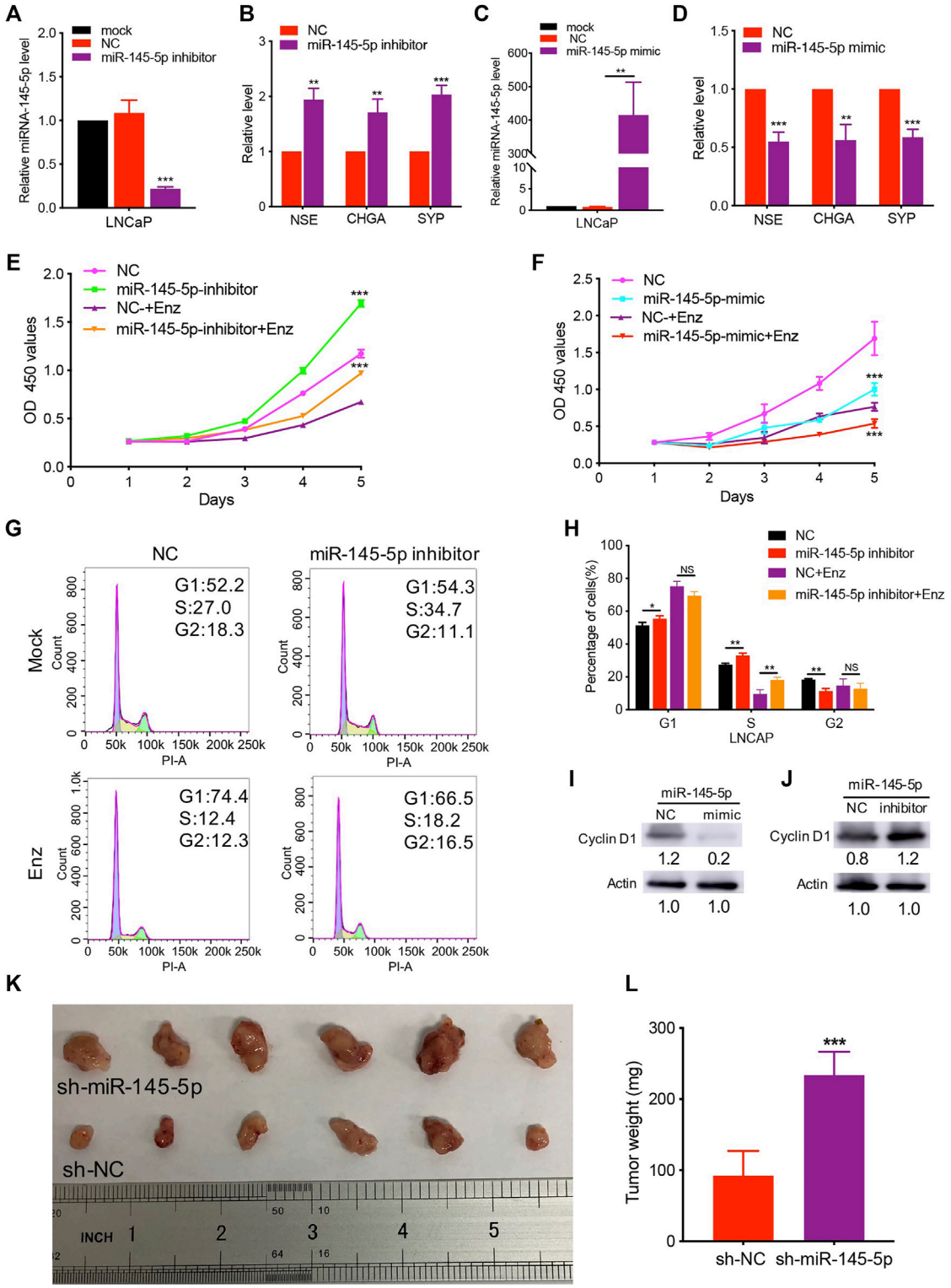

FIGURE 2 | Knockdown of miR-145-5p promoted neuroendocrine differentiation and proliferation of prostate cancer (PCa) cells. **(A)** The results of quantitative real-time polymerase chain reaction (qRT-PCR) show the efficiency of miR-145-5p knockdown. **(B)** qRT-PCR analysis of neuroendocrine (NE) markers in LNCaP cells transfected with miR-145-5p inhibitor or negative control (NC). **(C)** The results of the qPCR show the efficiency of miR-145-5p overexpression. **(D)** qRT-PCR analysis of NE markers in LNCaP cells transfected with miR-145-5p mimics or NC. **(E)** The Cell Counting Kit-8 (CCK-8) proliferation assay shows the proliferation ability of miR-145-5p-knockdown LNCaP cells or control cells with or without enzalutamide (Enz) exposure. **(F)** The CCK-8 proliferation assay shows the proliferation ability of miR-

(*Continued*)

FIGURE 2 | 145-5p-overexpressing LNCaP cells or control cells with or without Enz exposure. **(G, H)** Flow cytometry analysis of the cell cycle of miR-145-5p-knockdown LNCaP cells or control cells with or without Enz exposure. **(I)** Western blot analysis of Cyclin D1 proteins miR-145-5p-overexpressing LNCaP cells or control cells with Enz exposure. **(J)** Western blot analysis of Cyclin D1 proteins miR-145-5p-knockdown LNCaP cells or control cells with Enz exposure. **(K, L)** The results of the subcutaneous xenograft mouse model show that the knockdown of miR-145-5p promoted PCa growth *in vivo*. $^{*}p < 0.05$, $^{**}p < 0.01$, $^{***}p < 0.001$.

These findings showed that the downregulation of miR-145-5p expression promoted the NED and proliferation of PCa cells.

SOX11 Mediates Decreased miR-145-5p-Induced NED of LNCaP Cells

We predicted the targets of miR-145-5p using miRSystem and selected *SOX11* as a potential miR-145-5p target gene (**Supplementary Table S2**). **Figure 3A** illustrates the predicted miRNA interaction sites within the 3′UTR region of *SOX11*. The *SOX11* 3′UTR fragment containing the putative miRNA target site was incorporated into a luciferase reporter vector. *SOX11* luciferase vector and miRNA-145-5p mimics were co-transfected into HEK293T cells. When compared to NC, miR-145-5p significantly reduced the activity of the luciferase reporter gene ($p < 0.05$) under the regulatory control of the *SOX11* 3′UTR fragment (**Figure 3B**). SOX11 mRNA and protein levels were reduced as a result of the upregulation of miR-145-5p (**Figures 3C,D**). Furthermore, knocking down miR-145-5p could upregulate SOX11 mRNA and protein levels (**Figures 3E,F**). Using TCGA data, we validated our *in vitro* findings in a cohort of patients with PCa. In PCa, miR-145-5p has a negative correlation with SOX11 mRNA (**Figure 3G**). Furthermore, increased expression of *SOX11*is correlated to a higher N stage (**Figure 3H**). Subsequently, we performed a Kaplan–Meier analysis on 488 patients and found that higher expression of *SOX11* was associated with shorter disease-free survival (DFS) (log-rank test, $p = 0.0049$, **Figure 3I**).

Next, using RT-qPCR and western blot analysis, we discovered increased *SOX11* expression associated with NED of LNCaP (**Figure 4A**). In comparison to control cells, knockdown of *SOX11* inhibited the expression of NE markers (**Figures 4B,C**). Then, with a miR-145-5p knockdown *SOX11* knockdown rescued the sensitivity of LNCaP cells to Enz, resulting in the decreased proliferation of LNCaP cells compared to controls (**Figure 4D**). Compared with only miR-145-5p-knockdown cells, the proportion of S phase cells was significantly reduced in the double knockdown of miR-145-5p and *SOX11* with or without Enz exposure (**Figures 4E,F**), indicating that *SOX11* mediates knockdown of miR-145-5p and thus promotes cell cycle progression. Together, these findings show that the downregulation of miR-145-5p expression promotes the NED and proliferation of PCa cells by directly upregulating *SOX11*.

miR-145-5p Negatively Regulates *MYCN* by Repressing *SOX11* Expression in NED

We were interested in identifying which mediators are responsible for NED after *SOX11* is knocked out. Using the MatInspector and JASPAR datasets, multiple studies have revealed the *SOX11* targets (Cartharius et al., 2005; Mathelier et al., 2016). In contrast to controls, we found that overexpression of miR-145-5p repressed the expression of *MYCN* in PCa cell lines (**Figure 5A**). Knockdown of miR-145-5p, on the other hand, increased the expression of *MYCN* (**Figure 5B**). PCa samples from TCGA show that *MYCN* was positively correlated with SOX11 mRNA levels (**Figure 5C**). Furthermore, *MYCN* was significantly correlated with the expression of *SOX11* in the CRPC subgroup (**Figure 5D**) and shorter DFS (**Figure 5E**). Western blot analysis confirmed that *SOX11* knockdown decreased the expression of *MYCN* (**Figure 5F**). The double knockdown experiment showed that *SOX11* regulates *MYCN* through miR-145-5p to induce NED (**Figures 5G,H**). However, the luciferase reporter gene experiment showed that *SOX11* did not activate the expression of *MYCN* 2000 bp upstream of the *MYCN* promoter (**Supplementary Figure S1F**). These findings demonstrated that decreased miR-145-5p expression resulted in increased expression of *SOX11* and *MYCN,* promoting the NED and proliferation of PCa cells.

DISCUSSION

The histologic subtype of PCa known as NEPC is extremely aggressive. After treatment with ADT, PCa cells exhibit lineage plasticity, which is a common change in cellular phenotypes (Mu et al., 2017). The emergence and maintenance of NEPC have been linked to many molecular mechanisms, including gene mutations, apparent changes, transcription factors, and other pathways. Genomic alterations in *TP53, Rb1, PTEN,* and *MYCN* have been shown to play a critical role in the development of NEPC (Ge et al., 2020). Apart from these alterations, epigenetic changes, including the aberrant expression of EZH2, CBX2, and HOTAIR have been identified as key drivers of NEPC. Several transcription factors, including BRN2, SOX2, FOXA1, and REST, have been shown to enhance or repress the neuroendocrine lineage phenotype. Other regulators directly or indirectly involved in cell lineage plasticity, such as PRKCI, SRRM4, and AURKA, have been reported in NEPC in addition to genomic alterations, epigenetic regulators, and transcription factors (Wang et al., 2021). miR-145-5p is a well-studied tumor suppressor miRNA that is downregulated in many human cancers, including breast, bladder, and prostate cancer (Ye et al., 2019). Downregulation of miR-145 occurs as a result of DNA methylation and p53 mutation in PCa, suggesting that miR-145-5p might play an important role in the initiation and progression of PCa (Suh et al., 2011). According to emerging evidence, decreased miR-145-5p expression has been linked to the development of mCRPC and a shorter DFS in PCa (Avgeris et al., 2013; Zhu et al., 2015; Goto et al., 2017). Furthermore, by targeting pluripotency factors like OCT4, SOX2, and KLF4 in

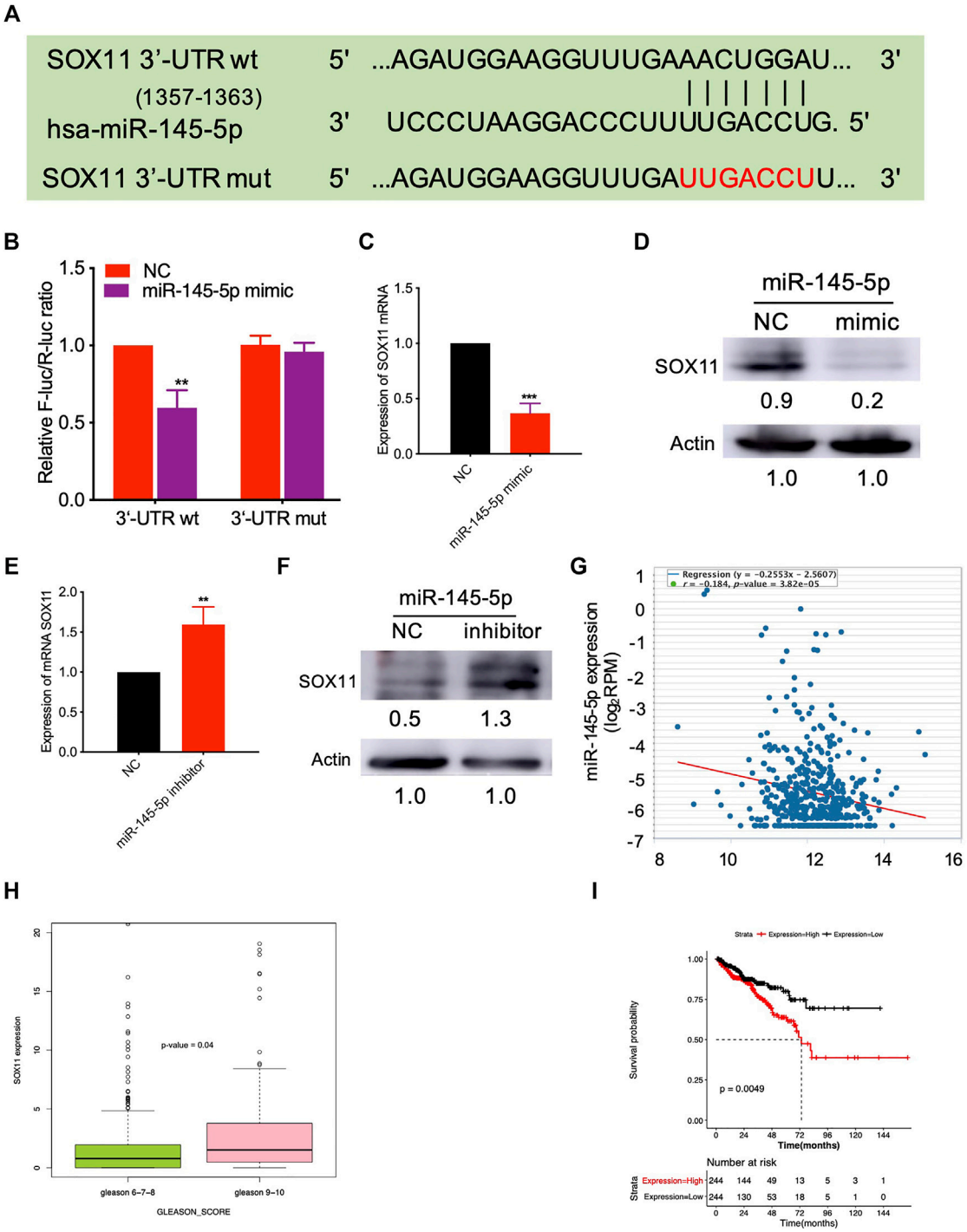

FIGURE 3 | miR-145-5p directly targets *SOX11*. **(A)** Schematic exhibiting the predicted miR-145-5p interaction sites in the 3′UTR region of *SOX11*. **(B)** The luciferase reporter gene assay showed the binding of miR-145-5p to *SOX11* 3′UTR compared to the empty reporter gene vector. **(C, D)** Quantitative real-time polymerase chain reaction (qRT-PCR) and western blot analysis of SOX11 mRNA and protein levels in miR-145-5p-overexpressing LNCaP cells or control cells. **(E, F)** qRT-PCR and western blot analysis of SOX11 mRNA and protein levels in miR-145-5p-knockdown LNCaP cells or control cells. **(G)** The correlation between miR-145-5p and SOX11 mRNA in prostate cancer (PCa) in The Cancer Genome Atlas (TCGA) data by starBase. **(H)** The correlation between SOX11 mRNA and Gleason score in PCa in TCGA data. **(I)** Kaplan–Meier analysis shows the association of *SOX11* expression with disease-free survival of 488 patients with PCa from TCGA data. $^{*}p < 0.05$, $^{**}p < 0.01$, $^{***}p < 0.001$.

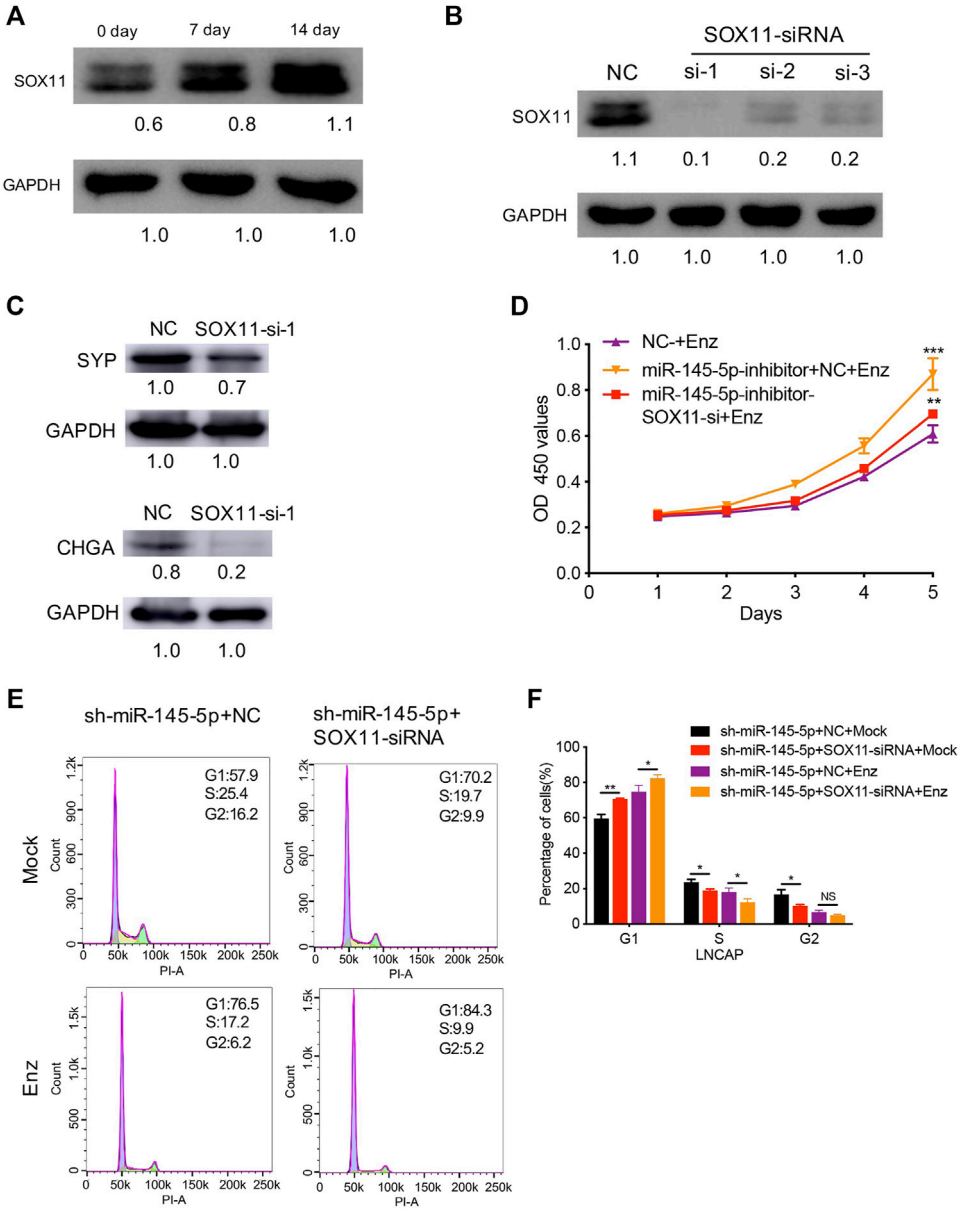

FIGURE 4 | *SOX11* mediates a decrease in miR-145-5p-induced neuroendocrine differentiation (NED) of LNCaP cells. **(A)** Western blot analysis of *SOX11* protein level during the NED of LNCaP. **(B)** The results of the western blot show the efficiency of *SOX11* knockdown. **(C)** Western blot analysis of neuroendocrine markers in *SOX11*-knockdown LNCaP cells or control cells upon enzalutamide (Enz) exposure. **(D)**. The Cell Counting Kit-8 proliferation assay shows the proliferation ability of miR-145-5p-knockdown LNCaP cells with *SOX11* knockdown upon Enz exposure. **(E, F)** Flow cytometry analysis showed that compared with miR-145-5p-knockdown cells, the proportion of S phase cells was significantly reduced in the double knockdown of miR-145-5p and SOX11 with or without Enz exposure. $^{*}p < 0.05$, $^{**}p < 0.01$, $^{***}p < 0.001$.

various cancers, miR-145-5p has been shown to suppress the cancer stem cell-like properties and contribute to chemotherapy and radiation sensitivity (Ye et al., 2019). As a result, the goal of this study was to identify the role and molecular mechanism of miR-145-5p in the development of NEPC.

Next, we discovered that miR-145-5p targets were correlated with the p53 mutation involved in NEPC. Furthermore, we found that miR-145-5p levels gradually decreased as LNCaP cells underwent NE transdifferentiation. Moreover, knockdown and overexpression of miR-145-5p promoted the upregulation and downregulation of NE markers, NSE, CHGA, and SYP. The proliferation assay revealed that downregulating miR-145-5p increased the proliferation of LNCaP cells while overexpressing miR-145-5p significantly decreased the proliferation of LNCaP cells. Subsequently, we found that knocking down miR-145-5p in PCa cells increased Cyclin E1 and Cyclin D1 while decreasing p21 and p27 expressions, explaining the increased cell cycle progression. Together, these

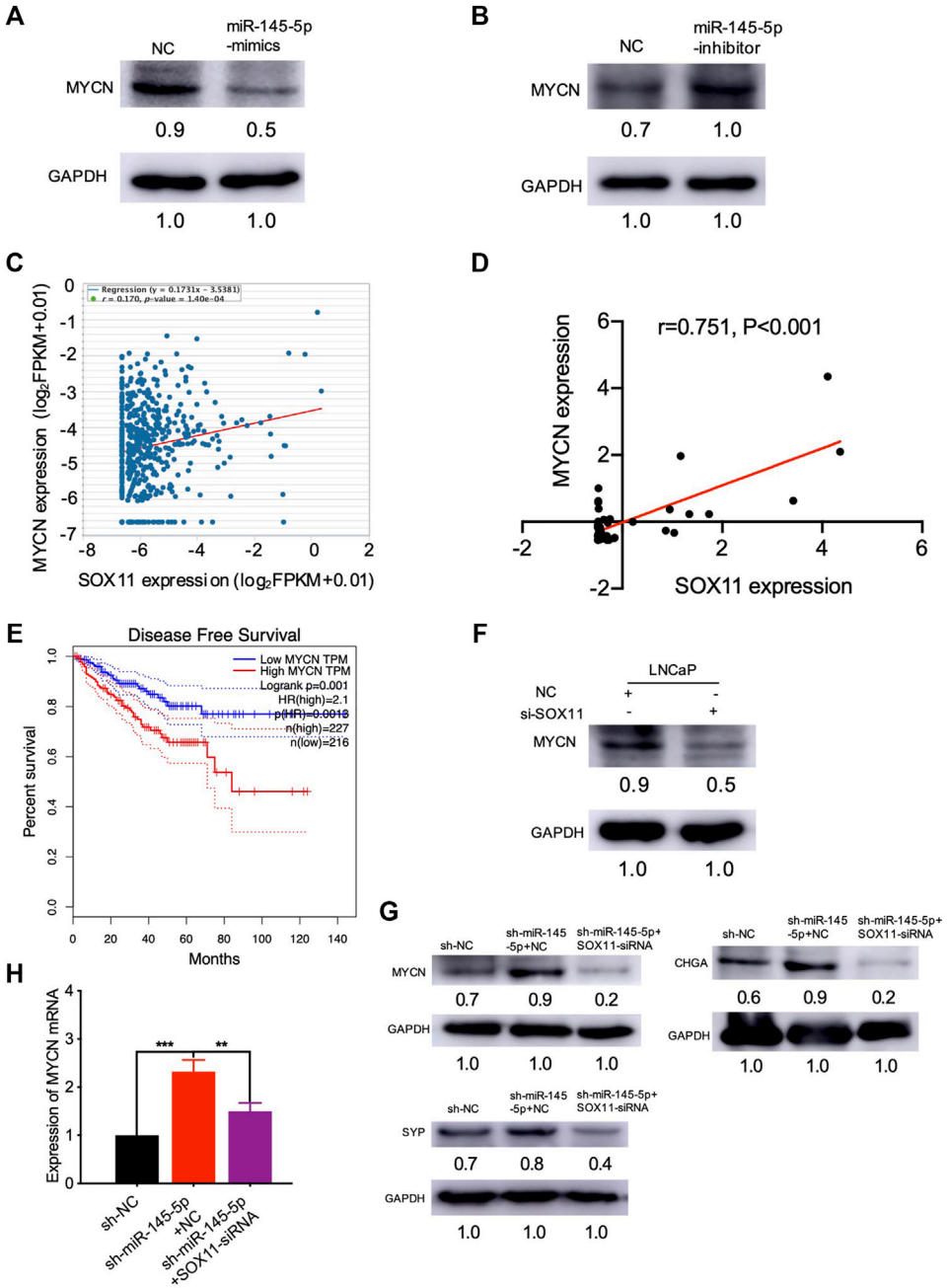

FIGURE 5 | miR-145-5p negatively regulates *MYCN* by repressing the expression of *SOX11* in neuroendocrine differentiation. **(A)** Western blot analysis of *MYCN* protein in miR-145-5p-overexpressing LNCaP cells or control cells upon enzalutamide (Enz) exposure. **(B)** Western blot analysis of *MYCN* protein in miR-145-5p-knockdown LNCaP cells or control cells upon Enz exposure. **(C)** The correlation between *SOX11* mRNA and *MYCN* expression in prostate cancer (PCa) in The Cancer Genome Atlas (TCGA) data by starBase. **(D)** The correlation between *SOX11* mRNA and *MYCN* expression in the castration-resistant prostate cancer subgroup in TCGA data. **(E)** Kaplan–Meier analysis shows the association of *MYCN* expression with disease-free survival of 488 patients with PCa from TCGA data by gene expression profiling interactive analysis. **(F)** Western blot analysis of *MYCN* protein in *SOX11*-knockdown LNCaP cells or control cells upon Enz exposure. **(G, H)** Western blot analysis and the quantitative real-time polymerase chain reaction of *MYCN* protein and neuroendocrine markers of miR-145-5p-knockdown and the double knockdown of miR-145-5p and *SOX11* LNCaP cells. $^{*}p < 0.05$, $^{**}p < 0.01$, $^{***}p < 0.001$.

findings demonstrated that decreased miR-145-5p expression promoted NED and proliferation of PCa cells.

miR-145-5p has been found to suppress cancer cell proliferation, invasion, stemness, chemotherapy, and radiation sensitivity in patients with PCa by targeting different regulators such as DNMT3a, TWIST1, ITPR2, AR, and NMT3b (Larne et al., 2015; Wang et al., 2015; Xue et al., 2015; Rajabi et al., 2020; Huang and Tang, 2021). Additionally, circular RNAs (circRNAs)

are a novel class of miR-145-5p target genes, according to a recent study using circRNA array analysis of LNCaP cells overexpressing miR-145 (He et al., 2018). According to bioinformatics and correlation analysis, *SOX11* is a downstream target gene of miR-145-5p in PCa. Recent studies also point out that miR-145-5p inhibits cell proliferation and induces cell apoptosis in the bladder and endometrial cancer cells by targeting *SOX11* (Chang et al., 2017; Wu et al., 2018). *SOX11* is a key modulator of NED in *TP53*-deficient CRPC (Zou et al., 2017). Coincidentally, this study also confirmed that decreased miR-145-5p expression directly upregulated *SOX11* to promote the NED and proliferation of PCa cells.

We also found that miR-145-5p overexpression suppressed the expression of *MYCN* in PCa. The induction of the NEPC histological phenotype was correlated to the overexpression of *MYCN* (Beltran et al., 2011; Lee et al., 2016). By binding to AR enhancers, *MYCN* functions to inhibit AR signaling and drives NEPC in human prostate epithelial cells (Dardenne et al., 2016; Lee et al., 2016). In the TCGA database, we found that *SOX11* was significantly correlated with the expression of *MYCN* in the CRPC subgroup. The double knockdown experiment showed that *SOX11* regulates *MYNC* to induce NE transdifferentiation, and thus mediates miR-145-5p. However, the luciferase reporter gene experiment showed that *SOX11* did not activate the expression of *MYCN*, suggesting that *SOX11* binds to sites other than the promoter region to directly or indirectly regulate the transcription of *MYCN*. These findings suggest that downregulation of miR-145-5p expression resulted in the increased expression of *SOX11* and *MYCN*, promoting the NED and proliferation of PCa cells.

In the present study, we found that miR-145-5p decreased gradually during androgen depletion, but the mechanism of its upstream regulation needs to be investigated further. AR was found to suppress the expression of miR-145 in renal cell carcinoma by directly binding to the AR element located on the promoter region of miR-145 and suppressing p53's induction of miR-145 (Chen et al., 2015). Previous research suggested that p53 could activate the miR-145 promoter by binding to the p53 response element (p53RE) (Sachdeva et al., 2009). According to recent studies, loss of *TP53* and *RB1* function confers antiandrogen resistance by inducing NED (Ku et al., 2017; Mu et al., 2017). As a result, we speculate that as ADT screening pressure increases, the proportion of cells with the p53 mutation gradually increases, failing to relieve AR-mediated transcriptional repression of miR-145, resulting in miR-145 decline. Additionally, in PCa, miR-145 has been implicated as a direct regulator of AR (Larne et al., 2015). These findings suggest that miR-145 may be involved in a negative feedback loop with AR signaling in PCa progression. However, when miR-145-5p was knocked down or overexpressed in LNCaP cells, there was no obvious change in the AR protein.

In conclusion, in this study, we found that decreased miR-145-5p expression is associated with PCa neuroendocrine transdifferentiation. Furthermore, we demonstrated that miR-145-5p inhibits the expression of *MYCN* by directly binding to *SOX11*, which prevents NED and inhibits the cell cycle progression of PCa cells. Our findings add to the growing body of evidence that miR-145-5p is a potential therapeutic target for NEPC in PCa, this is consistent with the report of Iscaife et al., who found that *in vivo* the therapeutic activity of the tumor suppressor miR-145 in treating metabolic PCa (Iscaife et al., 2018). More research is needed to prove its safety profile before it can be used in humans. Nevertheless, future research into the clinical significance of miR-145 in the treatment of patients with NEPC is needed.

DATA AVAILABILITY STATEMENT

The original contributions presented in the study are included in the article/**Supplementary Material**, further inquiries can be directed to the corresponding authors.

ETHICS STATEMENT

The animal study was reviewed and approved by The ethical standards of Shanghai Pudong Gongli Hospital.

AUTHOR CONTRIBUTIONS

Conception and design: FX, YL; Administrative support: FX, YL; Provision of study materials or patients: FX, SJ; Collection and assembly of data: FZ; LY; YS; Data analysis and interpretation: SJ; FZ; LY; Manuscript writing: All authors; Final approval of manuscript: All authors.

FUNDING

This study is supported by grants from Youth Foundation of Shanghai Pudong Gongli Hospital No. 2018YQNJJ-14.

SUPPLEMENTARY MATERIAL

The Supplementary Material for this article can be found online at: https://www.frontiersin.org/articles/10.3389/fgene.2022.790621/full#supplementary-material

REFERENCES

Avgeris, M., Stravodimos, K., Fragoulis, E. G., and Scorilas, A. (2013). The Loss of the Tumour-Suppressor miR-145 Results in the Shorter Disease-free Survival of Prostate Cancer Patients. *Br. J. Cancer* 108 (12), 2573–2581. doi:10.1038/bjc.2013.250

Beltran, H., Rickman, D. S., Park, K., Chae, S. S., Sboner, A., MacDonald, T. Y., et al. (2011). Molecular Characterization of Neuroendocrine Prostate Cancer and Identification of New Drug Targets. *Cancer Discov.* 1 (6), 487–495. doi:10.1158/2159-8290.CD-11-0130

Bishop, J. L., Thaper, D., Vahid, S., Davies, A., Ketola, K., Kuruma, H., et al. (2017). The Master Neural Transcription Factor BRN2 Is an Androgen Receptor-

Suppressed Driver of Neuroendocrine Differentiation in Prostate Cancer. *Cancer Discov.* 7 (1), 54–71. doi:10.1158/2159-8290.CD-15-1263

Cartharius, K., Frech, K., Grote, K., Klocke, B., Haltmeier, M., Klingenhoff, A., et al. (2005). MatInspector and beyond: Promoter Analysis Based on Transcription Factor Binding Sites. *Bioinformatics* 21 (13), 2933–2942. doi:10.1093/bioinformatics/bti473

Chang, L., Yuan, Z., Shi, H., Bian, Y., and Guo, R. (2017). miR-145 Targets the SOX11 3'UTR to Suppress Endometrial Cancer Growth. *Am. J. Cancer Res.* 7 (11), 2305–2317.

Chen, Y., Sun, Y., Rao, Q., Xu, H., Li, L., and Chang, C. (2015). Androgen Receptor (AR) Suppresses miRNA-145 to Promote Renal Cell Carcinoma (RCC) Progression Independent of VHL Status. *Oncotarget* 6 (31), 31203–31215. doi:10.18632/oncotarget.4522

Dardenne, E., Beltran, H., Benelli, M., Gayvert, K., Berger, A., Puca, L., et al. (2016). N-myc Induces an EZH2-Mediated Transcriptional Program Driving Neuroendocrine Prostate Cancer. *Cancer Cell* 30 (4), 563–577. doi:10.1016/j.ccell.2016.09.005

Ferlay, J., Colombet, M., Soerjomataram, I., Mathers, C., Parkin, D. M., Piñeros, M., et al. (2019). Estimating the Global Cancer Incidence and Mortality in 2018: GLOBOCAN Sources and Methods. *Int. J. Cancer* 144 (8), 1941–1953. doi:10.1002/ijc.31937

Ge, R., Wang, Z., Montironi, R., Jiang, Z., Cheng, M., Santoni, M., et al. (2020). Epigenetic Modulations and Lineage Plasticity in Advanced Prostate Cancer. *Ann. Oncol.* 31 (4), 470–479. doi:10.1016/j.annonc.2020.02.002

Giguère, V. (2020). DNA-PK, Nuclear mTOR, and the Androgen Pathway in Prostate Cancer. *Trends Cancer* 6 (4), 337–347. doi:10.1016/j.trecan.2020.01.015

Goto, Y., Kurozumi, A., Arai, T., Nohata, N., Kojima, S., Okato, A., et al. (2017). Impact of Novel miR-145-3p Regulatory Networks on Survival in Patients with Castration-Resistant Prostate Cancer. *Br. J. Cancer* 117 (3), 409–420. doi:10.1038/bjc.2017.191

He, J. H., Han, Z. P., Zhou, J. B., Chen, W. M., Lv, Y. B., He, M. L., et al. (2018). MiR-145 Affected the Circular RNA Expression in Prostate Cancer LNCaP Cells. *J. Cel Biochem* 119 (11), 9168–9177. doi:10.1002/jcb.27181

Huang, K., and Tang, Y. (2021). SChLAP1 Promotes Prostate Cancer Development through Interacting with EZH2 to Mediate Promoter Methylation Modification of Multiple miRNAs of Chromosome 5 with a DNMT3a-Feedback Loop. *Cell Death Dis* 12 (2), 188. doi:10.1038/s41419-021-03455-8

Iscaife, A., Reis, S. T., Morais, D. R., Viana, N. I., da Silva, I. A., Pimenta, R., et al. (2018). Treating Metastatic Prostate Cancer with microRNA-145. *Apoptosis* 23 (7-8), 388–395. doi:10.1007/s10495-018-1461-z

Ku, S. Y., Rosario, S., Wang, Y., Mu, P., Seshadri, M., Goodrich, Z. W., et al. (2017). Rb1 and Trp53 Cooperate to Suppress Prostate Cancer Lineage Plasticity, Metastasis, and Antiandrogen Resistance. *Science* 355 (6320), 78–83. doi:10.1126/science.aah4199

Larne, O., Hagman, Z., Lilja, H., Bjartell, A., Edsjö, A., and Ceder, Y. (2015). miR-145 Suppress the Androgen Receptor in Prostate Cancer Cells and Correlates to Prostate Cancer Prognosis. *Carcin* 36 (8), 858–866. doi:10.1093/carcin/bgv063

Lee, J. K., Phillips, J. W., Smith, B. A., Park, J. W., Stoyanova, T., McCaffrey, E. F., et al. (2016). N-myc Drives Neuroendocrine Prostate Cancer Initiated from Human Prostate Epithelial Cells. *Cancer Cell* 29 (4), 536–547. doi:10.1016/j.ccell.2016.03.001

Lu, T.-P., Lee, C.-Y., Tsai, M.-H., Chiu, Y.-C., Hsiao, C. K., Lai, L.-C., et al. (2012). miRSystem: an Integrated System for Characterizing Enriched Functions and Pathways of microRNA Targets. *PLoS One* 7 (8), e42390. doi:10.1371/journal.pone.0042390

Mao, S., Wu, Y., Wang, R., Guo, Y., Bi, D., Ma, W., et al. (2020). Overexpression of GAS6 Promotes Cell Proliferation and Invasion in Bladder Cancer by Activation of the PI3K/AKT Pathway. *OncoTargets Ther.* 13, 4813–4824. doi:10.2147/OTT.S237174

Mathelier, A., Fornes, O., Arenillas, D. J., Chen, C.-y., Denay, G., Lee, J., et al. (2016). JASPAR 2016: a Major Expansion and Update of the Open-Access Database of Transcription Factor Binding Profiles. *Nucleic Acids Res.* 44 (D1), D110–D115. doi:10.1093/nar/gkv1176

Mu, P., Zhang, Z., Benelli, M., Karthaus, W. R., Hoover, E., Chen, C.-C., et al. (2017). SOX2 Promotes Lineage Plasticity and Antiandrogen Resistance in TP53 - and RB1 -deficient Prostate Cancer. *Science* 355 (6320), 84–88. doi:10.1126/science.aah4307

Nguyen, H. G., Yang, J. C., Kung, H.-J., Shi, X.-B., Tilki, D., Lara, P. N., Jr., et al. (2014). Targeting Autophagy Overcomes Enzalutamide Resistance in Castration-Resistant Prostate Cancer Cells and Improves Therapeutic Response in a Xenograft Model. *Oncogene* 33 (36), 4521–4530. doi:10.1038/onc.2014.25

Rajabi, F., Liu-Bordes, W.-Y., Pinskaya, M., Dominika, F., Kratassiouk, G., Pinna, G., et al. (2020). CPEB1 Orchestrates a fine-tuning of miR-145-5p Tumor-Suppressive Activity on TWIST1 Translation in Prostate Cancer Cells. *Oncotarget* 11 (45), 4155–4168. doi:10.18632/oncotarget.27806

Sachdeva, M., Zhu, S., Wu, F., Wu, H., Walia, V., Kumar, S., et al. (2009). p53 Represses C-Myc through Induction of the Tumor Suppressor miR-145. *Proc. Natl. Acad. Sci.* 106 (9), 3207–3212. doi:10.1073/pnas.0808042106

Scher, H. I., Fizazi, K., Saad, F., Taplin, M.-E., Sternberg, C. N., Miller, K., et al. (2012). Increased Survival with Enzalutamide in Prostate Cancer after Chemotherapy. *N. Engl. J. Med.* 367 (13), 1187–1197. doi:10.1056/NEJMoa1207506

Suh, S. O., Chen, Y., Zaman, M. S., Hirata, H., Yamamura, S., Shahryari, V., et al. (2011). MicroRNA-145 Is Regulated by DNA Methylation and P53 Gene Mutation in Prostate Cancer. *Carcin* 32 (5), 772–778. doi:10.1093/carcin/bgr036

Wang, B.-D., Ceniccola, K., Yang, Q., Andrawis, R., Patel, V., Ji, Y., et al. (2015). Identification and Functional Validation of Reciprocal microRNA-mRNA Pairings in African American Prostate Cancer Disparities. *Clin. Cancer Res.* 21 (21), 4970–4984. doi:10.1158/1078-0432.CCR-14-1566

Wang, Y., Wang, Y., Ci, X., Choi, S. Y. C., Crea, F., Lin, D., et al. (2021). Molecular Events in Neuroendocrine Prostate Cancer Development. *Nat. Rev. Urol.* 18 (10), 581–596. doi:10.1038/s41585-021-00490-0

Wu, Z., Huang, W., Wang, X., Wang, T., Chen, Y., Chen, B., et al. (2018). Circular RNA CEP128 Acts as a Sponge of miR-145-5p in Promoting the Bladder Cancer Progression via Regulating SOX11. *Mol. Med.* 24 (1), 40. doi:10.1186/s10020-018-0039-0

Xu, N., Papagiannakopoulos, T., Pan, G., Thomson, J. A., and Kosik, K. S. (2009). MicroRNA-145 Regulates OCT4, SOX2, and KLF4 and Represses Pluripotency in Human Embryonic Stem Cells. *Cell* 137 (4), 647–658. doi:10.1016/j.cell.2009.02.038

Xu, W. X., Liu, Z., Deng, F., Wang, D. D., Li, X. W., Tian, T., et al. (2019). MiR-145: a Potential Biomarker of Cancer Migration and Invasion. *Am. J. Transl Res.* 11 (11), 6739–6753.

Xu, W., Hua, Y., Deng, F., Wang, D., Wu, Y., Zhang, W., et al. (2020). MiR-145 in Cancer Therapy Resistance and Sensitivity: A Comprehensive Review. *Cancer Sci.* 111 (9), 3122–3131. doi:10.1111/cas.14517

Xue, G., Ren, Z., Chen, Y., Zhu, J., Du, Y., Pan, D., et al. (2015). A Feedback Regulation between miR-145 and DNA Methyltransferase 3b in Prostate Cancer Cell and Their Responses to Irradiation. *Cancer Lett.* 361 (1), 121–127. doi:10.1016/j.canlet.2015.02.046

Yamada, Y., and Beltran, H. (2021). Clinical and Biological Features of Neuroendocrine Prostate Cancer. *Curr. Oncol. Rep.* 23 (2), 15. doi:10.1007/s11912-020-01003-9

Ye, D., Shen, Z., and Zhou, S. (2019). Function of microRNA-145 and Mechanisms Underlying its Role in Malignant Tumor Diagnosis and Treatment. *Cancer Manag. Res.* 11, 969–979. doi:10.2147/CMAR.S191696

Yuan, T.-C., Veeramani, S., and Lin, M.-F. (2007). Neuroendocrine-like Prostate Cancer Cells: Neuroendocrine Transdifferentiation of Prostate Adenocarcinoma Cells. *Endocr. Relat. Cancer* 14 (3), 531–547. doi:10.1677/ERC-07-0061

Zhu, J., Wang, S., Zhang, W., Qiu, J., Shan, Y., Yang, D., et al. (2015). Screening Key microRNAs for Castration-Resistant Prostate Cancer Based on miRNA/mRNA Functional Synergistic Network. *Oncotarget* 6 (41), 43819–43830. doi:10.18632/oncotarget.6102

Zou, M., Toivanen, R., Mitrofanova, A., Floch, N., Hayati, S., Sun, Y., et al. (2017). Transdifferentiation as a Mechanism of Treatment Resistance in a Mouse Model of Castration-Resistant Prostate Cancer. *Cancer Discov.* 7 (7), 736–749. doi:10.1158/2159-8290.CD-16-1174

Conflict of Interest: The authors declare that the research was conducted in the absence of any commercial or financial relationships that could be construed as a potential conflict of interest.

Publisher's Note: All claims expressed in this article are solely those of the authors and do not necessarily represent those of their affiliated organizations, or those of the publisher, the editors, and the reviewers. Any product that may be evaluated in this article, or claim that may be made by its manufacturer, is not guaranteed or endorsed by the publisher.

frontiers in Genetics

ORIGINAL RESEARCH
published: 18 March 2022
doi: 10.3389/fgene.2022.855557

Identification of Tissue-Specific Expressed Hub Genes and Potential Drugs in Rheumatoid Arthritis Using Bioinformatics Analysis

Xuewu Xing[1,2], *Qun Xia*[1], *Baoqi Gong*[3], *Zhongyang Shen*[4] *and Yingze Zhang*[2,5,6]*

[1]*Department of Orthopaedics, Tianjin First Central Hospital, Tianjin, China,* [2]*School of Medicine, Nankai University, Tianjin, China,* [3]*Department of Rheumatology, Tianjin First Central Hospital, Tianjin, China,* [4]*Department of Transplant Surgery, Tianjin First Central Hospital, Tianjin, China,* [5]*Department of Orthopaedic Surgery of Hebei Province, Third Hospital of Hebei Medical University, Shijiazhuang, China,* [6]*Chinese Academy of Engineering, Beijing, China*

Background: Rheumatoid arthritis (RA) is a common autoimmune disease characterized by progressive, destructive polyarthritis. However, the cause and underlying molecular events of RA are not clear. Here, we applied integrated bioinformatics to identify tissue-specific expressed hub genes involved in RA and reveal potential targeted drugs.

Methods: Three expression profiles of human microarray datasets involving fibroblast-like synoviocytes (FLS) were downloaded from the Gene Expression Omnibus (GEO) database, the differentially expressed mRNAs (DEGs), miRNAs (DEMs), and lncRNAs (DELs) between normal and RA synovial samples were screened using GEO2R tool. BioGPS was used to identified tissue-specific expressed genes. Functional and pathway enrichment analyses were performed for common DEGs using the DAVID database, and the protein-protein interaction (PPI) network of common DEGs was constructed to recognize hub genes by the STRING database. Based on receiver operating characteristic (ROC) curve, we further investigated the prognostic values of tissue-specific expressed hub genes in RA patients. Connectivity Map (CMap) was run to identify novel anti-RA potential drugs. The DEM–DEG pairs and ceRNA network containing key DEMs were established by Cytoscape.

Results: We obtain a total of 418 DEGs, 23 DEMs and 49 DELs. 64 DEGs were verified as tissue-specific expressed genes, most derive from the hematologic/immune system (20/64, 31.25%). GO term and KEGG pathway enrichment analysis showed that DEGs focused primarily on immune-related biological process and NF-κB pathway. 10 hub genes were generated via using MCODE plugin. Among them, SPAG5, CUX2, and THEMIS2 were identified as tissue-specific expressed hub genes, these 3 tissue-specific expressed hub genes have superior diagnostic value in the RA samples compared with osteoarthritis (OA) samples. 5 compounds (troleandomycin, levodopa, trichostatin A, LY-294002, and levamisole) rank among the top five in connectivity score. In addition, 5 miRNAs were identified to be key DEMs, the lncRNA–miRNA–mRNA network with five key DEMs was formed. The networks containing tissue-specific expressed hub genes are as follows: ARAP1-AS2/miR-20b-3p/TRIM3, ARAP1-AS2/miR-30c-3p/FRZB.

OPEN ACCESS

Edited by:
Rajesh Pandey,
CSIR-Institute of Genomics and Integrative Biology (CSIR-IGIB), India

Reviewed by:
Sergey V. Kozyrev,
Uppsala University, Sweden
Xueyuan Jiang,
Merck, United States

***Correspondence:**
Yingze Zhang
yzzhang2022@foxmail.com

Specialty section:
This article was submitted to RNA, a section of the journal Frontiers in Genetics

Received: *15 January 2022*
Accepted: *18 February 2022*
Published: *18 March 2022*

Citation:
Xing X, Xia Q, Gong B, Shen Z and Zhang Y (2022) Identification of Tissue-Specific Expressed Hub Genes and Potential Drugs in Rheumatoid Arthritis Using Bioinformatics Analysis. Front. Genet. 13:855557. doi: 10.3389/fgene.2022.855557

Conclusion: This study indicates that screening for identify tissue-specific expressed hub genes and ceRNA network in RA using integrated bioinformatics analyses could help us understand the mechanism of development of RA. Besides, SPAG5 and THEMIS2 might be candidate biomarkers for diagnosis of RA. LY-294002, trichostatin A, and troleandomycin may be potential drugs for RA.

Keywords: rheumatoid arthritis, GEO database, tissue specific, hub gene, competing endogenous RNA

INTRODUCTION

Rheumatoid arthritis (RA) is a chronic systemic autoimmune disease characterized by hyperplastic synovium, invasive synovitis, and progressive joint damage (Scott et al., 2010). The incidence of RA is approximately 1% in the adult population, mainly affecting middle-aged to elderly women (Stephenson et al., 2018). RA is the leading cause of disability worldwide and imposes a significant public health and economic burden (Schmidt et al., 2020). The etiology of RA is complex and multifactorial (McInnes and Schett, 2011). Despite there have been major advances in the understanding of RA development, the pathogenesis of RA remains incompletely elucidated.

Microarray analyses has improved the ability of human to study the pathogenesis of diseases, increasingly being used to explore disease epigenetics and to screen for effective biomarkers for disease diagnosis and treatment (Kulasingam and Diamandis, 2008). Although several genes, such as HLA-DR, PTPTN22, CTLA-4, and PADI4, have been identified as genetic factors that contribute to RA susceptibility, we still don't know the exact mechanisms by which these genes trigger RA (Moran-Moguel et al., 2018). Therefore, we can elucidate the pathogenesis of RA by identifying potential biomarkers and potential therapeutic targets. In addition, the competing endogenous RNA (ceRNA) hypothesis could facilitate the elucidation of molecular mechanisms underlying disease progression (Salmena et al., 2011). Tissue-specific expressed hub genes and regulatory networks of disease may be screened through transcriptome microarray and bioinformatic analysis (Cheng et al., 2021).

Del Rey et al. conducted transcriptional analysis of normal and pathological synoviocytes using microarray expression profiling (Del Rey et al., 2012). Georgel P et al. used high throughput expression analysis to evaluate the overall miRNA expression level in fibroblast-like synoviocytes (FLS) isolated from RA patients in comparison with FLS from osteoarthritic (OA) patients (Liu and Ren, 2020). Bi et al. assessed the differential expression profiles of lncRNA in FLSs between the RA group and the healthy control groups (Bi et al., 2019). In the present study, we downloaded the expression profiles of the above three different types of RNA from GEO database to screen the differentially expressed mRNAs (DEGs), miRNAs (DEMs), and lncRNAs (DELs) between normal and RA synovial samples. Hub genes, tissue-specific expressed genes, RNA regulatory networks, and novel anti-RA potential drugs were obtained by comprehensive analysis. This work provides a deeper understanding of the molecular mechanism underlying RA development and reveals novel biomarkers for disease diagnosis and potential drug for disease therapy.

MATERIALS AND METHODS

Datasets Collection

Three human microarray datasets involving fibroblast-like synoviocytes (FLS) were obtained by searching NCBI's Gene Expression Omnibus (GEO) database (http://www.ncbi.nlm.nih. gov/geo/). The mRNA, miRNA and lncRNA expression profiles were procured from GSE29746, GSE72564 and GSE128813 respectively, the description of these data sets was detailed below (**Table 1**).

Authentication of DEG, DEM, and DEL

Through GEO2R online tool, we obtained differentially expressed mRNAs (DEGs), miRNAs (DEMs) and lncRNAs (DELs). GEO2R is an interactive online tool that can be used to compare multiple expression data and then identify differentially expressed profiles. We selected differentially expressed RNAs according to the following criteria: $p < 0.05$ and $|\log2 \text{ (fold change)}| \geq 1$.

Authentication of the Tissue-specific Expressed Genes

We analyzed the distribution of DEGs using an online tool BioGPS (http://biogps.org/) which was created as a centralized gene-annotation portal for clustering distributed gene (Wu et al., 2009). Tissue-specific genes should qualify the following criteria: 1) the expression level of transcripts that mapped to a single organ system was >10 times the median, and 2) the highest expression level was more than half as high as the second highest level (Cheng et al., 2021).

Functional Enrichment Analysis

To identify the function of DEGs, the enrichment analysis was conducted by DAVID (version 6.8) using Gene Ontology (GO) and Kyoto Encyclopedia of Genes and Genomes (KEGG) pathways database (Huang et al., 2007). We defined enriched functions and pathways using a cutoff of $p < 0.05$.

Construction and Analysis of Protein–Protein Interaction (PPI) Network

A PPI network was constructed for the DEGs using STRING (https://string-db.org/) with a filter condition (interaction score>0.4), a online tool of known, and predicted PPIs. We use the Cytoscape to visualize the network. In order to screen the important pathways related to the development of RA, we

TABLE 1 | Details of the 3 human microarray datasets.

	GSE29746	GSE72564	GSE128813
Expression profiling	mRNA	miRNA	lncRNA
Public on	25 Oct 2011	01 Sep 2015	08 Jan 2020
Organization	Spain	France	China
Samples of RA group	9	4	3
Samples of control group	11	4	3
Platforms	GPL4133 Agilent	GPL20870 Qiagen	GPL21827 Agilent

RA, rheumatoid arthritis; OA, osteoarthritis.

constructed an interaction network between DEGs and the signaling pathway using the ClueGO plug-in of Cytoscape platform. We applied MCODE plug-in of Cytoscape to identify hub genes of significant modules with following criteria: MCODE scores >5, degree cut-off = 2, node score cut-off = 0.2, Max depth = 100, and k-score = 2.

CMap Analysis

We run Connectivity Map (CMap) to identify novel anti-RA potential drugs. Through the database which is available online (http://www.broadinstitute.org/cmap/), we can get the similarity between each researcher's DEGs and 7,056 gene expression profiles caused by 1,309 bioactive compounds (Huang et al., 2007). The similarity is assessed by the 'connectivity score'. The connectivity score ranges from −1 to +1; a positive score means a promoted effect, while a negative score means an inhibited effect (Peng et al., 2020).

Construction of kDEM-DEG Pairs

The potential microRNA binding to DEGs were predicted using TargetScan (http://www.targetscan.org/vert_72/). The key differentially expressed miRNAs (kDEM) were obtained by the intersection between predicted miRNAs and differentially expressed miRNAs found from the GSE72564 dataset. The kDEM–DEG pairs were constructed using Cytoscape.

Establishment of the ceRNA Network

The miRcode database (http://www.mircode.org/) was used to predict miRNA that can interact with DELs. We used Cytoscape to construct the ceRNA network by selecting lncRNA–miRNA–mRNA interaction that contain key DEMs.

RESULTS

Identification of DEGs

We reanalyzed the GEO data of GSE29746 in order to compare the expression pattern of differential genes between pathological synovial tissues from 9 rheumatoid arthritis (RA) patients and normal synovial tissues from 11 sex and age matched osteoarthritis (OA) patients. A total of 418 DEGs were obtained, comprising 206 upregulated genes and 212 downregulated genes. The data of DEGs was visualized as a volcano plot (**Figure 1A**), The top 10 DEGs were displayed in a heatmap (**Figure 1B**).

Authentication of the tissue-Specific Expressed Genes

We identified 64 tissue-specific expressed genes using BioGPS (**Table 2**). The system with the greatest distribution of tissue-specific expressed genes is the hematologic/immune system (20/46, 31.25%), followed by the digestive system (11), nervous system (10), endocrine system (7), genital system (6), respiratory system (6), urinary system (2), circulatory system (1) and motor system (1).

GO Term and KEGG Pathway Enrichment Analysis of DEGs

GO analysis showed that the biological processes (BP) of DEGs focused primarily on synapse assembly, synapse organization, positive regulation of neuron differentiation, cerebral cortex neuron differentiation, endocardial cushion development, positive regulation of neurogenesis, skeletal muscle organ development, negative regulation of blood coagulation, pallium development, and cell junction assembly (**Figures 2A,B**). The main cellular components (CC) include cell-cell junction, collagen-containing extracellular matrix, basement membrane, adherent junction, integral component of postsynaptic specialization membrane, integral component of presynaptic active zone membrane, intrinsic component of postsynaptic specialization membrane, MHC class II protein complex, synaptic membrane, and clathrin-coated endocytic vesicle (**Figure 2A**). The molecular functions (MF) include actin monomer binding, extracellular matrix structural constituent, channel activity, passive transmembrane transporter activity, ion channel activity, ligand-gated ion channel activity, ligand-gated channel activity, cation channel activity, protein binding involved in heterotypic cell-cell adhesion, and endopeptidase inhibitor activity (**Figure 2A**). Genes are mainly involved in the KEGG pathway termed Amoebiasis, Cell adhesion molecules (CAMs), Staphylococcus aureus infection, Asthma, Rheumatoid arthritis, Toxoplasmosis, Glycosphingolipid biosynthesis-ganglio series, Allograft rejection, Leishmaniasis, and Tryptophan metabolism (**Figure 2C**; **Table 3**).

Construction and Analysis of PPI Network

Based on the identified DEGs and the STRING database, we constructed a PPI network containing 364 nodes and 361 edges (**Figure 3A**). We found out that NF-κB pathway may be involved in the pathogenesis of RA through Gene-pathway network

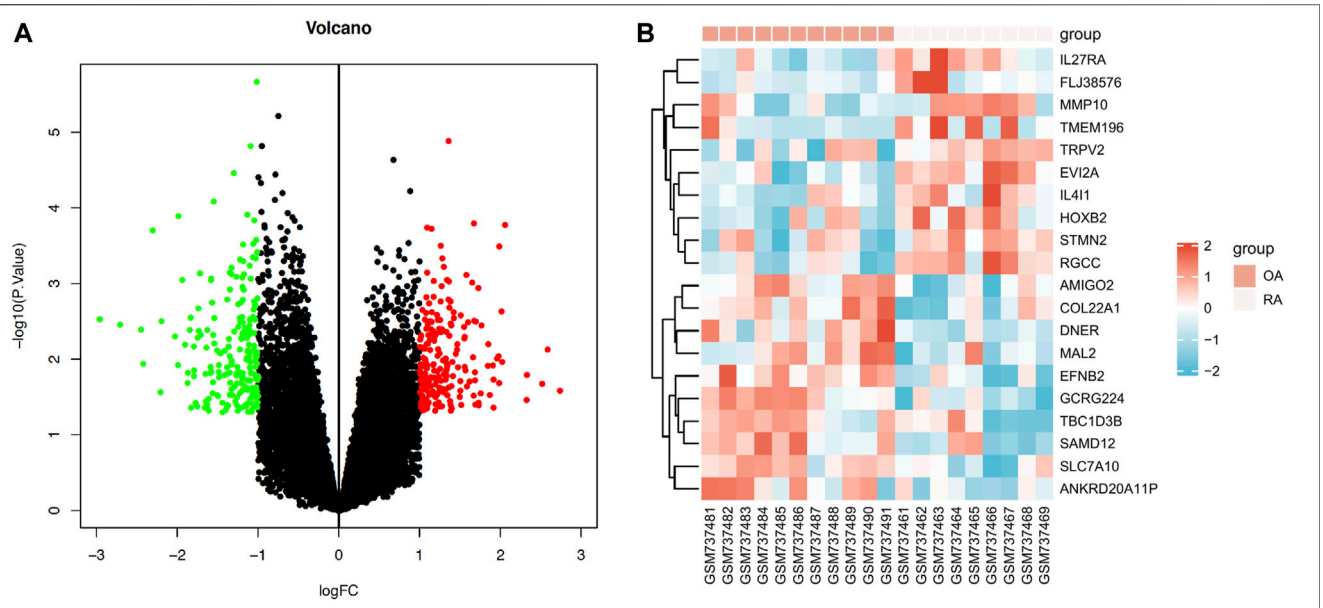

FIGURE 1 | Expression profiles of differentially expressed mRNAs (DEGs) in RA. **(A)** Volcano plot of DEGs (red: upregulated DEGs. green: downregulated DEGs.) **(B)** Heatmap of the top 10 upregulated DEGs and the top 10 downregulated DEGs (red: high expression; blue: low expression).

TABLE 2 | Distribution of tissue specific expressed genes identified by BioGPS.

system (counts)	Tissue	Genes
Hematologic/Immune (20)	CD56 + NK cells	TRPV2, PTGER2, ADGRG1, PREX1, NKG7
	BDCA4+dendritic cells	LAMP5, CUX2
	CD19 + B cells	VPREB3, BIRC3
	CD14 + monocytes	ADGRE1, TNFAIP8L2
	CD33 + myeloid	CCR1, TLR4, THEMIS2
	721 B lymphoblasts	IFI44L, SPAG5
	CD4+T cells	TRABD2A
	CD8+T cells	TBC1D10C
	whole blood	CLEC2B, KCNJ15
Digestive (11)	colorectal adenocarcinoma	HOXB7, MSX1, NGFR, KRT80, RBP1
	salivary gland	CST2, OPRPN
	small intestine	SLC5A1
	liver	HRG, HAAO, PLG
Nervous (10)	fetal brain	STMN2, LDLRAD4, DLX1
	whole brain	CRYM, BRINP1, MAPRE3
	prefrontal cortex	SHC3, CERCAM
	retina	FRZB, AOC2
Endocrine (7)	pineal	BEX5, CDH10, IGSF21, ASMT
	pancreatic islet	CRP
	thyroid	DUOX2, ID4
Genital (6)	testis germ cells	CHODL
	testis intersitial	SPATA8, LYZL6
	uterus	OGN
	uterus corpus	LEFTY2, MMP10
Respiratory (6)	lung	NEDD9, SFTPB, HEY1
	bronchial epithelial cells	PHLDA1, AMIGO2, FZD6
Urinary (2)	kidney	FMO1, CRYAA
Circulatory (1)	heart	HHATL
Motor (1)	skeletal muscle	ACTN3

CD, cluster differentiation.

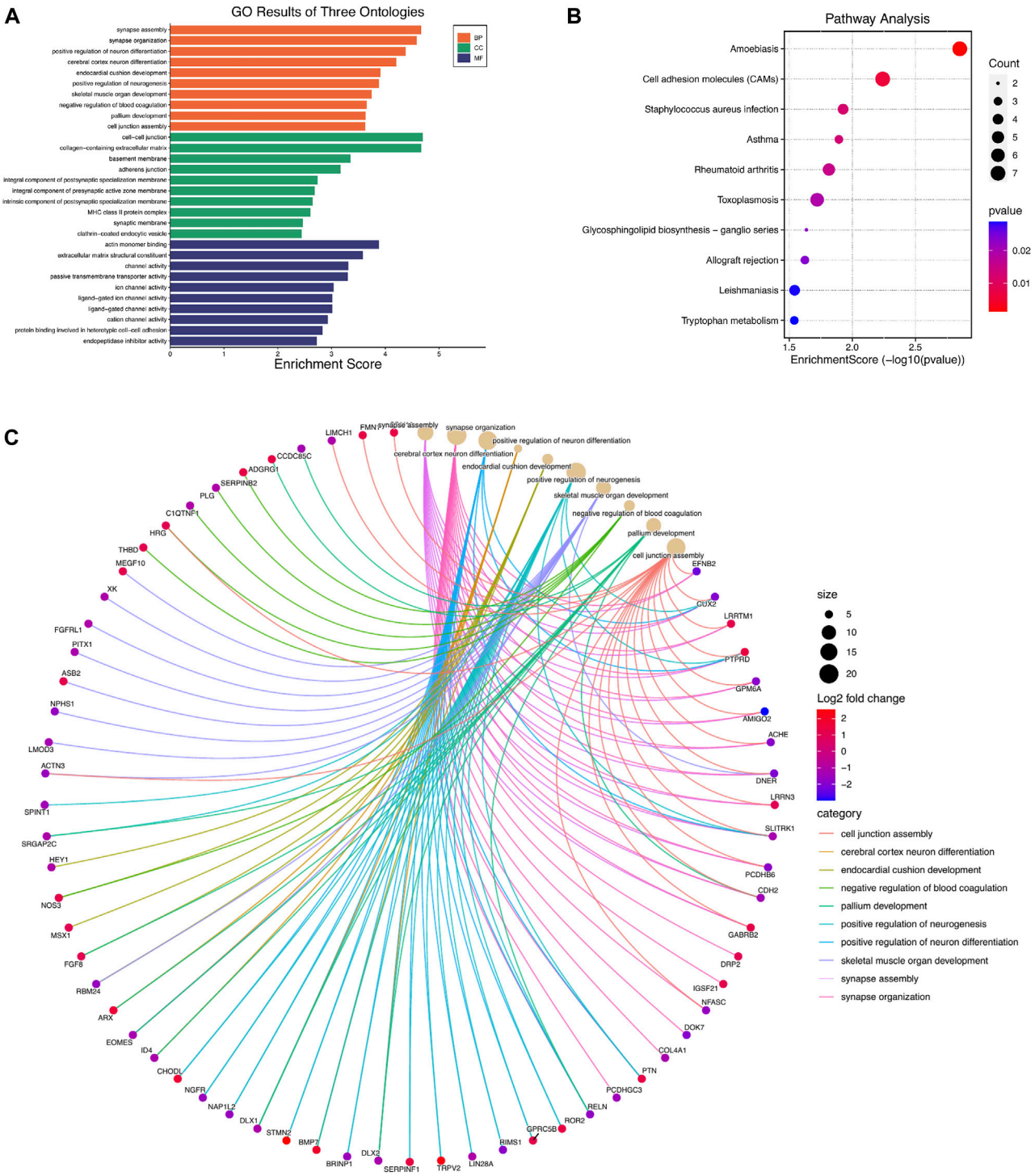

FIGURE 2 | GO and KEGG pathway enrichment analyses of differentially expressed mRNAs (DEGs). **(A)** Top 10 enriched GO terms of the DEGs. **(B)** cnetplot showing the top 10 enriched biological processes of DEGs **(C)**. The bubble plot showing top 10 enriched KEGG pathways of DEGs.

constructed by The ClueGO plugin of Cytoscape (**Figure 3B**). A total of 13 important module were generated via using MCODE plugin in Cytoscape, and 10 hub genes were obtained (**Table 4**).

ROC Curve of the 3 Tissue-Specific Expressed Hub Genes

Furthermore, we analyzed the performance of 3 tissue-specific expressed hub genes in diagnosing RA by means of receiver

TABLE 3 | Enrichment analysis of KEGG pathway.

KEGG ID	Term	GeneRatio	PValue	Genes
hsa05146	Amoebiasis	7/94	0.001414621	ACTN3/LAMA1/GNA14/TLR4/COL4A1/SERPINB4/SERPINB2
hsa04514	Cell adhesion molecules (CAMs)	7/94	0.005757522	HLA-DRB5/NCAM2/HLA-DQA2/HLA-DRB4/NFASC/CDH15/CDH2
hsa05150	Staphylococcus aureus infection	4/94	0.011840374	HLA-DRB5/HLA-DQA2/HLA-DRB4/PLG
hsa05310	Asthma	3/94	0.012784974	HLA-DRB5/HLA-DQA2/HLA-DRB4
hsa05323	Rheumatoid arthritis	5/94	0.015329475	HLA-DRB5/TLR4/HLA-DQA2/ATP6V1C2/HLA-DRB4
hsa05145	Toxoplasmosis	6/94	0.019005793	LAMA1/HLA-DRB5/BIRC3/TLR4/HLA-DQA2/HLA-DRB4
hsa00604	Glycosphingolipid biosynthesis - ganglio series	2/94	0.023088868	ST6GALNAC3/ST6GALNAC5
hsa05330	Allograft rejection	3/94	0.023727967	HLA-DRB5/HLA-DQA2/HLA-DRB4
hsa05140	Leishmaniasis	4/94	0.028621472	HLA-DRB5/TLR4/HLA-DQA2/HLA-DRB4
hsa00380	Tryptophan metabolism	3/94	0.028807929	ASMT/IL4I1/HAAO

KEGG , kyoto encyclopedia of genes and genomes.

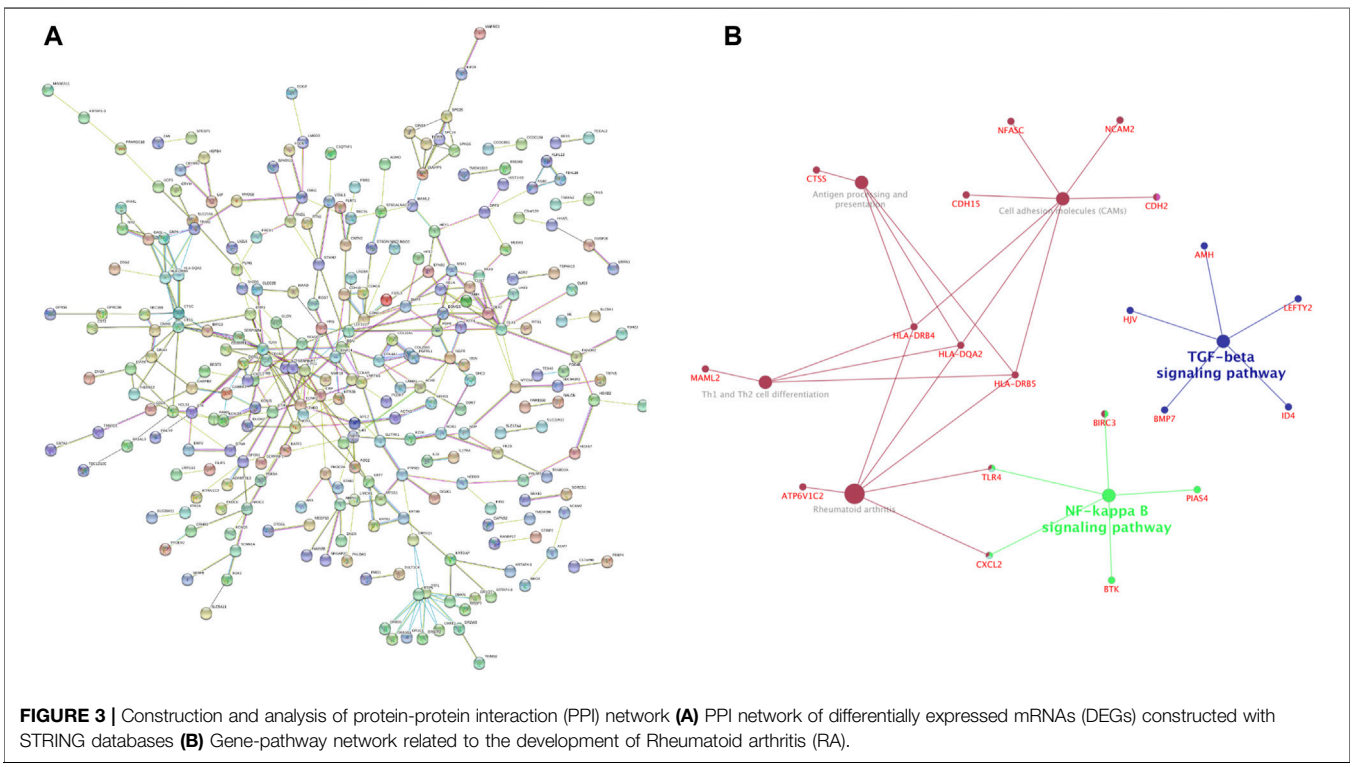

FIGURE 3 | Construction and analysis of protein-protein interaction (PPI) network **(A)** PPI network of differentially expressed mRNAs (DEGs) constructed with STRING databases **(B)** Gene-pathway network related to the development of Rheumatoid arthritis (RA).

TABLE 4 | Hub gene obtained by MCODE plug-in of Cytoscape.

No	Gene symbol	Log FC	*p* Value	Full name
1	MMP10	2.739087238	0.026051857	matrix metallopeptidase 10
2	TRIM3	−1.3827721	0.03985551	tripartite motif containing 3
3	THEMIS2	1.24876953	0.0083544	thymocyte selection associated family member 2
4	DLX2	−1.1895073	0.01692604	distal-less homeobox 2
5	SPAG5	1.03248394	0.0068909	sperm associated antigen 5
6	MIP	−1.1818731	0.00050311	major intrinsic protein of lens fiber
7	ASB2	1.20540696	0.0045946	ankyrin repeat and SOCS box containing 2
8	CXCL2	1.18019999	0.01749176	C-X-C motif chemokine ligand 2
9	CUX2	−1.9375622	0.00088542	cut like homeobox 2
10	FRZB	−1.5413208	0.00284952	frizzled-related protein

SOCS, suppressor of cytokine signalling.

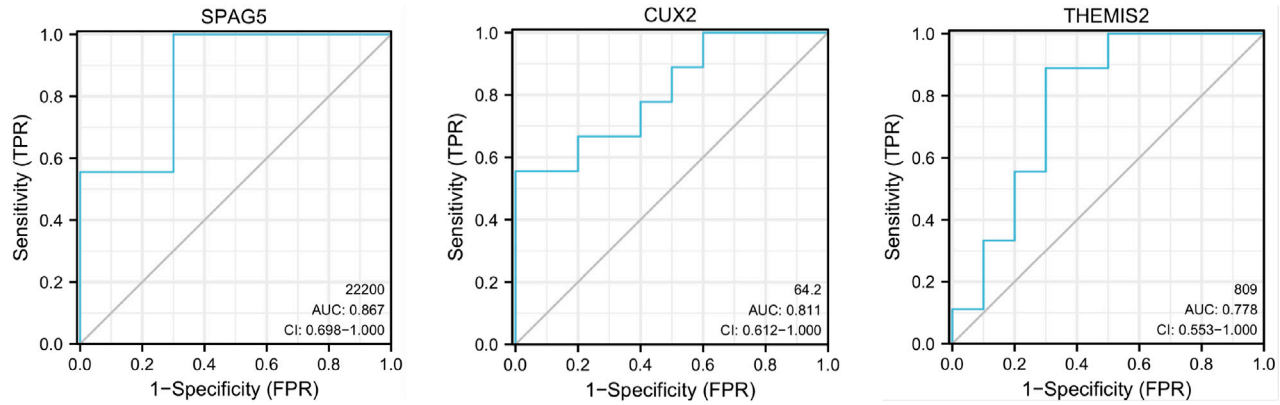

FIGURE 4 | ROC curve of the 3 specifically expressed hub genes in Rheumatoid arthritis (RA) samples. AUC area under the ROC curve.

TABLE 5 | The top five compounds with the highest scores in the CMap analysis.

CMap name	Dose	Cell line	Score	Instance ID	Description
Troleandomycin	5 μM	HL60	−1	1,965	inhibitors of CYP450 monooxygenases
Levodopa	20 μM	HL60	−0.998	1,972	the levorotatory form of dopa used in Parkinson's disease
Trichostatin A	100 nM	HL60	−0.971	2,949	HDAC inhibitor
LY-294002	10 μM	MCF7	−0.952	1,074	MTOR inhibitor
Levamisole	17 μM	HL60	−0.951	1,410	an anthelmintic drug $C_{11}H_{12}N_2S$

CYP450, Cytochrome P450; HDAC, histone deacetylase; MTOR, mammalian target of rapamycin.

operating characteristic (ROC) curve analysis in SPSS 23.0 software. The area under the ROC curve (AUC) was calculated to indicate diagnostic efficiency and predictive accuracy (Cheng et al., 2021). These 3 tissue-specific expressed hub genes have superior diagnostic value in the RA samples compared with OA samples. Specifically, SPAG5 showed the highest diagnostic performance (AUC: 0.867) in the RA samples, closely followed by CUX2 (AUC: 0.811), THEMIS2 ranks last (AUC: 0.778) (**Figure 4**). Based on the above data, these 3 tissue-specific expressed hub genes may serve as potential biomarkers for RA diagnosis.

Identification of Potential Targeted Drugs by CMap Analysis

We obtained a list of compounds after uploading DEGs tags to the CMap database. The top five compounds with the highest scores which may be potential drugs for RA are shown in **Table 5**.

Identification of DEMs and Construction of DEM-DEG Pairs

A total of 23 miRNAs were identified as DEMs, of which 17 miRNAs were upregulated and 6 miRNAs were downregulated (**Table 6**). A total of 147 miRNAs were predicted to combine with the DEGs. A total of five key DEMs were procured (**Figure 5A**), of which four were up-regulated, namely, miR-30c-2-3p, miR-20b-3p, miR-26a-1-3p, miR-218-5p, and miR-496 was the only down-regulated one. The kDEM–DEG pair is shown in **Figure 5B**.

TABLE 6 | differentially expressed miRNAs (DEMs) obtained from the GSE72564.

ID	adj.P.Val	P.Value	t	B	logFC	miRNA_ID
846	0.773	0.00181	5.08274	−0.98	1.5375	miR-670-5p
626	0.773	0.00365	4.44126	−1.51	2.0325	miR-26a-1-3p
958	0.773	0.00745	3.83781	−2.08	1.895	miR-2116-5p
63	0.773	0.02222	2.99059	−2.99	1.1625	miR-190a-5p
101	0.773	0.02336	2.95362	−3.03	1.5025	miR-548b-3p
119	0.773	0.02551	2.88896	−3.11	1.285	miR-579-3p
387	0.773	0.02961	2.78028	−3.24	1.7775	miR-1305
408	0.773	0.02995	2.77201	−3.25	1.6525	miR-30c-3p
620	0.773	0.03323	2.69675	−3.34	1.115	miR-20b-3p
797	0.773	0.03394	2.68158	−3.35	1.185	miR-4262
267	0.773	0.0345	2.66977	−3.37	1.165	miR-502-3p
666	0.773	0.0354	2.65136	−3.39	1.425	miR-1258
508	0.773	0.03672	2.62497	−3.42	2.1575	miR-708-5p
479	0.773	0.04256	2.51956	−3.55	1.6225	miR-1299
284	0.773	0.04671	2.45336	−3.63	2.745	miR-218-5p
731	0.773	0.04784	2.43638	−3.65	1.1275	miR-3116
636	0.773	0.04941	2.41358	−3.68	1.4275	miR-499a-5p
1	0.773	0.0471	−2.44742	−3.64	−1.02	miR-346
813	0.773	0.04084	−2.54889	−3.51	−1.475	miR-1193
1,067	0.773	0.03396	−2.68116	−3.35	−1.045	miR-4263
264	0.773	0.028	−2.82107	−3.19	−1.0725	miR-496
889	0.773	0.02301	−2.96491	−3.02	−1.8875	miR-2276-3p
560	0.773	0.01371	−3.35482	−2.58	−1.2775	miR-653-5p

DEG, differentially expressed mRNAs; DEM, differentially expressed miRNAs; DEL, differentially expressed lncRNAs; miR, miRNA; FC, fold change.

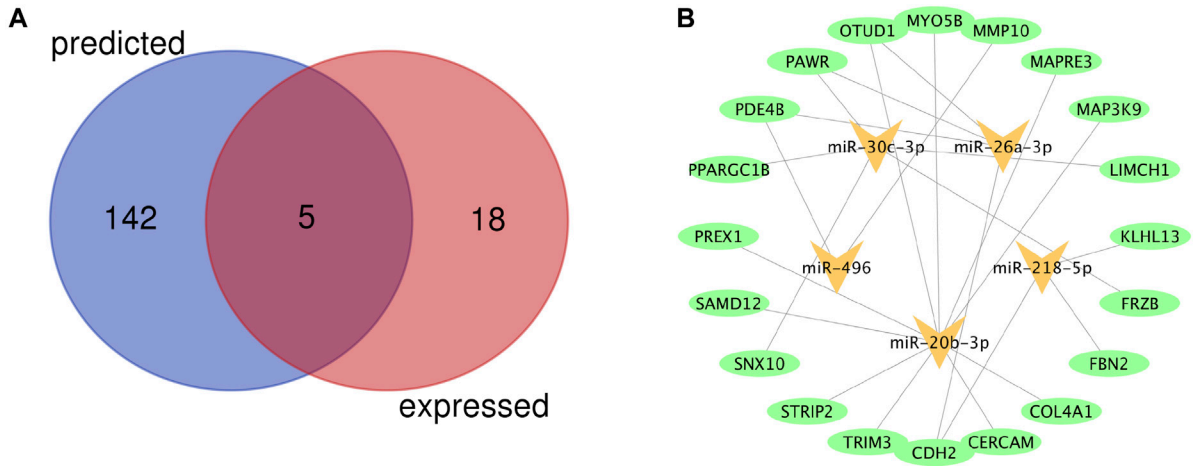

FIGURE 5 | Identification of key differentially expressed miRNAs (DEMs) and construction of DEM-DEG Pairs **(A)** Venn diagram of key differentially expressed miRNAs between predicted miRNAs and DEMs. **(B)** The kDEM–DEG pairs constructed by Cytoscape.

Identification of DELs and Establishment of the ceRNA Network

A total of 49 DELs were identified, of which 22 were up-regulated and 27 were down-regulated in GSE128813 (**Figure 6A**). The interactive miRNAs of DELs were predicted by mircode. Among these 49 lncRNAs, ARAP1-AS2, and AC104781 interacted with the five key miRNAs. ceRNA network was constructed by Cytoscape (**Figure 6B**). There are two networks containing hub gene: ARAP1-AS2/miR-20b-3p/TRIM3, ARAP1-AS2/miR-30c-3p/FRZB.

DISCUSSION

RA is one of the most common chronic autoimmune disease and is heterogeneous with complex pathogeneses. Although there is an accumulating evidence suggesting the involvement of novel transcripts in the development of RA, detailed mechanisms still remain elusive. In this study, we obtained the 418 DEGs in FLS from RA patients and OA patients. We further perform a tissue-specific expression analysis of DEGs, the result reveals that the hematologic/immune system is the greatest distribution system, which may explain the disease occurrence of RA.

Module analysis of the PPI network using ClueGO uncovered that NF-κB pathway may perform a significant role in RA pathogenesis. This has been confirmed by a number of studies. B cell activating factor of TNF family (BAFF) promoted synovial inflammation by activating of B cells in RA through NF-κB signaling pathway (Zhang et al., 2021). Growth differentiation factor 11 (GDF11) was able to significantly restrain the nuclear factor kappa-light-chain-enhancer of activated B cells (NF-κB) signaling pathway and prevent the development of RA (Li et al., 2019). Overexpression of miR-496 in RA-FLS may inhibit cell proliferation by inactivating the NF-κB pathway (Xing et al., 2021). CS-semi5, a semisynthetic chondroitin sulfate, may effectively improve synovial inflammation, and cartilage erosion in RA through NF-κB deactivation (Li et al., 2021). Hence, the intrinsic relationship between NF-κB pathway and RA needs to be further studied in the future.

Module analysis of the PPI network using MCODE identified 3 tissue-specific expressed hub genes involving in the hematologic/immune system. SPAG5 is a Protein Coding gene involved in the functional and dynamic regulation of mitotic spindles. There is growing evidence that it is upregulated in many human cancers, acting as an oncogene and promoting cell proliferation (Liu et al., 2018; He et al., 2020; Canu et al., 2021). CUX2 is a Protein Coding gene encoding a transcription factor which contains three CUT domains and a homeodomain. CUX2 functions as an accessory factor in the repair of oxidative DNA damage (Pal et al., 2015) and plays an important role in the neuron specification and spine development (Cubelos et al., 2010). THEMIS2, also known as ICB1 (Induced on contact with basement membrane 1), is a protein expressed in B cells and is associated with signaling proteins Grb2 and Vav1 (Hartweger et al., 2014). Themis2 is not required for B cell development and activation, but it lowers the threshold for activation of B cells in positive selection (Cheng et al., 2017). Themis2 may constitute a control point in macrophage inflammatory response (Peirce et al., 2010). There have been no reports of three tissue-specific expressed hub genes in RA-related research. Nonetheless, SPAG5 and THEMIS2 were overexpressed in the synovial samples of RA in our study. In addition, the results of ROC analysis revealed that these genes had an important diagnostic value for RA. Therefore, these findings suggest that SPAG5 and THEMIS2 may play an essential in progression of synovial hyperplasia.

After interacting 147 DEGs-related target miRNAs and 23 DEMs, 5 overlapping miRNAs were obtained as key miRNAs for further study. In addition to miR-20b and miR-30c, the roles of the other three miRNAs in RA have been reported. miR-496 can impair the proliferative ability and facilitate the apoptosis of

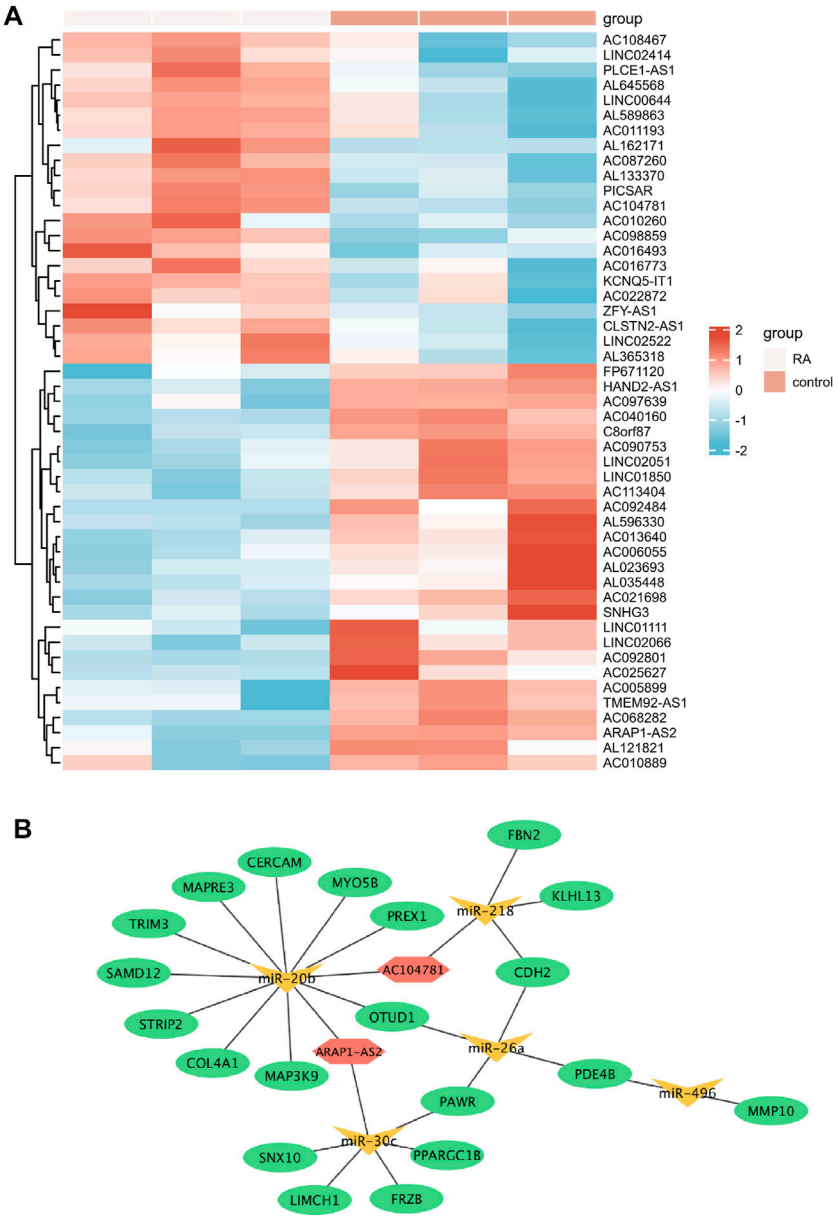

FIGURE 6 | Identification of differentially expressed lncRNAs (DELs) and Establishment of the ceRNA network **(A)** Heatmap of the DELs (red: high expression; blue: low expression) **(B)** The ceRNA network in Rheumatoid arthritis (RA) (ellipse: mRNA, triangle: miRNA, and hexagonal: lncRNA).

IL-1β-treated MH7A through regulating MMP10 expression and NF-κB signaling pathway (Xing et al., 2021). miR-218-5p knockdown could modulate the proliferation, apoptosis and autophagy of RASFs by upregulating KLF9, and suppressing the activation of the JAK2/STAT3 signaling pathway (Chen et al., 2021). MiR-218 regulates the osteogenic differentiation of RA-FLS via the ROBO1/DKK-1 axis (Iwamoto et al., 2018). miR-26a could enhances cells proliferation and attenuate apoptosis of chondrocytes in RA rats (Jiang and Cao, 2020). In addition, miR-26a ameliorates the arthritis severity of the rats through directly targeting TLR3 in rat macrophages (Jiang et al., 2014). Given its prominent role in RA, plasma miR-26a has been proposed as the most promising non-invasive biomarkers for disease detection (Liu et al., 2019). Although there is no relevant research on miR-20b and miR-30c in RA, studies have shown that both of them have a definite effect on inflammation. miR-30c-5p adjusts macrophage-mediated inflammation through pro-apoptotic signals (Ceolotto et al., 2017). knockdown of lncRNA HOTAIR inhibits inflammatory cytokine secretion by increasing the expression of miR-20b and decreasing the expression of NLRP3, thereby relieving ankle swelling caused by gouty arthritis (Liu et al., 2021). miR-20b can restraint T Cell proliferation and activation by regulating NFAT Signaling Pathway in Thymoma-Associated Myasthenia Gravis (Xin

et al., 2016). However, given that these results are based only on bioinformatics models and literature reports, further research is essential to validate the in-depth role of these 5 key miRNAs in RA.

We establish a ceRNA regulatory network was constructed based on five key miRNAs to investigate the role of lncRNA in RA. There are two regulatory axes involving hub genes among the network, including ARAP1-AS2/miR-20b-3p/TRIM3, ARAP1-AS2/miR-30c-3p/FRZB. Interestingly, the key miRNAs involved in these two regulatory networks are the same ones that have not been reported for RA. TRIM3 and FRZB are hub genes involved in the regulation of these two ceRNA axes, both are down regulated in our study. It is worth noting that our finding of FRZB differ from a prior study on circulating levels of FRZB in patients with early rheumatoid arthritis (Corallini et al., 2010). Experimental study has shown that TRIM3 expression in synovial tissue samples from patients with RA was lower than that of healthy controls, which is consistent with our findings, may play an anti-proliferative role in RA-FLS through the P38 signaling pathway (Wang et al., 2017). Our findings also offer insights into the roles of ARAP1-AS2. Unlike for rheumatoid arthritis, the study by Yang et al. showed that lncRNA-ARAP1-AS2 gradually up-regulated with the progression of diabetes (Yang et al., 2019). Mechanistically, lncRNA ARAP1-AS2 may participate in high glucose-induced proximal tubular cell injury by interacting with ARAP1 through persistent activation of EGFR/TGF-β/Smad3 pathway (Li X et al., 2020). ARAP1-AS2/ARAP1 may affect EMT processes and cytoskeleton rearrangement in human renal tubular epithelial cells via boosting of Cdc42-GTP levels (Li L et al., 2020). Although lncRNA ARAP1-AS2 has not been reported in RA, we assumed that ARAP1-AS2/miR-20b-3p/TRIM3 or ARAP1-AS2/miR-30c-3p/FRZB might be the key regulatory axes in the pathogenesis of RA based on the above analysis.

According to CMap analysis, five potential compounds for RA treatment were obtained, and their targets, and application scope were further searched. Troleandomycin (TAO) is one of cytochrome P-450 (CYP450) monooxygenases blockers, which is considered to be a novel drug in the treatment of human inflammatory bowel disease (Sasaki et al., 2003). This suggests that its therapeutic role in RA is also worth exploring. Antirheumatic agents are effective for Parkinson's symptoms, but not for levodopa (Lee et al., 2020). Nonselective HDAC inhibitor trichostatin A (TSA) shared multiple molecular mechanism in suppressing inflammation and may represent a new principle in the treatment of RA (Chung et al., 2003; Gillespie et al., 2012; Grabiec et al., 2012). As a PI3K/AKT inhibitor, LY294002 is often used in RA-related studies (Brennan et al., 2002; Kim et al., 2005; Xing et al., 2016). This presents a number of possibilities for therapeutic strategies. Levamisole was previously used to treat rheumatoid arthritis due to its immunomodulatory properties. However, it had been withdrawn from the US market because of serious side-effects (Cascio and Jen, 2018).

CONCLUSION

This study indicates that screening for identify tissue-specific expressed hub genes and ceRNA network in RA using integrated bioinformatics analyses could help us understand the mechanism of development of RA. Besides, SPAG5 and THEMIS2 might be candidate biomarkers for diagnosis of RA. LY-294002, trichostatin A, and troleandomycin may be potential drugs for RA.

DATA AVAILABILITY STATEMENT

The original contributions presented in the study are included in the article/Supplementary Material, further inquiries can be directed to the corresponding author.

AUTHOR CONTRIBUTIONS

XX and YZ conceived and designed the study. QX downloaded and analyzed the data. BG was responsible for the visualization of data. XX wrote the original draft of the manuscript. ZS and YZ supervised this work and revised the manuscript. All authors have read and approved the final manuscript.

FUNDING

The study was supported by Tianjin Applied basic Research project (No. 21JCYBJC00130), Science and Technology talent cultivation Project of Tianjin Health Commission (No. RC20156), and Science and Technology Fund of Tianjin First Central Hospital (No. 2020CM10).

ACKNOWLEDGMENTS

Thanks to the researchers who uploaded the data. We would like to thank the academic editor and reviewers for their important contributions that improved the quality of this article.

REFERENCES

Bi, X., Guo, X. H., Mo, B. Y., Wang, M. L., Luo, X. Q., Chen, Y. X., et al. (2019). LncRNA PICSAR Promotes Cell Proliferation, Migration and Invasion of Fibroblast-like Synoviocytes by Sponging miRNA-4701-5p in Rheumatoid Arthritis. *EBioMedicine* 50, 408–420. doi:10.1016/j.ebiom.2019.11.024

Brennan, F. M., Hayes, A. L., Ciesielski, C. J., Green, P., Foxwell, B. M., and Feldmann, M. (2002). Evidence that Rheumatoid Arthritis Synovial T Cells Are Similar to Cytokine-Activated T Cells: Involvement of Phosphatidylinositol 3-kinase and Nuclear Factor kappaB Pathways in Tumor Necrosis Factor Alpha Production in Rheumatoid Arthritis. *Arthritis Rheum.* 46, 31–41. doi:10.1002/1529-0131(200201)46:1<31::AID-ART10029>3.0.CO;2-5

Canu, V., Donzelli, S., Sacconi, A., Lo Sardo, F., Pulito, C., Bossel, N., et al. (2021). Aberrant Transcriptional and post-transcriptional Regulation of SPAG5, a

YAP-TAZ-TEAD Downstream Effector, Fuels Breast Cancer Cell Proliferation. *Cell Death Differ* 28, 1493–1511. doi:10.1038/s41418-020-00677-9

Cascio, M. J., and Jen, K.-Y. (2018). Cocaine/levamisole-associated Autoimmune Syndrome: A Disease Of Neutrophil-Mediated Autoimmunity. *Curr. Opin. Hematol.* 25, 29–36. doi:10.1097/moh.0000000000000393

Ceolotto, G., Giannella, A., Albiero, M., Kuppusamy, M., Radu, C., Simioni, P., et al. (2017). miR-30c-5p Regulates Macrophage-Mediated Inflammation and Pro-atherosclerosis Pathways. *Cardiovasc. Res.* 113, 1627–1638. doi:10.1093/cvr/cvx157

Chen, M., Li, M., Zhang, N., Sun, W., Wang, H., and Wei, W. (2021). Mechanism of miR-218-5p in Autophagy, Apoptosis and Oxidative Stress in Rheumatoid Arthritis Synovial Fibroblasts Is Mediated by KLF9 and JAK/STAT3 Pathways. *J. Investig. Med.* 69, 824–832. doi:10.1136/jim-2020-001437

Cheng, D., Deobagkar-Lele, M., Zvezdova, E., Choi, S., Uehara, S., Baup, D., et al. (2017). Themis2 Lowers the Threshold for B Cell Activation during Positive Selection. *Nat. Immunol.* 18, 205–213. doi:10.1038/ni.3642

Cheng, Q., Chen, X., Wu, H., and Du, Y. (2021). Three Hematologic/immune System-specific Expressed Genes Are Considered as the Potential Biomarkers for the Diagnosis of Early Rheumatoid Arthritis through Bioinformatics Analysis. *J. Transl Med.* 19, 18. doi:10.1186/s12967-020-02689-y

Chung, Y.-L., Lee, M.-Y., Wang, A.-J., and Yao, L.-F. (2003). A Therapeutic Strategy Uses Histone Deacetylase Inhibitors to Modulate the Expression of Genes Involved in the Pathogenesis of Rheumatoid Arthritis. *Mol. Ther.* 8, 707–717. doi:10.1016/s1525-0016(03)00235-1

Corallini, F., Secchiero, P., Castellino, G., Montecucco, M., Trotta, F., and Zauli, G. (2010). Circulating Levels of Frizzled-Related Protein (FRZB) Are Increased in Patients with Early Rheumatoid Arthritis and Decrease in Response to Disease-Modifying Antirheumatic Drugs. *Ann. Rheum. Dis.* 69, 1733–1734. doi:10.1136/ard.2009.125732

Cubelos, B., Sebastián-Serrano, A., Beccari, L., Calcagnotto, M. E., Cisneros, E., Kim, S., et al. (2010). Cux1 and Cux2 Regulate Dendritic Branching, Spine Morphology, and Synapses of the Upper Layer Neurons of the Cortex. *Neuron* 66, 523–535. doi:10.1016/j.neuron.2010.04.038

Del Rey, M. J., Usategui, A., Izquierdo, E., Cañete, J. D., Blanco, F. J., Criado, G., et al. (2012). Transcriptome Analysis Reveals Specific Changes in Osteoarthritis Synovial Fibroblasts. *Ann. Rheum. Dis.* 71, 275–280. doi:10.1136/annrheumdis-2011-200281

Gillespie, J., Savic, S., Wong, C., Hempshall, A., Inman, M., Emery, P., et al. (2012). Histone Deacetylases Are Dysregulated in Rheumatoid Arthritis and a Novel Histone Deacetylase 3-selective Inhibitor Reduces Interleukin-6 Production by Peripheral Blood Mononuclear Cells from Rheumatoid Arthritis Patients. *Arthritis Rheum.* 64, 418–422. doi:10.1002/art.33382

Grabiec, A. M., Korchynskyi, O., Tak, P. P., and Reedquist, K. A. (2012). Histone Deacetylase Inhibitors Suppress Rheumatoid Arthritis Fibroblast-like Synoviocyte and Macrophage IL-6 Production by Accelerating mRNA Decay. *Ann. Rheum. Dis.* 71, 424–431. doi:10.1136/ard.2011.154211

Hartweger, H., Schweighoffer, E., Davidson, S., Peirce, M. J., Wack, A., and Tybulewicz, V. L. J. (2014). Themis2 Is Not Required for B Cell Development, Activation, and Antibody Responses. *J.I.* 193, 700–707. doi:10.4049/jimmunol.1400943

He, J., Green, A. R., Li, Y., Chan, S. Y. T., and Liu, D.-X. (2020). SPAG5: An Emerging Oncogene. *Trends Cancer* 6, 543–547. doi:10.1016/j.trecan.2020.03.006

Huang, D., Sherman, B. T., Tan, Q., Collins, J. R., Alvord, W. G., Roayaei, J., et al. (2007). The DAVID Gene Functional Classification Tool: a Novel Biological Module-Centric Algorithm to Functionally Analyze Large Gene Lists. *Genome Biol.* 8, R183. doi:10.1186/gb-2007-8-9-r183

Iwamoto, N., Fukui, S., Takatani, A., Shimizu, T., Umeda, M., Nishino, A., et al. (2018). Osteogenic Differentiation of Fibroblast-like Synovial Cells in Rheumatoid Arthritis Is Induced by microRNA-218 through a ROBO/Slit Pathway. *Arthritis Res. Ther.* 20, 189. doi:10.1186/s13075-018-1703-z

Jiang, C., Zhu, W., Xu, J., Wang, B., Hou, W., Zhang, R., et al. (2014). MicroRNA-26a Negatively Regulates Toll-like Receptor 3 Expression of Rat Macrophages and Ameliorates Pristane Induced Arthritis in Rats. *Arthritis Res. Ther.* 16, R9. doi:10.1186/ar4435

Jiang, L., and Cao, S. (2020). Role of microRNA-26a in Cartilage Injury and Chondrocyte Proliferation and Apoptosis in Rheumatoid Arthritis Rats by Regulating Expression of CTGF. *J. Cel Physiol* 235, 979–992. doi:10.1002/jcp.29013

Kim, K.-W., Cho, M.-L., Park, M.-K., Yoon, C.-H., Park, S.-H., Lee, S.-H., et al. (2005). Increased Interleukin-17 Production via a Phosphoinositide 3-kinase/Akt and Nuclear Factor kappaB-dependent Pathway in Patients with Rheumatoid Arthritis. *Arthritis Res. Ther.* 7, R139–R148. doi:10.1186/ar1470

Kulasingam, V., and Diamandis, E. P. (2008). Strategies for Discovering Novel Cancer Biomarkers through Utilization of Emerging Technologies. *Nat. Rev. Clin. Oncol.* 5, 588–599. doi:10.1038/ncponc1187

Li, L., Xu, L., Wen, S., Yang, Y., Li, X., and Fan, Q. (2020). The Effect of lncRNA-ARAP1-AS2/ARAP1 on High Glucose-Induced Cytoskeleton Rearrangement and Epithelial-Mesenchymal Transition in Human Renal Tubular Epithelial Cells. *J. Cel Physiol* 235, 5787–5795. doi:10.1002/jcp.29512

Li, W., Wang, W., Liu, L., Qu, R., Chen, X., Qiu, C., et al. (2019). GDF11 Antagonizes TNF-α-Induced Inflammation and Protects against the Development of Inflammatory Arthritis in Mice. *FASEB j.* 33, 3317–3329. doi:10.1096/fj.201801375RR

Li, X., Ma, T. K., Wen, S., Li, L. L., Xu, L., Zhu, X. W., et al. (2020). LncRNA ARAP1-AS2 Promotes High Glucose-Induced Human Proximal Tubular Cell Injury via Persistent Transactivation of the EGFR by Interacting with ARAP1. *J. Cel. Mol. Med.* 24, 12994–13009. doi:10.1111/jcmm.15897

Li, X., Tang, X., Wang, Y., Chai, C., Zhao, Z., Zhang, H., et al. (2021). CS-semi5 Inhibits NF-Kb Activation to Block Synovial Inflammation, Cartilage Loss and Bone Erosion Associated with Collagen-Induced Arthritis. *Front. Pharmacol.* 12, 655101. doi:10.3389/fphar.2021.655101

Liou, L.-M., Lee, K.-W., Chien, C.-F., Wu, M.-N., and Lai, C.-L. (2020). Parkinsonism with Newly Diagnosed Flare-Up Rheumatoid Arthritis Mimicking Progressive Supranuclear Palsy. *Neurol. India* 68, 481–482. doi:10.4103/0028-3886.284382

Liu, B., and Ren, B. (2020). MiR-1193 Represses the Proliferation and Induces the Apoptosis of Interleukin-1β-Treated Fibroblast-like Synoviocytes via Targeting JAK3. *Int. J. Rheum. Dis.* 23, 1066–1075. doi:10.1111/1756-185x.13901

Liu, J. Y., Zeng, Q. H., Cao, P. G., Xie, D., Yang, F., He, L. Y., et al. (2018). SPAG5 Promotes Proliferation and Suppresses Apoptosis in Bladder Urothelial Carcinoma by Upregulating Wnt3 via Activating the AKT/mTOR Pathway and Predicts Poorer Survival. *Oncogene* 37, 3937–3952. doi:10.1038/s41388-018-0223-2

Liu, X., Ni, S., Li, C., Xu, N., Chen, W., Wu, M., et al. (2019). Circulating microRNA-23b as a New Biomarker for Rheumatoid Arthritis. *Gene* 712, 143911. doi:10.1016/j.gene.2019.06.001

Liu, Y.-F., Xing, G.-L., Chen, Z., and Tu, S.-H. (2021). Long Non-coding RNA HOTAIR Knockdown Alleviates Gouty Arthritis through miR-20b Upregulation and NLRP3 Downregulation. *Cell Cycle* 20, 332–344. doi:10.1080/15384101.2021.1874696

McInnes, I. B., and Schett, G. (2011). The Pathogenesis of Rheumatoid Arthritis. *N. Engl. J. Med.* 365, 2205–2219. doi:10.1056/NEJMra1004965

Moran-Moguel, M. C., Petarra-Del Rio, S., Mayorquin-Galvan, E. E., and Zavala-Cerna, M. G. (2018). Rheumatoid Arthritis and miRNAs: A Critical Review through a Functional View. *J. Immunol. Res.* 2018, 1–16. doi:10.1155/2018/2474529

Pal, R., Ramdzan, Z. M., Kaur, S., Duquette, P. M., Marcotte, R., Leduy, L., et al. (2015). CUX2 Protein Functions as an Accessory Factor in the Repair of Oxidative DNA Damage. *J. Biol. Chem.* 290, 22520–22531. doi:10.1074/jbc.M115.651042

Peirce, M. J., Brook, M., Morrice, N., Snelgrove, R., Begum, S., Lanfrancotti, A., et al. (2010). Themis2/ICB1 Is a Signaling Scaffold that Selectively Regulates Macrophage Toll-like Receptor Signaling and Cytokine Production. *PloS one* 5, e11465. doi:10.1371/journal.pone.0011465

Peng, P., Zhang, B., Huang, J., Xing, C., Liu, W., Sun, C., et al. (2020). Identification of a circRNA-miRNA-mRNA Network to Explore the Effects of circRNAs on Pathogenesis and Treatment of Spinal Cord Injury. *Life Sci.* 257, 118039. doi:10.1016/j.lfs.2020.118039

Salmena, L., Poliseno, L., Tay, Y., Kats, L., and Pandolfi, P. P. (2011). A ceRNA Hypothesis: the Rosetta Stone of a Hidden RNA Language? *Cell* 146, 353–358. doi:10.1016/j.cell.2011.07.014

Sasaki, M., Ostanin, D., Elrod, J. W., Oshima, T., Jordan, P., Itoh, M., et al. (2003). TNF-α-induced Endothelial Cell Adhesion Molecule Expression Is Cytochrome

P-450 Monooxygenase Dependent. *Am. J. Physiology-Cell Physiol.* 284, C422–C428. doi:10.1152/ajpcell.00271.2002

Schmidt, C. J., Wenndorf, K., Ebbers, M., Volzke, J., Müller, M., Strübing, J., et al. (2020). Infection with Clostridioides Difficile Attenuated Collagen-Induced Arthritis in Mice and Involved Mesenteric T(reg) and T(h2) Polarization. *Front. Immunol.* 11, 571049. doi:10.3389/fimmu.2020.571049

Scott, D. L., Wolfe, F., and Huizinga, T. W. (2010). Rheumatoid Arthritis. *The Lancet* 376, 1094–1108. doi:10.1016/s0140-6736(10)60826-4

Stephenson, W., Donlin, L. T., Butler, A., Rozo, C., Bracken, B., Rashidfarrokhi, A., et al. (2018). Single-cell RNA-Seq of Rheumatoid Arthritis Synovial Tissue Using Low-Cost Microfluidic Instrumentation. *Nat. Commun.* 9, 791. doi:10.1038/s41467-017-02659-x

Wang, M., Wu, J., Guo, Y., Chang, X., and Cheng, T. (2017). The Tripartite Motif-Containing Protein 3 on the Proliferation and Cytokine Secretion of Rheumatoid Arthritis Fibroblast-like Synoviocytes. *Mol. Med. Rep.* 15, 1607–1612. doi:10.3892/mmr.2017.6164

Wu, C., Orozco, C., Boyer, J., Leglise, M., Goodale, J., Batalov, S., et al. (2009). BioGPS: an Extensible and Customizable portal for Querying and Organizing Gene Annotation Resources. *Genome Biol.* 10, R130. doi:10.1186/gb-2009-10-11-r130

Xin, Y., Cai, H., Lu, T., Zhang, Y., Yang, Y., and Cui, Y. (2016). miR-20b Inhibits T Cell Proliferation and Activation via NFAT Signaling Pathway in Thymoma-Associated Myasthenia Gravis. *Biomed. Research International* 2016, 1–12. doi:10.1155/2016/9595718

Xing, R., Jin, Y., Sun, L., Yang, L., Li, C., Li, Z., et al. (2016). Interleukin-21 Induces Migration and Invasion of Fibroblast-like Synoviocytes from Patients with Rheumatoid Arthritis. *Clin. Exp. Immunol.* 184, 147–158. doi:10.1111/cei.12751

Xing, X.-W., Shi, H.-Y., Liu, S., Feng, S.-X., Feng, S.-Q., and Gong, B.-Q. (2021). miR-496/MMP10 Is Involved in the Proliferation of IL-1β-Induced Fibroblast-like Synoviocytes via Mediating the NF-Kb Signaling Pathway. *Inflammation* 44, 1359–1369. doi:10.1007/s10753-021-01421-2

Yang, Y., Lv, X., Fan, Q., Wang, X., Xu, L., Lu, X., et al. (2019). Analysis of Circulating lncRNA Expression Profiles in Patients with Diabetes Mellitus and Diabetic Nephropathy: Differential Expression Profile of Circulating lncRNA. *Cn* 92, 25–35. doi:10.5414/cn109525

Zhang, L.-l., Xiao, H., Zhang, F., Wu, Y.-j., Shu, J.-l., Li, Y., et al. (2021). BAFF, Involved in B Cell Activation through the NF-Kb Pathway, Is Related to Disease Activity and Bone Destruction in Rheumatoid Arthritis. *Acta Pharmacol. Sin* 42, 1665–1675. doi:10.1038/s41401-020-00582-4

Conflict of Interest: The authors declare that the research was conducted in the absence of any commercial or financial relationships that could be construed as a potential conflict of interest.

Publisher's Note: All claims expressed in this article are solely those of the authors and do not necessarily represent those of their affiliated organizations, or those of the publisher, the editors and the reviewers. Any product that may be evaluated in this article, or claim that may be made by its manufacturer, is not guaranteed or endorsed by the publisher.

frontiers in Genetics

ORIGINAL RESEARCH
published: 29 March 2022
doi: 10.3389/fgene.2022.837301

An Individualized Prognostic Signature for Clinically Predicting the Survival of Patients With Bladder Cancer

Qing Liu[1†], Yunchao Wang[2†], Huayu Gao[2], Fahai Sun[3], Xuan Wang[3], Huawei Zhang[1] and Jianning Wang[2*]*

[1]Department of Medical Ultrasound, Shandong Provincial Hospital Affiliated to Shandong First Medical University, Jinan, China, [2]Department of Urology, The First Affiliated Hospital of Shandong First Medical University, Jinan, China, [3]Department of Urology, Fifth Peoples Hospital Jinan, Jinan, China

OPEN ACCESS

Edited by:
Deepanjan Paul,
Children's Hospital of Philadelphia,
United States

Reviewed by:
Yuchen Liu,
Shenzhen University, China
Hifzur R Siddique,
Aligarh Muslim University, India
Disha Sharma,
Stanford Healthcare, United States

***Correspondence:**
Huawei Zhang
slyyzhw@163.com
Jianning Wang
docjianningwang@163.com

[†]These authors have contributed equally to this work

Specialty section:
This article was submitted to RNA,
a section of the journal Frontiers in Genetics

Received: 16 December 2021
Accepted: 02 March 2022
Published: 29 March 2022

Citation:
Liu Q, Wang Y, Gao H, Sun F, Wang X, Zhang H and Wang J (2022) An Individualized Prognostic Signature for Clinically Predicting the Survival of Patients With Bladder Cancer. Front. Genet. 13:837301. doi: 10.3389/fgene.2022.837301

Background: The tumor immune microenvironment (TIME) plays an important role in the development and prognosis of bladder cancer. It is essential to conduct a risk model to explore the prognostic value of the immunologic genes and establish an individualized prognostic signature for predicting the survival of patients with bladder cancer.

Method: The differentially expressed immunologic genes (DEGs) are identified in The Cancer Genome Atlas (TCGA). The nonnegative matrix factorization (NMF) was used to stratify the DEGs in TCGA. We used the least absolute shrinkage and selection operator (LASSO) Cox regression and univariate Cox analysis to establish a prognostic risk model. A nomogram was used to establish an individualized prognostic signature for predicting survival. The potential pathways underlying the model were explored.

Results: A total of 1,018 DEGs were screened. All samples were divided into two clusters (C1 and C2) by NMF with different immune cell infiltration, and the C2 subtype had poor prognosis. We constructed a 15-gene prognostic risk model from TCGA cohort. The patients from the high-risk group had a poor overall survival rate compared with the low-risk group. Time-dependent ROC curves demonstrated good predictive ability of the signature (0.827, 0.802, and 0.812 for 1-, 3-, and 5-year survival, respectively). Univariate and multivariate Cox regression analyses showed that the immunologic prognostic risk model was an independent factor. The decision curve demonstrated a relatively good performance of the risk model and individualized prognostic signature, showing the best net benefit for 1-, 3-, and 5-year OS. Gene aggregation analysis showed that the high-risk

Abbreviations: AUC, the area under the curve; BCG, bacillus Calmette–Guérin; CI, confidence interval; DCA, decision curve analysis; FDR, false discovery rate; GEO, Gene Expression Omnibus; GSEA, Gene Set Enrichment Analysis; HR, hazard ratio; ICIs, immune checkpoint inhibitors; LASSO, least absolute shrinkage and selection operator; MDSCs, myeloid-derived suppressor cells; OS, overall survival; PFS, progression-free survival; ROC, receiver operating characteristic curve; SNV, single-nucleotide variant; TCGA, The Cancer Genome Atlas; TIME, tumor immune microenvironment; TMB, tumor mutation burden; Treg, regulatory T cells.

group was mainly concentrated in tumorigenesis and migration and immune signaling pathways.

Conclusion: We established a risk model and an individualized prognostic signature, and these may be useful biomarkers for prognostic prediction of patients with bladder cancer.

Keywords: bladder cancer, prognostic model, tumor immune microenvironment, bioinformatics analysis, immunologic gene

INTRODUCTION

Bladder cancer is the most common type of cancer among urinary malignancies and adds approximately 550,000 new cases each year, with approximately 200,000 deaths (Antoni et al., 2017; Bray et al., 2018). The traditional treatments for bladder cancer mainly include transurethral resection and cisplatin-based chemotherapy (Tran et al., 2021). However, the 5-year overall survival rate remains at 40–60% for muscle-invasive bladder cancer (Alfred Witjes et al., 2017). Immunotherapy, such as bacillus Calmette–Guérin (BCG) and immune checkpoint inhibitors (ICIs), has become effective and showed promising antitumor activity (Balar et al., 2021). Studies demonstrated that immunotherapy might benefit some patients with bladder cancer, suggesting that the tumor immune microenvironment (TIME) may play an important role (Boorjian et al., 2021; Witjes et al., 2021).

The TIME, representing a complicated network of suppressing cancer immunity (Binnewies et al., 2018), is essential for tumor cells to avoid potential autoimmunity and tissue damage while generating a successful immune escape and is involved in restraining tumor development or tumor-promoting effects and affects the response to immunotherapy (Chen et al., 2017; Lenis et al., 2020). This regulation is orchestrated by different mechanisms, either intrinsic or extrinsic. The TIME has been demonstrated to predict the prognosis for patients with different tumor types, including hepatocellular carcinoma (Gong et al., 2021), breast (Keren et al., 2018), and ovarian cancers (Jiang et al., 2020). Immune gene expression patterns are also enriched in UBC. Although several clinical features and molecular biomarkers have been applied for the prognosis of bladder cancer, only limited data of patient cohorts have indicated positive prognostic relevance of the TIME for patient survival. Therefore, it is meaningful for us to find out high accurate prognostic biomarkers, which could guide patient selection and help evaluate likely disease outcomes.

In this study, we used data from The Cancer Genome Atlas (TCGA) and GEO database to analyze the differential expression of immunologic genes and constructed a consistent clustering. Then, we conducted a risk model to explore the prognostic value of the differentially expressed immunologic genes and established an individualized prognostic signature for predicting the survival of patients with bladder cancer. We also characterized the signature based on the differentially expressed immunologic gene scores as a prognostic stratification tool.

MATERIALS AND METHODS

Data Preparation

Gene expression data (FPKM format, normalized), related clinical information, and single-nucleotide variant (SNV) of the bladder cancer were obtained from The Cancer Genome Atlas (TCGA) database (https://portal.gdc.cancer.gov/). The data consisted of 414 bladder cancer samples and 19 normal case samples. RNA-seq data and clinical survival information of the GSE19423 dataset for additional bladder cancer samples were obtained from the Gene Expression Omnibus (GEO) (https://www.ncbi.nlm.nih.gov/geo/). GSE19423 had 48 tumor tissues with their associated follow-up information for subsequent validation of the prognostic gene signature. The samples with incomplete data on gender, age, survival time, survival status, and pathological grading were excluded. A total of 4061 immunologic gene sets (C7) were downloaded from Gene Set Enrichment Analysis (GSEA) (https://www.gsea-msigdb.org/gsea/msigdb/index.jsp) (Subramanian et al., 2005). The data were analyzed with the R (version 3.6.1) and R Bioconductor packages.

Screening of the Differentially Expressed Immunologic Genes

Immunologic gene sets (C7), GSE19423 dataset, and TCGA bladder cancer datasets are used to extract and sort out the expression of immunologic genes. The differentially expressed immunologic genes between tumor and normal tissues in TCGA bladder cancer datasets were screened using edgeR package (Robinson et al., 2010), with parameters of $|\log FC| > 1.0$ and p-value < 0.05. The differentially expressed immunologic genes were displayed by the volcano plot. ($n = 1018$)

Bladder Cancer Subtype Identification

The nonnegative matrix factorization (NMF) was used to stratify the differentially expressed immunologic genes in TCGA. The "NMF" R package was used to perform unsupervised NMF clustering (Gaujoux and Seoighe, 2010). According to cophenetic, dispersion, and silhouette coefficients, the best cluster number was chosen as the coexistence correlation coefficient K value 2. To explore the profiles of two subtypes, we used Kaplan–Meier analysis (R package "survival") to discriminate genes correlated with overall survival. Using the CIBERSORT algorithm (Newman et al., 2015), the infiltration levels of 23 kinds of immune cells were estimated, and we utilized the "MCPcounter" R package to evaluate the abundances of two

stromal cells and eight immune cells in two subtypes (Becht et al., 2016).

Construction of the Immunologic Prognostic Risk Model

To explore the prognostic value of the differentially expressed immunologic genes, we conducted a prognostic risk model. Before conducting the risk model, the randomly selected 70% samples from the differentially expressed immunologic genes were assigned as the training dataset, while the remaining 30% samples and GSE19423 dataset were used as the test set. The prognostic-related genes were identified by univariate and multivariate Cox regression analyses. After that, we conduct the least absolute shrinkage and selection operator (LASSO) Cox regression (R package "glmnet") to identify independent prognostic genes powerfully associated ($p < 0.05$) with OS in bladder cancer patients (Friedman et al., 2010). The risk score was calculated by the following formula:

$$Risk\ score = \sum (Coefficient\ of\ mRNAi * expression\ of\ mRNAi). \quad (1)$$

Based on the calculating formula, the training and the test sets were divided into low- and high-risk groups based on the median risk score. To validate the model, the receiver operating characteristic curve (ROC) analysis (R package "timeROC") and clinicopathological feature (age, gender, histological grade, and pathological T, N, and M) analysis (R package "survminer", "survival") were performed. Diagnosis of age, gender, histological grade, stage, and the risk score was included in this study for univariate and multivariate Cox regression analyses, which determined that the risk score was the independent prognostic factor for bladder cancer. We will also analyze which immunologic genes are related to the risk score. Then, we analyzed the relationship between the risk score and immune cell infiltration and tumor mutation burden (TMB) in bladder cancer through R package "corrplot" (Wei et al., 2017), and "circlize" (Gu et al., 2014).

Construct and Validate the Individualized Prognostic Signature

A previous study showed that clinical characteristics, including age, gender, histological grade, stage, and pathological T, N, and M, were risk predictors for OS in bladder cancer (Shinohara et al., 1995; Puente et al., 2003; Gupta et al., 2009). Diagnosis of age, gender, histological grade, stage, pathological T, N, M, and the risk score was used to build an individualized prognostic signature (R package "rms", "nomogramEx" and "regplot") to predict OS (Du et al., 2017; Arnhold, 2018). Next, we estimated whether the predicted survival outcome (1-, 3-, and 5-year survival) was close to the actual outcome with calibration curves. Furthermore, 1-, 3-, and 5-year decision curve analysis (DCA), which can assess and compare prediction signatures that incorporate clinicopathological features, was used to calculate whether our established nomogram was suitable for clinical utility.

Gene Set Enrichment Analyses and Identification of Significantly Mutated Genes

To identify the potential molecular mechanisms underlying the signature in the low-risk and high-risk groups, GSEA (Subramanian et al., 2005) was performed through the limma R package and clusterprofiler package. $p < 0.05$ was considered statistically significant.

Statistical Analyses

R software 4.1.1 was applied in this study for statistical analyses. Categorical variables were analyzed *via* the Wilcoxon rank-sum test. Continuous variables were analyzed using Student's t-test for paired samples. Univariate and multivariate Cox regression analyses were utilized to evaluate survival. The hazard ratio (HR) and 95% confidence interval (CI) were calculated to identify genes associated with OS. *p*-value < 0.05 was considered statistically significant.

RESULTS

Identification of Differentially Expressed Immunologic Genes

Our study flowchart is shown in **Figure 1**. 4061 immunologic gene sets were retrieved from "immunologic signature gene sets". After the preliminary screening, we matched 1,018 DEGs between tumor and normal tissues in TCGA database (**Supplementary Table S1**). 773 genes were found to be significantly upregulated, while 245 genes were significantly downregulated (**Figure 2A**).

Classification and Characterization of Bladder Cancer

Based on the expression profiles of the differentially expressed immunologic genes, bladder cancer samples from TCGA were clustered by using the NMF package. The optimal value of subtypes (K) was determined (K = 2, **Figure 2B**) on the grounds of the cophenetic correlation coefficient. Hence, the bladder cancer samples were clustered into two molecular subtypes C1 and C2. Bladder cancer patients with subtype 1 displayed good OS, while subtype 2 had poor prognosis (log-rank $p < 0.001$; **Figure 2C**). Interestingly, patients in subtype 2 had shorter PFS time than those in C1 (log-rank $p < 0.001$; **Figure 2D**).

To estimate the population abundance of tissue-infiltrating immune and stromal cell populations in two subtypes, we used the CIBERSORT algorithm and the MCPcounter method. As a result, activated B cell, activated CD4 T cell, activated CD8 T cell, activated dendritic cell, MDSC cell, macrophage, natural killer cell, type 1, 2 T helper cell, and regulatory T cell in cluster 2 were significantly higher than those in cluster 1 ($p < 0.01$), while

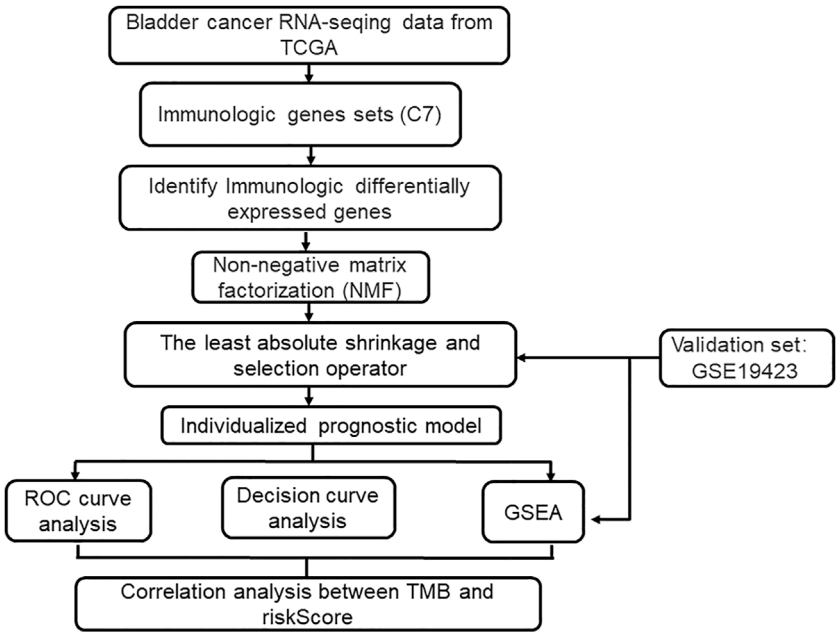

FIGURE 1 | Flow chart of this study.

monocyte ($p < 0.05$) and CD56 dim natural killer cell ($p < 0.001$) in cluster 1 were higher than those in cluster 2 (**Figure 2E**). The results from the MCPcounter method validated that given in **Supplementary Figure S1**.

Construction of the Immunologic Prognostic Risk Model

Then, we conducted a risk model to explore the value of differentially expressed immunologic genes. Among TCGA training cohort, 144 OS associated differentially expressed immunologic genes were identified through the univariate Cox regression analysis ($p < 0.05$) (**Supplementary Table S2**). In addition, the multivariate Cox regression analysis identified 15 OS associated differentially expressed immunologic genes in bladder cancer patients ($p < 0.05$) (**Supplementary Table S3**). Fifteen genes were screened using the LASSO regression algorithm (**Figures 3A,B**) to construct the immunologic prognostic risk model. Using the coefficients obtained from the expression levels and regression coefficients, patients from the training and the test set were divided into low-risk and high-risk groups based on the median risks score to assess the robustness of the prognostic risk model. The patients from the high-risk group had a poor overall survival rate compared with those in the low-risk group (**Figures 3C,D**) whether in the training or test set. Time-dependent ROC curves showed that the classifier had good accuracy with 0.827, 0.802, and 0.812 for 1-, 3-, and 5-year survival, respectively, in the training set while 0.661,0.742,0.740 in the test set. (**Figures 3E,F**). Moreover, the immunologic prognostic risk model had better predictive power and accuracy than other clinical factors (including age, gender, grade, and stage), indicating an independent prognostic risk factor (**Supplementary Figure S2**).

According to the analysis between immunologic genes and the risk score, we found that POLE2, FEN1, MCM6, MSH6, MSH2, and LOXL2 are positively correlated with the risk score, while PDCD1 and CTLA4 are negatively correlated with the risk score (**Figure 4A**). We also analyze the relationship between the risk score and immune cell infiltration and TMB (**Figure 4B**). The results showed that the risk score and TMB have a negative correlation and the risk score and endothelial cells have a positive correlation. In addition, we can also observe that except for endothelial cells, most immune cells have a negative relationship with the risk score. Univariate and multivariate Cox regression analyses showed that the immunologic prognostic risk model was an independent factor (**Table 1**).

We used the GSE19423 cohort to validate the predictive ability of the immunologic prognostic risk model. Kaplan–Meier analysis showed that the low-risk group has a greater chance of obtaining the same survival time than the high-risk score group in the GEO dataset (**Supplementary Figure S3**).

Establishment of an Individualized Prognostic Signature

Based on the results of the univariate and multivariate analyses, diagnosis of age, stage, and risk score were independent risk predictors for overall survival (OS) (**Supplementary Table**

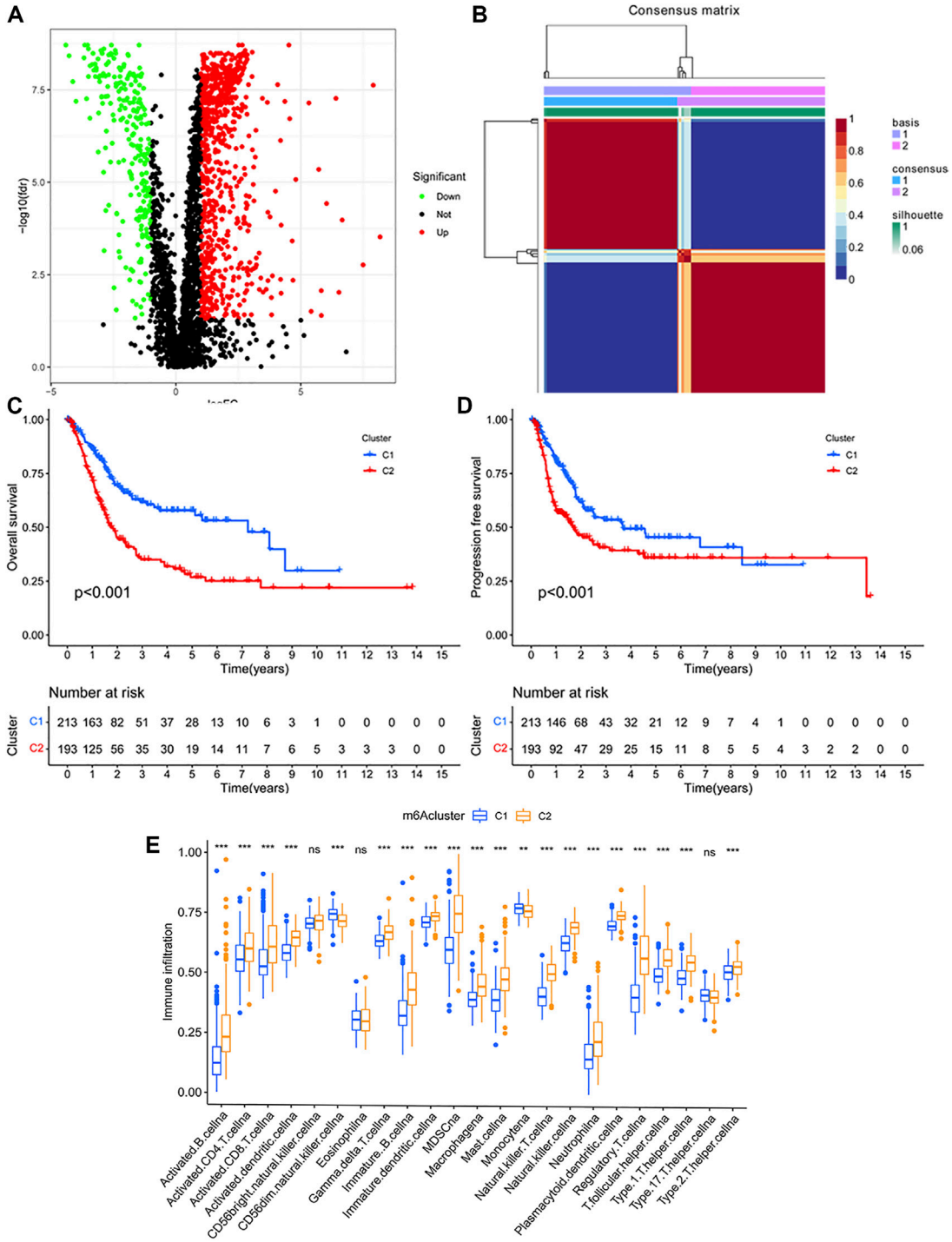

FIGURE 2 | (A) Identification of the differentially expressed immunologic genes in TCGA database. **(B)** Identification of clinically relevant subtypes of bladder cancer: samples were clustered by the nonnegative matrix factorization (NMF) method. **(C,D)** Survival curves of each immune subtype in the training set. **(E)** Immune cell infiltration in two subtypes.

S4). An individualized prognostic signature was generated to observe the relationship between these independent prognostic factors and personalized survival status (**Figure 5A**). The calibration curve was constructed to describe the prediction value of the nomogram, and the 45-degree line indicated the actual survival outcomes (**Figure 5B**). In the calibration curve, the signature had good predictive power for predicting OS at 1, 3, and 5 years.

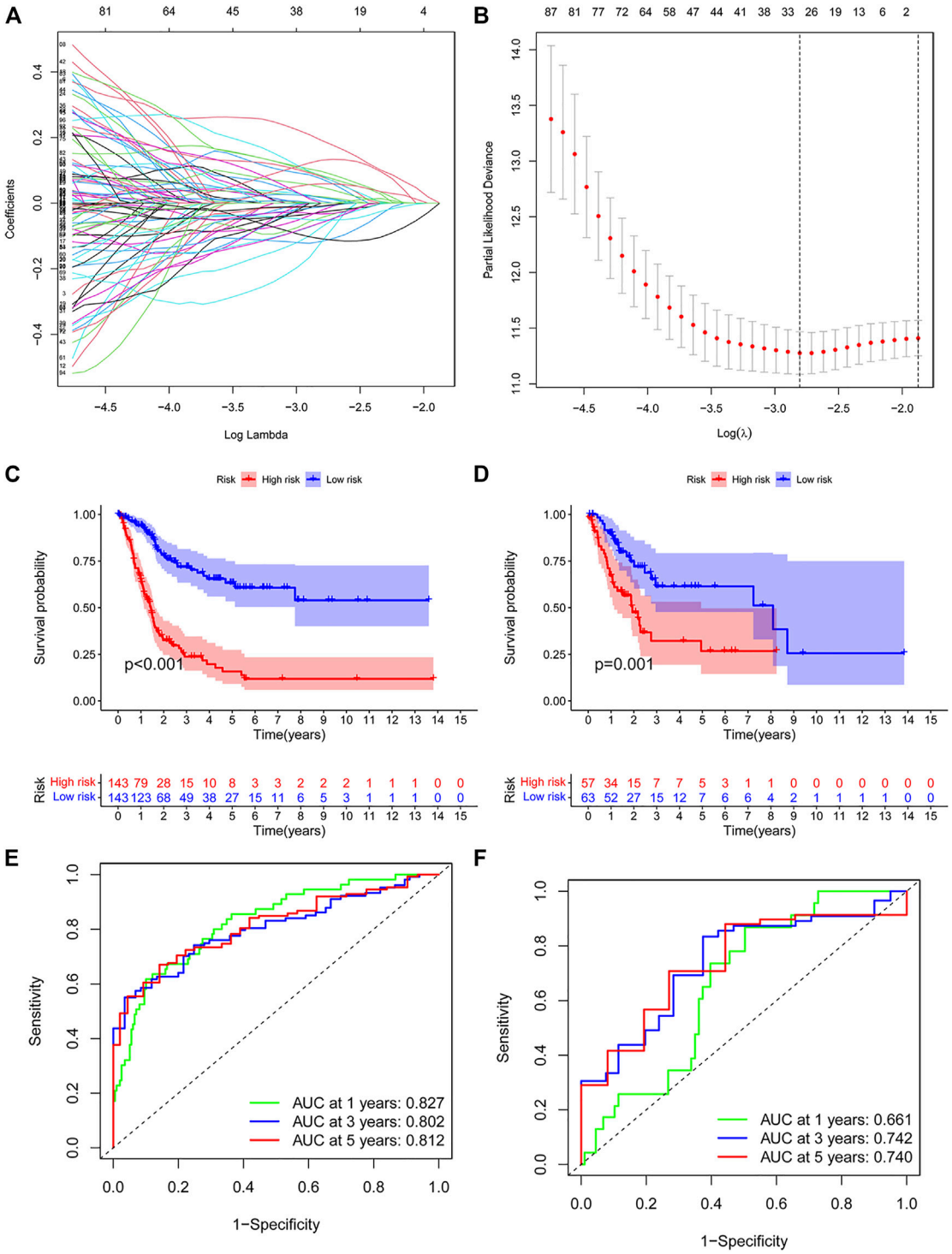

FIGURE 3 | (A,B) Risk model as prognostic factors for bladder cancer patients. **(C,D)** Kaplan–Meier survival curves show the OS of patients in the high- and low-risk groups in the training group. **(E,F)** Time-dependent ROC curves illustrated the ability of the risk model to predict OS in the training and test set (training dataset: 1-year AUC = 0.827, 3-year AUC = 0.802, 5-year AUC = 0.812; test dataset: 1-year AUC = 0.661, 3-year AUC = 0.742, 5-year AUC = 0.740).

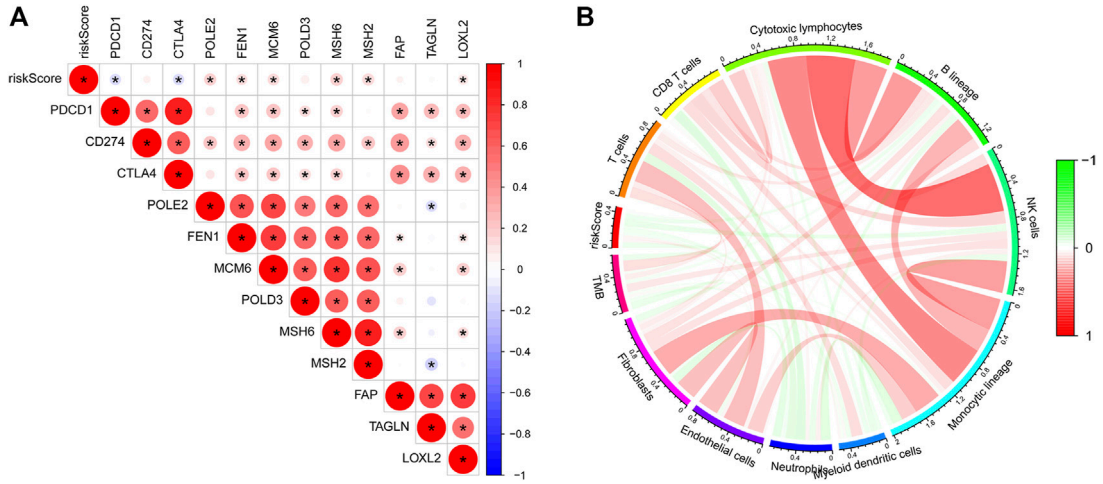

FIGURE 4 | (A) Correlations between the risk score and immunologic genes: a negative correlation was marked with blue and a positive correlation with red. **(B)** Correlation between the risk score and TMB and immune cells: a negative correlation was marked with blue and a positive correlation with red.

TABLE 1 | Cox analysis of clinicopathological parameters for OS in bladder cancer.

	Univariate			Multivariate		
	HR	**95% CI**	***p***	**HR**	**95% CI**	***p***
Age	1.03	1.02–1.05	0.00002	1.02	1.00–1.03	0.005
Stage	1.74	1.44–2.11	0.00000002	1.59	1.30–1.93	0.000004
RiskScore	1.11	1.09–1.13	0.005*	1.08	1.06–1.10	0.005*

**Statistically significant (p < 0.05).*

In addition, the ROC analysis result demonstrated that the AUC of individualized prognostic signature and nomogram signature increased to 0.791 and 0.784, respectively (**Figure 6A**). The DCA was performed for the clinicopathological features (including age, gender, grade, and stage), risk signature, and nomogram signature as shown in **Figure 6B**. The decision curve demonstrated relatively good performance of risk signature and individualized prognostic signature, showing the best net benefit for 1-, 3-, and 5-year OS (**Figures 6C,D**).

Functional Analysis of the Prognostic Signature

To understand the biological processes and KEGG pathways of the obtained 15 OS-associated differentially expressed immunologic genes, gene set enrichment analysis was performed (**Figures 6A,B**). As shown in **Figure 6A**, five biological processes relevant to ECM receptor interaction, focal adhesion, JAK-STAT, pathway in cancer, and regulation of actin cytoskeleton were enriched in the high-risk group. These results

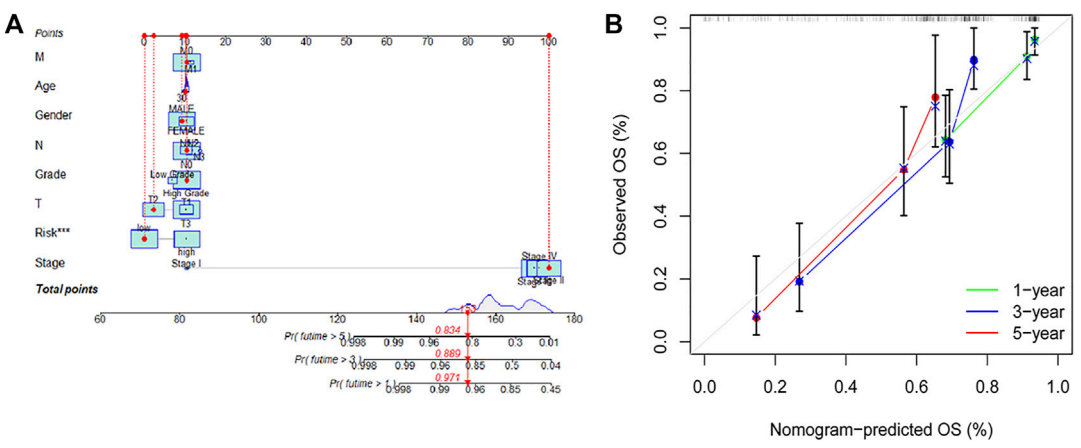

FIGURE 5 | An individualized prognostic signature incorporating the risk score and clinical factors for bladder cancer prognosis. **(A,B)** Construction of an individualized prognostic signature combining the subtype-specific signature and clinical features for prediction of OS. Calibration plots displayed the actual and signature-predicted probability of 1-, 3- and 5-year OS.

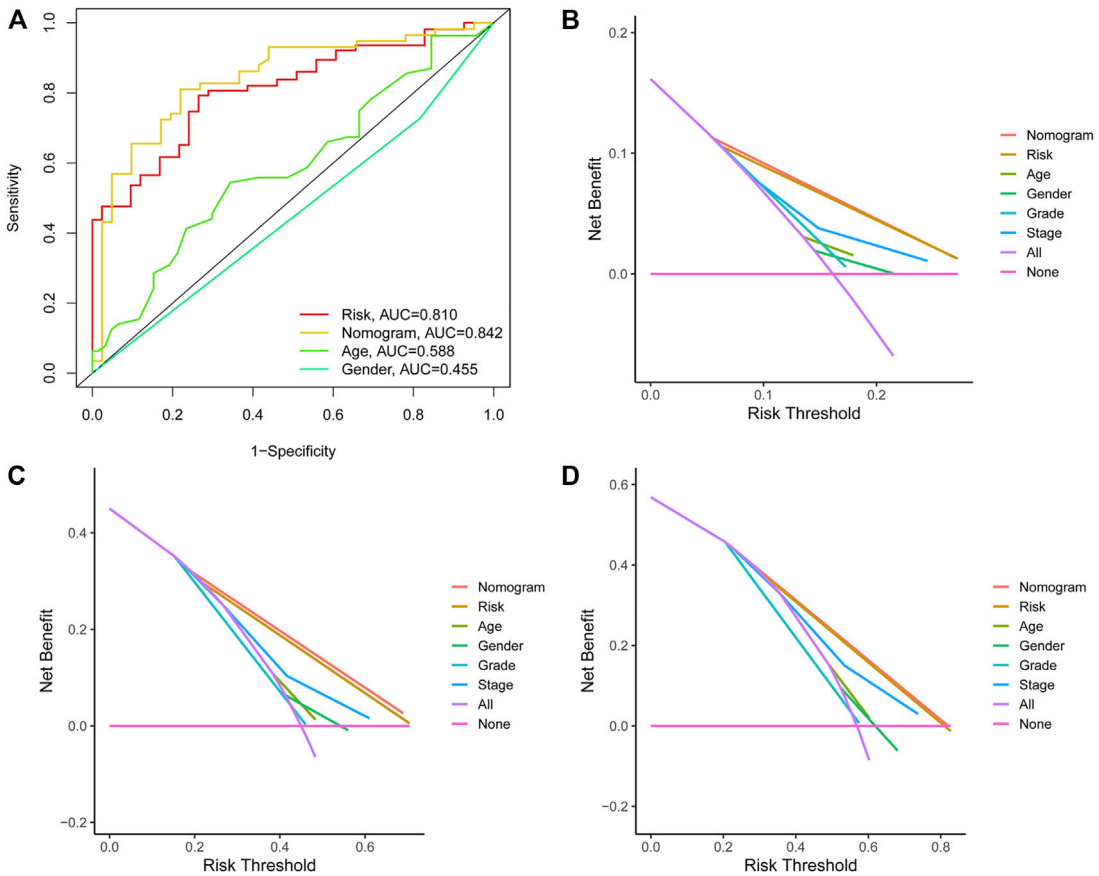

FIGURE 6 | (A) ROC curves illustrated the ability of the risk model and individualized prognostic signature to predict OS in the training set. **(B–D)** Decision curve analysis of the individualized prognostic signature and riskScore for the survival prediction of patients in 1-,3-, and 5-year survival benefit in the training cohort.

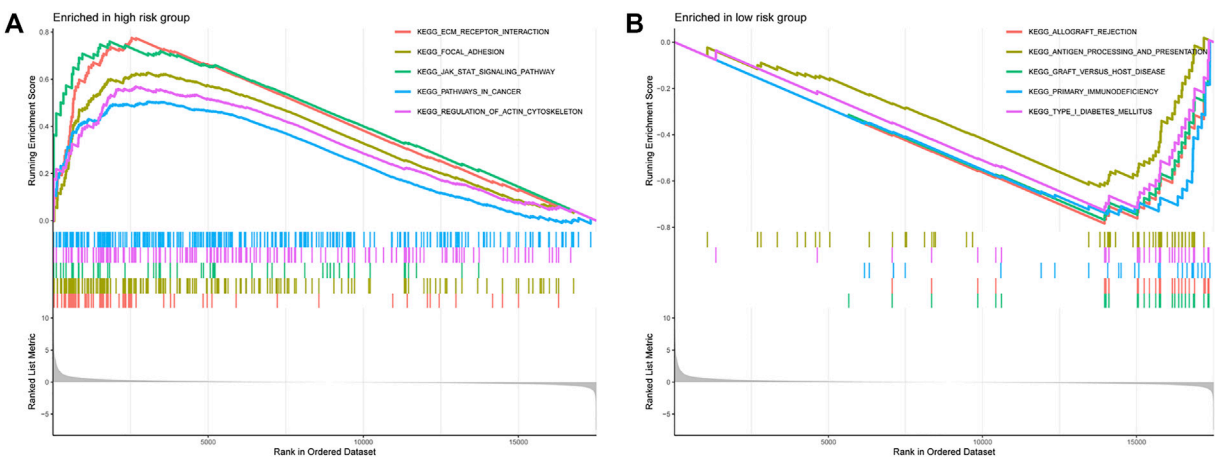

FIGURE 7 | (A,B) KEGG enrichment analysis of the high- and low-risk groups.

manifest that the functions of these genes are mainly embodied in the regulation of information transmission between cells and the transfer of nanoparticles and tumorigenesis.

DISCUSSION

Bladder cancer is one of the most prevalent cancers worldwide, with ~430,000 new diagnoses each year (Antoni et al., 2017). Although few advances have improved the clinical management of bladder cancer over the past 20 years, the overall incidence and mortality rates have changed little (Kamat et al., 2015). Immunotherapy has been used to treat bladder cancer for more than 40 years by using BCG. BCG was highly effective against bladder tumors and has been a part of the standard treatment for patients with bladder cancer. Cisplatin-ineligible patients or patients with metastatic urothelial carcinoma have limited treatment options. The ICIs have led to the advent of new classes of drugs, demonstrating promising results and improved response (Rosenberg et al., 2016). ICIs have become one of the most promising areas in cancer therapeutic development, but still not every patient achieves clinical benefit. Bladder cancer is one of the most significant genitourinary cancers with a high rate of somatic mutations. The TME has a critical influence on the immune response. In the TIME, there were distinct differences in immune cell infiltrations between subtypes. Tumor-infiltrating immune cells are linked to clinical outcomes and response to immunotherapy. Constructing reliable signatures to assess the clinicopathological features and analyze immune cell infiltration in bladder cancer patients is essential. **Figure 7**.

In this study, we identified the differentially expressed immunologic genes and divided bladder cancer samples into two subtypes by NMF cluster analysis. It was found that patients in subtype 1 had longer mPFS and mOS than those in C2. As we can see, cluster 2 contained more regulatory T cells (Treg), and myeloid-derived suppressor cells (MDSCs), which have a negative immunomodulatory effect (Siret et al., 2020). Our study focused on bioinformatics to predict the diagnostic, therapeutic, and prognostic value of immunologic genes in bladder cancer. Then, an immunologic prognostic risk model and individualized prognostic signature were constructed. We also identified 15 OS-related differentially expressed immunologic genes, and 10 genes (e.g., TSPAN7, PAQR6, TRIM59, RUNX2, AIM2, CGB5, FASN, FADS1, RAC3, and HLA-G′) (Prasad et al., 2013; Liu et al., 2018; Dumont et al., 2019; Cheng et al., 2020; Jiao et al., 2020; Liu et al., 2020; Piotr Białas et al., 2020; Cai et al., 2021; Yu et al., 2021) have been reported to be involved in the immune microenvironment. POLE2, FEN1, MCM6, MSH6, MSH2, and LOXL2 were considered to play a role in promoting cancer. A whole-genome CRISPR screen study found that MSH2 was involved in chemotherapy resistance in muscle-invasive bladder cancer and might be predictive biomarkers of response to platinum-based therapy (Goodspeed et al., 2019). The relationship between TMB and the risk score has also been explored, and it is found that the TMB and risk score have a negative correlation. TMB is defined as the total number of somatic mutations per megabase of an interrogated genomic sequence, and high TMB may produce many neoantigens to stimulate the antitumor immune response (Chan et al., 2019). In this study, we observe that endothelial cells have a positive relationship with the risk score. Studies showed that bladder cancer cells promoted tumor progression interacting with vascular endothelial cells through the VEGFR2 and EGFR signaling pathway (Huang et al., 2019). The differences in age, stage, gender, and grade did not reduce the accuracy of the classifier in predicting patient prognoses (**Supplementary Figure S2**). The nomogram incorporates an immunologic prognostic risk signature and clinicopathological parameters to help clinicians determine individual patient prognoses. Its graphical scoring system is easy to understand, facilitating the customized treatment and making of medical decisions. The ROC curves indicated that the immunologic prognostic risk signature and prognostic nomogram signature had high sensitivity and specificity. The results of the calibration curve and DCA demonstrated that the two signatures could be independent factors affecting the prognosis of bladder cancer and may be practical and reliable predictive tools for predicting bladder cancer prognosis.

In this study, we conducted GSEA to screen the most important signaling pathways. The results of GSEA indicated that the high-risk group was mainly concentrated in tumorigenesis and migration and immune signaling pathways, suggesting that bladder cancer in the high-risk group had a higher level of cell proliferation and immunosuppression.

Previous studies have reported different prognostic signatures of bladder cancer (Na et al., 2020; Qiu et al., 2020; Fu et al., 2021). However, most of them focused on building prognostic models. In this study, we comprehensively evaluated the prognostic value of immunologic genes in bladder cancer, identified two bladder cancer subtypes by unsupervised NMF clustering, and more importantly, established an individualized prognostic signature for predicting the survival of patients with bladder cancer. In this study, we also analyzed the relationship between the risk score and immune cell infiltration and TMB. It provides a new perspective for improving the response of bladder cancer to immunotherapy. Some limitations of this study should be noted. First, the study relied on retrospective data, so there was a lack of verification by multicenter prospective research. Second, the nomogram did not perform external validation as there was a lack of specific clinical data in the GEO database.

In conclusion, we established a risk model and an individualized prognostic signature, and this signature is more economical and clinically practical than whole-genome sequencing. The graphical scoring system of our nomogram is easy to understand, facilitating the customized treatment and making of medical decisions. Furthermore, this signature could be used to guide clinicians in decisions related to prognosis, clinical diagnosis, and medication for bladder cancer patients with different immunophenotypes. Understanding the TIME using the immune score provides important insights that will

improve the diagnosis and prognosis of patients with bladder cancer.

DATA AVAILABILITY STATEMENT

The original contributions presented in the study are included in the article/**Supplementary Material**, further inquiries can be directed to the corresponding authors.

AUTHOR CONTRIBUTIONS

JW and HZ designed the study. QL and YW conducted this study and wrote the original draft. HG, FS, and XW revised the original draft. QL and YW performed bioinformatics analysis. All authors participated in the discussion and data consolidation.

FUNDING

This work was supported by the medical and health plan of Shandong Province (2018WS265).

SUPPLEMENTARY MATERIAL

The Supplementary Material for this article can be found online at: https://www.frontiersin.org/articles/10.3389/fgene.2022.837301/full#supplementary-material

REFERENCES

Alfred Witjes, J., Lebret, T., Compérat, E. M., Cowan, N. C., De Santis, M., Bruins, H. M., et al. (2017). Updated 2016 EAU Guidelines on Muscle-Invasive and Metastatic Bladder Cancer. *Eur. Urol.* 71 (3), 462–475. doi:10.1016/j.eururo.2016.06.020

Antoni, S., Ferlay, J., Soerjomataram, I., Znaor, A., Jemal, A., and Bray, F. (2017). Bladder Cancer Incidence and Mortality: A Global Overview and Recent Trends. *Eur. Urol.* 71 (1), 96–108. doi:10.1016/j.eururo.2016.06.010

Arnhold, E. (2018). R-environment Package for Regression Analysis. *Pesq. Agropec. Bras.* 53, 870–873. doi:10.1590/s0100-204x2018000700012

Balar, A. V., Kamat, A. M., Kulkarni, G. S., Uchio, E. M., Boormans, J. L., Roumiguié, M., et al. (2021). Pembrolizumab Monotherapy for the Treatment of High-Risk Non-muscle-invasive Bladder Cancer Unresponsive to BCG (KEYNOTE-057): an Open-Label, Single-Arm, Multicentre, Phase 2 Study. *Lancet Oncol.* 22 (7), 919–930. doi:10.1016/S1470-2045(21)00147-9

Becht, E., Giraldo, N. A., Lacroix, L., Buttard, B., Elarouci, N., Petitprez, F., et al. (2016). Estimating the Population Abundance of Tissue-Infiltrating Immune and Stromal Cell Populations Using Gene Expression. *Genome Biol.* 17 (1), 218. doi:10.1186/s13059-016-1070-5

Binnewies, M., Roberts, E. W., Kersten, K., Chan, V., Fearon, D. F., Merad, M., et al. (2018). Understanding the Tumor Immune Microenvironment (TIME) for Effective Therapy. *Nat. Med.* 24 (5), 541–550. doi:10.1038/s41591-018-0014-x

Boorjian, S. A., Alemozaffar, M., Konety, B. R., Shore, N. D., Gomella, L. G., Kamat, A. M., et al. (2021). Intravesical Nadofaragene Firadenovec Gene Therapy for BCG-Unresponsive Non-muscle-invasive Bladder Cancer: a Single-Arm, Open-Label, Repeat-Dose Clinical Trial. *Lancet Oncol.* 22 (1), 107–117. doi:10.1016/S1470-2045(20)30540-4

Bray, F., Ferlay, J., Soerjomataram, I., Siegel, R. L., Torre, L. A., and Jemal, A. (2018). Global Cancer Statistics 2018: GLOBOCAN Estimates of Incidence and Mortality Worldwide for 36 Cancers in 185 Countries. *CA: A Cancer J. Clinicians* 68 (6), 394–424. doi:10.3322/caac.21492

Cai, Z., Chen, H., Bai, J., Zheng, Y., Ma, J., Cai, X., et al. (2021). Copy Number Variations of CEP63, FOSL2 and PAQR6 Serve as Novel Signatures for the Prognosis of Bladder Cancer. *Front. Oncol.* 11, 674933. doi:10.3389/fonc.2021.674933

Chan, T. A., Yarchoan, M., Jaffee, E., Swanton, C., Quezada, S. A., Stenzinger, A., et al. (2019). Development of Tumor Mutation burden as an Immunotherapy Biomarker: Utility for the Oncology Clinic. *Ann. Oncol.* 30 (1), 44–56. doi:10.1093/annonc/mdy495

Chen, Y.-P., Zhang, Y., Lv, J.-W., Li, Y.-Q., Wang, Y.-Q., He, Q.-M., et al. (2017). Genomic Analysis of Tumor Microenvironment Immune Types across 14 Solid Cancer Types: Immunotherapeutic Implications. *Theranostics* 7 (14), 3585–3594. doi:10.7150/thno.21471

Cheng, C., Song, D., Wu, Y., and Liu, B. (2020). RAC3 Promotes Proliferation, Migration and Invasion via PYCR1/JAK/STAT Signaling in Bladder Cancer. *Front. Mol. Biosci.* 7, 218. doi:10.3389/fmolb.2020.00218

Du, Z., Hao, Y., Du, M. Z., and LazyData, T. (2017). "Package" nomogramEx".).

Dumont, C., Jacquier, A., Verine, J., Noel, F., Goujon, A., Wu, C.-L., et al. (2019). CD8+PD-1-ILT2+ T Cells Are an Intratumoral Cytotoxic Population Selectively Inhibited by the Immune-Checkpoint HLA-G. *Cancer Immunol. Res.* 7 (10), 1619–1632. doi:10.1158/2326-6066.CIR-18-0764

Friedman, J., Hastie, T., and Tibshirani, R. (2010). Regularization Paths for Generalized Linear Models via Coordinate Descent. *J. Stat. Softw.* 33 (1), 1–22. doi:10.18637/jss.v033.i01

Fu, Y., Sun, S., Bi, J., Kong, C., and Yin, L. (2021). A Novel Immune-Related Gene Pair Prognostic Signature for Predicting Overall Survival in Bladder Cancer. *BMC Cancer* 21 (1), 810. doi:10.1186/s12885-021-08486-0

Gaujoux, R., and Seoighe, C. (2010). A Flexible R Package for Nonnegative Matrix Factorization. *BMC Bioinformatics* 11, 367. doi:10.1186/1471-2105-11-367

Gong, J., Li, R., Chen, Y., Zhuo, Z., Chen, S., Cao, J., et al. (2021). HCC Subtypes Based on the Activity Changes of Immunologic and Hallmark Gene Sets in Tumor and Nontumor Tissues. *Brief Bioinform* 22 (5). doi:10.1093/bib/bbaa427

Goodspeed, A., Jean, A., and Costello, J. C. (2019). A Whole-Genome CRISPR Screen Identifies a Role of MSH2 in Cisplatin-Mediated Cell Death in Muscle-Invasive Bladder Cancer. *Eur. Urol.* 75 (2), 242–250. doi:10.1016/j.eururo.2018.10.040

Gu, Z., Gu, L., Eils, R., Schlesner, M., and Brors, B. (2014). Circlize Implements and Enhances Circular Visualization in R. *Bioinformatics* 30 (19), 2811–2812. doi:10.1093/bioinformatics/btu393

Huang, Z., Zhang, M., Chen, G., Wang, W., Zhang, P., Yue, Y., et al. (2019). Bladder Cancer Cells Interact with Vascular Endothelial Cells Triggering EGFR Signals to Promote Tumor Progression. *Int. J. Oncol.* 54 (5), 1555–1566. doi:10.3892/ijo.2019.4729

Jiang, Y., Wang, C., and Zhou, S. (2020). Targeting Tumor Microenvironment in Ovarian Cancer: Premise and Promise. *Biochim. Biophys. Acta (Bba) - Rev. Cancer* 1873 (2), 188361. doi:10.1016/j.bbcan.2020.188361

Jiao, F., Sun, H., Yang, Q., Sun, H., Wang, Z., and Chen, M. J. (2020). Identification of FADS1 through Common Gene Expression Profiles for Predicting Survival in Patients with Bladder Cancer. *Cmar* Vol. 12, 8325–8339. doi:10.2147/cmar.s254316

Kamat, A. M., Flaig, T. W., Grossman, H. B., Konety, B., Lamm, D., O'Donnell, M. A., et al. (2015). Expert Consensus Document: Consensus Statement on Best Practice Management Regarding the Use of Intravesical Immunotherapy with BCG for Bladder Cancer. *Nat. Rev. Urol.* 12 (4), 225–235. doi:10.1038/nrurol.2015.58

Keren, L., Bosse, M., Marquez, D., Angoshtari, R., Jain, S., Varma, S., et al. (2018). A Structured Tumor-Immune Microenvironment in Triple Negative Breast Cancer Revealed by Multiplexed Ion Beam Imaging. *Cell* 174 (6), 1373–1387. doi:10.1016/j.cell.2018.08.039

Lenis, A. T., Lec, P. M., Chamie, K., and Mshs, M. (2020). Bladder Cancer. *JAMA* 324 (19), 1980–1991. doi:10.1001/jama.2020.17598

Liu, J., Yu, X., Liu, B., Yu, H., and Li, Z. (2020). Phosphorylated MAPK14 Promotes the Proliferation and Migration of Bladder Cancer Cells by Maintaining

RUNX2 Protein Abundance. *Cmar* Vol. 12, 11371–11382. doi:10.2147/CMAR.S274058

Liu, Y., Dong, Y., Zhao, L., Su, L., Diao, K., and Mi, X. J. M. C. (2018). TRIM59 Overexpression Correlates with Poor Prognosis and Contributes to Breast Cancer Progression through AKT Signaling Pathway. *Mol. Carcinogenesis* 57, 1792–1802. doi:10.1002/mc.22897

Mandhani, A., Gupta, P., Jain, M., Kapoor, R., Muruganandham, K., and Srivastava, A. (2009). Impact of Age and Gender on the Clinicopathological Characteristics of Bladder Cancer. *Indian J. Urol.* 25 (2), 207–210. doi:10.4103/0970-1591.52916

Na, L., Bai, Y., Sun, Y., Wang, Z., Wang, W., Yuan, L., et al. (2020). Identification of 9-Core Immune-Related Genes in Bladder Urothelial Carcinoma Prognosis. *Front. Oncol.* 10, 1142. doi:10.3389/fonc.2020.01142

Newman, A. M., Liu, C. L., Green, M. R., Gentles, A. J., Feng, W., Xu, Y., et al. (2015). Robust Enumeration of Cell Subsets from Tissue Expression Profiles. *Nat. Methods* 12 (5), 453–457. doi:10.1038/nmeth.3337

Piotr Białas, A. Ś., Anna, S., and Anna, J. (2020). The Study of the Expression of CGB1 and CGB2. *Hum. Cancer Tissues* 11 (9).

Prasad, A., Ramirezortiz, Z., and Means, T. J. J. o. I. (2013). Mechanisms of AIM2 Inflammasome Regulation. *J. Immunol.* 190.

Puente, D., Malats, N., Cecchini, L., Tardón, A., Garcı´a-Closas, R., Serra, C., et al. (2003). Gender-related Differences in Clinical and Pathological Characteristics and Therapy of Bladder Cancer. *Eur. Urol.* 43 (1), 53–62. doi:10.1016/s0302-2838(02)00496-7

Qiu, H., Hu, X., He, C., Yu, B., Li, Y., and Li, J. (2020). Identification and Validation of an Individualized Prognostic Signature of Bladder Cancer Based on Seven Immune Related Genes. *Front. Genet.* 11, 12. doi:10.3389/fgene.2020.00012

Robinson, M. D., McCarthy, D. J., and Smyth, G. K. (2010). edgeR: a Bioconductor Package for Differential Expression Analysis of Digital Gene Expression Data. *Bioinformatics* 26 (1), 139–140. doi:10.1093/bioinformatics/btp616

Rosenberg, J. E., Hoffman-Censits, J., Powles, T., van der Heijden, M. S., Balar, A. V., Necchi, A., et al. (2016). Atezolizumab in Patients with Locally Advanced and Metastatic Urothelial Carcinoma Who Have Progressed Following Treatment with Platinum-Based Chemotherapy: a Single-Arm, Multicentre, Phase 2 Trial. *The Lancet* 387, 1909–1920. doi:10.1016/s0140-6736(16)00561-4

Shinohara, M., Okazawa, A., Suzuki, M., Itakura, H., Munakata, A., and Kinoshita, K. (1995). Clinical Investigation of Renal Pelvic and Ureteral Cancer with Special Reference to Adjuvant Chemotherapy. *Jpn. J. Urol.* 86 (8), 1375–1382. doi:10.5980/jpnjurol1989.86.1375

Siret, C., Collignon, A., Silvy, F., Robert, S., Cheyrol, T., André, P., et al. (2020). Deciphering the Crosstalk between Myeloid-Derived Suppressor Cells and Regulatory T Cells in Pancreatic Ductal Adenocarcinoma. *Front. Immunol.* 10, 3070. doi:10.3389/fimmu.2019.03070

Subramanian, A., Tamayo, P., Mootha, V. K., Mukherjee, S., Ebert, B. L., Gillette, M. A., et al. (2005). Gene Set Enrichment Analysis: a Knowledge-Based Approach for Interpreting Genome-wide Expression Profiles. *Proc. Natl. Acad. Sci. U.S.A.* 102 (43), 15545–15550. doi:10.1073/pnas.0506580102

Tran, L., Xiao, J.-F., Agarwal, N., Duex, J. E., and Theodorescu, D. (2021). Advances in Bladder Cancer Biology and Therapy. *Nat. Rev. Cancer* 21 (2), 104–121. doi:10.1038/s41568-020-00313-1

Wei, T., Simko, V., Levy, M., Xie, Y., Jin, Y., and Zemla, J. J. S. (2017). Package. *corrplot'* 56 (316), e24.

Witjes, J. A., Bruins, H. M., Cathomas, R., Compérat, E. M., Cowan, N. C., Gakis, G., et al. (2021). European Association of Urology Guidelines on Muscle-Invasive and Metastatic Bladder Cancer: Summary of the 2020 Guidelines. *Eur. Urol.* 79 (1), 82–104. doi:10.1016/j.eururo.2020.03.055

Yu, X., Li, S., Pang, M., Du, Y., Xu, T., Bai, T., et al. (2021). TSPAN7 Exerts Anti-tumor Effects in Bladder Cancer through the PTEN/PI3K/AKT Pathway. *Front. Oncol.* 10, 613869. doi:10.3389/fonc.2020.613869

Conflict of Interest: The authors declare that the research was conducted in the absence of any commercial or financial relationships that could be construed as a potential conflict of interest.

Publisher's Note: All claims expressed in this article are solely those of the authors and do not necessarily represent those of their affiliated organizations, or those of the publisher, the editors, and the reviewers. Any product that may be evaluated in this article, or claim that may be made by its manufacturer, is not guaranteed or endorsed by the publisher.

frontiers | Frontiers in Genetics

ORIGINAL RESEARCH
published: 13 April 2022
doi: 10.3389/fgene.2022.827559

Identification and Validation of Ferroptosis-Related Biomarkers in Septic Cardiomyopathy via Bioinformatics Analysis

Cheng-Wu Gong[1,2†], Ming-Ming Yuan[2,3†], Bai-Quan Qiu[1,2], Li-Jun Wang[1,2], Hua-Xi Zou[1,2], Tie Hu[1,2], Song-Qing Lai[2,3] and Ji-Chun Liu[1,2*]*

[1]Department of Cardiothoracic Surgery, The Second Affiliated Hospital of Nanchang University, Nanchang, China, [2]Department of Cardiothoracic Surgery, The First Affiliated Hospital of Nanchang University, Nanchang, China, [3]Institute of Cardiovascular Diseases, Jiangxi Academy of Clinical Medical Sciences, The First Affiliated Hospital of Nanchang University, Nanchang, China

Septic cardiomyopathy (SCM) is a cardiac dysfunction caused by severe sepsis and septic shock that increases the risk of heart failure and death and its molecular mechanism remains unclear. Ferroptosis, a novel form of programmed cell death, has been reported to be present in the heart tissue of patients with sepsis, which demonstrated that ferroptosis may be a potential mechanism of myocardial injury in SCM. Therefore, we explored the role of ferroptosis-related genes (FRGs) in SCM and aimed to identify pivotal ferroptosis-related targets in SCM and potential therapeutic targets involved in the pathological process of SCM. To explore the regulatory mechanisms of ferroptosis in SCM, we identified differentially expressed genes (DEGs) in SCM and FRGs by bioinformatics analysis, and further identified hub genes. And the crucial microRNAs (miRNAs)-FRGs regulatory network was subsequently constructed. Finally, several candidate drugs associated with the hub genes were predicted, and Real-time quantitative reverse Transcription PCR (qRT-PCR) and western blotting analysis were performed to confirm the abnormal expression of hub genes. In this study, we identified several FRGs that may be involved in the pathogenesis of SCM, which helps us further clarify the role of ferroptosis in SCM and deeply understand the molecular mechanisms and potential therapeutic targets of SCM.

Keywords: septic cardiomyopathy, ferroptosis, miRNA, mRNA, public database

OPEN ACCESS

Edited by:
William C. Cho,
QEH, Hong Kong SAR, China

Reviewed by:
Megha Lal,
Children's Hospital of Philadelphia, United States
Aniello Maiese,
Sapienza University of Rome, Italy

***Correspondence:**
Ji-Chun Liu
liujichun999@163.com
Song-Qing Lai
ndyfy03743@ncu.edu.cn

[†]These authors have contributed equally to this work

Specialty section:
This article was submitted to RNA, a section of the journal Frontiers in Genetics

Received: *02 December 2021*
Accepted: *24 March 2022*
Published: *13 April 2022*

Citation:
Gong C-W, Yuan M-M, Qiu B-Q, Wang L-J, Zou H-X, Hu T, Lai S-Q and Liu J-C (2022) Identification and Validation of Ferroptosis-Related Biomarkers in Septic Cardiomyopathy via Bioinformatics Analysis. Front. Genet. 13:827559. doi: 10.3389/fgene.2022.827559

INTRODUCTION

Sepsis, a syndrome of physiologic, pathologic, and biochemical abnormalities induced by infection (Cecconi et al., 2018), has been identified by the World Health Organization as a global healthy priority (Reinhart et al., 2017). Septic cardiomyopathy (SCM) is a significant morbid component of severe sepsis and septic shock (Balija and Lowry 2011). Myocardial cell injury and cardiomyocyte contractile dysfunction are the main pathophysiological processes in SCM, and clinical diagnosis can only rely on myocardial damage factors and echocardiography, which limits early intervention in patients with SCM (Crouser 2004; Rudiger and Singer 2007; Hassoun et al., 2008; Werdan et al., 2009; Celes et al., 2010). Therefore, it is crucial to select appropriate predictive biomarkers for early intervention in SCM.

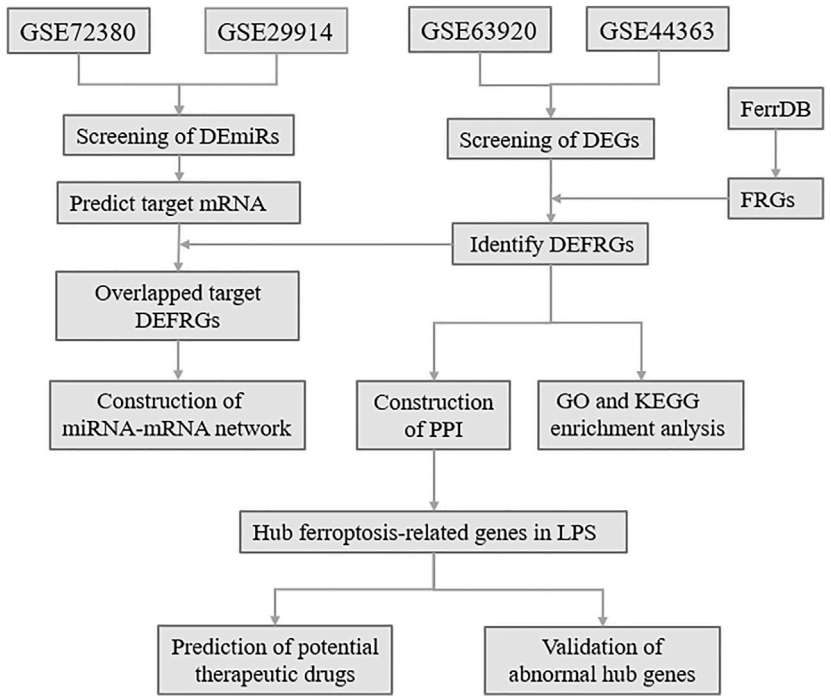

FIGURE 1 | The overall protocol of this study. DEmiRs, differentially expressed microRNA; DEmRs, differentially expressed mRNA; FRGs, ferroptosis-related genes; DEFRGs, differentially expressed FRGs; PPI, protein-protein interaction.

TABLE 1 | The primer sequences of hub genes.

Primer	Sequence
GAPDH-F	GGTCGGTGTGAACGGATTT
GAPDH-R	TGAACTTGCCGTGGGTAGA
Cdkn1a-F	GCAAAGTGTGCCGTTGTCTC
Cdkn1a-R	CGTCTCCGTGACGAAGTCAA
Vim-F	TTCTCTGGCACGTCTTGACC
Vim-R	CTTTCATACTGCTGGCGCAC
Rela-F	CAAGACACACCCCACCATCA
Rela-R	CTCTATAGGAACTATGGATACTGCG
Arntl-F	GATCGCGGAGGAAATCATGG
Arntl-R	TGAGCCTGCCCTGGTAATAG
Nfe2l2-F	AGCCAGCTGACCTCCTTAGA
Nfe2l2-R	AGTGACTGACTGATGGCAGC
Socs1-F	CAACGGAACTGCTTCTTCGC
Socs1-R	AGCTCGAAAAGGCAGTCGAA
Slc39a14-F	GATATCGGGACCTTGGCCTG
Slc39a14-R	AGAGAATGGCCACTGACGTG
Ptgs2-F	GGTGCCTGGTCTGATGATGTATGC
Ptgs2-R	GGATGCTCCTGCTTGAGTATGTCG

MiRNAs, small, single-stranded, non-coding RNAs (18–24 nucleotides), well conserved in eukaryotic organisms, play biological roles in inflammation, metabolism, and development (Mendell and Olson 2012; Manetti et al., 2021). What's more, in inflammatory heart diseases and sepsis-induced cardiac dysfunction, circulating miRNAs were proposed as biomarkers for diagnosis and disease monitoring (Mirna et al., 2019; Manetti et al., 2020; Chiti et al., 2021). With the development of high-throughput gene expression profiling technology, Microarray analysis has been developed as detection technology to simultaneously monitor the differential expression of numerous genes or miRNAs in various studies, including in the field of SCM (Vogelstein et al., 2013; Zhang et al., 2019a; Reyes et al., 2020).

Ferroptosis is an iron-dependent, novel form of programmed cell death that differs from apoptosis, cell necrosis, and autophagy (Tang et al., 2021). Ferroptosis was proposed in 2012 by Dixon, S.J. et al. (Dixon et al., 2012), and is characterized essentially by iron-dependent lipid peroxidation. Ferroptosis is mainly related to pathological cell death associated with mammalian degenerative diseases, carcinogenic effects, cerebral hemorrhage, local ischemia-reperfusion injury, and kidney degeneration (Stockwell et al., 2017; Fang et al., 2020). Wang et al. (Wang et al., 2020) reported that the reduction of ferroptosis via enhancing GPX4, may be the major mechanisms via which Dexmedetomidine alleviates sepsis-induced myocardial cellular injury. It is suggested that ferroptosis may be an important part of myocardial injury in SCM. However, the exact mechanism of ferroptosis in LPS-induced myocardial injury remains unclear. Here, to determine the role of ferroptosis in SCM, we identified FRGs based on relevant databases and analyzed the differential expression of FRGs among SCM and normal samples, and further identified differentially expressed FRGs (DEFRGs) by bioinformatic analysis. GO and KEGG Pathway enrichment analysis of DEFRGs were performed subsequently. After screening out the differentially expressed miRNAs (DEmiRs), we obtained the target mRNAs of DEmiRs from the relevant databases. The crucial miRNAs-FRGs regulatory network was subsequently constructed.

TABLE 2 | Characteristics for GEO microarray in LPS hearts tissues.

Data Sourse	Type	Sourse	LPS/Control	Platform	Annotation of Platform
GSE72380	miRNA	heart samples	6/6	GPL19324	Agilent-038112 mouse miRNA microarray, Release 18.0 (miRNA ID version)
GSE29914	miRNA	hearts samples	4/4	GPL13715	ORB Sanger15 Multispecies MIcroRNA Microarray
GSE63920	mRNA	hearts samples	4/4	GPL19507	MI mouse exonic evidence-based oligonucleotide (MEEBO) microarray
GSE44363	mRNA	hearts samples	4/4	GPL1261	[Mouse430_2] Affymetrix Mouse Genome 430 2.0 Array

GEO, Gene expression omnibus; LPS, Lipopolysaccharide; miRNA, microrna; Mrna, messenger RNA.

TABLE 3 | Key DE miRs accessed from GSE72380 and GSE29914.

miRNA_ID	Log FC	*p* Value
mmu-miR-21-3p	5.018872	3.19E-07
mmu-miR-155-5p	1.056015	4.70E-05
mmu-miR-2132	1.18572	0.00656
mmu-miR-155	1.264	0.00757
mmu-miR-125b-3p	−1.89198	0.02283
mmu-miR-1892	−1.02102	0.03988
mmu-miR-2137	1.23337	0.03988
mmu-miR-341	−1.69248	0.04126

Based on the STRING online database, we established a protein-protein interaction (PPI) network, and Hub genes were screened out from PPI network, and further identified potential therapeutic drugs of SCM by DSigDB database. Furthermore, qRT-PCR and Western Blotting Analysis were performed to confirm the abnormal expression of hub genes. The flow chart of the whole study was shown in **Figure 1**.

MATERIALS AND METHODS

Data Collection

The microarray data were obtained from GEO database (http://www.ncbi.nlm.nih.gov/geo/). Two miRNA expression profiles (GSE72380 and GSE29914) and two mRNA expression profiles (GSE63920 and GSE44363) between LPS and Saline were downloaded and investigated. The FRGs were identified from FerrDb (https://www.zhounan.org/ferrdb) and GeneCards (https://www.genecards.org). After deduplication of genes, the merged FRGs set contains 442 FRGs, listed in **Supplementary Table S1**. The GSE72380 dataset was comprised of 6 mice hearts tissue treated with LPS and 6 mice hearts tissue treated with saline (Wang et al., 2016); GSE29914 contained 4 LPS treated mice hearts tissue and 4 saline treated mice hearts tissue sample miRNA expression profiles (Drosatos et al., 2011); GSE63920 included 4 LPS treated mice hearts tissue and 4 saline treated mice hearts tissue sample mRNA expression profiles (Drosatos et al., 2016); and GSE44363 contained 24 mice hearts tissue samples, including 4 LPS samples and 4 saline samples. All datasets were downloaded in a processed and normalized format.

Data Processing

The R-based GEO online tool GEO2R (http://www.ncbi.nlm.nih.gov/geo/geo2r/) was used to identify the differentially expressed miRNAs (DEmiRs) and mRNAs (DEmRs) between LPS and saline treated mice hearts tissue expression profiles, with the thresholds of $|\log2\ (\text{fold-change})| > 1.0$ and adjusted p-value < 0.05.

Functional and Pathway Analysis

Database for Annotation, Visualization, and Integrated Discovery (DAVID) (https://david.ncifcrf.gov/) was used to perform Gene Ontology (GO) and Kyoto Encyclopedia of Genes and Genomes (KEGG) analysis with DEFRGs. $p < 0.05$ was applied as the cut-off criterion.

Construction of Protein-Protein Interaction Network and Identification of Hub Genes

The STRING Database (Szklarczyk et al., 2015) (https://string-db.org/) is a flexible and user-friendly website for generating hypotheses about gene function, analyzing gene lists, and prioritizing genes for functional assays. In this study, the network of DEFRGs was constructed using the STRING Database. Minimum required interaction score was selected as medium confidence (0.4). In addition, cytoHubba app of Cytoscape was used to determine hub genes. The plot displayed the ranking of the 10 molecules by the shade of each color: The darkest red marked the first, the lightest yellow marked the last.

Prediction of the Target Genes of Differentially Expressed miRs and Construction miRNA-mRNA Networks

The target mRNAs of DEmiRs were obtained from TargetScan (www.targetscan.org/) (Fehlmann et al., 2019) and miRDB (http://www.mirdb.org/) (Wong and Wang 2015). And the Overlapped target DEFRGs between predicted mRNAs and DEFRGs were identified. And the miRNA-mRNA pairs were identified based on the connection between DEmiRs and DEFRGs. Then, the miRNA-mRNA pairs were imported into Cytoscape software to construct the initial miRNA-mRNA network. Finally, the miRNA-mRNA interaction network was depicted and visualized using cytoscape 3.8.2 software.

Drug Prediction of Differentially Expressed mRs

The DSigDB database (http://dsigdb.tanlab.org/) contains 22 527 gene sets, consists of 17 389 unique compounds covering 19 531 genes The DSigDB database aids the identification of novel drug targets and the comparison of drug structures with potential mechanisms of action

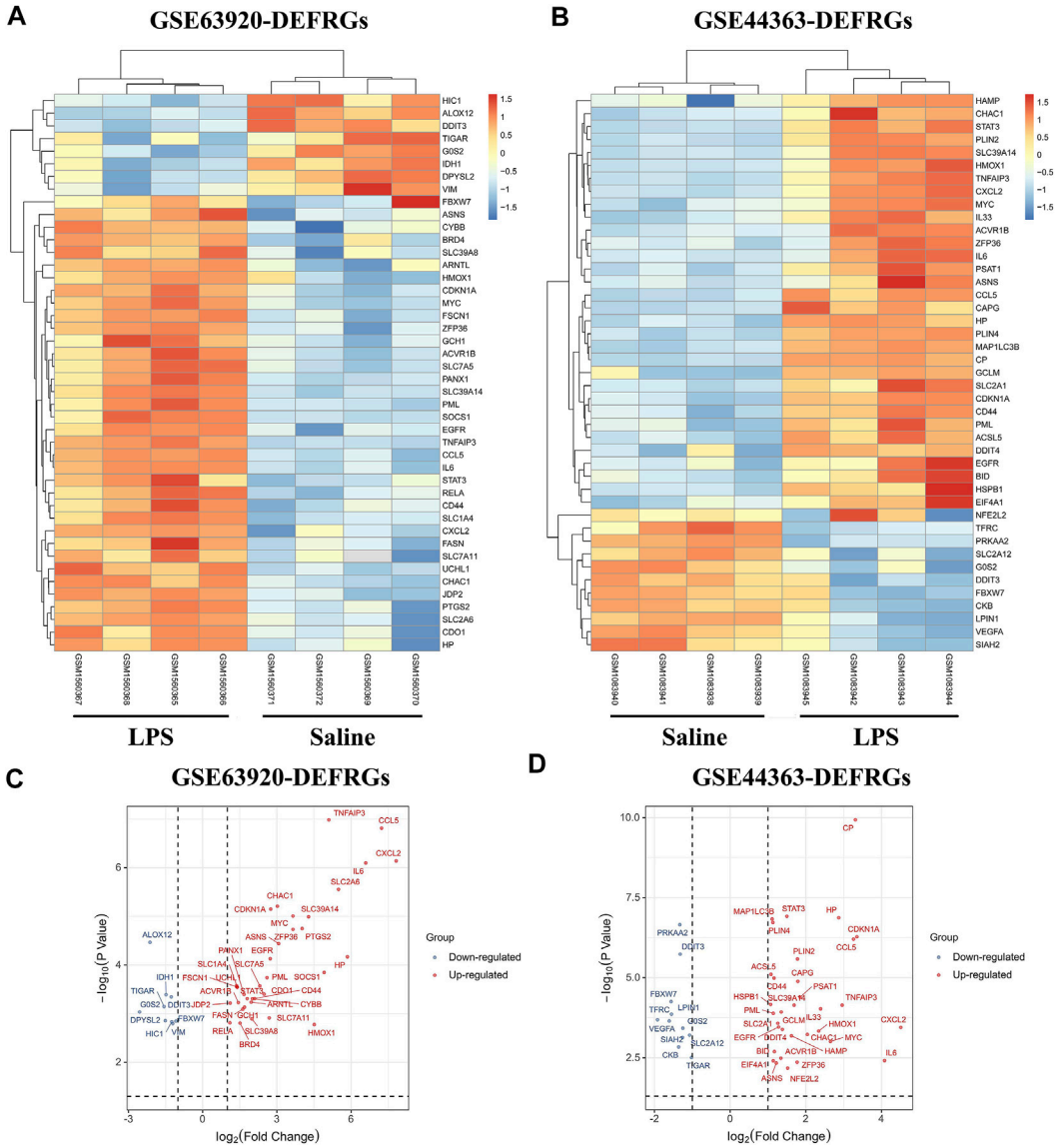

FIGURE 2 | The heatmaps and volcano plots of DEFRGs. **(A)** The heatmap of DEFRGs in GSE63920; **(B)** The heatmap of DEFRGs in GSE44363; **(C)** The volcano plot of DEFRGs in GSE63920; **(D)** The volcano plot of DEFRGs in GSE44363. FRGs, ferroptosis-related genes; DEFRGs, differentially expressed FRGs.

(Yoo et al., 2015). The hub genes were input into DSigDB database to examine their association with potential targeted drugs.

Construction of the Cardiomyocyte Injury Model

To verify our results, we constructed an LPS-induced myocardial injury model of SCM. Lipopolysaccharide (LPS) was purchased from Sigma (United States); ferrostatin-1 (Fer-1) (≥99.72% purity) was obtained from Solarbio (Shanghai, China). HL-1 cells (a cardiac muscle cell line that contracts and retains phenotypic characteristics of the adult cardiomyocyte) were provided by the Cell Bank of the Chinese Academy of Sciences. Cells were cultured in MEM Alpha Modification containing 10% fetal bovine serum (FBS). LPS (5 μg/ml) was added into the cell culture medium to induce an *in vitro* cardiomyocyte injury model. In addition, to further increase the confidence of the results, we used Cdkn1a small interfering RNA (Si-Cdkn1a) to validate our predicted results. HL-1 cells were transfected with Si-Cdkn1a by riboFECT™ CP Reagent (RIBOBIO, China) according to protocol for 24 or 36 h. HL-1 cells were pretreated with Fer-1 (1 μmol/L) for 1 h before LPS stimulation.

Real-Time Quantitative Reverse Transcription PCR

Total RNA was isolated from HL-1 cells with Trizol reagent (Invitrogen, CA, United States), and was reverse transcribed into cDNA using Revert Aid First Strand cDNA Synthesis Kit

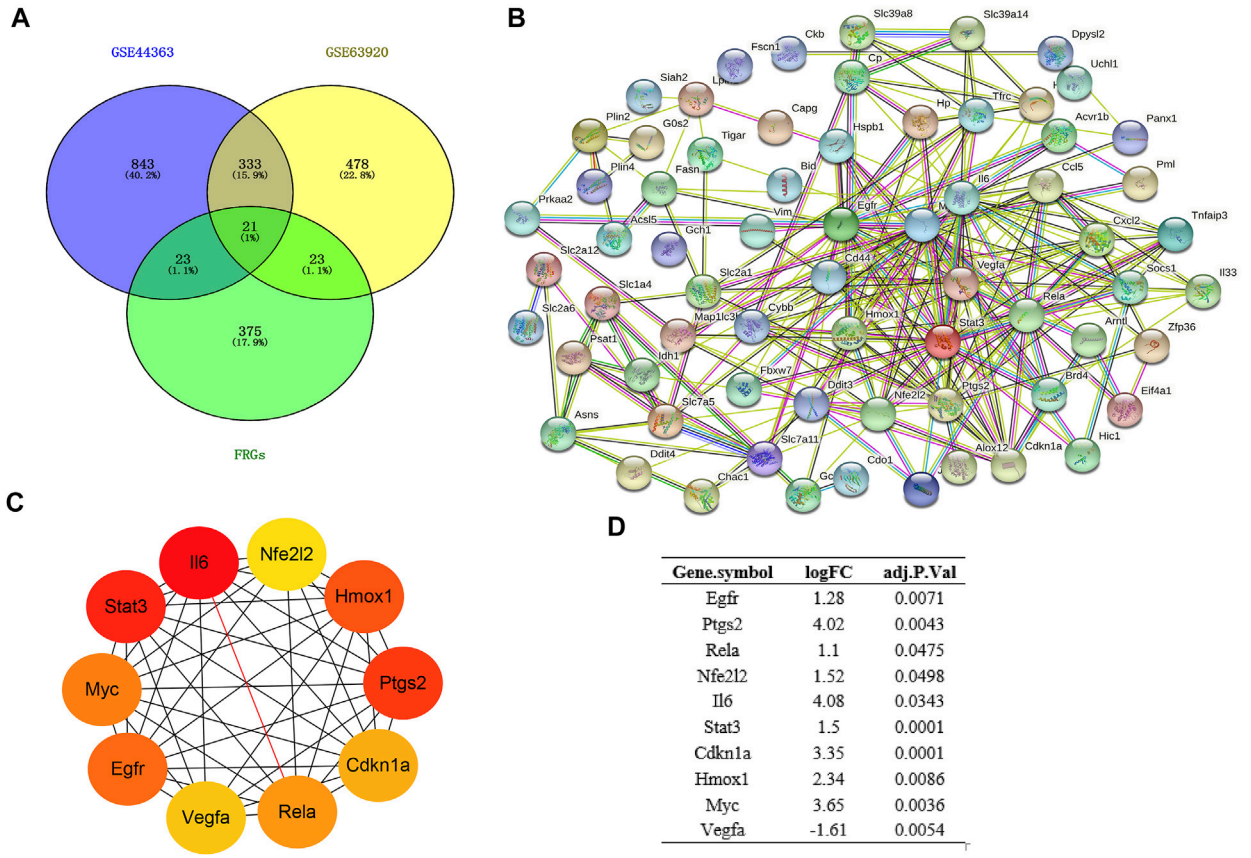

Gene.symbol	logFC	adj.P.Val
Egfr	1.28	0.0071
Ptgs2	4.02	0.0043
Rela	1.1	0.0475
Nfe2l2	1.52	0.0498
Il6	4.08	0.0343
Stat3	1.5	0.0001
Cdkn1a	3.35	0.0001
Hmox1	2.34	0.0086
Myc	3.65	0.0036
Vegfa	-1.61	0.0054

FIGURE 3 | Construction of PPI network and Identification of hub genes. **(A)** Venn diagram of DEGs between DEmRs and FRGs; **(B)** PPI network of DEFRGs constructed by STRING database; **(C)** the top 10 hub genes were identified by MCC; **(D)** the logFC and adjusted *p*-value of the hub genes. DEGs, differentially expressed genes; FRGs, ferroptosis-related genes; DEFRGs, differentially expressed FRGs.

(Thermo Fisher Scientific, Shanghai, China). Real-time PCR assays were performed using SYBR rapid quantitative PCR Kit (Thermo Fisher Scientific, Shanghai, China). The mRNA and miRNA primers were designed and synthesized by The Beijing Genomics Institute (BGI). The primer sequences were supplemented in **Table 1**. The target genes were quantified relative to internal control using $2^{-\triangle CT}$ algorithm (GAPDH/U6), and the differences between the different groups were confirmed.

Western Blotting Analysis

Total protein from HL-1 cells was extracted using RIPA lysis buffer. Proteins in the samples (20 μg) were separated by 12% SDS-PAGE and subsequently transferred to PVDF membranes. The membranes were then incubated with 5% non-fat milk for 1 h at room temperature to block nonspecific binding and incubated with primary antibodies against GPX4 (1:1,000, ZENBIO, chain), FTH1 (1:1,000, ZENBIO, chain), Caspase-3 (1:1,000, Abcam), Bcl-2 (1:5,000, Proteintech), Cdkn1a (Proteintech), Bax (1:2,000, cell Signaling Technology),, and *β*-actin (1:1,000, Abcam) at 4 °C overnight, followed by incubation with goat anti-rabbit HRP-conjugated secondary antibody (1:5,000, Abcam) at room temperature for 1 h. Protein bands were visualized using an enhanced chemiluminescence kit (Beyotime, China), and *β*-actin was used as an internal control for the relative protein expression. Protein bands were quantified using the ImageJ software.

Statistical Analysis

Data are presented as the mean ± SEMs or SDs. Statistical analyses were performed in GraphPad Prism 7 (GraphPad Software, Inc.) using unpaired two-tailed Student's t-test to compare differences between two groups with significance of $p < 0.05$. One-way analysis of variance with multiple comparisons tests was used to compare three or more groups with significance of $p < 0.05$.

RESULTS

Identification of Differentially Expressed miRs and Differentially Expressed mRs

The total number of miRNAs were 1,200 and 318 from GSE72380 and GSE29914, while the total number of mRNAs were 34945 and 45101 from GSE63920 and GSE44363, respectively (**Table 2**). According to the predetermined threshold (|log2FC| > 1.0 and adjusted $p < 0.05$), we identified 2 DEmiRs (2 upregulated) from

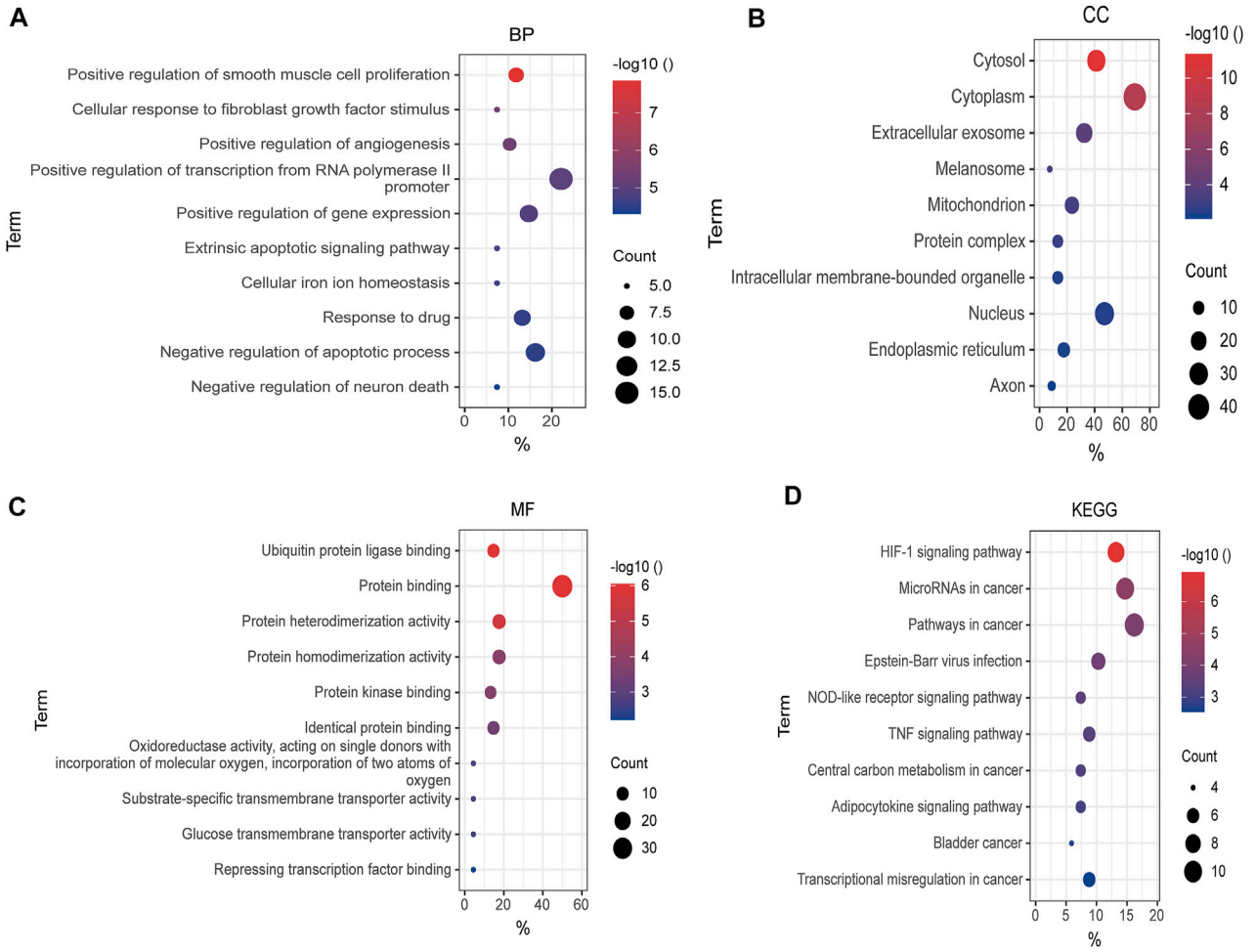

FIGURE 4 | GO and KEGG enrichment analysis of DEFRGs. **(A)** GO enrichment analysis of DEFRGs in the biological process category (BP); **(B)** the cellular component category (CC); **(C)** the molecular function category (MF); **(D)** KEGG enrichment analysis of DEFRGs. DEFRGs, differentially expressed FRGs.

GSE72380 dataset and 6 DEmiRs (3 upregulated and 3 downregulated) from GSE29914 dataset (**Table 3**, **Supplementary Tables S2–S3**). Also, 1,206 DEmRs (878 upregulated and 328 downregulated) in GSE63920 and 1,690 DEmRs (901 upregulated and 789 downregulated) in GSE44363 were identified **(Supplementary Tables S4–S5)**. Then, a heatmap of the top 25 DEmiRs and DEmRs were constructed (**Supplementary Figure S1)**, while the volcano plots of DEmiRs and DEmRs are shown in **Supplementary Figure S2**. Finally, 67 overlapping DEFRGs were found between DEGs and FRGs (**Figure 3A**). Subsequently, the heatmaps and volcano plots of DEFRGs in dataset GSE44363 and GSE63920 were constructed, respectively (**Figure 2**).

Establishment of Protein-Protein Interaction Network and Identification of Hub Genes

Based on the STRING database, the visual PPI network of DEFRGs was constructed (**Figure 3B**). Furthermore, the STRING database analysis showed that these genes were significantly associated with oxidoreductase activity. In the PPI network, some key nodes are closely linked and the Cytohubba plugin of Cytoscape software was used to screen these hub genes. Then, ten hub genes were screened out with MCC algorithms, including Egfr, Ptgs2, Cdkn1a, Nfe2l2, Rela, Il6, Hmox1, Stat3, Myc and Vegfa (**Figure 3C**). And **Figure 3D** shows the logFC and adjusted *p*-value of the hub genes.

Gene Ontology and Kyoto Encyclopedia of Genes and Genomes Pathway Enrichment Analysis of Differentially Expressed FRGs

To make a thorough understanding of the function of DEFRGs, GO and KEGG Pathway enrichment analysis of DEFRGs were performed. These duplicated functions or pathways present in both results were shown below. Biological processes (BP) included "positive regulation of smooth muscle cell proliferation", "cellular response to fibroblast growth factor

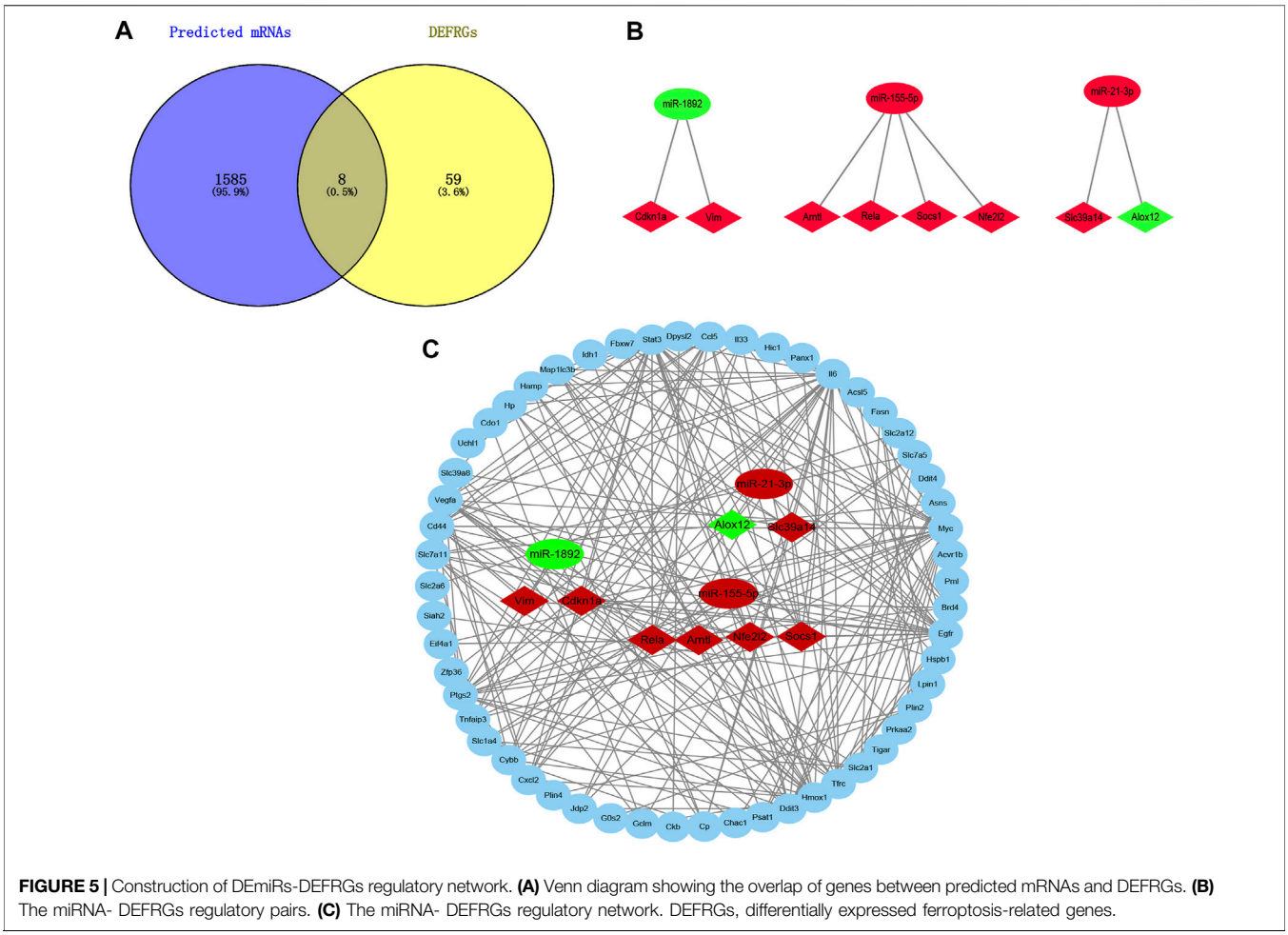

FIGURE 5 | Construction of DEmiRs-DEFRGs regulatory network. **(A)** Venn diagram showing the overlap of genes between predicted mRNAs and DEFRGs. **(B)** The miRNA- DEFRGs regulatory pairs. **(C)** The miRNA- DEFRGs regulatory network. DEFRGs, differentially expressed ferroptosis-related genes.

TABLE 4 | The predicted drugs of DEmRs.

Term	Groups	*p*-Value	Adj *p*-value	Genes
glutathione	Approved	1.51E-22	3.63E-19	IL6; CDKN1A; MYC; STAT3; HMOX1; PTGS2; EGFR; RELA; NFE2L2; VEGFA
1,9-Pyrazoloanthrone	Experimental	2.86E-21	3.45E-18	IL6; CDKN1A; MYC; STAT3; HMOX1; PTGS2; EGFR; RELA; NFE2L2; VEGFA
Capsaicin	Approved	1.08E-20	8.66E-18	IL6; CDKN1A; MYC; STAT3; HMOX1; PTGS2; EGFR; RELA; NFE2L2; VEGFA
PD 98059	Approved	1.25E-19	7.55E-17	IL6; CDKN1A; MYC; STAT3; HMOX1; PTGS2; EGFR; RELA; NFE2L2; VEGFA
170,449–18-0	Experimental	6.66E-19	3.21E-16	IL6; CDKN1A; STAT3; HMOX1; PTGS2; EGFR; NFE2L2; VEGFA
N-Acetyl-L-cysteine	Approved, Investigational	8.14E-19	3.27E-16	IL6; CDKN1A; MYC; STAT3; HMOX1; PTGS2; EGFR; RELA; NFE2L2; VEGFA
LY 294002	Experimental	2.64E-17	9.09E-15	IL6; CDKN1A; STAT3; HMOX1; PTGS2; EGFR; RELA; NFE2L2; VEGFA
Celecoxib	Approved Investigational	4.46E-17	1.34E-14	IL6; CDKN1A; MYC; STAT3; PTGS2; RELA; NFE2L2; VEGFA
Chromium	Approved	1.14E-16	3.05E-14	IL6; MYC; STAT3; HMOX1; PTGS2; EGFR; RELA; VEGFA
curcumin	Approved	1.51E-16	3.51E-14	IL6; CDKN1A; MYC; STAT3; HMOX1; PTGS2; EGFR; RELA; NFE2L2; VEGFA

stimulus", "positive regulation of angiogenesis", "positive regulation of transcription from RNA polymerase II promoter", and "positive regulation of gene expression" (**Figure 4A**). Besides, "cytosol", "cytoplasm", "extracellular exosome", "melanosome", "mitochondrion" and "protein complex" were contained in Cellular Components (**Figure 4B**), while Molecular Functions (MF) included "ubiquitin protein ligase binding", "protein binding", "protein heterodimerization activity", "protein homodimerization activity", "protein kinase binding" and "identical protein binding" (**Figure 4C**). In addition, these genes were both significantly associated with 6 KEGG pathways, including "HIF-1 signaling pathway", "MicroRNAs in cancer", "Pathways in cancer", "Epstein-Barr virus infection", "NOD-like receptor signaling pathway" and "TNF signaling pathway". (**Figure 4D**).

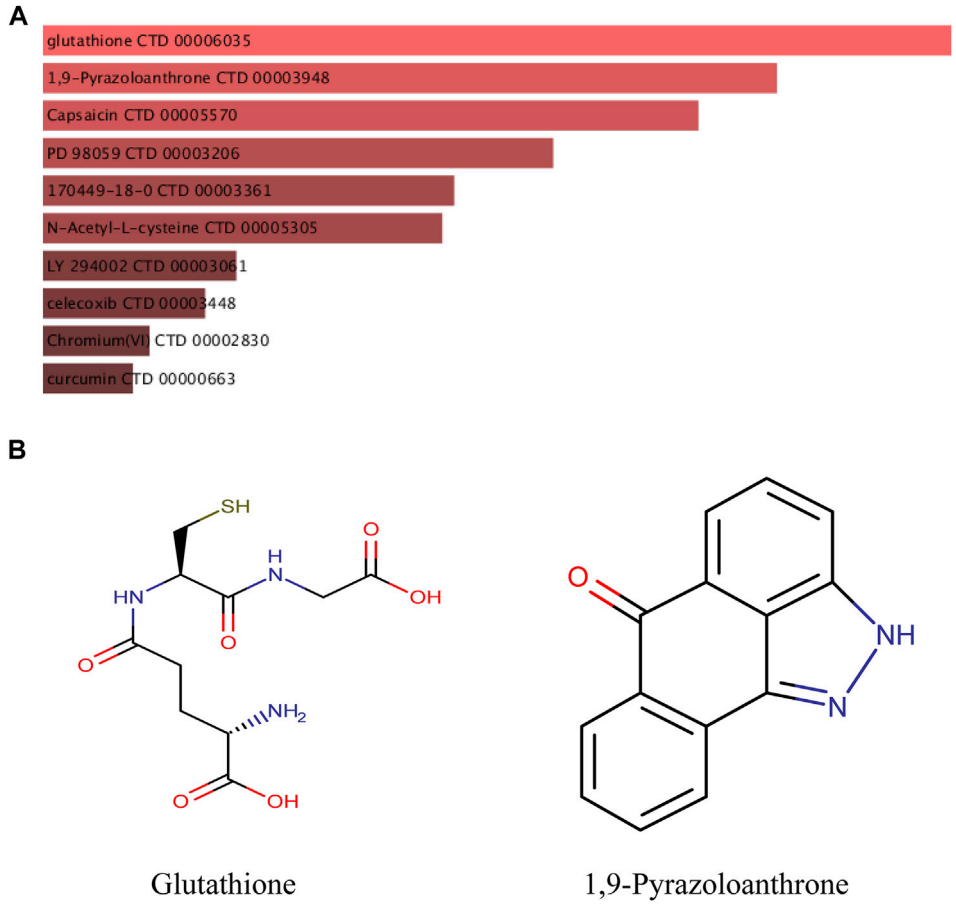

FIGURE 6 | Targeted drugs prediction. **(A)** The top 10 predicted target drugs ranked according to *p* values in the DSigDB database. **(B)** The chemical structures of glutathione and 1,9-Pyrazoloanthrone.

Prediction of the Target Genes of Differentially Expressed miRs and Construction miRNA-mRNA Networks

The target mRNAs of those 8 DEmiRs were gained from two miRNA target prediction websites (TargetScan and miRDB). A total of 1,593 predicted mRNAs were subsequently identified. And 8 Overlapped target DEFRGs between predicted mRNAs and DEFRGs were found, including Cdkn1a, Nfe2l2, Rela, Vim, Arntl, Socs1, Slc39a14 and Alox12. (**Figure 5A**). Next, based on the association between DEmiRs and the DEFRGs, the miRNA-DEFRGs pairs were identified (**Figure 5B**). Subsequently, we merged the miRNA- DEFRGs pairs and PPI network into the final miRNA-mRNA network by using Cytoscape software (**Figure 5C**).

Drug Prediction of Differentially Expressed mRs

The DSigDB database can combine detailed drug data with comprehensive drug targets and drug action information. Its main functions included promotion of silicon-chip drug target discovery, drug design, drug docking or screening, drug metabolism prediction, drug interaction prediction, and general pharmacy education. The 10 hub genes were inserted into DSigDB database, and the targeted drugs of these genes were predicted. The top 10 candidate drugs related to the DEmRs were chosen according to the *p*-value and adjusted *p*-value and all these drugs have been approved by Food and Drug Administration or have been experimental stage (**Table 4**). The 10 drugs were shown in **Figure 6A** and the structure of the top two drugs were shown in **Figure 6B**. The effects of these drugs were consistent with the international guidelines for management of sepsis (29).

Validation of Abnormal Hub Genes

Based on the miRNA–mRNA network, we validated several hub genes to increase the confidence of our results. We constructed an LPS-induced myocardial injury model of SCM and determined the expression of differential mRNAs using real-time PCR. The results are shown in **Figure 7**. Compared with the control group, the expression of FRGs Cdkn1a, Vim, Rela, Arntl, Nfe2l2, Socs1, Ptgs2 and Slc39a14 were upregulated in HL-1 cells treated with LPS (**Figure 7A**). In addition, the expression of mmu-miR-1892 was significantly down-regulated in LPS-treated HL-1 cells (**Figure 7B**).

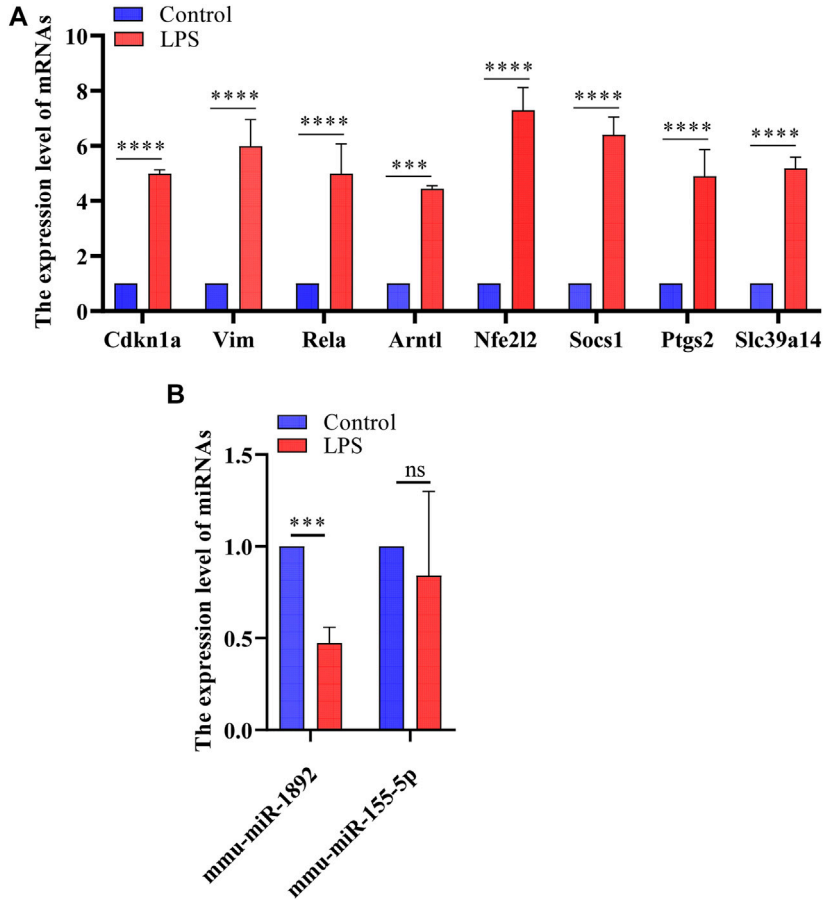

FIGURE 7 | The results of real-time PCR. **(A)** Detection of FRGs expression in control and LPS treat HL-1 cells using RT-qPCR (n = 3), compared with the control group, the expression of FRGs was upregulated in HL-1 cells treated with LPS. **(B)** Detection of miRNAs expression using RT-qPCR (*n* = 3), the expression of mmu-miR-1892 was significantly down-regulated in LPS-treated HL-1 cells. ***, $p < 0.001$; ****, $p < 0.0001$; ns, no significant. Error bars represent the mean ± SD of triplicate experiments.

These findings were consistent with our predicted results. Based on the above results, we selected mmu-miR-1892 -Cdkn1a, a regulatory pair, for further protein-level validation. To verify the protein levels of Cdkn1a and to further explore the effect of Cdkn1a on ferroptosis in SCM, we performed western blotting analysis. As shown in **Figure 8A**, the expression of Cdkn1a was up-regulated in HL-1 cells treated with LPS, but the expression of Gpx4 and FTH1, ferroptosis-related proteins, were down-regulated in LPS-treated HL-1 cells, however, Si- Cdkn1a treatment reversed this discrepancy, suggesting that Cdkn1a may be a potential regulatory target of LPS-induced ferroptosis in cardiomyocytes. Furthermore, to further explore the effect of Cdkn1a on LPS-induced myocardial injury, we simultaneously examined the levels of apoptosis-related proteins. As shown in **Figure 8B**, the expression of Caspase-3 and Bax were significantly up-regulated, but the expression of Bcl-2 was down-regulated in LPS-treated HL-1 cells. Interestingly, Si- Cdkn1a inhibited the expression of apoptosis-associated proteins and increased the expression of Bcl-2, indicating that Cdkn1a may be inhibiting LPS-induced cardiomyocyte injury through diverse pathways, and the specific mechanism of action needs to be further studied.

DISCUSSION

Sepsis is a manifestation of the body's dysfunctional response to infection, which may eventually lead to multi-organ failure, disability and even death (Deutschman and Tracey 2014). SCM is a serious complication of sepsis and is directly associated with high sepsis mortality (Liu et al., 2017). Despite great efforts and numerous clinical trials, there is still a major need for effective therapies for SCM. Therefore, it is crucial to diagnose SCM early and intervene promptly to avoid the development of severe SCM. However, the diagnosis of SCM relies mainly on myocardial damage factors and echocardiography, which limits early intervention in SCM patients. Therefore, it is urgent to find new predictive biomarkers for the early diagnosis and intervention of SCM. In recent years, with the development of targeted gene therapy, targeted gene technology has achieved significant success in the early diagnosis, treatment, and prediction of prognosis in a variety of diseases (Bakhshinejad et al., 2014; Zeng et al., 2021), which provides a direction for early diagnosis of SCM. Ferroptosis is closely associated with the development of various

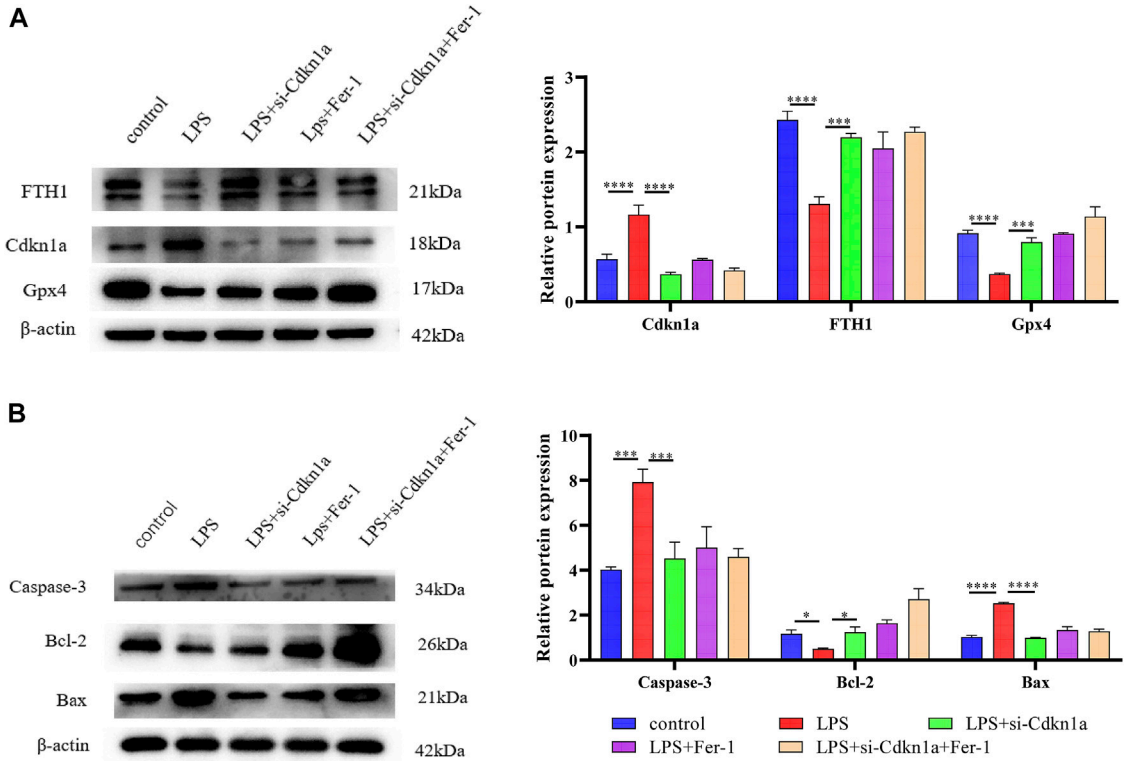

FIGURE 8 | The results of Western Blotting Analysis. This part of the study was based on the untreated HL-1 cells and LPS-treated HL-1 cells that were treated with Si- Cdkn1a or Fer-1 ($n = 3$). **(A)** Western blotting was used for detecting GPX4, FTH1 and Cdkn1a expression in different HL-1 cells; **(B)** Western blotting was used for detecting Caspase-3, Bcl-2 and Bax expression in different HL-1 cells. *, $p < 0.05$; ***, $p < 0.001$; ****, $p < 0.0001$, Error bars represent the mean ± SD of triplicate experiments.

cardiovascular diseases, including coronary artery disease, myocardial infarction and SCM (Fang et al., 2019; Wang et al., 2020). Recent studies have found that iron overload, an important pathological process of ferroptosis, is present in the heart tissue of septic mice (Sae-Khow et al., 2020), suggesting that ferroptosis may be a potential mechanism for the development of SCM. However, the impact of ferroptosis in the development of SCM is unclear. Therefore, we performed bioinformatics analysis based on SCM-related datasets to explore the role of ferroptosis in the pathogenesis of SCM.

With the development of public databases, microarray analysis is emerging as an effective method for identifying key molecules in various diseases, including septic cardiomyopathy (Ivandic et al., 2012). Therefore, in this study, we combined differentially expressed genes profiling in septic cardiomyopathy and FRGs analysis to construct PPI and miRNA-mRNA regulatory networks to improve our understanding of the molecular mechanisms of septic cardiomyopathy and to explore potential biomarkers.

After the construction of the PPI network, we identified 10 differentially expressed ferroptosis-related mRNA (Egfr, Ptgs2, Cdkn1a, Nfe2l2, Rela, Il6, Hmox1, Stat3, Myc and Vegfa) using cytoHubba. These hub genes may be potential targets for the regulation of ferroptosis in SCM. After validation, Cdkn1a, Ptgs2, Nfe2l2, Rela, and Vim were finally identified as key genes. These genes have been demonstrated to be involved in tumorigenesis, lipid peroxidation, inflammatory stress, or oxidative stress. Cdkn1a, an oncogene that encodes a potent cyclin-dependent kinase inhibitor, was reported to be specifically cleaved by CASP3-like caspases, which thus leaded to a dramatic activation of cyclin-dependent kinase2 and may be instrumental in the execution of apoptosis following caspase activation (Torgovnick et al., 2018). Moreover, Cdkn1a was upregulated in ferroptosis--related necrotizing enterocolitis (Bein et al., 2017) However, the role of Cdkn1a in SCM has not been investigated. In the present study, we further explored the effect of Cdkn1a on ferroptosis in SCM by western blotting analysis. The results show that the expression of Cdkn1a was up-regulated in HL-1 cells treated with LPS, but the expression of Gpx4 and FTH1, ferroptosis-related proteins, were down-regulated in LPS-treated HL-1 cells, however, Si-Cdkn1a treatment reversed this discrepancy, suggesting that Cdkn1a may be a potential regulatory target of LPS-induced ferroptosis in cardiomyocytes. Also, Ptgs2, also known as cyclooxygenase, was the marker gene of ferroptosis. Ptgs2 was reported to be significantly upregulated in LPS-induced septic cardiomyopathy mice (Li et al., 2020), which was consistent with our prediction, while PCR results further validated our prediction. Moreover, Nfe2l2 (Nuclear Factor, Erythroid 2 Like 2) is a Protein Coding gene. Li et al. reported that Curcumin

alleviates LPS-induced oxidative stress, in bovine mammary epithelial cells via the Nfe2l2 signaling pathway (Li et al., 2021). However, the role of Nfe2l2 in LPS-induced myocardial injury has not been studied. These were consistent with our predicted results, and our PCR results further confirmed this. In addition, we found that the relationship between some mRNAs and sepsis is still poorly studied. Therefore, these key mRNAs are expected to be new biomarkers and therapeutic targets in future sepsis research.

Currently, many researchers have demonstrated that ferroptosis was associated with sepsis (Wei et al., 2020; Wang et al., 2021; Xiao et al., 2021). However, it is not common to construct miRNA-mRNA regulatory networks of FRGs in SCM and to predict its biomarkers. Here, we constructed a miRNA-FRGs network to explore the potential regulation of FRG by miRNAs in SCM. And 3 miRNA-miRNA regulatory pairs (mmu-miR-21-3p, mmu-miR-155-5p and mmu-miR-1892) were identified by bioinformatic analysis. And most of these miRNAs have been studied. Recent research implied that mmu-miR-21-3p was involved in oxidative stress during carcinogenesis (Kushwaha et al., 2020), while Zhou et al. found that miR-21-3p mediated angiogenesis in inflammatory states (Zhou et al., 2019). In addition, Zhang et al. reported that mmu-miR-155 promoted mastitis induced by *staphylococcus aureus* in mice (Zhang et al., 2019b). Finally, mmu-miR-1892-Cdkn1a was identified as key regulatory pair via validation. The PCR results showed that mmu-miR-1892 was downregulated in the LPS-induced myocardial injury model, which was consistent with our prediction. In addition, western blotting analysis results showed that Cdkn1a was up-regulated in the LPS-induced myocardial injury model, and interestingly, inhibition of its expression attenuated myocardial injury, suggesting that Cdkn1a may be a potential regulatory target in SCM. However, the specific mechanism of mmu-miR-1892-Cdkn1a in SCM has not been reported yet, and further studies are needed.

Sepsis is life-threatening organ dysfunction caused by a dysregulated host response to infection. Early identification and appropriate management in the initial hours after sepsis develops improves outcomes. Therefore, it is critical to select the most appropriate candidate drug intervention. At present, the main therapeutic drugs for sepsis are antimicrobials, norepinephrine, and hydrocortisone (Rhodes et al., 20162017). In this study, we used an online website to predict potential therapeutic agents associated with key genes and which may provide a reference for the pharmacological treatment of SCM.

CONCLUSION

In the present study, we identified differentially expressed genes in SCM and analyzed the differential expression of FRGs in SCM by bioinformatics analysis. We constructed a miRNA-mRNA regulatory network in SCM and further obtained key FRGs and key miRNA-mRNA regulatory pair that may be potential regulatory mechanisms of myocardial ferroptosis in SCM. In addition, qRT-PCR and western blotting analysis were performed to confirm the abnormal expression of hub genes. The current study will contribute to the discovery of ferroptosis-related biomarkers in SCM and provide an important reference for further studies.

DATA AVAILABILITY STATEMENT

The original contributions presented in the study are included in the article/**Supplementary Material**, further inquiries can be directed to the corresponding authors.

AUTHOR CONTRIBUTIONS

Conception and design: S-QL; administrative support: J-CL; collection and assembly of data: H-XZ, L-JW; data analysis and interpretation: C-WG, M-MY and B-QQ; cellular experiments: M-MY, TH; manuscript writing: all authors; final approval of manuscript: all authors. All authors have read and agreed to the published version of the manuscript.

FUNDING

This work was supported in part by grants from the National Natural Science Foundation of China (No. 82070303), the Natural Science Foundation of Jiangxi Province, China (No. 20202BAB206007)

SUPPLEMENTARY MATERIAL

The Supplementary Material for this article can be found online at: https://www.frontiersin.org/articles/10.3389/fgene.2022.827559/full#supplementary-material

REFERENCES

Bakhshinejad, B., Karimi, M., and Sadeghizadeh, M. (2014). Bacteriophages and Medical Oncology: Targeted Gene Therapy of Cancer. *Med. Oncol.* 31 (8), 110. doi:10.1007/s12032-014-0110-9

Balija, T. M., and Lowry, S. F. (2011). Lipopolysaccharide and Sepsis-Associated Myocardial Dysfunction. *Curr. Opin. Infect. Dis.* 24 (3), 248–253. doi:10.1097/QCO.0b013e32834536ce

Bein, A., Zilbershtein, A., Golosovsky, M., Davidov, D., and Schwartz, B. (2017). LPS Induces Hyper-Permeability of Intestinal Epithelial Cells. *J. Cel. Physiol.* 232 (2), 381–390. doi:10.1002/jcp.25435

Cecconi, M., Evans, L., Levy, M., and Rhodes, A. (2018). Sepsis and Septic Shock. *The Lancet* 392 (10141), 75–87. doi:10.1016/s0140-6736(18)30696-2

Celes, M. R. N., Torres-Dueñas, D., Malvestio, L. M., Blefari, V., Campos, E. C., Ramos, S. G., et al. (2010). Disruption of Sarcolemmal Dystrophin and β-dystroglycan May Be a Potential Mechanism for Myocardial Dysfunction in Severe Sepsis. *Lab. Invest.* 90 (4), 531–542. doi:10.1038/labinvest.2010.3

Chiti, E., Paolo, M., Turillazzi, E., and Rocchi, A. (2021). MicroRNAs in Hypertrophic, Arrhythmogenic and Dilated Cardiomyopathy. *Diagnostics* 11 (9), 1720. doi:10.3390/diagnostics11091720

Crouser, E. D. (2004). Mitochondrial Dysfunction in Septic Shock and Multiple Organ Dysfunction Syndrome. *Mitochondrion* 4 (5-6), 729–741. doi:10.1016/j.mito.2004.07.023

Deutschman, C. S., and Tracey, K. J. (2014). Sepsis: Current Dogma and New Perspectives. *Immunity* 40 (4), 463–475. doi:10.1016/j.immuni.2014.04.001

Dixon, S. J., Lemberg, K. M., Lamprecht, M. R., Skouta, R., Zaitsev, E. M., Gleason, C. E., et al. (2012). Ferroptosis: an Iron-dependent Form of Nonapoptotic Cell Death. *Cell* 149 (5), 1060–1072. doi:10.1016/j.cell.2012.03.042

Drosatos, K., Drosatos-Tampakaki, Z., Khan, R., Homma, S., Schulze, P. C., Zannis, V. I., et al. (2011). Inhibition of C-Jun-N-Terminal Kinase Increases Cardiac Peroxisome Proliferator-Activated Receptor α Expression and Fatty Acid Oxidation and Prevents Lipopolysaccharide-Induced Heart Dysfunction. *J. Biol. Chem.* 286 (42), 36331–36339. doi:10.1074/jbc.M111.272146

Drosatos, K., Pollak, N. M., Pol, C. J., Ntziachristos, P., Willecke, F., Valenti, M.-C., et al. (2016). Cardiac Myocyte KLF5 Regulates Ppara Expression and Cardiac Function. *Circ. Res.* 118 (2), 241–253. doi:10.1161/circresaha.115.306383

Fang, X., Cai, Z., Wang, H., Han, D., Cheng, Q., Zhang, P., et al. (2020). Loss of Cardiac Ferritin H Facilitates Cardiomyopathy via Slc7a11-Mediated Ferroptosis. *Circ. Res.* 127 (4), 486–501. doi:10.1161/circresaha.120.316509

Fang, X., Wang, H., Han, D., Xie, E., Yang, X., Wei, J., et al. (2019). Ferroptosis as a Target for protection against Cardiomyopathy. *Proc. Natl. Acad. Sci. U.S.A.* 116 (7), 2672–2680. doi:10.1073/pnas.1821022116

Fehlmann, T., Sahay, S., Keller, A., and Backes, C. (2019). A Review of Databases Predicting the Effects of SNPs in miRNA Genes or miRNA-binding Sites. *Brief. Bioinformatics* 20 (3), 1011–1020. doi:10.1093/bib/bbx155

Hassoun, S. M., Marechal, X., Montaigne, D., Bouazza, Y., Decoster, B., Lancel, S., et al. (2008). Prevention of Endotoxin-Induced Sarcoplasmic Reticulum Calcium Leak Improves Mitochondrial and Myocardial Dysfunction*. *Crit. Care Med.* 36 (9), 2590–2596. doi:10.1097/CCM.0b013e3181844276

Ivandic, B. T., Mastitsky, S. E., Schönsiegel, F., Bekeredjian, R., Eils, R., Frey, N., et al. (2012). Whole-genome Analysis of Gene Expression Associates the Ubiquitin-Proteasome System with the Cardiomyopathy Phenotype in Disease-Sensitized Congenic Mouse Strains. *Cardiovasc. Res.* 94 (1), 87–95. doi:10.1093/cvr/cvs080

Kushwaha, P. P., Gupta, S., Singh, A. K., Prajapati, K. S., Shuaib, M., and Kumar, S. (2020). MicroRNA Targeting Nicotinamide Adenine Dinucleotide Phosphate Oxidases in Cancer. *Antioxid. Redox Signaling* 32 (5), 267–284. doi:10.1089/ars.2019.7918

Li, N., Wang, W., Zhou, H., Wu, Q., Duan, M., Liu, C., et al. (2020). Ferritinophagy-mediated Ferroptosis Is Involved in Sepsis-Induced Cardiac Injury. *Free Radic. Biol. Med.* 160, 303–318. doi:10.1016/j.freeradbiomed.2020.08.009

Li, R., Fang, H., Shen, J., Jin, Y., Zhao, Y., Wang, R., et al. (2021). Curcumin Alleviates LPS-Induced Oxidative Stress, Inflammation and Apoptosis in Bovine Mammary Epithelial Cells via the NFE2L2 Signaling Pathway. *Toxins* 13 (3), 208. doi:10.3390/toxins13030208

Liu, Y.-C., Yu, M.-M., Shou, S.-T., and Chai, Y.-F. (2017). Sepsis-Induced Cardiomyopathy: Mechanisms and Treatments. *Front. Immunol.* 8, 1021. doi:10.3389/fimmu.2017.01021

Manetti, A. C., Maiese, A., Baronti, A., Mezzetti, E., Frati, P., Fineschi, V., et al. (2021). MiRNAs as New Tools in Lesion Vitality Evaluation: A Systematic Review and Their Forensic Applications. *Biomedicines* 9 (11), 1731. doi:10.3390/biomedicines9111731

Manetti, A. C., Maiese, A., Paolo, M. D., De Matteis, A., La Russa, R., Turillazzi, E., et al. (2020). MicroRNAs and Sepsis-Induced Cardiac Dysfunction: A Systematic Review. *Ijms* 22 (1), 321. doi:10.3390/ijms22010321

Mendell, J. T., and Olson, E. N. (2012). MicroRNAs in Stress Signaling and Human Disease. *Cell* 148 (6), 1172–1187. doi:10.1016/j.cell.2012.02.005

Mirna, M., Paar, V., Rezar, R., Topf, A., Eber, M., Hoppe, U. C., et al. (2019). MicroRNAs in Inflammatory Heart Diseases and Sepsis-Induced Cardiac Dysfunction: A Potential Scope for the Future? *Cells* 8 (11), 1352. doi:10.3390/cells8111352

Reinhart, K., Daniels, R., Kissoon, N., Machado, F. R., Schachter, R. D., and Finfer, S. (2017). Recognizing Sepsis as a Global Health Priority - A Who Resolution. *N. Engl. J. Med.* 377 (5), 414–417. doi:10.1056/NEJMp1707170

Reyes, M., Filbin, M. R., Bhattacharyya, R. P., Billman, K., Eisenhaure, T., Hung, D. T., et al. (2020). An Immune-Cell Signature of Bacterial Sepsis. *Nat. Med.* 26 (3), 333–340. doi:10.1038/s41591-020-0752-4

Rhodes, A., Evans, L. E., Alhazzani, W., Levy, M. M., Antonelli, M., Ferrer, R., et al. (20162017). Surviving Sepsis Campaign: International Guidelines for Management of Sepsis and Septic Shock: 2016. *Intensive Care Med.* 43 (3), 304–377. doi:10.1007/s00134-017-4683-6

Rudiger, A., and Singer, M. (2007). Mechanisms of Sepsis-Induced Cardiac Dysfunction. *Crit. Care Med.* 35 (6), 1599–1608. doi:10.1097/01.Ccm.0000266683.64081.02

Sae-Khow, K., Charoensappakit, A., Visitchanakun, P., Saisorn, W., Svasti, S., Fucharoen, S., et al. (2020). Pathogen-Associated Molecules from Gut Translocation Enhance Severity of Cecal Ligation and Puncture Sepsis in Iron-Overload β-Thalassemia Mice. *Jir* Vol. 13, 719–735. doi:10.2147/jir.S273329

Stockwell, B. R., Friedmann Angeli, J. P., Bayir, H., Bush, A. I., Conrad, M., Dixon, S. J., et al. (2017). Ferroptosis: A Regulated Cell Death Nexus Linking Metabolism, Redox Biology, and Disease. *Cell* 171 (2), 273–285. doi:10.1016/j.cell.2017.09.021

Szklarczyk, D., Franceschini, A., Wyder, S., Forslund, K., Heller, D., Huerta-Cepas, J., et al. (2015). STRING V10: Protein-Protein Interaction Networks, Integrated over the Tree of Life. *Nucleic Acids Res.* 43, D447–D452. doi:10.1093/nar/gku1003

Tang, D., Chen, X., Kang, R., and Kroemer, G. (2021). Ferroptosis: Molecular Mechanisms and Health Implications. *Cell Res* 31 (2), 107–125. doi:10.1038/s41422-020-00441-1

Torgovnick, A., Heger, J. M., Liaki, V., Isensee, J., Schmitt, A., Knittel, G., et al. (2018). The Cdkn1aSUPER Mouse as a Tool to Study P53-Mediated Tumor Suppression. *Cel Rep.* 25 (4), 1027–1039. doi:10.1016/j.celrep.2018.09.079

Vogelstein, B., Papadopoulos, N., Velculescu, V. E., Zhou, S., Diaz, L. A., Jr., and Kinzler, K. W. (2013). Cancer Genome Landscapes. *Science* 339 (6127), 1546–1558. New York, NY. doi:10.1126/science.1235122

Wang, C., Yuan, W., Hu, A., Lin, J., Xia, Z., Yang, C., et al. (2020). Dexmedetomidine Alleviated Sepsis-induced M-yocardial F-erroptosis and S-eptic H-eart I-njury. *Mol. Med. Rep.* 22 (1), 175–184. doi:10.3892/mmr.2020.11114

Wang, H., Bei, Y., Shen, S., Huang, P., Shi, J., Zhang, J., et al. (2016). miR-21-3p Controls Sepsis-Associated Cardiac Dysfunction via Regulating SORBS2. *J. Mol. Cell. Cardiol.* 94, 43–53. doi:10.1016/j.yjmcc.2016.03.014

Wang, N., Ma, H., Li, J., Meng, C., Zou, J., Wang, H., et al. (2021). HSF1 Functions as a Key Defender against Palmitic Acid-Induced Ferroptosis in Cardiomyocytes. *J. Mol. Cell. Cardiol.* 150, 65–76. doi:10.1016/j.yjmcc.2020.10.010

Wei, S., Bi, J., Yang, L., Zhang, J., Wan, Y., Chen, X., et al. (2020). Serum Irisin Levels Are Decreased in Patients with Sepsis, and Exogenous Irisin Suppresses Ferroptosis in the Liver of Septic Mice. *Clin. translational Med.* 10 (5), e173. doi:10.1002/ctm2.173

Werdan, K., Schmidt, H., Ebelt, H., Zorn-Pauly, K., Koidl, B., Hoke, R. S., et al. (2009). Impaired Regulation of Cardiac Function in Sepsis, SIRS, and MODSThis Article Is One of a Selection of Papers from the NATO Advanced Research Workshop on Translational Knowledge for Heart Health (Published in Part 2 of a 2-part Special Issue). *Can. J. Physiol. Pharmacol.* 87 (4), 266–274. doi:10.1139/y09-012

Wong, N., and Wang, X. (2015). miRDB: an Online Resource for microRNA Target Prediction and Functional Annotations. *Nucleic Acids Res.* 43, D146–D152. doi:10.1093/nar/gku1104

Xiao, Z., Kong, B., Fang, J., Qin, T., Dai, C., Shuai, W., et al. (2021). Ferrostatin-1 Alleviates Lipopolysaccharide-Induced Cardiac Dysfunction. *Bioengineered* 12 (2), 9367–9376. doi:10.1080/21655979.2021.2001913

Yoo, M., Shin, J., Kim, J., Ryall, K. A., Lee, K., Lee, S., et al. (2015). DSigDB: Drug Signatures Database for Gene Set Analysis: Fig. 1. *Bioinformatics* 31 (18), 3069–3071. doi:10.1093/bioinformatics/btv313

Zeng, X., Li, Z., Zhu, C., Xu, L., Sun, Y., and Han, S. (2021). Research Progress of Nanocarriers for Gene Therapy Targeting Abnormal Glucose and Lipid Metabolism in Tumors. *Drug Deliv.* 28 (1), 2329–2347. doi:10.1080/10717544.2021.1995081

Zhang, T.-N., Yang, N., Goodwin, J. E., Mahrer, K., Li, D., Xia, J., et al. (2019). Characterization of Circular RNA and microRNA Profiles in Septic Myocardial Depression: a Lipopolysaccharide-Induced Rat Septic Shock Model. *Inflammation* 42 (6), 1990–2002. doi:10.1007/s10753-019-01060-8

Zhang, Z.-b., Guo, Y.-f., Li, C.-y., Qiu, C.-w., and Guo, M.-y. (2019). Selenium Influences Mmu-miR-155 to Inhibit Inflammation inStaphylococcus Aureus-Induced Mastitis in Mice. *Food Funct.* 10 (10), 6543–6555. doi:10.1039/c9fo01488h

Zhou, Y., Yang, Y., Liang, T., Hu, Y., Tang, H., Song, D., et al. (2019). The Regulatory Effect of microRNA-21a-3p on the Promotion of Telocyte Angiogenesis Mediated by PI3K (p110α)/AKT/mTOR in LPS Induced Mice ARDS. *J. Transl Med.* 17 (1), 427. doi:10.1186/s12967-019-02168-z

Conflict of Interest: The authors declare that the research was conducted in the absence of any commercial or financial relationships that could be construed as a potential conflict of interest.

Publisher's Note: All claims expressed in this article are solely those of the authors and do not necessarily represent those of their affiliated organizations, or those of the publisher, the editors and the reviewers. Any product that may be evaluated in this article, or claim that may be made by its manufacturer, is not guaranteed or endorsed by the publisher.

frontiers | Frontiers in Genetics

REVIEW
published: 13 April 2022
doi: 10.3389/fgene.2022.834367

Long Non Coding RNA Based Regulation of Cerebrovascular Endothelium

Samatha Mathew[1,2] *and Sridhar Sivasubbu*[1,2]*

[1]CSIR Institute of Genomics and Integrative Biology (CSIR-IGIB), New Delhi, India, [2]Academy of Scientific and Innovative Research (AcSIR), Ghaziabad, India

The rapid and high throughput discovery of long non coding RNAs (lncRNAs) has far outstripped the functional annotation of these novel transcripts in their respective cellular contexts. The cells of the blood brain barrier (BBB), especially the cerebrovascular endothelial cells (CVECs), are strictly regulated to maintain a controlled state of homeostasis for undisrupted brain function. Several key pathways are understood in CVEC function that lead to the development and maintenance of their barrier properties, the dysregulation of which leads to BBB breakdown and neuronal injury. Endothelial lncRNAs have been discovered and functionally validated in the past decade, spanning a wide variety of regulatory mechanisms in health and disease. We summarize here the lncRNA-mediated regulation of established pathways that maintain or disrupt the barrier property of CVECs, including in conditions such as ischemic stroke and glioma. These lncRNAs namely regulate the tight junction assembly/disassembly, angiogenesis, autophagy, apoptosis, and so on. The identification of these lncRNAs suggests a less understood mechanistic layer, calling for further studies in appropriate models of the blood brain barrier to shed light on the lncRNA-mediated regulation of CVEC function. Finally, we gather various approaches for validating lncRNAs in BBB function in human organoids and animal models and discuss the therapeutic potential of CVEC lncRNAs along with the current limitations.

Keywords: long non coding RNAs, blood brain barrier, neurovascular unit, cerebrovascular endothelial cells, organoids, animal models, lncRNA therapeutics

OPEN ACCESS

Edited by:
William C. Cho,
QEH, Hong Kong SAR, China

Reviewed by:
H. S. Jeffrey Man,
University of Toronto, Canada
Navjot Kaur,
Yale University, United States

***Correspondence:**
Sridhar Sivasubbu
sridhar@igib.in

Specialty section:
This article was submitted to RNA, a section of the journal Frontiers in Genetics

Received: *13 December 2021*
Accepted: *24 March 2022*
Published: *13 April 2022*

Citation:
Mathew S and Sivasubbu S (2022) Long Non Coding RNA Based Regulation of Cerebrovascular Endothelium. Front. Genet. 13:834367. doi: 10.3389/fgene.2022.834367

INTRODUCTION

Endothelial cells (ECs) lining the blood vessel walls display functional, structural and biochemical heterogeneity across the body, depending on the cellular environment and blood flow ((Aird, 2007a), (Aird, 2007b)). Using endothelial cell-specific translating ribosome affinity purification, a recent study cataloged the *in vivo* translatomes of ECs of mice, showing the endothelial heterogeneity across vascular beds (Cleuren et al., 2019). Spatial transcriptomics of the brain in a cerebral cavernous malformation (CCM) mouse model could identify the differential involvement of arterial ECs versus venous ECs in the disease (Orsenigo et al., 2020). Endothelial cells also exhibit considerable plasticity in response to a variety of endothelial permeability modulators (Claesson-Welsh et al., 2021). Moreover, tissue-specific phenotype of the endothelium is not only decided by the environmental milieu, but is encoded by epigenetic marks as well (Aird, 2007a). The discovery of non-coding RNA (ncRNA) mediated regulation of epigenetic modifications and other cellular processes provide new

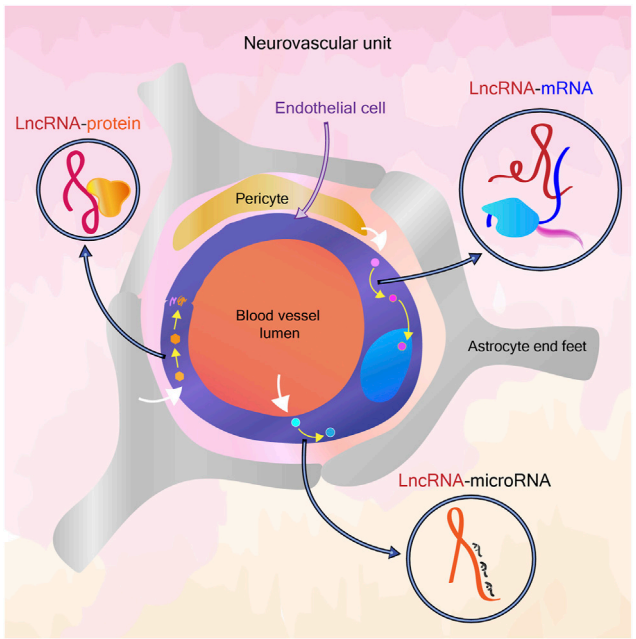

Graphical Abstract | Long non coding RNAs regulate the cerebrovascular endothelial processes.

avenues to explore the mechanisms of heterogeneity and plasticity of endothelial cells. With the availability of single cell endothelial transcriptomic data (Khan et al., 2019), there are many prospects ahead to decipher the complex network of the noncoding RNA and protein coding factor interplay in endothelial cells.

CEREBROVASCULAR ENDOTHELIAL CELLS

The heightened sensitivity of the brain tissue and neuronal signaling to pathogens, toxins and ionic imbalance, coupled with the inability to rapidly regenerate post damage has led to the evolution of a highly selective blood brain barrier (BBB) between blood and the brain parenchyma (Strange, 1992). Cerebrovascular endothelial cells (CVECs) are non-fenestrated, with exceptions in certain areas of the brain, and undergo very low rates of transcytosis allowing only lipid soluble molecules to pass through, sieving the movement of water-soluble solutes. CVECs are marked by abundant tight junctions at endothelial cell-cell boundaries, and express a large number of efflux proteins to exclude toxins and fewer leukocyte adhesion molecules to prevent inflammation. Additionally, they contain higher numbers of mitochondria (Obermeier et al., 2013; Daneman and Prat, 2015).

The cellular anatomy of the blood brain barrier consists of a conjugated system of endothelial cells, mural cells and glial cells, along with the basement lamina and glycocalyx. The signals sent by supporting cells to the endothelial cells determine the composition and permeability of the blood brain barrier. The signaling of the support cells are also influenced by the triggers from neurons (Obermeier et al., 2013). This neurovascular unit (NVU) is maintained throughout the life of a vertebrate for the normal functioning of the brain. The cerebrovascular endothelial cells rapidly respond to cues from the NVU, from both the luminal and abluminal sides. Apart from the regulation of angiogenesis and permeability during development by neurons, in adults, neuronal activity can send signals that affect the BBB permeability during stresses such as chronic sleep deprivation (Sweeney et al., 2019). In addition, in neuroinflammatory conditions such as ischemic stroke and psychiatric disorders, several cues lead to alteration in BBB permeability (Yang et al., 2019; Kealy et al., 2020).

INTERPLAY OF MOLECULAR PATHWAYS IN CVEC FUNCTION

During development, the Vascular Endothelial Growth Factor (VEGF) pathway is central to guidance and migration of endothelial cells into the neural tissue, during which time they possess tight junctions and transporter proteins, however with high levels of transcytosis and expression of leukocyte adhesion molecules (Bauer et al., 2014). Wnt/beta-catenin signaling pathway is specifically activated in the central nervous system (CNS), and regulates expression of nutrient transport molecules. The sonic hedgehog pathway further plays a role in the maintenance of the barrier properties (Obermeier et al., 2013). Signals from the pericytes and astrocytes and basement membrane also influence the maintenance of BBB (Daneman et al., 2010; Obermeier et al., 2013). The different cellular pathways involved in BBB establishment and permeability have been summarized recently (Tjakra et al., 2019).

THE UNKNOWNS OF BBB: CAN LONG NON CODING RNA ANSWER?

An elegant set of questions on the dynamicity of BBB have been raised by the Daneman group recently (Profaci et al., 2020). It is well understood that the BBB is not uniform in different parts of the brain and that the "breakdown" of BBB is also a non-uniform process. The non-coding RNA mediated regulation of the NVU has been known for more than a decade (Wang S.-W. et al., 2018). LncRNAs can exert a regulatory role at epigenetic, post-transcriptional, translational and post-translational levels (Xie and Wei, 2021), (Huang et al., 2021) while some lncRNAs are also known to function by coding for short peptides (Choi et al., 2019), (Hartford and Lal, 2020). LncRNAs are in particular known to be highly cell-type specific, unlike mRNA (Quinn and Chang, 2016), which could act as a potential factor in the variability of endothelial cells in general and variability within brain endothelial cells depending on brain region, age and disease conditions. Also, the abundance of a lncRNA can influence its functional role, which can add another tier of fine-tuning for cell-type specific properties (Grammatikakis and Lal, 2021). The tissue-specific transcriptomic and epigenomic signatures that

differentiate CNS endothelial cells and other endothelial cells have been explored earlier (Sabbagh et al., 2018). The availability of transcriptomic data from the NVU at single cell resolution further opens up avenues to uncover novel regulators of cell function, including the less abundantly expressed lncRNAs (Kiss et al., 2020), (Mäe et al., 2021). In this review, we particularly focus on functionally validated lncRNAs associated with cerebrovascular endothelial cell pathways.

LONG NON CODING RNAS IN ENDOTHELIAL FUNCTION

Of the thousands of RNAs in a eukaryotic cell that defy the central dogma of biology, long non coding RNAs (lncRNAs) form a considerable proportion. NONCODEv5 has put together nearly 550 thousand lncRNA transcripts from 17 species, of which 172 thousand are of human origin (Fang et al., 2018). The ANGIOGENES database has catalogued protein coding RNAs and noncoding RNAs in endothelial cells from human, and the model organisms, mouse and zebrafish (Müller et al., 2016). Endothelial lncRNAs are known in development, function and vascular disease (Kok and Baker, 2019), (Jaé and Dimmeler, 2020). A recent review has classified vascular-associated lncRNAs based on their mechanism of action (Ono et al., 2021). Here we introduce some recent studies to spotlight the diverse regulation of endothelial function by lncRNAs:

The lncRNA *PUNISHER* or *AGAP2-AS1* is enriched in small extracellular vesicles (sEV) released by endothelial cells in the plasma of coronary artery disease (CAD) patients. *PUNISHER* interacts with *Heterogeneous Nuclear Ribonucleoprotein K* (*hnRNPK*), an RNA binding protein, and subsequently regulates the levels of VEGFA and endothelial cell proliferation in sEV recipient endothelial cells (Hosen et al., 2021). Another recent report shows lncRNA *NORAD* has a detrimental effect in CAD models by facilitating endothelial cell injury. *NORAD* is a nuclear lncRNA known to have multiple binding partners earlier, but in the said study was found to bind to HDAC6, through the RNA binding protein FUS. The *NORAD*-FUS-HDAC6 complex leads to H3K9 deacetylation at *VEGF* promoter and suppresses its transcription. The effects of *Norad* on endothelial cell injury were also demonstrated in atherosclerotic mice (Kai et al., 2021). In an oxidized LDL (oxLDL)-induced aortic endothelial cell model of atherosclerosis, the knockdown of lncRNA *AK087124* inhibited apoptosis and inflammation. *AK087124* acts as a sponge for *miR-224-5p*, which targets PTEN, a pro-apoptotic factor in the atherosclerotic model of aortic endothelial cells (Zhai et al., 2021).

LncRNA *VEAL2* was shown to interact with the kinase Protein kinase C beta 2 (PRKCB2) and prevent hyper-activation of the kinase by the small molecule diacylglycerol (DAG). This interplay regulates the turnover of junctional proteins VE-cadherin and beta-catenin, altering the permeability and angiogenic properties of human umbilical vein endothelial cells (HUVECs). *VEAL2* was found to be upregulated in the blood of diabetic retinopathy patients, and overexpression of the lncRNA in hyperglycemia model of HUVECs could attenuate PRKCB2-mediated hyper-permeability. A zebrafish knockout model for the ortholog *veal2* caused cranial hemorrhage, which could be rescued by the PRKCB2 inhibitor Enzastaurin (Sehgal et al., 2021). Aging related lncRNA *AERRIE* is important to maintain endothelial function and angiogenesis *in vitro*. Silencing of *AERRIE* led to DNA damage response mediated by YBX1. The study showed further that depletion of *AERRIE* induced DNA damage, and the damage response was activated by YBX1 as a consequence. Rescue with *AERRIE* could improve DNA repair in a doxorubicin mediated DNA damage model of endothelial spheroids (Pham et al., 2020). Endothelial-cell enriched lncRNA *LINC00961* encodes a micropeptide Small regulatory polypeptide of amino acid response (SPAAR). Knockdown of *LINC00961* in HUVECs prevents cell proliferation and angiogenesis. The lncRNA alone prevents angiogenesis while SPAAR induces vessel network formation and increases permeability, indicating that both the lncRNA and micropeptide have distinct functional roles, with independent protein partners (Spencer et al., 2020).

THE EVOLVING ROLES OF LNCRNA IN BBB FUNCTION

A plethora of noncoding RNAs are known to govern the BBB function and dysfunction, including small, long and circular non coding RNAs (Wang S.-W. et al., 2018), (Liu et al., 2021), (Gan et al., 2020). LncRNAs in BBB dysfunction have been extensively reported, with a view of identification of potential biomarkers. Here we attempt to collate the mechanistic role of lncRNA expressed in cerebrovascular endothelial cells and how they elicit regulation in known pathways.

CVE LncRNAs Involved in Tight Junction Dynamics

Tight junctions (TJs) allow CVECs to form a size and charge selective barrier and many membrane complexes are assembled around TJs, helping in cell signaling and polarization of the endothelial cells. Three types of transmembrane proteins comprise TJs: Claudins, MARVEL-motif containing proteins such as occludin and immunoglobulin super family membrane proteins such as junctional adhesion molecule (JAM) isoforms. BBB usually contains claudin-3, 5 or 12, claudin-5 being the most abundant. Claudins interact with zona occludens (ZO) proteins via their C- terminals and their turnover is determined by phosphorylation marks. Zona occludens 1, 2 and 3 act as scaffold proteins and are instrumental in the formation of TJs, with ZO-1 and ZO-2 present in endothelial cells. Occludin interacts with the ZO proteins and cytoskeleton. Phosphorylation mediated marking of degradation of occludin regulates the permeability of the barrier. JAM B and C are known to be endothelial specific and loss of JAM-C causes cerebral hemorrhage. JAMs also mediate the transcellular migration of leukocytes in endothelial cells. The downregulation of TJ proteins have been reported in BBB disruption (Bauer et al., 2014). Several

lncRNAs have been reported to regulate TJ protein levels and can affect barrier permeability and trans-endothelial electrical resistance (TEER).

Lnc00462717 regulates levels of occludin in a blood-tumor barrier (BTB) model of brain microvascular endothelial cells (BMECs) by binding to polypyrimidine tract binding protein (PTBP1) and downregulating *miR-186-5p*. *miR-186-5p* directly binds to occludin 3′UTR and regulates its expression levels, thus altering the endothelial permeability (Zhang C. et al., 2020). LncRNA *HOTAIR* interacts with transcription factor upstream stimulatory factor 1 (USF1) and regulates levels of ZO-1, claudin-5 and occludin. *miR-148b-3p* binds to *HOTAIR* and USF1 transcripts and modulates the levels of the TJ proteins (Sa et al., 2017).

Linc00174 titers the expression levels of the FOS Like 2, AP-1 Transcription Factor (FOSL2), which can regulate expressions of ZO-1, occludin and claudin-5. MicroRNAs *miR-138-5p* and *miR-150-5p* bind to both *Linc00174* and FOSL2 transcripts and bring down their levels, increasing permeability in the BTB model. It was seen that FOSL2 also has a feedback loop with *Linc00174* and binds to its promoter (Guo et al., 2019). *NEAT1* is a miRNA sponge of *miR-181d-5p* which regulates levels of RY-Box Transcription Factor 5 (SOX5) by binding to its 3' UTR. SOX5 modulates levels of the tight junction proteins ZO-1, occludin and claudin-5 and thus *NEAT1* regulates BTB permeability (Guo et al., 2017).

LncRNA *MIAT* acts as a competing endogenous RNA (ceRNA) for miRNA *miR-140-3p*. ZO-1-associated kinase (ZAK) which phosphorylates NFκB-p65 is a target of *miR-140-3p*. NFκB-p65 is a transcription suppressor for the TJ proteins ZO-1, occludin, and claudin-5 (He et al., 2020). *LINC00094* sponges *miR-224-5p/miR-497-5p* in an Alzheimer's disease (AD) microenvironment BBB model. *miR-224-5p/miR-497-5p* regulates Endophilin-1 post-translationally, which is a known factor in modulation of BBB permeability by altering expressions of ZO-1, claudin-5 and occludin through EGFR-ERK1/2 pathway (Zhu et al., 2019). LncRNA *XIST* is downregulated on ischemic insult while it is upregulated in the post-ischemic phase in patients and in a mouse model of cerebral ischemic stroke. In oxygen-glucose deprivation and restoration (OGD/R) model of ischemia in the murine brain endothelial cells, bEnd.3 cells, similar results were observed. Downregulation of *XIST* caused reduced expressions of integrin-α5, Kruppel-like transcription factor 4 (KLF4), claudin-5 and ZO-1 in ischemic conditions/OGD/R. Additionally, knockdown of *Xist* in bEnd.3 cells enhanced NF-κB activation and stalled angiogenesis. *Xist* acts as a sponge for *miR-92a*, which in turn regulates levels of integrin-α5 and KLF4. KLF4 overexpression can reduce levels of E-selectin, VCAM-1, ICAM-1 and p- NFκB (Wang C. et al., 2021).

CVE lncRNAs Involved in VEGFA Signaling and Hypoxic Response

Signaling of the angiogenic Vascular Endothelial Growth Factor-A (VEGFA) is highly polarized in the cerebral vasculature, through the differential expression of the receptors VEGFR1 and VEGFR2 on the luminal and abluminal cell surfaces, respectively. In many scenarios, VEGFA signaling can induce disruption of the BBB by junctional turnovers, also altering TEER. Of note, VEGFA ligand binding on the abluminal side leads to leakage, while VEGFA binding on the luminal side has a protective role. VEGFR1 on the luminal side induces Akt pathway, and has a cytoprotective role by preventing apoptosis (Gerber et al., 1998), while VEGFR2 on the abluminal side activates p38 and increases barrier permeability (Dragoni and Turowski, 2018). VEGFA downregulates expressions of occludin and claudin-5, leading to the disassembly of TJs and increase in paracellular permeability of BBB (Argaw et al., 2009). VEGFA is also known to cause BBB breakdown through the eNOS pathway during CNS inflammation in a multiple sclerosis (MS) mouse model (Argaw et al., 2012). During hypoxic conditions, VEGF is shown to activate MMP-9, disrupting BBB (Valable et al., 2005). Pericytes and astrocytes release VEGF during hypoxic conditions of ischemia and stroke, leading to BBB disruption (Bai et al., 2015), (Li Y.-N. et al., 2014). Many lncRNAs are known to regulate VEGFA expression and thus affect angiogenesis and blood brain barrier permeability.

One of the earliest lncRNAs reported to have a function in cerebrovascular angiogenesis was *Meg3*, through the classical reverse genetic technique of generating a knockout. Whole gene knockout of lncRNA *Meg3* led to elevated levels of VEGF in brains of mice. Other VEGF pathway genes also showed differential expression in the brains of *Meg3*-null mice, which led to increase in microvessel density (Gordon et al., 2010). The overexpression of lncRNA *Anril* was shown to increase VEGF expression in the brains from Diabetes mellitus rat model with cerebral infarction. Apart from VEGF, the levels of NF-κB and p-IκB/IκB were also elevated in the brain tissues of this model, along with VEGFR1 and VEGFR2. This elevation in expression levels of genes of the VEGF pathway was then reflected as an increase in the microvessel density in the brain (Zhang B. et al., 2017).

LncRNA *MIAT* knockdown reduced levels of VEGF in HUVECs and reduced microvessel number and showed reduction in TJs in brains of an AD mouse model (Jiang et al., 2016). *MIAT* is a ceRNA sponge for *miR-150-5p*, which targets VEGF ((Yan B. et al., 2015). LncRNA *Meg8* is expressed in high levels in OGD challenged BMECs and its silencing inhibits proliferation and angiogenesis. Silencing of *Meg8* could be correlated with lower levels of VEGFA. *Meg8* acts as a sponge for *miR-130a-5p* which targets VEGFA. Injection of *Meg8* could diminish cerebral infarct volumes in middle cerebral artery occlusion (MCAO) model in rats (Sui et al., 2021).

LncRNA *Snhg1* which expresses abundantly in cerebral microvessels of ischemic mouse model and OGD induced BMECs is a ceRNA for *miR-18a*. Hypoxia-inducible factor 1-alpha (HIF1A) mediated activation of VEGF pathway is regulated by the *Snhg1/miR-18a* axis by the binding of *miR-18a* to suppress HIF1A expression and to determine the apoptosis and homeostasis of BMECs (Zhang L. et al., 2018). *Snhg1* is also known to act as a sponge for *miR-199a* in the OGD/R BMEC model, which can downregulate both HIF1A and VEGF and inhibit capillary formation by BMECs (Wang Z. et al., 2018). A

third miRNA, *miR-338* is also sponged by lncRNA *Snhg1* in OGD-treated BMECs. *miR-338* binds to 3' UTR of HIF1A and induces apoptotic pathways in the BMEC model of ischemia (Yang and Zi, 2019).

CVE LncRNAs in PI3K-Akt Pathway

Depending on the factor that activates PI3K/Akt pathway, and the downstream effector of Akt, the outcomes of endothelial permeability can vary through assembly or disassembly of TJs (Cong and Kong, 2020). For instance, in ischemic hypoxia in rat neonates, the hematopoietic factor Granulocyte stimulating factor (G-CSF) activates PI3K/Akt/GSK-3β axis to increase BBB barrier properties and is anti-inflammatory. The authors of the study note that the protective effects of PI3K/Akt pathway were shown previously, which is mediated by reducing levels of VCAM-1, ICAM-1 and beta catenin, while upregulating claudin 3 and 5 (Li et al., 2015). On the contrary, in a rat model of brain injury and a parallel *in vitro* hypoxic model, PI3K/Akt/GSK-3β axis activation led to apoptosis of brain endothelial cells (Chen et al., 2017). Certain lncRNAs elicit the PI3K/Akt pathway to exert their regulatory action on CVECs.

LncRNA *MALAT1*, a ceRNA for *miR-126* in the OGD model of ischemia in human (HBMECs), has a positive effect on angiogenesis and cell viability via regulating PI3K-Akt pathway activation. *MALAT1* leads to endothelial cell apoptosis and inhibition of PI3K-Akt pathway in OGD HBMECs by sponging *miR-126* (Zhang L. et al., 2020). LncRNA *FAL1* has a protective effect against oxidative stress in OGD/R challenged HBVMECs. *FAL1* overexpression inhibits expressions of interleukin-6 (IL-6), monocyte chemotactic protein-1 (MCP-1) and high mobility group box-1 (HMGB1). Further, *FAL1* overexpression restored lowered phosphorylation levels of p21 (RAC1) activated kinase 1 (PAK1) and Akt in the OGD/R cells, and increased expression of proliferating cell nuclear antigen (PCNA), a downstream target. Thus, *FAL1* overexpression reversed cell injury induced by OGD/R (Gao M. et al., 2020).

CVE lncRNAs in STAT3 Activation

Sphingosine-1-phosphate (S1P) pathway is activated in OGD/R and MCAO models of cerebral ischemia. Signal Transducer And Activator Of Transcription 3 (STAT3) gets activated downstream of S1P pathway and its inhibition protects BBB from OGD/R induced dysfunction (Nakagawa and Aruga, 2020). JAK/STAT3 pathway induction and microRNA mediated regulation of S1P receptor was also shown to cause BBB damage in rat model of septic encephalopathy (Chen S.-L. et al., 2020). Following are two examples of CVE lncRNAs with the potential to activate STAT3.

The abundant expression of lncRNA *Snhg3* in the BMVEC model of intracerebral hemorrhage (ICH) led to inhibition of proliferation and migration, apoptosis and loss of barrier properties. *Snhg3* overexpression increased levels of Tumor necrosis factor-like weak inducer of apoptosis (TWEAK) mRNA and protein and its receptor fibroblast growth factor-inducible 14 (Fn14). This then activated the STAT3 pathway by phosphorylation of STAT3 protein. STAT3 pathway activation led to the secretion of MMP-3 and MMP-9, increasing permeability. Combined inhibition of TWEAK, Fn14 and STAT3 could reverse effects of high expression of *Snhg3* in ICH BMVECs (Zhang J. et al., 2019). LncRNA *Malat1* knockdown reversed the upregulation of 15-lipoxygenase 1 (15-LOX1), pSTAT3 and VEGF in OGD/R BMECs. This suggested that *Malat1* induces angiogenesis through activation of STAT3 pathway in OGD/R BMECs (Wang C. et al., 2019).

CVE LncRNAs in Autophagy

The process of autophagy is a systematic house-keeping process to remove damaged organelles or misfolded proteins by lysosomal degradation and in case of irreparable damage, the self-destruction of cells containing those (Mathiassen et al., 2017). Occludin degradation and subsequent increase in permeability has been shown to be induced via autophagy in OGD/R treated bEnd.3 cells and MCAO rat models (Kim et al., 2020). Autophagy mediated degradation of ZO-1 is known in high glucose conditioned BMECs in the OGD/R model (Zhang S. et al., 2018). Alternatively, protective effect of autophagy in OGD/R BMVECs by redistribution of ZO-1 on the membrane has also been shown (Li H. et al., 2014). In short term hypoxia injury, autophagy protects cerebrovascular endothelial cells from increased permeability and loss of TEER. Effect of autophagy in endothelial damage during ischemic stroke has been reviewed earlier (Kim et al., 2018). A couple of lncRNAs are known to modulate CVEC function through the regulation of the autophagy pathway.

In the OGD/R model of BMECs, *Malat1* sponges *miR-26b* which in turn regulates Unc-51 Like Autophagy Activating Kinase 2 (ULK2). Knockdown of ULK2 prevents autophagy in OGD/R BMECs. Hence *Malat1* acts as a protective agent in OGD/R by activating autophagy (Li Z. et al., 2017). Additionally in OGD induced bEnd.3 cells, *Malat1* is shown to act as a sponge for *miR-200c-3p* which binds to Sirtuin 1 (SIRT1) mRNA. Knockdown of SIRT1 inhibited LCB3II and increased p62 expression and increased cell death in bEnd.3 OGD/R cells. By maintaining the levels of SIRT1, *Malat1* protects bEnd.3 cells from cell death by inducing autophagy (Wang S. et al., 2019). LncRNA *PVT1* negatively regulates *miR-186* in glioma endothelial cells. *PVT1* overexpression induces formation of autophagosomes in the BTB model. *miR-186* binds to 3' UTRs of Autophagy related 7 (Atg7) and Beclin1, preventing autophagy, while *PVT1* reverses this effect and facilitates endothelial cell autophagy in the BTB model (Ma et al., 2017a).

CVE LncRNAs in Apoptosis

Once the vessels migrate into the nascent neural tissue, and the formation of the neural tissue is complete, the associated endothelial cells become quiescent. Apoptosis plays a major role in homeostasis of quiescent BMECs by removal of the dysfunctional cells. Apoptotic signals also directly regulate angiogenesis, and are particularly important during adult neurogenesis coupled with angiogenesis (Pozhilenkova et al., 2017). In disease conditions like stroke, apoptosis of BMECs leads to neuronal injury via increased BBB permeability and leads to vascular edema. Apoptosis of CVECs can occur through both intrinsic and extrinsic pathways of apoptosis, owing to various

TABLE 1 | List of lncRNAs expressed in cerebrovascular endothelial cells and their functional roles.

LncRNA Name	Associated Pathway in Cerebrovas-cular endothelial Cells	Interacting Partner	Effect on BBB	Mechanism	Disease/Condition	Model	References
Lnc00462717	Tight junction turn over	PTBP1	+	Regulation of occludin levels	Glioma	Co-culture BTB model	Zhang et al. (2020a)
HOTAIR	Tight junction turn over	miR-148b-3p	+	Modulation of ZO-1, claudin-5 and occludin levels	Glioma	Co-culture BTB model	Sa et al. (2017)
XIST	Tight junction turn over	miR-137	+	Modulation of levels of ZO-2 and CXCR7	Glioma	Co-culture BTB model	Yu et al. (2017)
TUG1	Tight junction turn over	miR-144	+	Modulation of ZO-1, claudin-5 and occludin levels	Glioma	Co-culture BTB model	Cai et al. (2015)
MALAT1	Tight junction turn over	miR-140	+	Modulation of ZO-1, claudin-5 and occludin levels	Glioma	Co-culture BTB model	Ma et al. (2016)
Linc00174	Tight junction turn over	miR-138-5p and miR-150-5p	+	Modulation of ZO-1, claudin-5 and occludin levels	Glioma	Co-culture BTB model	Guo et al. (2019)
NEAT1	Tight junction turn over	miR-181daysay-5p	+	Modulation of ZO-1, claudin-5 and occludin levels	Glioma	Co-culture BTB model	Guo et al. (2017)
MEG3	Tight junction turn over	miR-330-5p	-	Modulation of ZO-1, claudin-5 and occludin levels	Glioma	Co-culture BTB model	Shen et al. (2018)
MIAT	Tight junction turn over	miR-140-3p	-	Modulation of ZO-1, claudin-5 and occludin levels	Glioma	Co-culture BTB model	He et al. (2020)
LINC00094	Tight junction turn over	miR-224-5p/ miR-497-5p	-	Modulation of ZO-1 and occludin levels	Alzheimer's disease microenvironment	Co-culture BTB model	Zhu et al. (2019)
LncRSPH9-4	Tight junction turn over	miR-17-5p	-	Modulation of ZO-1 and occludin levels	Meningitic *E. coli* Infection	Human BMECs	Xu et al. (2021a)
Xist	Tight junction turn over	miR-92a	+	Modulation of ZO-1 and claudin-5 occludin levels	Cerebral ischemia	OGD/R murine brain endothelial cells and bEnd.3 cells	Wang et al. (2021a)
Miat	VEGF pathway, Tight junction turn over	None	+	Modulation of ZO-1 and occludin levels	Alzheimer's disease	Mice	Jiang et al. (2016)
Meg3	VEGF pathway	None	*	Modulation of VEGF levels in brain	MEG3 knockout	MEG3 null mice	Gordon et al. (2010)
Anril	VEGF pathway	None	*	Modulation of VEGF levels in brain	Diabetes mellitus with cerebral infarction	Rats	Zhang et al. (2017a)
MALAT1	VEGF pathway	miR-205-5p	*	Modulation of VEGF levels	Cerebral ischemia	OGD/R HBMEC	Gao et al. (2020a)
Snhg12	VEGF pathway	miR-150	*	Modulation of VEGF levels	Cerebral ischemia	OGD bEnd.3 cells, MCAO mice	Zhao et al. (2018)
SNHG15	VEGF pathway	miR-153	*	Modulation of VEGFA levels	Glioma	Glioma-conditioned hCMECs	Ma et al. (2017b)
Meg8	VEGF pathway	miR-130a-5p	*	Modulation of VEGFA levels	Cerebral ischemia	OGD bEnd.3 cells, MCAO rats	Sui et al. (2021)
Snhg1	Hypoxia pathway	miR-18a	*	Modulation of HIF1A levels	Cerebral ischemia	OGD mice BMECs, MCAO mice	Zhang et al. (2018a)
Snhg1	VEGF-Hypoxia pathway	miR-199a	*	Modulation of VEGF and HIF1A levels	Cerebral ischemia	OGD/R model of mice BMECs	Wang et al. (2018b)
Snhg1	Hypoxia pathway	miR-338	*	Modulation of HIF1A levels	Cerebral ischemia	OGD mice BMECs	Yang and Zi, (2019)
MALAT1	PI3K-Akt pathway	miR-126	*	Activation of PI3K and Akt	Cerebral ischemia	OGD human BMECs	Zhang et al. (2020b)
FAL1	PAK1-Akt pathway	None	*	Activation of PAK1 and Akt	Cerebral ischemia	OGD/R human BMECs	Gao et al. (2020c)
Snhg3	STAT3 pathway	None	+	Activation of STAT3	Intracerebral hemorrhage	ICH rats, OGD plus themin rat BMVECs	Zhang et al. (2019a)
Malat1	STAT3 pathway	none	*	Activation of 15-LOX1/ STAT3 pathway	Cerebral ischemia	OGD/R mice BMECs, MCAO mice	Wang et al. (2019a)
Malat1	Autophagy	miR-26b	*	Modulation of ULK2 levels	Cerebral ischemia	OGD/R mice BMECs	Li et al. (2017b)

(Continued on following page)

TABLE 1 | (*Continued*) List of lncRNAs expressed in cerebrovascular endothelial cells and their functional roles.

LncRNA Name	Associated Pathway in Cerebrovas-cular endothelial Cells	Interacting Partner	Effect on BBB	Mechanism	Disease/Condition	Model	References
Malat1	Autophagy	miR-200c-3p	*	Modulation of SIRT1 levels	Cerebral ischemia	OGD bEnd.3 cells	Wang et al. (2019b)
PVT1	Autophagy	miR-186	*	Modulation of Atg7 and Beclin1 levels	Glioma	Glioma-conditioned human CMECs	Ma et al. (2017a)
Malat1	Apoptosis	Bim and E-selectin	*	Modulation of Bim levels and pro-inflammatory cytokines	Cerebral ischemia	OGD mice BMECs, MCAO mice	Zhang et al. (2017b)
Malat1	VEGF pathway, Apoptosis	miR-143	*	Modulation of VEGF, ET-1, vWF, and MMP-9 levels	Intracranial aneurysm	IA rats, Vascular endothelial cells from IA rat tissue	Gao et al. (2020b)
MALAT1	Apoptosis	none	*	Modulation of MDM2, p53 and BAX levels	Cerebral ischemia	OGD/R human BMECs, MCAO mice	Zhang et al. (2018c)
SNHG16	Apoptosis	miR-15a-5p	*	Modulation of Bcl-2 levels	Cerebral ischemia	OGD/R human BMECs	Teng et al. (2020)
LncOGD-1006	Apoptosis	miR-184-5p	*	Modulation of CAAP1 levels	Cerebral ischemia	OGD bEnd.3 cells	Chen et al. (2020a)
Neat1	Apoptosis, VEGF pathway	miR-377	*	Modulation of SIRT1, VEGFA, and BCL-XL levels	Cerebral ischemia	OGD mice BMECs	Zhou et al. (2019)
Meg3	Apoptosis, VEGF pathway, Hypoxia pathway	p53	*	Modulation of p53 and NOX4 levels	Cerebral ischemia	OGD/R rat BMVECs	Zhan et al. (2017)
FENDRR	Apoptosis, VEGF pathway	miR-126	*	Modulation of VEGFA levels	Hypertensive intracerebral hemorrhage	Human BMECs treated with thrombin	Dong et al. (2018)
Gas5	Apoptosis	miR-34b-3p	*	Modulation of EPHA4 levels	Cerebral ischemia	OGD/R bEnd.3 cells	Shen et al. (2021)
Snhg1	Apoptosis	miR-298	*	Modulation of SIK1 levels	Cerebral ischemia	OGD/R bEnd.3 cells	Zhou et al. (2021)
Rmst	Apoptosis	miR-150	*	Modulation of MMP2 and MMP9 levels, change in caspase-3 activity	Cerebral ischemia	OGD bEnd.3 cells	Qiao et al. (2020)
RMST	Apoptosis	miR-204-5p	*	Modulation of VCAM1 levels	Cerebral ischemia	OGD human BMECs and bEnd.3 cells	Yin et al. (2021)
MIAT	Apoptosis	MYC	*	Modulation of ENC1 levels	Intracranial aneurysm	Vascular endothelial cells HBEC-5i, IA rats	Li et al. (2020)
Meg3	Ferroptosis	None	*	Modulation of p53 and GPX4 levels	Cerebral ischemia with hyperglycemia	OGD rat BMVECs with hyperglycemia	Chen et al. (2021b)
H19	Ferroptosis	miR-106b-5p	*	Modulation of ACSL4 levels	Intracerebral hemorrhage	ICH human BMVECs	Chen et al. (2021a)
LINC00346	Angiogenesis	ANKHD1	*	Modulation of EGFL7 and ROBO4 levels	Glioma	Glioma-conditioned human CMECs	Yang et al. (2020)
Dancr	Angiogenesis	miR-33a-5p	*	Modulation of XBP1 levels	Cerebral ischemia	OGD rat BMECs	Zhang et al. (2020c)
Miat	Angiogenesis	miR-204-5p	-	Modulation of HMGB1 levels	Cerebral ischemia	OGD rat CMECs, MCAO rats	Deng et al. (2020)

*BTB, blood tumor barrier; BMECs/BMVECs, brain microvascular endothelial cells; OGD/R, oxygen-glucose deprivation and restoration; OGD, oxygen-glucose deprivation; MCAO, middle cerebral artery occlusion; CMECs, cerebral microvascular endothelial cells; IA, intracranial aneurysm. Effect on BBB is represented as + (maintains the BBB), –(induces BBB permeability), * (no information in the study).*

stimuli such as infections, amyloid proteins, inflammation, ischemia, and so on. Studies have shown that elevated levels of p53 and Bax, lower levels of Bcl-2, and activation of caspase-3 bring about apoptosis in BMECs. The ERK, JNK and p38-MAPK pathways are implicated in apoptosis induction in BMECs (Rizzo and Leaver, 2010). Several lncRNAs are known to perform anti-apoptotic or pro-apoptotic roles to determine outcomes of cerebrovascular endothelial cells in disease conditions.

Malat1 is upregulated in the OGD model of BMECs and cerebral microvessels of ischemic mice after reperfusion. Knockout of *Malat1* amplifies ischemic injury in mice model. *Malat1* has an anti-apoptotic role in cerebral microvasculature by regulating the expression of the pro-apoptotic factor Bim. *Malat1* knockdown also increased levels of inflammatory cytokines like E-Selectin, MCP1 and IL-6. Further, *Malat1* was shown to directly interact with both Bim and E-selectin proteins (Zhang

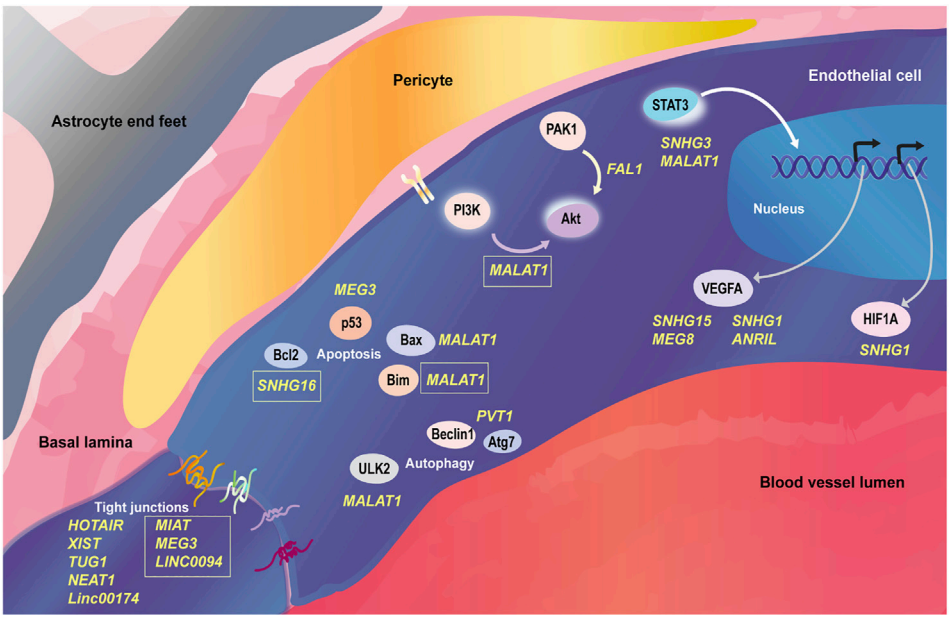

FIGURE 1 | LncRNAs regulating cellular processes in cerebrovascular endothelial cells. The cerebrovascular endothelial cells of the neurovascular unit are governed by signaling pathways that respond to distinct cues from luminal and abluminal sides. Several lncRNAs have been discovered to regulate the protein coding gene players in cerebrovascular endothelial cells at post-transcriptional and post-translational levels within the signaling involving tight junction turn over, VEGF pathway, PI3K-Akt pathway, STAT3 activation, autophagy and apoptosis. LncRNAs are mentioned in yellow font in the figure; the ones in boxes negatively regulate their cognate pathways, while the rest have a positive role in their cognate pathways. All the references to the mentioned lncRNAs can be found in **Table 1**.

X. et al., 2017). LncRNA *SNHG16* acts as a sponge for *miR-15a-5p* in OGD/R HBMECs. *miR-15a-5p* binds to and targets Bcl-2 post transcriptionally. Hence *SNHG16* protects HBMECs from OGD/R apoptosis (Teng et al., 2020). *LncOGD-1006* is upregulated in OGD BMECs and is protective against apoptosis. Overexpression of *LncOGD-1006* increased expression of Bcl-2 and BCL2 associated agonist of cell death (BAD) proteins and downregulated cleaved caspase-3. *miR-184-5p* is sponged by *LncOGD-1006* which regulates expression of Caspase Activity And Apoptosis Inhibitor 1 (CAAP1). CAAP1 knockdown reversed effects of *LncOGD-1006* overexpression (Chen JY. et al., 2020). LncRNA *Neat1* was upregulated in OGD BMECs and is a sponge for *miR-377*. Knockdown of *Neat1* leads to apoptosis in OGD BMECs, increasing BAX expression and downregulating VEGF, SIRT1 and Bcl-xl. *miR-377* was shown to bind to 3′UTRs of VEGF, SIRT1 and Bcl-xl and hence *Neat1* acts anti-apoptotic by sponging *miR-377* (Zhou et al., 2019).

LncRNA *Meg3* knockdown protects rat BVMECs (RBMVECs) from OGD/R mediated apoptosis. *Meg3* directly interacts with p53 and modulates its downstream targets. The study showed that the p53 target NADPH Oxidase 4 (NOX4) expression is elevated in OGD/R RBVMECs and is regulated by *Meg3* via p53. NOX4 regulates levels of HIF1A and VEGF. Thus knockdown of *Meg3* acts anti-apoptotic and angiogenic in OGD/R RBVMECs (Zhan et al., 2017). LncRNA *FENDRR* induces apoptosis in hypertensive intracerebral hemorrhage (HIHC) model of HBMECs treated with thrombin. *FENDRR* acts as a sponge for *miR-126*, which can regulate VEGF levels. The study showed that VEGF downregulation could prevent apoptosis of thrombin-treated HBMECs (Dong et al., 2018).

LncRNA *Rmst* is abundantly expressed in OGD bEnd.3 cells and has a positive correlation with apoptosis while acting as a sponge for *miR-150* (Qiao et al., 2020). Another study showed *RMST* as a ceRNA for *miR-204-5p* in OGD models for promoting apoptosis. *miR-204-5p* was shown to target VCAM1 which induced permeability and apoptosis in CVECs (Yin et al., 2021). Overexpression of lncRNA *MIAT* induced apoptosis in intracranial aneurysm (IA) model of HBEC-5i cells by upregulating cleaved caspase-3, cleaved PARP1 and Bax, while downregulating Bcl-2. *MIAT* directly interacts with the MYC proto-oncogene and modulates the expression of the downstream gene Ectodermal-Neural Cortex 1 (ENC1). Silencing *Miat* and ENC1 independently could prevent apoptosis of cerebrovascular endothelial cells and protect against IA in a rat model (Li et al., 2020).

Apart from the afore-mentioned pathways, several other cerebrovascular endothelial lncRNAs have been reported to date. The entire list of lncRNAs reviewed here can be found in **Table 1**. We attempt to capture a snapshot of the lncRNA mediated regulation of CVEC pathways in **Figure 1**.

STUDYING LNCRNAS IN DIFFERENT BBB MODELS

This review has compiled studies on lncRNAs in BBB cell culture models and animal models, mostly in various disease contexts.

However, it is widely accepted that the cell culture models of cerebrovascular endothelial cell monolayers or even co-cultures with glial/mural cells are inadequate in representing the blood brain barrier, which is closely regulated by other components of the neurovascular unit. The 2-D and 3-D *in vitro* models of BBB and *in vivo* animal models such as rodent and zebrafish models of BBB and their applicability were summarized recently (Bhalerao et al., 2020), (Jackson et al., 2019). Of particular interest in *in vitro* models is human induced pluripotent stem cell (iPSC)-derived brain microvascular endothelial cell model and multi-cellular organoids which incorporate various cell types of the NVU (Logan et al., 2019), (Lacalle-Aurioles et al., 2020). An intriguing humanized model which involves introduction of human BBB organoids into murine systems has also been explored (Waldau, 2019).

Near identical brain microvasculature across species corresponding to the number of neurons gives a hint that non-human models are good candidates to study BBB function (Wong et al., 2013). Rodent models such as mice and rats are popular models owing to BBB architecture similar to humans, and their evaluation can be done post-mortem or through live techniques such as PET, MRI or two-photon imaging (Jackson et al., 2019). Tissue clearing techniques such as CLARITY and PACT have additionally opened up the possibility of visualizing fixed but intact rodent brain (Tomer et al., 2014), (Woo et al., 2016). The well-annotated invertebrate model *Drosophila*, has been used to understand BBB dysfunction and drug delivery despite the limited similarity with mammalian system of having only a glial barrier (Cuddapah et al., 2019), (Schirmeier and Klämbt, 2015). In zebrafish, the blood brain barrier genesis occurs between 3 and 10 days post fertilization and this gives an opportunity to study the progressive selective permeability over time using dye diffusion based assays. Adult zebrafish BBB is known to be highly similar to human BBB (Li Y. et al., 2017). Zebrafish has also been shown to be an amicable model to understand the role of pericytes and smooth muscle cells in BBB development and maintenance (Bahrami and Childs, 2018). Similarly, the utility of transparent *Xenopus* tadpoles to study blood brain permeability has also been proven (De Jesús Andino et al., 2016). Despite the availability of a range of animal models to study BBB, it is known that the human BBB has unique biochemical signatures which cannot be recapitulated completely (Wong et al., 2013). Hence a combined approach of using animal models and human BBB organoids may be a rational approach to study BBB phenomena.

FUTURE PERSPECTIVES FOR STUDYING LNCRNA IN BBB FUNCTION

The advancements in deep sequencing, with the latest introduction of single-cell sequencing have led to the recording of thousands of novel lncRNAs. The rapidly developing bioinformatic frameworks have also allowed the prediction of biological interactions and functions of lncRNAs. These ambiguous molecules however are experimentally validated in disproportionately lower numbers and this acts as a bottle-neck in understanding their physiologically relevant roles. The past decades have seen the use of genome-editing tools such as TALENs and CRISPR-Cas9 systems to probe functions of novel genes. CRISPR based systems for RNA interference, activation and gene editing have already been tested for high throughput functional screening of lncRNA in erstwhile contexts (Esposito et al., 2019). Further, innovative systems to circumvent effects of conventional CRISPR-Cas9 approaches, including epigenetic silencing and post-transcriptional editing can also help study lncRNA function (Awwad, 2019), (Nuñez et al., 2021). In recent times RNA-editing versions of Cas protein have also emerged, which could be used as a novel strategy (Xu et al., 2020).

A majority of lncRNA functional studies are carried out in cell lines which are amenable to relatively less cumbersome methods of screening. However, as discussed in the previous section, the complex neurovascular unit and the blood brain barrier property as its function is captured limitedly by cell culture based models. Three-dimensional hydrogel based organoids are being explored for modeling the NVU (Potjewyd et al., 2021). The 3D structure will allow emulating the mechanical and biochemical properties of the neurovascular milieu. A recent study successfully developed a vascularized brain organoid model in mice with necessary BBB properties (Cakir et al., 2019). Another recent study has shown the editing using CRISPR-Cas9 systems in BBB organoids to identify receptor mediated transcytosis in brain endothelial cells (Simonneau et al., 2021). Therefore in order to study functions of novel lncRNA, BBB organoids can be leveraged by creating gene edited models to understand the role of lncRNA in BBB establishment and maintenance. Further such organoid models can be used for drug screening to identify small molecules that can modulate BBB permeability and function (Bergmann et al., 2018).

In lieu of the poor sequence conservation of lncRNAs, identification of lncRNAs in animal models can illuminate hitherto unknown regulatory angles in well studied pathways. Identification of functionally conserved human lncRNA has been exemplified in the case of lncRNAs *jpx* (mouse) (Karner et al., 2020) and *veal2* (zebrafish) (Sehgal et al., 2021) even in the absence of sequence or structural conservation, albeit with a conserved interacting protein partner. This provides a framework to look beyond sequence-based conservation for identifying lncRNA candidates that regulate well-conserved pathways. Rodent models, which are the most popular models to study BBB physiology have been used to study endothelial and BBB-related lncRNA (Cleuren et al., 2019), (Orsenigo et al., 2020). The very recent cell-type atlas release by the BRAIN Initiative Cell Census Network (BRAIN Initiative Cell Census Network, 2021) that captures nuclear transcriptomic signatures, along with epigenetic state information from mouse motor cortex, adds another powerful dataset for understanding novel transcripts including lncRNA in mammalian brain (BRAIN Initiative Cell Census Network (BICCN), 2021). Zebrafish can be deployed for large functional screens, using anti-sense oligos like morpholinos and CRISPR-based systems (Gut et al., 2017),

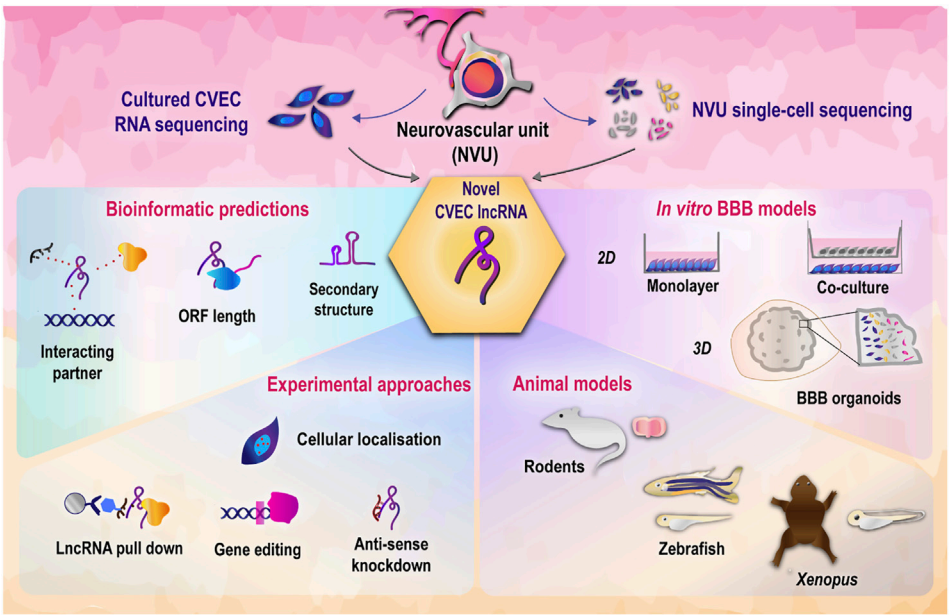

FIGURE 2 | Strategies to decipher functional roles of cerebrovascular endothelial lncRNAs. LncRNAs discovered from cerebrovascular endothelial cells through transcriptomic studies can be functionally validated using a combination of bioinformatics and experimental approaches (Jalali et al., 2015), (McDonel and Guttman, 2019). *In vitro* and *in vivo* model systems employed in tandem will allow in deciphering the physiological roles of lncRNA in cerebrovascular endothelial function (Jackson et al., 2019). CVEC, cerebrovascular endothelial cells; BBB, blood brain barrier.

(Ranjan et al., 2021). Endothelial lncRNA datasets from zebrafish have been reported by several groups (Sehgal et al., 2021), (Müller et al., 2016), while an entire compendium of zebrafish conserved lncRNA is available on the ZFLNC database (Hu et al., 2018). A transcriptome wide sgRNA-guide design may be attempted in zebrafish, coupled with *in vivo* imaging to track modulations in BBB integrity. The CRISPR toolkit has been proven to be efficient in *Xenopus* and *Drosophila* as well, and may well be exploited for understanding lncRNA function in BBB (Bhattacharya et al., 2015), (Port et al., 2020). The drug-based alterations in lncRNA levels in different model systems (Jiang et al., 2019) can further have potential applications in deriving drug-targets among lncRNA identified from BBB.

It can be seen from **Table 1** that currently redundant roles have been assigned to a handful of lncRNAs, leaving open the door for functionally validating novel and unannotated candidates. Of note, many of the referred studies have observed that the lncRNA function is exclusive to the respective disease model and does not hold true in the context of homeostasis. Hence, orthogonal validations are needed to strengthen the understanding of lncRNA-mediated regulation of CVEC function. A recent study invalidated several ncRNA studies, underscoring the need to thoroughly test predicted interactions and mechanisms of ncRNA (Mitschka and Mayr, 2021). Stringent and parallel functional validation approaches will allow in confidently placing the lncRNA-mediated regulatory mechanisms in the bigger picture of cerebrovascular endothelial function. We provide a glimpse of the different strategies and models that can be employed for studying lncRNA in cerebrovascular endothelial function in **Figure 2**.

THERAPEUTIC POTENTIAL OF CVEC LNCRNA

LncRNAs are expected to be effective biomarkers and drug targets, due to their low and spatio-temporally restricted expression patterns. This section discusses the expression patterns and levels of lncRNAs and how these correlate with function and ultimately the therapeutic applicability of lncRNA candidates. We further attempt to understand how lncRNAs can be potential therapeutic targets in the context of CVECs.

Expression Patterns of lncRNAs

From 24 human tissues and cell types, Cabili et al. showed that long intergenic RNA (lincRNA), a subset of lncRNA, have highly tissue-specific expression patterns, with the majority having low expression levels. In particular, the brain and testes expressed lncRNAs that are highly tissue-specific. The study reported 4,200 plus lincRNA, and concluded that 78% of lincRNA are tissue-specific, compared to 19% of protein coding genes, after normalizing for expression levels (Cabili et al., 2011). Based on transcriptomic data of 15 human cell lines, compared to protein coding genes, lncRNAs show greater unique expression in cell types (Djebali et al., 2012). The study showed that 10% lncRNA transcripts were found in all cell lines, compared to 29% found in only a single cell line. The corresponding numbers for protein coding transcripts were 53 and 7%. The lower and tissue restricted expression of lncRNAs was replicated during the ENCODE phase 2 project using 16 human tissue samples from RNA-seq data. About 11% of lncRNAs were found in all tissue types, with 65% being the

corresponding proportion for protein coding transcripts. The study cautions that the tissue-restricted expression may be a false read out owing to the lower expression levels of lncRNAs. The study also used custom microarrays for five human cell lines, 17 tissues and nine region-wise brain samples-all representing a total of 31 cell types-which confirmed lower expression of lncRNAs with respect to protein coding transcripts (Derrien et al., 2012). Further an expression analysis of lncRNAs from The Cancer Genome Atlas (TCGA) including 5,037 samples corresponding to 13 cancer types showed cancer type-specific differential expression of lncRNA (Yan X. et al., 2015). In summary, the understanding of the tissue-specific nature of lncRNAs could be dictated by technical limitations of the detection techniques, however even considering these limitations, the relative abundance is relevant to biological function of lncRNA (Grammatikakis and Lal, 2021). In particular, studies have shown on comparing bulk RNA-sequencing and single cell sequencing that certain lncRNAs are relatively abundantly expressed in a very specific subset of cells, but predictably may show a lower signal in the data from a pool of cells from a tissue (Yan et al., 2013), (Liu et al., 2016).

LncRNA Expression and Apparent Functional Correlation

Depending on the type of function and mode of action, the cellular abundance of a lncRNA may vary. For instance, nuclear localized lncRNAs may be of low abundance if they are *cis*-acting or *trans*-acting with specific targets, while *trans*-acting lncRNAs with genome-wide roles or cytoplasmically localized lncRNA may have relatively higher copy numbers in a cell (~1,000 or more copies per cell) (Grammatikakis and Lal, 2021). Chromatin associated lncRNAs are known to be expressed as low as ~0.3 copies per cell. In comparison protein coding transcript copy numbers lie in the ranges of approximately 10–800 thousands. Thus, the copy number of lncRNA is directly dependent on the kind of function a lncRNA performs (Wu et al., 2021). The quantification of abundance of lncRNA at cellular and tissue-level contexts will be paramount in both determining the function and therapeutic targeting (Kopp and Mendell, 2018). Given that lncRNAs are an amorphous class of molecules with a wide range of functions and varying spatio-temporal abundance, the therapeutic targeting of individual lncRNAs may need customized approaches.

Strategies for Therapeutic Applications of lncRNAs

Clinical trials around the therapeutic potential of lncRNAs have picked up in the past few years. Therapeutic targeting of small non coding RNA such as miRNA has been demonstrated earlier (Winkle et al., 2021), and is being explored in many disease contexts including cerebrovascular conditions such as stroke (Xu Y. et al., 2021). A search for the key word "long non coding RNA" retrieved 69 results on https://www.clinicaltrials.gov/(As on 27 February 2022). Most of these studies have assessed/intend to assess the potential of lncRNAs as biomarkers in various conditions. Several lncRNAs have already shown potential as biomarkers in cancers (Gutschner et al., 2018). Of note, lncRNAs such as *ANRIL* and *MIAT* were primarily identified as differentially expressed transcripts in cardiovascular diseases (Holdt et al., 2010), (Ishii et al., 2006). Hence the applicability of lncRNAs as biomarkers has been well documented and with the increasingly explored transcriptomic data, more and more lncRNA biomarkers may come to the fore.

For considering the potential of lncRNAs as druggable targets, various strategies have been adopted. It has been shown in a phase I clinical trial that lncRNAs of mitochondrial origin can be targeted successfully. FDA approved the use of single-stranded phosphorothioate anti-sense oligo (ASO) against anti-sense mitochondrial lncRNA for treatment of solid tumors in advanced metastatic cancer and the ASO was shown to be well tolerated (Chen Y. et al., 2021). A cell-type specific targeting of cancer cells with higher levels of EGFR was shown to be possible by coupling an anti-EGFR aptamer with anti-*HOTAIR* siRNA in a cell line model of triple-negative breast cancer (Wang YL. et al., 2021). The strategies to explore the therapeutic potential of lncRNAs have been reviewed earlier (Renganathan and Felley-Bosco, 2017), (Winkle et al., 2021), (Schwarzmueller et al., 2020). RNA interference, ASO based targeting and CRISPR based targeting are slated to be most effective for modulating levels of lncRNAs (Arun et al., 2018). ASOs have been shown to be effective in mouse disease models against lncRNAs *anti-GATA6* (Zhu et al., 2018) and *MALAT1* (Arun et al., 2016). Small molecule targeting has also been shown to have some application against lncRNAs such as *GAS5* and *MALAT1* (Winkle et al., 2021). This mode of targeting of lncRNAs can be facilitated by understanding the secondary and tertiary structures of lncRNAs and sterically blocking functional motifs (Arun et al., 2018). Combining different approaches of lncRNA targeting have also been attempted (Chen Y. et al., 2021). On the other end, RNA therapeutics where non coding RNAs are used to target another transcript has also been explored. RNA therapeutics can be delivered to the system of interest using carriers and adjuvants, or using viral vectors (Poller et al., 2018). In addition, exosome based and nano-particle based delivery approaches of RNA therapeutics including delivery of lncRNA in cardiovascular disease are also being tested. Exosome-based delivery can in particular help in cell-specific targeting of RNA therapeutics by incorporating molecules on the exosome membranes that can detect and bind to cell-type specific markers (Lu and Thum, 2019). Intravenous delivery of ncRNAs involved in cardiac functioning has been shown to successfully have a therapeutic effect in a mouse model of cardiovascular disease (Quattrocelli et al., 2013).

Targeting CVEC lncRNAs for Therapeutic Applications

The therapeutic applicability of lncRNAs in cerebrovascular diseases has been revealed from transcriptomic analyses. In conditions such as ischemic stroke, differential expression of several lncRNAs could be seen (Deng et al., 2018), and the levels of *H19*, *ANRIL*, *NEAT1* and other candidate lncRNAs

seem to correlate with the severity of stroke (Gan et al., 2020). These lncRNAs showed marked upregulation in ischemic stroke and are considered as biomarkers. Possibilities of targeting lncRNAs across cardiovascular diseases have been reviewed earlier (Gomes et al., 2017). Small molecule based targeting in cardiac arrhythmias have been shown to lead to lowering of the levels of lncRNAs exacerbating the disease (Zhang Y. et al., 2019).

As described before, BBB dysfunction can lead to neurological conditions and vice versa. It is therefore important to look at therapeutic interventions that can manage potential breach of the blood brain barrier. Some of the approaches to prevent excessive permeability of the BBB is by targeting the VEGF pathway players and the downstream matrix metalloproteases. Further the use of antago-miRs and small molecules that can elevate levels of junctional proteins of the endothelial cells have also been proven effective (Archie et al., 2021). Engineered Wnt ligands have also been shown to be effective in preventing deterioration of BBB properties in conditions such as glioblastoma and stroke (Martin et al., 2022). This review has described CVEC lncRNAs across different pathways including VEGF and Wnt-related pathways. Targeting of lncRNAs that are potential modulators of such pathways which have already been shown to have drug targets to modulate BBB function provides a framework to explore novel therapeutic mechanisms in BBB dysfunction.

Increasing number of transcriptomic studies, especially at single cell resolution, are identifying unique EC differentiating patterns providing opportunities to specifically target ECs subtypes such as CVECs. Single cell sequencing of cells from brain vasculature of mice could identify unique transcriptomic signatures in endothelial cells, microglia, oligodendrocytes and fibroblasts (Lin et al., 2021). Cerebrovascular endothelial cells themselves have been shown to be heterogeneous in a cerebral cavernous malformation mouse model (Orsenigo et al., 2020). Five distinct EC types were identified from single cell sequencing of glioblastoma (GBM) tumor vessels from human patients. The EC phenotypes showed varying breakdown extents of the blood brain barrier property. Additionally, the ECs isolated from GBM tissue showed different gene signatures than ECs isolated from peripheral brain tissue (Xie et al., 2021). While these studies did not explicitly shed light on the non-coding RNA players, it will be interesting to see future studies on the lncRNA markers across CVEC sub-populations. This can pave the way for cell type-specific targeting of CVEC lncRNA using approaches such as exosome-based delivery of ASOs or RNA therapeutics (Lu and Thum, 2019).

Current Challenges in Therapeutic Targeting of lncRNAs

While low copy numbers of lncRNAs that can be targeted can be an advantage because they may need lower dosages of targeting agents, there are several challenges to be tackled. One of the primary considerations in lncRNA targeting is the appropriate classification of lncRNAs based on abundance, processing, function and structure for designing therapeutics to each class for better effectiveness (Poller et al., 2018). As mentioned earlier, signals from bulk RNA sequencing may give a misleading read out on the cell types from expressing lncRNA. With the widespread use of single cell sequencing, this limitation can be overcome in the near future. Alternatively, visualization techniques such as fluorescence *in situ* hybridization can hint at a cellular subset-specific origin of a lncRNA. Further, a known functional relevance of lncRNA and proven conserved function if discovered in a model organism can be factors imperative for selection of a lncRNA therapeutic target (Gutschner et al., 2018). An additional consideration for RNA therapeutics based targeting of lncRNAs is the immunogenicity and toxicity of such agents, apart from issues of stability, specificity and delivery (Winkle et al., 2021), (Chen Y. et al., 2021). Hence, testing the therapeutic potential of lncRNAs may need several layers of examination and clear understanding of the molecular mechanism across a variety of models and conditions.

CONCLUSION

The homeostasis of cerebrovascular endothelial cells forming the blood brain barrier is under the complex regulation of multiple pathways, which are primarily dictated by surrounding cells and various local environmental cues. This allows CVECs to exhibit dynamicity and plasticity in response to cues in the neurovascular milieu. Many lncRNAs have been shown to perform a regulatory role in cellular processes of CVECs, suggesting the presence of an under-studied mechanistic layer added by lncRNAs in CVEC function. Adopting appropriate models mimicking the cerebrovascular endothelial cells, blood-brain barrier and neurovascular unit can be an important strategy to gain a true picture of the underlying mechanisms of lncRNAs. The past decades have seen lncRNA studies that have mostly focused on a small subset of highly and ubiquitously expressed lncRNAs that are technically easier to probe with the available strategies to understand lncRNA function. This review is a compendium of several such studies that have cataloged the functional mechanism of lncRNAs in CVECs that could have redundant or overlapping roles in other cell types as well. With an increase in the annotation of the thousands of novel lncRNAs identified from bulk RNA sequencing and cell-type specific sequencing, in the future CVEC specific lncRNA signature may emerge that can be specifically targeted in the context of maintaining and modulating the blood brain barrier.

AUTHOR CONTRIBUTIONS

SM performed the literature review. The manuscript was written by SM and SS. The figures were illustrated by SM.

FUNDING

This work was supported by Council of Scientific and Industrial Research (CSIR), India (Grant number MLP 2001). SM acknowledges CSIR, India, for Senior Research Fellowship.

REFERENCES

Aird, W. C. (2007a). Phenotypic Heterogeneity of the Endothelium. *Circ. Res.* 100, 158–173. doi:10.1161/01.RES.0000255691.76142.4a

Aird, W. C. (2007b). Phenotypic Heterogeneity of the Endothelium. *Circ. Res.* 100, 174–190. doi:10.1161/01.RES.0000255690.03436.ae

Archie, S. R., Al Shoyaib, A., and Cucullo, L. (2021). Blood-Brain Barrier Dysfunction in CNS Disorders and Putative Therapeutic Targets: An Overview. *Pharmaceutics* 13, 1779. doi:10.3390/pharmaceutics13111779

Argaw, A. T., Asp, L., Zhang, J., Navrazhina, K., Pham, T., Mariani, J. N., et al. (2012). Astrocyte-derived VEGF-A Drives Blood-Brain Barrier Disruption in CNS Inflammatory Disease. *J. Clin. Invest.* 122, 2454–2468. doi:10.1172/JCI60842

Argaw, A. T., Gurfein, B. T., Zhang, Y., Zameer, A., and John, G. R. (2009). VEGF-mediated Disruption of Endothelial CLN-5 Promotes Blood-Brain Barrier Breakdown. *Proc. Natl. Acad. Sci. U.S.A.* 106, 1977–1982. doi:10.1073/pnas.0808698106

Arun, G., Diermeier, S., Akerman, M., Chang, K.-C., Wilkinson, J. E., Hearn, S., et al. (2016). Differentiation of Mammary Tumors and Reduction in Metastasis upon Malat1 lncRNA Loss. *Genes Dev.* 30, 34–51. doi:10.1101/gad.270959.115

Arun, G., Diermeier, S. D., and Spector, D. L. (2018). Therapeutic Targeting of Long Non-coding RNAs in Cancer. *Trends Mol. Med.* 24, 257–277. doi:10.1016/j.molmed.2018.01.001

Awwad, D. A. (2019). Beyond Classic Editing: Innovative CRISPR Approaches for Functional Studies of Long Non-coding RNA. *Biol. Methods Protoc.* 4, bpz017. doi:10.1093/biomethods/bpz017

Bahrami, N., and Childs, S. J. (2018). Pericyte Biology in Zebrafish. *Adv. Exp. Med. Biol.* 1109, 33–51. doi:10.1007/978-3-030-02601-1_4

Bai, Y., Zhu, X., Chao, J., Zhang, Y., Qian, C., Li, P., et al. (2015). Pericytes Contribute to the Disruption of the Cerebral Endothelial Barrier via Increasing VEGF Expression: Implications for Stroke. *PLoS One* 10, e0124362. doi:10.1371/journal.pone.0124362

Bauer, H.-C., Krizbai, I. N. A., Bauer, H., and Traweger, A. (2014). â€œYou Shall Not Passâ€â€"tight Junctions of the Blood Brain Barrier. *Front. Neurosci.* 8, 392. doi:10.3389/fnins.2014.00392

Bergmann, S., Lawler, S. E., Qu, Y., Fadzen, C. M., Wolfe, J. M., Regan, M. S., et al. (2018). Blood-brain-barrier Organoids for Investigating the Permeability of CNS Therapeutics. *Nat. Protoc.* 13, 2827–2843. doi:10.1038/s41596-018-0066-x

Bhalerao, A., Sivandzade, F., Archie, S. R., Chowdhury, E. A., Noorani, B., and Cucullo, L. (2020). *In Vitro* modeling of the Neurovascular Unit: Advances in the Field. *Fluids Barriers CNS* 17, 22. doi:10.1186/s12987-020-00183-7

Bhattacharya, D., Marfo, C. A., Li, D., Lane, M., and Khokha, M. K. (2015). CRISPR/Cas9: An Inexpensive, Efficient Loss of Function Tool to Screen Human Disease Genes in Xenopus. *Developmental Biol.* 408, 196–204. doi:10.1016/j.ydbio.2015.11.003

BRAIN Initiative Cell Census Network (BICCN) (2021). A Multimodal Cell Census and Atlas of the Mammalian Primary Motor Cortex. *Nature* 598, 86–102. doi:10.1038/s41586-021-03950-0

Cabili, M. N., Trapnell, C., Goff, L., Koziol, M., Tazon-Vega, B., Regev, A., et al. (2011). Integrative Annotation of Human Large Intergenic Noncoding RNAs Reveals Global Properties and Specific Subclasses. *Genes Dev.* 25, 1915–1927. doi:10.1101/gad.17446611

Cai, H., Xue, Y., Wang, P., Wang, Z., Li, Z., Hu, Y., et al. (2015). The Long Noncoding RNA TUG1 Regulates Blood-Tumor Barrier Permeability by Targeting miR-144. *Oncotarget* 6, 19759–19779. doi:10.18632/oncotarget.4331

Cakir, B., Xiang, Y., Tanaka, Y., Kural, M. H., Parent, M., Kang, Y.-J., et al. (2019). Engineering of Human Brain Organoids with a Functional Vascular-like System. *Nat. Methods* 16, 1169–1175. doi:10.1038/s41592-019-0586-5

Chen, B., Wang, H., Lv, C., Mao, C., and Cui, Y. (2021a). Long Non-coding RNA H19 Protects against Intracerebral Hemorrhage Injuries via Regulating microRNA-106b-5p/acyl-CoA Synthetase Long Chain Family Member 4 axis. *Bioengineered* 12, 4004–4015. doi:10.1080/21655979.2021.1951070

Chen, C., Huang, Y., Xia, P., Zhang, F., Li, L., Wang, E., et al. (2021b). Long Noncoding RNA Meg3 Mediates Ferroptosis Induced by Oxygen and Glucose Deprivation Combined with Hyperglycemia in Rat Brain Microvascular Endothelial Cells, through Modulating the p53/GPX4 axis. *Eur. J. Histochem.* 65, 3224. doi:10.4081/ejh.2021.3224

Chen, J. Y., Chen, H., Li, T., Yang, L., Ye, X. M., Gao, W. Y., et al. (2020a). LncRNA LncOGD-1006 Alleviates OGD-Induced Ischemic Brain Injury Regulating Apoptosis through miR-184-5p/CAAP1 axis. *Eur. Rev. Med. Pharmacol. Sci.* 24, 12324–12333. doi:10.26355/eurrev_202012_24025

Chen, K., Wang, N., Diao, Y., Dong, W., Sun, Y., Liu, L., et al. (2017). Hydrogen-Rich Saline Attenuates Brain Injury Induced by Cardiopulmonary Bypass and Inhibits Microvascular Endothelial Cell Apoptosis via the PI3K/Akt/GSK3β Signaling Pathway in Rats. *Cell Physiol Biochem* 43, 1634–1647. doi:10.1159/000484024

Chen, S.-L., Cai, G.-X., Ding, H.-G., Liu, X.-Q., Wang, Z.-H., Jing, Y.-W., et al. (2020b). JAK/STAT Signaling Pathway-Mediated microRNA-181b Promoted Blood-Brain Barrier Impairment by Targeting Sphingosine-1-Phosphate Receptor 1 in Septic Rats. *Ann. Transl. Med.* 8, 1458. doi:10.21037/atm-20-7024

Chen, Y., Li, Z., Chen, X., and Zhang, S. (2021c). Long Non-coding RNAs: From Disease Code to Drug Role. *Acta Pharmaceutica Sinica B* 11, 340–354. doi:10.1016/j.apsb.2020.10.001

Choi, S.-W., Kim, H.-W., and Nam, J.-W. (2019). The Small Peptide World in Long Noncoding RNAs. *Brief. Bioinform* 20, 1853–1864. doi:10.1093/bib/bby055

Claesson-Welsh, L., Dejana, E., and McDonald, D. M. (2021). Permeability of the Endothelial Barrier: Identifying and Reconciling Controversies. *Trends Mol. Med.* 27, 314–331. doi:10.1016/j.molmed.2020.11.006

Cleuren, A. C. A., van der Ent, M. A., Jiang, H., Hunker, K. L., Yee, A., Siemieniak, D. R., et al. (2019). The *In Vivo* Endothelial Cell Translatome Is Highly Heterogeneous across Vascular Beds. *Proc. Natl. Acad. Sci. U.S.A.* 116, 23618–23624. doi:10.1073/pnas.1912409116

Cong, X., and Kong, W. (2020). Endothelial Tight Junctions and Their Regulatory Signaling Pathways in Vascular Homeostasis and Disease. *Cell Signal.* 66, 109485. doi:10.1016/j.cellsig.2019.109485

Cuddapah, V. A., Zhang, S. L., and Sehgal, A. (2019). Regulation of the Blood-Brain Barrier by Circadian Rhythms and Sleep. *Trends Neurosciences* 42, 500–510. doi:10.1016/j.tins.2019.05.001

Daneman, R., and Prat, A. (2015). The Blood-Brain Barrier. *Cold Spring Harb. Perspect. Biol.* 7, a020412. doi:10.1101/cshperspect.a020412

Daneman, R., Zhou, L., Kebede, A. A., and Barres, B. A. (2010). Pericytes Are Required for Blood-Brain Barrier Integrity during Embryogenesis. *Nature* 468, 562–566. doi:10.1038/nature09513

De Jesús Andino, F., Jones, L., Maggirwar, S. B., and Robert, J. (2016). Frog Virus 3 Dissemination in the Brain of Tadpoles, but Not in Adult Xenopus, Involves Blood Brain Barrier Dysfunction. *Sci. Rep.* 6, 22508. doi:10.1038/srep22508

Deng, Q.-W., Li, S., Wang, H., Sun, H.-L., Zuo, L., Gu, Z.-T., et al. (2018). Differential Long Noncoding RNA Expressions in Peripheral Blood Mononuclear Cells for Detection of Acute Ischemic Stroke. *Clin. Sci. Lond. Engl.* 132, 1597–1614. doi:10.1042/CS20180411

Deng, W., Fan, C., Shen, R., Wu, Y., Du, R., and Teng, J. (2020). Long Noncoding MIAT Acting as a ceRNA to Sponge microRNA-204-5p to Participate in Cerebral Microvascular Endothelial Cell Injury after Cerebral Ischemia through Regulating HMGB1. *J. Cel. Physiol.* 235, 4571–4586. doi:10.1002/jcp.29334

Derrien, T., Johnson, R., Bussotti, G., Tanzer, A., Djebali, S., Tilgner, H., et al. (2012). The GENCODE V7 Catalog of Human Long Noncoding RNAs: Analysis of Their Gene Structure, Evolution, and Expression. *Genome Res.* 22, 1775–1789. doi:10.1101/gr.132159.111

Djebali, S., Davis, C. A., Merkel, A., Dobin, A., Lassmann, T., Mortazavi, A., et al. (2012). Landscape of Transcription in Human Cells. *Nature* 489, 101–108. doi:10.1038/nature11233

Dong, B., Zhou, B., Sun, Z., Huang, S., Han, L., Nie, H., et al. (2018). LncRNA-FENDRR Mediates VEGFA to Promote the Apoptosis of Brain Microvascular Endothelial Cells via Regulating miR-126 in Mice with Hypertensive Intracerebral Hemorrhage. *Microcirculation* 25, e12499. doi:10.1111/micc.12499

Dragoni, S., and Turowski, P. (2018). Polarised VEGFA Signalling at Vascular Blood-Neural Barriers. *Ijms* 19, 1378. doi:10.3390/ijms19051378

Esposito, R., Bosch, N., Lanzós, A., Polidori, T., Pulido-Quetglas, C., and Johnson, R. (2019). Hacking the Cancer Genome: Profiling Therapeutically Actionable Long Non-coding RNAs Using CRISPR-Cas9 Screening. *Cancer Cell* 35, 545–557. doi:10.1016/j.ccell.2019.01.019

Fang, S., Zhang, L., Guo, J., Niu, Y., Wu, Y., Li, H., et al. (2018). NONCODEV5: a Comprehensive Annotation Database for Long Non-coding RNAs. *Nucleic Acids Res.* 46, D308–D314. doi:10.1093/nar/gkx1107

Gan, L., Liao, S., Xing, Y., and Deng, S. (2020). The Regulatory Functions of lncRNAs on Angiogenesis Following Ischemic Stroke. *Front. Mol. Neurosci.* 13, 613976. doi:10.3389/fnmol.2020.613976

Gao, C., Zhang, C.-C., Yang, H.-X., and Hao, Y.-N. (2020a). MALAT1 Protected the Angiogenesis Function of Human Brain Microvascular Endothelial Cells (HBMECs) under Oxygen Glucose Deprivation/re-Oxygenation (OGD/R) Challenge by Interacting with miR-205-5p/VEGFA Pathway. *Neuroscience* 435, 135–145. doi:10.1016/j.neuroscience.2020.03.027

Gao, G., Zhang, Y., Yu, J., Chen, Y., Gu, D., Niu, C., et al. (2020b). Long Non-coding RNA MALAT1/microRNA-143/VEGFA Signal Axis Modulates Vascular Endothelial Injury-Induced Intracranial Aneurysm. *Nanoscale Res. Lett.* 15, 139. doi:10.1186/s11671-020-03357-2

Gao, M., Fu, J., and Wang, Y. (2020c). The lncRNA FAL1 Protects against Hypoxia-Reoxygenation- Induced Brain Endothelial Damages through Regulating PAK1. *J. Bioenerg. Biomembr.* 52, 17–25. doi:10.1007/s10863-019-09819-2

Gerber, H.-P., McMurtrey, A., Kowalski, J., Yan, M., Keyt, B. A., Dixit, V., et al. (1998). Vascular Endothelial Growth Factor Regulates Endothelial Cell Survival through the Phosphatidylinositol 3′-Kinase/Akt Signal Transduction Pathway. *J. Biol. Chem.* 273, 30336–30343. doi:10.1074/jbc.273.46.30336

Gomes, C. P. C., Spencer, H., Ford, K. L., Michel, L. Y. M., Baker, A. H., Emanueli, C., et al. (2017). The Function and Therapeutic Potential of Long Non-coding RNAs in Cardiovascular Development and Disease. *Mol. Ther. - Nucleic Acids* 8, 494–507. doi:10.1016/j.omtn.2017.07.014

Gordon, F. E., Nutt, C. L., Cheunsuchon, P., Nakayama, Y., Provencher, K. A., Rice, K. A., et al. (2010). Increased Expression of Angiogenic Genes in the Brains of Mouse Meg3-Null Embryos. *Endocrinology* 151, 2443–2452. doi:10.1210/en.2009-1151

Grammatikakis, I., and Lal, A. (2021). Significance of lncRNA Abundance to Function. *Mamm. Genome* 1, 1. doi:10.1007/s00335-021-09901-4

Guo, J., Cai, H., Zheng, J., Liu, X., Liu, Y., Ma, J., et al. (2017). Long Non-coding RNA NEAT1 Regulates Permeability of the Blood-Tumor Barrier via miR-181d-5p-Mediated Expression Changes in ZO-1, Occludin, and Claudin-5. *Biochim. Biophys. Acta (Bba) - Mol. Basis Dis.* 1863, 2240–2254. doi:10.1016/j.bbadis.2017.02.005

Guo, J., Shen, S., Liu, X., Ruan, X., Zheng, J., Liu, Y., et al. (2019). Role of linc00174/miR-138-5p (miR-150-5p)/FOSL2 Feedback Loop on Regulating the Blood-Tumor Barrier Permeability. *Mol. Ther. - Nucleic Acids* 18, 1072–1090. doi:10.1016/j.omtn.2019.10.031

Gut, P., Reischauer, S., Stainier, D. Y. R., and Arnaout, R. (2017). Little Fish, Big Data: Zebrafish as a Model for Cardiovascular and Metabolic Disease. *Physiol. Rev.* 97, 889–938. doi:10.1152/physrev.00038.2016

Gutschner, T., Richtig, G., Haemmerle, M., and Pichler, M. (2018). From Biomarkers to Therapeutic Targets-The Promises and Perils of Long Non-coding RNAs in Cancer. *Cancer Metastasis Rev.* 37, 83–105. doi:10.1007/s10555-017-9718-5

Hartford, C. C. R., and Lal, A. (2020). When Long Noncoding Becomes Protein Coding. *Mol. Cel. Biol.* 40, e00528–19. doi:10.1128/MCB.00528-19

He, J., Xue, Y., Wang, Q., Zhou, X., Liu, L., Zhang, T., et al. (2020). Long Non-coding RNA MIAT Regulates Blood Tumor Barrier Permeability by Functioning as a Competing Endogenous RNA. *Cell Death Dis* 11, 936. doi:10.1038/s41419-020-03134-0

Holdt, L. M., Beutner, F., Scholz, M., Gielen, S., Gäbel, G., Bergert, H., et al. (2010). ANRIL Expression Is Associated with Atherosclerosis Risk at Chromosome 9p21. *Atvb* 30, 620–627. doi:10.1161/ATVBAHA.109.196832

Hosen, M. R., Li, Q., Liu, Y., Zietzer, A., Maus, K., Goody, P., et al. (2021). CAD Increases the Long Noncoding RNA PUNISHER in Small Extracellular Vesicles and Regulates Endothelial Cell Function via Vesicular Shuttling. *Mol. Ther. - Nucleic Acids* 25, 388–405. doi:10.1016/j.omtn.2021.05.023

Hu, X., Chen, W., Li, J., Huang, S., Xu, X., Zhang, X., et al. (2018). ZFLNC: a Comprehensive and Well-Annotated Database for Zebrafish lncRNA. *Database J. Biol. Databases Curation* 2018, bay114. doi:10.1093/database/bay114

Huang, S.-F., Peng, X.-F., Jiang, L., Hu, C. Y., and Ye, W.-C. (2021). LncRNAs as Therapeutic Targets and Potential Biomarkers for Lipid-Related Diseases. *Front. Pharmacol.* 12, 729745. doi:10.3389/fphar.2021.729745

Ishii, N., Ozaki, K., Sato, H., Mizuno, H., Susumu Saito, S., Takahashi, A., et al. (2006). Identification of a Novel Non-coding RNA, MIAT, that Confers Risk of Myocardial Infarction. *J. Hum. Genet.* 51, 1087–1099. doi:10.1007/s10038-006-0070-9

Jackson, S., Meeks, C., Vézina, A., Robey, R. W., Tanner, K., and Gottesman, M. M. (2019). Model Systems for Studying the Blood-Brain Barrier: Applications and Challenges. *Biomaterials* 214, 119217. doi:10.1016/j.biomaterials.2019.05.028

Jaé, N., and Dimmeler, S. (2020). Noncoding RNAs in Vascular Diseases. *Circ. Res.* 126, 1127–1145. doi:10.1161/CIRCRESAHA.119.315938

Jalali, S., Kapoor, S., Sivadas, A., Bhartiya, D., and Scaria, V. (2015). Computational Approaches towards Understanding Human Long Non-coding RNA Biology. *Bioinformatics* 31, 2241–2251. doi:10.1093/bioinformatics/btv148

Jiang, Q., Shan, K., Qun-Wang, X., Zhou, R.-M., Yang, H., Liu, C., et al. (2016). Long Non-coding RNA-MIAT Promotes Neurovascular Remodeling in the Eye and Brain. *Oncotarget* 7, 49688–49698. doi:10.18632/oncotarget.10434

Jiang, W., Qu, Y., Yang, Q., Ma, X., Meng, Q., Xu, J., et al. (2019). D-lnc: a Comprehensive Database and Analytical Platform to Dissect the Modification of Drugs on lncRNA Expression. *RNA Biol.* 16, 1586–1591. doi:10.1080/15476286.2019.1649584

Kai, H., Wu, Q., Yin, R., Tang, X., Shi, H., Wang, T., et al. (2021). LncRNA NORAD Promotes Vascular Endothelial Cell Injury and Atherosclerosis through Suppressing VEGF Gene Transcription via Enhancing H3K9 Deacetylation by Recruiting HDAC6. *Front. Cel Dev. Biol.* 9, 701628. doi:10.3389/fcell.2021.701628

Karner, H., Webb, C.-H., Carmona, S., Liu, Y., Lin, B., Erhard, M., et al. (2020). Functional Conservation of LncRNA JPX Despite Sequence and Structural Divergence. *J. Mol. Biol.* 432, 283–300. doi:10.1016/j.jmb.2019.09.002

Kealy, J., Greene, C., and Campbell, M. (2020). Blood-brain Barrier Regulation in Psychiatric Disorders. *Neurosci. Lett.* 726, 133664. doi:10.1016/j.neulet.2018.06.033

Khan, S., Taverna, F., Rohlenova, K., Treps, L., Geldhof, V., de Rooij, L., et al. (2019). EndoDB: a Database of Endothelial Cell Transcriptomics Data. *Nucleic Acids Res.* 47, D736–D744. doi:10.1093/nar/gky997

Kim, K.-A., Kim, D., Kim, J.-H., Shin, Y.-J., Kim, E.-S., Akram, M., et al. (2020). Autophagy-mediated Occludin Degradation Contributes to Blood-Brain Barrier Disruption during Ischemia in bEnd.3 Brain Endothelial Cells and Rat Ischemic Stroke Models. *Fluids Barriers CNS* 17, 21. doi:10.1186/s12987-020-00182-8

Kim, K.-A., Shin, D., Kim, J.-H., Shin, Y.-J., Rajanikant, G. K., Majid, A., et al. (2018). Role of Autophagy in Endothelial Damage and Blood-Brain Barrier Disruption in Ischemic Stroke. *Stroke* 49, 1571–1579. doi:10.1161/STROKEAHA.117.017287

Kiss, T., Nyúl-Tóth, Á., Balasubramanian, P., Tarantini, S., Ahire, C., DelFavero, J., et al. (2020). Single-cell RNA Sequencing Identifies Senescent Cerebromicrovascular Endothelial Cells in the Aged Mouse Brain. *GeroScience* 42, 429–444. doi:10.1007/s11357-020-00177-1

Kok, F. O., and Baker, A. H. (2019). The Function of Long Non-coding RNAs in Vascular Biology and Disease. *Vasc. Pharmacol.* 114, 23–30. doi:10.1016/j.vph.2018.06.004

Kopp, F., and Mendell, J. T. (2018). Functional Classification and Experimental Dissection of Long Noncoding RNAs. *Cell* 172, 393–407. doi:10.1016/j.cell.2018.01.011

Lacalle-Aurioles, M., Cassel de Camps, C., Zorca, C. E., Beitel, L. K., and Durcan, T. M. (2020). Applying hiPSCs and Biomaterials towards an Understanding and Treatment of Traumatic Brain Injury. *Front. Cel. Neurosci.* 14, 594304. doi:10.3389/fncel.2020.594304

Li, H., Gao, A., Feng, D., Wang, Y., Zhang, L., Cui, Y., et al. (2014a). Evaluation of the Protective Potential of Brain Microvascular Endothelial Cell Autophagy on Blood-Brain Barrier Integrity during Experimental Cerebral Ischemia-Reperfusion Injury. *Transl. Stroke Res.* 5, 618–626. doi:10.1007/s12975-014-0354-x

Li, L., McBride, D. W., Doycheva, D., Dixon, B. J., Krafft, P. R., Zhang, J. H., et al. (2015). G-CSF Attenuates Neuroinflammation and Stabilizes the Blood-Brain Barrier via the PI3K/Akt/GSK-3β Signaling Pathway Following Neonatal Hypoxia-Ischemia in Rats. *Exp. Neurol.* 272, 135–144. doi:10.1016/j.expneurol.2014.12.020

Li, X., Zhao, H., Liu, J., and Tong, J. (2020). Long Non-coding RNA MIAT Knockdown Prevents the Formation of Intracranial Aneurysm by Downregulating ENC1 via MYC. *Front. Physiol.* 11, 572605. doi:10.3389/fphys.2020.572605

Li, Y.-N., Pan, R., Qin, X.-J., Yang, W.-L., Qi, Z., Liu, W., et al. (2014b). Ischemic Neurons Activate Astrocytes to Disrupt Endothelial Barrier via Increasing VEGF Expression. *J. Neurochem.* 129, 120–129. doi:10.1111/jnc.12611

Li, Y., Chen, T., Miao, X., Yi, X., Wang, X., Zhao, H., et al. (2017a). Zebrafish: A Promising *In Vivo* Model for Assessing the Delivery of Natural Products, Fluorescence Dyes and Drugs across the Blood-Brain Barrier. *Pharmacol. Res.* 125, 246–257. doi:10.1016/j.phrs.2017.08.017

Li, Z., Li, J., and Tang, N. (2017b). Long Noncoding RNA Malat1 Is a Potent Autophagy Inducer Protecting Brain Microvascular Endothelial Cells against Oxygen-Glucose Deprivation/reoxygenation-Induced Injury by Sponging miR-26b and Upregulating ULK2 Expression. *Neuroscience* 354, 1–10. doi:10.1016/j.neuroscience.2017.04.017

Lin, W.-W., Xu, L.-T., Chen, Y.-S., Go, K., Sun, C., and Zhu, Y.-J. (2021). Single-Cell Transcriptomics-Based Study of Transcriptional Regulatory Features in the Mouse Brain Vasculature. *Biomed. Res. Int.* 2021, 1–15. doi:10.1155/2021/7643209

Liu, S. J., Nowakowski, T. J., Pollen, A. A., Lui, J. H., Horlbeck, M. A., Attenello, F. J., et al. (2016). Single-cell Analysis of Long Non-coding RNAs in the Developing Human Neocortex. *Genome Biol.* 17, 67. doi:10.1186/s13059-016-0932-1

Liu, X., Shen, L., Han, B., and Yao, H. (2021). Involvement of Noncoding RNA in Blood-Brain Barrier Integrity in central Nervous System Disease. *Non-coding RNA Res.* 6, 130–138. doi:10.1016/j.ncrna.2021.06.003

Logan, S., Arzua, T., Canfield, S. G., Seminary, E. R., Sison, S. L., Ebert, A. D., et al. (2019). Studying Human Neurological Disorders Using Induced Pluripotent Stem Cells: From 2D Monolayer to 3D Organoid and Blood Brain Barrier Models. *Compr. Physiol.* 9, 565–611. doi:10.1002/cphy.c180025

Lu, D., and Thum, T. (2019). RNA-based Diagnostic and Therapeutic Strategies for Cardiovascular Disease. *Nat. Rev. Cardiol.* 16, 661–674. doi:10.1038/s41569-019-0218-x

Ma, J., Wang, P., Yao, Y., Liu, Y., Li, Z., Liu, X., et al. (2016). Knockdown of Long Non-coding RNA MALAT1 Increases the Blood-Tumor Barrier Permeability by Up-Regulating miR-140. *Biochim. Biophys. Acta (Bba) - Gene Regul. Mech.* 1859, 324–338. doi:10.1016/j.bbagrm.2015.11.008

Ma, Y., Wang, P., Xue, Y., Qu, C., Zheng, J., Liu, X., et al. (2017a). PVT1 Affects Growth of Glioma Microvascular Endothelial Cells by Negatively Regulating miR-186. *Tumour Biol.* 39, 101042831769432. doi:10.1177/1010428317694326

Ma, Y., Xue, Y., Liu, X., Qu, C., Cai, H., Wang, P., et al. (2017b). SNHG15 Affects the Growth of Glioma Microvascular Endothelial Cells by Negatively Regulating miR-153. *Oncol. Rep.* 38, 3265–3277. doi:10.3892/or.2017.5985

Mäe, M. A., He, L., Nordling, S., Vazquez-Liebanas, E., Nahar, K., Jung, B., et al. (2021). Single-Cell Analysis of Blood-Brain Barrier Response to Pericyte Loss. *Circ. Res.* 128, e46–e62. doi:10.1161/CIRCRESAHA.120.317473

Martin, M., Vermeiren, S., Bostaille, N., Eubelen, M., Spitzer, D., Vermeersch, M., et al. (2022). Engineered Wnt Ligands Enable Blood-Brain Barrier Repair in Neurological Disorders. *Science* 375, eabm4459. doi:10.1126/science.abm4459

Mathiassen, S. G., De Zio, D., and Cecconi, F. (2017). Autophagy and the Cell Cycle: A Complex Landscape. *Front. Oncol.* 7, 51. doi:10.3389/fonc.2017.00051

McDonel, P., and Guttman, M. (2019). Approaches for Understanding the Mechanisms of Long Noncoding RNA Regulation of Gene Expression. *Cold Spring Harb. Perspect. Biol.* 11, a032151. doi:10.1101/cshperspect.a032151

Mitschka, S., and Mayr, C. (2021). Endogenous P53 Expression in Human and Mouse Is Not Regulated by its 3′UTR. *eLife* 10, e65700. doi:10.7554/eLife.65700

Müller, R., Weirick, T., John, D., Militello, G., Chen, W., Dimmeler, S., et al. (2016). ANGIOGENES: Knowledge Database for Protein-Coding and Noncoding RNA Genes in Endothelial Cells. *Sci. Rep.* 6, 32475. doi:10.1038/srep32475

Nakagawa, S., and Aruga, J. (2020). Sphingosine 1-Phosphate Signaling Is Involved in Impaired Blood-Brain Barrier Function in Ischemia-Reperfusion Injury. *Mol. Neurobiol.* 57, 1594–1606. doi:10.1007/s12035-019-01844-x

Nuñez, J. K., Chen, J., Pommier, G. C., Cogan, J. Z., Replogle, J. M., Adriaens, C., et al. (2021). Genome-wide Programmable Transcriptional Memory by CRISPR-Based Epigenome Editing. *Cell* 184, 2503–2519. e17. doi:10.1016/j.cell.2021.03.025

Obermeier, B., Daneman, R., and Ransohoff, R. M. (2013). Development, Maintenance and Disruption of the Blood-Brain Barrier. *Nat. Med.* 19, 1584–1596. doi:10.1038/nm.3407

Ono, K., Horie, T., Baba, O., Kimura, M., Tsuji, S., Rodriguez, R. R., et al. (2021). Functional Non-coding RNAs in Vascular Diseases. *FEBS J.* 288, 6315–6330. doi:10.1111/febs.15678

Orsenigo, F., Conze, L. L., Jauhiainen, S., Corada, M., Lazzaroni, F., Malinverno, M., et al. (2020). Mapping Endothelial-Cell Diversity in Cerebral Cavernous Malformations at Single-Cell Resolution. *eLife* 9, e61413. doi:10.7554/eLife.61413

Pham, T. P., Bink, D. I., Stanicek, L., van Bergen, A., van Leeuwen, E., Tran, Y., et al. (2020). Long Non-coding RNA Aerrie Controls DNA Damage Repair via YBX1 to Maintain Endothelial Cell Function. *Front. Cel Dev. Biol.* 8, 619079. doi:10.3389/fcell.2020.619079

Poller, W., Dimmeler, S., Heymans, S., Zeller, T., Haas, J., Karakas, M., et al. (2018). Non-coding RNAs in Cardiovascular Diseases: Diagnostic and Therapeutic Perspectives. *Eur. Heart J.* 39, 2704–2716. doi:10.1093/eurheartj/ehx165

Port, F., Strein, C., Stricker, M., Rauscher, B., Heigwer, F., Zhou, J., et al. (2020). A Large-Scale Resource for Tissue-specific CRISPR Mutagenesis in Drosophila. *eLife* 9, e53865. doi:10.7554/eLife.53865

Potjewyd, G., Kellett, K. A. B., and Hooper, N. M. (2021). 3D Hydrogel Models of the Neurovascular Unit to Investigate Blood-Brain Barrier Dysfunction. *Neuronal Signal.* 5, NS20210027. doi:10.1042/NS20210027

Pozhilenkova, E. A., Lopatina, O. L., Komleva, Y. K., Salmin, V. V., and Salmina, A. B. (2017). Blood-brain Barrier-Supported Neurogenesis in Healthy and Diseased Brain. *Rev. Neurosci.* 28, 397–415. doi:10.1515/revneuro-2016-0071

Profaci, C. P., Munji, R. N., Pulido, R. S., and Daneman, R. (2020). The Blood-Brain Barrier in Health and Disease: Important Unanswered Questions. *J. Exp. Med.* 217, e20190062. doi:10.1084/jem.20190062

Qiao, P., Yan, H., and Wang, J. (2020). EGb761 Protects Brain Microvascular Endothelial Cells against Oxygen-Glucose Deprivation-Induced Injury through lncRNA Rmst/miR-150 Axis. *Neurochem. Res.* 45, 2398–2408. doi:10.1007/s11064-020-03099-8

Quattrocelli, M., Crippa, S., Montecchiani, C., Camps, J., Cornaglia, A. I., Boldrin, L., et al. (2013). Long-Term miR-669a Therapy Alleviates Chronic Dilated Cardiomyopathy in Dystrophic Mice. *Jaha* 2, e000284. doi:10.1161/JAHA.113.000284

Quinn, J. J., and Chang, H. Y. (2016). Unique Features of Long Non-coding RNA Biogenesis and Function. *Nat. Rev. Genet.* 17, 47–62. doi:10.1038/nrg.2015.10

Ranjan, G., Sehgal, P., Sharma, D., Scaria, V., and Sivasubbu, S. (2021). Functional Long Non-coding and Circular RNAs in Zebrafish. *Brief. Funct. Genomics* 1, elab014. doi:10.1093/bfgp/elab014

Renganathan, A., and Felley-Bosco, E. (2017). Long Noncoding RNAs in Cancer and Therapeutic Potential. *Adv. Exp. Med. Biol.* 1008, 199–222. doi:10.1007/978-981-10-5203-3_7

Rizzo, M. T., and Leaver, H. A. (2010). Brain Endothelial Cell Death: Modes, Signaling Pathways, and Relevance to Neural Development, Homeostasis, and Disease. *Mol. Neurobiol.* 42, 52–63. doi:10.1007/s12035-010-8132-6

Sa, L., Li, Y., Zhao, L., Liu, Y., Wang, P., Liu, L., et al. (2017). The Role of HOTAIR/miR-148b-3p/USF1 on Regulating the Permeability of BTB. *Front. Mol. Neurosci.* 10, 194. doi:10.3389/fnmol.2017.00194

Sabbagh, M. F., Heng, J. S., Luo, C., Castanon, R. G., Nery, J. R., Rattner, A., et al. (2018). Transcriptional and Epigenomic Landscapes of CNS and Non-CNS Vascular Endothelial Cells. *eLife* 7, e36187. doi:10.7554/eLife.36187

Schirmeier, S., and Klämbt, C. (2015). The Drosophila Blood-Brain Barrier as Interface between Neurons and Hemolymph. *Mech. Development* 138 (Pt 1), 50–55. doi:10.1016/j.mod.2015.06.002

Schwarzmueller, L., Bril, O., Vermeulen, L., and Léveillé, N. (2020). Emerging Role and Therapeutic Potential of lncRNAs in Colorectal Cancer. *Cancers* 12, 3843. doi:10.3390/cancers12123843

Sehgal, P., Mathew, S., Sivadas, A., Ray, A., Tanwar, J., Vishwakarma, S., et al. (2021). LncRNA VEAL2 Regulates PRKCB2 to Modulate Endothelial Permeability in Diabetic Retinopathy. *EMBO J.* 40, e107134. doi:10.15252/embj.2020107134

Shen, B., Wang, L., Xu, Y., Wang, H., and He, S. (2021). LncRNA GAS5 Silencing Attenuates Oxygen-Glucose Deprivation/Reperfusion-Induced Injury in Brain Microvascular Endothelial Cells via miR-34b-3p-dependent Regulation of EPHA4. *Ndt* 17, 1667–1678. doi:10.2147/NDT.S302314

Shen, S., Yu, H., Liu, X., Liu, Y., Zheng, J., Wang, P., et al. (2018). PIWIL1/piRNA-DQ593109 Regulates the Permeability of the Blood-Tumor Barrier via the

MEG3/miR-330-5p/RUNX3 Axis. *Mol. Ther. - Nucleic Acids* 10, 412–425. doi:10.1016/j.omtn.2017.12.020

Simonneau, C., Duschmalé, M., Gavrilov, A., Brandenberg, N., Hoehnel, S., Ceroni, C., et al. (2021). Investigating Receptor-Mediated Antibody Transcytosis Using Blood-Brain Barrier Organoid Arrays. *Fluids Barriers CNS* 18, 43. doi:10.1186/s12987-021-00276-x

Spencer, H. L., Sanders, R., Boulberdaa, M., Meloni, M., Cochrane, A., Spiroski, A.-M., et al. (2020). The LINC00961 Transcript and its Encoded Micropeptide, Small Regulatory Polypeptide of Amino Acid Response, Regulate Endothelial Cell Function. *Cardiovasc. Res.* 116, 1981–1994. doi:10.1093/cvr/cvaa008

Strange, K. (1992). Regulation of Solute and Water Balance and Cell Volume in the central Nervous System. *Jasn* 3, 12–27. doi:10.1681/ASN.V3112

Sui, S., Sun, L., Zhang, W., Li, J., Han, J., Zheng, J., et al. (2021). LncRNA MEG8 Attenuates Cerebral Ischemia after Ischemic Stroke through Targeting miR-130a-5p/VEGFA Signaling. *Cell. Mol. Neurobiol.* 41, 1311–1324. doi:10.1007/s10571-020-00904-4

Sweeney, M. D., Zhao, Z., Montagne, A., Nelson, A. R., and Zlokovic, B. V. (2019). Blood-Brain Barrier: From Physiology to Disease and Back. *Physiol. Rev.* 99, 21–78. doi:10.1152/physrev.00050.2017

Teng, H., Li, M., Qian, L., Yang, H., and Pang, M. (2020). Long Non-coding RNA SNHG16 I-nhibits the O-xygen-glucose D-eprivation and R-eoxygenation-induced A-poptosis in H-uman B-rain M-icrovascular E-ndothelial C-ells by R-egulating miR-15a-5p/bcl-2. *Mol. Med. Rep.* 22, 2685–2694. doi:10.3892/mmr.2020.11385

Tjakra, M., Wang, Y., Vania, V., Hou, Z., Durkan, C., Wang, N., et al. (2019). Overview of Crosstalk between Multiple Factor of Transcytosis in Blood Brain Barrier. *Front. Neurosci.* 13, 1436. doi:10.3389/fnins.2019.01436

Tomer, R., Ye, L., Hsueh, B., and Deisseroth, K. (2014). Advanced CLARITY for Rapid and High-Resolution Imaging of Intact Tissues. *Nat. Protoc.* 9, 1682–1697. doi:10.1038/nprot.2014.123

Valable, S., Montaner, J., Bellail, A., Berezowski, V., Brillault, J., Cecchelli, R., et al. (2005). VEGF-induced BBB Permeability Is Associated with an MMP-9 Activity Increase in Cerebral Ischemia: Both Effects Decreased by Ang-1. *J. Cereb. Blood Flow Metab.* 25, 1491–1504. doi:10.1038/sj.jcbfm.9600148

Waldau, B. (2019). Using Miniature Brain Implants in Rodents for Novel Drug Discovery. *Expert Opin. Drug Discov.* 14, 379–386. doi:10.1080/17460441.2019.1577816

Wang, C., Dong, J., Sun, J., Huang, S., Wu, F., Zhang, X., et al. (2021a). Silencing of lncRNA XIST Impairs Angiogenesis and Exacerbates Cerebral Vascular Injury after Ischemic Stroke. *Mol. Ther. - Nucleic Acids* 26, 148–160. doi:10.1016/j.omtn.2021.06.025

Wang, C., Qu, Y., Suo, R., and Zhu, Y. (2019a). Long Non-coding RNA MALAT1 Regulates Angiogenesis Following Oxygen-glucose Deprivation/reoxygenation. *J. Cel. Mol. Med.* 23, 2970–2983. doi:10.1111/jcmm.14204

Wang, S.-W., Liu, Z., and Shi, Z.-S. (2018a). Non-Coding RNA in Acute Ischemic Stroke: Mechanisms, Biomarkers and Therapeutic Targets. *Cel Transpl.* 27, 1763–1777. doi:10.1177/0963689718806818

Wang, S., Han, X., Mao, Z., Xin, Y., Maharjan, S., and Zhang, B. (2019b). MALAT1 lncRNA Induces Autophagy and Protects Brain Microvascular Endothelial Cells against Oxygen-Glucose Deprivation by Binding to miR-200c-3p and Upregulating SIRT1 Expression. *Neuroscience* 397, 116–126. doi:10.1016/j.neuroscience.2018.11.024

Wang, Y. L., Chang, L. C., Chen, K. B., and Wang, S. C. (2021b). Aptamer-guided Targeting of the Intracellular Long-Noncoding RNA HOTAIR. *Am. J. Cancer Res.* 11, 945–954.

Wang, Z., Wang, R., Wang, K., and Liu, X. (2018b). Upregulated Long Noncoding RNA Snhg1 Promotes the Angiogenesis of Brain Microvascular Endothelial Cells after Oxygen-Glucose Deprivation Treatment by Targeting miR-199a. *Can. J. Physiol. Pharmacol.* 96, 909–915. doi:10.1139/cjpp-2018-0107

Winkle, M., El-Daly, S. M., Fabbri, M., and Calin, G. A. (2021). Noncoding RNA Therapeutics - Challenges and Potential Solutions. *Nat. Rev. Drug Discov.* 20, 629–651. doi:10.1038/s41573-021-00219-z

Wong, A. D., Ye, M., Levy, A. F., Rothstein, J. D., Bergles, D. E., and Searson, P. C. (2013). The Blood-Brain Barrier: an Engineering Perspective. *Front. Neuroeng.* 6, 7. doi:10.3389/fneng.2013.00007

Woo, J., Lee, M., Seo, J. M., Park, H. S., and Cho, Y. E. (2016). Optimization of the Optical Transparency of Rodent Tissues by Modified PACT-Based Passive Clearing. *Exp. Mol. Med.* 48, e274. doi:10.1038/emm.2016.105

Wu, M., Yang, L.-Z., and Chen, L.-L. (2021). Long Noncoding RNA and Protein Abundance in lncRNPs. *Rna* 27, 1427–1440. doi:10.1261/rna.078971.121

Xie, Y., He, L., Lugano, R., Zhang, Y., Cao, H., He, Q., et al. (2021). Key Molecular Alterations in Endothelial Cells in Human Glioblastoma Uncovered through Single-Cell RNA Sequencing. *JCI Insight* 6, 150861. doi:10.1172/jci.insight.150861

Xie, Y., and Wei, Y. (2021). A Novel Regulatory Player in the Innate Immune System: Long Non-coding RNAs. *Ijms* 22, 9535. doi:10.3390/ijms22179535

Xu, B., Yang, R., Fu, J., Yang, B., Chen, J., Tan, C., et al. (2021a). LncRSPH9-4 Facilitates Meningitic Escherichia Coli-Caused Blood-Brain Barrier Disruption via miR-17-5p/MMP3 Axis. *Ijms* 22, 6343. doi:10.3390/ijms22126343

Xu, D., Cai, Y., Tang, L., Han, X., Gao, F., Cao, H., et al. (2020). A CRISPR/Cas13-based Approach Demonstrates Biological Relevance of Vlinc Class of Long Non-coding RNAs in Anticancer Drug Response. *Sci. Rep.* 10, 1794. doi:10.1038/s41598-020-58104-5

Xu, Y., Hu, Y., Xu, S., Liu, F., and Gao, Y. (2021b). Exosomal microRNAs as Potential Biomarkers and Therapeutic Agents for Acute Ischemic Stroke: New Expectations. *Front. Neurol.* 12, 747380. doi:10.3389/fneur.2021.747380

Yan, B., Yao, J., Liu, J.-Y., Li, X.-M., Wang, X.-Q., Li, Y.-J., et al. (2015a). lncRNA-MIAT Regulates Microvascular Dysfunction by Functioning as a Competing Endogenous RNA. *Circ. Res.* 116, 1143–1156. doi:10.1161/CIRCRESAHA.116.305510

Yan, L., Yang, M., Guo, H., Yang, L., Wu, J., Li, R., et al. (2013). Single-cell RNA-Seq Profiling of Human Preimplantation Embryos and Embryonic Stem Cells. *Nat. Struct. Mol. Biol.* 20, 1131–1139. doi:10.1038/nsmb.2660

Yan, X., Hu, Z., Feng, Y., Hu, X., Yuan, J., Zhao, S. D., et al. (2015b). Comprehensive Genomic Characterization of Long Non-coding RNAs across Human Cancers. *Cancer Cell* 28, 529–540. doi:10.1016/j.ccell.2015.09.006

Yang, C., Hawkins, K. E., Doré, S., and Candelario-Jalil, E. (2019). Neuroinflammatory Mechanisms of Blood-Brain Barrier Damage in Ischemic Stroke. *Am. J. Physiology-Cell Physiol.* 316, C135–C153. doi:10.1152/ajpcell.00136.2018

Yang, C., Zheng, J., Liu, X., Xue, Y., He, Q., Dong, Y., et al. (2020). Role of ANKHD1/LINC00346/ZNF655 Feedback Loop in Regulating the Glioma Angiogenesis via Staufen1-Mediated mRNA Decay. *Mol. Ther. - Nucleic Acids* 20, 866–878. doi:10.1016/j.omtn.2020.05.004

Yang, X., and Zi, X.-H. (2019). LncRNA SNHG1 Alleviates OGD Induced Injury in BMEC via miR-338/HIF-1α axis. *Brain Res.* 1714, 174–181. doi:10.1016/j.brainres.2018.11.003

Yin, D., Xu, F., Lu, M., and Li, X. (2021). Long Non-coding RNA RMST Promotes Oxygen-Glucose Deprivation-Induced Injury in Brain Microvascular Endothelial Cells by Regulating miR-204-5p/VCAM1 axis. *Life Sci.* 284, 119244. doi:10.1016/j.lfs.2021.119244

Yu, H., Xue, Y., Wang, P., Liu, X., Ma, J., Zheng, J., et al. (2017). Knockdown of Long Non-coding RNA XIST Increases Blood-Tumor Barrier Permeability and Inhibits Glioma Angiogenesis by Targeting miR-137. *Oncogenesis* 6, e303. doi:10.1038/oncsis.2017.7

Zhai, C., Sun, Y., Qian, G., Pan, H., Xie, S., Sun, Z., et al. (2021). LncRNA AK087124/miR-224-5p/PTEN axis Modulates Endothelial Cell Injury in Atherosclerosis through Apoptosis and AKT Signaling Pathway. *Arch. Biochem. Biophys.* 705, 108916. doi:10.1016/j.abb.2021.108916

Zhan, R., Xu, K., Pan, J., Xu, Q., Xu, S., and Shen, J. (2017). Long Noncoding RNA MEG3 Mediated Angiogenesis after Cerebral Infarction through Regulating p53/NOX4 axis. *Biochem. Biophysical Res. Commun.* 490, 700–706. doi:10.1016/j.bbrc.2017.06.104

Zhang, B., Wang, D., Ji, T.-F., Shi, L., and Yu, J.-L. (2017a). Overexpression of lncRNA ANRIL Up-Regulates VEGF Expression and Promotes Angiogenesis of Diabetes Mellitus Combined with Cerebral Infarction by Activating NF-Kb Signaling Pathway in a Rat Model. *Oncotarget* 8, 17347–17359. doi:10.18632/oncotarget.14468

Zhang, C., Zhang, X., Wang, J., Di, F., Xue, Y., Lin, X., et al. (2020a). Lnc00462717 Regulates the Permeability of the Blood-brain Tumor Barrier through Interaction with PTBP1 to Inhibit the miR-186-5p/Occludin Signaling Pathway. *FASEB j.* 34, 9941–9958. doi:10.1096/fj.202000045R

Zhang, J., Dong, B., Hao, J., Yi, S., Cai, W., and Luo, Z. (2019a). LncRNA Snhg3 Contributes to Dysfunction of Cerebral Microvascular Cells in Intracerebral Hemorrhage Rats by Activating the TWEAK/Fn14/STAT3 Pathway. *Life Sci.* 237, 116929. doi:10.1016/j.lfs.2019.116929

Zhang, L., Luo, X., Chen, F., Yuan, W., Xiao, X., Zhang, X., et al. (2018a). LncRNA SNHG1 Regulates Cerebrovascular Pathologies as a Competing Endogenous RNA through HIF-1α/VEGF Signaling in Ischemic Stroke. *J. Cel. Biochem.* 119, 5460–5472. doi:10.1002/jcb.26705

Zhang, L., Yang, H., Li, W.-J., and Liu, Y.-H. (2020b). LncRNA MALAT1 Promotes OGD-Induced Apoptosis of Brain Microvascular Endothelial Cells by Sponging miR-126 to Repress PI3K/Akt Signaling Pathway. *Neurochem. Res.* 45, 2091–2099. doi:10.1007/s11064-020-03071-6

Zhang, M., Tang, M., Wu, Q., Wang, Z., Chen, Z., Ding, H., et al. (2020c). LncRNA DANCR Attenuates Brain Microvascular Endothelial Cell Damage Induced by Oxygen-Glucose Deprivation through Regulating of miR-33a-5p/XBP1s. *Aging* 12, 1778–1791. doi:10.18632/aging.102712

Zhang, S., An, Q., Wang, T., Gao, S., and Zhou, G. (2018b). Autophagy- and MMP-2/9-Mediated Reduction and Redistribution of ZO-1 Contribute to Hyperglycemia-Increased Blood-Brain Barrier Permeability during Early Reperfusion in Stroke. *Neuroscience* 377, 126–137. doi:10.1016/j.neuroscience.2018.02.035

Zhang, T., Wang, H., Li, Q., Fu, J., Huang, J., and Zhao, Y. (2018c). MALAT1 Activates the P53 Signaling Pathway by Regulating MDM2 to Promote Ischemic Stroke. *Cel Physiol Biochem* 50, 2216–2228. doi:10.1159/000495083

Zhang, X., Tang, X., Liu, K., Hamblin, M. H., and Yin, K.-J. (2017b). Long Noncoding RNA Malat1 Regulates Cerebrovascular Pathologies in Ischemic Stroke. *J. Neurosci.* 37, 1797–1806. doi:10.1523/JNEUROSCI.3389-16.2017

Zhang, Y., Du, W., and Yang, B. (2019b). Long Non-coding RNAs as New Regulators of Cardiac Electrophysiology and Arrhythmias: Molecular Mechanisms, Therapeutic Implications and Challenges. *Pharmacol. Ther.* 203, 107389. doi:10.1016/j.pharmthera.2019.06.011

Zhao, M., Wang, J., Xi, X., Tan, N., and Zhang, L. (2018). SNHG12 Promotes Angiogenesis Following Ischemic Stroke via Regulating miR-150/VEGF Pathway. *Neuroscience* 390, 231–240. doi:10.1016/j.neuroscience.2018.08.029

Zhou, X., Xu, B., Gu, Y., Ji, N., Meng, P., and Dong, L. (2021). Long Noncoding RNA SNHG1 Protects Brain Microvascular Endothelial Cells against Oxygen-Glucose Deprivation/reoxygenation-Induced Injury by Sponging miR-298 and Upregulating SIK1 Expression. *Biotechnol. Lett.* 43, 1163–1174. doi:10.1007/s10529-021-03096-z

Zhou, Z.-W., Zheng, L.-J., Ren, X., Li, A.-P., and Zhou, W.-S. (2019). LncRNA NEAT1 Facilitates Survival and Angiogenesis in Oxygen-Glucose Deprivation (OGD)-induced Brain Microvascular Endothelial Cells (BMECs) via Targeting miR-377 and Upregulating SIRT1, VEGFA, and BCL-XL. *Brain Res.* 1707, 90–98. doi:10.1016/j.brainres.2018.10.031

Zhu, L., Lin, M., Ma, J., Liu, W., Gao, L., Wei, S., et al. (2019). The Role of LINC 00094/miR-224-5p (miR-497-5p)/Endophilin-1 axis in Memantine Mediated Protective Effects on Blood-brain Barrier in AD Microenvironment. *J. Cel. Mol. Med.* 23, 3280–3292. doi:10.1111/jcmm.14214

Zhu, P., Wu, J., Wang, Y., Zhu, X., Lu, T., Liu, B., et al. (2018). LncGata6 Maintains Stemness of Intestinal Stem Cells and Promotes Intestinal Tumorigenesis. *Nat. Cel Biol.* 20, 1134–1144. doi:10.1038/s41556-018-0194-0

Conflict of Interest: The authors declare that the research was conducted in the absence of any commercial or financial relationships that could be construed as a potential conflict of interest.

Publisher's Note: All claims expressed in this article are solely those of the authors and do not necessarily represent those of their affiliated organizations, or those of the publisher, the editors and the reviewers. Any product that may be evaluated in this article, or claim that may be made by its manufacturer, is not guaranteed or endorsed by the publisher.

GLOSSARY

15-LOX1 15-lipoxygenase 1

AERRIE Age and EndMT Regulated RNA In Endothelium

Akt Protein kinase B

ANRIL Antisense non-coding RNA in the INK4 locus

Atg7 Autophagy related 7

BAD BCL2 associated agonist of cell death

BBB Blood brain barrier

Bcl-2 B-cell lymphoma 2

BMECs/BMVECs Brain microvascular endothelial cells

BTB Blood tumor barrier

CAAP1 Caspase Activity and Apoptosis Inhibitor 1

ceRNA competing endogenous RNA

CMECs Cerebral microvascular endothelial cells

CRISPR Clustered regularly interspaced short palindromic repeats

CVECs Cerebrovascular endothelial cells

DAG Diacyl glycerol

DANCR Differentiation Antagonizing Non-Protein Coding RNA

EC Endothelial cells

EGFR Epidermal growth factor

ENC1 Ectodermal-Neural Cortex 1

eNOS Endothelial nitric oxide synthase

ERK Extracellular signal-regulated kinase

FAL1 Focally amplified lncRNA on chromosome 1

FENDRR FOXF1 Adjacent Non-Coding Developmental Regulatory RNA

Fn14 Fibroblast growth factor-inducible 14

FOSL2 FOS Like 2, AP-1 Transcription Factor

FUS Fused in sarcoma

GAS5 Growth Arrest Specific 5

G-CSF Granulocyte stimulating factor

GSK-3β Glycogen synthase kinase 3 beta

H19 H19 Imprinted Maternally Expressed Transcript

HBEC-5i Human Brain Endothelial Cell line-5i

HDAC6 Histone deacetylase 6

HIF1A Hypoxia-inducible factor 1-alpha

HIHC Hypertensive intracerebral hemorrhage

HOTAIR HOX antisense intergenic RNA

HUVECs Human umbilical vein endothelial cells

IA Intracranial aneurysm

ICAM-1 Intercellular adhesion molecule-1

ICH Intracerebral hemorrhage

JAK Janus kinase

JAM Junctional adhesion molecule

KLF4 Kruppel-like transcription factor 4

LncRNA long non coding RNA

MALAT1 Metastasis Associated Lung Adenocarcinoma Transcript 1

MAPK Mitogen-activated protein kinase

MARVEL MAL and related proteins for vesicle trafficking and membrane link

MCAO Middle cerebral artery occlusion

MCP-1 Monocyte chemotactic protein-1

MEG3 Maternally expressed 3

MEG8 Maternally Expressed 8

MIAT Myocardial infarction associated transcript

MMP Matrix metalloproteinase

MRI Magnetic resonance imaging

MYC MYC Proto-Oncogene, BHLH Transcription Factor

NEAT1 Nuclear Enriched Abundant Transcript 1

NORAD Non-Coding RNA Activated by DNA Damage

NOX4 NADPH Oxidase 4

NVU Neurovascular unit

OGD Oxygen-glucose deprivation

OGD/R Oxygen-glucose deprivation and restoration

OxLDL Oxidized LDL

PAK1 p21 (RAC1) activated kinase 1

PARP1 Poly [ADP-ribose] polymerase 1

PCNA Proliferating cell nuclear antigen

PET Positron emission tomography

PI3K Phosphoinositide 3-kinase

PRKCB2 Protein kinase C beta 2

PTEN Phosphatase and tensin homolog

PVT1 Plasmacytoma variant translocation 1

RMST Rhabdomyosarcoma 2 associated transcript

S1P Sphingosine-1-phosphate

SIRT1 Sirtuin 1

SNHG Small Nucleolar RNA Host Gene

SOX5 RY-Box Transcription Factor 5

SPAAR Small regulatory polypeptide of amino acid response

STAT3 Signal Transducer and Activator Of Transcription 3

TALEN Transcription activator-like effector nucleases

TEER Transendothelial electrical resistance

TWEAK Tumor necrosis factor-like weak inducer of apoptosis

ULK2 Unc-51 Like Autophagy Activating Kinase 2
USF1 Upstream stimulatory factor 1
VCAM-1 Vascular cell adhesion protein 1
VEAL2 Vascular endothelial associated lncRNA-2
VEGF Vascular endothelial growth factor
VEGFR Vascular endothelial growth factor receptor
XIST X-inactive specific transcript
YBX1 Y box binding protein 1
ZAK ZO-1-associated kinase
ZO Zona occludens

frontiers | Frontiers in Genetics

ORIGINAL RESEARCH
published: 29 April 2022
doi: 10.3389/fgene.2022.854097

A Circ-0007022/miR-338-3p/Neuropilin-1 Axis Reduces the Radiosensitivity of Esophageal Squamous Cell Carcinoma by Activating Epithelial-To-Mesenchymal Transition and PI3K/AKT Pathway

*Junpeng Zhang[1,2], Yanyan Yu[3], Xiaoyang Yin[1,2], Lei Feng[1,2], Zhe Li[1,2], Xiaomeng Liu[2], Xinshuang Yu[4] and Baosheng Li[2]**

[1]Department of Graduate, Shandong First Medical University and Shandong Academy of Medical Sciences, Jinan, China, [2]Department of Radiation Oncology, Shandong Cancer Hospital and Institute, Shandong First Medical University and Shandong Academy of Medical Sciences, Jinan, China, [3]Department of Neurology, The First Affiliated Hospital of Shandong First Medical University and Shandong Provincial Qianfoshan Hospital, Jinan, China, [4]Department of Oncology, The First Affiliated Hospital of Shandong First Medical University and Shandong Provincial Qianfoshan Hospital, Jinan, China

OPEN ACCESS

Edited by:
William C. Cho, QEH, Hong Kong SAR, China

Reviewed by:
Aniket Bhattacharya, Rutgers, The State University of New Jersey, United States
Gisela Ceballos, Instituto Nacional de Medicina Genómica (INMEGEN), Mexico

***Correspondence:**
Baosheng Li
bsli@sdfmu.edu.cn

Specialty section:
This article was submitted to RNA, a section of the journal Frontiers in Genetics

Received: *13 January 2022*
Accepted: *24 March 2022*
Published: *29 April 2022*

Citation:
Zhang J, Yu Y, Yin X, Feng L, Li Z, Liu X, Yu X and Li B (2022) A Circ-0007022/miR-338-3p/Neuropilin-1 Axis Reduces the Radiosensitivity of Esophageal Squamous Cell Carcinoma by Activating Epithelial-To-Mesenchymal Transition and PI3K/AKT Pathway. Front. Genet. 13:854097. doi: 10.3389/fgene.2022.854097

Radiotherapy resistance is an important cause of treatment failure in esophageal squamous cell carcinoma (ESCC). Circular RNAs have attracted a lot of attention in cancer research, but their role in ESCC radiosensitivity has not been elucidated yet. Here, we aimed to evaluated the functional impacts of circ-0007022 on ESCC radiosensitivity. In this study, a stable radiotherapy-resistant cell line was established and verified by a series of functional experiments. Subsequently, high-throughput sequencing revealed that circ-0007022 was significantly overexpressed in the radiotherapy-resistant cell line and this conclusion was verified in ESCC patients' tumor tissues by real-time quantitative PCR. Moreover, loss-of-function and overexpression experiments *in vitro* and *in vivo* revealed that, after irradiation, the abilities of proliferation and migration in circ-0007022-overexpressing stable transgenic strain were significantly higher than that in circ-0007022-knockdown stable transgenic strain. Additionally, RNA Immunoprecipitation, RNA pull-down, luciferase reporter assays, and fluorescence *in situ* hybridization experiments demonstrated the mechanism of how circ-0007022 could sponge miR-338-3p and upregulate downstream target of miR-338-3p, neuropilin-1 (NRP1). Moreover, NRP1 led to poor prognosis for ESCC patients receiving radiotherapy, and NRP1 knock-down enhanced radiosensitivity of ESCC cells. Furthermore, circ-0007022 overexpression activated Epithelial-to-mesenchymal transition and PI3K/Akt pathway, and NRP1 knock-down could reversed this phenomenon. Finally, Akt Inhibitor reversed circ-0007022s role in radiotherapy in ESCC cells. Taken together, the circ-0007022/miR-338-3p/NRP1 axis enhances the radiation resistance of ESCC cells *via* regulating EMT and PI3K/Akt pathway. The new circRNA circ-0007022 is thus expected to be a therapeutic target for ESCC patients.

Keywords: circ-0007022, miR-338-3p, neuropilin-1, radiosensitivity, ESCC

INTRODUCTION

Esophageal cancer ranks seventh in terms of incidence and sixth overall in mortality, in other words, one of every 18 deaths from tumors is due to esophageal cancer (Sung et al., 2021). Esophageal squamous cell carcinoma (ESCC) is a common pathological type of esophageal cancer, especially in Asia. Surgery, radiotherapy and chemotherapy are the most important treatment methods for esophageal cancer, among which, radiotherapy plays a key role in the local treatment of esophageal cancer (Ajani et al., 2019), but the 5-years survival rate of ESCC is only 21% due to radiotherapy resistance (Murphy et al., 2017). Therefore, finding a molecular target to increase the sensitivity of ESCC radiotherapy is urgently needed.

Circular RNAs (circRNAs) are non-coding RNAs without a 5′-end cap and a 3′-end poly(A) tail, where the 5′ end and 3′ end form a ring structure *via* an end-to-end covalent connection (Yang C. et al., 2021). The expression range of circRNAs is very wide, including in tissues, blood, and exosomes (Fan et al., 2019; Chen et al., 2020; Luo et al., 2021). Moreover, because they are resistant to digestion by nucleic acid exonucleases (RNase R), they are more stable than linear RNAs (Hansen, 2018). In recent years, circRNAs have been demonstrated to play important roles in the occurrence, development, diagnosis, and treatment of tumors, cardiovascular diseases, endocrine diseases, and inflammation, mainly by sponging miRNAs, regulating the translation, directly regulating the transcription, splicing, and expression of parental genes (Li et al., 2015; Du et al., 2017; Liu et al., 2017; Yu et al., 2018; Cao et al., 2020; Zhang et al., 2020). CircRNAs could be reliable and important targets for the treatment of carcinomas. Recent studies had found that circRNAs could modulate the radiosensitivity of various tumors (Li H. et al., 2020; Gao et al., 2021; Yang et al., 2022), however, the interaction between circRNAs and ESCC radiosensitivity has rarely been reported.

In our study, circ-0007022, a new circRNA, was determined to be remarkably upregulated in radiotherapy-resistant ESCC cells and patients, and the phenotypic changes in ESCC cells were closely related to aberrant circ-0007022 expression.

In this study, we aimed to explore the potential functions and mechanisms of circ-0007022, which might be a crucial target to improve existing clinical therapeutic strategies against radiotherapy-resistant ESCC. This study provides new insights into the mechanisms of radiotherapy resistance in ESCC.

MATERIALS AND METHODS

Patients and Tissue Specimens

Two independent cohorts were used in present study as follows: 1) 20 total ESCC patients who received neoadjuvant chemoradiation containing platinum-based chemotherapy drugs were divided into partial response (PR, n = 10) and stable disease (SD, n = 10) groups based on their imaging examinations before surgery, and tumor tissues of these patients, obtained by endoscopy before they accepted any anti-tumor therapy, were frozen in liquid nitrogen and stored at −80°C; 2) another 22 ESCC patients who had accepted radical radiotherapy with or without concurrent chemotherapy were enrolled in this study, and their baseline characteristics are presented in **Supplementary Table S1**. Their tumor tissue samples were obtained before they received any treatment, and they were fixed with paraffin for subsequent histological examination. Follow-up was performed over the phone, and the deadline was March 2021. The time between radiotherapy and disease recurrence was defined as progression-free survival (PFS). All patients enrolled in this study accepted radiotherapy treatment at the Shandong Cancer Hospital and Institute (Jinan, China) and had provided written informed consent. The study was approved by the institutional review board of Shandong Cancer Hospital and the Institute for Scientific and Ethical Integrity (approval number: SDTHEC201803).

Cell Culture and Establishment of Radioresistant Cell Line

The 293T cells and the human ESCC cell lines Kyse30, Kyse150, Kyse410, Kyse450, Kyse510, and TE1 were obtained from the Cell Bank of Shanghai Institutes for Biological Sciences, Chinese Academy of Sciences (Shanghai, China) and authenticated based on short tandem repeats. All cell lines were maintained in Dulbecco's modified Eagle's medium (DMEM; Gibco, Grand Island, NY, United States) with 1% penicillin/streptomycin (Biosharp, Hefei, Anhui, China) and 10% fetal bovine serum (Gibco) with 5% CO2 at 37°C. Kyse30 cell were continuously irradiated with a radiation gradient as follows: 2 Gy/f × 3f, 4 Gy/f × 3f, 6 Gy/f × 3f, and 8 Gy/f × 3f. The established radioresistant cell lines were designated as Kyse30R. ESCC cells were incubated with AKT inhibitor MK-2206 (Selleck, Shanghai, China) for 48 h before next experiments, and named as cell-AKT-Inh.

Colony Formation Assay

Cells (1×10^3) were seeded into 60 mm cell culture dishes (NEST, Wuxi, China), treated with X-rays at doses of 0, 2, 4, or 6 Gy, and then cultured for 14 days to allow colonies to grow. Then, colonies were fixed with 4% paraformaldehyde (Biosharp), stained with 0.1% crystal violet solution (Biosharp), and counted using ImageJ software (National Institutes of Health, Bethesda, MD, United States).

Cell Survival Assays

Cell survival was analyzed using Cell Counting Kit-8 (CCK-8, Bioss, Beijing, China). Cells with or without irradiation were seeded and incubated in 96-well plates at a density of approximately 3,000 cells/well. At 0, 24, 48, 72, or 96 h, the CCK-8 reagent was added, and the optical absorbance of each sample was measured at 450 nm using an enzyme-labeling instrument (Thermo Fisher Scientific, Waltham, MA, United States) to reflect cell survival.

Flow Cytometry

At 24 h after a dose of 4Gy irradiation, the cells were collected, washed with cold phosphate-buffered saline (PBS), and fixed overnight at 4°C with pre-cooled 70% ethanol, which was followed by propidium iodide staining. The cells were

analyzed using a flow cytometer (BD, Franklin Lakes, NJ, United States). Next, 48 h after a dose of 4Gy irradiation, the cells were collected and analyzed using a Annexin V FITC Apoptosis Detection Kit I (BD), following the manufacturer's instructions. Subsequently, apoptosis rates was analyzed using FlowJo (v 10.0, BD).

Western Blot Analysis

Total proteins were extracted using RIPA buffer (KenGEN, Shanghai, China) with a cocktail inhibitor (Beyotime, Shanghai, China). After electrophoresis and transfer, the proteins were blocked with 5% BSA and incubated with primary antibodies as follows: anti-cyclin B1 (Cell Signaling Technology, Danvers, MA, United States; 12231, dilution 1: 1,000), anti-cleaved PARP (Cell Signaling Technology; 5625, dilution 1:1,000), anti-cleaved-caspase-3 (Abcam, Cambridge, MA; ab2302, dilution 1:500), anti-γ-H2AX (Abcam; ab26350, dilution 1:1,000), anti-Bax (Cell Signaling Technology; 5023, dilution 1:2000), anti-Argonaute2 (Ago2; Cell Signaling Technology; 2897, dilution 1:1,000), anti-neuropilin-1 (NRP1) (Abcam; ab81321, dilution 1:1,000), anti-E-cadherin (Cell Signaling Technology; 3195, dilution 1:1,000), anti-N-cadherin (Cell Signaling Technology; 5741, dilution 1:500), anti-Akt (Cell Signaling Technology; 4691, dilution 1:1,000), anti-Phospho-Akt (Ser473) (Cell Signaling Technology; 4060, dilution 1:5000), anti-PI3 Kinase catalytic subunit alpha (Abcam; ab40776, dilution 1: 1,000), anti-PI3K p85 (phospho Y458)+PI3K p55 (phospho Y199) (Abcam; ab278545, dilution 1:500) and anti-GAPDH (Cell Signaling Technology; 5174, dilution 1:1,000) at 4°C overnight. After incubation with secondary antibodies for 1 h, the membranes were visualized using the ChemiDoc XRS + Gel Imaging System (Bio-Rad, Hercules, CA, United States).

Immunofluorescence Analysis

For immunofluorescence analysis, the cells were incubated in 24-well plates with or without treatment with radiation at a dose of 6 Gy. Cells were then fixed with 4% paraformaldehyde (Biosharp) for 30min, permeabilized with 1% TritonX-100 (Biosharp) for 30min, blocked with 5% BSA for 1 h, and then incubated overnight at 4°C with primary antibodies (anti-γ-H2AX (Abcam; ab26350, dilution 1:500), anti- Vimentin (Cell Signaling Technology, 5741, dilution 1:500), and primary antibodies were diluted by primary antibody dilution buffer for immunol staining (Beyotime). Subsequently, the cells were incubated for 1 h at 37°C with the secondary antibody. Nuclei were stained with 4′,6-diamidino-2-phenylindole dihydrochloride (DAPI; Solarbio, Beijing, China). Three areas were selected randomly for photography and calculation. Single-staining and merged images were acquired using laser confocal microscopy (LSM 900 with Airyscan 2, Carl Zeiss, Jena, Germany) using Zen 3.0 (blue edition) imaging software (Carl Zeiss).

Neutral Comet Assay

A neutral comet assay was performed using the CometAssay Kit (Trevigen, Gaithersburg, Maryland, United States). At 4 h after administering radiation therapy at 4 Gy, Kyse30 and Kyse30R cells were mixed with low-density agarose, fixed on the comet slide, and lysed overnight; this was followed by electrophoresis at 21 V for 45 min in a neutral electrophoresis buffer. Gels were then immersed in DNA Precipitation Solution for 30 min at 37°C before staining with SYBR Gold (Invitrogen, Carlsbad, CA, United States). After being photographed using a fluorescence microscope (Carl Zeiss), the olive tail moment was measured using comet score software.

RNA Extraction, Quantitative Reverse Transcription-Polymerase Chain Reaction, and High-Throughput Sequencing

Total RNA was isolated from cells and tumor tissues using SuperpureTotal RNA Kit (SPARKeasy, Shandong, China), and the reverse transcriptions were performed according to the manuals to obtain the cDNA using miRNA 1st strand cDNA synthesis kit (AG, Changsha, China, for miRNA) and PrimeScript™ RT reagent Kit (Takara, Shiga-Ken, Japan, for mRNA and cirRNA). Then, qRT-PCR was performed in triplicate using SYBR Premix Ex Taq (Takara) and by applying the 2−ΔΔCt method with GAPDH and U6, which were used for normalizing these data. The primers used in the qRT-PCR are listed in **Supplementary Table S2**. Kyse30 and Kyse30R cells were used to perform High-throughput sequencing to identify circRNAs, according to a previous study (Zhang et al., 2017): Briefly, after RNA quantification and qualification, a total of 3 μg RNA per sample was used as the input material for the RNA sample preparation. Sequencing libraries were generated using the NEBNext® UltraTM RNA Library Prep Kit for Illumina® (NEB, United States). Fragmentation was carried out using divalent cations under elevated temperature in the NEBNext First-Strand Synthesis Reaction Buffer (5X). After first-strand and directional second-strand synthesis, a tailing/adapter ligation approach was performed using the purified cDNA, following amplification. Finally, products were purified, and the Agilent Bioanalyzer 2100 system was used to assess library quality. After cluster generation using the TruSeq PE Cluster Kit v3-cBot-HS (Illumina), library preparations were sequenced using an Illumina Hiseq platform to generate 125 bp/150 bp paired-end reads, followed by Quality control, Mapping to the reference genome, circRNA identification and differential expression analysis for the samples with biological replicates.

RNase R Digestion, Nucleic Acid Electrophoresis, and Sanger Sequencing

Total RNA (2 μg) was incubated with RNase R (20 U/μL, Lucigen, Wisconsin, United States) for 20 min at 37°C. Control samples were exposed to the same experimental steps as those used for the experimental samples, except for the addition of RNase R. The qRT-PCR products were added to 6 loading buffer (Beyotime) with the nucleic acid dye Gel-Green (Beyotime). After agarose gel (2%) electrophoresis at 60 V for 40 min, DNA fragments were visualized using UV transillumination. Moreover, qRT-PCR amplification products were excised from the agarose gel and

purified using a GeneJET Gel Purification Kit (Thermo Fisher Scientific). Subsequently, following the standard approach detailed by Geneseed (Guangzhou, China), the nucleotide sequences of the purified products were determined *via* Sanger sequencing.

Cell Transfection and Lentiviral Transduction

The circ-0007022-overexpression/knockdown plasmids and the corresponding vectors were successfully constructed using GENE (Shanghai, China), and the miR-338-3p mimic, siRNA-NRP1, and their corresponding negative controls were purchased from GenePharma (Shanghai, China). Kyse150 and TE1 cells (1.5×10^5 cells/well) were seeded into six-well plates and incubated for 8 h before transfection. 20 ul of 1×10^7 TU/ml of plasmids were infected into cells and cultured with 1 ml DMEM with 10% FBS and 6 ug/ml polybrene (GENE) for 48 h, followed by selection using 8 μg/ml puromycin (Thermo Fisher Scientific). 2.5 ul of 20 um miRNA mimics, miRNA labeled with biotin at the 3′ end or siRNAs were injected into cells with 7.5 ul of Lipofectamine 3000 Reagent (Invitrogen) and 500ul of opti-MEM (Gibco), and the transfection efficiency was determined by qRT-PCR analysis after 24 h of transfection. Sequences of mimic, inhibitor, and vectors were listed in **Supplementary Table S2**.

Wound Healing Assay

Cells after transfection (2.5×10^5 cells/well) were seeded into 12-well plates and incubated for 24 h. Following 4 Gy irradiation, a 200 μL pipette was used to wound cells, and cells were washed once using PBS to remove cell debris. At 0 and 36 h, cells were photographed, and the wound area was measured.

Transwell Migration Assays

A transwell assay was also used to assess cell migration. Initially, 2×10^4 cells seeded in the upper chambers of every 8 mm transwell (Millipore, Billerica, MA, United States) were irradiated with 4 Gy of X-rays. The cells in the upper chamber were incubated in serum-free medium, whereas medium with 10% serum was added to the lower chamber. After removing cells on the upper surface of the filter after 48 h, cells attached to the lower chamber were fixed with 4% paraformaldehyde (Biosharp) for 30 min, stained with 0.1% crystal violet solution (Biosharp)for 30 min. Three areas were selected randomly for photography and calculation using an inverted microscope (Carl Zeiss).

In vivo Xenograft Mouse Model

BALB/C nude mice (5–6-week-old) were purchased from Vital River Laboratory (Beijing, China) and subcutaneously injected with transfected cells (1×10^7 transfected cells, $n = 5$ for each group). When tumors reached the intended size, mice were divided randomly into two groups as follows: 1) the irradiation group, which received radiotherapy at a single dose of 8 Gy, and 2) the non-irradiated group. Tumor size was measured using calipers, and the greatest longitudinal diameter (length) and transverse diameter (width) were recorded three times per week. The mice were sacrificed 30 days after injection. Animal experiments were approved by the Institutional Animal Care and Use Committee of Shandong Cancer Hospital and Institute, Shandong First Medical University and Shandong Academy of Medical Sciences (approval number: SDTHEC201803).

Bioinformatics Analysis

The Circular RNA Interactome (https://circinteractome.nia.nih.gov/) and CircBank Database (www.circbank.cn/) were used to predict circRNAs–miRNA associations. For miRNA–gene interactions, miRDB (http://www.mirdb.org/), miRTarBase (http://mirtarbase.mbc.nctu.edu.tw/php/index.php), TargetScan (http://www.targetscan.org/vert_71/), and miRWalk (http://mirwalk.umm.uni-heidelberg.de/) were used. Gene expression data of human ESCC and corresponding clinical information were obtained from the Cancer Genome Atlas (TCGA) database. All data were downloaded and processed by the R software (version 3.6.1).

Luciferase Reporter Assay

The wild-type and mutant fragments in the 3′-untranslated region of circ-0007022 and NRP1 related to the miR-338-3p-binding site were generated using GenePharma (Shanghai, China) and subcloned into the pMIR-REPORT vectors. In brief, 5×10^3 cells/well 293T cells transfected with circ-0007022 or circ-0007022-mutant and NRP1 or NRP1-mutant were seeded in 96-well plates and co-transfected with 50 nM miR-NC or miR-338-3p-mimics and the reporter vector using Lipofectamine 2000 (Invitrogen) for 48 h. Then, Firefly and Renilla luciferase activities were measured by a dual-luciferase reporter assay system (Promega, WI, United States) and Relative luciferase activity was normalized to the Renilla luciferase internal control.

Fluorescence *In Situ* Hybridization

Circ-0007022 and miR-338-3p probes, as well as the FISH kit used in this assay, were all purchased from GenePharma, Sequences of probes were listed in **Supplementary Table S2**. FISH was performed according to the manufacturer's instructions. Briefly, 5×10^4 cells/well cells were seeded in 12-well plates and incubated for 24 h. Cells were then fixed with 4% paraformaldehyde (Biosharp) for 15 min, permeabilized with 1% TritonX-100 (Biosharp) for 15 min. Then cells were hybridized at 4°C in hybrid solution containing circ-0007022 and miR-338-3p probes overnight. After washing, cell nuclei were stained with DAPI (Solarbio) at 37°C for 20 min. The single-staining and merged images were captured using a laser confocal microscopy (Carl Zeiss).

RNA Immunoprecipitation

To analyze the relationships among circ-0007022, miR-338-3p, and NRP1, a RIP experiment was conducted with an RNA Immunoprecipitation Kit (Geneseed, Guangzhou, China). Briefly, 1×10^7 Kyse150 and TE1 cells were lysed in RIP buffer at 4°C for 20 min, and the supernatant incubated overnight with magnetic beads coupled with 5 ug anti-Ago2 (Cell Signaling Technology; 2897) or anti-IgG (Proteintech,

Rosemont, United States; 16402-1-AP) at 4°C. Then, after washing, the RNA was extracted from immunoprecipitated complexes and subjected to qRT-PCR.

RNA Pulldown Assay

Kyse150 and TE1 cells were used to perform the RNA pull-down assay according to a previous study (Phatak and Donahue, 2017). MiR-338-3p-Bio and miR-NC-Bio were constructed by GenePharma (Shanghai, China).

5-Ethynyl-2′-Deoxyuridine Assay

The EDU assay was performed using an EDU Kit (Beyotime), according to the manufacturer's instructions. 5×10^4 cells/well Kyse150 and TE1 cells transfected with si-negative-control or si-NRP1 were seeded onto 12-well plates, irradiated with 4 Gy, and cultured for 48 h, and then, the medium was switched to fresh DMEM supplemented with EDU (50 mmol/L). The cells were then incubated for 2 h, followed by fixation, permeabilization, and EDU staining with Azide 488 (Beyotime). After staining cell nuclei with DAPI, five areas were selected randomly for photography and calculation. And the EDU-positive cells were identified using Zen 3.0 (blue edition) imaging software (Carl Zeiss).

Immunohistochemistry

NRP1 was detected in 5 μm-thick paraffin sections using the indicated antibodies as previous description (Zeng et al., 2016). Briefly, the sections were incubated with primary antibodies (Abcam; ab81321, dilution 1:500) overnight at 4°C and secondary antibodies (Abcam; ab6789, dilution 1:500) at 37°C for 30 min and then developed using a chromogen (DAB, Biosharp) for 5 min. The staining intensity scoring method was the same as that used in a previous study (Yang Q. et al., 2021).

Statistical Analysis

Statistical analysis was performed using SPSS (version 22.0; SPSS Inc., Chicago, IL, United States) and GraphPad Prism 8.0.1 (GraphPad Software, San Diego, California, United States). All data were generated from at least three independent experiments, and the results were described as the mean ± standard deviation. Statistical significance was analyzed using a two-tailed Student's t-test and Mann Whitney U test. Survival rates were calculated using the Kaplan-Meier method, and the Cox proportional hazards regression model was performed for the univariate and multivariate analyses.

RESULTS

Confirmation of Radioresistant Cell Line Establishment

Kyse30 cells were exposed to radiation based on a gradient, the cumulative dose reached 60 Gy, and the surviving cells, named Kyse30R, were in a stable state. The radiation sensitivity of Kyse30 cells was determined by several functional experiments. Colony formation and CCK-8 assays revealed that after irradiation, the proliferation of Kyse30 cells was significantly reduced, compared to that of Kyse30R cells ($p < 0.05$, **Supplementary Table S3**, **Figures 1A–C**). Following X-ray exposure, the proportion of cells in the G2/M phases of the cell cycle was lower in Kyse30R cells than in parental Kyse30 cells (**Figure 1D**). Simultaneously, expression of the cycle-related molecule cyclin B1 was higher in Kyse30 cells, compared to that in Kyse30R cells (**Figure 1E**, **Supplementary Figure S1A**). Further, expressions of several apoptosis-related proteins were significantly higher in Kyse30 cells, compared to that in Kyse30R cells, with radiation (**Figure 1F**, **Supplementary Figure S1B**). Moreover, apoptosis analysis revealed that there were fewer Kyse30R apoptotic cells than Kyse30 apoptotic cells after irradiation ($p < 0.05$, **Figures 1G,H**). In addition, we found that both the frequency of γ-H2AX-positive cells and the expression of γ-H2AX in Kyse30 cells were also significantly increased, compared to those in Kyse30R cells, following exposure to irradiation ($p < 0.05$, **Figures 1I,J**, **Supplementary Figures S1C,D**), which indicated more extensive DNA damage in Kyse30 cells. Furthermore, the neutral comet assays revealed DNA double-strand breaks in both Kyse30 and Kyse30R cells after irradiation. Kyse30 cells had longer Olive tails (comets) after electrophoresis, indicating an obviously higher number of double-strand breaks ($p < 0.001$), whereas the damage in Kyse30R cells was not apparent (**Figures 1K,L**). In summary, the radioresistant cell line was successfully established and could be used for further exploration.

Identification and Characterization of Circ-0007022 in Radioresistant ESCC Cells

After the radioresistant cell line was established, the Kyse30 and Kyse30R cell lines were subjected to high-throughput sequencing to explore the potential circRNAs that might play a role in radiation resistance. There were a total of 1,343 known circRNAs differently expressed in both Kyse30R and Kyse30 cells (log2 fold-change ^{3}1, $p < 0.05$). Among these circRNAs, 668 upregulated and 675 downregulated circRNAs were identified in the Kyse30R cell line, compared to levels in the Kyse30 cell line ($p < 0.05$, **Figure 2A**). Among the upregulated circRNAs, circ-0003380, circ-0007022, circ-0023637, circ-0003646, and circ-0007317 were ranked as the top five according to the largest fold-change in expression. Then, we measured the level of expression of the top five circRNAs in tumor tissues of patients who received neoadjuvant chemoradiation, and it was found that circ-0007022, circ-0023637, circ-0003646, and circ-0007317 were significantly upregulated in the SD group compared with expression in the PR group ($p < 0.05$, **Figure 2B**). Thus, combining the fold-change ranking in the high-throughput results and the expression level measured in tumor tissues of patients insensitive to radiotherapy, we finally selected circ-0007022 for further analysis in our study. The expression level of circ-0007022 in the Kyse30R cell line was verified as significantly higher than that in multiple ESCC cell lines ($p < 0.05$, **Figure 2C**). According to the circRNA annotation in the circBase database (http://www.circbase.org/), back-splicing of circ-0007022 corresponds to 635 bp in length and exon 2 of the SAE1 gene on chromosome 19 (chr19:47646750-47673180) (**Figures 2D,E**). The back-splicing sequence was identified

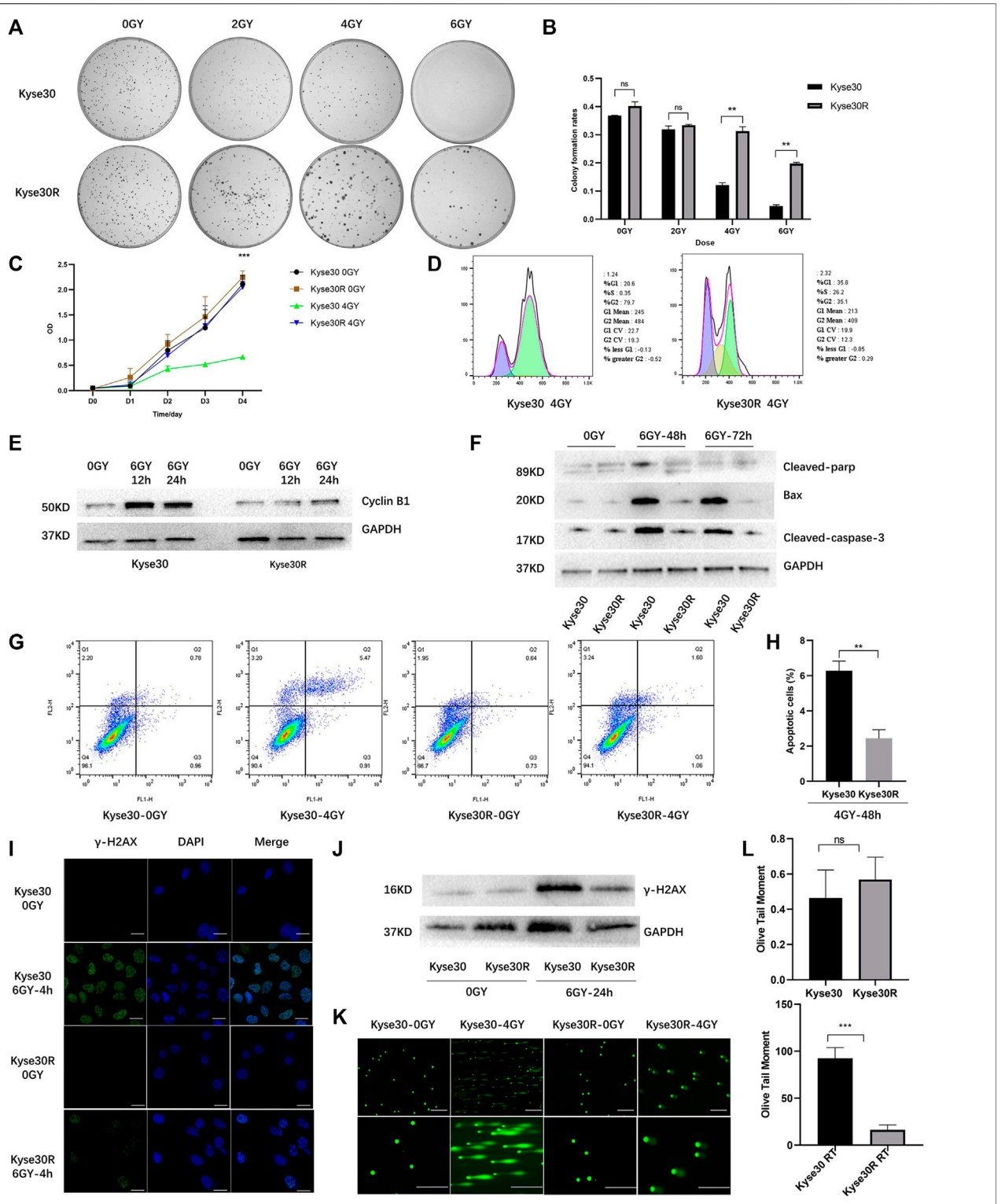

FIGURE 1 | Radioresistant ESCC cell line was established. **(A,B)** Clone formation shown the number of colonies of Kyse30R and Kyse30 cells after irradiation (The Y axis was the ratio of the number of clones to that of cells seeded). **(C)** CCK-8 assays shown the proliferation abilities of Kyse30R and Kyse30 cells after irradiation. **(D,E)** Radiotherapy induced cell cycle arrest in Kyse30R and Kyse30 cells. **(F)** Expressions of several apoptosis-related proteins in Kyse30R and Kyse30 cells. **(G,H)** Radiotherapy induced cell apoptosis in Kyse30R and Kyse30 cells (FL1: Annexin V-FITC, FL2: PI; Q2: Late apoptosis, Q3: Early apoptosis). Immunofluorescence **(I)** (Green, γ-H2AX staining; Blue, DAPI nuclear staining; Scale bar 30 μm), Western blot **(J)** and neutral comet assays **(K, L)** (Scale bar 150 and 100 μm) shown DNA damage in both Kyse30R and Kyse30 cells after radiotherapy. Data are expressed as mean ± SD, ns > 0.05, $^{**}p < 0.01$, $^{***}p < 0.001$.

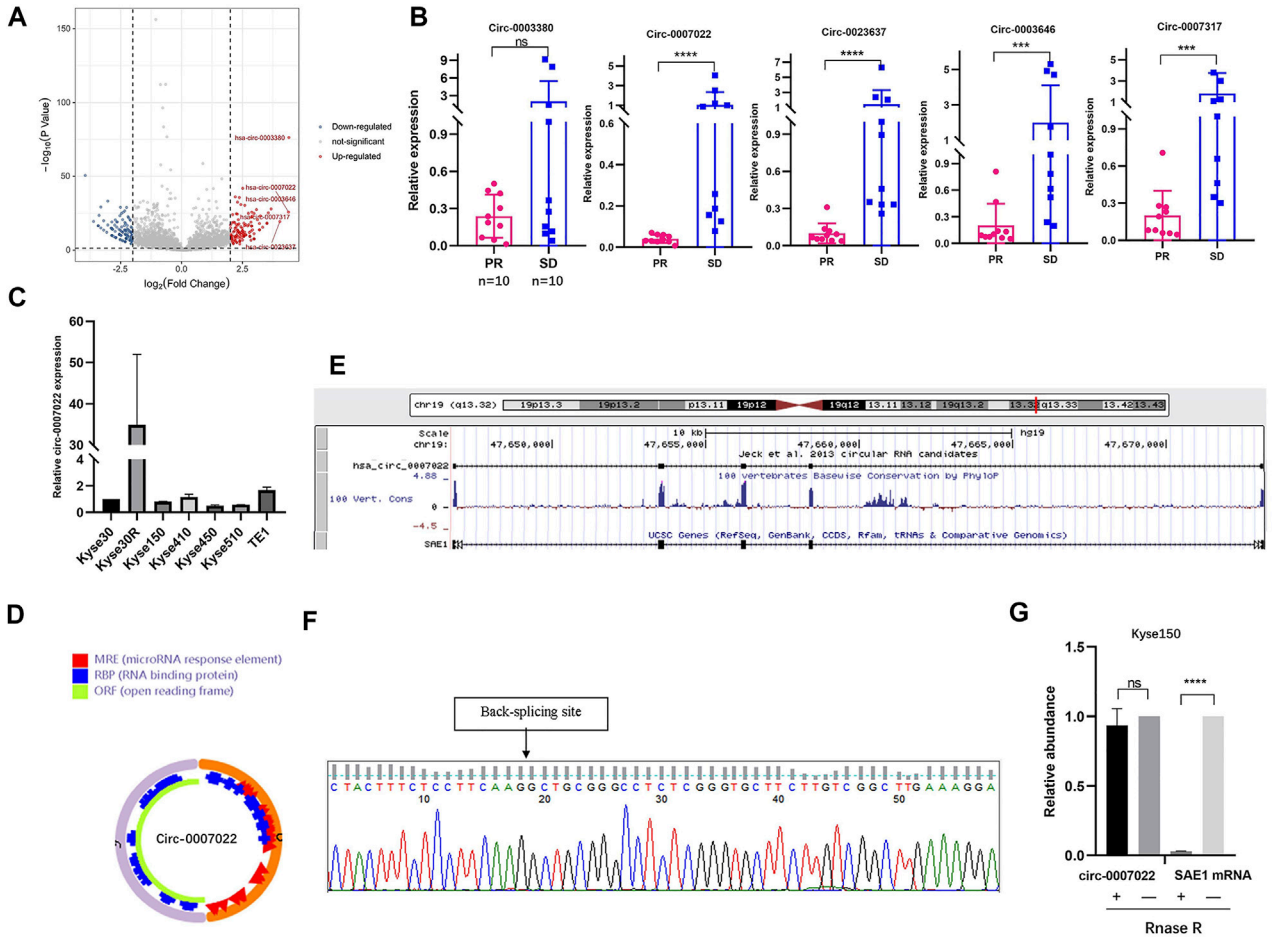

FIGURE 2 | Circ-0007022 expression was upregulated in radioresistant ESCC cell line. **(A)** Volcano plot shown difference in known circRNA expression profiles between Kyse30R and Kyse30 cell lines. **(B)** The qRT-PCR confirmed the different levels of circ-0003380, circ-0007022, circ-0023637, circ-0003646, and circ-0007317 in tumor tissues of ESCC patients. **(C)** The qRT-PCR assay detected the expression of circ-0007022 in multiple ESCC cell lines. **(D,E)** Schematic illustration shown the ring structure of circ-0007022 was composed of two exons (the orange and pink semicircular lines) and the genomic loci circ-0007022. **(F)** Sanger sequencing revealed the "head to tail" splicing sites of circ-0007022 where the arrow pointed. **(G)** RNase R treatment revealed that circ-0007022RNA was resistant to RNase R in ESCC cells, but not mSAE1. Data are expressed as mean ± SD, ns > 0.05, ***$p < 0.001$, ****$p < 0.0001$.

using Sanger sequencing, as described in the circBase database (**Figure 2F**). Moreover, the ability to resist RNase R-mediated digestion of circ-0007022, but not of mSAE1, was verified through qRT-PCR (**Figure 2G**).

Circ-0007022 Reduces the Radiosensitivity of ESCC Cells *In Vitro* and *In Vivo*

To estimate the function of circ-0007022 in ESCC cells, Kyse150 and TE1 cells were transfected with the circ-0007022-overexpression/knockdown plasmids and the corresponding negative controls, named Kyse150-OE, Kyse150-OE-nc, Kyse150-KD, Kyse150-KD-nc, TE1-OE, TE1-OE-nc, TE1-KD, and TE1-KD-nc. In the aforementioned cells, the expression of circ-0007022 changed significantly with the corresponding transfection ($p < 0.05$), but the expression of mSAE1 showed no obvious change (**Figures 3A,B**). The proliferation of both cell lines after radiotherapy was enhanced upon circ-0007022 overexpression, whereas circ-0007022 knockdown suppressed their proliferation (**Figures 3C,D**, **Supplementary Figure S2A**, **Supplementary Table S3**). Circ-0007022 overexpression showed the same effect on migration (**Figures 3E,F**, **Supplementary Figure S2B,C**). To explore whether circ-0007022 regulates the radiosensitivity of ESCC cells *in vivo*, TE1-OE-nc, TE1-OE, Kyse150-OE-nc, and Kyse150-OE cells were injected into BALB/C nude mice subcutaneously, followed by irradiation and analysis. The overexpression of circ-0007022 remarkably increased the growth and weights of the ESCC tumors with radiation ($p < 0.01$, **Figures 3G,H**, **Supplementary Figure S2D**).

Circ-0007022 Functions as a Sponge for miR-338-3p, and NRP1 is a Direct Target of miR-338-3p

RNA interaction prediction tools, including Circular RNA Interactome and Circbank were used to predict the targets of

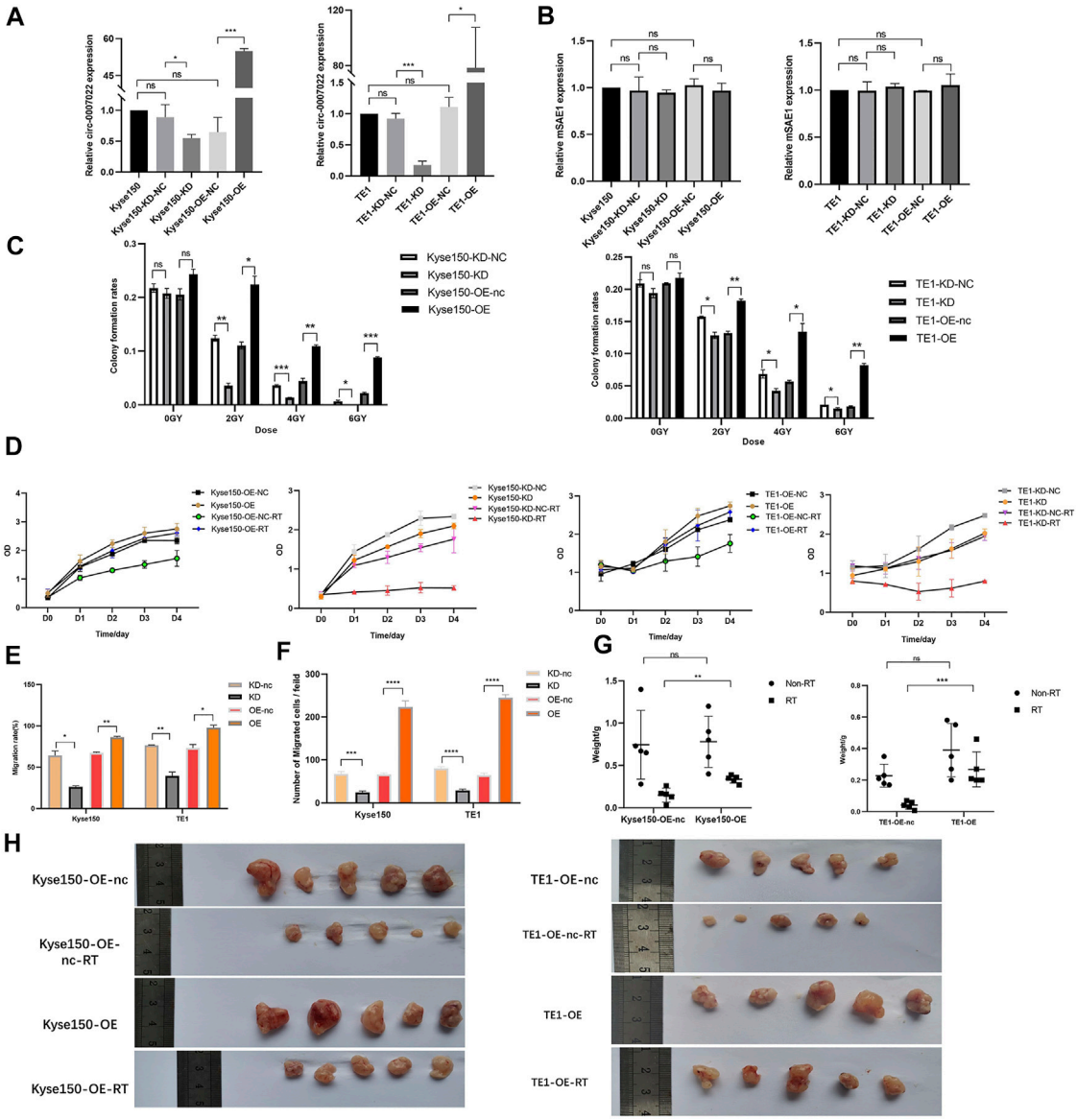

FIGURE 3 | Circ-0007022 reduced radiosensitivity of ESCC cells *in vitro* and *in vivo*. **(A,B)** The qRT-PCR indicated expression levels of circ-0007022 and mSAE1 expression in Kyse150 and TE1 cells after transfection of the overexpression or knockdown plasmids. **(C,D)** Clone formation and CCK-8 assays revealed the proliferation capabilities of Kyse150 and TE1 cells transfected with the overexpression or knockdown plasmids after radiotherapy. **(E,F)** Wound healing and transwell assays assessed cell migration abilities of Kyse150 and TE1 cells, transfected with the overexpression or knockdown plasmids, after radiotherapy. **(G,H)** BALB/C nude mice were treated injected with Kyse150/TE1 cells with transfection of overexpression plasmids or corresponding negative control and received radiation therapy. Tumor wight were detected in each group. Data are expressed as mean ± SD, ns > 0.05, *p < 0.05, **p < 0.01, ***p < 0.001, ****p < 0.0001.

circ-0007022, and the potential interactions between circ-0007022 and four miRNAs are shown (**Supplementary Figure S3A**). Then, qRT-PCR further revealed that in both Kyse150-OE and TE1-OE cell lines, only the expression of miR-338-3p was negatively altered by circ-0007022, but miR-1283, miR-1248 and miR-583 had no stable relationship with the change of circ-0007022 level in these two cell lines (**Figure 4A**). To validate our findings, a dual-luciferase reporter assay was performed, which suggested that the miR-338-3p mimic significantly reduced the relative luciferase activity of the wild-type circ-0007022 reporter vector (circ-0007022-WT vector) compared to that with the circ-0007022-MUT vector (p < 0.05, **Figure 4B**, **Supplementary Figure S3B**). The RIP assay indicated that both circ-0007022 and miR-338-3p were significantly enriched in the immunoprecipitated complexes of Ago2 groups compared to that in IgG groups (**Figure 4C**), which indicated that circ-0007022 functions as a competing endogenous RNA (ceRNA) by recruiting Ago2 to interact with miR-338-3p. Next, the interaction between circ-0007022 and miR-338-3p was also confirmed by RNA pulldown assay (**Figure 4D**). Additionally,

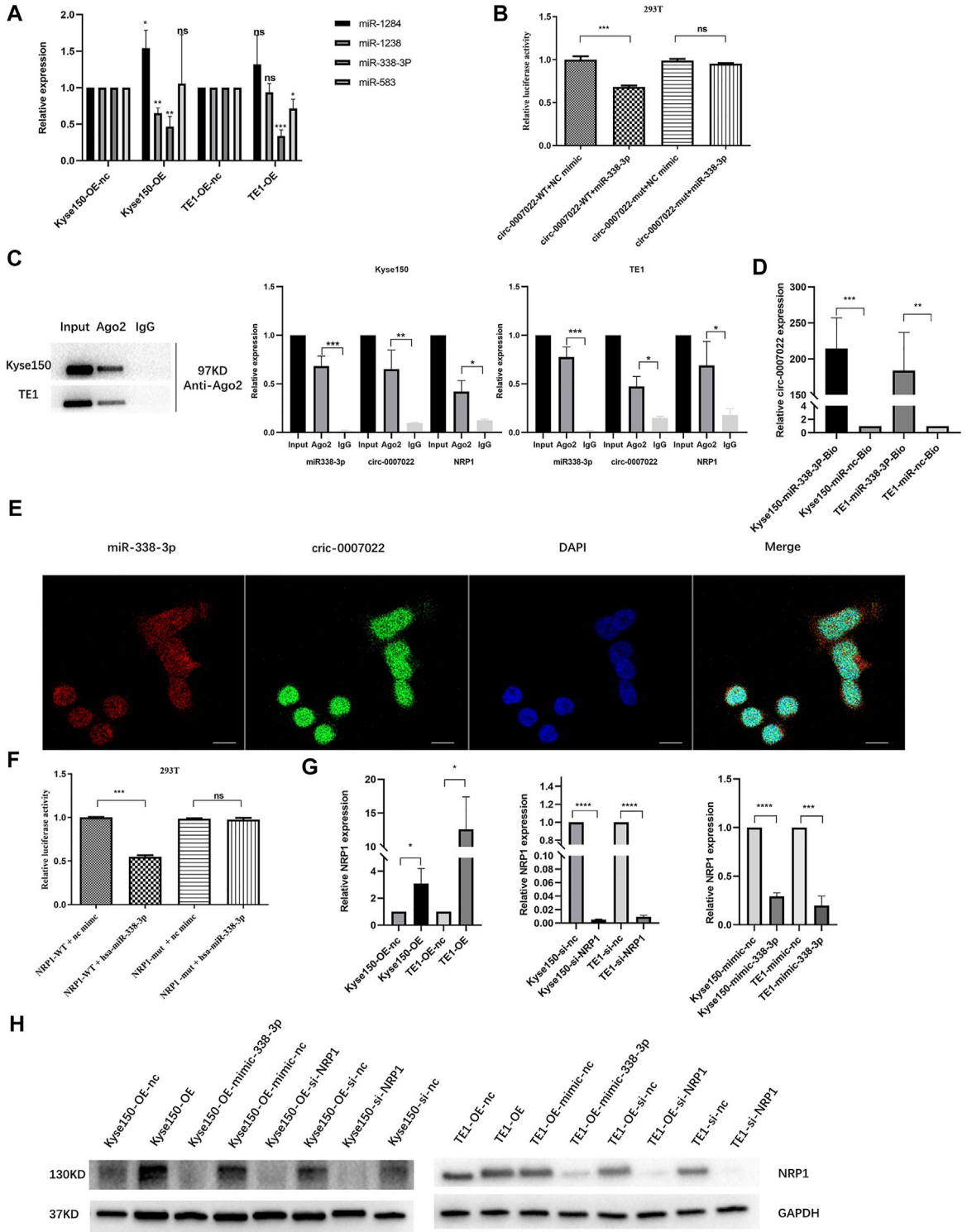

FIGURE 4 | Circ-0007022 functions as a sponge for miR-338-3p, and NRP1 is a direct target of miR-338-3p. **(A)** The qRT-PCR detected relative expression of candidate miRNAs in Kyse150 and TE1 cells transfected with circ-0007022 overexpression or knockdown plasmids. **(B)** The dual luciferase reporter assay indicated that miR-338-3p mimics significantly decreased the luciferase activity of the circ-0007022-WT construct. **(C)** RNA Immunoprecipitation (RIP) analyzed the relationship between circ-0007022 and miR-338-3p, miR-338-3p and NRP1. **(D)** RNA pulldown assays analyzed the relationship between circ-0007022 and miR-338-3p. **(E)** FISH images shown locations of circ-0007022 and miR-338-3p in Kyse150 cells (Red, miR-338-3p probe; Green, circ-0007022 probe; Blue, DAPI nuclear staining; Scale bar 20 μm). **(F)** Luciferase reporter assay confirmed the relationship between miR-338-3p and NRP1. **(G,H)** The qRT-PCR and Western blot revealed NRP1 expression in Kyse150 and TE1 cells after circ-0007022 overexpression, miR-338-3p overexpression or NRP1 knocking down. Data are expressed as mean ± SD, ns > 0.05, *p < 0.05, **p < 0.01, ***p < 0.001, ****p < 0.0001.

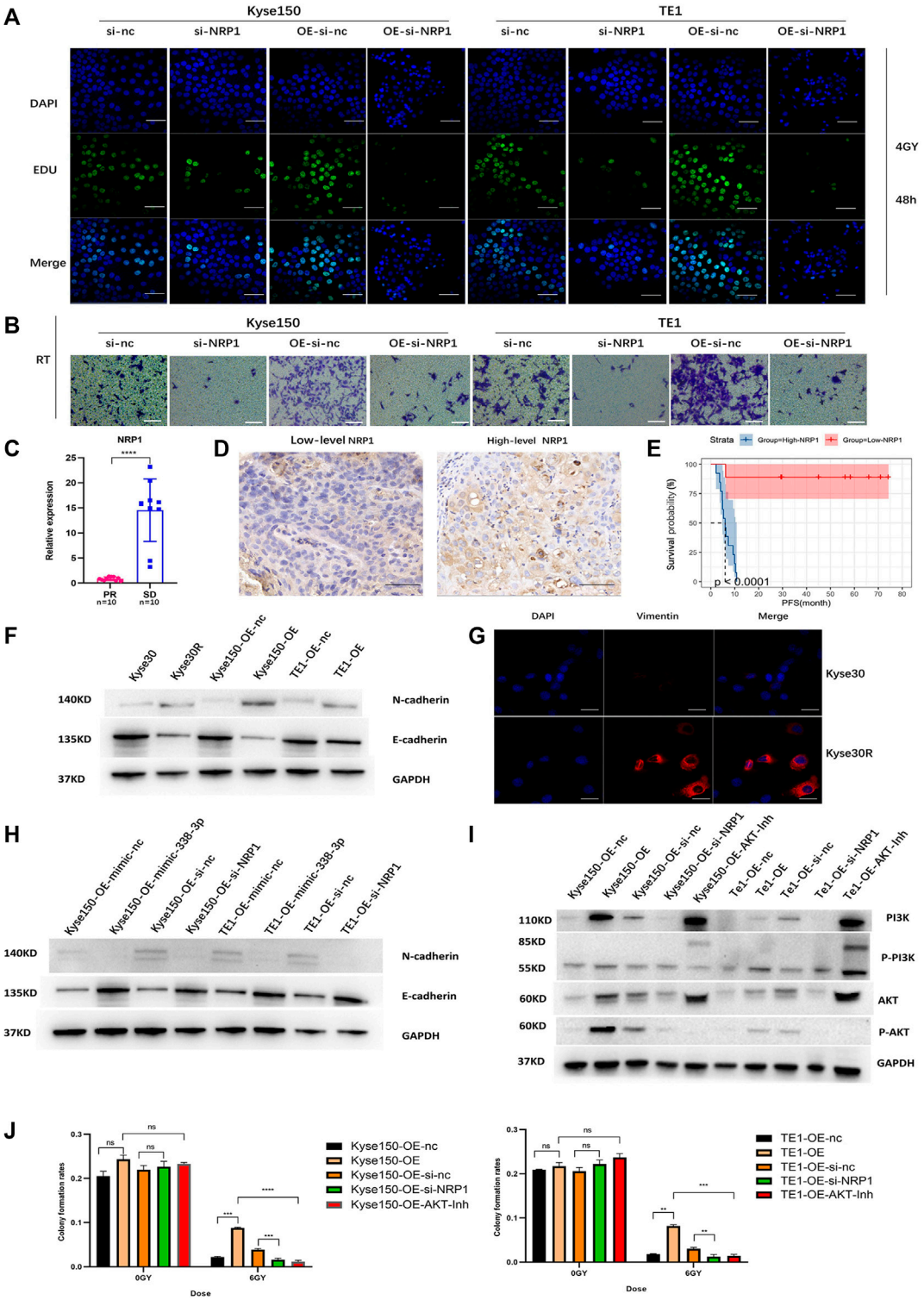

FIGURE 5 | Circ-0007022 activates EMT and PI3K/AKT pathway by regulating the miR-338-3p-NRP1 axis, leading to radio-resistance of ESCC cells. **(A,B)** EDU assay (Green, EDU staining; Blue, DAPI nuclear staining; Scale bar 50 μm) and Transwell assays (Scale bar 50 μm) assessed cell migration and proliferation abilities of Kyse150, TE1, Kyse150-OE and TE1-OE cells, transfected with NRP1 siRNAs, after radiotherapy. **(C)** The qRT-PCR detected the expression level of NRP1 in tumor tissues of patients. **(D)** Immunohistochemical staining image of NRP1 was acquired on tumor tissues from High/Low level group (Scale bar 50 μm). **(E)** Kaplan-Meier analysis showed that the level of NRP1 was predictive of PFS in ESCC patients receiving radiotherapy (PFS, progression-free survival). **(F,G)** Western blot and Immunofluorescence (Red, Vimentin staining; Blue, DAPI nuclear staining; Scale bar 30 μm) analyzed expression change of EMT-related proteins (N-cadherin,

(*Continued*)

FIGURE 5 | E-cadherin and Vimentin) in ESCC cells with circ-0007022 overexpression. **(H)** The relative expressions of N-cadherin and E-cadherin in Kyse150 or TE1 cells after indicated transfection were analyzed by western blot. **(I)** Western blot analyzed expression change of PI3K/AKT pathway related proteins (PI3K, p-PI3K, AKT and p-AKT) in ESCC cells after indicated transfection or AKT inhibitor incubation. **(J)** Clone formation shown the proliferation ability of Kyse150-OE and TE1-OE cells, with si-NRP1 transfection or AKT inhibitor incubation, after irradiation. Data are expressed as mean ± SD, ns > 0.05, $^{**}p < 0.01$, $^{***}p < 0.001$, $^{****}p < 0.0001$.

FISH was performed to validate that circ-0007022 and miR-338-3p were both localized in the same area (**Figure 4E**). NRP1 was identified as one of the potential downstream targets of miR-338-3p after analysis using four authoritative bioinformatics programs, including miRTarBase, miRwalk, miRDB, and TargetScan (**Supplementary Figure S3C**). Additionally, the RIP assay and the dual-luciferase reporter assay also validated their interaction (**Figures 4C,F**, **Supplementary Figure S3D**). Furthermore, qRT-PCR and western blotting revealed changes in NRP1 levels in Kyse150 and TE1 cell lines following circRNA-0007022 and miR-338-3p overexpression and si-NRP1 transfection (**Figure 4G, H**). To summarize, these data suggest that circ-0007022 could sponges miR-338-3p to enhance NRP1 translation, and this ceRNA network might be able to explain how circ-0007022 could reduce the radiosensitivity of ESCC.

Circ-0007022 Activates Epithelial-To-Mesenchymal Transition and PI3K/AKT Pathway by Regulating the miR-338-3p-NRP1 Axis, Leading to Radio-Resistance of ESCC Cells

The EDU and transwell migration assays indicated that silencing NRP1 remarkably decreased the proliferation and migration of Kyse150, TE1, Kyse150-OE and TE1-OE cells exposed to radiation ($p < 0.05$, **Figures 5A,B**, **Supplementary Figure S4A,B**). Subsequently, we analyzed the relationship between the NRP1 level and the prognosis of ESCC patients receiving radiotherapy. On one hand, for ESCC patients administered neoadjuvant chemoradiation, NRP1 was significantly upregulated in the SD group compared with levels in the PR group ($p < 0.05$, **Figure 5C**). On the other hand, for ESCC patients receiving radical radiotherapy with or without concurrent chemotherapy, those with high NRP1 expression had a more unfavorable PFS than those with lower NRP1 expression ($p < 0.0001$, **Figures 5D,E**). Multivariate analysis showed that NRP1 and AJCC staging were independent prognostic indicators for PFS (**Supplementary Table S1**). In order to deeply explore the relationship between NRP1 and radiosensitivity in ESCC, GO (Gene Ontology) analysis (**Supplementary Figure S4C**) and gene set enrichment analysis (**Supplementary Figure S4D**) were performed and found that high NRP1 expression was closely and positively related to EMT activation, indicating EMT might account for the role of NRP1 in ESCC radiotherapy resistance. As expected, western blotting demonstrated increased protein levels of a mesenchymal molecular marker (N-cadherin) but decreased protein levels of an epithelial molecular marker (E-cadherin) following circ-0007022 overexpression (**Figure 5F**, **Supplementary Figure S4E**). Moreover, another mesenchymal molecular marker (Vimentin) was also be found overexpressed in the Kyse30R cell line (**Figure 5G**). Additionally, rescue experiments revealed that the co-transfection of miR-338-3p mimic or si-NRP1 significantly reversed the positive effect on EMT induced by circ-0007022 upregulation (**Figure 5H**, **Supplementary Figure S4F**). Furthermore, inhibition of the PI3K/Akt/mTOR signaling pathway had been found to enhance radiosensitivity of tumor cells. Thus, western blot (**Figure 5I**, **Supplementary Figure S4G**) was performed and shown that, p-AKT was up-regulated with circ-0007022 overexpression, but down-regulated with silencing NRP1 or AKT inhibitor incubated. PI3K had the same changes as p-AKT with circ-0007022 or NRP1 changed. Otherwise, in TE1 cells, AKT inhibitor would enhance the expression of PI3K and p-PI3K, and si-NRP1 also could upregulate the level of p-PI3K. However, there was little difference of the expression of AKT between groups in both two cells or the expression of p-PI3k between groups in Kyse150 cells. Additionally, rescue experiments indicated that both si-NRP1 and AKT inhibitor could reversed radioresistant ability of Kyse150-OE and TE1-OE cells (**Figure 5J**, **Supplementary Figure S4H**). Collectively, the circ-0007022/miR-338-3p/NRP1 axis promotes ESCC radiotherapy-resistance by activating EMT and PI3K/AKT pathway (**Figure 6**).

DISCUSSION

As important non-coding RNAs, circRNAs were considered to have no regulatory effects in the early days of their discovery (Hsu and Coca-Prados, 1979). With the development of RNA sequencing technology, many circRNAs have been identified and been found that they can take part in biological processes, as with linear RNAs (Goodall and Wickramasinghe, 2021). ESCC studies have shown that multiple circRNAs are related to metastasis, migration, invasion, progression, and diagnosis (Hu et al., 2019; Ma et al., 2020; Shi et al., 2020; Zhou et al., 2021). Nevertheless, there is very little research on the role of circRNAs in ESCC radiosensitivity, and there are no reports on the role of circ-0007022 in cancer. Hence, in this study, we first time explored the promoting effect of circ-0007022 on radiotherapy resistance and verified the regulatory network of circ-0007022/miR-338-3p/NRP1 in ESCC.

In this study, we found that patients who were not sensitive to neoadjuvant chemoradiation had a high level of circ-0007022, a new circRNA, indicating that circ-0007022 might be involved in the radioresistance of ESCC. In contrast with a similar previous study (Liu J. et al., 2019), we chose two different ESCC cell lines to explore the function of circ-0007022. Functionally, the downregulation of circ-0007022 inhibited the migration and proliferation of cells after radiation *in vitro* and *in vivo*, whereas circ-0007022 overexpression increased resistance to

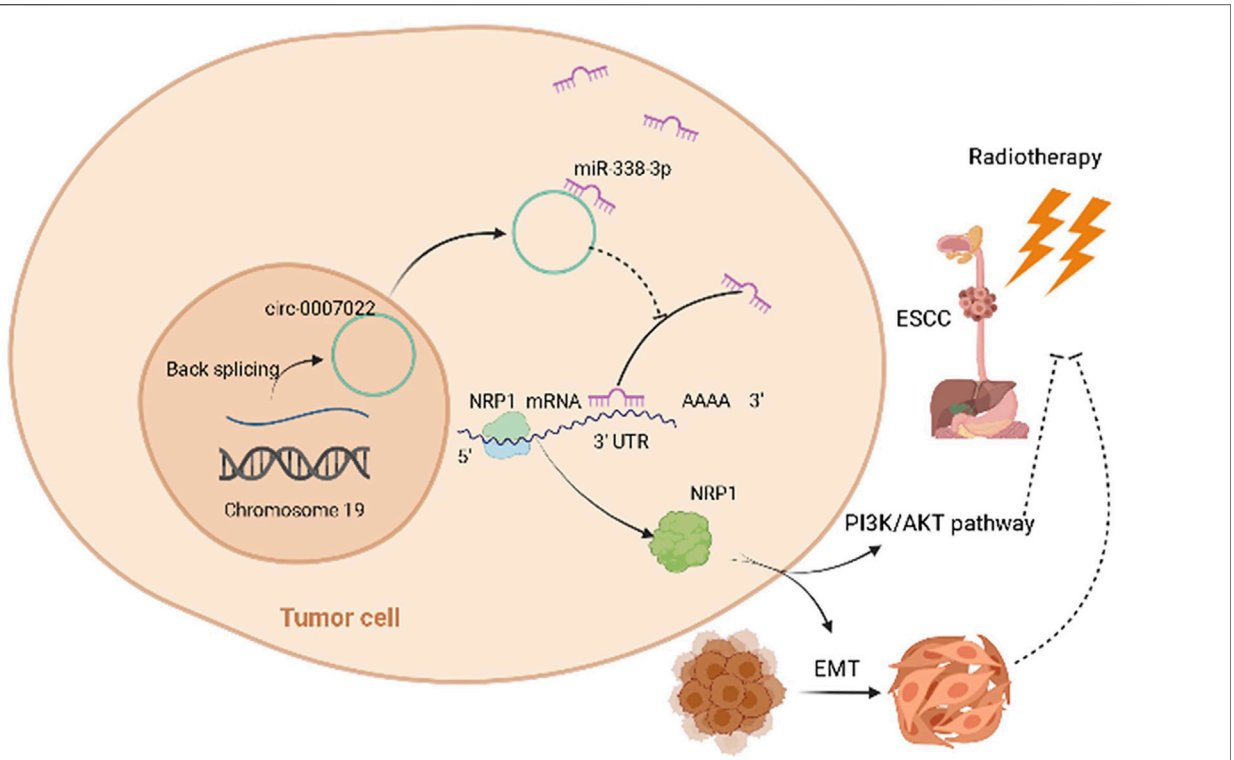

FIGURE 6 | Schematic of the mechanisms of circ-0007022 in the regulation of radiotherapy resistance in ESCC. Circ-0007022/miR-338-3p/NRP1 axis promotes ESCC radiotherapy-resistance by activating EMT and PI3K/AKT pathway.

radiation in ESCC cells. Consequently, our results indicated that circ-0007022 might play a key role in ESCC radiosensitivity. In recent years, studies have found that the most common form of circRNA acts as an miRNA sponge to establish a circRNA/miRNA/mRNA axis (Ng et al., 2018). For example, by sponging miR-200c-3p, circ-001783 regulates the progression of breast cancer (Liu Z. et al., 2019). CircNRIP1 promotes cervical cancer migration and invasion by sponging miR-629-3p and regulating the PTP4A1/ERK1/2 pathway (Li X. et al., 2020). Thus, dual-luciferase reporter assays, RIP, pull-down, and FISH assays were used in the present study to prove the direct association between circ-0007022 and miR-338-3p. We also found that miR-338-3p was significantly downregulated in ESCC cells overexpressing circ-0007022. Moreover, the expression of mSAE1 in ESCC cells overexpressing circ-0007022 was similar to that in ESCC cells after transfection of the corresponding negative control, and thus we reasoned that radiosensitivity was affected by circ-0007022 sponging miR-338-3p, instead of mSAE1 sponging miR-338-3p. In multiple cancers, miR-338-3p functions as a tumor suppressor (Sun et al., 2018; Wang and Qin, 2018; Song et al., 2021). Moreover, miR-338-3p is sponged by circRNAs in tumors, which is consistent with our findings (Xiong et al., 2019; Liu et al., 2020a; Liu et al., 2020b). These findings show that circ-0007022 might exert a negative effect on ESCC radiosensitivity by sponging miR-338-3p.

The ceRNA hypothesis represents a new model of gene expression regulation. Compared with miRNA, the ceRNA regulation network is more sophisticated and complex, and circRNAs can act as ceRNAs to regulate miRNA target gene expression (Salmena et al., 2011). NRP1, a non-tyrosine kinase transmembrane receptor, is highly expressed in many cancers, especially in gastrointestinal cancers, promoting metastasis and proliferation (Li et al., 2016; Zhang et al., 2018; Ding et al., 2019; De Vlaeminck et al., 2020; Abdullah et al., 2021; Wang et al., 2021). A series of experiments indicated that NRP1 is a functional target of miR-338-3p. Meanwhile, circ-0007022 overexpression also increased the expression of NRP1 at the mRNA and protein levels, whereas miR-338-3p mimics had an opposing effect, indicating that the ceRNA network circ-0007022-miR338-3p-NRP1 was stable. Silencing NRP1 led to a decrease in the proliferation and migration of ESCC cells exposed to radiation, and patients with higher NRP1 expression in ESCC tissues exhibited shorter PFS after radiotherapy. All these confirmed our conjecture, specifically that the mechanism of radiation resistance might be associated with an increase in NRP1 expression. In addition, conforming with our bioinformatics analysis, previous research found that NRP1 might modulate EMT to not only contribute to the growth and metastasis of tumors (Chen et al., 2018; Ma et al., 2019; Ding et al., 2020), but also induce drug-resistance and radiation resistance in cancers (Abdullah et al., 2021; Cong et al., 2021). Our results showed that the expression levels of EMT-related markers, including N-cadherin and vimentin, were significantly increased, accompanied by a decrease in E-cadherin, in cells with

radiation resistance and circ-0007022 overexpression. Subsequently, silencing NRP1 reversed the positive effect of circ-0007022 upregulation on EMT. Furthermore, it is known that NRP1 was associated with AKT pathways (Jin et al., 2020), we found circ-0007022-OE upregulated the expression of p-AKT and PI3K, and si-NRP1 may reverse this phenomenon, suggesting that NRP1 upregulated by circ-0007022 could activate PI3K/AKT pathway. Moreover, AKT inhibitor decreased radiation resistance of circ-0007022 overexpression ESCC cells, indicating circ-0007022 could regulate radiosensitivity through PI3K/AKT pathway. In addition, in TE1 cells, the phenomenon that AKT inhibitor and si-NRP1could enhance the expression of p-PI3K might be the result of negative feedback after AKT pathways inhibited. All of these results indicate that the ceRNA network, composed of circ-0007022, miR-338-3p, and NRP1, could affect sensitivity of radiotherapy in ESCC by activating EMT and PI3K/AKT Pathway. In addition, previous studies have found that NRP1 could affect the sensitivity of radiotherapy through NF-κB pathway in non-small cell lung cancer (Dong et al., 2015), so whether other pathways also involved in the process of circ-0007022/miR-338-3p/NRP1 axis' regulation of radiotherapy resistance in ESCC still needs further research explore in the further.

To sum up, our results first time corroborate the hypothesis that the circ-0007022/miR-338-3p/NRP1 axis leads to radiation resistance by activating EMT and PI3K/AKT pathway in ESCC, establishing a circRNA-miRNA-mRNA network. These findings provide new evidence that circRNAs exert functions in ESCC and present several new potential therapeutic targets for reducing radiotherapy failure in patients with ESCC.

DATA AVAILABILITY STATEMENT

The datasets presented in this study can be found in online repositories. The names of the repository/repositories and accession number(s) can be found below:https://www.ncbi.nlm.nih.gov/bioproject/PRJNA808226.

ETHICS STATEMENT

The studies involving human participants were reviewed and approved by the institute ethical committee of Shandong Cancer Hospital and Institute, Shandong First Medical University and Shandong Academy of Medical Sciencese. The patients/participants provided their written informed consent to participate in this study. The animal study was reviewed and approved by the Institutional Animal Care and Use Committee of Shandong Cancer Hospital and Institute, Shandong First Medical University and Shandong Academy of Medical Sciences.

AUTHOR CONTRIBUTIONS

JZ and BL: conception and design; JZ, XY, LF and ZL: carried out the experiments; JZ and XY: acquisition of data; XL and YY: analysis and interpretation of data; JZ, BL, and YY: Writing and revision of the paper. All authors read and approved the final paper.

FUNDING

This study was supported by grants from the National Key Research and Development Program of China (2016YFC0105106); National Natural Science Foundation of China, China (81874224); Academic promotion program of Shandong First Medical University, China (2019LJ004); Taishan Scholar Project of Shandong Province, China (ts20120505); The tumor prevention and control Joint Fund of Shandong province natural science fund, China (ZR2019LZL008); Shandong province post-doctoral innovation projects Jinan (202003083).

ACKNOWLEDGMENTS

The authors thank all members for assistance in various aspects of this work.

SUPPLEMENTARY MATERIAL

The Supplementary Material for this article can be found online at: https://www.frontiersin.org/articles/10.3389/fgene.2022.854097/full#supplementary-material

REFERENCES

Abdullah, A., Akhand, S. S., Paez, J. S. P., Brown, W., Pan, L., Libring, S., et al. (2021). Epigenetic Targeting of Neuropilin-1 Prevents Bypass Signaling in Drug-Resistant Breast Cancer. *Oncogene* 40 (2), 322–333. doi:10.1038/s41388-020-01530-6

Ajani, J. A., D'Amico, T. A., Bentrem, D. J., Chao, J., Corvera, C., Das, P., et al. (2019). Esophageal and Esophagogastric Junction Cancers, Version 2.2019, NCCN Clinical Practice Guidelines in Oncology. *J. Natl. Compr. Canc Netw.* 17 (7), 855–883. doi:10.6004/jnccn.2019.0033

Cao, Y., Mi, X., Zhang, D., Wang, Z., Zuo, Y., and Tang, W. (2020). Transcriptome Sequencing of Circular RNA Reveals a Novel Circular RNA-Has_circ_0114427 in the Regulation of Inflammation in Acute Kidney Injury. *Clin. Sci. (Lond)* 134 (2), 139–154. doi:10.1042/CS20190990

Chen, W., Quan, Y., Fan, S., Wang, H., Liang, J., Huang, L., et al. (2020). Exosome-transmitted Circular RNA Hsa_circ_0051443 Suppresses Hepatocellular Carcinoma Progression. *Cancer Lett.* 475, 119–128. doi:10.1016/j.canlet.2020.01.022

Chen, Z.-P., Wei, J.-C., Wang, Q., Yang, P., Li, W.-L., He, F., et al. (2018). Long Non-coding RNA 00152 F-unctions as a C-ompeting E-ndogenous RNA to R-egulate NRP1 E-xpression by S-ponging with miRNA-206 in C-olorectal C-ancer. *Int. J. Oncol.* 53 (3), 1227–1236. doi:10.3892/ijo.2018.4451

Cong, L., Yi, J., Qiu, S., Wang, R., Jin, S., Jiang, R., et al. (2021). Effect of EG00229 on Radiation Resistance of Lung Adenocarcinoma Cells. *J. Cancer* 12 (20), 6105–6117. doi:10.7150/jca.56123

De Vlaeminck, Y., Bonelli, S., Awad, R. M., Dewilde, M., Rizzolio, S., Lecocq, Q., et al. (2020). Targeting Neuropilin-1 with Nanobodies Reduces Colorectal Carcinoma Development. *Cancers* 12 (12), 3582. doi:10.3390/cancers12123582

Ding, Z., Du, W., Lei, Z., Zhang, Y., Zhu, J., Zeng, Y., et al. (2020). Neuropilin 1 Modulates TGF-β1-induced E-pithelial-mesenchymal T-ransition in N-on-small C-ell L-ung C-ancer. *Int. J. Oncol.* 56 (2), 531–543. doi:10.3892/ijo.2019.4938

Ding, Z., Zhu, J., Zeng, Y., Du, W., Zhang, Y., Tang, H., et al. (2019). The Regulation of Neuropilin 1 Expression by miR-338-3p Promotes Non-small Cell Lung Cancer via Changes in EGFR Signaling. *Mol. Carcinog* 58 (6), 1019–1032. doi:10.1002/mc.22990

Dong, J. C., Gao, H., Zuo, S. Y., Zhang, H. Q., Zhao, G., Sun, S. L., et al. (2015). Neuropilin 1 Expression Correlates with the Radio-Resistance of Human Non-small-cell Lung Cancer Cells. *J. Cel. Mol. Med.* 19 (9), 2286–2295. doi:10.1111/jcmm.12623

Du, W. W., Yang, W., Chen, Y., Wu, Z.-K., Foster, F. S., Yang, Z., et al. (2017). Foxo3 Circular RNA Promotes Cardiac Senescence by Modulating Multiple Factors Associated with Stress and Senescence Responses. *Eur. Heart J.* 38 (18), ehw001–1412. doi:10.1093/eurheartj/ehw001

Fan, L., Cao, Q., Liu, J., Zhang, J., and Li, B. (2019). Circular RNA Profiling and its Potential for Esophageal Squamous Cell Cancer Diagnosis and Prognosis. *Mol. Cancer* 18 (1), 16. doi:10.1186/s12943-018-0936-4

Gao, C., Zhang, Y., Tian, Y., Han, C., Wang, L., Ding, B., et al. (2021). Circ_0055625 Knockdown Inhibits Tumorigenesis and Improves Radiosensitivity by Regulating miR-338-3p/MSI1 axis in colon Cancer. *World J. Surg. Onc* 19 (1), 131. doi:10.1186/s12957-021-02234-1

Goodall, G. J., and Wickramasinghe, V. O. (2021). RNA in Cancer. *Nat. Rev. Cancer* 21 (1), 22–36. doi:10.1038/s41568-020-00306-0

Hansen, T. B. (2018). Improved circRNA Identification by Combining Prediction Algorithms. *Front. Cel Dev. Biol.* 6, 20. doi:10.3389/fcell.2018.00020

Hsu, M.-T., and Coca-Prados, M. (1979). Electron Microscopic Evidence for the Circular Form of RNA in the Cytoplasm of Eukaryotic Cells. *Nature* 280 (5720), 339–340. doi:10.1038/280339a0

Hu, X., Wu, D., He, X., Zhao, H., He, Z., Lin, J., et al. (2019). circGSK3β Promotes Metastasis in Esophageal Squamous Cell Carcinoma by Augmenting β-catenin Signaling. *Mol. Cancer* 18 (1), 160. doi:10.1186/s12943-019-1095-y

Jin, Y., Che, X., Qu, X., Li, X., Lu, W., Wu, J., et al. (2020). CircHIPK3 Promotes Metastasis of Gastric Cancer via miR-653-5p/miR-338-3p-NRP1 Axis under a Long-Term Hypoxic Microenvironment. *Front. Oncol.* 10, 1612. doi:10.3389/fonc.2020.01612

Li, H., Zhi, Y., Ma, C., Shen, Q., Sun, F., and Cai, C. (2020a). Circ_0062020 Knockdown Strengthens the Radiosensitivity of Prostate Cancer Cells. *Cmar* 12, 11701–11712. doi:10.2147/CMAR.S273826

Li, L., Jiang, X., Zhang, Q., Dong, X., Gao, Y., He, Y., et al. (2016). Neuropilin-1 Is Associated with Clinicopathology of Gastric Cancer and Contributes to Cell Proliferation and Migration as Multifunctional Co-receptors. *J. Exp. Clin. Cancer Res.* 35, 16. doi:10.1186/s13046-016-0291-5

Li, X., Ma, N., Zhang, Y., Wei, H., Zhang, H., Pang, X., et al. (2020b). Circular RNA circNRIP1 Promotes Migration and Invasion in Cervical Cancer by Sponging miR-629-3p and Regulating the PTP4A1/ERK1/2 Pathway. *Cell Death Dis* 11 (5), 399. doi:10.1038/s41419-020-2607-9

Li, Y., Zheng, Q., Bao, C., Li, S., Guo, W., Zhao, J., et al. (2015). Circular RNA Is Enriched and Stable in Exosomes: a Promising Biomarker for Cancer Diagnosis. *Cell Res* 25 (8), 981–984. doi:10.1038/cr.2015.82

Liu, C., Yao, M.-D., Li, C.-P., Shan, K., Yang, H., Wang, J.-J., et al. (2017). Silencing of Circular RNA-Znf609 Ameliorates Vascular Endothelial Dysfunction. *Theranostics* 7 (11), 2863–2877. doi:10.7150/thno.19353

Liu, G., Guo, W., Rao, M., Qin, J., Hu, F., and Li, K. (2020a). circRNA Hsa_circ_104566 Sponged miR-338-3p to Promote Hepatocellular Carcinoma Progression. *Cel Transpl.* 29, 096368972096394. doi:10.1177/0963689720963948

Liu, G., Wan, Q., Li, J., Hu, X., Gu, X., and Xu, S. (2020b). Circ_0038467 Regulates Lipopolysaccharide-induced Inflammatory Injury in Human Bronchial Epithelial Cells through Sponging miR-338-3p. *Thorac. Cancer* 11 (5), 1297–1308. doi:10.1111/1759-7714.13397

Liu, J., Xue, N., Guo, Y., Niu, K., Gao, L., Zhang, S., et al. (2019a). CircRNA_100367 Regulated the Radiation Sensitivity of Esophageal Squamous Cell Carcinomas through miR-217/Wnt3 Pathway. *Aging* 11 (24), 12412–12427. doi:10.18632/aging.102580

Liu, Z., Zhou, Y., Liang, G., Ling, Y., Tan, W., Tan, L., et al. (2019b). Circular RNA Hsa_circ_001783 Regulates Breast Cancer Progression via Sponging miR-200c-3p. *Cel Death Dis* 10 (2), 55. doi:10.1038/s41419-018-1287-1

Luo, Q., Guo, F., Fu, Q., and Sui, G. (2021). hsa_circ_0001018 Promotes Papillary Thyroid Cancer by Facilitating Cell Survival, Invasion, G1/S Cell Cycle Progression, and Repressing Cell Apoptosis via Crosstalk with miR-338-3p and SOX4. *Mol. Ther. - Nucleic Acids* 24, 591–609. doi:10.1016/j.omtn.2021.02.023

Ma, L., Zhai, B., Zhu, H., Li, W., Jiang, W., Lei, L., et al. (2019). The miR-141/neuropilin-1 axis Is Associated with the Clinicopathology and Contributes to the Growth and Metastasis of Pancreatic Cancer. *Cancer Cel Int* 19, 248. doi:10.1186/s12935-019-0963-2

Ma, Y., Zhang, D., Wu, H., Li, P., Zhao, W., Yang, X., et al. (2020). Circular RNA PRKCI Silencing Represses Esophageal Cancer Progression and Elevates Cell Radiosensitivity through Regulating the miR-186-5p/PARP9 axis. *Life Sci.* 259, 118168. doi:10.1016/j.lfs.2020.118168

Murphy, G., McCormack, V., Abedi-Ardekani, B., Arnold, M., Camargo, M. C., Dar, N. A., et al. (2017). International Cancer Seminars: a Focus on Esophageal Squamous Cell Carcinoma. *Ann. Oncol.* 28 (9), 2086–2093. doi:10.1093/annonc/mdx279

Ng, W. L., Mohd Mohidin, T. B., and Shukla, K. (2018). Functional Role of Circular RNAs in Cancer Development and Progression. *RNA Biol.* 15 (8), 1–11. doi:10.1080/15476286.2018.1486659

Phatak, P., and Donahue, J. (2017). Biotinylated Micro-RNA Pull Down Assay for Identifying miRNA Targets. *Bio-protocol* 7 (9), e2253. doi:10.21769/BioProtoc.2253

Salmena, L., Poliseno, L., Tay, Y., Kats, L., and Pandolfi, P. P. (2011). A ceRNA Hypothesis: the Rosetta Stone of a Hidden RNA Language? *Cell* 146 (3), 353–358. doi:10.1016/j.cell.2011.07.014

Shi, Y., Fang, N., Li, Y., Guo, Z., Jiang, W., He, Y., et al. (2020). Circular RNA LPAR3 Sponges microRNA-198 to Facilitate Esophageal Cancer Migration, Invasion, and Metastasis. *Cancer Sci.* 111 (8), 2824–2836. doi:10.1111/cas.14511

Song, Y., Zhang, F., Li, L., Song, B., Xu, J., Wang, G., et al. (2021). MiR-338-3p Inhibits Growth of Glioblastoma through Targeting MAP4K3. *Minerva Med.* 112 (4), 531–533. doi:10.23736/S0026-4806.19.06251-7

Sun, F., Yu, M., Yu, J., Liu, Z., Zhou, X., Liu, Y., et al. (2018). miR-338-3p Functions as a Tumor Suppressor in Gastric Cancer by Targeting PTP1B. *Cel Death Dis* 9 (5), 522. doi:10.1038/s41419-018-0611-0

Sung, H., Ferlay, J., Siegel, R. L., Laversanne, M., Soerjomataram, I., Jemal, A., et al. (2021). Global Cancer Statistics 2020: GLOBOCAN Estimates of Incidence and Mortality Worldwide for 36 Cancers in 185 Countries. *CA A. Cancer J. Clin.* 71 (3), 209–249. doi:10.3322/caac.21660

Wang, S., Zhang, Z., and Gao, Q. (2021). Transfer of microRNA-25 by Colorectal Cancer Cell-Derived Extracellular Vesicles Facilitates Colorectal Cancer Development and Metastasis. *Mol. Ther. - Nucleic Acids* 23, 552–564. doi:10.1016/j.omtn.2020.11.018

Wang, Y., and Qin, H. (2018). miR-338-3p Targets RAB23 and Suppresses Tumorigenicity of Prostate Cancer Cells. *Am. J. Cancer Res.* 8 (12), 2564–2574. doi:10.1186/s13578-018-0252-0

Xiong, Z., Zhou, C., Wang, L., Zhu, R., Zhong, L., Wan, D., et al. (2019). Circular RNA SMO Sponges miR-338-3p to Promote the Growth of Glioma by Enhancing the Expression of SMO. *Aging* 11 (24), 12345–12360. doi:10.18632/aging.102576

Yang, C., Mou, Z., Wu, S., Ou, Y., Zhang, Z., Chen, X., et al. (2021a). High-throughput Sequencing Identified Circular RNA circUBE2K Mediating RhoA Associated Bladder Cancer Phenotype via Regulation of miR-516b-5p/ARHGAP5 axis. *Cel Death Dis* 12 (8), 719. doi:10.1038/s41419-021-03977-1

Yang, Q., Zhang, J., Zhang, X., Miao, L., Zhang, W., Jiang, Z., et al. (2021b). C-C Motif Chemokine Ligand 2/C-C Receptor 2 Is Associated with Glioma Recurrence and Poor Survival. *Exp. Ther. Med.* 21 (6), 564. doi:10.3892/etm.2021.9996

Yang, Z., Wu, H., Zhang, K., Rao, S., Qi, S., Liu, M., et al. (2022). Circ_0007580 Knockdown Strengthens the Radiosensitivity of Non-small Cell Lung Cancer via the miR -598-dependent Regulation of THBS2. *Thorac. Cancer* 13, 678–689. doi:10.1111/1759-7714.14221

Yu, J., Xu, Q.-g., Wang, Z.-g., Yang, Y., Zhang, L., Ma, J.-z., et al. (2018). Circular RNA cSMARCA5 Inhibits Growth and Metastasis in Hepatocellular Carcinoma. *J. Hepatol.* 68 (6), 1214–1227. doi:10.1016/j.jhep.2018.01.012

Zeng, K., Wang, Z., Ohshima, K., Liu, Y., Zhang, W., Wang, L., et al. (2016). BRAFV600E Mutation Correlates with Suppressive Tumor Immune Microenvironment and Reduced Disease-free Survival in Langerhans Cell Histiocytosis. *Oncoimmunology* 5 (7), e1185582. doi:10.1080/2162402X.2016.1185582

Zhang, C., Han, X., Yang, L., Fu, J., Sun, C., Huang, S., et al. (2020). Circular RNA circPPM1F Modulates M1 Macrophage Activation and Pancreatic Islet Inflammation in Type 1 Diabetes Mellitus. *Theranostics* 10 (24), 10908–10924. doi:10.7150/thno.48264

Zhang, G., Chen, L., Khan, A. A., Li, B., Gu, B., Lin, F., et al. (2018). miRNA-124-3p/neuropilin-1(NRP-1) axis Plays an Important Role in Mediating Glioblastoma Growth and Angiogenesis. *Int. J. Cancer* 143 (3), 635–644. doi:10.1002/ijc.31329

Zhang, S., Zhu, D., Li, H., Li, H., Feng, C., and Zhang, W. (2017). Characterization of circRNA-Associated-ceRNA Networks in a Senescence-Accelerated Mouse Prone 8 Brain. *Mol. Ther.* 25 (9), 2053–2061. doi:10.1016/j.ymthe.2017.06.009

Zhou, P. L., Wu, Z., Zhang, W., Xu, M., Ren, J., Zhang, Q., et al. (2021). Circular RNA Hsa_circ_0000277 Sequesters miR-4766-5p to Upregulate LAMA1 and Promote Esophageal Carcinoma Progression. *Cel Death Dis* 12 (7), 676. doi:10.1038/s41419-021-03911-5

Conflict of Interest: The authors declare that the research was conducted in the absence of any commercial or financial relationships that could be construed as a potential conflict of interest.

Publisher's Note: All claims expressed in this article are solely those of the authors and do not necessarily represent those of their affiliated organizations, or those of the publisher, the editors and the reviewers. Any product that may be evaluated in this article, or claim that may be made by its manufacturer, is not guaranteed or endorsed by the publisher.

frontiers | Frontiers in Genetics

ORIGINAL RESEARCH
published: 09 May 2022
doi: 10.3389/fgene.2022.804614

N6-Methyladenosine-Related lncRNAs Are Novel Prognostic Markers and Predict the Immune Landscape in Acute Myeloid Leukemia

Lulu Zhang[1], Wen Ke[2], Pin Hu[1], Zhangzhi Li[1], Wei Geng[1], Yigang Guo[1], Bin Song[1], Hua Jiang[1], Xia Zhang[1] and Chucheng Wan[1]*

[1]Department of Hematology, Taihe Hospital, Hubei University of Medicine, Shiyan, China, [2]Department of Osteology, Taihe Hospital, Hubei University of Medicine, Shiyan, China

Background: Acute myelocytic leukemia (AML) is one of the hematopoietic cancers with an unfavorable prognosis. However, the prognostic value of N 6-methyladenosine-associated long non-coding RNAs (lncRNAs) in AML remains elusive.

Materials and Methods: The transcriptomic data of m6A-related lncRNAs were collected from The Cancer Genome Atlas (TCGA) and the Gene Expression Omnibus (GEO) database. AML samples were classified into various subgroups according to the expression of m6A-related lncRNAs. The differences in terms of biological function, tumor immune microenvironment, copy number variation (CNV), and drug sensitivity in AML between distinct subgroups were investigated. Moreover, an m6A-related lncRNA prognostic model was established to evaluate the prognosis of AML patients.

Results: Nine prognosis-related m6A-associated lncRNAs were selected to construct a prognosis model. The accuracy of the model was further determined by the Kaplan–Meier analysis and time-dependent receiver operating characteristic (ROC) curve. Then, AML samples were classified into high- and low-risk groups according to the median value of risk scores. Gene set enrichment analysis (GSEA) demonstrated that samples with higher risks were featured with aberrant immune-related biological processes and signaling pathways. Notably, the high-risk group was significantly correlated with an increased ImmuneScore and StromalScore, and distinct immune cell infiltration. In addition, we discovered that the high-risk group harbored higher IC50 values of multiple chemotherapeutics and small-molecule anticancer drugs, especially TW.37 and MG.132. In addition, a nomogram was depicted to assess the overall survival (OS) of AML patients. The model based on the median value of risk scores revealed reliable accuracy in predicting the prognosis and survival status.

Conclusion: The present research has originated a prognostic risk model for AML according to the expression of prognostic m6A-related lncRNAs. Notably, the signature might also serve as a novel biomarker that could guide clinical applications, for example, selecting AML patients who could benefit from immunotherapy.

Keywords: m6A modification, long non-coding RNA, acute myeloid leukemia, prognosis, immune infiltration, copy number variation

OPEN ACCESS

Edited by:
Rajesh Pandey,
CSIR-Institute of Genomics and Integrative Biology (CSIR-IGIB), India

Reviewed by:
Ezhilarasi Chendamarai,
Washington University in St. Louis, United States
Christos K. Kontos,
National and Kapodistrian University of Athens, Greece

****Correspondence:***
Lulu Zhang
zhanglulu@hbmu.edu.cn

Specialty section:
This article was submitted to RNA, a section of the journal Frontiers in Genetics

Received: *29 October 2021*
Accepted: *06 April 2022*
Published: *09 May 2022*

Citation:
Zhang L, Ke W, Hu P, Li Z, Geng W, Guo Y, Song B, Jiang H, Zhang X and Wan C (2022) N6-Methyladenosine-Related lncRNAs Are Novel Prognostic Markers and Predict the Immune Landscape in Acute Myeloid Leukemia. Front. Genet. 13:804614. doi: 10.3389/fgene.2022.804614

INTRODUCTION

Acute myelocytic leukemia (AML) is one of the most common hematopoietic malignancies in adults. AML is featured with the infiltration of malignant myeloid progenitor cells into the peripheral blood, bone marrow, and other tissues, which often progress rapidly leading to poor prognosis (De Kouchkovsky and Abdul-Hay, 2016; Papaemmanuil et al., 2016). In the past 15 years, basic and translational research, such as large-scale genomic analyses, has greatly improved our understanding of the molecular and genetic pathogenesis of AML. As a result, many new and effective targeted therapies have been developed. These include protein kinase small-molecule inhibitors such as gilteritinib (Perl et al., 2019), enasidenib (Stein et al., 2017), and ivosidenib (Dinardo et al., 2018); immune checkpoint antibody such as gemtuzumab (Vago and Gojo, 2020); and mitochondrial inhibitor venetoclax (Candon, 2018; Ram et al., 2019). Despite these advances, the prognosis of AML is still poor with a 5-year overall survival (OS) rate of approximately 10% (Dewolf and Tallman, 2020). Therefore, there is a great need to learn more insights into the molecular pathogenesis of AML for the development of novel therapies.

N 6-Methyladenosine (m6A) RNA modification has been reported to play an important role in AML *via* multiple pathophysiological mechanisms (Zheng and Gong, 2021). Numerous studies have described that methyltransferases ("writers") [METTL3 (Vu et al., 2017), METTL14 (Weng et al., 2018), WTAP (Naren et al., 2021)], demethylases ("erasers") [FTO (Qing et al., 2021a), ALKBH5 (Shen et al., 2020; Wang et al., 2020)], and the common m6A binding protein ("reader") [YTHDF2 (Paris et al., 2019)] were significantly upregulated in different subtypes of AML. These findings indicated that the transcriptome level of m6A regulators may be important diagnostic and prognostic biomarkers for AML patients. Moreover, the overexpression of IGF2BP1 ("reader") promoted the chemotherapeutic resistance of tumor cells by activating many stemness-related signaling *via* transcription regulation or metabolic reprogramming (Elcheva et al., 2020). Interestingly, the inhibition of METTL14, FTO, ALKBH,5 or YTHDF2 only weakly interrupted normal hematopoiesis compared with leukemogenesis. In addition, m6A was reported to be crucial in the initiation and progression of AML, indicating that targeting m6A regulators could be used for the elimination of leukemia cells. It has been reported that inhibiting FTO could decrease the expression level of immune checkpoints in an m6A-dependent manner, which significantly increased the AML cell sensitivity to T-cell-based killing and overcoming decitabine-mediated immune evasion (Su et al., 2020). Nonetheless, the underlying mechanisms by which m6A regulate AML pathophysiology remains to be clarified in order to develop effective and safe pharmaceutical inhibitors targeting m6A regulators.

There were several long non-coding RNAs (lncRNAs) that have been implicated with the growth, metastasis, and apoptotic cell death of AML cells, thus affecting the progression of AML and patient's survival. For example, linc00239 has been shown to downregulate the efficacy of doxorubicin and negatively regulate the apoptosis of AML cells (Yang et al., 2019). lncRNA HOTTIP (Zhuang et al., 2019) was specifically upregulated in the microenvironment of bone marrow in patients with the AML M5 subtype. Furthermore, some lncRNAs were considered as tumor-resistant factors in AML. For example, lncRNA H22954 was decreased in the bone marrow of AML patients, which was correlated with an increased risk of disease relapse. H22954 upregulation blocked AML proliferation and promoted cell apoptosis. Furthermore, H22954 overexpression decreased tumor growth in animal models *via* the BCL-2-dependent mechanism (Qi et al., 2019). Nonetheless, the role of m6A-associated lncRNAs in AML remains unclear. Thus, understanding the expression pattern and prognostic role of m6A-associated lncRNAs in AML is of great importance.

In the present study, we established an m6A-related lncRNA-based prognostic model (FAM30A, HCP5, LINC00342, LINC00963, MEG3, HCG18, TMEM147-AS1, N4BP2L2-IT2, and TTTY15) which harbored a satisfied accuracy in predicting the OS of patients with AML in an independent manner. We also divided the AML patients into two clusters based on the risk scores of the model. Gene set enrichment analysis (GSEA) indicated that increased risk scores were associated with immune-related biological processes and signaling pathways. Our results also demonstrated a higher risk score was highly related to increased ImmuneScore and StromalScore, and distinct immune cell infiltration. The analysis of copy number data showed that the low-risk group was mainly manifested with gene amplification; however, the high-risk group was more associated with the censoring of gene copy numbers. Notably, the samples with increased risk scores harbored higher IC50 values of multiple chemotherapeutic drugs.

MATERIALS AND METHODS

Data Preparation and Preprocessing

Transcriptome materials in fragments per kilobase of transcript per million mapped reads (FPKM) form of AML was collected from The Cancer Genome Atlas (TCGA) GDC data portal (https://portal.gdc.cancer.gov/). Then, transcripts were labeled with either mRNA or lncRNA and extracted as an independent matrix, respectively. Furthermore, the FPKM value was converted to transcripts per million read (TPM) value. Clinical information, including age, gender, and survival of the corresponding patients, was acquired from TCGA. After the deletion of samples with incomplete clinical information, 130 tumor tissues were included in the present study. In addition, the copy number variations (CNVs) of these patients were downloaded in masked somatic mutation annotation, which was utilized to visualize somatic mutations using R package "maftools" (Mayakonda et al., 2018).

Microarray data GSE37642 (Li et al., 2013; Herold et al., 2014; Kuett et al., 2015; Herold et al., 2018) was extracted from the Gene Expression Omnibus (GEO) database (http://www.ncbi.nlm.nih.gov/geo). GSE37642 was retrieved from the GPL570 platform (HG-U133_Plus_2) Affymetrix Human Genome U133 Plus 2.0 Array and GPL96 platform (HG-U133A) Affymetrix Human

Genome U133A Array. The data type was microarray data, and the species was *Homo sapiens*, which included 562 tissue samples of AML (**Supplementary Table S1**). After the deletion of samples with incomplete survival information, 553 AML tissue samples were obtained. Subsequently, the mRNA and lncRNA expression data from TCGA and GEO were merged separately, and R package "sva" was applied for standardization and removing batch effects.

M6A-Related lncRNA Risk Model Construction

The expression and co-expression of m6A-related genes in AML were studied. Next, we calculated the correlation coefficient and *p* value between m6A-related genes and lncRNA profiles, and m6A-related lncRNAs were identified according to the standard of $p < 0.05$ in the correlation analysis as mentioned in previous studies (Zhang P. et al., 2021; Zhao et al., 2021). Moreover, we incorporated the expression of m6A-related lncRNA in TCGA and the GEO database into model construction. R package "random Forest" was utilized to build a random forest model, which was an m6A-related lncRNA risk assessment model for AML patients, and divided AML patients into high- and low-risk groups according to the median of risk scores.

Differentially Expressed Gene Analysis Based on Related Risk Scoring Model of m6A-Related lncRNA Genes

The DESeq2 algorithm (Love et al., 2014) and limma package (Ritchie et al., 2015) in Bioconductor were conducted for sequencing and microarray matrix to screen the DEGs between high- and low-risk groups of AML patients. The cutoff value for screening was $|\log \text{fold change (FC)}| > 0.5$ and adjusted *p* value <0.05. Then, the selected DEGs were used to draw a heatmap and volcano plot. The Venn diagram displayed overlapped DEGs between two datasets.

Functional and Pathway Enrichment Analysis

Gene ontology (GO) analysis serves as a bioinformatics tool that provides systematic annotations, containing molecular functions (MFs), biological processes (BPs), and cellular components (CCs). Kyoto encyclopedia of genes and genomes (KEGG) is a widely utilized database for understanding information about biological pathways, genomes, drugs, and diseases. GO annotations and KEGG pathway enrichment analysis of overlapped DEGs were conducted using the R package "clusterProfiler" (Yu et al., 2012), and items with a false discovery rate (FDR) < 0.05 were considered statistically significant.

In order to explore the differences in biological processes between different groups, we performed gene set enrichment analysis (GSEA) according to the gene expression profiles of AML samples. GSEA is a statistical algorithm to evaluate whether *a priori*-defined gene sets showed statistically significant and consistent differences between two different biological statuses (Subramanian et al., 2005). It is usually performed to estimate variations in pathway and biological process activity samples undergoing high-through sequencing. GSEA was performed based on the "h.all.v7.2.symbols.gmt" gene set (Subramanian et al., 2005) downloaded using the MSigDB database. Adjusted p value < 0.05 was considered as statistically significant.

Identification of Intra-Tumoral Infiltrated Immune Cells and Correlation Analysis

The CIBERSORT algorithm and LM22 matrix (Newman et al., 2015) were applied to assess the percentage of immune–stromal components in the tumor microenvironment (TME) for each AML sample. A total of 22 distinct immune cell types in the TME of AML samples were distinguished as highly sensitive and specific. CIBERSORT is a deconvolution algorithm using transcriptomic data (with 547 characteristic genes) (Newman et al., 2015), which was considered to be the smallest representative of each cell type. We calculated the cellular components of tumor samples according to the gene expression profile of the tissue using CIBERSORT.

Meanwhile, the R package "ESTIMATE" (Yoshihara et al., 2013) was implemented to assess the immune activity in tumors. ESTIMATE analysis quantified the infiltrated immune cells in the tumor tissues according to their gene expression values and obtained the immune score for each sample. The differences in the features of immune infiltration in AML patients between the high- and low-risk groups were compared.

Copy Number Variation Analysis

In order to analyze the copy number changes in groups with different risk scores of TCGA-AML patients, masked copy number segment data were downloaded using TCGAbiolinks package. GISTIC 2.0 was applied to perform analysis with downloaded CNV fragments through GenePattern5. During the analysis, except for a few parameters (e.g., the confidence setting is 0.99; the X chromosome is not excluded prior to the analysis), GISTIC 2.0 analysis chose the default settings. In the end, the Maftools package (Mayakonda et al., 2018) was conducted to visualize the analysis results of GISTIC 2.0.

Analysis of Drug Sensitivity in Cancer

The Genomics of Drug Sensitivity in Cancer (GDSC) database (https://www.cancerrxgene.org/) (Yang et al., 2013) is a public database for cancer molecular therapy and mutation exploration. The cell line gene mutation data and IC50 values of different anticancer drugs were downloaded using R package "pRRophetic" (Geeleher et al., 2014), and then a ridge regression model was constructed to perform a correlation between patients with different risk scores and the sensitivity to different anticancer drugs.

Construction of Clinical Prognostic Model Based on m6A-Related lncRNA Risk Model

In order to investigate whether the risk scores could reflect patients' prognoses and serve as independent factors beyond

clinicopathological characteristics, univariate and multivariate Cox regression analyses were thereafter conducted. A nomogram was depicted with risk scores and clinicopathological features incorporated. Harrell's consistency index (C-index) was generated to quantify the discrimination performance. Subsequently, a calibration curve was generated to test the performance of the constructed nomogram by comparing the difference between the predicted and real OS of patients with AML. Moreover, decision curve analysis (DCA) was employed to evaluate the clinical values of the model.

Statistical Analysis

Statistical analyses were conducted *via* R software (version4.0.2, http://www.R-project.org). When comparing two groups of continuous variables, Student's t-test was utilized to study variables with normal distribution; however, variables without normal distribution were addressed using the Wilcoxon test. The chi-square test or Fisher's exact test was applied to analyze the statistical difference between two groups of categorical variables. The correlation coefficient was calculated between different genes through Pearson correlation analysis. The Kaplan–Meier survival curves were depicted by R package "survival" and the differences of OS between different cohorts were assessed using the log-rank test. Univariate and multivariate Cox analyses were conducted to determine the independent factors for prognosis. $p < 0.05$ was considered statistically significant.

RESULTS

Data Preprocessing

In order to explore the influence of m6A-related lncRNA on the occurrence and development of AML, we downloaded the transcriptome matrix of AML samples from TCGA and the GSE37642 dataset from the GEO database. Considering that the GSE37642 dataset contains two different annotation platforms, we organized the data of the two platforms and standardized for the gene expression (**Supplementary Figures S1A–D**). We further merged the transcriptome information from two platforms and removed batch effects (**Supplementary Figures S1E, F**).

Construction of Risk Model According to the Expression Pattern of m6A-Related lncRNAs

To investigate the expression pattern of m6A-related lncRNAs in AML, we first performed the comprehensive analysis according to the expression level of m6A-related genes in TCGA and GEO database and removed the batch effect. Heatmap and correlation analysis demonstrated the expression pattern of different m6A-related genes in AML (**Figure 1A**), even if the expressions of different m6A-related genes were mainly positively correlated, there was a negative association between METTL3 and WTAP with statistical significance (**Figure 1B**). According to the correlation analysis, we further searched for m6A-related lncRNA. A number of 41 m6A-related lncRNAs were finally obtained, and $p < 0.05$ was considered as significantly correlated genes (**Figure 1C**). Moreover, we conducted correlation analysis for m6A-related lncRNAs (**Figure 1D**).

We integrated the expression level of 41 m6A-related lncRNAs and implemented univariate Cox regression, of which 9 lncRNAs were prognosis-related, given the *p*-value was less than 0.05. Among them, the expressions of four lncRNAs were protective factors for the prognosis of patients, while other five lncRNAs were unfavorable factors (**Figure 2A**). According to the expression level of nine prognostic-related m6A lncRNAs, a risk scoring system was constructed by the random forest model. The risk score of the m6A-related lncRNAs that can quantitatively evaluate the impact on the prognosis of each AML patient was obtained (**Figures 2B,C**). Dividing all AML patients in TCGA dataset and GEO dataset into the high- and low-risk groups based on the cutoff value, which was the median of the risk scores for all samples. The K–M curve showed that compared to patients with higher risk scores, low-risk patients displayed a better prognosis (Log-rank $p < 0.001$, **Figure 2D**). The time-dependent receiver operating characteristic (ROC) curve further proved the accuracy of the prognostic model. The area under the curve (AUC) at 1-year, 2-year, and 3-year OS was 0.626, 0.676, and 0.690, respectively (**Figure 2E**). The distribution of risk scores, survival status, and the expression pattern of characteristic genes are presented in **Figure 2F**.

Differentially Expressed Genes and Functional Enrichment Analysis Between High-Risk and Low-Risk Acute Myelocytic Leukemia

In order to illuminate the role of m6A-related lncRNA risk model on occurrence and progress of AML patients, AML samples included in the present study were divided into high- and low-risk groups based on the median of risk scores. We conducted differential analysis for the samples in two groups with the cutoff value set as log fold change $|(FC)| > 0.5$ and adjusted *p*-value <0.05. A total of 1,162 genes were significantly upregulated, while 651 genes were otherwise downregulated (**Figures 3A,B**) in the high-risk group of TCGA-AML cohort. In addition, 36 genes were definitely upregulated, while 16 genes, on the contrary, were dramatically downregulated (**Figures 3C,D**) in the high-risk group of the GEO cohort. Moreover, the intersection analysis displayed by the Venn plot showed 22 DEGs between two datasets (**Figure 3E**).

Subsequently, we conducted the functional enrichment analysis for the identified 22 DEGs. GO analysis showed that the significant DEGs were related to biological processes such as response to the external biotic stimulus, defense response, and humoral immune response (**Figure 3F-H**, **Supplementary Table S2**). KEGG analysis suggested that DEGs were mainly associated with the viral protein interaction with cytokine and cytokine receptors, chemokine signaling pathway, transcriptional misregulation in cancers, cytokine–cytokine receptor interaction pathways, and so on (**Figure 3I**, **Supplementary Table S3**). Furthermore, according to the differential analysis of TCGA cohort, the GSEA results indicated that myc targets, allograft rejection, apical junction,

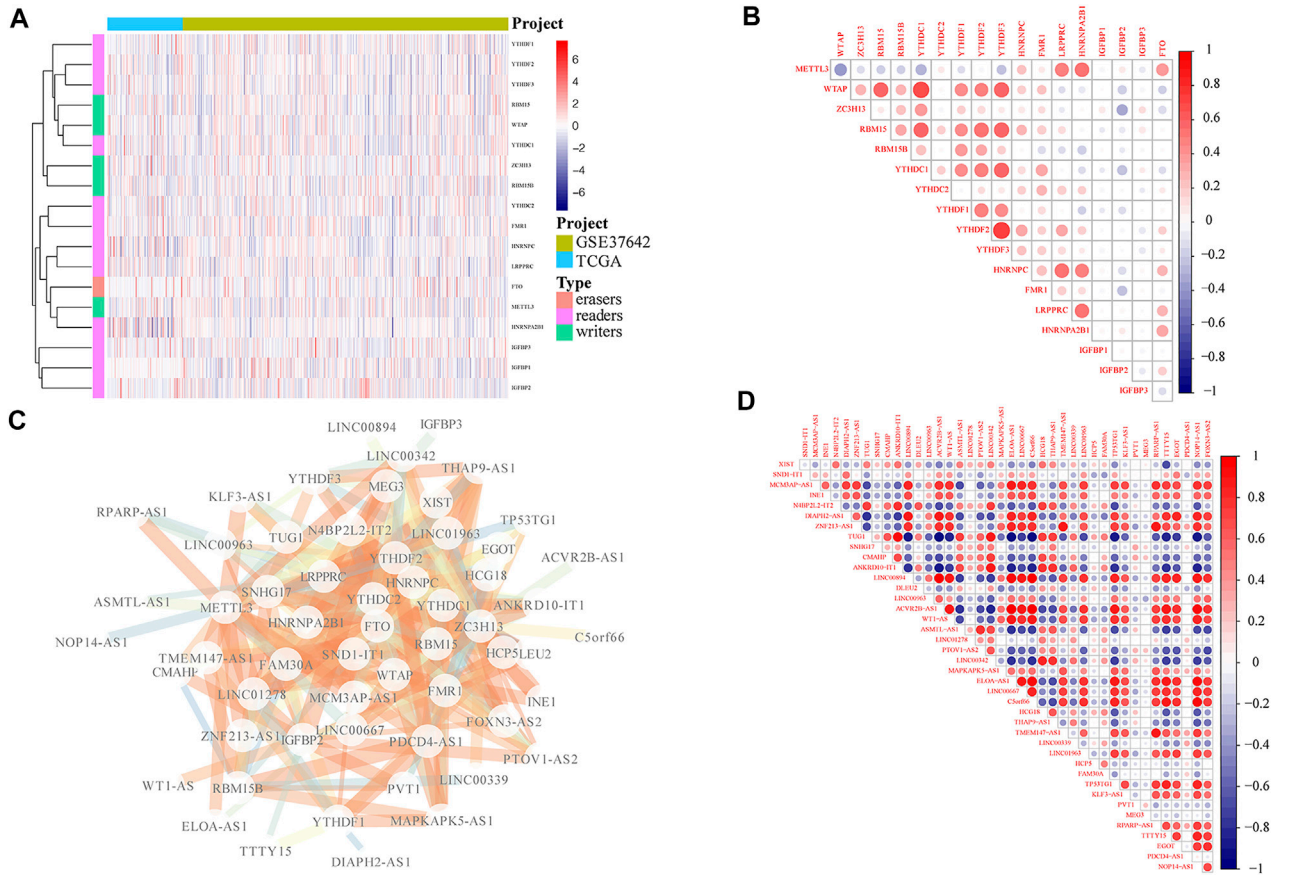

FIGURE 1 | Screening of m6A-related lncRNAs. **(A)** Expression of m6A-related genes in AML patients from TCGA and GEO databases. **(B)** Heatmap showing the co-expression correlation of m6A-related gene in AML patients. **(C)** Based on correlation screening, 41 significant m6A-related lncRNAs were obtained. **(D)** Correlation analysis of the expression level of 41 significant m6A-related lncRNAs in AML patients in TCGA and GEO datasets, in which the color intensity was proportional to the degree of correlation; the deeper red color indicates more positive correlation, and the deeper blue color represents more negative correlation.

hypoxia, and PI3K/Akt/mTOR signaling pathway were significantly enriched in high-risk AML samples. The enrichment analysis of related pathways was displayed in **Supplementary Figures S2A–I**, **Supplementary Table S4**. All these demonstrated that increased risk scores were closely related to the cancer hallmark, malignancy, and immune pathways.

Immune Cell Differentially Infiltrated in Samples With High- and Low-Risk Acute Myelocytic Leukemia Samples

We investigated the impact of the m6A-related lncRNA risk model on the overall immune characteristics and immune cell infiltration in AML samples with different risk scores. Compared with the low-risk group, high-risk samples demonstrated higher ImmuneScore and StromalScore (ImmuneScore: p = 0.00012, StromalScore: p = 0.0098; **Figure 4A**). We further implemented the CIBERSORT algorithm to evaluate the infiltration level of 22 distinct immune cells (**Figure 4B**). Differential infiltrations were found in multiple immune cell subgroups between high- and low-risk groups, including naive B cells, eosinophils, activated mast cells, neutrophils, naive CD4 T cells, CD8 T cells, follicular helper T cells, and Tregs (**Figure 4C–J**).

The Influence of Risk Score on the Genomic Changes of Acute Myelocytic Leukemia Patients

Next, we evaluated the impact of m6A-related lncRNA risk score on the level of genetic variation, consisting of single-nucleotide polymorphism (SNP) and CNV among AML patients. The SNP analysis of driver genes in the occurrence of common tumors demonstrated that the SNP level of different driver genes was different between high- and low-risk groups (**Figure 5A**). Although patients with a higher risk had a relatively high tumor mutation burden (TMB), no significant differences were found between the two groups (p = 0.65; **Figure 5B**). We further discovered the overall CNV change level of TCGA-AML patients (**Figure 5C**). The results of CNV changing frequency suggested that patients with increased risk scores were mainly concentrated in the censoring of gene copy numbers (**Figure 5D**), while patients in the low-risk group were majorly manifested as gene amplification.

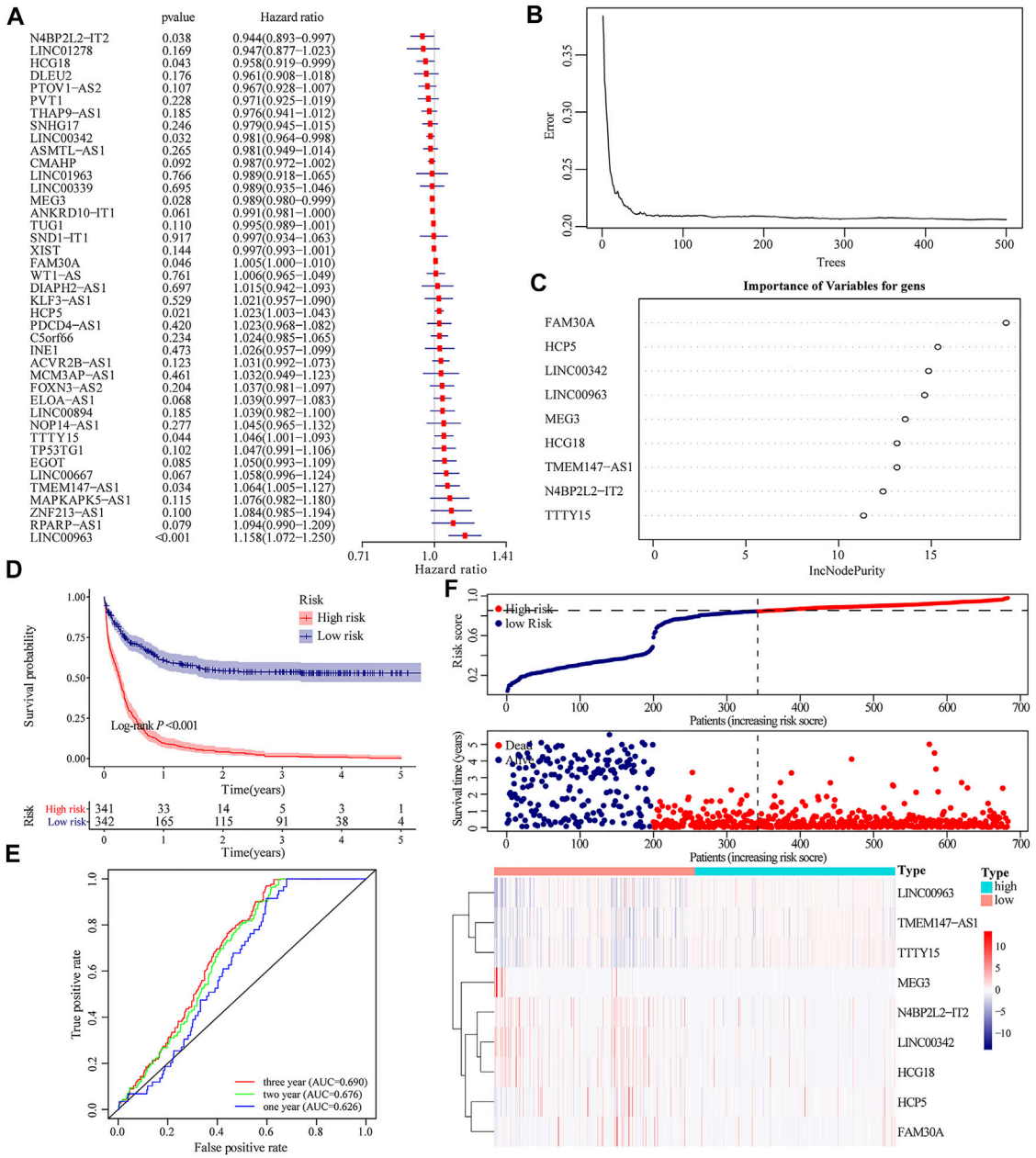

FIGURE 2 | Construction of m6A-related lncRNA-based prognosis model. **(A)**Univariate Cox regression demonstrating that the expression level of nine lncRNAs were dramatically associated with the prognosis of AML patients. **(B)** Generating a random forest model according to the expression of m6A-related lncRNAs. **(C)** Weights of nine different m6A-related lncRNAs in the random forest model. **(D)** Kaplan–Meier curve assessing the impact of risk score on the OS rate of AML patients in TCGA and GEO database. **(E)** Time-dependent ROC curve evaluating the accuracy of the prognostic model. **(F)** Risk score distribution of AML patients in TCGA and GEO databases, and the heatmap shows the patient's survival status and expression of characteristic genes.

Sensitivity of Acute Myelocytic Leukemia Patients to Different Small-Molecule Drugs Assessed by Risk Score Model

In order to explore the sensitivity of patients with different risk scores to different drugs and small molecules, we downloaded the cell line gene mutation data and the IC50 values of different anticancer drugs from the GDSC database. The IC50 values of AML patients to different drugs were predicted based on the responsiveness of cell lines to 138 different chemotherapeutic drugs and small-molecule anticancer drugs. Taken together, our data indicated that the IC50 values of multiple chemotherapeutics and small-molecule anticancer drugs were obviously distinct between high- and low-risk samples ($p < 0.01$; **Figure 6**), especially TW.37 and MG.132.

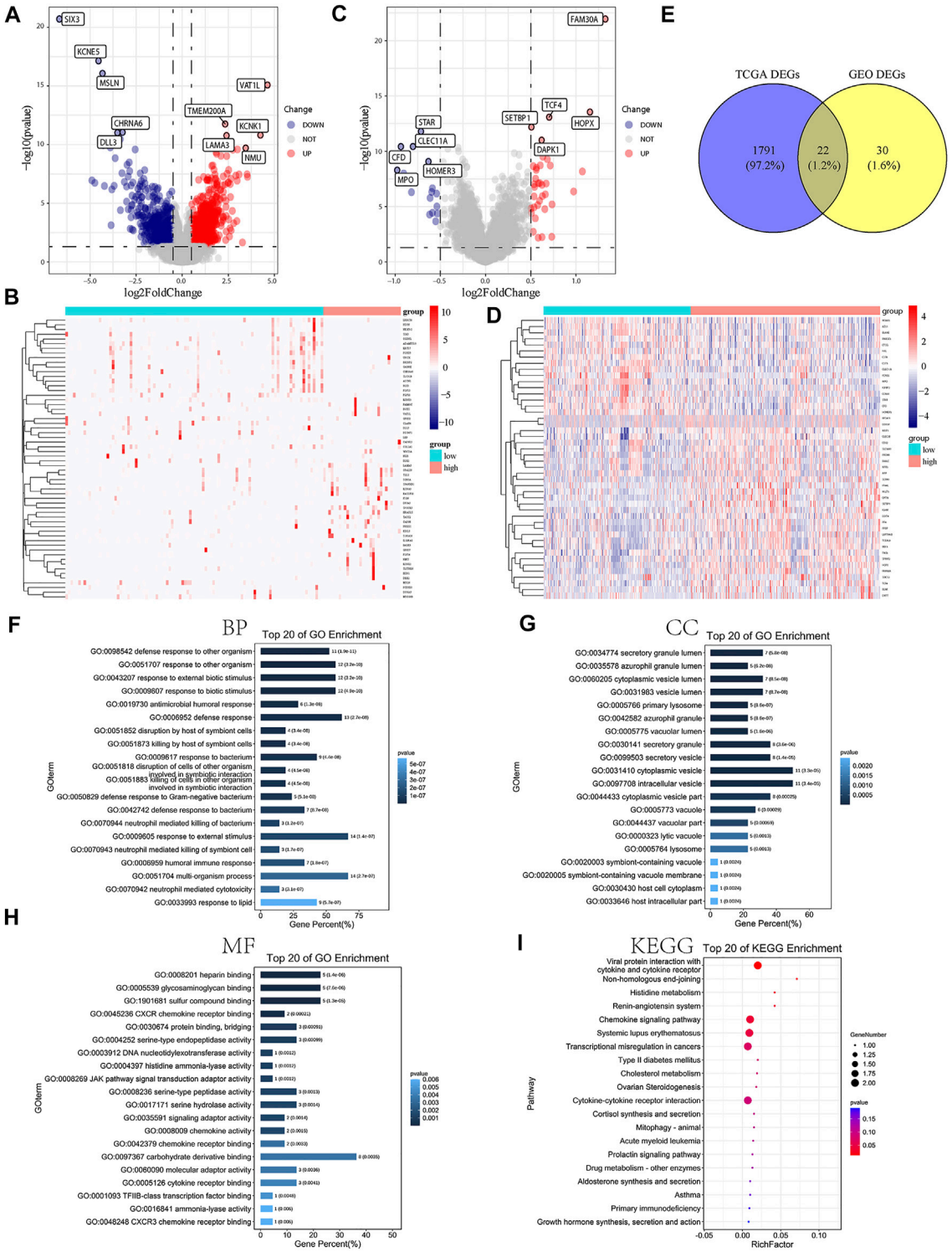

FIGURE 3 | DEG analysis and functional enrichment analysis based on the related risk score model of m6A-related lncRNAs. **(A,B)** Volcano map and heatmap presenting the differential expression of DEGs between high- and low-risk AML patients in TCGA-AML dataset. **(C,D)** Volcano map and heatmap demonstrating the expression level of DEGs between high- and low-risk AML patients in the GEO dataset. **(E)** Venn diagram exhibiting 22 overlapped DEGs between TCGA-AML and GEO datasets. **(F)** GO BP terms suggesting the top 20 enriched biological processes. **(G)** GO CC terms demonstrating the top 20 enriched cellular components. **(H)** GO MF terms indicating the top 20 enriched molecular functions. **(I)** KEGG enrichment analysis showing the top 20 enriched pathways.

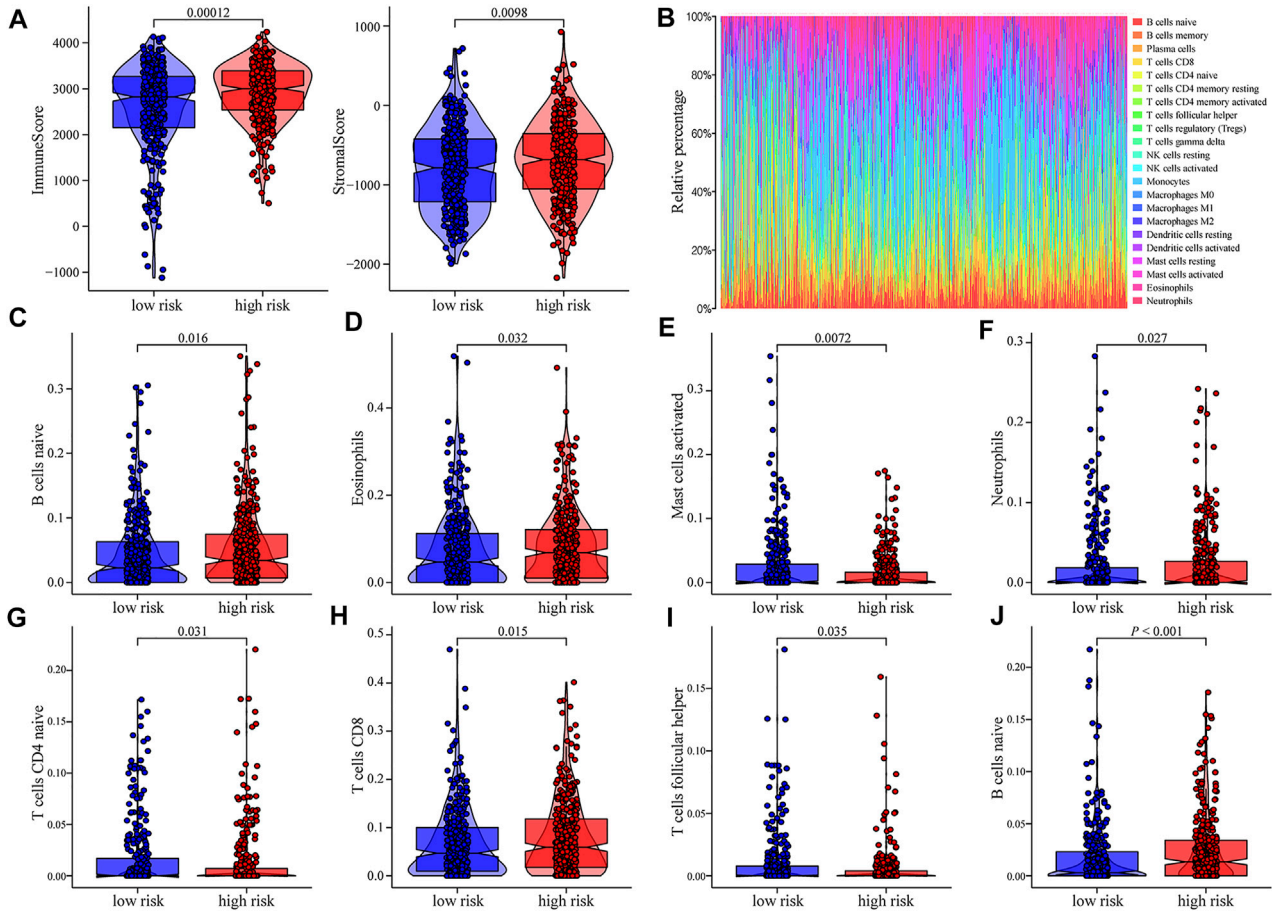

FIGURE 4 | Relationship between risk scores and distinct immune cell infiltration. **(A)** Scatter diagram indicating the immune-related scores, and matrix-related scores of high-risk patient group were significantly increased ($p < 0.05$). **(B)** CIBERSORT was conducted to show the level of overall immune cell infiltration of AML patients in TCGA and GEO database. **(C–J)** Correlation analyses indicating that there were obvious differences in the expression of multiple immune cell subtypes between high- and low-risk groups of AML patients.

Construction of Clinical Prognostic Model Based on m6A-Related lncRNA Risk Score

Subsequently, we assessed the impact of the risk score on the OS of AML patients. Univariate and multivariate Cox regression analyses demonstrated that m6A-related lncRNA risk scores, age, and M5 subgroup were independent prognostic markers predicting the OS of AML patients (**Figure7A**, **Supplementary Table S5**). A nomogram was further depicted to predict the survival expectancy of AML patients by incorporating both the risk scores and clinicopathological characteristics (**Figure 7B**). We applied the C-Index to evaluate the predictive capability of the nomogram. The results showed that the nomogram harbored a high degree of discrimination 0.736. The calibration curve demonstrated that there was a good agreement between the estimated OS values of 1, 3, and 5 years and the actual observations of patients (**Figure 7C**). Moreover, DCA indicated that about 20–90% of patients could be benefited from the predictive model (**Figure 7D**).

DISCUSSION

Currently, the therapeutic approaches for AML remained limited and chemotherapy was still one of the most common first-line treatment modalities (Cai and Levine, 2019). Although an increasing number of targeted drugs emerged in recent years, including protein kinase inhibitors (Dinardo et al., 2018; Dogra et al., 2018; Perl et al., 2019), immune checkpoint antibodies (Vago and Gojo, 2020), and mitochondrial inhibitors (Ram et al., 2019), the percentage of responders was not satisfied. In this context, it is essential to clarify the molecular mechanisms underlying the AML progression and explore novel targets for AML treatment.

According to previous reports, m6A-related lncRNAs were associated with the development and deterioration of many human malignancies, including hepatocellular carcinoma (Li L. et al., 2021), bladder cancer (Li Z. et al., 2021), colon adenocarcinoma (Zhang P. et al., 2021), adrenocortical carcinoma (Jin et al., 2021), and breast cancer (Zhang X. et al., 2021). However, to our knowledge, few studies have focused on

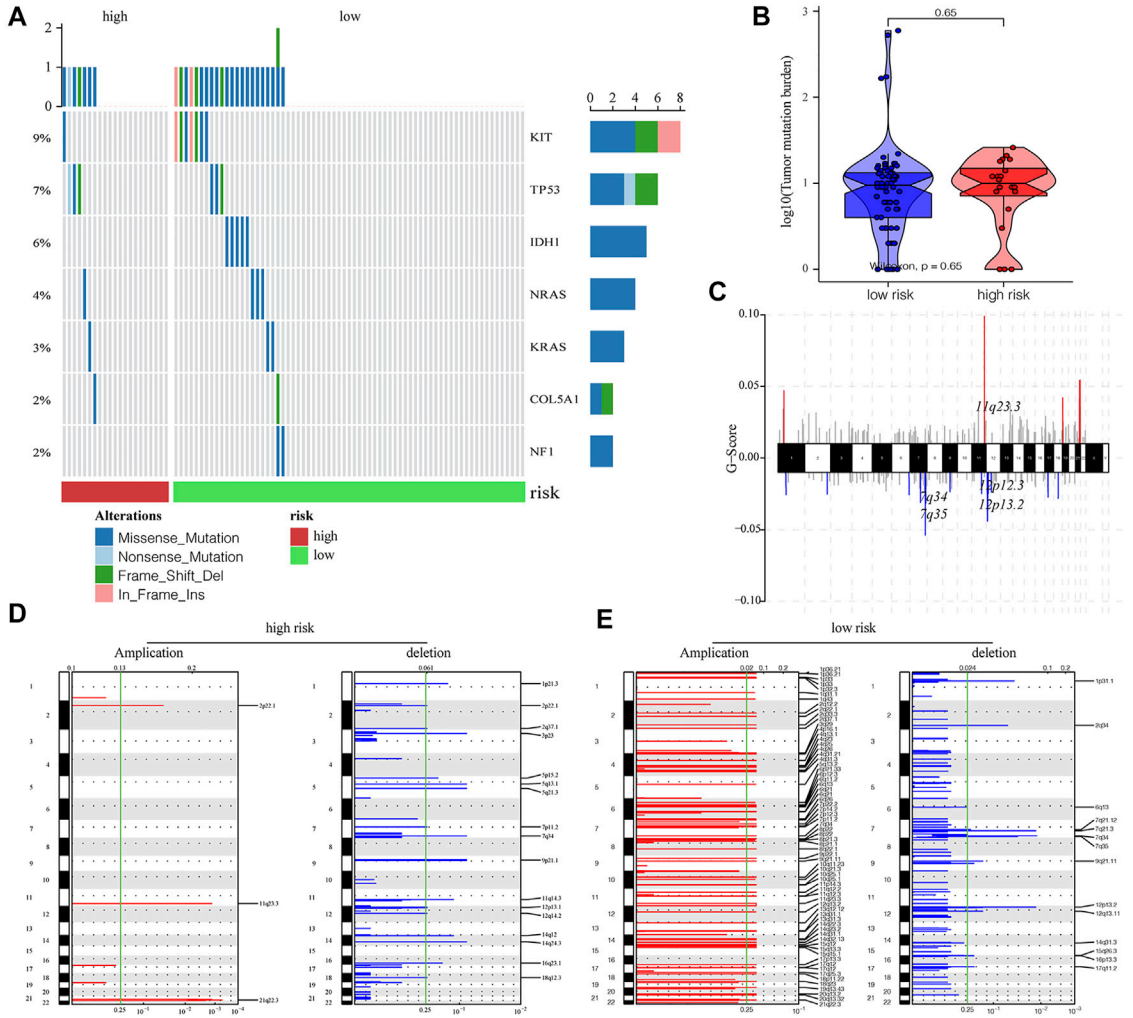

FIGURE 5 | Influence of different m6A-related lncRNAs risk groups on the genetic variation of AML patients. **(A)** Mutation maps of common cancer driver genes between high- and low-risk groups. The waterfall chart displays the mutation information of every gene in each sample, of which various colors indicated different mutation types. The subsection before the legend demonstrated mutational burden. **(B)** Compared with the low-risk group, the high-risk group obtained a higher tumor mutation level, but the difference was not statistically significant ($p = 0.65$). **(C)** Overall level of CNV in TCGA-LAML patients. **(D,E)** Changes in the copy number levels of different genes between the high- and low-risk groups, among which red color represents the genes with significantly increased copy number, and blue color represents genes with significantly missing copy number.

the role of m6A-related lncRNAs in AML. Hence, in the present study, we identified m6A-associated lncRNAs and provided a reliable platform for future studies that focused on the inner relationship between non-coding RNA and epigenetic modification. In detail, we first investigated the expression pattern of m6A genes in TCGA-AML and GEO cohorts. A strong co-expression correlation between distinct m6A regulators was detected. The METTL3–WTAP pair harbored the highest correlation coefficient. The expression level of WTAP turned to be increased when the expression of METTL3 decreased. Most m6A regulators were considered to be dysregulated and play an essential role in leukemia (Yao et al., 2021). Accumulating evidence indicated that m6A "writers," METTL3, METTL14, and WTAP were all oncogenic in AML (Qing et al., 2021b). Melissa Sorci et al. reported that METTL3 levels were crucial for WTAP protein stabilization, but WTAP activation was not enough to trigger cell proliferation in the absence of a functional METTL3 in AML (Sorci et al., 2018). A plausible explanation was that although m6A writers could exert dual roles in the same cancer, m6A modification is not consistently pro-tumorigenic or antitumorigenic. The downstream effect was determined by the stability or translational efficiency of m6A motif-contained transcripts. These m6A motif contained oncogenes or tumor suppressors that could be influenced by differentially expressed m6A regulators would determine the biological processes of tumor cells. A similar phenomenon is observed in research involved with DNA methylation.

Then, we screened the deregulated lncRNAs from TCGA and GEO database. A lot of articles have reported that m6A-related

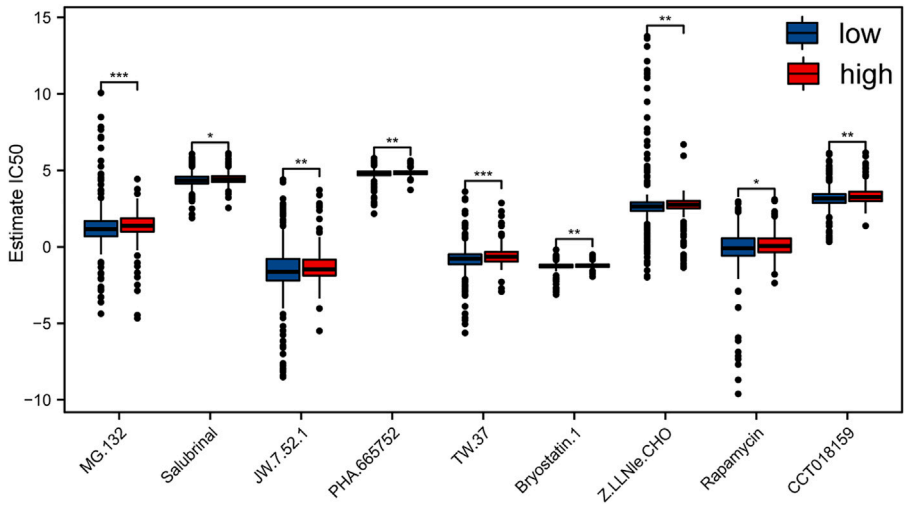

FIGURE 6 | Evaluation of the sensitivity to different chemotherapeutics and small-molecule anticancer drugs with risk score of m6A-related lncRNAs according to the GDSC database.

lncRNAs were able to regulate cancer initiation and progression (Ni et al., 2019; Wen et al., 2020; Yang et al., 2020). Wen Ni et al. reported that m6A-modified transcripts of lncRNA GAS5 could regulate YAP activation in colorectal cancer progression (Ni et al., 2019). In another study, m6A modification in lncRNA NEAT1 played an oncogenic role in bone metastatic prostate cancer and was correlated with the poor prognosis (Wen et al., 2020). On the contrary, as an essential component of m6A writer, METTL14 has been shown to suppress proliferation and metastasis of colorectal cancer by downregulating oncogenic lncRNA XIST (Yang et al., 2020), suggesting the regulatory network of m6A and lncRNA in tumor pathophysiology was extremely complicated. Meanwhile, their relationships with m6A regulators were analyzed and a total of 41 m6A-related lncRNAs were identified in the end. Next, through univariate and multivariate Cox regression, we selected nine m6A-related lncRNAs that were associated with OS and further constructed an m6A-related lncRNA-based prognosis model based on their expression level. Among them, FAM30A, HCP5, LINC00963, TMEM147-AS1, and TTTY15 indicated a worse prognosis, but LINC00342, MEG3, HCG18, and N4BP2L2-IT2 demonstrated a better tumor prognosis. FAM30A was included in a prognostic model for AML, which was significantly correlated with the European Leukemia Net 2017 recommended prognostic genetic abnormalities (Guo et al., 2021). According to reports, HCP5 was overexpressed in AML and was positively associated with poor prognosis (Lei et al., 2020), it was significantly overexpressed in AML, and HCP5 upregulation promoted the progression of AML cells *via* the miR-1291/PIK3R5 axis (Liu Y. et al., 2021). Wenli Zuo et al. have shown that LINC00963 promoted AML development by regulating miR-608/MMP-15 (Zuo et al., 2020). Multiple lncRNAs have been reported to be both oncogenic and anti-oncogenic in AML. On one side, MEG3 was overexpressed in acute promyelocytic leukemia (APL), while exerting antitumor function in AML cell lines (Liu et al., 2019; Zimta et al., 2019). The aforementioned lncRNAs have been reported to be involved with AML, but TMEM147-AS1, TTTY15, LINC00342, HCG18, and N4BP2L2-IT2 have not been studied in AML yet.

Moreover, the pathophysiological role of 22 DEGs was investigated in the present study. AML tissues were grouped into high- and low-risk subgroups according to the median of risk scores. DEGs were mainly enriched in the viral protein interaction with cytokine and cytokine receptors, chemokine signaling pathway, transcriptional misregulation in cancers, and cytokine–cytokine receptor interaction pathways, which were shown by KEGG functional analysis. By GO analysis, multiple pathways involved with immune surveillance and defending were enriched, suggesting these genes may be associated with alteration in antitumor immunity. GSEA results revealed that myc targets, allograft rejection, apical junction, hypoxia, and PI3K/Akt/mTOR signaling pathway may be associated with the high-risk group. Among these signal pathways, the PI3K/Akt/mTOR signaling pathway has been reported to be aberrantly hyperactivated in multiple cancers such as AML, which is required to sustain the oncogenic potential of leukemia stem cell populations (Darici et al., 2020; Nepstad et al., 2020). The PI3K/Akt/mTOR signaling pathway was found to be potentially affected by m6A regulators in most cancers such as gastrointestinal cancer (Zhao Q. et al., 2020) and ovarian cancer (Bi et al., 2021), which was consistent with our results. M6A modification of lncRNAs may affect the occurrence and development of tumors, lncRNAs may also target m6A regulators as competitive endogenous RNAs, affecting tumor invasive progression (Xu F. et al., 2021; Zhao et al., 2021). Taken together, these findings implied potential correlation between m6A-modified lncRNAs and AML initiation or progression. It would be interesting to clarify the potential biological mechanism by which the abnormal expressions of m6A-related lncRNAs deteriorate AML.

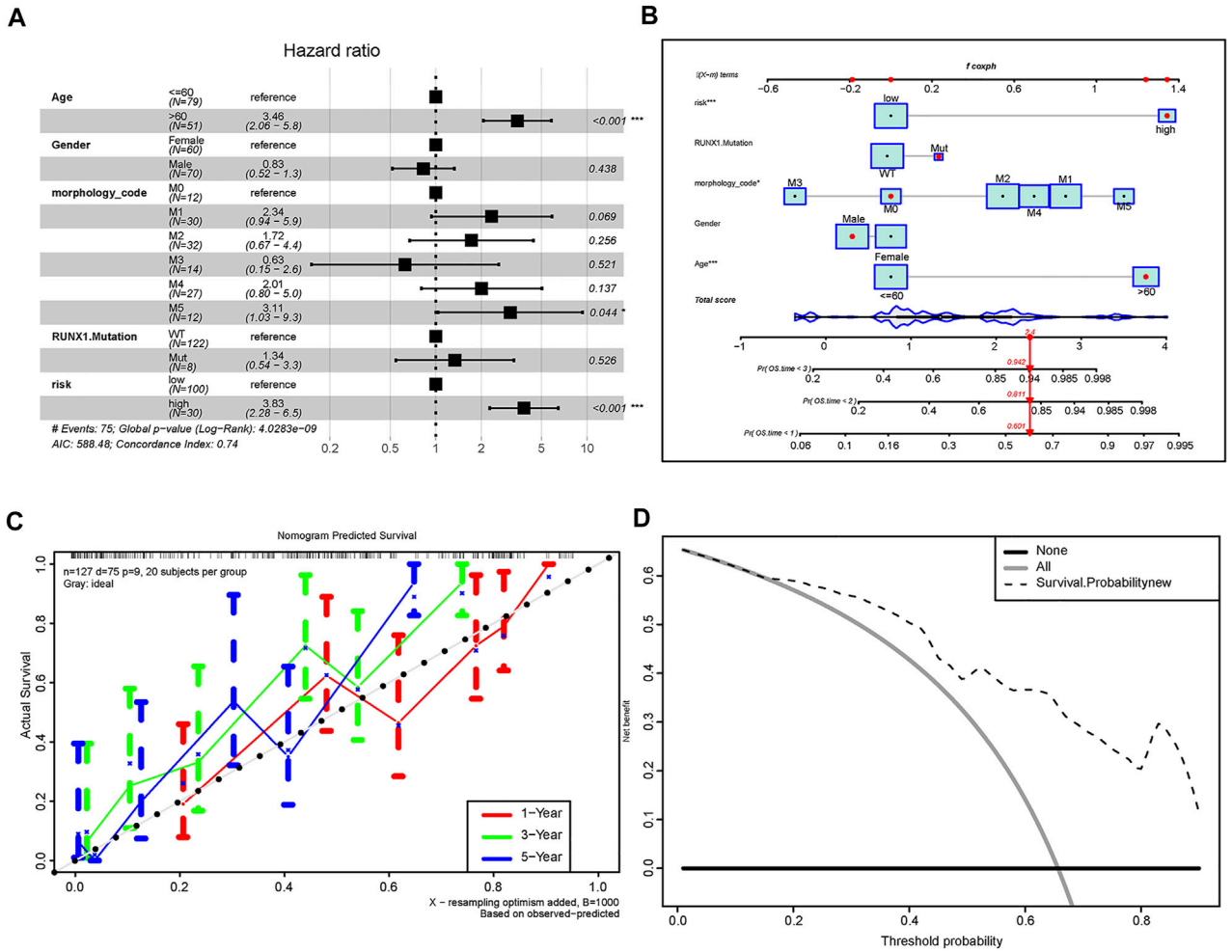

FIGURE 7 | Predictive ability of the constructed model for the OS of AML patients. **(A)** Multivariate Cox regression analysis of risk scores combined with clinicopathological characteristics, which indicate that risk score, age, and M5 subgroup are independent risk factors for the prognosis of AML patients. **(B)** Nomogram showing clinicopathological characteristics such as age, gender, morphological subtype, RUNX1 mutation, and risk scores and manifesting great predictive accuracy for 1-, 2-, and 3-year survival rates. **(C)** Calibration curve of nomogram. X-axis indicates the survival situation predicted by the nomogram, and Y-axis indicates actual observed survival. Repeated 1,000 times in each run, the curve demonstrate that the model had an excellent predictive value for the prognosis of patients at 1, 3, and 5 years. **(D)** Decision curve analysis of nomogram; Y-axis indicates the net benefit, the dotted line indicates the benefit predicted by the model, the gray curve represents the benefit rate of all patients receiving the intervention, and the horizontal line indicates the benefit rate of the whole patients not received intervention. Take the intersection of the dotted line and all as the starting point, and the intersection with none as the end. Patients within this range can benefit from intervention.

In addition, we explored the association between the risk scores and the BMM of AML. Compared with the low-risk samples, AML in the high-risk group exhibited increased ImmuneScore and StromalScore. Another significant discovery was that certain immune cells, including naive B cells, eosinophils, activated mast cells, neutrophils, naive CD4 T cells, CD8 T cells, follicular helper T cells, and T-regulatory cells (Tregs), were enriched in high-risk groups. Infiltrated immune and stromal cells are vital components of the BM microenvironment and exert significant function in the progression of AML (Dufva et al., 2020). CD8-positive T cells were more abundant in bone marrow aspirates (BMAs) from patients with multiple relapses than in BMAs from those who had first relapsed or newly diagnosed AML (Williams et al., 2019). NFATC4 was an essential immune-related regulator in AML, and predicted worse survival by recruiting more Tregs (Zhao C. et al., 2020) and hence formed an immunosuppressive microenvironment, suggesting that Tregs were associated with a poor prognosis in AML patients. Interestingly, Yingxi Xu et al. revealed that Tregs promoted the stemness of leukemia cells *via* the IL10/IL10R/PI3K/AKT signaling pathway (Xu Y. et al., 2021). These findings were consistent with the results in the present

study; however, other immune cells involved in immune imbalance remained unclear in AML. Therefore, elucidating the biological mechanisms based on the immune microenvironment may facilitate exploring novel therapeutic targets for AML.

The screening of gene signatures or biomarkers that could accurately predict the AML prognosis was still a huge challenge. We could identify the gene signals associated with the prognosis of AML *via* bioinformatics approaches. Thus, we evaluated the impact of m6A-related lncRNA risk score on the level of genetic variation, which consisted of SNP and CNV in AML patients. We found that patients in the high-risk group majorly harbored censoring of gene copy number. Conversely, patients in the low-risk group were majorly manifested as gene amplification. Na Li et al. illustrated that alterations in CNVs influenced the m6A-related gene expression in non-lung cancer genes (Li N. et al., 2021). A similar study found substantial prognostic values of the CNV of m6A regulatory genes in hepatocellular carcinoma (Liu G.-M. et al., 2021). However, according to the literature in PubMed, few studies have investigated the role of m6A-related lncRNA risk score on the level of CNV in AML. In the current study, AML was grouped into three prognostic risk groups: favorable, intermediate, and adverse. These clusters are according to both cytogenetics and relatively recent recognition of molecular disease subtypes that are distinct from the contribution of the cytogenetic risk (Pelcovits and Niroula, 2020). Our results may facilitate the invention of a new method for predicting the OS of AML patients.

Subsequently, we found that the high-risk group was featured with the higher IC50 values of multiple chemotherapeutics and small-molecule anticancer drugs, notably TW.37 and MG.132. It was reported that epigallocatechin-3-gallate (EGCG) increases ATRA-induced APL cell line (NB4) differentiation *via* phosphatase and tensin homolog (PTEN). The expression of PTEN was decreased in NB4 cells and could be rescued by proteases inhibitor MG132 (Yao et al., 2017). This indicated that MG132 may be a promising strategy for APL, which was a favorable group of AML. Our results suggested that the low-risk group may be more sensitive to MG132, which was consistent with previous results. These drugs may provide potential clues for precise treatment for AML patients with different risk scores. Finally, for the sake of better comprehension of the function of m6A-related lncRNA risk score in the survival of AML patients, we established a clinical prognostic model, which revealed good accuracy in predicting the survival expectancy of AML patients. Notably, the prognosis model constructed in the present study has the potential to be translated into clinical practices given its high predictive accuracy. Clinicians could refer to the risk score given by our model to assess the survival expectancy of AML patients and make appropriate clinical decisions.

Certainly, there were some limitations in the present study. First, the biological function of the m6A-related lncRNAs remained indistinct and warranted further exploration to determine approaches to reprogram the immune microenvironment and promote precision immunotherapy for AML. Second, this clinical prognostic model was only validated in TCGA and GSE37642, and more external validations based on RNA-seq cohorts are expected in the future to evaluate whether it can be applied to AML patients. Further experimental verifications are necessary to fully clarify the role of m6A-related lncRNAs and the potential mechanisms of AML. We would like to perform more careful examinations of the diagnosis and treatment effect of these predicted m6A-related lncRNAs in AML by combining *in vivo* and *in vitro* techniques.

In conclusion, the present study was the first systematic screening and comprehensive analysis of m6A-related lncRNAs in AML samples. We identified m6A-related lncRNAs with survival implications and constructed a novel and accurate prognostic model. The risk score was extremely associated with the malignant clinicopathological characteristics of AML and could be recognized as a novel biomarker. For the first time, the research of m6A-related lncRNAs has been published to exert essential roles in the immune infiltration and CNV of AML. The present study offered a potentially theoretical basis for further research demonstrating the role of m6A-related lncRNAs in AML, which provided new guidance for the valid treatment guidelines for AML.

DATA AVAILABILITY STATEMENT

The datasets presented in this study can be found in online repositories. The names of the repository/repositories and accession number(s) can be found in the article.

AUTHOR CONTRIBUTIONS

LZ was the principal investigator and took primary responsibility for the manuscript. LZ and WK conceived and designed the study. LZ, WK, PH, and ZL performed the literature search, generated the figures and tables, and wrote the manuscript. LZ, WG, YG, BS, HJ, XZ, and CW revised the manuscript. All authors read and approved the final manuscript version.

FUNDING

This work was supported by the National Natural Science Foundation of China (Grant No. 81900141).

ACKNOWLEDGMENTS

We would like to acknowledge the contributions from TCGA project and the GEO datasets.

SUPPLEMENTARY MATERIAL

The Supplementary Material for this article can be found online at: https://www.frontiersin.org/articles/10.3389/fgene.2022.804614/full#supplementary-material

REFERENCES

Bi, X., Lv, X., Liu, D., Guo, H., Yao, G., Wang, L., et al. (2021). METTL3-mediated Maturation of miR-126-5p Promotes Ovarian Cancer Progression via PTEN-Mediated PI3K/Akt/mTOR Pathway. *Cancer Gene Ther.* 28, 335–349. doi:10.1038/s41417-020-00222-3

Cai, S. F., and Levine, R. L. (2019). Genetic and Epigenetic Determinants of AML Pathogenesis. *Semin. Hematol.* 56, 84–89. doi:10.1053/j.seminhematol.2018.08.001

Candon, D. (2018). The Effect of Cancer on the Labor Supply of Employed Men over the Age of 65. *Econ. Hum. Biol.* 31, 184–199. doi:10.1016/j.ehb.2018.08.010

Darici, S., Alkhaldi, H., Horne, G., Jørgensen, H. G., Marmiroli, S., and Huang, X. (2020). Targeting PI3K/Akt/mTOR in AML: Rationale and Clinical Evidence. *Jcm* 9, 2934. doi:10.3390/jcm9092934

De Kouchkovsky, I., and Abdul-Hay, M. (2016). 'Acute Myeloid Leukemia: a Comprehensive Review and 2016 Update'. *Blood Cancer J.* 6, e441. doi:10.1038/bcj.2016.50

Dewolf, S., and Tallman, M. S. (2020). How I Treat Relapsed or Refractory AML. *Blood* 136, 1023–1032. doi:10.1182/blood.2019001982

Dinardo, C. D., Stein, E. M., De Botton, S., Roboz, G. J., Altman, J. K., Mims, A. S., et al. (2018). Durable Remissions with Ivosidenib inIDH1-Mutated Relapsed or Refractory AML. *N. Engl. J. Med.* 378, 2386–2398. doi:10.1056/NEJMoa1716984

Dogra, R., Bhatia, R., Shankar, R., Bansal, P., and Rawal, R. K. (2019). Enasidenib: First Mutant IDH2 Inhibitor for the Treatment of Refractory and Relapsed Acute Myeloid Leukemia. *Acamc* 18, 1936–1951. doi:10.2174/1871520618666181025091128

Dufva, O., Pölönen, P., Brück, O., Keränen, M. A. I., Klievink, J., Mehtonen, J., et al. (2020). Immunogenomic Landscape of Hematological Malignancies. *Cancer Cell* 38, 380–399. e313. doi:10.1016/j.ccell.2020.06.002

Elcheva, I. A., Wood, T., Chiarolanzio, K., Chim, B., Wong, M., Singh, V., et al. (2020). RNA-binding Protein IGF2BP1 Maintains Leukemia Stem Cell Properties by Regulating HOXB4, MYB, and ALDH1A1. *Leukemia* 34, 1354–1363. doi:10.1038/s41375-019-0656-9

Geeleher, P., Cox, N., and Huang, R. S. (2014). pRRophetic: an R Package for Prediction of Clinical Chemotherapeutic Response from Tumor Gene Expression Levels. *PLoS One* 9, e107468. doi:10.1371/journal.pone.0107468

Guo, C., Gao, Y.-y., Ju, Q.-q., Zhang, C.-x., Gong, M., and Li, Z.-l. (2021). The Landscape of Gene Co-expression Modules Correlating with Prognostic Genetic Abnormalities in AML. *J. Transl Med.* 19, 228. doi:10.1186/s12967-021-02914-2

Herold, T., Jurinovic, V., Batcha, A. M. N., Bamopoulos, S. A., Rothenberg-Thurley, M., Ksienzyk, B., et al. (2018). A 29-gene and Cytogenetic Score for the Prediction of Resistance to Induction Treatment in Acute Myeloid Leukemia. *Haematologica* 103, 456–465. doi:10.3324/haematol.2017.178442

Herold, T., Metzeler, K. H., Vosberg, S., Hartmann, L., Röllig, C., Stölzel, F., et al. (2014). Isolated Trisomy 13 Defines a Homogeneous AML Subgroup with High Frequency of Mutations in Spliceosome Genes and Poor Prognosis. *Blood* 124, 1304–1311. doi:10.1182/blood-2013-12-540716

Jin, Y., Wang, Z., He, D., Zhu, Y., Hu, X., Gong, L., et al. (2021). Analysis of m6A-Related Signatures in the Tumor Immune Microenvironment and Identification of Clinical Prognostic Regulators in Adrenocortical Carcinoma. *Front. Immunol.* 12, 637933. doi:10.3389/fimmu.2021.637933

Kuett, A., Rieger, C., Perathoner, D., Herold, T., Wagner, M., Sironi, S., et al. (2015). IL-8 as Mediator in the Microenvironment-Leukaemia Network in Acute Myeloid Leukaemia. *Sci. Rep.* 5, 18411. doi:10.1038/srep18411

Lei, M., Jingjing, Z., Tao, J., Jianping, M., Yuanxin, Z., Jifeng, W., et al. (2020). LncRNA HCP5 Promotes LAML Progression via PSMB8-Mediated PI3K/AKT Pathway Activation. *Naunyn-schmiedeberg's Arch. Pharmacol.* 393, 1025–1032. doi:10.1007/s00210-019-01788-y

Li, L., Xie, R., and Lu, G. (2021a). Identification of m6A Methyltransferase-Related lncRNA Signature for Predicting Immunotherapy and Prognosis in Patients with Hepatocellular Carcinoma. *Biosci. Rep.* 41. doi:10.1042/BSR20210760

Li, N., Chen, X., Liu, Y., Zhou, T., and Li, W. (2021b). Gene Characteristics and Prognostic Values of m6A RNA Methylation Regulators in Nonsmall Cell Lung Cancer. *J. Healthc. Eng.* 2021, 1–12. doi:10.1155/2021/2257066

Li, Z., Herold, T., He, C., Valk, P. J. M., Chen, P., Jurinovic, V., et al. (2013). Identification of a 24-gene Prognostic Signature that Improves the European LeukemiaNet Risk Classification of Acute Myeloid Leukemia: an International Collaborative Study. *Jco* 31, 1172–1181. doi:10.1200/JCO.2012.44.3184

Li, Z., Li, Y., Zhong, W., and Huang, P. (2021c). m6A-Related lncRNA to Develop Prognostic Signature and Predict the Immune Landscape in Bladder Cancer. *J. Oncol.* 2021, 1–16. doi:10.1155/2021/7488188

Liu, G.-M., Zeng, H.-D., Zhang, C.-Y., and Xu, J.-W. (2021a). Identification of METTL3 as an Adverse Prognostic Biomarker in Hepatocellular Carcinoma. *Dig. Dis. Sci.* 66, 1110–1126. doi:10.1007/s10620-020-06260-z

Liu, Y., Cheng, Z., Pang, Y., Cui, L., Qian, T., Quan, L., et al. (2019). Role of microRNAs, circRNAs and Long Noncoding RNAs in Acute Myeloid Leukemia. *J. Hematol. Oncol.* 12, 51. doi:10.1186/s13045-019-0734-5

Liu, Y., Jing, X.-B., Wang, Z.-C., and Han, Q.-K. (2021b). HCP5, as the Sponge of miR-1291, Facilitates AML Cell Proliferation and Restrains Apoptosis via Increasing PIK3R5 Expression. *Hum. Genomics* 15, 38. doi:10.1186/s40246-021-00340-5

Love, M. I., Huber, W., and Anders, S. (2014). Moderated Estimation of Fold Change and Dispersion for RNA-Seq Data with DESeq2. *Genome Biol.* 15, 550. doi:10.1186/s13059-014-0550-8

Mayakonda, A., Lin, D.-C., Assenov, Y., Plass, C., and Koeffler, H. P. (2018). Maftools: Efficient and Comprehensive Analysis of Somatic Variants in Cancer. *Genome Res.* 28, 1747–1756. doi:10.1101/gr.239244.118

Naren, D., Yan, T., Gong, Y., Huang, J., Zhang, D., Sang, L., et al. (2021). High Wilms' Tumor 1 Associating Protein Expression Predicts Poor Prognosis in Acute Myeloid Leukemia and Regulates m6A Methylation of MYC mRNA. *J. Cancer Res. Clin. Oncol.* 147, 33–47. doi:10.1007/s00432-020-03373-w

Nepstad, I., Hatfield, K. J., Grønningsæter, I. S., and Reikvam, H. (2020). The PI3K-Akt-mTOR Signaling Pathway in Human Acute Myeloid Leukemia (AML) Cells. *Ijms* 21, 2907. doi:10.3390/ijms21082907

Newman, A. M., Liu, C. L., Green, M. R., Gentles, A. J., Feng, W., Xu, Y., et al. (2015). Robust Enumeration of Cell Subsets from Tissue Expression Profiles. *Nat. Methods* 12, 453–457. doi:10.1038/nmeth.3337

Ni, W., Yao, S., Zhou, Y., Liu, Y., Huang, P., Zhou, A., et al. (2019). Long Noncoding RNA GAS5 Inhibits Progression of Colorectal Cancer by Interacting with and Triggering YAP Phosphorylation and Degradation and Is Negatively Regulated by the m6A Reader YTHDF3. *Mol. Cancer* 18, 143. doi:10.1186/s12943-019-1079-y

Papaemmanuil, E., Gerstung, M., Bullinger, L., Gaidzik, V. I., Paschka, P., Roberts, N. D., et al. (2016). Genomic Classification and Prognosis in Acute Myeloid Leukemia. *N. Engl. J. Med.* 374, 2209–2221. doi:10.1056/NEJMoa1516192

Paris, J., Morgan, M., Campos, J., Spencer, G. J., Shmakova, A., Ivanova, I., et al. (2019). Targeting the RNA m6A Reader YTHDF2 Selectively Compromises Cancer Stem Cells in Acute Myeloid Leukemia. *Cell Stem Cell* 25, 137–148. e136. doi:10.1016/j.stem.2019.03.021

Pelcovits, A., and Niroula, R. (2020). Acute Myeloid Leukemia: A Review. *R. Med. J. (2013)* 103, 38–40.

Perl, A. E., Martinelli, G., Cortes, J. E., Neubauer, A., Berman, E., Paolini, S., et al. (2019). Gilteritinib or Chemotherapy for Relapsed or Refractory FLT3-Mutated AML. *N. Engl. J. Med.* 381, 1728–1740. doi:10.1056/NEJMoa1902688

Qi, X., Jiao, Y., Cheng, C., Qian, F., Chen, Z., and Wu, Q. (2019). H22954, a Novel Long Non-coding RNA Down-Regulated in AML, Inhibits Cancer Growth in a BCL-2-dependent Mechanism. *Cancer Lett.* 454, 26–36. doi:10.1016/j.canlet.2019.03.055

Qing, Y., Dong, L., Gao, L., Li, C., Li, Y., Han, L., et al. (2021a). R-2-hydroxyglutarate Attenuates Aerobic Glycolysis in Leukemia by Targeting the FTO/m6A/PFKP/LDHB axis. *Mol. Cel* 81, 922–939. doi:10.1016/j.molcel.2020.12.026

Qing, Y., Su, R., and Chen, J. (2021b). RNA Modifications in Hematopoietic Malignancies: A New Research Frontier. *Blood* 138, 637–648. doi:10.1182/blood.2019004263

Ram, R., Amit, O., Zuckerman, T., Gurion, R., Raanani, P., Bar-On, Y., et al. (2019). Venetoclax in Patients with Acute Myeloid Leukemia Refractory to Hypomethylating Agents-A Multicenter Historical Prospective Study. *Ann. Hematol.* 98, 1927–1932. doi:10.1007/s00277-019-03719-6

Ritchie, M. E., Phipson, B., Wu, D., Hu, Y., Law, C. W., Shi, W., et al. (2015). Limma powers Differential Expression Analyses for RNA-Sequencing and Microarray Studies. *Nucleic Acids Res.* 43, e47. doi:10.1093/nar/gkv007

Shen, C., Sheng, Y., Zhu, A. C., Robinson, S., Jiang, X., Dong, L., et al. (2020). RNA Demethylase ALKBH5 Selectively Promotes Tumorigenesis and Cancer Stem

Cell Self-Renewal in Acute Myeloid Leukemia. *Cell Stem Cell* 27, 64–80. e69. doi:10.1016/j.stem.2020.04.009

Sorci, M., Ianniello, Z., Cruciani, S., Larivera, S., Ginistrelli, L. C., Capuano, E., et al. (2018). METTL3 Regulates WTAP Protein Homeostasis. *Cell Death Dis* 9, 796. doi:10.1038/s41419-018-0843-z

Stein, E. M., Dinardo, C. D., Pollyea, D. A., Fathi, A. T., Roboz, G. J., Altman, J. K., et al. (2017). Enasidenib in Mutant IDH2 Relapsed or Refractory Acute Myeloid Leukemia. *Blood* 130, 722–731. doi:10.1182/blood-2017-04-779405

Su, R., Dong, L., Li, Y., Gao, M., Han, L., Wunderlich, M., et al. (2020). Targeting FTO Suppresses Cancer Stem Cell Maintenance and Immune Evasion. *Cancer Cell* 38, 79–96. doi:10.1016/j.ccell.2020.04.017

Subramanian, A., Tamayo, P., Mootha, V. K., Mukherjee, S., Ebert, B. L., Gillette, M. A., et al. (2005). Gene Set Enrichment Analysis: a Knowledge-Based Approach for Interpreting Genome-wide Expression Profiles. *Proc. Natl. Acad. Sci. U.S.A.* 102, 15545–15550. doi:10.1073/pnas.0506580102

Vago, L., and Gojo, I. (2020). Immune Escape and Immunotherapy of Acute Myeloid Leukemia. *J. Clin. Invest.* 130, 1552–1564. doi:10.1172/JCI129204

Vu, L. P., Pickering, B. F., Cheng, Y., Zaccara, S., Nguyen, D., Minuesa, G., et al. (2017). The N6-Methyladenosine (m6A)-Forming Enzyme METTL3 Controls Myeloid Differentiation of normal Hematopoietic and Leukemia Cells. *Nat. Med.* 23, 1369–1376. doi:10.1038/nm.4416

Wang, J., Li, Y., Wang, P., Han, G., Zhang, T., Chang, J., et al. (2020). Leukemogenic Chromatin Alterations Promote AML Leukemia Stem Cells via a KDM4C-ALKBH5-AXL Signaling Axis. *Cell Stem Cell* 27, 81–97. e88. doi:10.1016/j.stem.2020.04.001

Wen, S., Wei, Y., Zen, C., Xiong, W., Niu, Y., and Zhao, Y. (2020). Long Non-coding RNA NEAT1 Promotes Bone Metastasis of Prostate Cancer through N6-Methyladenosine. *Mol. Cancer* 19, 171. doi:10.1186/s12943-020-01293-4

Weng, H., Huang, H., Wu, H., Qin, X., Zhao, B. S., Dong, L., et al. (2018). METTL14 Inhibits Hematopoietic Stem/Progenitor Differentiation and Promotes Leukemogenesis via mRNA m6A Modification. *Cell Stem Cell* 22, 191–205. doi:10.1016/j.stem.2017.11.016

Williams, P., Basu, S., Garcia-Manero, G., Hourigan, C. S., Oetjen, K. A., Cortes, J. E., et al. (2019). The Distribution of T-cell Subsets and the Expression of Immune Checkpoint Receptors and Ligands in Patients with Newly Diagnosed and Relapsed Acute Myeloid Leukemia. *Cancer* 125, 1470–1481. doi:10.1002/cncr.31896

Xu, F., Huang, X., Li, Y., Chen, Y., and Lin, L. (2021a). m6A-related lncRNAs Are Potential Biomarkers for Predicting Prognoses and Immune Responses in Patients with LUAD. *Mol. Ther. - Nucleic Acids* 24, 780–791. doi:10.1016/j.omtn.2021.04.003

Xu, Y., Mou, J., Wang, Y., Zhou, W., Rao, Q., Xing, H., et al. (2021b). Regulatory T Cells Promote the Stemness of Leukemia Stem Cells through IL10 Cytokine-Related Signaling Pathway. *Leukemia* 36, 403–415. doi:10.1038/s41375-021-01375-2

Yang, W., Soares, J., Greninger, P., Edelman, E. J., Lightfoot, H., Forbes, S., et al. (2013). Genomics of Drug Sensitivity in Cancer (GDSC): a Resource for Therapeutic Biomarker Discovery in Cancer Cells. *Nucleic Acids Res.* 41, D955–D961. doi:10.1093/nar/gks1111

Yang, X., Zhang, S., He, C., Xue, P., Zhang, L., He, Z., et al. (2020). METTL14 Suppresses Proliferation and Metastasis of Colorectal Cancer by Down-Regulating Oncogenic Long Non-coding RNA XIST. *Mol. Cancer* 19, 46. doi:10.1186/s12943-020-1146-4

Yang, Y., Dai, W., Sun, Y., and Zhao, Z. (2019). Long Non-coding RNA L-inc00239 P-romotes M-alignant B-ehaviors and C-hemoresistance against D-oxorubicin P-artially via A-ctivation of the PI3K/Akt/mTOR P-athway in A-cute M-yeloid L-eukaemia C-ells. *Oncol. Rep.* 41, 2311–2320. doi:10.3892/or.2019.6991

Yao, L., Yin, H., Hong, M., Wang, Y., Yu, T., Teng, Y., et al. (2021). RNA Methylation in Hematological Malignancies and its Interactions with Other Epigenetic Modifications. *Leukemia* 35, 1243–1257. doi:10.1038/s41375-021-01225-1

Yao, S., Zhong, L., Chen, M., Zhao, Y., Li, L., Liu, L., et al. (2017). Epigallocatechin-3-gallate Promotes All-Trans Retinoic Acid-Induced Maturation of Acute Promyelocytic Leukemia Cells via PTEN. *Int. J. Oncol.* 51, 899–906. doi:10.3892/ijo.2017.4086

Yoshihara, K., Shahmoradgoli, M., Martínez, E., Vegesna, R., Kim, H., Torres-Garcia, W., et al. (2013). Inferring Tumour Purity and Stromal and Immune Cell Admixture from Expression Data. *Nat. Commun.* 4, 2612. doi:10.1038/ncomms3612

Yu, G., Wang, L.-G., Han, Y., and He, Q.-Y. (2012). clusterProfiler: an R Package for Comparing Biological Themes Among Gene Clusters. *OMICS: A J. Integr. Biol.* 16, 284–287. doi:10.1089/omi.2011.0118

Zhang, P., Liu, G., and Lu, L. (2021a). N6-Methylandenosine-Related lncRNA Signature Is a Novel Biomarkers of Prognosis and Immune Response in Colon Adenocarcinoma Patients. *Front. Cel Dev. Biol.* 9, 703629. doi:10.3389/fcell.2021.703629

Zhang, X., Shen, L., Cai, R., Yu, X., Yang, J., Wu, X., et al. (2021b). Comprehensive Analysis of the Immune-Oncology Targets and Immune Infiltrates of N6-Methyladenosine-Related Long Noncoding RNA Regulators in Breast Cancer. *Front. Cel Dev. Biol.* 9, 686675. doi:10.3389/fcell.2021.686675

Zhao, C., Yang, S., Lu, W., Liu, J., Wei, Y., Guo, H., et al. (2020a). Increased NFATC4 Correlates with Poor Prognosis of AML through Recruiting Regulatory T Cells. *Front. Genet.* 11, 573124. doi:10.3389/fgene.2020.573124

Zhao, J., Lin, X., Zhuang, J., and He, F. (2021). Relationships of N6-Methyladenosine-Related Long Non-coding RNAs with Tumor Immune Microenvironment and Clinical Prognosis in Lung Adenocarcinoma. *Front. Genet.* 12, 714697. doi:10.3389/fgene.2021.714697

Zhao, Q., Zhao, Y., Hu, W., Zhang, Y., Wu, X., Lu, J., et al. (2020b). m6A RNA Modification Modulates PI3K/Akt/mTOR Signal Pathway in Gastrointestinal Cancer. *Theranostics* 10, 9528–9543. doi:10.7150/thno.42971

Zheng, X., and Gong, Y. (2021). Functions of RNA N6-Methyladenosine Modification in Acute Myeloid Leukemia. *Biomark Res.* 9, 36. doi:10.1186/s40364-021-00293-w

Zhuang, M. F., Li, L. J., and Ma, J. B. (2019). LncRNA HOTTIP Promotes Proliferation and Cell Cycle Progression of Acute Myeloid Leukemia Cells. *Eur. Rev. Med. Pharmacol. Sci.* 23, 2908–2915. doi:10.26355/eurrev_201904_17569

Zimta, A.-A., Tomuleasa, C., Sahnoune, I., Calin, G. A., and Berindan-Neagoe, I. (2019). Long Non-coding RNAs in Myeloid Malignancies. *Front. Oncol.* 9, 1048. doi:10.3389/fonc.2019.01048

Zuo, W., Zhou, K., Deng, M., Lin, Q., Yin, Q., Zhang, C., et al. (2020). LINC00963 Facilitates Acute Myeloid Leukemia Development by Modulating miR-608/MMP-15. *aging* 12, 18970–18981. doi:10.18632/aging.103252

Conflict of Interest: The authors declare that the research was conducted in the absence of any commercial or financial relationships that could be construed as a potential conflict of interest.

Publisher's Note: All claims expressed in this article are solely those of the authors and do not necessarily represent those of their affiliated organizations, or those of the publisher, the editors, and the reviewers. Any product that may be evaluated in this article, or claim that may be made by its manufacturer, is not guaranteed or endorsed by the publisher.

GLOSSARY

AML acute myeloid leukemia
APL acute promyelocytic leukemia
AUC area under the curve
BMAs bone marrow aspirates
BMM bone marrow microenvironment
BPs biological processes
CCs cellular components
C-index consistency index
CNV copy number variation
DCA decision curve analysis
DDA1 DET1- and DDB1-associated protein 1
DEGs differentially expressed genes
EGCG pigallocatechin-3-gallate
FDR false discovery rate
FPKM fragments per kilobase of transcript per million mapped reads
GDSC Genomics of Drug Sensitivity in Cancer
GEO Gene Expression Omnibus
GO gene ontology
GSEA gene set enrichment analysis
KEGG Kyoto Encyclopedia of Genes and Genomes
lncRNAs long non-coding RNAs
m6A N 6-methyladenosine
MFs molecular functions
OS overall survival
PTEN phosphatase and tensin homolog
ROC receiver operating characteristic
SNP single-nucleotide polymorphism
TCGA The Cancer Genome Atlas
TMB tumor mutation burden
TME tumor microenvironment
TPM transcripts per million reads
Tregs T-regulatory cells

frontiers | Frontiers in Genetics

ORIGINAL RESEARCH
published: 08 June 2022
doi: 10.3389/fgene.2022.873230

The Novel lncRNA ENST00000530525 Affects ANO1, Contributing to Blood–Brain Barrier Injury in Cultured hCMEC/D3 Cells Under OGD/R Conditions

*Wen Jiang[1], Jie Li[2], Yuefang Cai[1], Wenchen Liu[3], Mei Chen[3], Xiaoying Xu[4], Minzhen Deng[3], Jingbo Sun[1,3,5,6], Lihua Zhou[4], Yan Huang[1,3,5,6], Shuang Wu[1] and Xiao Cheng[1,3,5,6]**

[1]Department of Second Institute of Clinical Medicine, Guangzhou University of Traditional Chinese Medicine, Guangzhou, China, [2]Department of Anesthesiology, Guangdong Provincial Hospital of Traditional Chinese Medicine/The Second Affiliated Hospital of Guangzhou University of Chinese Medicine, Guangzhou, China, [3]Department of Neurology, Guangdong Provincial Hospital of Traditional Chinese Medicine/The Second Affiliated Hospital of Guangzhou University of Chinese Medicine, Guangzhou, China, [4]Department of Anatomy, Sun Yat-Sen School of Medicine, Sun Yat-Sen University, Shenzhen, China, [5]State Key Laboratory of Dampness Syndrome of Chinese Medicine, The Second Affiliated Hospital of Guangzhou University of Chinese Medicine, Guangzhou, China, [6]Guangdong Provincial Key Laboratory of Research on Emergency in TCM, Guangzhou, China*

OPEN ACCESS

Edited by:
William C. Cho, QEH, Hong Kong SAR, China

Reviewed by:
Malgorzata Burek, Julius Maximilian University of Würzburg, Germany
Ravi K. Sajja, Nelson Laboratories, United States
Abraham Jacob Al-Ahmad, Jerry H. Hodge School of Pharmacy, United States

***Correspondence:**
Xiao Cheng
chengxiaolucky@126.com

Specialty section:
This article was submitted to RNA, a section of the journal Frontiers in Genetics

Received: *10 February 2022*
Accepted: *19 May 2022*
Published: *08 June 2022*

Citation:
Jiang W, Li J, Cai Y, Liu W, Chen M, Xu X, Deng M, Sun J, Zhou L, Huang Y, Wu S and Cheng X (2022) The Novel lncRNA ENST00000530525 Affects ANO1, Contributing to Blood–Brain Barrier Injury in Cultured hCMEC/D3 Cells Under OGD/R Conditions. Front. Genet. 13:873230. doi: 10.3389/fgene.2022.873230

Ischemic stroke (IS) is a major neurological disease with high fatality and residual disability burdens. Long noncoding RNAs (lncRNAs) have been found to play an important role in IS. However, the roles and significance of most lncRNAs in IS are still unknown. This study was performed to identify differentially expressed (DE) lncRNAs using a lncRNA microarray in whole blood samples of patients suffering from acute cerebral ischemia. Bioinformatics analyses, including GO, KEGG pathway enrichment analysis, and proximity to putative stroke risk location analysis were performed. The novel lncRNA, ENST00000530525, significantly decreased after IS. Furthermore, we evaluated lncRNA ENST00000530525 expression in cultured hCMEC/D3 cells under oxygen-glucose deprivation/reoxygenation (OGD/R) conditions using fluorescent *in situ* hybridization (FISH) and quantitative real-time polymerase chain reaction (RT–qPCR) analysis. To investigate the function of lncRNA ENST00000530525, its over-expression (OE) and negative control (NC) plasmids were transfected into hCMEC/D3 cells, and cell viability was detected by a cell counting kit-8 (CCK-8) assay after OGD/R. LncRNA ENST00000530525 and ANO1 expression were investigated using RT–qPCR and immunofluorescence. For blood–brain barrier (BBB) permeability, FITC-dextran transendothelial permeability assay and tight junction (TJ) protein immunofluorescence assays were performed. There were 3352 DE lncRNAs in the blood samples of acute IS patients. The validation results were consistent with the gene chip data. The GO and KEGG results showed that these lncRNAs were mainly related to oxygen

Abbreviations: ANO1, Anoctamin-1; BBB, Blood-brain barrier; CCK-8, cell counting kit-8; CT, Computed tomographic; CFTR, Cystic fibrosis transmembrane conductance regulator; CSF, Codon substitution frequency; DE, Differential expressed; ECG, Electrocardiograph; FE, Feature Extraction; FISH, Fluorescent *in situ* hybridization; IS, Ischemic stroke; lncRNAs, Long noncoding RNAs; NC, Negative control; OE, Over-expression; ORF, Open reading frame; OGD/R, Oxygen-glucose deprivation/reoxygenation; RT-qPCR, Quantitative real-time polymerase chain reaction; TMEM16A, Transmembrane protein 16A; TJ, Tight junction.

and glucose metabolism, leukocyte transendothelial migration, mitophagy and cellular senescence. Among these, lncRNA ENST00000530525 was the most highly downregulated lncRNA and it was mapped within the IS-associated gene anoctamin-1 (ANO1). We further found that lncRNA ENST00000530525 was downregulated in hCMEC/D3 cells under 4 h OGD and 20 h reoxygenation (OGD4/R20) conditions. Upregulating lncRNA ENST00000530525 by plasmid transfection decreased cell viability while increasing ANO1 expression and it contributed to BBB injury in hCMEC/D3 cells after OGD4/R20. The lncRNA ENST00000530525 might play deleterious roles in post-stroke pathogenesis. These results show that some DE lncRNAs in humans participate through characteristic roles in post-stroke pathogenesis; thus, the roles and significance of some novel lncRNAs in IS warrant further study.

Keywords: ischemic stroke, ANO1, lncRNA, ENST00000530525, oxygen-glucose deprivation and reperfusion, human cerebrovascular endothelial cells

INTRODUCTION

Stroke is a high risk factor for death and disability worldwide. IS is the most prevalent, accounting for up to 80% of all stroke cases (Wang et al., 2017). Hypertension, diabetes, dyslipidemia, atrial fibrillation, and obesity are prevalent among Chinese individuals aged 40 years and older (Li et al., 2017). This makes stroke a very important health issue.

Cerebral blood flow interruption initiates a cascade of complex and poorly understood pathophysiologic processes, including oxidative stress, inflammation and apoptosis (Schaukowitch and Kim, 2014; Ren and Yang, 2018). Therefore, many scientists have turned to epigenetics to understand the molecular mechanisms, regulation of the complex stroke-induced pathophysiological processes as well as the elucidation of new therapeutic targets and the design of new treatment modalities (Dharap et al., 2012; Liu et al., 2018)). The most promising theme thus far is the alteration of the expression of some noncoding RNAs that could participate in post-stroke processes, both neuroprotective and neurodegenerative.

Long noncoding RNAs (lncRNAs) are more than 200 nucleotides long and do not encode any proteins. Previous studies showed lncRNAs could modulate cell survival, inflammation, and angiogenesis (Bao et al., 2018). They appear to perform these varied functions by interacting with multiple elements involved in the central dogma of biology, such as other RNAs, DNA, and proteins (Akella et al., 2019). Recently, a number of abnormally expressed lncRNAs have been identified in IS though microarrays, high-throughput deep sequencing, and RNA-seq (Bao et al., 2018). However, the importance and significance of most lncRNAs remain poorly understood and warrant further study in IS.

Therefore, this research was performed to evaluate lncRNA expression in patients' whole blood samples after acute cerebral ischemia. Bioinformatics analyses were also used for the dysregulated genes to reveal the predicted connections and functions of the DE lncRNAs. Furthermore, we found that lncRNA ENST00000530525 is highly decreased in stroke patients relative to controls, and the high conservation of lncRNA ENST00000530525 suggests that it may be important in stroke pathology.

LncRNA ENST00000530525 is located intragenically with its neighbor gene ANO1. However, the role of lncRNA ENST00000530525 and the regulatory mechanism linking lncRNAs and ANO1 signaling in stroke remain enigmatic. ANO1 (also known as transmembrane protein 16A, TMEM16A) widely expresses in eukaryotes and is a molecular indicator of calcium-activated chloride channels. Recent studies have shown that the upregulation of ANO1 is related to the development of many diseases, such as IS (Wang et al., 2012; Wu et al., 2014; Deng et al., 2016). Recently, it was found that ANO1 is strongly expressed in cerebrovascular endothelial cells, IS-induced BBB injury is accompanied by upregulation of ANO1. Inhibiting ANO1 significantly rescued OGD/R-induced downregulation of TJ proteins and upregulation of BBB permeability *in vitro* (Liu et al., 2019). And the present studies showed that ANO1 affects the functions of brain capillary endothelial cells, which are involved in BBB functions (Suzuki et al., 2020; Liu et al., 2021; Ma et al., 2021; Suzuki et al., 2021).

As we know, BBB is part of the neurovascular unit that plays a vital role in regulating blood-to-brain flux of endogenous and exogenous xenobiotics and associated metabolites. Because of the TJ protein between the endothelial cells of the BBB, blood-borne substances and cells have restricted access to the brain. Under IS condition, the BBB can be destroyed and loss of the TJ integrity, followed by the extravasation of blood components into the brain and compromise of normal neuronal function, future research on the BBB is likely to reveal promising potential therapeutic targets for protecting the BBB and improving patient outcome after IS (Jiang et al., 2018).

Based on the above, the underlying mechanisms and targets of lncRNA ENST00000530525 in hCMEC/D3 cells under OGD/R injury were investigated, which may provide a novel idea for us to better understand the function and significance of lncRNAs in the pathophysiological mechanism of IS. Further studies of these lncRNAs in biological systems after IS may provide opportunities to identify biomarkers and new therapeutic targets.

TABLE 1 | Demographics and the distribution of the comorbid conditions in the study sample.

Characteristics	Non-stroke group (*n* = 20)	Stroke group (*n* = 10)
Age (years)	64.54 ± 11.83	63.58 ± 10.20
Gender (Male)	14 (70%)	8 (80%)
Hypertension history	10 (50%)	7 (70%)*
Diabetes history	1 (5%)	3 (30%)*
Smoking history	3 (15%)	4 (40%)*
Cardiovascular disease history	3 (15%)	1 (5%)
Hyperlipidemia	5 (25%)	5 (5%)

The table shows the age of study participants along with the distribution of their comorbid conditions such as hypertension, diabetes, smoking, cardiovascular disease and hyperlipidemia.

MATERIALS AND METHODS

Study Subjects

Ten patients with a diagnosis of IS who were seen at Guangdong Province Traditional Chinese Medical Hospital from September 2016 to November 2017 along with 20 control subjects were recruited to join the study. The protocol was approved by the ethics committee of Guangdong Provincial Hospital of Chinese Medicine (B2016-149-01). After explaining study details, patients and their immediate caregivers or significant others provided written informed consent to participate. There was no incentive to participate.

Patients' histories, examinations, and evaluations were collected after qualified neurologists diagnosed them as acute IS. Standard stroke assessments performed at our hospital included computed tomographic (CT), electrocardiography (ECG), magnetic resonance imaging (MRI), carotid Doppler, Holter monitor and computed tomographic angiography or magnetic resonance arteriogram of extracranial and intracranial vessels according to the clients' clinical data. Acute IS patients who presented with a rare pathogenesis other than atherosclerosis and cardiogenic stroke, psychopathology, pregnancy and lactation or those patients who were in other clinical trials when they suffered a stroke were not eligible to participate in this study. The age and sex of the 20 control subjects were matched to those of the stroke patients; the control patients were without a history of stroke and did not have severe heart disease, cardiac insufficiency, hepatitis, renal insufficiency, respiratory failure, malignant tumor or gastrointestinal bleeding.

Derivation and Validation Group

Ten IS patients and 20 non-stroke subjects were recruited to detect DE lncRNAs and randomly distributed them to the derivation group or the validation group. All patients' race, sex, age, and vascular risk factors (diabetes mellitus, hypertension, and hyperlipidemia) were matching. Exclusion criteria included prior stroke; treatment with thrombolysis or anticoagulant before sample collection;

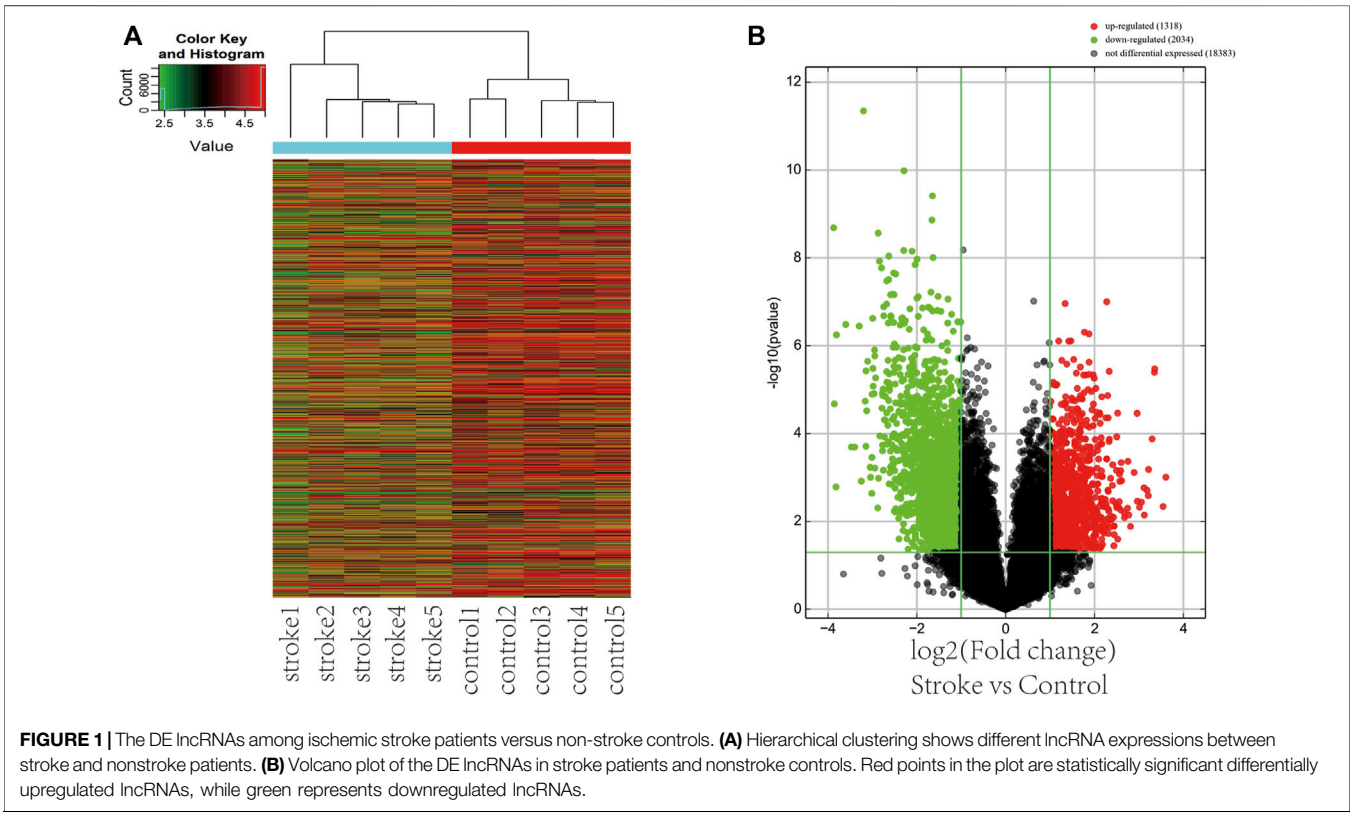

FIGURE 1 | The DE lncRNAs among ischemic stroke patients versus non-stroke controls. **(A)** Hierarchical clustering shows different lncRNA expressions between stroke and nonstroke patients. **(B)** Volcano plot of the DE lncRNAs in stroke patients and nonstroke controls. Red points in the plot are statistically significant differentially upregulated lncRNAs, while green represents downregulated lncRNAs.

TABLE 2 | The top 10 highly up- and downregulated lncRNAs.

Seq-Name	*p*-value	Fold change	Regulation	Gene symbol
A				
T120068	0.0010	12.2021	up	G028344
T346481	0.0045	11.6843	up	G081575
uc002vbb.3	0.0001	10.2441	up	BC047484
T333126	0.0001	10.2030	up	G078089
ENST00000530249	0.0001	9.8429	up	CTD-3138F19.1
ENST00000597530	0.0007	9.3130	up	RP11-251M1.1
T224664	0.0026	9.2702	up	G051903
ENST00000447488	0.0019	9.0912	up	AC073254.1
NR_046,612	0.0071	8.7159	up	HTR2A-AS1
T344288	0.0017	8.6688	up	G080966
B				
ENST00000530525	0.0001	14.6300	down	RP11-805J14.3
T198099	0.0001	14.4622	down	G045690
ENST00000523658	0.0016	14.0950	down	RP11-402L5.1
T235708	0.0001	12.1118	down	G054213
T328914	0.0002	11.0822	down	G077138
NR_132,119	0.0002	10.5270	down	GTF2IP20
T024196	0.0001	9.8059	down	G005224
ENST00000458252	0.0012	9.4884	down	AC123886.2
T056136	0.0001	9.1733	down	G012959
TCONS_00010056	0.0001	8.9389	down	XLOC_004,504

hemorrhagic infarction; infection before or after stroke; subarachnoid hemorrhage; recreational drug abuse; dialysis; cancer; and immunosuppressive therapy for blood abnormalities or steroids. The validation set was used to prove the microarray analysis results. The primer sequences used are provided in **Supplementary Table S1**.

Blood Collection and RNA Isolation

Venipuncture was performed once on all study participants, and their whole blood was drawn into EDTA tubes (Jingxin Biotechnology Co., Ltd., China). For stroke patients, blood collection time varied from a few hours to 2 weeks after symptom onset. For the control samples, the time of extraction was not applicable. And then the tubes was rapidly frozen with liquid nitrogen and put at -80°C until use. RNA isolation was performed by using TRIzol (Invitrogen, United States), which was added to every cryopreserved serum supernatant sample according to the protocol.

Array Hybridization

Arraystar Human lncRNA V4.0 chip (Arraystar, United States) was used, which can test 20,730 protein-coding and 40,173 lncRNA transcripts. Sample marking and chip hybridization were based on the recommended experimental procedure of Agilent One-Color Microarray-Based Gene Expression Analysis (Agilent Technology, United States). Briefly, a mRNA-ONLY™ Eukaryotic mRNA Isolation Kit (Epicenter, United States) was used to remove the rRNA from mRNA, which was then amplified and transcribed into cRNA with fluorescence by random priming. The marked cRNAs was purified by the RNeasy Mini Kit (Qiagen 74104, Germany). The RNA was quantified by a NanoDrop ND-1000 spectrophotometer (NanoDrop Technologies, Thermo Fisher, United States), and an Agilent 2100 Bioanalyzer (Agilent, United States) was used to assess the quality of the samples. The GenePix 4000B chip scanner (Agilent, United States) was used to wash and process arrays. DAT file formats were used to save raw values. The scanned results were transformed into digital data and then saved.

Differential Expression Analysis

To identify DE lncRNAs, cuffdiff was used for the differential expression analysis. Only probes with a fold-change higher than 2 and $p < 0.05$ were selected as significantly DE lncRNAs or mRNAs. To obtain the overall characteristics of the lncRNA and mRNA expression profiles, we used the R package for hierarchical clustering analysis of normalized values of all DE lncRNAs to generate heatmaps. Bioinformatics analyses, including the Gene Ontology project (GO, http://geneontology.org/), the database Kyoto Encyclopedia of Genes and Genomes (KEGG) pathway enrichment analysis (http://www.kegg.jp/kegg/), and network analysis, were also performed for the identified DE genes. Through a literature review, NONCODE, UCSC Genome Browser, and OMIM®—Online Mendelian Inheritance in Man® databases, we further explained the biology of the differential lncRNAs.

Data Normalization

The original data were exported by GeneSpring GX v12.1 software (Agilent, United States). The data were normalized by preprocess Core in the R package, and log2 transformation was performed to obtain the final normalized data. The standardized data were further analyzed by screening high-

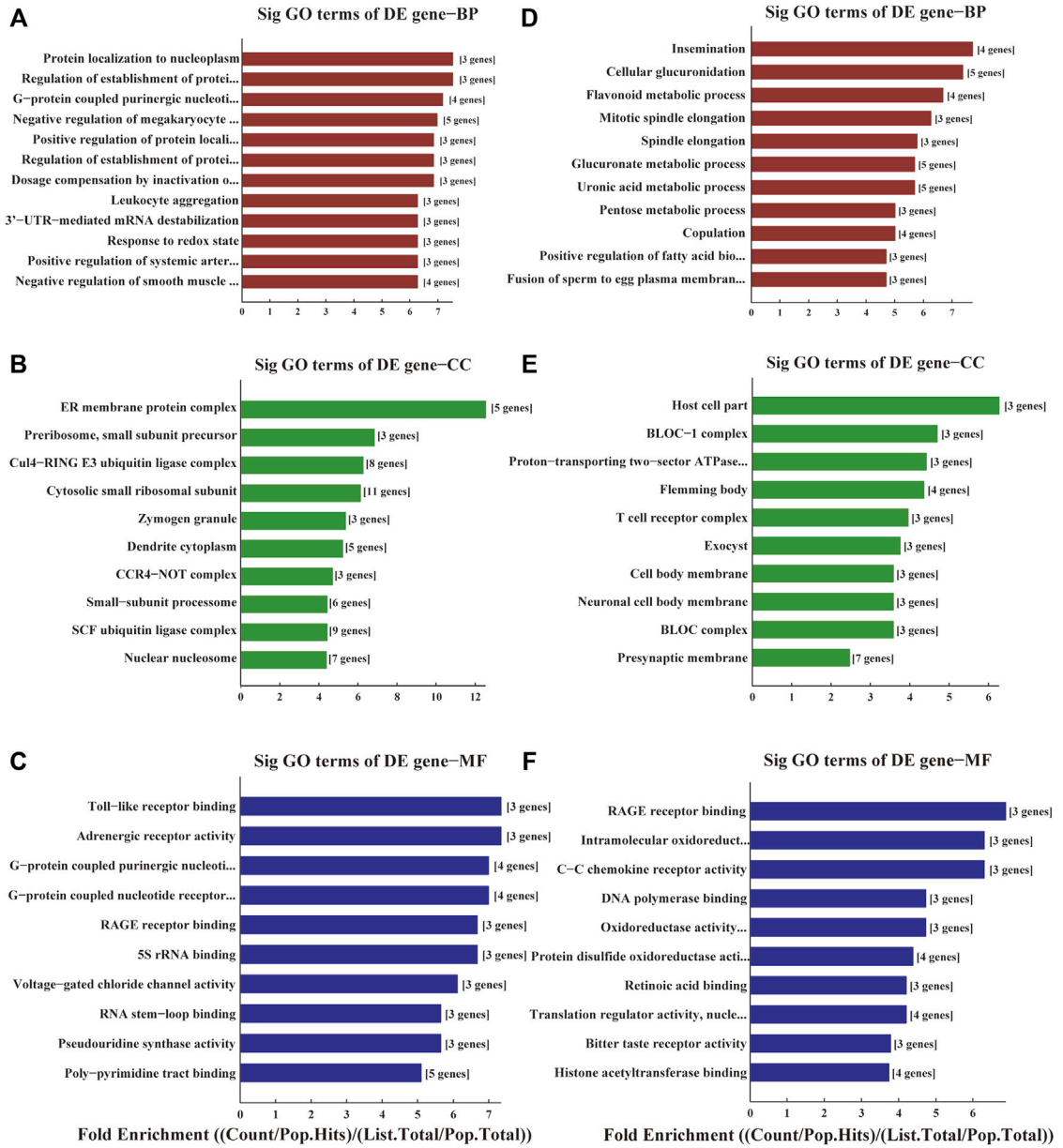

FIGURE 2 | GO analyses of the DE genes among ischemic stroke patients versus non-stroke controls. GO terms of Biological Process (BP), Cellular Component (CC) and Molecular Function (MF) for the DE upregulated **(A–C)** and downregulated genes **(D–F).**

quality probes marked as detected in at least three samples out of six. Hierarchical clustering was conducted using R script. Finally, the lncRNAs expressed at significantly different levels between the two groups of samples were screened by volcano plots.

hCMEC/D3 Cell Culture

HCMEC/D3 cells (FuHeng Biology, FH1110, Shanghai, China) were cultured in endothelial cell medium (ECM,ScienCell, Carlsbad, United States) and added fetal bovine serum (FBS, Gibco, Australia) into ECM to making its concentration to 10%, and then incubated the cells in humidified atmosphere at 37°C with 5% CO_2. All experiments with hCMEC/D3 cells were used below 15 passages.

OGD/R Condition

To mimic acute IS *in vitro*, hCMEC/D3 cells were subjected to OGD/R. The establishment of OGD model in this paper refers to the literatures (Fan et al., 2021; Xu et al., 2021). When the cells became confluent, glucose-free DMEM (Cienry, Zhejiang, China) was used to replace the culture medium, and the cells were put into an anaerobic incubator (94% N_2, 5% CO_2, 1% O_2) for 2, 4, 6, and 8 h. After incubation, the cells were

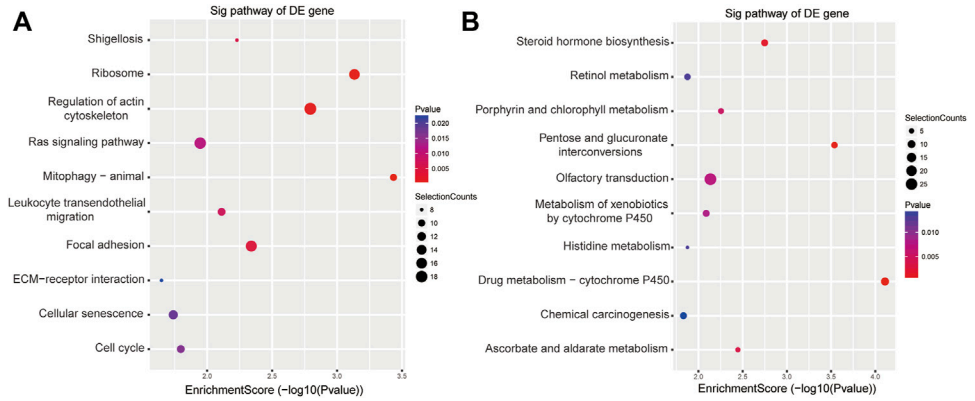

FIGURE 3 | KEGG analyses of the DE genes among ischemic stroke patients versus non-stroke controls. KEGG terms for the DE upregulated **(A)** and downregulated genes **(B)**.

returned to regular conditions and normal medium for reoxygenation. The total time of oxygen glucose deprivation and reoxygenation was 24 h.

CCK-8 Assay

The cell counting kit-8 assay (Dojindo, Tokyo, Honshu, Japan) was used to detect cell viability. All of the procedures followed the manufacturer's instructions. Cell suspensions (100 μl, 1 × 10^4 cells/mL) were added to a 96-well plate. After incubating with NC or OE (MOI = 50 nM) in 96-well microtiter plates, CCK-8 solution (10 μl) was put into 96-well plate after OGD for 4 h and reoxygenation for 20 h. Finally, absorbance at 450 nm of the wells was measured by the microplate reader (SYNERGY H1, BioTek), and five replicate wells were assessed in each experiment.

RNA FISH

Subcellular localization of the lncRNA ENST00000530525 was detected by the FISH Kit (RiboBio, China). The Cy3-labeled lncRNA ENST00000530525 probe and the control probe 18S were all designed by RiboBio (Guangzhou, China). Briefly, 4% paraformaldehyde was used to fix hCMEC/D3 cells for 15 min at room temperature and washed with PBS three times for 5 min each time. The cells were incubated in proteinase K for 5 min at 4°C and washed as before. Then, prehybridization buffer was added to the cells for incubation at 37°C and then they were incubated in hybridization buffer with specific probes for lncRNA ENST00000530525 and 18S at 37°C overnight. After extensive washing with SSC, the cell nucleus was stained by DAPI for 5 min. The images were took by the fluorescence microscope (Nikon Ti2-E, Japan).

Plasmid Transfection

RiboBio company (Guangzhou, China) provided the lncRNA ENST00000530525 (OE) overexpression plasmid, negative control plasmid (NC) and transfection kit (riboFECT™ CP, C10511-05). HCMEC/D3 cells were cultured and incubated for 3 days with OE or NC (MOI = 50 nM), which was then replaced by glucose-free DMEM for OGD 4 h. RT–qPCR was used to detect the transfection efficiency of lncRNA ENST00000530525.

FITC-Dextran Transendothelial Permeability Assay

In brief, cell suspension was added into polycarbonate 12-well Transwell inserts with a 0.4 μm pore size (Corning, United States) at a density of 4 × 10^4 cells/cm^2. When cells grown to approximately 70% confluence, they were transfected with plasmid. Then FITC-labeled dextran (0.1 mg/ml, MW, 70000, Sigma-Aldrich) was added to the upper chamber and 500 μL PBS was added to the lower cavity after OGD/R. Then we put them in a cell incubator for 5 min. The microplate reader was used to analyze the supernatant from the lower chamber (excitation at 490 nm, emission at 520 nm).

Quantitative Real-Time PCR for lncRNA and mRNA

The protocol of RT-qPCR are as follows. We used TRIzol (Thermo Fisher Scientific, Waltham, MA, United States) to separate total RNA from hCMEC/D3 cells. For reverse transcriptase, we used cDNA synthesis kits (Takara, Dalian, China) to synthesize cDNA. SYBR® Premix Ex Taq™II (Takara, Dalian, China) was used for amplification. The internal reference is human β-actin gene. Comparative quantification was performed by using the $2^{-\Delta\Delta Ct}$ method. The primer sequences used are shown in **Supplementary Table S1**.

Immunofluorescence

Cells were cultured on 24-well plates for immunofluorescence staining at a seeding density of 7 × 10^4 cells per well (Shin et al., 2016). For immunofluorescent staining, 4% paraformaldehyde was used to fix the cell at 4°C overnight. After blocking with 5% BSA, the first antibodies:

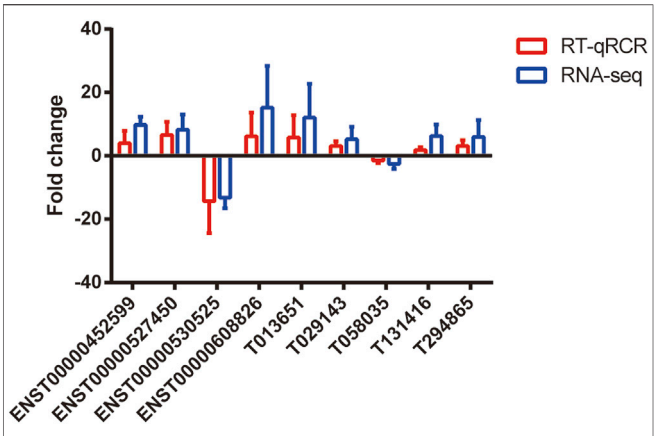

FIGURE 4 | Validation of differential expression of lncRNAs. RT-qPCR was used to verify the expression levels of these selected lncRNAs ($p < 0.05$). The blue points represent RT-qPCR, while the red points represent the gene chip of RNA-seq. $n = 5$.

rabbit monoclonal anti-ANO1 (1:200), rabbit monoclonal anti-ZO1 (1:200), rabbit anti-occludin (1:100), and rabbit anti-claudin-5 (1:200) were added to the cells at 4°C overnight. Then the cells were incubated with the corresponding secondary antibody in a dark chamber at 37°C for 1 h. The antibodies and secondary antibodies were obtained from Abcam. After stained with DAPI (1: 500, Beyotime), the fluorescence microscope (Nikon TI2-E) was used to take the images.

Transfection and Luciferase Assays

293T cells were inoculated in 24-well plates and cultured until the degree of cell fusion reached over 60%. Plasmid transfections for luciferase assays were performed with 1 μg plasmid and 2 μL X-tremegene HP reagent (ROCHE, Switzerland) as described by the manufacturer. The expression of fluorescent-labeled genes on the plasmid was observed 24–48 h after transfection to determine the transfection efficiency. And then 48 h post transfection, luminescence was detected using the Dual-Luciferase Reporter Assay System as described by the manufacturer (Promega, United States). Data were normalized to the Renilla luminescence and presented relative to control transfected group.

Statistical Analysis

All quantitative experiments were performed at least three times, and the data are showed as the mean ± SD. Statistical tests were performed using SPSS 24.0 statistical software and Graphed Prism 6 was used for graphic representations. The comparisons of patient characteristics between two groups were analyzed by the chi-square test (sex, hypertension history, diabetes history, smoking history, cardiovascular history, and hyperlipidemia) and unpaired two-tailed Student's t-test (age). One-way ANOVA was used to analyze the comparisons among multiple groups. $p < 0.05$ was considered statistically significant.

RESULTS

Characteristics

The characteristics of 10 stroke patients and 20 non-stroke cases are shown in **Table 1**. There were significantly more stroke patients with a positive history of hypertension, diabetes, and smoking.

Differential lncRNA Expression and GO and KEGG Analyses Among IS Patients versus Non-stroke Patients

We used the Arraystar Human lncRNA V4.0 chip to analyze the DE lncRNAs between two groups. Unsupervised hierarchical clustering analysis generated from the expression profile of the lncRNAs showed the different expression levels between non-stroke and stroke patients (**Figure 1A**). Volcano plots were used to show the statistically significant differences expression of lncRNAs. There were 3352 DE lncRNAs, with 1318 upregulated and 2034 downregulated lncRNAs (**Figure 1B**). The top 10 most significantly up and downregulated lncRNAs are listed in **Table 2**. T120068 (fold change 12.2021) was the most highly upregulated lncRNAs. ENST00000530525 (fold change -14.63) was the most highly downregulated lncRNAs.

The functions of these lncRNAs were predicted with the co-expressed mRNAs using GO and KEGG pathway annotations. In GO annotation, the upregulated genes were mainly related to ER membrane protein complexes, Toll-like receptor binding, protein localization to the nucleoplasm (**Figures 2A–C**). The downregulated genes were manly related to RAGE receptor binding, intramolecular oxidoreductase activity, cellular glucuronidation, cellular glucuronation and T cell receptor complexes (**Figures 2D–F**).

The results of KEGG enrichment showed that these DE genes were related to pathways in pathophysiological processes underpinning acute cerebral infarction, such as pentose and glucuronate interconversions, regulation of the actin cytoskeleton, RAS signal pathway, focal adhesion, leukocyte transendothelial migration, mitophagy and cellular senescence (**Figures 3A,B**).

Validation of the DE lncRNAs

We selected nine DE lncRNAs at random and used RT–qPCR analysis to prove our gene chip performance (**Figure 4**). There were seven upregulated (ENST00000452599, ENST00000527450, ENST00000608826, T013651, T029143, T131416, and T294865) and two downregulated lncRNA transcripts (ENST00000530525 and T058035). The RT–qPCR results were consistent with the gene chip data in the two groups.

Biological Interpretation-Proximity to Putative Stroke Genes

Among the upregulated lncRNAs, ASHGV40004037 was annotated to NR_046612 that mapped to the putative

TABLE 3 | Up and downregulated lncRNAs and proximity to putative stroke genes.

Probe name	lncRNA ID	Cyto-band	Gene in region	lncRNA Up-/down-stream	lncRNA Distance (kb) from gene	FC
ASHGV40004037	NR_046612	13q14.2	HTR2A	within	within	8.7159
ASHGV40013775	NR_002312	14q11.2	PARP2	down	45	6.1135
ASHGV40056557	NR_037932	19q13.32	APOC2	down	416.9	4.7449
			APOC4	down	419.2	
			APOE	down	461.9	
ASHGV40056142	T111838	14q32.33	MTA1	within	within	4.6273
ASHGV40042838	T294865	5q35.3	ADAMTS2	up	346.4	4.0617
ASHGV40043041	T297706	6p23	SIRT5	down	5.7	3.9144
ASHGV40008778	ENST00000530525	11q13.3	ANO1	within	within	−14.6300
ASHGV40001758	ENST00000395996	8q22.2	VPS13B	within	within	−14.0950
ASHGV40037155	NR_045414	4p16.3	HTT	down	7.6	−6.3636
ASHGV40053990	ENST00000416061	XP11.23	SUV39H1	down	3.4	−4.9941

Significant DE lncRNA probe sets in stroke vs. non-stroke groups and their proximity to putative stroke genes ("-" means downregulated, fold change (FC) ≥ 2.0, $p < 0.05$*).*

ischemic risk locus HTR2A at cytoband 13q14.2. Similarly, ASHGV40013775 was annotated to NR_002312, which has genomic coordinates 45 kb downstream of the PARP2 cerebral ischemic injury-associated gene at 14q11.2. ASHGV40056557 is expressed as NR_037932, which maps to the stroke-associated genes apolipoprotein C and E within 420 kb, while T111838 (ASHGV40056142) maps at 14q32.33 within metastasis-associated protein 1 (MTA1), a transcriptional regulator-associated gene modifing master chromatin. Additionally, T294865 (ASHGV40042838) mapped within 350 kb of another gene ADAMTS2 associating with stroke at 5q35.3, while T297706 (ASHGV40043041) mapped to Sirtuin 5 (SIRT5) within 6 kb at 6p23. Among the downregulated lncRNAs, the annotation of ASHGV40008778 identified the validated lncRNA ENST00000530525, which is within anoctamin-1 (ANO1), a chloride ion channel gene related to cerebrovascular remodeling. ENST00000395996 (ASHGV40001758) is within VPS13B and is associated with cerebral ischemic injury. Furthermore, NR_045414 (ASHGV40037155) at 4p16.3 mapped within 8 kb of HTT and is associated with post-stroke depression (PSD), while ENST00000416061 (ASHGV40053990)'s genomic coordinates were 3.4 kb downstream of SUV39H1, a histone methyltransferase related to stroke (**Table 3**).

LncRNA ENST00000530525 was Located Intragenically with ANO1

To futher detect the expression trend of lncRNA ENST00000530525 in stroke patients, we expanded the samples and randomly chose 40 blood samples from stroke patients and 20 blood samples from controls. LncRNA ENST00000530525 expression was significantly decreased in IS group compared with the control group (**Supplementary Figure S1**). To further research the function of lncRNA ENST00000530525 in stroke pathology, the noncoding nature of lncRNA ENST00000530525 was first confirmed by coding-potential analysis (**Supplementary Figure S2**) (Qu et al., 2016). Then, we checked Ensembl (Abdillahi et al., 2012), an online database used to predict gene location (Yates et al., 2020), and found that the lncRNA ENST00000530525 is located intragenically with ANO1 (**Supplementary Figure S3A**). ANO1 is strongly expressed in cerebrovascular endothelial cells (Liu et al., 2019), and study showed that ANO1 contributed to the proliferation and migration of brain capillary endothelial cells, which are involved in BBB functions (Suzuki et al., 2020). We also checked STRING (Lo et al., 2007), an online database, to summarize the network of predicted associations for this protein (Szklarczyk et al., 2015). ANO1 is known to have strong links to epithelial ion channels, such as cystic fibrosis transmembrane conductance regulator (CFTR) and the Bestrophin family (**Supplementary Figure S3B**). Thus, we further speculated that lncRNA ENST00000530525 and ANO1 are involved in the pathology of stroke. Because ANO1 is strongly expressed in cerebrovascular endothelial cells, in the following study, the cells undergo OGD/R was chosen to mimic IS.

LncRNA ENST00000530525 was DownRegulated in hCMEC/D3 Cells After OGD/R

To investigate lncRNA ENST00000530525 expression in hCMEC/D3 cells after OGD/R injury, CCK-8 assays were used to test cell vitality. The results indicated that the longer the OGD time was, the worse the cell vitality (**Figure 5A**). The RT–qPCR results showed lncRNA ENST00000530525 expression was significantly downregulated in hCMEC/D3 cells after OGD/R compared with control cells, which is consistent with the results of ChIP sequencing (**Figure 5B**). The expression of lncRNA ENST00000530525 was highly downregulated after 4 h OGD and 20 h reoxygenation.

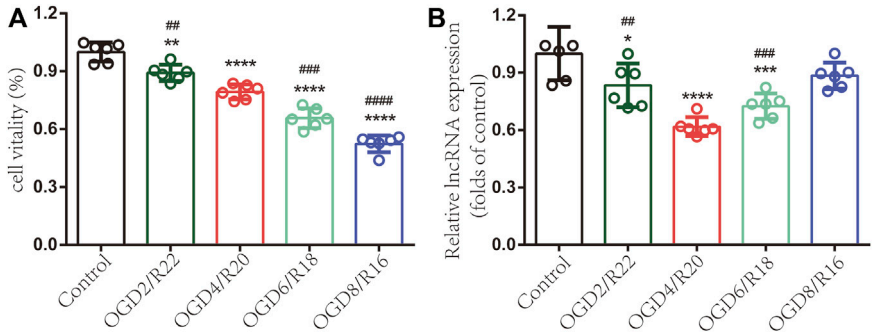

FIGURE 5 | LncRNA ENST00000530525 is downregulated in hCMEC/D3 cells under OGD/R condition. Cells were exposed to OGD for 2, 4, 6 or 8 h and reoxygenate for 22, 20, 18 or 16 h. Each bar represents a different OGD duration and reoxygenation time (e.g., OGD2/R22 represents 2 h of OGD and 22 h of reoxygenation). **(A)** The cell vitality worsened as the OGD time increased **(B)** LncRNAs highly downregulated under OGD4/R20 conditions. *$p < 0.05$, **$p < 0.01$, ****$p < 0.0001$ (vs. control); ##$p < 0.01$, ###$p < 0.001$, ####$p < 0.0001$ (vs. OGD4/R20), $n = 6$, one-way ANOVA.

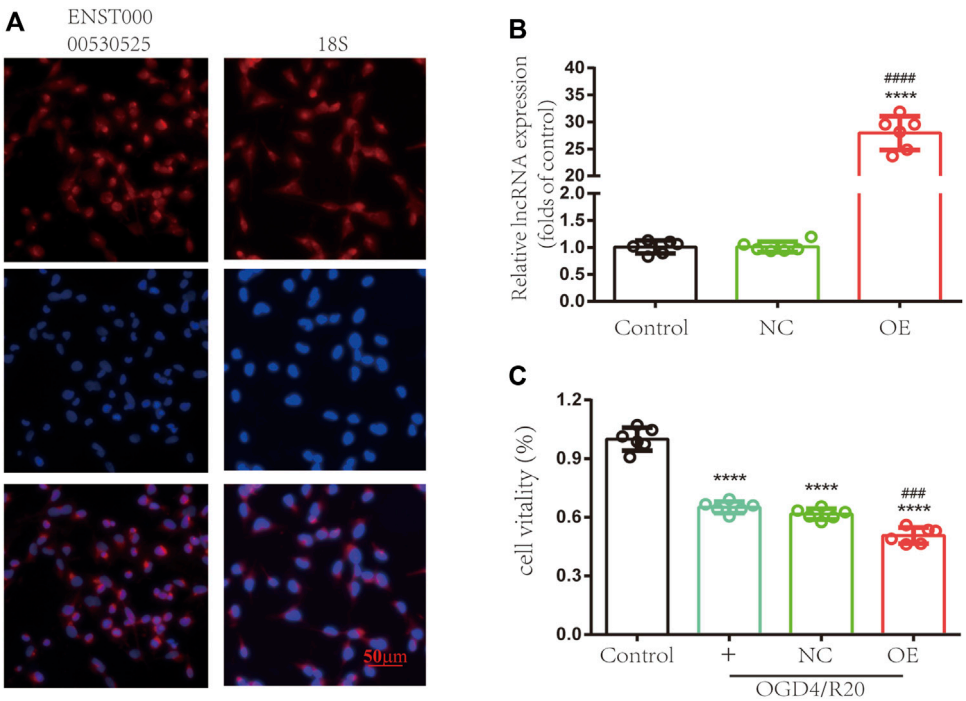

FIGURE 6 | Upregulating the expression of lncRNA ENST00000530525 affects the vitality of hCMEC/D3 cells. **(A)** FISH showed that ENST00000530525 was mainly distributed in the cytoplasm, similar to the control group 18S. Scale bar: 50 μm. **(B)** The transduction efficiency detected by RT–qPCR. **(C)** The CCK-8 assay revealed cell vitality. NC: negative control; OE: over expression; OGD4/R20: 4 h of OGD and 20 h of reoxygenation. ****$p < 0.0001$ (vs. control); ###$p < 0.001$, ####$p < 0.0001$ (vs. NC), $n = 6$, one-way ANOVA.

Upregulating lncRNA ENST00000530525 Expression Affected the Viability of hCMEC/D3 Cells After OGD/R

To explore the functions of lncRNA ENST00000530525 in hCMEC/D3 cells after OGD/R, lncRNA ENST00000530525 was upregulated by transfection of an overexpression plasmid. The location of lncRNA ENST00000530525 was tested by FISH. The results showed lncRNA ENST00000530525 was mostly distributed in the cytoplasm, similar to the control group-18S, which means overexpression plasmid transfection would effectively promote the lncRNA's function (**Figure 6A**).

The RT–qPCR results uncovered lncRNA ENST00000530525 expression in the OE group was effectively upregulated by 28-fold compared to it in the NC group after 72 h of transfection in hCMEC/D3 cells, while there was no difference between the control and NC-

treated groups (**Figure 6B**). This result suggested that the transient plasmid transfection of lncRNA into cultured hCMEC/D3 cells could selectively upregulate lncRNA ENST00000530525 expression.

We investigated whether overexpression of lncRNA ENST00000530525 can influence the viability of hCMEC/D3 cells after OGD/R. The results revealed the cell viability was 1.00 ± 0.05 in untreated cells as a control, 0.65 ± 0.03 in the normal control group, 0.62 ± 0.03 in the NC-treated group, and 0.51 ± 0.04 in the OE-treated group. Statistical analysis showed the cell viability of the OE-treated group was decreased compared to that of the NC-treated group after OGD/R injury (**Figure 6C**), which indicated that overexpression of lncRNA ENST00000530525 in cultured hCMEC/D3 cells could lead to more severe OGD/R ischemia injury.

Upregulating lncRNA ENST00000530525 Increased the Expression of ANO1

To test whether upregulation of lncRNA ENST00000530525 affects the expression of ANO1, RT–qPCR and immunofluorescence were used. RT–qPCR results showed the expression of ANO1 in the OGD4/R20 group was upregulated. Meanwhile, the ANO1 expression in the OE group was effectively upregulated by 4.27-fold compared to that in the NC-treated cells after 72 h of transfection in hCMEC/D3 cells, but there was no significant difference between OGD4/R20 group and NC group (**Figure 7A**).

Immunofluorescence showed that the protein expression of ANO1 increased after OGD4/R20. Meanwhile, when lncRNA ENST00000530525 was upregulated by transfection of the overexpression plasmid, ANO1 protein expression in the OE group increased almost 2-fold compared to that in the NC group, while there was no significant difference between OGD4/R20 group and NC group (**Figures 7B,C**). These results demonstrated that altered expression of lncRNA ENST00000530525 could influence the expression of ANO1 in hCMEC/D3 cells after OGD4/R20.

Targeted Increases in lncRNA ENST00000530525 Deteriorated BBB Disruption After OGD4/R20

FITC-dextran permeability was used to evaluate BBB permeability. The results showed in the OGD4/R20 group FITC-dextran permeability was upregulated compared to the control group. However, FITC-dextran permeability in the OE group was effectively upregulated by 1.41-fold compared to that in the NC-

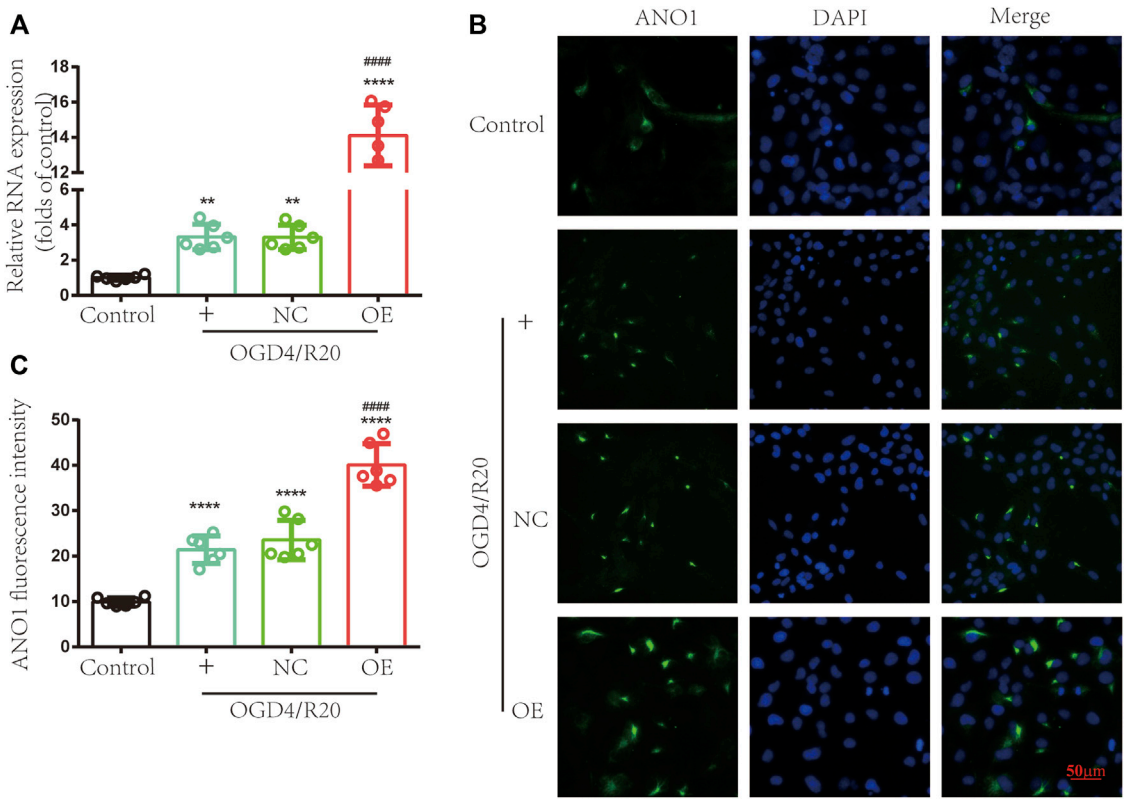

FIGURE 7 | Upregulating lncRNA ENST00000530525 increased the expression of ANO1. The effects of lncRNA ENST00000530525 upregulation by plasmid on the gene and protein expression of ANO1 in hCMEC/D3 cells after OGD4/R20 conditions. **(A)** The RT–qPCR results show that ANO1 increased after OGD4/R20, which increased more significantly when lncRNA ENST00000530525 was upregulated by the plasmid. **(B,C)** The immunofluorescence results show that transfecting a plasmid into hCMEC/D3 cells resulted in an increase in ANO1 protein expression. Scale bar: 50 μm. NC: negative control; OE: over expression; OGD4/R20: 4 h of OGD and 20 h of reoxygenation. $^{**}p < 0.01$, $^{****}p < 0.0001$ (vs. Control); ####$p < 0.0001$ (vs. NC), $n = 6$, one-way ANOVA.

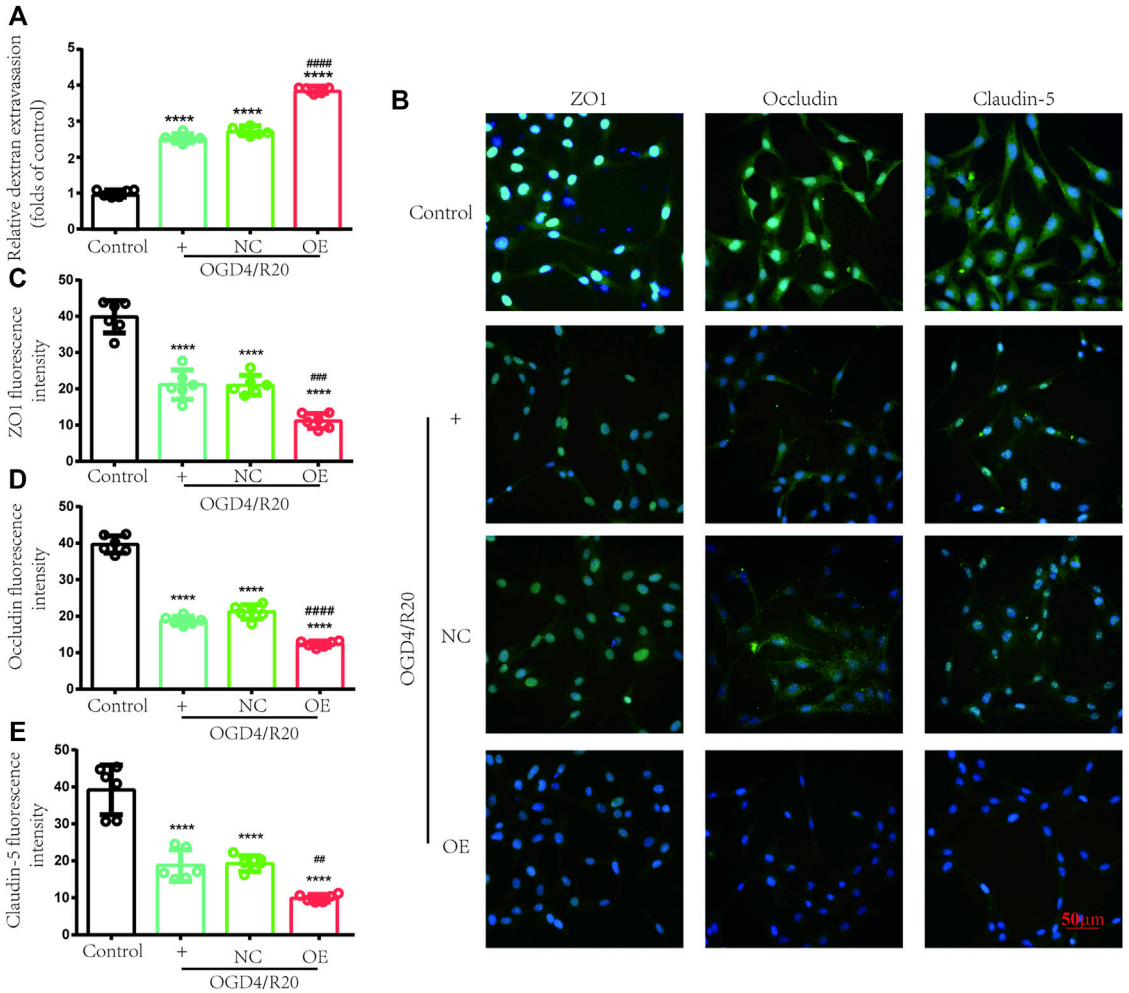

FIGURE 8 | Increasing lncRNA ENST00000530525 deteriorated transendothelial permeability under OGD/R condition. **(A)** FITC-dextran leakage was used to quantificat transendothelial permeability. **(B–E)** Representative immunofluorescence indensity of ZO-1, occludin and claudin-5. Scale bar: 50 μm. NC: negative control; OE: over expression; OGD4/R20: 4 h of OGD and 20 h of reoxygenation. ****$p < 0.0001$ (vs. Control); #$p < 0.001$, ##$p < 0.01$; ###$p < 0.001$, ####$p < 0.0001$ (vs. NC), $n = 6$, one-way ANOVA.

treated cells 72 h after plasmid transfection, while there was no difference between the OGD4/R20 group and NC group (**Figure 8A**).

Endothelial cells, which were connected by TJ proteins, are a major component of BBB. TJ proteins (ZO-1, occludin, and claudin-5) were evaluated by immunofluorescence to assess the state of BBB. After OGD4/R20, the fluorescence intensity of these proteins significantly decreased compared to the control group. Meanwhile, lncRNA ENST00000530525 overexpression futher decreased the fluorescence intensity of these proteins compared to the NC group (**Figures 8B–E**). These results also showed that lncRNA ENST00000530525 overexpression downregulated the expression of ZO-1, occludin and claudin-5 under OGD4/R20 condition.

LncRNA ENST00000530525 Not Directly Bind to 3′UTR of ANO1

In order to investigate whether lncRNA ENST00000530525 directly bind to 3′UTR of ANO1 and affect its expression, a double luciferase assay was used. Luc-ANO1-NC, Luc-ANO1-mimic, lncRNA-NC, and lncRNA-OE plasmids were constructed and transfected into 293T cells. After 48 h transfection, firefly luminescence and renilla luminescence were detected. However, there was no significant difference between Luc-ANO1-mimic group and Luc-ANO1-NC group when lncRNA ENST00000530525 was over-expressed ($p < 0.05$ but the difference was less than 20%), which indicated that lncRNA could not directly bind to the target gene ANO1 and affect its expression (**Supplementary Figure S4**).

DISCUSSION

In our study, we uncovered lncRNA ENST00000530525 was downregulated after OGD4/R20, but ANO1 was upregulated. After IS, ANO1 was showed to be upregulated and to destroy the

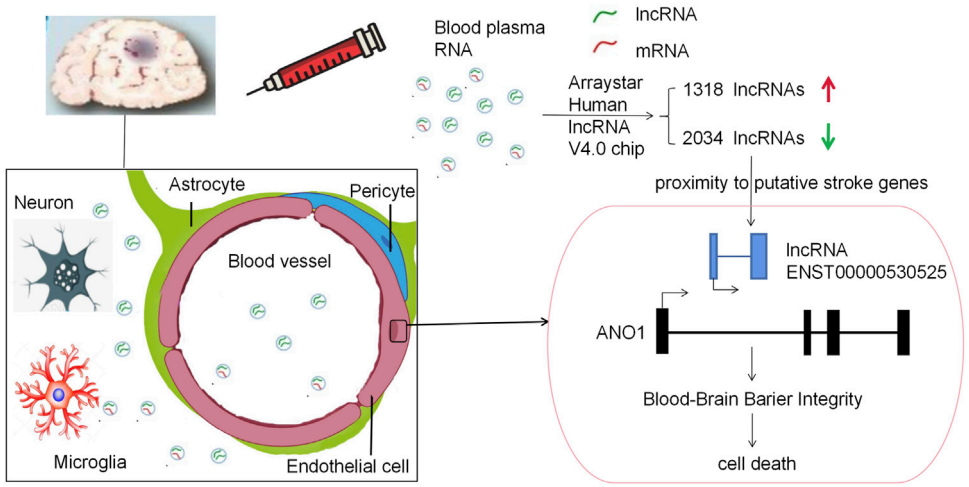

FIGURE 9 | Schematic diagram of this paper. This study used a RNA-chip sequencing in whole blood samples of patients suffering from acute cerebral ischemia to identify DE lncRNAs. The Arraystar Human lncRNA V4.0 chip results showed there were 3352 lncRNA transcripts DE, with 1318 upregulated and 2034 downregulated lncRNAs. LncRNA ENST00000530525 was the highest downregulated lncRNA, while ANO1 was in proximity to the putative stroke gene. Upregulating lncRNA ENST00000530525 improved the expression of ANO1, which further destroyed the BBB integrity, in the hCMEC/D3 cells after OGD4/R20.

BBB integrity by regulating the NF-kB signaling pathway (Liu et al., 2019). This study was consistent with these researches. Notably, when lncRNA ENST00000530525 was upregulated by plasmid transfection, the RNA and protein expression of ANO1 was also increased, while the vitality of hCMEC/D3 cells and the BBB integrity were inhibited. This indicated that lncRNA ENST00000530525 might affect its neighbor gene ANO1 to play an important role in BBB integrity (**Figure 9**).

Stroke is a high risk factor for death and disability worldwide. However, the narrow time window for treatment of its standard therapy and the difficulty in making a quick diagnosis in most low-resource medical facilities (no brain imaging) indicates a need to understand the molecular regulation of stroke and the identification of its biomarkers. Such knowledge would enable the identification of biomarkers among the DE proteins and mRNAs as well as to provide new opinions to the mechanisms of stroke pathogenesis in patients (ENCODE Project Consortium, 2012; Falcione et al., 2020). Consequently, this study identified several stroke-induced changes in the expression of some circulating lncRNAs and their probable target genes.

Among the upregulated lncRNAs, NR_002312 at 14q11.2 is 45 kb away from poly (ADP-ribose) polymerase-2 (PARP2). PARP2 is responsive to DNA damage and drives cell death pathways in IS (Kofler et al., 2006). Additionally, lncRNA NR_037,932 (upregulated) was mapped to APOC2 and APOC4 within 420 kb and APOE within 462 kb at 19q13.32. APOE is central to the transport and metabolism of lipids and plays an important role in both cerebral IS and coronary heart disease (Satizabal et al., 2018). APOC4 correlates with stroke recovery, while APOC2 is involved in the pathophysiology of post-stroke depression (Zhan et al., 2014; Plubell et al., 2020). These associations may be key to the functions of lncRNAs in the evolution of stroke and can serve as potential biomarkers if pursued further. Another significant DE lncRNA, T297706, is within 6 kb of SIRT5 at 6p23, which increases blood–brain barrier permeability by degrading occludins (Diaz-Cañestro et al., 2018) and it promotes arterial thrombosis *via* endothelial PAI-1 expression (Liberale et al., 2020).

Among the downregulated lncRNAs, ENST00000395996 is within vacuolar protein sorting 13 homolog B (VPS13B). VPS13B participates in the pathoevolution of atherosclerosis-induced IS (Ruan et al., 2020). The HTT gene is less than 8 kb away from the downregulated lncRNA NR_045414, while the upregulated lncRNA is within the HTR2A gene. Both HTT and HTR2A are associated with post-stroke disease (Kim et al., 2012). The highly downregulated lncRNA ENST00000530525 is within the ANO1 gene. It is plausible that the lncRNA ENST00000530525 may affect the expression of the ANO1 gene after IS due to proximity. Our guess was identified by plasmid transfection assays, which mean upregulation of the lncRNA ENST00000530525 could influence the expression of ANO1. But the double luciferase assay result showed, the lncRNA ENST00000530525 could not directly bind to and regulate its neighbor gene ANO1.

Previous studies in rodents revealed the mechanisms of action of some of the dysregulated lncRNAs. There are four archetypes of molecular functions that lncRNAs execute: decoys, guides, signals, and scaffolds (Wang and Chang, 2011). For instance, *cis*-regulation, which means lncRNA can somehow bind to adjacent DNA in chromosomes and regulate its expression, is one kind of signal and plays a crucial role in stroke (Yan et al., 2017). LncRNA Peril acts in this manner to positively regulate the expression of two genes 1.5 million base pairs (Mb) away from its transcription location (Groff et al., 2018). Accordingly, it is possible that other cis-lncRNAs may regulate cerebral ischemic stroke genes in this way, as several significantly DE lncRNAs in our study

mapped within or to the neighboring genes associated with IS (**Table 3**).

Recent studies have provided intriguing evidence for decoy lncRNAs. LncRNA U90926 binds directly to malate dehydrogenase 2 (MDH2), competitively inhibiting the binding of MDH2 to the untranslated region (UTR) of CXCL2, thereby protecting the mRNA of CXCL2 from MDH2-mediated attenuation (Chen et al., 2021). As for signal, the lncRNAs in this archetype can act as markers of functionally significant biological events. For example, HOTTIP, a lncRNA found at the distal end of the human HOXA cluster, directly binds the adaptor protein WDR5 and targets WDR5/MLL complexes across HOXA, driving histone H3 lysine 4 trimethylation and gene transcription (Wang et al., 2011). Another archetype of lncRNA is the guide—RNA binds proteins (usually transcription factors), then directs the protein complex to specific targets. Engreitz found that 5 of 12 lncRNA loci regulate their neighboring gene transcription. In most of these lncRNA, local effects are mediated by enhancer-like functions of DNA elements, while in one locus perhaps by recruit more transcription-associated factors (Engreitz et al., 2016). In conclusion, the lncRNA ENST00000530525 may recruit transcription factors or enhancers to promote ANO1 gene transcription. In this study, the mechanism by which lncRNA ENST00000530525 affects its target gene ANO1 requires further research.

There are still some problems being worthy of consideration and in-depth exploration in this study. The basic disease of stroke patients is complex and diverse in clinical, the incidence of ischemia stroke is common in the middle-aged and elderly who have high-risk factors (such as Hypertension, diabetes, and hyperlipidemia). The race, sex, age, and vascular risk factors (diabetes mellitus, hypertension, and hyperlipidemia) were matching of all patients enrolled in this study and there were significantly more stroke patients with a positive history of hypertension, diabetes, and smoking in **Table 1**, the expression of the novel lncRNA ENST00000530525 in stroke patients without risk factors has not been verified due to the limitation of sample, However, we are randomly sampling 40 blood samples from stroke patients and 20 blood samples from controls to detect the expression trend of lncRNA ENST00000530525, which is downregulated in stroke group compared with the control group (See **Supplementary Figure S1**). Moreover, the gene chip results were gotten from patients' blood, but our further validation used hCMEC/D3 cells. It is not clear how the reduced circulating levels of lncRNA in patients' blood is linked to the downregulation of its expression in the hCMEC/D3 cells, and the relationship between them needs to be further studied. In addition, there are varying times of BBB permeability detection according to the literatures. In Cowan's study, FITC-dextran was added to the inserts, which were then transferred every 5 min over 30 min to a series of collecting wells to measure the BBB permeability (Cowan and Easton, 2010). Gerhartl used FITC-dextran to assess BBB permeability after transferring 30 min (Gerhartl et al., 2020). While in Liu's study, the BBB permeability test is performed for 20 min (Liu et al., 2019). There were still other researchers added FITC-Dextran the upper chamber and then incubated for 1 h to test (Ni et al., 2017; Bergman et al., 2021). BBB permeability test just performed for 5 min in our study, the test time may need further verification. In this study, if the expression of ANO1 and cell viability under upregulating and downregulating lncRNA conditions by transfection, and also ANO1 expression in lncRNA overexpressed cells under normal conditions (not just OGD/R pathological condition) were investigated, the conclusion would be more convincing.

Due to the relatively recent discoveries, the expression and functions of the majority of lncRNAs in the post-stroke brain are largely unknown. However, numerous lncRNAs are emerging as important regulators of transcription and translation. These findings of dysregulated lncRNAs may help to guide evidence-based preventive measures and the search for a cure. Further studies will be needed to establish whether these remaining lncRNAs can modulate theis neighboring and stroke-associated genes *in vivo* or *in vitro*.

DATA AVAILABILITY STATEMENT

The datasets presented in this study can be found in online repositories. The names of the repository/repositories and accession number(s) can be found below: GEO—GSE198710

ETHICS STATEMENT

The studies involving human participants were reviewed and approved by the ethics committee of Guangdong Provincial Hospital of Chinese Medicine Guangdong Provincial Hospital of Chinese Medicine. The patients/participants provided their written informed consent to participate in this study.

AUTHOR CONTRIBUTIONS

WJ performed the experiments, data statistics, and was a major contributor in writing the manuscript. JL and YC participated in drafting and revised the manuscript. WL analyzed and interpreted the patient data regarding the stroke patients. MC, XX, MD, and WS carried out experiments and analyzed the data. JS, LZ, YH, and XC supervised the design of the study and reviewed this manuscript. All authors reviewed and approved the final version of this paper. All authors read and approved the final manuscript.

FUNDING

This study was financially supported by the State key R & D Program (No. 2019YFC1708601), the National Natural Science Foundation of China, Nos. 81303115, 81774042, 81771353, and 81904104; the Pearl River S & T Nova Program of Guangzhou, No. 201806010025; the Youth Pilot

Project of Chinese Society of Traditional Chinese Medicine, No. CACM-2018-QNRC2-C09; the Science and Technology Program of Guangzhou City of China, Nos. 201604020003 and 202102010268; Guangdong Provincial Key Laboratory of Research on Emergency in TCM, No. 2017B030314176; 2018-75 and 2019-140; the Administration of Traditional Chinese Medicine of Guangdong Province, No. 20211203; Postdoctoral Science Foundation of China, No. 2021M690759. Guangzhou Science and Technology Project (Nos. 202102010268 and 202102010339). The Specialty Program of Guangdong Province Hospital of Traditional Chinese Medicine of China, Nos. YN2016MJ07, 2015KT1294, YN2015MS02, and YN2018ZD07.

ACKNOWLEDGMENTS

We thank AJE (https://www.aje.cn/) for editing this manuscript. The content of this manuscript has previously appeared online in a preprint. Available at: https://www.researchsquare.com/article/rs-968571/v1 (Accessed 10 January 2022).

SUPPLEMENTARY MATERIAL

The Supplementary Material for this article can be found online at: https://www.frontiersin.org/articles/10.3389/fgene.2022.873230/full#supplementary-material

REFERENCES

Abdillahi, M., Ananthakrishnan, R., Vedantham, S., Shang, L., Zhu, Z., Rosario, R., et al. (2012). Aldose Reductase Modulates Cardiac Glycogen Synthase Kinase-3β Phosphorylation during Ischemia-Reperfusion. *Am. J. Physiology-Heart Circulatory Physiology* 303 (3), H297–H308. doi:10.1152/ajpheart.00999.2011

Akella, A., Bhattarai, S., and Dharap, A. (2019). Long Noncoding RNAs in the Pathophysiology of Ischemic Stroke. *Neuromol Med.* 21 (4), 474–483. doi:10.1007/s12017-019-08542-w

Bao, M.-H., Szeto, V., Yang, B. B., Zhu, S.-z., Sun, H.-S., and Feng, Z.-P. (2018). Long Non-coding RNAs in Ischemic Stroke. *Cell Death Dis.* 9 (3), 281. doi:10.1038/s41419-018-0282-x

Bergman, L., Acurio, J., Leon, J., Gatu, E., Friis, T., Nelander, M., et al. (2021). Preeclampsia and Increased Permeability over the Blood-Brain Barrier: A Role of Vascular Endothelial Growth Receptor 2. *Am. J. Hypertens.* 34 (1), 73–81. doi:10.1093/ajh/hpaa142

Chen, J., Jin, J., Zhang, X., Yu, H., Zhu, X., Yu, L., et al. (2021). Microglial Lnc-U90926 Facilitates Neutrophil Infiltration in Ischemic Stroke via MDH2/CXCL2 axis. *Mol. Ther.* 29 (9), 2873–2885. doi:10.1016/j.ymthe.2021.04.025

Cowan, K. M., and Easton, A. S. (2010). Neutrophils Block Permeability Increases Induced by Oxygen Glucose Deprivation in a Culture Model of the Human Blood-Brain Barrier. *Brain Res.* 1332, 20–31. doi:10.1016/j.brainres.2010.03.066

Deng, L., Yang, J., Chen, H., Ma, B., Pan, K., Su, C., et al. (2016). Knockdown of TMEM16A Suppressed MAPK and Inhibited Cell Proliferation and Migration in Hepatocellular Carcinoma. *Onco Targets Ther.* 9, 325–333. doi:10.2147/OTT.S95985

Dharap, A., Nakka, V. P., and Vemuganti, R. (2012). Effect of Focal Ischemia on Long Noncoding RNAs. *Stroke* 43 (10), 2800–2802. doi:10.1161/strokeaha.112.669465

Diaz-Cañestro, C., Merlini, M., Bonetti, N. R., Liberale, L., Wüst, P., Briand-Schumacher, S., et al. (2018). Sirtuin 5 as a Novel Target to Blunt Blood-Brain Barrier Damage Induced by Cerebral Ischemia/reperfusion Injury. *Int. J. Cardiol.* 260, 148–155. doi:10.1016/j.ijcard.2017.12.060

Engreitz, J. M., Haines, J. E., Perez, E. M., Munson, G., Chen, J., Kane, M., et al. (2016). Local Regulation of Gene Expression by lncRNA Promoters, Transcription and Splicing. *Nature* 539 (7629), 452–455. doi:10.1038/nature20149

Falcione, S., Kamtchum-Tatuene, J., Sykes, G., and Jickling, G. C. (2020). RNA Expression Studies in Stroke: what Can They Tell Us about Stroke Mechanism? *Curr. Opin. neurology* 33 (1), 24–29. doi:10.1097/wco.0000000000000786

Fan, X.-D., Yao, M.-J., Yang, B., Han, X., Zhang, Y.-H., Wang, G.-R., et al. (2021). Chinese Herbal Preparation SaiLuoTong Alleviates Brain Ischemia via Nrf2 Antioxidation Pathway-dependent Cerebral Microvascular Protection. *Front. Pharmacol.* 12, 748568. doi:10.3389/fphar.2021.748568

Gerhartl, A., Pracser, N., Vladetic, A., Hendrikx, S., Friedl, H.-P., and Neuhaus, W. (2020). The Pivotal Role of Micro-environmental Cells in a Human Blood-Brain Barrier *In Vitro* Model of Cerebral Ischemia: Functional and Transcriptomic Analysis. *Fluids Barriers CNS* 17 (1), 19. doi:10.1186/s12987-020-00179-3

Groff, A. F., Barutcu, A. R., Lewandowski, J. P., and Rinn, J. L. (2018). Enhancers in the Peril lincRNA Locus Regulate Distant but Not Local Genes. *Genome Biol.* 19 (1), 219. doi:10.1186/s13059-018-1589-8

ENCODE Project Consortium (2012). An Integrated Encyclopedia of DNA Elements in the Human Genome. *Nature* 489(7414), 57–74. doi:10.1038/nature11247

Jiang, X., Andjelkovic, A. V., Zhu, L., Yang, T., Bennett, M. V. L., Chen, J., et al. (2018). Blood-brain Barrier Dysfunction and Recovery after Ischemic Stroke. *Prog. Neurobiol.* 163-164, 144–171. doi:10.1016/j.pneurobio.2017.10.001

Kim, J.-M., Stewart, R., Bae, K.-Y., Kim, S.-W., Kang, H.-J., Shin, I.-S., et al. (2012). Serotonergic and BDNF Genes and Risk of Depression after Stroke. *J. Affect. Disord.* 136 (3), 833–840. doi:10.1016/j.jad.2011.09.029

Kofler, J., Otsuka, T., Zhang, Z., Noppens, R., Grafe, M. R., Koh, D. W., et al. (2006). Differential Effect of PARP-2 Deletion on Brain Injury after Focal and Global Cerebral Ischemia. *J. Cereb. Blood Flow. Metab.* 26 (1), 135–141. doi:10.1038/sj.jcbfm.9600173

Li, Q., Wu, H., Yue, W., Dai, Q., Liang, H., Bian, H., et al. (2017). Prevalence of Stroke and Vascular Risk Factors in China: a Nationwide Community-Based Study. *Sci. Rep.* 7 (1), 6402. doi:10.1038/s41598-017-06691-1

Liberale, L., Akhmedov, A., Vlachogiannis, N. I., Bonetti, N. R., Nageswaran, V., Miranda, M. X., et al. (2020). Sirtuin 5 Promotes Arterial Thrombosis by Blunting the Fibrinolytic System. *Cardiovasc. Res.* 117 (10), 2275–2288. doi:10.1093/cvr/cvaa268

Liu, C., Yang, J., Zhang, C., Liu, M., Geng, X., Ji, X., et al. (2018). Analysis of Long Non-coding RNA Expression Profiles Following Focal Cerebral Ischemia in Mice. *Neurosci. Lett.* 665, 123–129. doi:10.1016/j.neulet.2017.11.058

Liu, P.-y., Zhang, Z., Liu, Y., Tang, X.-l., Shu, S., Bao, X.-y., et al. (2019). TMEM16A Inhibition Preserves Blood-Brain Barrier Integrity after Ischemic Stroke. *Front. Cell. Neurosci.* 13, 360. doi:10.3389/fncel.2019.00360

Liu, Y., Liu, Z., and Wang, K. (2021). The Ca2+-Activated Chloride Channel ANO1/TMEM16A: An Emerging Therapeutic Target for Epithelium-Originated Diseases? *Acta Pharm. Sin. B* 11 (6), 1412–1433. doi:10.1016/j.apsb.2020.12.003

Lo, A. C., Cheung, A. K., Hung, V. K., Yeung, C.-M., He, Q.-Y., Chiu, J.-F., et al. (2007). Deletion of Aldose Reductase Leads to Protection against Cerebral Ischemic Injury. *J. Cereb. Blood Flow. Metab.* 27 (8), 1496–1509. doi:10.1038/sj.jcbfm.9600452

Ma, K., Liu, S., Liang, H., Wang, G., Wang, T., Luo, S., et al. (2021). Ca2+-activated Cl− Channel TMEM16A Inhibition by Cholesterol Promotes Angiogenesis in Endothelial Cells. *J. Adv. Res.* 29, 23–32. doi:10.1016/j.jare.2020.09.003

Ni, Y., Teng, T., Li, R., Simonyi, A., Sun, G. Y., and Lee, J. C. (2017). TNFα Alters Occludin and Cerebral Endothelial Permeability: Role of p38MAPK. *PLoS One* 12 (2), e0170346. doi:10.1371/journal.pone.0170346

Plubell, D. L., Fenton, A. M., Rosario, S., Bergstrom, P., Wilmarth, P. A., Clark, W. M., et al. (2020). High-Density Lipoprotein Carries Markers that Track with Recovery from Stroke. *Circ. Res.* 127 (10), 1274–1287. doi:10.1161/circresaha.120.316526

Qu, L., Ding, J., Chen, C., Wu, Z.-J., Liu, B., Gao, Y., et al. (2016). Exosome-Transmitted lncARSR Promotes Sunitinib Resistance in Renal Cancer by Acting as a Competing Endogenous RNA. *Cancer Cell* 29 (5), 653–668. doi:10.1016/j.ccell.2016.03.004

Ren, W., and Yang, X. (2018). Pathophysiology of Long Non-coding RNAs in Ischemic Stroke. *Front. Mol. Neurosci.* 11, 96. doi:10.3389/fnmol.2018.00096

Ruan, W., Wu, J., Su, J., Jiang, Y., Pang, T., and Li, J. (2020). Altered lncRNAs Transcriptomic Profiles in Atherosclerosis-Induced Ischemic Stroke. *Cell Mol. Neurobiol.* 42 (1), 265–278. doi:10.1007/s10571-020-00918-y

Satizabal, C. L., Samieri, C., Davis-Plourde, K. L., Voetsch, B., Aparicio, H. J., Pase, M. P., et al. (2018). APOE and the Association of Fatty Acids with the Risk of Stroke, Coronary Heart Disease, and Mortality. *Stroke* 49 (12), 2822–2829. doi:10.1161/strokeaha.118.022132

Schaukowitch, K., and Kim, T.-K. (2014). Emerging Epigenetic Mechanisms of Long Non-coding RNAs. *Neuroscience* 264, 25–38. doi:10.1016/j.neuroscience.2013.12.009

Shin, J. A., Yoon, J. C., Kim, M., and Park, E.-M. (2016). Activation of Classical Estrogen Receptor Subtypes Reduces Tight Junction Disruption of Brain Endothelial Cells under Ischemia/reperfusion Injury. *Free Radic. Biol. Med.* 92, 78–89. doi:10.1016/j.freeradbiomed.2016.01.010

Suzuki, T., Suzuki, Y., Asai, K., Imaizumi, Y., and Yamamura, H. (2021). Hypoxia Increases the Proliferation of Brain Capillary Endothelial Cells via Upregulation of TMEM16A Ca2+-Activated Cl− Channels. *J. Pharmacol. Sci.* 146 (1), 65–69. doi:10.1016/j.jphs.2021.03.002

Suzuki, T., Yasumoto, M., Suzuki, Y., Asai, K., Imaizumi, Y., and Yamamura, H. (2020). TMEM16A Ca2+-Activated Cl- Channel Regulates the Proliferation and Migration of Brain Capillary Endothelial Cells. *Mol. Pharmacol.* 98 (1), 61–71. doi:10.1124/mol.119.118844

Szklarczyk, D., Franceschini, A., Wyder, S., Forslund, K., Heller, D., Huerta-Cepas, J., et al. (2015). STRING V10: Protein-Protein Interaction Networks, Integrated over the Tree of Life. *Nucleic Acids Res.* 43 (Database issue), D447–D452. doi:10.1093/nar/gku1003

Wang, K. C., and Chang, H. Y. (2011). Molecular Mechanisms of Long Noncoding RNAs. *Mol. Cell* 43 (6), 904–914. doi:10.1016/j.molcel.2011.08.018

Wang, K. C., Yang, Y. W., Liu, B., Sanyal, A., Corces-Zimmerman, R., Chen, Y., et al. (2011). A Long Noncoding RNA Maintains Active Chromatin to Coordinate Homeotic Gene Expression. *Nature* 472 (7341), 120–124. doi:10.1038/nature09819

Wang, M., Yang, H., Zheng, L.-Y., Zhang, Z., Tang, Y.-B., Wang, G.-L., et al. (2012). Downregulation of TMEM16A Calcium-Activated Chloride Channel Contributes to Cerebrovascular Remodeling during Hypertension by Promoting Basilar Smooth Muscle Cell Proliferation. *Circulation* 125 (5), 697–707. doi:10.1161/circulationaha.111.041806

Wang, W., Jiang, B., Sun, H., Ru, X., Sun, D., Wang, L., et al. (2017). Prevalence, Incidence, and Mortality of Stroke in China. *Circulation* 135 (8), 759–771. doi:10.1161/circulationaha.116.025250

Wu, M. M., Lou, J., Song, B. L., Gong, Y. F., Li, Y. C., Yu, C. J., et al. (2014). Hypoxia Augments the Calcium-activated Chloride Current Carried by Anoctamin-1 in Cardiac Vascular Endothelial Cells of Neonatal Mice. *Br. J. Pharmacol.* 171 (15), 3680–3692. doi:10.1111/bph.12730

Xu, S. y., Bian, H. j., Shu, S., Xia, S. n., Gu, Y., Zhang, M. j., et al. (2021). AIM2 Deletion Enhances Blood-brain Barrier Integrity in Experimental Ischemic Stroke. *CNS Neurosci. Ther.* 27 (10), 1224–1237. doi:10.1111/cns.13699

Yan, P., Luo, S., Lu, J. Y., and Shen, X. (2017). Cis- and Trans-acting lncRNAs in Pluripotency and Reprogramming. *Curr. Opin. Genet. Dev.* 46, 170–178. doi:10.1016/j.gde.2017.07.009

Yates, A. D., Achuthan, P., Akanni, W., Allen, J., Allen, J., Alvarez-Jarreta, J., et al. (2020). Ensembl 2020. *Nucleic acids Res.* 48 (D1), D682–8. doi:10.1093/nar/gkz966

Zhan, Y., Yang, Y.-T., You, H.-M., Cao, D., Liu, C.-Y., Zhou, C.-J., et al. (2014). Plasma-based Proteomics Reveals Lipid Metabolic and Immunoregulatory Dysregulation in Post-stroke Depression. *Eur. Psychiatr.* 29 (5), 307–315. doi:10.1016/j.eurpsy.2014.03.004

Conflict of Interest: The authors declare that the research was conducted in the absence of any commercial or financial relationships that could be construed as a potential conflict of interest.

Publisher's Note: All claims expressed in this article are solely those of the authors and do not necessarily represent those of their affiliated organizations, or those of the publisher, the editors and the reviewers. Any product that may be evaluated in this article, or claim that may be made by its manufacturer, is not guaranteed or endorsed by the publisher.

frontiers | Frontiers in Genetics

ORIGINAL RESEARCH
published: 07 July 2022
doi: 10.3389/fgene.2022.840060

Deletion of microRNA-183-96-182 Cluster in Lymphocytes Suppresses Anti-DsDNA Autoantibody Production and IgG Deposition in the Kidneys in C57BL/6-Fas$^{lpr/lpr}$ Mice

Zhuang Wang[1], Bettina Heid[1], Ran Lu[1], Mohit Sachdeva[2†], Michael R. Edwards[1], JingJing Ren[1], Thomas E. Cecere[1], Deena Khan[1], Taschua Jeboda[1], David G. Kirsch[3], Christopher M. Reilly[1,4], Rujuan Dai[1] and S. Ansar Ahmed[1]**

[1]Department of Biomedical Sciences and Pathobiology, Virginia-Maryland College of Veterinary Medicine (VMCVM), Virginia Tech, Blacksburg, VA, United States, [2]Preclinical Lead Immunology, Spark Theraprutics, Philadelphia, PA, United States, [3]Department of Pharmacology and Cancer Biology, Duke University Medical Center, Durham, NC, United States, [4]Edward Via College of Osteopathic Medicine, Blacksburg, VA, United States

Dysregulated miRNAs have been implicated in the pathogenesis of systemic lupus erythematosus (SLE). Our previous study reported a substantial increase in three miRNAs located at the miR-183-96-182 cluster (miR-183C) in several autoimmune lupus-prone mice, including MRL/lpr and C57BL/6-lpr (B6/lpr). This study reports that *in vitro* inhibition of miR-182 alone or miR-183C by specific antagomirs in activated splenocytes from autoimmune-prone MRL/lpr and control MRL mice significantly reduced lupus-related inflammatory cytokines, interferon-gamma (IFNγ), and IL-6 production. To further characterize the role of miR-182 and miR-183C cluster *in vivo* in lupus-like disease and lymphocyte phenotypes, we used hCD2-iCre to generate B6/lpr mice with conditional deletion of miR-182 or miR-183C in CD2$^+$ lymphocytes (miR-182$^{-/-}$B6/lpr and miR-183C$^{-/-}$B6/lpr). The miR-182$^{-/-}$B6/lpr and miR-183C$^{-/-}$B6/lpr mice had significantly reduced deposition of IgG immunocomplexes in the kidney when compared to their respective littermate controls, although there appeared to be no remarkable changes in renal pathology. Importantly, we observed a significant reduction of serum anti-dsDNA autoantibodies in miR-183C$^{-/-}$B6/lpr mice after reaching 24 weeks-of age compared to age-matched miR-183C$^{fl/fl}$B6/lpr controls. *In vitro* activated splenocytes from miR-182$^{-/-}$B6/lpr mice and miR-183C$^{-/-}$B6/lpr mice showed reduced ability to produce lupus-associated IFNγ. Forkhead box O1(Foxo1), a previously validated miR-183C miRNAs target, was increased in the splenic CD4$^+$ cells of miR-182$^{-/-}$B6/lpr and miR-183C$^{-/-}$B6/lpr mice. Furthermore, *in vitro* inhibition of Foxo1 with siRNA in splenocytes from miR-182$^{-/-}$B6/lpr and miR-183C$^{-/-}$B6/lpr mice significantly increased IFNγ expression following anti-CD3/CD28 stimulation, suggesting that miR-182 and miR-183C miRNAs regulate the inflammatory IFNγ in splenocytes via targeting Foxo1. The deletion of either miR-182 alone or the whole miR-183C cluster, however, had no marked effect on the composition of T and B cell subsets in the spleens of B6/lpr mice. There were similar percentages of CD4$^+$, CD8$^+$, CD19$^+$, as well as Tregs, follicular helper T (T_{FH}), germinal center B (GCB), and plasma cells in the miR-

OPEN ACCESS

Edited by:
Deepanjan Paul,
Children's Hospital of Philadelphia,
United States

Reviewed by:
Sathi Babu Chodisetti,
Biocon Bristol Myers Squibb Research & Development Center (BBRC), India
Mary Kaileh,
National Institute on Aging (NIH),
United States
Trine N. Jorgensen,
Case Western Reserve University,
United States

***Correspondence:**
Rujuan Dai
rdai05@vt.edu
S. Ansar Ahmed
ansrahmd@vt.edu

†Present address:
Preclinical Lead Immunology,
Spark Therapeutics, Philadelphia, PA,
United States

Specialty section:
This article was submitted to RNA,
a section of the journal
Frontiers in Genetics

Received: 20 December 2021
Accepted: 03 March 2022
Published: 07 July 2022

Citation:
Wang Z, Heid B, Lu R, Sachdeva M, Edwards MR, Ren J, Cecere TE, Khan D, Jeboda T, Kirsch DG, Reilly CM, Dai R and Ahmed SA (2022) Deletion of microRNA-183-96-182 Cluster in Lymphocytes Suppresses Anti-DsDNA Autoantibody Production and IgG Deposition in the Kidneys in C57BL/6-Fas$^{lpr/lpr}$ Mice. Front. Genet. 13:840060. doi: 10.3389/fgene.2022.840060

183C$^{-/-}$B6/lpr and miR-182$^{-/-}$B6/lpr mice and their respective littermate controls, miR-183C$^{fl/fl}$B6/lpr and miR-182$^{fl/fl}$B6/lpr mice. Together, our data demonstrate a role of miR-183C in the regulation of anti-dsDNA autoantibody production *in vivo* in B6/lpr mice and the induction of IFNγ in *in vitro* activated splenocytes from B6/lpr mice.

Keywords: epigenetics, miR-183-96-182 cluster, autoantibody, inflammatory cytokine, systemic lupus erythematosus, murine model

INTRODUCTION

Systemic lupus erythematosus (SLE) is a prototypical autoimmune disease characterized by autoantibodies against cellular components and systemic damage to multiple organs, especially kidneys. However, due to the complexity of this disease, the cause of SLE remains unclear. Various risk factors, including genetic, epigenetic, environmental, and hormonal factors, are believed to contribute to the pathogenesis of SLE (Ansar Ahmed et al., 1985; Squatrito et al., 2014; Parks et al., 2017; Goulielmos et al., 2018). Recently, there has been a significant focus on the epigenetic regulation of SLE, especially the role of microRNAs (miRNA), in lupus pathogenesis (Honarpisheh et al., 2018; Dai et al., 2021).

The evolutionally conserved miRNAs play crucial roles in various biological processes, including the development and function of the immune system (Baltimore et al., 2008; Baumjohann and Ansel, 2013; Danger et al., 2014; Mehta and Baltimore, 2016). Dysregulated miRNA expression and function have been identified and implicated in the pathogenesis of various human diseases. Signature lupus-related miRNAs have been implicated in disease pathogenesis by regulating the key molecules and signaling pathways involved in lupus, such as DNA methylation and type I interferon pathways, leading to abnormal production of inflammatory cytokines, chemokines, and antibodies (Tang et al., 2009; Pan et al., 2010; Dai and Ahmed, 2011; Shen et al., 2012; Zan et al., 2014; Dai and Ahmed, 2016; Schell and Rahman, 2021). In our previous miRNA profiling study with three genetically different murine lupus models (C57BL/6-lpr or B6/lpr, NZB/NZW$_{F1}$, and MRL/lpr), we identified a common upregulation of a group of miRNAs, including three miRNAs from the highly conserved miR-183-96-182 cluster (miR-183C) (Dai et al., 2010). Notably, the upregulation of miR-182 and miR-183 of miR-183C has also been identified in human lupus in the recent studies (Chen J. Q. et al., 2017; Lin et al., 2020).

The miR-183 cluster was initially identified as a sensory organ-specific miRNA cluster (Xu et al., 2007). The high expression of miR-183C has been identified in mouse sensory organs such as the inner ear, eye, and olfactory bulb (Weston et al., 2006; Bak et al., 2008; Pierce et al., 2008; Li et al., 2010). Typically, the miR-183C expression is very low in the lymphoid tissues in resting state (Xu et al., 2007). However, miR-183C miRNAs are highly expressed in activated immune cells (Stittrich et al., 2010; Pucella et al., 2015; Li et al., 2016). Current studies have revealed that miR-183C miRNAs are critically involved in immunity and autoimmunity by regulating B cell functions, T cell expansion and activation, the differentiation and function of Tregs, and pathogenic Th17 cells (Stittrich et al., 2010; Ichiyama et al., 2016; Li et al., 2016; Wan et al., 2016; Ichiyama and Dong, 2019). While miR-182 knockout B6 mice have normal B cell and T cell development, these mice have impaired extrafollicular B cell antibody response (Li et al., 2016). *In vitro* studies have shown that miR-182 is highly induced by IL-2 to promote T helper (Th) cell expansion and proliferation by targeting Foxo1 (Stittrich et al., 2010). Specific inhibition of miR-182 in Th cells suppressed Th cell expansion and decreased ovalbumin (OVA)-induced arthritis in mice. A positive correlation between miR-182 expression and the severity of induced experimental autoimmune encephalomyelitis (EAE) was demonstrated in B6 mice (Wan et al., 2016). The authors demonstrated that during EAE development, miR-182 suppressed CD4$^+$CD25$^+$Foxp3$^+$ Tregs differentiation by targeting Foxo1 (Wan et al., 2016). Another study reported that miR-183C cluster miRNAs were highly induced by IL-6-STAT3 signaling, which promoted the differentiation of pathogenic Th17 cell differentiation by targeting Foxo1 (Ichiyama et al., 2016). The deletion of miR-183C significantly reduced the severity of EAE disease by suppressing the pathogenic function of Th17 cells (Ichiyama et al., 2016).

In SLE, we have reported that the miR-183C miRNAs were highly upregulated in splenic lymphocytes in three different murine lupus models and correlated with the disease development (Dai et al., 2010). Additionally, Choi and coworkers reported highly upregulated miR-183C in another murine lupus model, the C3. MRL-Faslpr/J model, which further validates the association of miR-183C with murine lupus (Choi et al., 2016). The treatment of C3. MRL-Faslpr/J mice with cyclophosphamide or human-derived mesenchymal stem cells reduced not only classical lupus parameters (anti-dsDNA, immune complex C3 deposition, and CD138$^+$ cells) but also the miR-182 and miR-96 expression (Choi et al., 2016). Inhibition of miR-182 *in vivo* in MRL/lpr mice with the antagomir-182 treatment resulted in the amelioration of lupus nephritis, which provided additional support for a potential role of miR-182 in lupus (Wang X. et al., 2018).

The miR-182 has been shown to be largely dispensable for adaptive immune cell development and function in B6 mice (Pucella et al., 2015). This may likely be due to the functional compensation by the other two miRNAs (miR-96 and miR-183) within the miR-183C since they have similar seed sequences and could target the same gene, such as Foxo1. On the other hand, the minor differences in the seed sequences will allow individual miR-183C miRNA specific unique targets (Dambal et al., 2015). Individual miR-183C miRNA may play a distinct role in different aspects of immune function. For example, miR-96, but not miR-182 and miR-183, was critical for the induction of pathogenic Th17 cytokines (Ichiyama et al., 2016), while miR-182, but not miR-96 and miR-183, was involved in IL-2 driven helper T cell expansion and function (Stittrich et al., 2010). Therefore, in this study, to further characterize the role of miR-183C and miR-182 in lupus *in vivo*, we

derived both miR-183C$^{-/-}$B6/lpr and miR-182$^{-/-}$B6/lpr mice with conditional deletion of whole miR-183C or miR-182 alone in CD2^{+} lymphocytes. Here, we report the immunological and pathological consequences of *in vivo* deletion of miR-182 and miR-183C in B6/lpr mice.

MATERIAL AND METHODS

Mice

All animal experimental procedures and housing have been approved by the Institutional Animal Care and Use Committee (IACUC) of Virginia Polytechnic Institute and State University. In this study, MRL/lpr (MRL/MpJ-Fas^{lpr}/J, Stock No. 000485), B6/lpr (B6. MRL-Fas^{lpr}/J, Stock No. 000482), MRL (MRL/MpJ, Stock No.000486), B6 (C57BL/6J, Stock No. 000664) and hCD2-iCre (B6-Cg-Tg (CD2-icre)4Kio/J, Stock No. 008520) mice were purchased from Jackson Laboratory (JAX, Maine, United States) and bred in-house.

Although the MRL/lpr model has been widely used to study human lupus, it has several drawbacks that prevent it from being easy to generate MRL/lpr mice with specific gene deletion. This include that MRL/lpr mice have a mixed genetic background. Consequently, multiple generations of backcross are needed to generate knockout mice in MRL/lpr background. It is even more difficult and time-consuming for generating conditional knockout MRL/lpr mice since the commercially available CRE transgenic mouse stains are in B6 background. We, therefore, generated autoinflammatory-prone B6/lpr mice with conditional deletion of either miR-183C cluster or miR-182 in lymphocytes to investigate the role of miR-183C and miR-182 in lupus *in vivo*. We bred hCD2-iCre mice with B6/lpr mice in-house to generate CD2-CreB6/lpr mice. The miR-183C$^{fl/fl}$ and miR-182$^{fl/fl}$ mice in a B6-129/SvJ mixed genetic background were generated by Dr. David G. Kirsch's group at Duke University Medical Center. The development and characterization of miR-182$^{fl/fl}$ mice on a B6-129/SvJ mixed genetic background have been described in detail in a previous report (Sachdeva et al., 2014). An identical strategy was used to generate the miR-183C$^{fl/fl}$ mice on a B6-129/SvJ mixed genetic background (**Supplementary Figure S1**) except that the loxP sites flank the entire miR-183, miR-96, miR-182 cluster instead of only miR-182. The miR-183C$^{fl/fl}$ and miR-182$^{fl/fl}$ mice in the mixed background were backcrossed with B6 mice for at least eight generations. The miR-183C$^{fl/fl}$ and miR-182$^{fl/fl}$ mice in a B6 background were crossbred with B6/lpr to generate miR183C$^{fl/fl}$B6/lpr and miR-182$^{fl/fl}$B6/lpr mice, which were then crossbred with CD2-CreB6/lpr mice to generate CD2-CremiR-183C$^{fl/fl}$B6/lpr (miR183C$^{-/-}$B6/lpr) and CD2-CremiR-182$^{fl/fl}$B6/lpr (miR-182$^{-/-}$B6/lpr) mice. The miR183C$^{-/-}$B6/lpr and miR-182$^{-/-}$B6/lpr mice were bred with miR-183C$^{fl/fl}$B6/lpr and miR-182$^{fl/fl}$B6/lpr mice, respectively to obtain experimental miR183C$^{-/-}$B6/lpr and miR-182$^{-/-}$B6/lpr mice. The littermate miR183C$^{fl/fl}$B6/lpr and miR-182$^{fl/fl}$B6/lpr, which do not carry the hCD2-iCre gene, served as wild-type control B6/lpr mice for conditional miR183 and miR-182 knockout B6/lpr mice. Due to the female predominance of lupus, only female mice were used in this study.

All mice were housed in our Association for Assessment and Accreditation of Laboratory Animal Care (AAALAC)-certified animal facility at the Virginia-Maryland College of Veterinary Medicine (VMCVM), Virginia Tech. Mice were fed with a commercial 7013 NIH-31 Modified 6% Mouse/Rat Sterilizable Diet (Harlan Laboratory, Madison, WI, United States) and given water *ad libitum*. The mice at designated age were euthanized by CO_2 asphyxiation according to the IACUC approved protocol.

Measurement of Proteinuria

Proteinuria was measured by dipstick analysis using Chemistrip-2GP (Roche Diagnostics Corporation, Indianapolis, IN, United States). The semi-quantitative scale was demonstrated as follows: "-": negative or trace; "+" 30 mg/dl; "++": 100 mg/dl and "+++": ≥500 mg/dl.

Blood Collection and Serum Preparation

Peripheral blood was collected every 4 weeks by retro-orbital bleeding following IACUC requirements. Freshly-collected blood was maintained in 4°C refrigerator overnight to clot, and then centrifuged at 1,500× g for 15 min at 4°C to remove clots and collect supernatant as serum. The serum was stored at −80°C freezer.

Splenic Lymphocyte Preparation, Splenic T and B Cell Purification, and Cell Culture

Whole splenocytes were prepared by following standard laboratory procedures described in detail previously (Lengi et al., 2007; Edwards et al., 2017; Dai et al., 2019; Edwards et al., 2020). Per the manufacturer's protocol, splenic CD4^{+} cells (T cells) and CD19^{+} cells (B cells) were purified from splenic lymphocytes with anti-CD4 (L3T4) and anti-CD19 MicroBeads (Miltenyi Biotec, San Diego, CA, United States), respectively. The purity of CD4^{+} (93.84% ± 2.03%) and CD19^{+} (91.88% ± 1.81%) cells were confirmed by flow cytometry.

To activate splenic lymphocytes, 2.5 × 10^{6} cells were seeded in 24-well plates and stimulated with 500 ng/ml of Lipopolysaccharide (LPS, from Sigma-Aldrich, St Louis, MO, United States) or anti-mouse CD3ε (plate coated at 5 μg/ml, Bio X cell, Lebanon, NH, United States) plus 2 μg/ml soluble anti-mouse CD28 (Bio X cell) for 24 h h, or 50 ng/ml phorbol 12-myristate 13-acetate (PMA) (Sigma-Aldrich) and 1 μg/ml ionomycin (Sigma-Aldrich) for 6 h. For the induction of IL-17, the splenocytes were stimulated with either non-pathogenic T helper 17 (Th17) stimuli (20 ng/ml IL-6 (BioLegend) plus 3 ng/ml TGFβ 1 (R&D System Inc., Minneapolis, MN, United States) and 1 μg/ml anti-CD3) or pathogenic Th17 stimuli (20 ng/ml IL-6 plus 10 ng/ml IL-1β (BioLegend), 10 ng/ml IL-23 (Invitrogen) and 1 μg/ml anti-CD3) for 72 h. The cell culture supernatants were collected for ELISA assay.

In Vitro Transfection of Antagomir

As previously described (Krützfeldt et al., 2005; Dai et al., 2016), the specific antagomirs against certain miR-182, miR-183, and miR-96 were designed based on mature murine miRNA

TABLE 1 | Scrambled control and specific miR-183, -96, -182 antagomirs sequences.

Antagomir ID	Sequences
Scrambled Control	5′mU (*)mC (*)mAmCmGmCmAmGmAmUmUmCmAmUmAmA (*)mC (*)mG (*)mU (*)-3′-Chl
Antagomir-183	5′ mA (*)mG (*)mUmG mAmAmU mUmCmU mAmCmC mAmGmUmGmCmC (*)mA (*) mU (*)mA (*) -3′-Chl
Antagomir-96	5′ mA (*)mG (*)mCmA mAmAmA mAmUmG mUmGmC mUmAmG mUmGmC mC (*)mA (*)mA (*) mA (*) -3′-Chl
Antagomir-182	5′mC (*)mG (*)mGmUmGmUmGmAmGmUmUmCmUmAmCmCmAmUmUmGmCmC(*) mA (*)mA (*)mA (*)-3′-Chl

All ribonucleotides are 2′-O-methyl modified (mN). (*) represents a phosphorothioate modification of the backbone. A cholesterol molecule was added at the 3′ end (-3′-Chl).

sequences from miRbase (http://www.mirbase.org/) and shown in **Table 1**. The scramble control antagomir (Stittrich et al., 2010) and specific antagomirs were synthesized by GE Dharmacon (Lafayette, CO, United States). Antagomirs were delivered into splenic lymphocytes using a serum-free Accell siRNA delivery medium (GE Dharmacon) as we reported previously (Dai et al., 2016). Twenty-four hours after antagomir treatment, the cells were stimulated with concanavalin A (Con A; 5 μg/ml) or LPS (500 ng/ml) for 24 h or 48 h, the culture supernatants were collected to measure the cytokine levels by ELISA. The cell pellets were collected for Western blot.

RNA Extraction

As we reported previously (Dai et al., 2016; Wang Z. et al., 2018; Dai et al., 2019), total RNA containing small RNA was extracted from cells using the miRNeasy Mini Kit (Qiagen) following the manufacturer's protocol. On-column DNA digestion was performed to remove any residual DNA in the RNA samples during RNA extraction. Concentration and purity of RNA were determined by NANODROP 2000 spectrophotometer (Thermo Fisher Scientific, United States) and samples with the OD260/280 ratio at around 2.0 were used for TaqMan miRNA Assay and RT-qPCR analysis.

Quantitative RT-PCR Analysis of miRNA and mRNA

As we previously reported (Dai et al., 2010; Dai et al., 2016; Wang Z. et al., 2018; Dai et al., 2019), TaqMan microRNA assays (Applied Biosystems, Waltham, MA, United States) were used to quantify miR-183C miRNAs (miR-182 ID 002599; miR-183 ID 00269; miR-96 ID 000186; snoRNA202 ID 001232, Applied Biosystems) expression levels according to the manufacturer's instruction. For miRNA analysis, RNA samples were reverse transcribed with TaqMan microRNA reverse transcription kit, followed by quantitative real-time PCR (qPCR) with TaqMan miRNA assay reagent. For RT-qPCR of protein-coding genes, total RNA samples were reverse transcribed using High-Capacity cDNA Reverse Transcription Kit (Applied Biosystems, Waltham, MA, United States) followed by qPCR using Power SYBR green PCR master mix (Applied Biosystems). The qPCR reactions were performed with a 7,500 Fast Real-Time PCR system (Applied Biosystems, Waltham, MA, United States). The relative expression level of miRNAs and mRNAs was normalized to endogenous small nucleolar RNA 202 (snoRNA202) and house-keeping gene β–actin respectively and calculated relative expression level using the $2^{-\Delta\Delta Ct}$ method. The primers for quantitative RT-PCR were as follows, Foxo1: (Forward) 5′-CGTGCCCTACTTCAA GGATAAG-3′, (Reverse) 5′-GCACTCGAATAAACTTGCTGT G-3'; β–actin: (Forward) 5′-CGCGAGCACAGCTTCTT-3′, (Reverse) 5′-GCAGCGATATCGTCATCCAT-3'.

ELISA

The production level of interferon-gamma (IFNγ), interleukin 6 (IL-6), and interleukin 17 (IL-17) in cell culture supernatant were detected ELISA kits from BioLegend and ThermoFisher Scientific) respectively. Serum levels of IL-6, IFNγ, IL-17, TNF-a, and IL-10 were determined by the SP-X (previously Ciraplex®) multiplex Chemiluminescent Assay kit (Quanterix, Billerica, MA, United States) as we previously reported (Dai et al., 2019; Edwards et al., 2020). The image of the chemiluminescent array plate was captured with the Aushon Cirascan™ Imaging system (Aushon BioSystems, InC., Billerica, MA, United States) and the image data was processed with Cirasoft software.

Anti-dsDNA autoantibody ELISA was performed to detect serum anti-dsDNA autoantibody production levels as we previously reported (Dai et al., 2010; Edwards et al., 2017). The plates were read at 380 nm with a Versa microplate reader (Molecular Devices).

Flow Cytometry

The relative proportion of subsets of immune cells was quantified by flow cytometric analysis with specific cell surface markers as we previously reported (Dai et al., 2019; Dai et al., 2020). Briefly, the freshly-isolated splenocytes were blocked with purified anti-mouse CD16/CD32 antibody (eBiosciences/ThermoFisher Scientific), and stained with cell surface markers in MACS buffer (Phosphate-buffered saline (PBS, pH 7.2) supplemented with 0.5% bovine serum albumin (BSA) and 2 mM EDTA) for 15–20 min at 4°C. After washing, the stained cells were resuspended in 100 μl MACS buffer for flow cytometry analysis. Anti-CD3-FITC, anti-CD4-eFluor 450, anti-CD8a-Percp-Cy5.5, anti-CD19-Percp-Cy5.5, anti-B220-PE, anti-CD25-Percp/Cy5.5, anti-Foxp3-APC, and anti-GL7-eFluor660 were purchased from eBiosciences/ThermoFisher Scientific. Anti-CXCR5-APC/Cy7, anti-CD138-APC (PE), anti-IgD-PE were obtained from BioLegend, anti-PD1-BV421 was obtained from BD biosciences. FACSAria Flow cytometer (BD Biosciences, San Jose, CA) was used for stained cell profiling. Data were analyzed by FlowJo software (FlowJo LLC, BD Life Sciences).

Western Blot Analysis

Western blotting was performed by following the lab-established protocol (Dai et al., 2007; Dai et al., 2009). Briefly, whole cell

extracts were prepared by lysing the cell pellets with CelLytic™ M Cell Lysis Reagent (Sigma-Aldrich). Protein lysates were separated by 4%–15% Criterion™ TGX™ Precast sodium dodecyl sulfate-polyacrylamide gel electrophoresis (SDS-PAGE) (Bio-Rad Laboratories, Inc.) and then transferred onto a polyvinylidene difluoride (PVDF) membrane. Membranes were blocked with 5% non-fat milk in PBST, incubated with a primary antibody, and subsequently a secondary horseradish peroxidase-conjugated antibody. After applying ECL plus western blot substrate (GE Healthcare, Cleveland, OH, United States), the blot images were captured with iBright CL1000 Imaging System (ThermoFisher Scientific). The Foxo1 antibody was purchased from Cell Signaling Technology, Inc. United States. β–actin antibody (Santa Cruz Biotechnology) was used as a reference protein.

Renal Histopathology and Renal Immunofluorescence

Renal histopathology and immunofluorescence analysis were performed as we previously reported (Dai et al., 2013; Edwards et al., 2017; Edwards et al., 2020). Frozen section slides and hematoxylin and eosin (H&E) stained slides were prepared by the histopathology laboratory at VMCVM, Virginia Tech. The H&E renal sections were assessed by a board-certified pathologist in a blinded fashion. A grade of 0–4 (0 = perfect, no change; 1 = minimal; 2 = moderate, 3 = marked; 4 = severe) was given to reflect the glomerular, tubular, interstitium, and vessel inflammation and lesions, respectively.

The OCT frozen kidneys were cut to 5 μM sections in the histopathology laboratory at VMCVM. The frozen slide sections were stored at −80°C for immunofluorescent staining. Briefly, the frozen slides were air-dried, fixed with cold acetone for 10 min at room temperature, followed by blocking with PBS containing 1% BSA (Fisher) and anti-mouse CD16/32 for 20–30 min. The slides were then incubated with FITC-conjugated IgG (eBioscience, San Diego, CA, United States) and PE-conjugated Complement Component C3 (Cedarlane, Burlington, NC, United States) for 1–2 h at room temperature in a dark chamber. The stained slides were mounted with coverslips using Prolong Gold anti-fade reagent with DAPI (Invitrogen, Grand Island, NY, United States). The stained kidney sections were assessed for IgG and C3 deposition under a fluorescent microscope. Fiji/ImageJ image processing program (Schindelin et al., 2015) was used to measure the fluorescent intensity of the selected area as we previously described (Edwards et al., 2017; Edwards et al., 2020).

siRNA Transfection

The Foxo1 specific Dicer substrate siRNA (Foxo1 siRNA) and negative control DsiRNA (NC) were purchased from Integrated DNA Technologies (Coralville, IA, United States) and reconstituted with distilled water to a stock concentration at 10 μM. The DsiRNAs were transfected into splenic lymphocytes with Lipofectamine RNAiMAX transfection reagent (ThermoFisher Scientific) per the manufacturer's protocol as we recently reported (Dai et al., 2020). Forty-eight hours after transfection, the transfected cells were stimulated with anti-mouse CD3ε (plate coated at 5 μg/ml) plus 2 μg/ml soluble anti-mouse CD28 (Bio X cell) for 24 h h, or 50 ng/ml phorbol 12-myristate 13-acetate (PMA) plus 1 μg/ml ionomycin for 6 h. The cell culture supernatants were collected for ELISA assay.

Statistical Analysis

All the values in the graphs were given as means ± SD. Unpaired student t-test and one-way ANOVA with Tukey-Kramer all pair's comparisons were performed to determine the statistical significance for two or multiple group comparisons, respectively. "*," "**," and "***" indicate $p < 0.05$, $p < 0.01$, and $p < 0.001$, respectively. The graphic presentations of data were performed in GraphPad Prism software (v.8.10 for Windows).

RESULTS

Inhibition of Either miR-182 Alone or miR-183C *In Vitro* in Splenocytes Reduces Inflammatory Cytokines IFNγ and IL-6 Expression Level

We have previously reported a significant upregulation of miR-183C miRNAs in the splenocytes of different murine lupus models (Dai et al., 2010). To determine whether miR-183C miRNAs play a role in regulating lupus-related inflammatory cytokines such as IFNγ and IL-6, we inhibited miR-182 alone or miR-183C miRNAs with specific antagomirs *in vitro* in splenocytes (**Figure 1A**). The antagomir-treated cells from MRL (control) and MRL/lpr (lupus-prone) were stimulated with two different stimuli, LPS and Con A, which activated immune cells to elicit cytokine production via distinct signaling pathways. As indicated, the inhibition of miR-182 alone or the miR-183C whole cluster significantly suppressed LPS-induced IFNγ and IL-6 production in both MRL and MRL/lpr splenocytes (**Figure 1B**). In Con A-stimulated cells, miR-182 and miR-183C inhibition significantly reduced both IFNγ and IL-6 in MRL splenocytes, while in MRL/lpr splenocytes only IL-6 was significantly reduced (**Figure 1C**). The antagomir treatment did not affect the cell viability (**Supplementary Figure S2A**). We also noticed that silencing miR-182, but not miR-96 and miR-183 alone, had a similar suppression on IFNγ and IL-6 production as silencing the three miR-183C miRNAs (**Supplementary Figure S2B**). This suggests that of the three miR-183C miRNAs, miR-182 likely plays a major role in regulating inflammatory cytokine production.

Conditional Deletion of miR-183C Significantly Suppresses Anti-dsDNA Autoantibodies in B6/lpr Mice

To further investigate the role of upregulated miR-183C cluster miRNAs *in vivo* in autoinflammation-prone mice, we generated miR-183C$^{-/-}$B6/lpr mice with conditional deletion of miR-183C miRNA cluster in both T and B lymphocytes (**Figure 2A**). As previously reported (de Boer et al., 2003; Siegemund et al., 2015), the hCD2-iCre deleted the floxed-target gene in both T and B

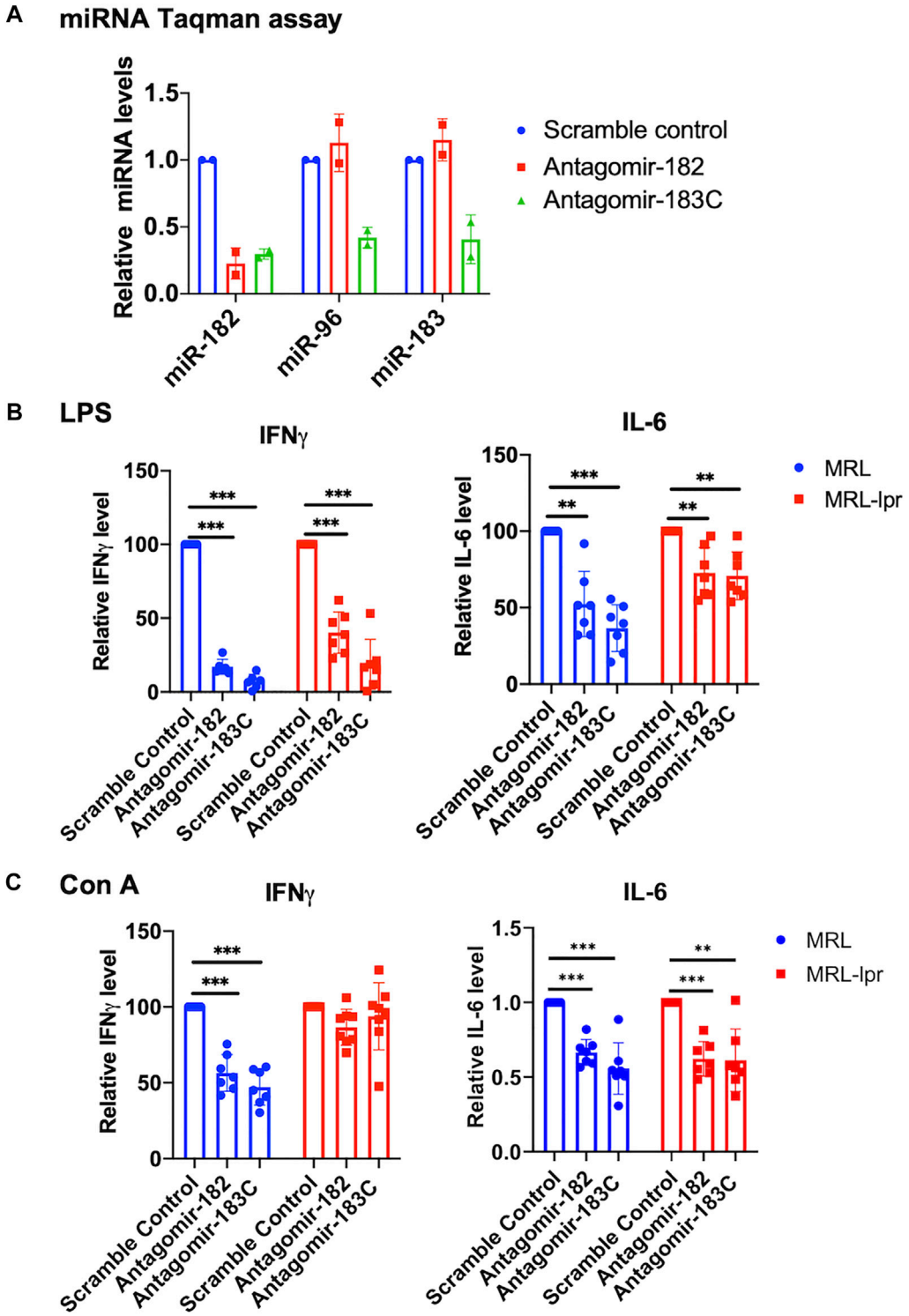

FIGURE 1 | *In vitro* inhibition of miR-182 alone and miR-183C miRNAs in splenocytes reduces inflammatory cytokines IFNγ and IL-6 expression level. **(A)** Antagomir-182, -96, -183 inhibited the respective miRNA efficiently and specifically. Freshly-isolated splenocytes from MRL/lpr mice were transfected with either scramble control, antagomir-182, or the mixture of antagomir-182, -96, and -183 (antagomir-183C). Twenty-four hours after transfection, the cells were collected for TaqMan miRNA assays. The graph showed means ± SD ($n = 2$ each). **(B,C)** Inhibition of miR-182 or miR-183C reduced IFNγ and IL-6 production in LPS or Con A-activated splenocytes. Freshly-isolated splenocytes from MRL and autoimmune-prone MRL/lpr mice at 14–15 weeks of age were treated with control antagomir and specific antagomir for 24 h, and then stimulated with LPS (500 ng/ml) for 48 h or Con A (5 μg/ml) for 24 h. The IFNγ and IL-6 levels in the culture supernatant were measured by ELISA. The graphs showed means ± SD ($n \geq 6$). The cytokine level in specific antagomir treated samples were shown as the percentage of paired scrambled control antagomir treated cells. Paired student *t* tests were performed (scrambled control vs. antagomir-182 or antagomir-183C); **, $p < 0.01$; and ***, $p < 0.001$.

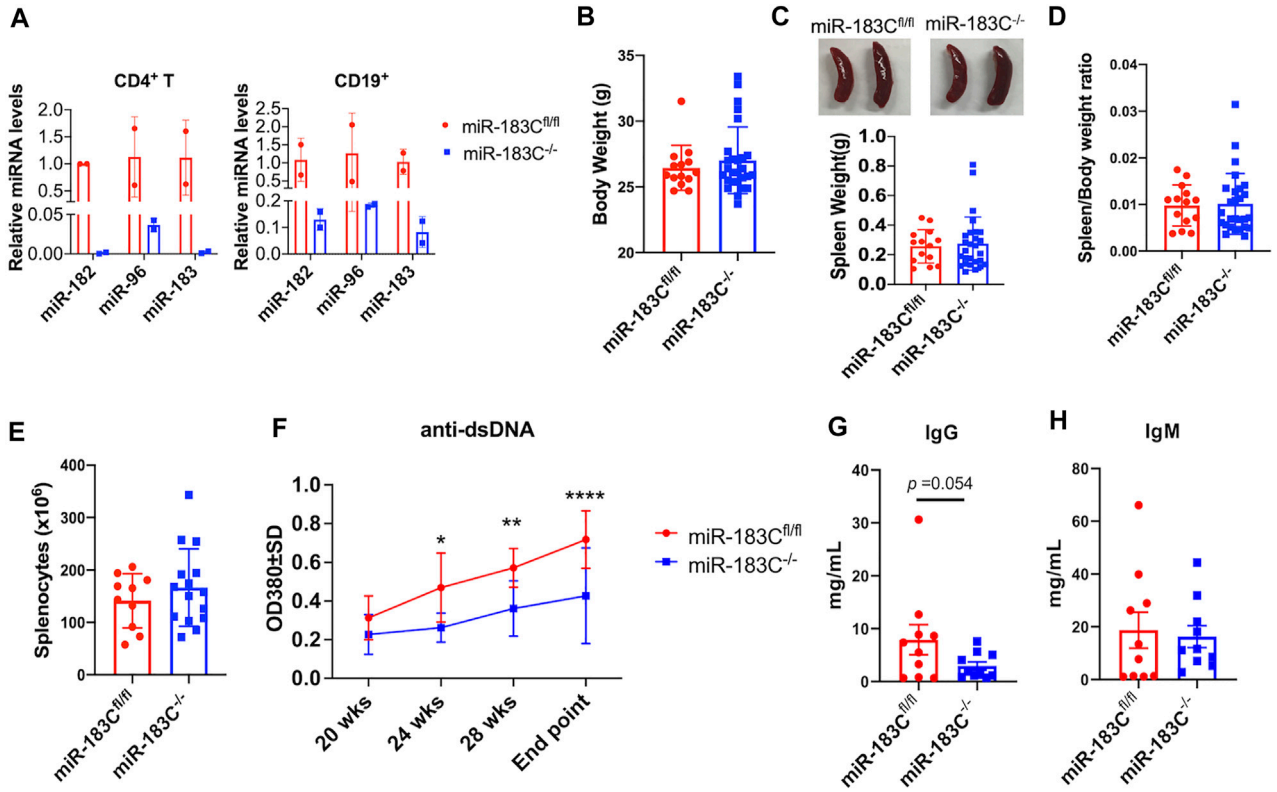

FIGURE 2 | Analysis of the effect of miR-183C deletion on body weight, spleen weight, and antibody production. **(A)** miRNA TaqMan assay was performed to validate the deletion of miR-182, -96, -183 miRNAs in purified CD4$^+$ T and CD19$^+$ B cells from conditional miR-183C$^{-/-}$B6/lpr (miR-183C$^{-/-}$) mice. Data are presented as means ± SD (n = 2 each). **(B–E)** Deletion of miR-183C had no obvious effect on body weight **(B)**, spleen weight **(C)**, spleen/body weight ratio **(D)**, and splenocyte counts **(E)**. The miR-183C$^{-/-}$ and control miR-183C$^{fl/fl}$B6/lpr (miR-183C$^{fl/fl}$) mice were euthanized at 29–32 weeks of age (end point) for the assay. Data are displayed as means ± SD ($n \geq 10$). **(F)** Deletion of miR-183C miRNAs significantly reduced serum anti-dsDNA autoantibodies. The serum anti-dsDNA autoantibody levels in miR-183C$^{-/-}$ and control miR-183C$^{fl/fl}$ mice were monitored every 4 weeks starting at 20 weeks of age. The graph showed means ± SD (n = 6 for miR-183C$^{-/-}$ mice at different time points except n = 12 for the end point; n = 10 for 183C$^{fl/fl}$ mice at different time points except n = 15 for the end point). **(G,H)** Evaluation of serum levels of total IgG **(G)** and IgM **(H)** antibodies in miR-183C$^{-/-}$ and control mice at the end point. Graphs showed means ± SD (n = 10 each). Unpaired student t tests were performed (miR-183C$^{fl/fl}$ vs. miR-183C$^{-/-}$); *, $p < 0.05$; **, $p < 0.01$.

lymphocytes. Nevertheless, the deletion efficiency in CD4$^+$ T (about 99% reduction) is higher than that in CD19$^+$ B (about 90% reduction) cells (**Figure 2A**). After the mice reached 20 weeks of age, blood samples were collected at 4 weeks intervals to monitor the serum level of anti-double strand DNA (anti-dsDNA) autoantibody in miR-183C$^{-/-}$B6/lpr and control miR183C$^{fl/fl}$B6/lpr mice. The mice were euthanized at 29–32 weeks of age (endpoint) for the experimental analysis. Conditional deletion of miR-183C had no obvious effect on the body weight, spleen weight, and absolute splenocyte counts (**Figures 2B–E**). Impressively, we found that miR-183C deletion significantly reduced serum anti-dsDNA autoantibody level in miR-183C$^{-/-}$B6/lpr mice compared to age-matched miR183C$^{fl/fl}$B6/lpr control mice (**Figure 2F**). There was a trend of reduced total IgG in miR-183C$^{-/-}$B6/lpr mice (p = 0.054, **Figure 2G**). There was no difference in the serum IgM levels (**Figure 2H**).

The *in vitro* antagomir inhibition data indicated that inhibition miR-182 alone and inhibition of the whole miR-183C had a similar suppressive effect on activation induced inflammatory cytokines production (**Figure 1**). We, therefore, derived miR-182$^{-/-}$B6/lpr to determine whether deletion of miR-182 alone *in vivo* has a similar effect as the deletion of whole cluster *in vivo* in B6/lpr mice. As expected, miR-182 was specifically deleted in the splenocytes of miR-182$^{-/-}$B6/lpr mice (**Figure 3A**). There was no change in the expression of miR-96 and miR-183 in the splenocytes of miR-182$^{-/-}$B6/lpr mice when compared to control miR182$^{fl/fl}$B6/lpr mice (**Figure 3A**). Conditional deletion of miR-182 alone did not affect the body weight (**Figure 3B**). There was a trend of decreased spleen weight (p = 0.076) and spleen/body weight ratio (p = 0.082) in miR-182$^{-/-}$B6/lpr mice when compared to controls (**Figures 3C,D**). However, there was no obvious change in the absolute splenocytes count in miR-182$^{-/-}$B6/lpr compared to control miR-182$^{fl/fl}$B6/lpr mice (**Figure 3E**). We only observed a reduction of serum anti-dsDNA levels in miR-182$^{-/-}$B6/lpr mice at 28 weeks of age compared to age-matched controls (**Figure 3F**). Deletion of miR-182 significantly decreased serum IgM levels and demonstrated a trend of reduced total IgG (p = 0.062) in B6/lpr mice (**Figures 3G,H**).

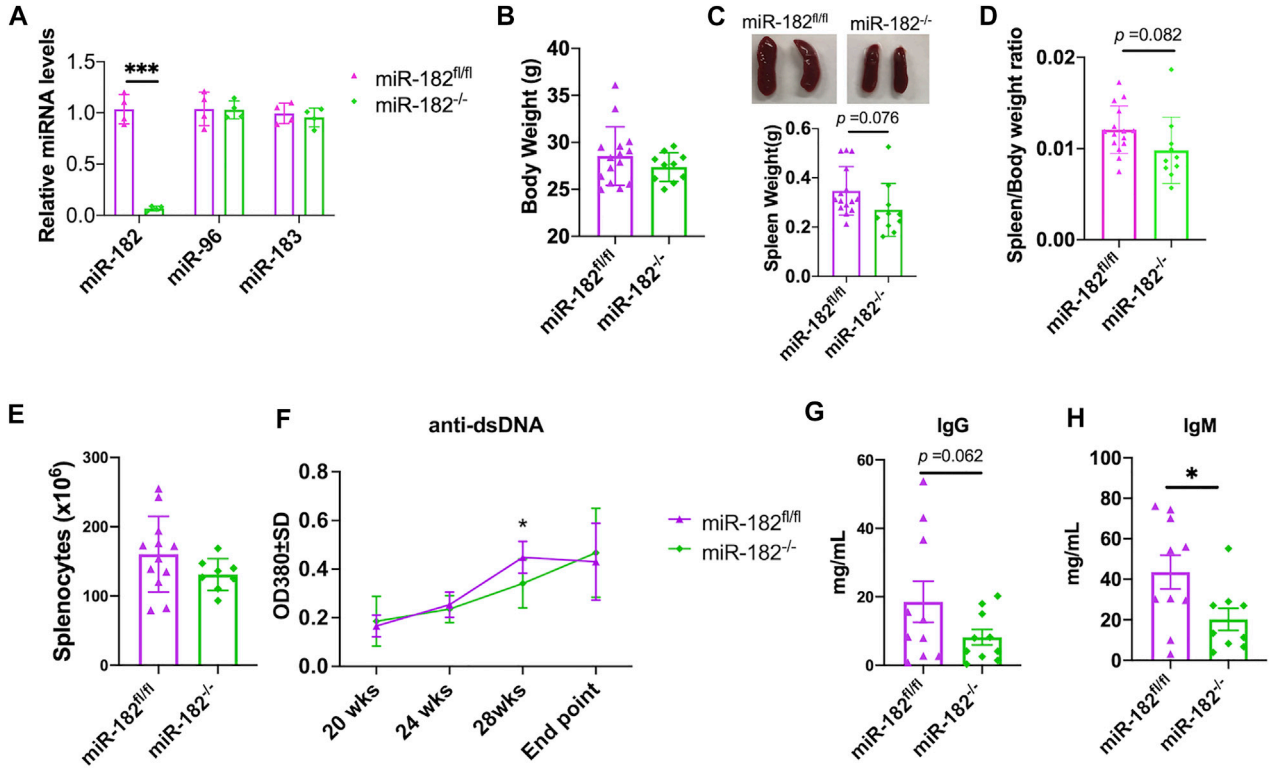

FIGURE 3 | Analysis of the effect of miR-182 deletion on body weight, spleen weight, and antibody production. **(A)** miRNA TaqMan assay was performed to validate the specific deletion of miR-182, but not miR-96 and miR-183 in splenocytes of miR-182$^{-/-}$B6/lpr (miR-182$^{-/-}$) mice. The graph showed means ± SD (n = 4 each). **(B–E)** Deletion of miR-182 alone had no obvious effect on body weight **(B)** and splenocyte counts **(E)**, but led a trend of reduction of spleen weight **(C)** and spleen/body weight ratio **(D)**. The miR-182$^{-/-}$ and control miR-182$^{fl/fl}$B6/lpr (miR-182$^{fl/fl}$) mice were euthanized at 29–32 weeks of age (end point) for sample collections. Graphs showed means ± SD ($n \geq 8$). **(F)** Deletion of miR-182 had minimal effect on serum anti-dsDNA autoantibodies. The serum anti-dsDNA autoantibody levels in miR-182$^{-/-}$ and miR-182$^{fl/fl}$ mice were monitored every 4 weeks starting at 20 weeks of age. Data were shown as means ± SD (n = 6 for miR-182$^{-/-}$ mice at different time points except n = 15 for the end point; n = 7 for miR-182$^{fl/fl}$ mice at different time points except n = 15 for the end point) **(G,H)** Evaluation of serum levels of total IgG **(G)** and IgM **(H)** antibodies in miR-182$^{-/-}$ and miR-182$^{fl/fl}$ mice at the end point. Graphs showed means ± SD (n = 10 each). Unpaired student t tests were performed (miR-182$^{fl/fl}$ vs. miR-182$^{-/-}$); *, $p < 0.05$; ***, $p < 0.001$.

Conditional Deletion of miR-183C or miR-182 Reduces IgG Immune Complex Deposition in the Kidneys of B6/lpr Mice

The effect of miR-183C deletion on the renal function of B6/lpr was determined by examining proteinuria and blood urea nitrogen (BUN) levels. There was no difference in the proteinuria or BUN levels between miR-183C$^{-/-}$B6/lpr and control miR-183C$^{fl/fl}$B6/lpr mice (**Figures 4A,B**). The renal histopathology analysis also showed no obvious difference in the kidney inflammation and damages in the miR-183C$^{-/-}$B6/lpr mice compared to control miR-183C$^{fl/fl}$B6/lpr mice (**Table 2**). However, we observed a significant reduction of IgG and complement component C3 immunocomplex deposition in the kidneys of miR-183C$^{-/-}$B6/lpr mice compared to age-matched control mice (**Figures 4C,D**). We also examined the effect of miR-182 deletion on renal pathology and function in B6/lpr mice. Similar to the data with miR-183C deletion, deletion of miR-182 had no effect on renal histopathology, proteinuria levels, serum BUN levels and C3 immunocomplex deposition in the kidneys in B6/lpr mice (**Figures 4E,F,H**), but significantly reduced IgG immune complex deposition in the kidneys of B6/lpr mice (**Figure 4G**).

Conditional Deletion of miR-183C or miR-182 Does Not Change Lymphocyte Composition in the Spleens of B6/lpr Mice

Previous studies have reported that deletion of miR-182 *in vivo* had no obvious effects on adaptive immune cell development in normal B6 mice (Pucella et al., 2015; Ichiyama and Dong, 2019). Flow cytometric evaluation was performed to determine whether miR-182 and miR-183C deletion affected immune cell composition in B6/lpr mice (**Supplementary Figure S3**). Consistently, we found that in the autoinflammatory-prone B6/lpr mice, conditional deletion of either miR-182 alone or miR-183C cluster in lymphocytes also did not change the adaptive immune cell development and lymphocyte subset composition in the spleens (**Figures 5A,B**). The development of CD4$^-$CD8$^-$CD3$^+$B220$^+$ double-negative T cells (DN T) is a specific characteristic cell type in *lpr* lupus mice (Morse et al., 1985; Giese et al., 1993; Hamad et al., 2003). There were no obvious differences in the percentage of DN T cells in the splenocytes between the knockout and control B6/*lpr* mice (**Figures 5A,B**). While the previous study has shown that

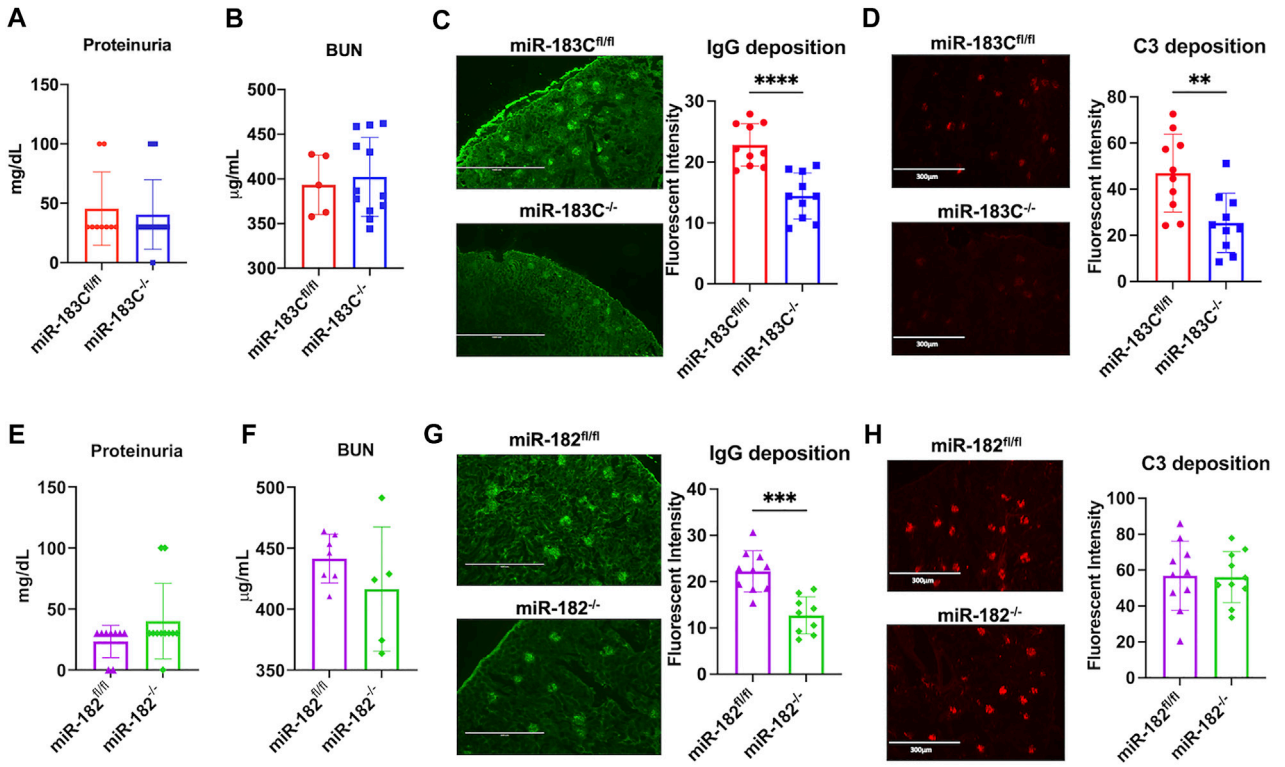

FIGURE 4 | Deletion of either miR-183C or miR-182 alone reduces IgG antibody deposition in kidney. **(A,B)** Summary graphs show no significant difference in the proteinuria **(A)** and blood urea nitrogen (BUN, **(B)** levels between miR-183C$^{-/-}$B6/lpr and control miR-183C$^{fl/fl}$B6/lpr mice. Graphs showed means ± SD ($n \geq 5$) **(C,D)** Representing IF images and summary data show significantly reduced IgG **(C)** and complement C3 **(D)** immune complex deposition in the kidneys of miR-183C$^{-/-}$. Graphs showed means ± SD ($n = 10$ each) **(E,F)** Summary graphs show no significant difference in the proteinuria **(E)** and blood urea nitrogen (BUN, **(F)**) levels between miR-182$^{-/-}$B6/lpr and control miR-182$^{fl/fl}$B6/lpr mice. Graphs showed means ± SD ($n \geq 5$) **(G,H)** Representing images and summary data show significantly reduced IgG **(G)** and complement C3 **(H)** immune complex deposition in the kidneys of miR-182$^{-/-}$. Graphs showed means ± SD ($n = 10$ each). Unpaired student t tests were performed (miR-183C$^{fl/fl}$ vs. miR-183C$^{-/-}$, miR-182$^{fl/fl}$ vs. miR-182$^{-/-}$); *, $p < 0.05$; and **, $p < 0.01$.

TABLE 2 | Renal histopathological scores.

Strains	Glomeruli	Tubules	Interstitium	Vessels	Kidney Scores
miR183C$^{fl/fl}$B6/lpr ($n = 8$)	1.13 ± 0.64	0.13 ± 0.35	0 ± 0	0.63 ± 0.52	1.88 ± 1.13
miR183C$^{-/-}$B6/lpr ($n = 11$)	0.73 ± 0.65	0 ± 0	0 ± 0	0.91 ± 0.83	1.64 ± 1.29
miR182$^{fl/fl}$B6/lpr ($n = 9$)	1 ± 0.5	0 ± 0	0.22 ± 0.44	0.78 ± 0.67	2 ± 1.41
miR182$^{-/-}$B6/lpr ($n = 8$)	1.25 ± 1.04	0 ± 0	0 ± 0	0.38 ± 0.52	1.63 ± 1.19

Evaluation and scoring of the formalin-fixed renal tissue section. H&E-stained slides were evaluated by veterinary pathologists in a blinded fashion. Scores were averaged for each group and each structure. Data are shown as Mean ± SD.

miR-182 regulates Treg cell development during murine EAE development (Wan et al., 2016), we did not observe any notable change of Tregs percentage in the splenocytes in either the miR-183C$^{-/-}$B6/lpr or the miR-182$^{-/-}$B6/lpr mice compared to their respective controls (**Figures 5C,G**). Furthermore, we found that conditional deletion of miR-183C or miR-182 did not affect the differentiation of germinal center B cells (GCB), follicular helper T cells (T_{FH}), or plasma cells in the spleens. The percentages of GCB, T_{FH}, and plasma cells in the splenocytes of the miR-183C$^{-/-}$B6/lpr (**Figures 5D–F**) and the miR-182$^{-/-}$B6/lpr (**Figures 5H–J**) mice were similar to their respective controls.

Deletion of miR-183C and miR-182 *In Vivo* in B6/lpr Mice Significantly Reduces IFNγ, but Not IL-6 Production in *In Vitro* Activated Splenocytes

We showed that *in vitro* inhibition of either miR-182 alone or miR-183C significantly suppressed IFNγ and IL-6 production in activated splenocytes (**Figure 1**). We then checked IFNγ and IL-6 cytokine production in *in vitro* activated splenocytes from miR-183C$^{-/-}$B6/lpr and control miR-183C$^{fl/fl}$B6/*lpr* mice. We found that in response to either anti-CD3 plus anti-CD28 or PMA plus ionomycin stimulation, there was a significantly lower IFNγ

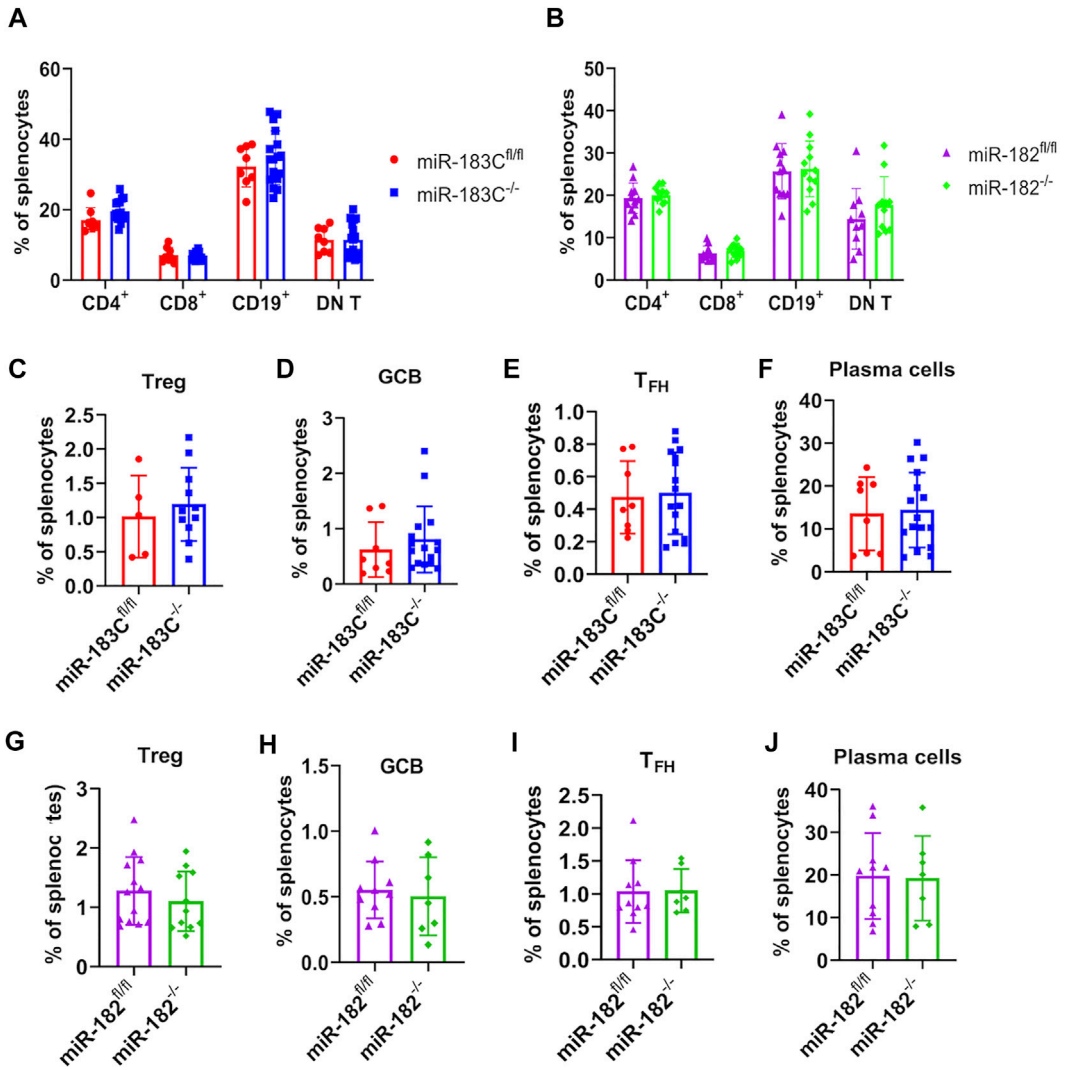

FIGURE 5 | Evaluate the effect of miR-182 and miR-183C deletion on splenic lymphocyte composition in B6/lpr mice. The different lymphocyte subsets in the freshly-isolated splenocytes were analyzed by flow cytometry. Please see **Supplementary Figure S3** for the gating of different immune cell subsets in the splenocytes. **(A,B)** Summary data of the frequency of $CD4^+$ T cells, $CD8^+$ T cells, $CD19^+$ cells, and $CD3^+B220^+CD4^-CD8^-$ double negative T cells (DN T cells) in the splenocytes of miR-183C$^{-/-}$ and control miR-183C$^{fl/fl}$ B6/lpr **(A)**, miR-182$^{-/-}$ and control miR-182$^{fl/fl}$ B6/lpr **(B)**. The graphs show means ± SD ($n \geq 8$). **(C–J)** Summary data of the frequency of differentiated $CD4^+CD25^+Foxp3^+$ **(C,G)**, $CD19^+GL7^+IgD^-$ GCB **(D,H)**, $CD3^+CD4^+CXCR5^+PD1^+$ T_{FH} **(E,I)**, $CD19^-CD138^+$ plasma **(F,J)** cells in the splenocytes of miR-183C$^{-/-}$ and miR-183C$^{fl/fl}$ **(C–F)**, miR-182$^{-/-}$ and miR-182$^{fl/fl}$ **(G–J).** The graphs show means ± SD ($n \geq 5$). Unpaired student *t* tests were performed (miR-183C$^{fl/fl}$ vs. miR-183C$^{-/-}$, miR-182$^{fl/fl}$ vs. miR-182$^{-/-}$) for statistical analysis. No significant differences were observed in the difference immune cell subsets between knockout and control mice.

production in splenocytes from miR-183C$^{-/-}$B6/lpr and miR-182$^{-/-}$B6/lpr mice compared to splenocytes from their respective control mice (**Figures 6A,B**). *In vivo* deletion of miR-183C or miR-182 alone had no effect on IL-6 production in splenocytes in response to anti-CD3 plus anti-CD28 stimulation (**Figures 6B,E**). There was an increase of IL-6 in PMA plus ionomycin-activated splenocytes from miR-183C$^{-/-}$B6/lpr mice, but not from miR-182$^{-/-}$B6/lpr compared to their respective controls (**Figures 6B,E**). A recent study revealed that miR-183C was highly induced by IL-6-STAT3 signaling to promote the differentiation and function of pathogenic Th17 cells (Ichiyama et al., 2016). We found that deletion of miR-183C or miR-182 *in vivo* did not affect IL-17 production in B6/lpr splenocytes in response to either non-pathogenic (IL-6 plus TGFβ1) or pathogenic (IL-6, IL-23 plus IL-1β) Th17 stimuli (**Figures 6C,F**). *In vitro* inhibition of either miR-183C or miR-182 alone suppressed LPS-induced IFNγ and IL-6 production in splenocytes from MRL and MRL/lpr mice (**Figure 1**). However, we found that deletion of miR-183C *in vivo* did not affect LPS-induced IFNγ and IL-6 production, and the deletion of miR-182 only inhibited LPS-induced IFNγ, but not IL-6 in splenocytes from B6/lpr mice (data not shown).

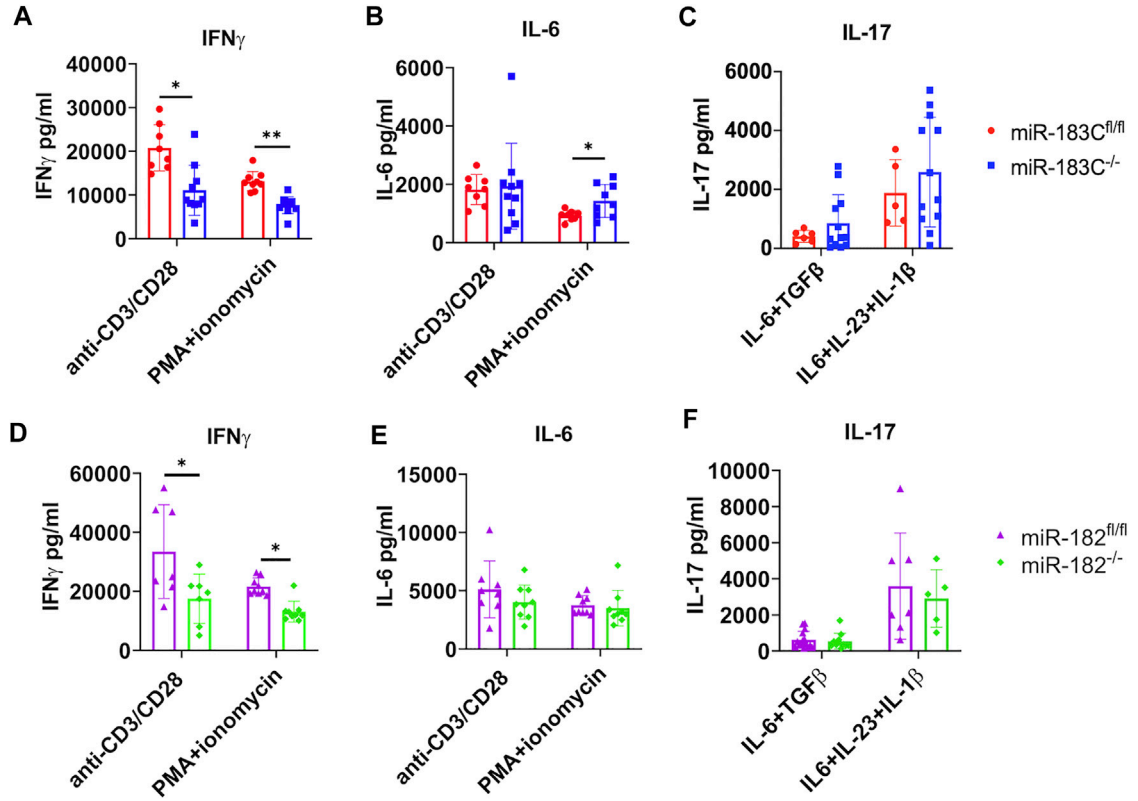

FIGURE 6 | Exam the effect of miR-182 and miR-183C deletion on IFNγ, IL-6, and IL-17 production in *in vitro* activated splenocytes with different stimuli. The freshly isolated splenocytes from miR-183C$^{-/-}$B6/lpr **(A–C)**, miR-182$^{-/-}$B6/lpr **(D–F)** and their respective littermate control miR-miR-183C$^{fl/fl}$ and miR-182$^{fl/fl}$B6/lpr mice were stimulated with anti-CD3 plus anti-CD28 for 24 h, PMA plus ionomycin for 6 h, non-pathogenic Th17 stimuli or pathogenic Th17 stimuli for 72 h. The production specific cytokines in culture supernatant were measured by ELISA. **(A–C)** Summary graphs show deletion of miR183C *in vivo* in B6/lpr mice suppressed IFNγ, but not IL-6 and IL-17 in splenocytes following *in vitro* stimulation with specific stimuli. **(D–F)** Summary graphs show deletion of miR182 alone *in vivo* in B6/lpr mice suppressed IFNγ, but not IL-6 and IL-17 in *in vitro* activated splenocytes with specific stimuli. The graphs were shown as means ± SD ($n \geq 5$). Unpaired student t tests were performed (miR-183C$^{fl/fl}$ vs. miR-183C$^{-/-}$, miR-182$^{fl/fl}$ vs. miR-182$^{-/-}$) for statistical analysis; *, $p < 0.05$; **, $p < 0.01$; and ***, $p < 0.005$.

miR-183C miRNAs Regulate Inflammatory Cytokine IFNγ *via* Targeting Foxo1

Previous studies have shown that miR-183C cluster miRNAs play an immune- and autoimmune-regulatory role through targeting Foxo1 directly (Stittrich et al., 2010; Ichiyama et al., 2016; Wang X. et al., 2018). We found an inverse relationship between the miR-183C miRNAs expression and Foxo1 protein expression in the splenocytes of MRL and MRL/lpr mice (**Figure 7A**). Consistent with the marked increase of miR-183C miRNAs, there was a significant decrease in the Foxo1 protein expression in MRL/lpr splenocytes. Knocking down miR-182 *in vitro* alone with antagomir-182 or miR-183C cluster with the mixes of antagomir-182, -96, -183 in MRL/lpr splenocytes increased Foxo1 protein expression (**Figure 7B**). Further, Foxo1 protein expression was significantly increased in CD4$^+$ T cells from miR-182$^{-/-}$B6/lpr and miR-183$^{-/-}$B6/lpr compared to the CD4$^+$ T cells from control mice (**Figure 7C**). Together, these data demonstrated that Foxo1 is the target of miR-183C miRNAs in splenocytes and T cells of MRL/lpr and B6/lpr mice. Deletion of miR-182 or miR-183C increased Foxo1 expression (**Figure 7C**) and reduced IFNγ in B6/lpr splenocytes in response to anti-CD3 plus anti-CD28 or PMA plus ionomycin stimulation (**Figures 6A,D**). To determine whether miR-183C regulates the production of cytokines in splenocytes through targeting Foxo1, we inhibited Foxo1 expression with Foxo1 siRNA *in vitro* in splenocytes from miR-183C$^{-/-}$B6/lpr and miR-182$^{-/-}$B6/lpr. We confirmed the significant reduction of Foxo1 mRNA expression level in the Foxo1 siRNA transfected cells (**Figure 7D**). In Foxo1 siRNA transfected cells, there was a significantly increased IFNγ production in response to anti-CD3 plus anti-CD28 or PMA plus ionomycin stimulation when compared to control siRNA transfected cells (**Figures 7E,G**). Suppression of Foxo1 *in vitro* has minimal effect on IL-6 production in activated splenocytes from miR-183C$^{-/-}$B6/lpr and miR-182$^{-/-}$B6/lpr mice (**Figures 7F,H**). This is consistent with the finding that deletion of miR-182 or miR-183C *in vivo* has minimal effect on IL-6 in *in vitro* activated splenocytes (**Figures 6B,E**). Together, our data suggested that miR-183C acts through Foxo1 to regulate the production of inflammatory cytokine IFNγ, a key pathogenic cytokine in the *lpr* lupus model.

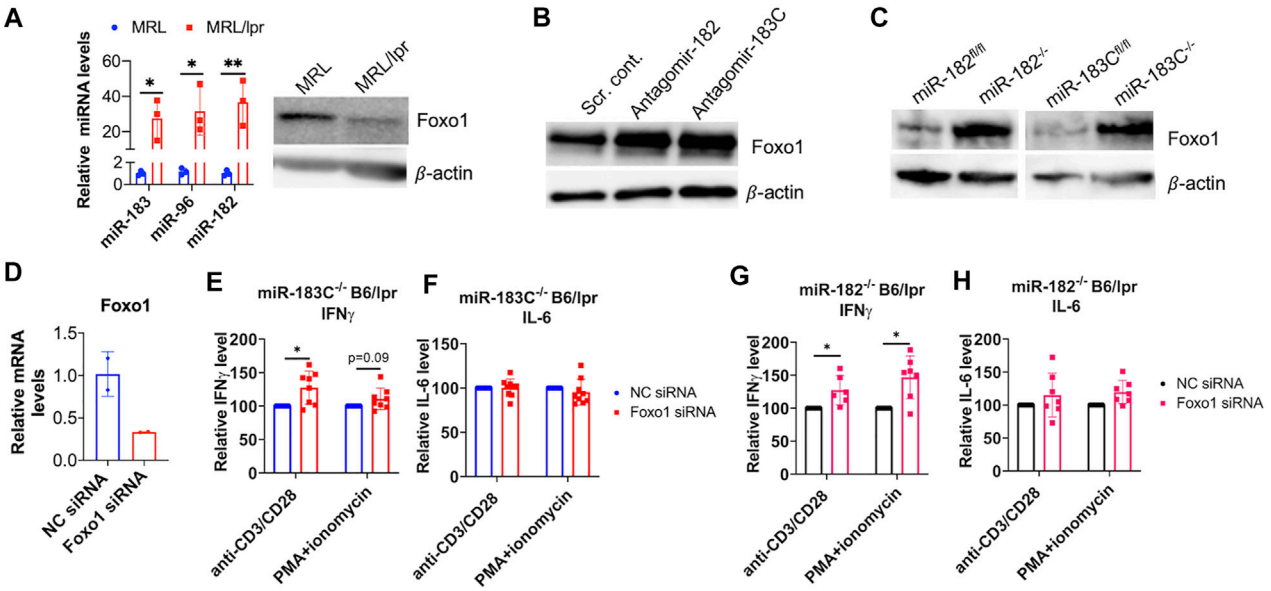

FIGURE 7 | miR-183C and miR-182 miRNAs regulate IFNγ production via targeting Foxo1. **(A)** An inverse relationship between miR-183 miRNAs expression of Foxo1 protein expression in control MRL and autoimmune-prone MRL/lpr mice splenocytes. The left graph showed relative miR-183, -96, -182 miRNAs expression in the splenocytes of MRL and MRL/lpr mice (14–15 weeks of age). The graph showed means ± SD ($n = 3$ each). Unpaired student t -test (MRL vs. MRL/lpr); *, $p < 0.05$; **, $p < 0.01$. The right panel showed western blotting of Foxo1 and β-actin (loading control) protein expression in MRL and MRL/lpr splenocytes. The representative western blotting image from three independent experiment was shown. **(B)** Increased Foxo1 protein in antagomir-182 or antagomir-183C treated splenocytes from MRL/lpr mice. The representative western blotting image from two independent experiments was shown. **(C)** Increased Foxo1 protein expression in splenic $CD4^+$ T cells from miR-183C$^{-/-}$B6/lpr (miR-183C$^{-/-}$), miR-182$^{-/-}$B6/lpr (miR-182$^{-/-}$) mice when compared to the cells from their respective control miR-183C$^{fl/fl}$B6/lpr (miR-183C$^{fl/fl}$) and miR-182$^{fl/fl}$B6/lpr (miR-182$^{fl/fl}$) mice. The representative western blotting image from at least three independent experiments was shown. **(D)** Reduced Foxo1 mRNA expression in Foxo1 siRNA treated cells when compared to negative control siRNA (NC siRNA) treated cells. The graph showed means ± SD ($n = 2$ each). **(E–H)** Inhibition of Foxo1 *in vitro* in splenocytes of miR-183$^{-/-}$ **(E,F)** and miR-182$^{-/-}$ **(G,H)** mice increased IFNγ, but not IL-6 production in response to anti-CD3/anti-CD28 or PMA/ionomycin stimulation. The cytokine level in Foxo1 siRNA treated samples were shown as the percentage of paired NC siRNA treated cells. The graphs were shown as means ± SD ($n \geq 4$). Paired student t tests were performed (NC siRNA vs. Foxo1 siRNA); *, $p < 0.05$ and **, $p < 0.01$.

DISCUSSION

Several studies have revealed that miR-183C miRNAs are critically involved in immunity and autoimmunity via regulating T cell activation, inflammatory cytokine IFNγ production, Tregs, and pathogenic Th17 cells differentiation and function (Stittrich et al., 2010; Kelada et al., 2013; Ichiyama et al., 2016; Wan et al., 2016; Thiel et al., 2019). Dysregulated miR-183C miRNAs expression has been identified in lupus and other human diseases (Dai et al., 2010; Chen J. Q. et al., 2017; Chen Y. J. et al., 2017; Liguori et al., 2018; Thiel et al., 2019). This study demonstrated that *in vitro* inhibition and *in vivo* deletion of miR-183C or miR-182 alone significantly reduces inflammatory cytokine IFNγ production in *in vitro* activated splenic lymphocytes from *lpr* lupus mice. This finding was significant as IFNγ is a key pathogenic cytokine in *lpr* lupus mice (Fan and Wüthrich, 1997; Peng et al., 1997). We further demonstrated that miR-183C and miR-182 regulate inflammatory IFNγ production in *in vitro* activated splenocytes *via* targeting Foxo1. Deletion of either miR-183C or miR-182 alone had no changes on the serum levels of IFNγ, IL-6, or other selected lupus-related cytokines, such as TNFα, IL-10, and IL-17 (**Supplementary Figures S4A,B**). Consistent with the previous data showing that miR-182 is largely dispensable for adaptive immune cell development, deletion of either miR-182 alone or miR-183C cluster did not affect lymphocyte composition in the spleens of B6/lpr mice. Importantly, we found that deletion of the miR-183C cluster significantly reduced serum anti-dsDNA level and IgG and C3 immunocomplex deposition in the kidneys of B6/lpr mice. Deletion of miR-182 alone suppressed immunocomplex IgG deposition in the B6/lpr kidneys but had only minor effects on the serum level of anti-dsDNA autoantibodies.

A previous study has shown that inhibition of miR-182 with antagomir-182 attenuated lupus nephritis in MRL/lpr mice via targeting Foxo1 (Wang X. et al., 2018). Our study revealed that deletion of miR-183C suppressed anti-dsDNA production and kidney IgG immunocomplex deposition in B6/lpr but had no obvious effect in renal function and histopathology (**Figures 2**, **4**, and **Table 2**). This could be due to the observation that B6/lpr mice, unlike MRL/lpr, do not show significant clinical pathology and lupus nephritis development (Santiago-Raber et al., 2007). In contrast to the upregulated miR-183 in MRL/lpr splenocytes, a recent study showed that the expression of miR-183 was decreased in renal tissues of MRL/lpr mice and human patients with LN (Li et al., 2019). Intraperitoneal delivery of miR-183 mimics to MRL/lpr mice attenuated murine lupus nephritis with reduced anti-dsDNA

antibodies, BUN through targeting mTOR (Li et al., 2019). These data suggested a tissue-specific dysregulation and function of miR-183 in lupus. The reason of why both administration of miR-183 mimic (Li et al., 2019) and deletion of miR-183-96-182 cluster have a suppressive effect on anti-dsDNA antibodies (**Figure 2F**) is unknown and perplexing. The previous studies have shown that deletion of miR-182 *in vivo* could not confirm the role of miR-182 on T cell-mediated immune responses that were determined by *in vitro* and *ex vivo* inhibition of miR-182 with antagomir (Stittrich et al., 2010; Pucella et al., 2015). It should be noted the off-target effect of systemic administration of antagomir and miRNA mimic *in vivo* is one possibility for the discrepancy of the data (Ichiyama and Dong, 2019).

miR-183C miRNAs have been shown to be involved in autoimmunity through promoting Tregs and Th17 cells differentiation and function. In our studies, we found that deletion of either miR-182 or miR-183C did not affect Treg development (**Figures 5C,G**). Also, compared to controls, there were no significant differences in the production of IL-17 in splenocytes from miR-182$^{-/-}$B6/lpr and miR-183C$^{-/-}$B6/lpr mice, which were stimulated with either non-pathogenic or pathogenic Th17 stimuli (**Figures 6C,F**). A previous study showed that the B6 mice with miR-182 deficiency had normal B cell development and antibody response to the T cell-dependent antigen NP-CGG (Pucella et al., 2015). However, Li et al. (2016) reported that miR-182 deficiency impaired early T cell-dependent immune response. The miR-182$^{-/-}$ B6 mice had reduced production of antigen-specific IgM and IgG1 at early time point but not late time point after immunization with NP-CGG. Mechanistically, Li et al. (2016) showed that miR-182 deficiency impaired the antigen-specific antibody response by suppressing the generation of extra-follicular plasma cells without perturbing the expansion of T_{FH} and GCB cells. The authors further confirmed the critical role of miR-182 in extra-follicular B cell response by showing that the miR-182 knockout B6 mice were not able to respond to T-cell-independent type 2 antigen NP-Ficoll, which typically elicited an extrafollicular B-cell response (Li et al., 2016). Consistent with this report (Li et al., 2016), we found that deletion of miR-182 or miR-183C did not affect T_{FH}, GCB and CD19^{-}CD138^{+}plasma cells (**Figure 5**). Further investigation of T cell-dependent and independent B cell responses is necessary to understand the mechanism underlying reduced serum levels of IgG/IgM in miR-182$^{-/-}$ B6/lpr and anti-dsDNA in miR-183C$^{-/-}$ B6/lpr mice.

Foxo1 is a well-defined target of miR-183C miRNAs in immune cells. In our studies, we confirmed that miR-182 and miR-183C miRNAs targeted Foxo1 in splenic lymphocytes of *lpr* lupus mice. Moreover, we demonstrated that inhibition of Foxo1 *in vitro* was able to reverse the suppressive effect of miR-183C and miR-182 deletion on IFNγ production in anti-CD3 plus anti-CD28 or PMA plus ionomycin activated splenocytes (**Figures 7E,G**). This suggested that miR-182 and miR-183C regulate IFNγ production in splenocytes *via* targeting Foxo1. Further studies to determine other specific target genes of miR-183C and miR-182, in addition to *Foxo1*, may help us to better understand the similar and divergent role of miR-182 and miR-183C in regulation of autoinflammatory response.

In conclusion, our data demonstrated that deletion of miR-183C reduced anti-dsDNA autoantibody production, IgG and C3 immunocomplex deposition in B6/lpr kidneys. Although the cellular and molecular mechanism of miR-183C regulating anti-dsDNA autoantibody production remains to be clarified, these data revealed a regulatory role of miR-183C on anti-dsDNA production in lupus. Furthermore, our data validated that Foxo1 is an important target gene of miR-183C miRNAs and miR-182, by which miR-183C and miR-182 regulate IFNγ production in splenocytes following antigen stimulation.

DATA AVAILABILITY STATEMENT

The original contributions presented in the study are included in the article/**Supplementary Material**, further inquiries can be directed to the corresponding authors.

ETHICS STATEMENT

The animal study was reviewed and approved by Institutional Animal Care and Use Committee (IACUC) of Virginia Polytechnic Institute and State University.

AUTHOR CONTRIBUTIONS

RD and SA conceived the study and secured the fund for the research. ZW and RD designed, executed experiments and performed data analysis with assistance from BH, RL, JR, DeK, ME, TC, TJ, and CR. MS and DaK generated and provided miR-182$^{fl/fl}$ and miR-183C$^{fl/fl}$ mice for the study. ZW, RD, and SA drafted, wrote, and finalized the manuscript. CR critically reviewed and edited manuscript. All authors reviewed and approved the manuscript.

FUNDING

This work was supported by Alliance for Lupus Research (ALR, Award ID: 219631) and Virginia-Maryland College of Veterinary Medicine (VMCVM) Intramural Research Competition Grant. DaK was supported by NCI grant R35 CA197616. The miR-183C$^{fl/fl}$ mice were generated by the Duke Transgenic Core, which is supported by P30 CA014236 DHHS/NCI Cancer Center Support Grant (CCSG). TJ was funded by the NIH T35 OD011887. The article processing charges (APC) is partially funded by VT Open Access Subvention Fund. The funders had no role in study design, data collection and analysis, decision to publish, or preparation of the manuscript.

ACKNOWLEDGMENTS

We thank our colleagues and all the animal care staff at Virginia-Maryland College of Veterinary Medicine Facility. Meanwhile, the authors would like to thank Melissa Makris for technical support with flow cytometry.

SUPPLEMENTARY MATERIAL

The Supplementary Material for this article can be found online at: https://www.frontiersin.org/articles/10.3389/fgene.2022.840060/full#supplementary-material

REFERENCES

Ansar Ahmed, S., Penhale, W. J., and Talal, N. (1985). Sex Hormones, Immune Responses, and Autoimmune Diseases. Mechanisms of Sex Hormone Action. *Am. J. Pathol.* 121 (3), 531–551. https://pubmed.ncbi.nlm.nih.gov/3907369. https://www.ncbi.nlm.nih.gov/pmc/articles/PMC1887926/.

Bak, M., Silahtaroglu, A., Møller, M., Christensen, M., Rath, M. F., Skryabin, B., et al. (2008). MicroRNA Expression in the Adult Mouse Central Nervous System. *Rna* 14 (3), 432–444. doi:10.1261/rna.783108

Baltimore, D., Boldin, M. P., O'Connell, R. M., Rao, D. S., and Taganov, K. D. (2008). MicroRNAs: New Regulators of Immune Cell Development and Function. *Nat. Immunol.* 9 (8), 839–845. doi:10.1038/ni.f.209

Baumjohann, D., and Ansel, K. M. (2013). MicroRNA-mediated Regulation of T Helper Cell Differentiation and Plasticity. *Nat. Rev. Immunol.* 13 (9), 666–678. doi:10.1038/nri3494

Chen, J.-Q., Papp, G., Póliska, S., Szabó, K., Tarr, T., Bálint, B. L., et al. (2017). MicroRNA Expression Profiles Identify Disease-specific Alterations in Systemic Lupus Erythematosus and Primary Sjögren's Syndrome. *PLoS One* 12 (3), e0174585. doi:10.1371/journal.pone.0174585

Chen, Y.-J., Chang, W.-A., Hsu, Y.-L., Chen, C.-H., and Kuo, P.-L. (2017). Deduction of Novel Genes Potentially Involved in Osteoblasts of Rheumatoid Arthritis Using Next-Generation Sequencing and Bioinformatic Approaches. *Ijms* 18 (11), 2396. https://www.mdpi.com/1422-0067/18/11/2396. doi:10.3390/ijms18112396

Choi, E. W., Lee, M., Song, J. W., Shin, I. S., and Kim, S. J. (2016). Mesenchymal Stem Cell Transplantation Can Restore Lupus Disease-Associated miRNA Expression and Th1/Th2 Ratios in a Murine Model of SLE. *Sci. Rep.* 6, 38237. doi:10.1038/srep38237

Dai, R., and Ahmed, S. A. (2011). MicroRNA, a New Paradigm for Understanding Immunoregulation, Inflammation, and Autoimmune Diseases. *Transl. Res.* 157 (4), 163–179. S1931-5244(11)00039-9 [pii]. doi:10.1016/j.trsl.2011.01.007

Dai, R., and Ahmed, S. A. (2016). "microRNA, an Important Epigenetic Regulator of Immunity and Autoimmunity," in *Translating MicroRNAs to the Clinic*. Editor J. Laurence (Elsevier), 223–258.

Dai, R., Edwards, M. R., Heid, B., and Ahmed, S. A. (2019). 17β-Estradiol and 17α-Ethinyl Estradiol Exhibit Immunologic and Epigenetic Regulatory Effects in NZB/WF1 Female Mice. *Endocrinology* 160 (1), 101–118. doi:10.1210/en.2018-00824

Dai, R., Heid, B., Xu, X., Xie, H., Reilly, C. M., and Ahmed, S. A. (2020). EGR2 Is Elevated and Positively Regulates Inflammatory IFNγ Production in Lupus CD4+ T Cells. *BMC Immunol.* 21 (1), 41. doi:10.1186/s12865-020-00370-z

Dai, R., Lu, R., and Ahmed, S. A. (2016). The Upregulation of Genomic Imprinted DLK1-Dio3 miRNAs in Murine Lupus Is Associated with Global DNA Hypomethylation. *PLoS One* 11 (4), e0153509. doi:10.1371/journal.pone.0153509

Dai, R., McReynolds, S., Leroith, T., Heid, B., Liang, Z., and Ahmed, S. (2013). Sex Differences in the Expression of Lupus-Associated miRNAs in Splenocytes from Lupus-Prone NZB/WF1 Mice. *Biol. Sex. Dif.* 4 (1), 19. doi:10.1186/2042-6410-4-19

Dai, R., Phillips, R. A., and Ahmed, S. A. (2007). Despite Inhibition of Nuclear Localization of NF-Kb P65, C-Rel, and RelB, 17-β Estradiol Up-Regulates NF-Kb Signaling in Mouse Splenocytes: The Potential Role of Bcl-3. *J. Immunol.* 179 (3), 1776–1783. http://www.ncbi.nlm.nih.gov/entrez/query.fcgi?cmd=Retrieve&db=PubMed&dopt=Citation&list_uids=17641044. doi:10.4049/jimmunol.179.3.1776

Dai, R., Phillips, R. A., Karpuzoglu, E., Khan, D., and Ahmed, S. A. (2009). Estrogen Regulates Transcription Factors STAT-1 and NF-Kb to Promote Inducible Nitric Oxide Synthase and Inflammatory Responses. *J. Immunol.* 183 (11), 6998–7005. doi:10.4049/jimmunol.0901737

Dai, R., Wang, Z., and Ahmed, S. A. (2021). Epigenetic Contribution and Genomic Imprinting Dlk1-Dio3 miRNAs in Systemic Lupus Erythematosus. *Genes.* 12 (5), 680. doi:10.3390/genes12050680

Dai, R., Zhang, Y., Khan, D., Heid, B., Caudell, D., Crasta, O., et al. (2010). Identification of a Common Lupus Disease-Associated microRNA Expression Pattern in Three Different Murine Models of Lupus. *PLoS One* 5 (12), e14302. doi:10.1371/journal.pone.0014302

Dambal, S., Shah, M., Mihelich, B., and Nonn, L. (2015). The microRNA-183 Cluster: the Family that Plays Together Stays Together. *Nucleic Acids Res.* 43 (15), 7173–7188. doi:10.1093/nar/gkv703

Danger, R., Braza, F., Giral, M., Soulillou, J.-P., and Brouard, S. (2014). MicroRNAs, Major Players in B Cells Homeostasis and Function. *Front. Immunol.* 5, 98. doi:10.3389/fimmu.2014.00098

de Boer, J., Williams, A., Skavdis, G., Harker, N., Coles, M., Tolaini, M., et al. (2003). Transgenic Mice with Hematopoietic and Lymphoid Specific Expression of Cre. *Eur. J. Immunol.* 33 (2), 314–325. doi:10.1002/immu.200310005

Edwards, M. R., Dai, R., Heid, B., Cecere, T. E., Khan, D., Mu, Q., et al. (2017). Commercial Rodent Diets Differentially Regulate Autoimmune Glomerulonephritis, Epigenetics and Microbiota in MRL/lpr Mice. *Int. Immunol.* 29 (6), 263–276. doi:10.1093/intimm/dxx033

Edwards, M. R., Dai, R., Heid, B., Cowan, C., Werre, S. R., Cecere, T., et al. (2020). Low-dose 17α-Ethinyl Estradiol (EE) Exposure Exacerbates Lupus Renal Disease and Modulates Immune Responses to TLR7/9 Agonists in Genetically Autoimmune-Prone Mice. *Sci. Rep.* 10 (1), 5210. doi:10.1038/s41598-020-62124-6

Fan, X., and Wüthrich, R. P. (1997). Upregulation of Lymphoid and Renal Interferon-Gamma mRNA in Autoimmune MRL-Fas(lpr) Mice with Lupus Nephritis. *Inflammation* 21 (1), 105–112.http://www.ncbi.nlm.nih.gov/entrez/query.fcgi?cmd=Retrieve&db=PubMed&dopt=Citation&list_uids=9179626. doi:10.1023/a:1027399027170

Giese, T., Allison, J. P., and Davidson, W. F. (1993). Functionally Anergic Lpr and Gld B220+ T Cell Receptor (TCR)-alpha/beta+ Double-Negative T Cells Express CD28 and Respond to Costimulation with Phorbol Myristate Acetate and Antibodies to CD28 and the TCR. *J. Immunol.* 151 (2), 597–609. https://www.ncbi.nlm.nih.gov/pubmed/7687618

Goulielmos, G. N., Zervou, M. I., Vazgiourakis, V. M., Ghodke-Puranik, Y., Garyfallos, A., and Niewold, T. B. (2018). The Genetics and Molecular Pathogenesis of Systemic Lupus Erythematosus (SLE) in Populations of Different Ancestry. *Gene* 668, 59–72. doi:10.1016/j.gene.2018.05.041

Hamad, A. R. A., Mohamood, A. S., Trujillo, C. J., Huang, C.-T., Yuan, E., and Schneck, J. P. (2003). B220+Double-Negative T Cells Suppress Polyclonal T Cell Activation by a Fas-independent Mechanism that Involves Inhibition of IL-2 Production. *J. Immunol.* 171 (5), 2421–2426. doi:10.4049/jimmunol.171.5.2421

Honarpisheh, M., Köhler, P., von Rauchhaupt, E., and Lech, M. (2018). The Involvement of MicroRNAs in Modulation of Innate and Adaptive Immunity in Systemic Lupus Erythematosus and Lupus Nephritis. *J. Immunol. Res.* 2018, 1–15. doi:10.1155/2018/4126106

Ichiyama, K., and Dong, C. (2019). The Role of miR-183 Cluster in Immunity. *Cancer Lett.* 443, 108–114. doi:10.1016/j.canlet.2018.11.035

Ichiyama, K., Gonzalez-Martin, A., Kim, B.-S., Jin, H. Y., Jin, W., Xu, W., et al. (2016). The MicroRNA-183-96-182 Cluster Promotes T Helper 17 Cell Pathogenicity by Negatively Regulating Transcription Factor Foxo1 Expression. *Immunity* 44 (6), 1284–1298. doi:10.1016/j.immuni.2016.05.015

Kelada, S., Sethupathy, P., Okoye, I. S., Kistasis, E., Czieso, S., White, S. D., et al. (2013). miR-182 and miR-10a Are Key Regulators of Treg Specialisation and Stability during Schistosome and Leishmania-Associated Inflammation. *PLoS Pathog.* 9 (6), e1003451. doi:10.1371/journal.ppat.1003451

Krützfeldt, J., Rajewsky, N., Braich, R., Rajeev, K. G., Tuschl, T., Manoharan, M., et al. (2005). Silencing of microRNAs *In Vivo* with 'antagomirs'. *Nature* 438 (7068), 685–689. http://www.ncbi.nlm.nih.gov/entrez/query.fcgi?cmd=Retrieve&db=PubMed&dopt=Citation&list_uids=16258535. doi:10.1038/nature04303

Lengi, A. J., Phillips, R. A., Karpuzoglu, E., and Ahmed, S. A. (2007). Estrogen Selectively Regulates Chemokines in Murine Splenocytes. *J. Leukoc. Biol.* 81 (4), 1065–1074. http://www.ncbi.nlm.nih.gov/entrez/query.fcgi?cmd=Retrieve&db=PubMed&dopt=Citation&list_uids=17185357. doi:10.1189/jlb.0606391

Li, H., Kloosterman, W., and Fekete, D. M. (2010). MicroRNA-183 Family Members Regulate Sensorineural Fates in the Inner Ear. *J. Neurosci.* 30 (9), 3254–3263. doi:10.1523/jneurosci.4948-09.2010

Li, X., Luo, F., Li, J., and Luo, C. (2019). MiR-183 Delivery Attenuates Murine Lupus Nephritis-related Injuries via Targeting mTOR. *Scand. J. Immunol.* 90 (5), e12810. doi:10.1111/sji.12810

Li, Y.-F., Ou, X., Xu, S., Jin, Z.-B., Iwai, N., and Lam, K.-P. (2016). Loss of miR-182 Affects B-Cell Extrafollicular Antibody Response. *Immunology* 148 (2), 140–149. doi:10.1111/imm.12592

Liguori, M., Nuzziello, N., Licciulli, F., Consiglio, A., Simone, M., Viterbo, R. G., et al. (2018). Combined microRNA and mRNA Expression Analysis in Pediatric Multiple Sclerosis: an Integrated Approach to Uncover Novel Pathogenic Mechanisms of the Disease. *Hum. Mol. Genet.* 27 (1), 66–79. doi:10.1093/hmg/ddx385

Lin, L. J., Mai, L. J., Chen, G., Zhao, E. N., Xue, M., and Su, X. D. (2020). Expression and Diagnostic Value of Plasma miR-145 and miR-183 in Children with Lupus Nephritis. *Zhongguo Dang Dai Er Ke Za Zhi* 22 (6), 632–637. doi:10.7499/j.issn.1008-8830.2001013

Mehta, A., and Baltimore, D. (2016). MicroRNAs as Regulatory Elements in Immune System Logic. *Nat. Rev. Immunol.* 16 (5), 279–294. doi:10.1038/nri.2016.40

Morse, H. C., 3rd, Roths, J. B., Davidson, W. F., Langdon, W. Y., Fredrickson, T. N., and Hartley, J. W. (1985). Abnormalities Induced by the Mutant Gene, Lpr. Patterns of Disease and Expression of Murine Leukemia Viruses in SJL/J Mice Homozygous and Heterozygous for Lpr. *J. Exp. Med.* 161 (3), 602–616. doi:10.1084/jem.161.3.602

Pan, W., Zhu, S., Yuan, M., Cui, H., Wang, L., Luo, X., et al. (2010). MicroRNA-21 and MicroRNA-148a Contribute to DNA Hypomethylation in Lupus CD4+T Cells by Directly and Indirectly Targeting DNA Methyltransferase 1. *J. Immunol.* 184 (12), 6773–6781. [pii]. doi:10.4049/jimmunol.0904060

Parks, C. G., de Souza Espindola Santos, A., Barbhaiya, M., and Costenbader, K. H. (2017). Understanding the Role of Environmental Factors in the Development of Systemic Lupus Erythematosus. *Best Pract. Res. Clin. Rheumatology* 31 (3), 306–320. doi:10.1016/j.berh.2017.09.005

Peng, S. L., Moslehi, J., and Craft, J. (1997). Roles of Interferon-Gamma and Interleukin-4 in Murine Lupus. *J. Clin. Invest.* 99 (8), 1936–1946.http://www.ncbi.nlm.nih.gov/entrez/query.fcgi?cmd=Retrieve&db=PubMed&dopt=Citation&list_uids=9109438. doi:10.1172/jci119361

Pierce, M. L., Weston, M. D., Fritzsch, B., Gabel, H. W., Ruvkun, G., and Soukup, G. A. (2008). MicroRNA-183 Family Conservation and Ciliated Neurosensory Organ Expression. *Evol. Dev.* 10 (1), 106–113. doi:10.1111/j.1525-142X.2007.00217.x

Pucella, J. N., Yen, W.-F., Kim, M. V., van der Veeken, J., Socci, N. D., Naito, Y., et al. (2015). miR-182 Is Largely Dispensable for Adaptive Immunity: Lack of Correlation between Expression and Function. *J. Immunol.* 194 (6), 2635–2642. doi:10.4049/jimmunol.1402261

Sachdeva, M., Mito, J. K., Lee, C.-L., Zhang, M., Li, Z., Dodd, R. D., et al. (2014). MicroRNA-182 Drives Metastasis of Primary Sarcomas by Targeting Multiple Genes. *J. Clin. Invest.* 124 (10), 4305–4319. doi:10.1172/JCI77116

Santiago-Raber, M.-L., Haraldsson, M. K., Theofilopoulos, A. N., and Kono, D. H. (2007). Characterization of Reciprocal Lmb1-4 Interval MRL-Faslpr and C57BL/6-Faslpr Congenic Mice Reveals Significant Effects from Lmb3. *J. Immunol.* 178 (12), 8195–8202. doi:10.4049/jimmunol.178.12.8195

Schell, S. L., and Rahman, Z. S. M. (2021). miRNA-Mediated Control of B Cell Responses in Immunity and SLE. *Front. Immunol.* 12, 683710. doi:10.3389/fimmu.2021.683710

Schindelin, J., Rueden, C. T., Hiner, M. C., and Eliceiri, K. W. (2015). The ImageJ Ecosystem: An Open Platform for Biomedical Image Analysis. *Mol. Reprod. Dev.* 82 (7-8), 518–529. doi:10.1002/mrd.22489

Shen, N., Liang, D., Tang, Y., de Vries, N., and Tak, P.-P. (2012). MicroRNAs-novel Regulators of Systemic Lupus Erythematosus Pathogenesis. *Nat. Rev. Rheumatol.* 8 (12), 701–709. doi:10.1038/nrrheum.2012.142

Siegemund, S., Shepherd, J., Xiao, C., and Sauer, K. (2015). hCD2-iCre and Vav-iCre Mediated Gene Recombination Patterns in Murine Hematopoietic Cells. *PLoS One* 10 (4), e0124661. doi:10.1371/journal.pone.0124661

Squatrito, D., Emmi, G., Silvestri, E., Ciucciarelli, L., D'Elios, M. M., Prisco, D., et al. (2014). Pathogenesis and Potential Therapeutic Targets in Systemic Lupus Erythematosus: from Bench to Bedside. *Autoimmun. Highlights* 5 (2), 33–45. doi:10.1007/s13317-014-0058-y

Stittrich, A.-B., Haftmann, C., Sgouroudis, E., Kühl, A. A., Hegazy, A. N., Panse, I., et al. (2010). The microRNA miR-182 Is Induced by IL-2 and Promotes Clonal Expansion of Activated Helper T Lymphocytes. *Nat. Immunol.* 11 (11), 1057–1062. [pii]. doi:10.1038/ni.1945

Tang, Y., Luo, X., Cui, H., Ni, X., Yuan, M., Guo, Y., et al. (2009). MicroRNA-146A Contributes to Abnormal Activation of the Type I Interferon Pathway in Human Lupus by Targeting the Key Signaling Proteins. *Arthritis Rheum.* 60 (4), 1065–1075. doi:10.1002/art.24436

Thiel, J., Alter, C., Luppus, S., Eckstein, A., Tan, S., Führer, D., et al. (2019). MicroRNA-183 and microRNA-96 Are Associated with Autoimmune Responses by Regulating T Cell Activation. *J. Autoimmun.* 96, 94–103. doi:10.1016/j.jaut.2018.08.010

Wan, C., Ping, C.-Y., Shang, X.-Y., Tian, J.-T., Zhao, S.-H., Li, L., et al. (2016). MicroRNA 182 Inhibits CD4+CD25+Foxp3+ Treg Differentiation in Experimental Autoimmune Encephalomyelitis. *Clin. Immunol.* 173, 109–116. doi:10.1016/j.clim.2016.09.008

Wang, X., Wang, G., Zhang, X., Dou, Y., Dong, Y., Liu, D., et al. (2018). Inhibition of microRNA-182-5p Contributes to Attenuation of Lupus Nephritis via Foxo1 Signaling. *Exp. Cell. Res.* 373 (1-2), 91–98. doi:10.1016/j.yexcr.2018.09.026

Wang, Z., Heid, B., Dai, R., and Ahmed, S. A. (2018). Similar Dysregulation of Lupus-Associated miRNAs in Peripheral Blood Mononuclear Cells and Splenic Lymphocytes in MRL/lpr Mice. *Lupus Sci. Med.* 5 (1), e000290. doi:10.1136/lupus-2018-000290

Weston, M. D., Pierce, M. L., Rocha-Sanchez, S., Beisel, K. W., and Soukup, G. A. (2006). MicroRNA Gene Expression in the Mouse Inner Ear. *Brain Res.* 1111 (1), 95–104. doi:10.1016/j.brainres.2006.07.006

Xu, S., Witmer, P. D., Lumayag, S., Kovacs, B., and Valle, D. (2007). MicroRNA (miRNA) Transcriptome of Mouse Retina and Identification of a Sensory Organ-specific miRNA Cluster. *J. Biol. Chem.* 282 (34), 25053–25066. M700501200 [pii]. doi:10.1074/jbc.m700501200

Zan, H., Tat, C., and Casali, P. (2014). MicroRNAs in Lupus. *Autoimmunity* 47 (4), 272–285. doi:10.3109/08916934.2014.915955

Conflict of Interest: The authors declare that the research was conducted in the absence of any commercial or financial relationships that could be construed as a potential conflict of interest.

Publisher's Note: All claims expressed in this article are solely those of the authors and do not necessarily represent those of their affiliated organizations, or those of the publisher, the editors and the reviewers. Any product that may be evaluated in this article, or claim that may be made by its manufacturer, is not guaranteed or endorsed by the publisher.

frontiers | Frontiers in Genetics

REVIEW
published: 22 July 2022
doi: 10.3389/fgene.2022.837343

Emerging Roles of *Circ-ZNF609* in Multiple Human Diseases

Songbo Wang†, Jiajin Wu†, Zhongyuan Wang†, Zixuan Gong, Yiyang Liu and Zengjun Wang**

Department of Urology, First Affiliated Hospital of Nanjing Medical University, Nanjing, China

Circular RNAs (circRNAs) are a special type of endogenous RNAs with extensive roles in multiple human diseases. They are formed by back-splicing of partial sequences of the parental precursor mRNAs. Unlike linear RNAs, their covalently closed loop structure without a 5′ cap and a 3′ polyadenylated tail confers on them high stability and they are difficult to be digested by RNase R. Increasing evidence has proved that aberrant expressions of many circRNAs are detected and that circRNAs exert essential biological functions in disease development and progression *via* acting as a molecular sponge of microRNA, interacting with proteins as decoys or scaffolds, or self-encoding small peptides. Circular RNA zinc finger protein 609 (*circ-ZNF609*) originates from exon2 of ZNF609, which is located at chromosome 15q22.31, and it has recently been proved that it can translate into a protein. Being aberrantly upregulated in various diseases, it could promote malignant progression of human tumors, as well as tumor cell proliferation, migration, and invasion. Here in this review, we concluded the biological functions and potential mechanisms of *circ-ZNF609* in multiple diseases, which could be further explored as a targetable molecule in future accurate diagnosis and prognosis.

Keywords: circular RNA, ZNF609, human diseases, tumor malignant progression, mechanism

OPEN ACCESS

Edited by:
Deepanjan Paul,
Children's Hospital of Philadelphia, United States

Reviewed by:
Chunlin Ou,
Central South University, China
Christos K. Kontos,
National and Kapodistrian University of Athens, Greece
Gopal Pandi,
Madurai Kamaraj University, India

****Correspondence:***
Yiyang Liu
liu820700@163.com
Zengjun Wang
zengjunwang@njmu.edu.cn

†These authors have contributed equally to this work.

Specialty section:
This article was submitted to RNA, a section of the journal Frontiers in Genetics.

Received: *16 December 2021*
Accepted: *03 June 2022*
Published: *22 July 2022*

Citation:
Wang S, Wu J, Wang Z, Gong Z, Liu Y and Wang Z (2022) Emerging Roles of Circ-ZNF609 in Multiple Human Diseases. Front. Genet. 13:837343. doi: 10.3389/fgene.2022.837343

INTRODUCTION

In 1976, circular RNAs (circRNAs) were found in viroids and eukaryotic cells (Kolakofsky, 1976; Sanger et al., 1976). In the process of transcription from parental gene to RNA, circular RNAs are back-spliced to form a loop structure without a 5′ cap and a 3′ polyadenylated tail (Jeck et al., 2012; Chen and Yang, 2015). The special circular structure endows them with a characteristic so that they can resist the digestion of exonuclease RNase R and become a class of relatively stable RNAs (Suzuki et al., 2006; Xiao and Wilusz, 2019).

With the development of high-throughput RNA sequencing and bioinformatics, the mechanisms and functions of circRNAs have been gradually elucidated (Memczak et al., 2013; Chen and Yang, 2015). According to the current research, circRNAs are generally divided into three subtypes: exonic circRNAs (ecircRNAs) (Jeck et al., 2012), exon–intron circRNAs (eicircRNAs) (Li et al., 2015), and intronic circRNAs (ciRNAs) (Zhang et al., 2013). The majority is ecircRNAs located in the cytoplasm mostly, and the other two exist in the nucleus mostly (Jeck et al., 2012; Zhang et al., 2013; Li et al., 2015). CircRNAs are ubiquitous in tissue cells, blood cells, serum, and exosomes (Salzman et al., 2012; Rong et al., 2019; Shi et al., 2020a). The primary functions of circRNAs are as follows: the ability to regulate the transcription of parental mRNAs (Li et al., 2015); acting as molecular sponges to regulate the expressions of target genes (Thomson and Dinger, 2016); binding to and sequestering proteins to regulate the expressions of the associated proteins (Kristensen et al., 2019; Chen, 2020); and translating into proteins to perform their functions (Legnini et al., 2017; Shi et al., 2020b). CircRNAs play important roles in the occurrence and development of human diseases, such as

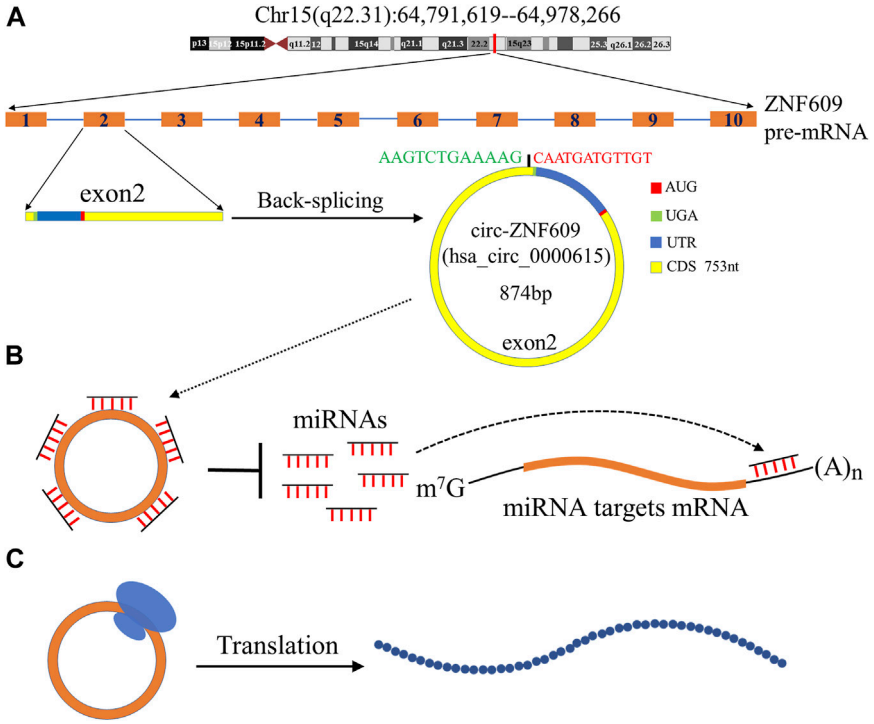

FIGURE 1 | Biogenesis and biological functions of *circ-ZNF609*. **(A)** ZNF609 is located in chromosome 15q22.31 in humans; the red line indicates its approximate location. ZNF609 contains 10 exons, and the exon2 is spliced in reverse to form *circ-ZNF609*. The total length of *circ-ZNF609* is 874nt and contains a 753nt coding region, the promoter of *circ-ZNF609* is at position 128, and the terminator is at position 6. **(B)** *Circ-ZNF609* as a molecular sponge to adsorb microRNAs, reducing its binding to the 3′ UTR of the target mRNA, and regulate gene expression. **(C)** *Circ-ZNF609* can be translated into a protein.

promoting cell proliferation, migration, and invasion in tumors, regulating drug resistance, and the progression of cardiovascular disease, as well as regulating neovascularization (Liu et al., 2017; Aufiero et al., 2019; Rossi et al., 2019; Li et al., 2020a; Xiao et al., 2020; Ding et al., 2021; Kim et al., 2021; Verduci et al., 2021).

Circular RNA zinc finger protein 609 (*circ-ZNF609*) is highly expressed in normal human neurons and maintains physiological functions (Rybak-Wolf et al., 2015; Legnini et al., 2017). It is differentially expressed in a variety of human diseases, as a competitive endogenous RNA to regulate target genes and affect disease progression. In the present review, we aim to gain insights into the relationship between *circ-ZNF609* and human diseases and provide a theoretical basis for clinical diagnosis and targeted therapy.

Structure and Biological Function of *Circ-ZNF609*

Circ-ZNF609 is a covalently closed circular RNA, which originates from the primary transcript of exon2 of ZNF609 located on chromosome 15q22.31. It is usually formed by back-splicing, a downstream splice-donor site is joined to an upstream splice-acceptor site, resulting in the loop structure of *circ-ZNF609* and containing a specific junction site. It contains 874 bp nucleotides (Legnini et al., 2017); as a kind of circRNA that could be translated, its coding sequence contains 753 bp nucleotides, the start codon is located at position 128, and the stop codon is located at position 6 (**Figure 1**). There is one of the RNA binding proteins that can regulate the biogenesis of *circ-ZNF609*. Liu et al. (Liu et al., 2021a) reported that the expression of *circ-ZNF609* could be upregulated by RNA binding protein fused in sarcoma (FUS), which could modulate the back-splicing reaction (Liu et al., 2021a). The FUS protein could induce the splicing and circularization of *circ-ZNF609* by binding to the upstream exon2 of ZNF609 pre-mRNA (Liu et al., 2021a).

Considering the loop structure of *circ-ZNF609* without a 5′ cap, its translation relies on a splicing-dependent/cap-independent manner (Legnini et al., 2017). However, Hung et al. (Ho-Xuan et al., 2020a) found that its translation may be originated from trans-splicing the byproducts of the overexpression of artificial circRNAs. They thought while performing functional studies of overexpression constructs of circRNA, it should be evaluated carefully (Ho-Xuan et al., 2020a). The primary biological function of *circ-ZNF609* was to act as a molecular sponge of endogenous microRNAs to sequester and inhibit the microRNA activity, which led to regulating the target gene expression (Chen, 2020; Xiao et al., 2020). As in hepatocellular carcinoma, *circ-ZNF609* inhibits *miR-15a-5p/15b-5p* expression and then elevates *GLI2* (a key protein molecule concerning the Hedgehog pathway) expression,

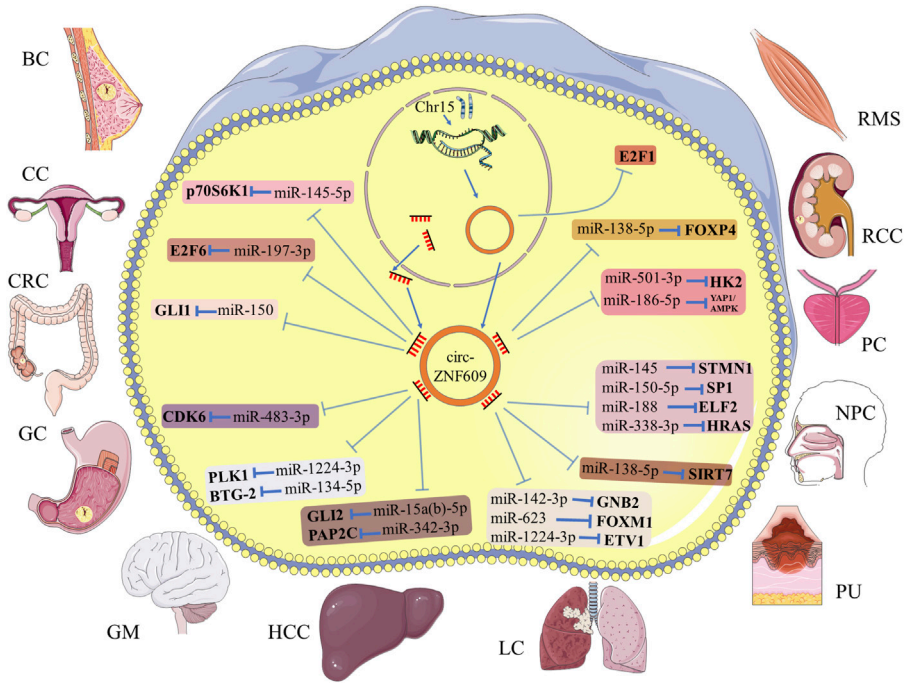

FIGURE 2 | Schematic diagram for the molecular mechanism of *circ-ZNF609* in human cancers. *Circ-ZNF609* acts as a molecular sponge of specific miRNA to regulate the expression of targeted genes in multiple cancers. T-shaped bars represent inhibition.

activating the Hedgehog pathway to promote hepatocellular carcinoma (HCC) proliferation and metastasis (He et al., 2020).

Circ-ZNF609 in Multiple Human Cancers

The present studies suggested that the main function of *circ-ZNF609* is the posttranscriptional regulation, by acting as a molecular sponge of target microRNA (**Figure 2**; **Table 1**). As a carcinogen, *circ-ZNF609* was abnormally upregulated in tumor tissues and cell lines. It also promoted tumor proliferation, migration, invasion, and other malignant phenotypes. The following content describes the molecular mechanisms of *circ-ZNF609* in human cancers, in order by cancer names.

Breast Cancer

Breast cancer is the most common cancer and the second leading cause of cancer lethality among women (DeSantis et al., 2017). In comparison with conventional surgery, neoadjuvant therapy has become a more widely used option, and novel targeted therapies play an important role in long-term disease control of metastatic breast cancer (Harbeck and Gnant, 2017). Being highly expressed in breast tumor tissues; *circ-ZNF609* leads to a poor outcome in the overall survival and is closely associated with lymph node metastasis and advanced TNM stage (Wang et al., 2018a). Wang et al. proved that *circ-ZNF609* knockdown inhibits the formation of malignant phenotypes of breast cancer cells and delays the tumor growth rate *in vivo*. It exerted biological function by sponging *miR145-5p*, which targeted oncogenic ribosomal protein S6 kinase, polypeptide 1 (*p70S6K1*), and promoted breast cancer progression (Wang et al., 2018a). They demonstrated that *circ-ZNF609* regulated the *miR-145-5p/p70S6K1* axis and could become a potential posttreatment prognostic biomarker in breast cancer.

Cervical Cancer

Each year, more than 500,000 women are diagnosed with cervical cancer. Advances in radiotherapy technology have significantly reduced treatment-related toxicity (Cohen et al., 2019); however, the overall survival of metastatic cervical tumors is still poor. Gu et al. (Gu et al., 2021) found that *circ-ZNF609* was overexpressed in cervical cancer tissues and cell lines, and knockdown of *circ-ZNF609* suppresses the malignant phenotype of the tumor. Circ-ZNF609 acted as the sponge of *miR-197-3p*, directly upregulating the expression of E2F transcription factor 6 (*E2F6*). The overexpression of *E2F6* can partially reverse the inhibition of cell proliferation, migration, and invasion caused by *circ-ZNF609* depletion (Gu et al., 2021). Their research suggested that the *circ-ZNF609/miR-197-3p/E2F6* regulatory axis proposed a new insight into the progression of cervical cancer.

Colorectal Cancer

Colorectal cancer is the third most commonly diagnosed cancer in males and the second in females (Torre et al., 2015). Exploring the potential diagnostic biomarkers of colorectal cancer is of great significance to contemporary medicine. Emerging evidence has shown the vital role of *circ-ZNF609* in colorectal cancer development and progression. The expression level of circ-ZNF609 was reported to be positively correlated with GLI family zinc finger 1 (*GLI1*) and negatively correlated with

TABLE 1 | Mechanism of *circ-ZNF609* in human cancers.

Cancers	Expression Change	Targeted miRNAs	Targeted Genes	Tumor's progression	Clinicopathological Features	References
Breast cancer (BC)	Upregulated	miR-145-5p	p70S6K1	Promoting	Lymph node metastasis, advanced TNM stage, poor overall survival	Wang et al. (Wang et al., 2018a)
Cervical cancer (CC)	Upregulated	miR-197-3p	E2F6	Promoting	—	Gu et al. (Gu et al., 2021)
Colorectal cancer (CRC)	Upregulated	miR-150	GLI1	Promoting	Lymph node metastasis, Dukes stage	Wu et al. (Wu et al., 2018)
Gastric cancer (GC)	Upregulated	miR-483-3p	CDK6	Promoting	Advanced TNM stage, poor overall survival	Wu et al. (Wu et al., 2019)
Glioma (GM)	Upregulated	miR-1224-3p	PLK1	Promoting	Advanced clinical grade	Du et al. (Du et al., 2021)
		miR-134-5p	BTG-2	Promoting	—	Tong et al. (Tong et al., 2019)
Hepatocellular carcinoma (HCC)	Upregulated	miR-15a(b)-5p	GLI2	Promoting	—	He et al. (He et al., 2020)
		miR-342-3p	PAP2C	Promoting	Lymph node metastasis, advanced TNM stage, poor overall survival	Liao et al. (Liao et al., 2020)
Lung cancer (LC)	Upregulated	miR-142-3p	GNB2	Promoting	—	Liu et al. (Liu et al., 2021a)
		miR-623	FOXM1	Promoting	Lymph node metastasis, advanced TNM stage, poor overall survival	Wang et al. (Wang et al., 2021a)
		miR-1224-3p	ETV1	Promoting	—	Zuo et al. (Zuo et al., 2020)
Melanoma (MM)	Upregulated	miR-138-5p	SIRT7	Promoting	—	Liu et al. (Liu et al., 2021b)
Nasopharyngeal carcinoma (NPC)	Upregulated	miR-145	STMN1	Promoting	Lymph node metastasis, advanced clinical stage	Wang et al. (Wang et al., 2021b)
		miR-150-5p	SP1	Promoting	—	Zhu et al. (Zhu et al., 2019)
		miR-188	ELF2	Promoting	—	Li et al. (Li et al., 2020b)
		miR-338-3p	HRAS	Promoting	Poor overall survival	Liu et al. (Liu et al., 2021c)
Prostate cancer (PC)	Upregulated	miR-186-5p	YAP1/AMPK	Promoting	—	Jin et al. (Jin et al., 2019)
		miR-501-3p	HK2	Promoting	Advanced TNM stage, metastasis	Du et al. (Du et al., 2020)
Renal cell carcinoma (RCC)	Upregulated	miR-138-5p	FOXP4	Promoting	—	Xiong et al. (Xiong et al., 2019)
Rhabdomyosarcoma (RMS)	Upregulated	—	E2F1	Promoting	—	Rossi et al. (Rossi et al., 2019)

miR-150. In particular, it acted as a molecular sponge of *miR-150* to downregulate the expression of *GLI1* and then promoted colorectal cancer cell proliferation and migration (Wu et al., 2018). Later, Hung et al. (Ho-Xuan et al., 2020b) found that *circ-ZNF609* acted as an oncogene during colorectal cancer progression and metastasis. The overexpression of circ-ZNF609 leads to increased tumor growth, while knockdown led to contrasting effects in mouse xenograft models. However, Zhang et al. (Zhang et al., 2019a) reported discrepant results that *circ-ZNF609* is downregulated in colorectal cancer tissues and patient serum samples, and it also induced cell apoptosis *via* upregulating *p53*. To summarize, the specific role and regulating mechanism of *circ-ZNF609* in colorectal cancer are still unclear, requiring further elucidation.

Gastric Cancer

Gastric cancer is the second leading cause of cancer-related deaths and the incidence ranks fourth worldwide, which mainly relies on pathological examination (Torre et al., 2015; Sitarz et al., 2018). Surgical resection and chemotherapy are the principal treatment approaches; however, lymph node and distant metastases during advanced stages limit the therapeutic effect (Sitarz et al., 2018). Therefore, seeking early biomarkers of gastric cancer makes all the difference between accurate diagnosis and treatment (Zhang and Zhang, 2017). Wu et al. (Wu et al., 2019) proved that *circ-ZNF609* is overexpressed in cancer tissues and cell lines of gastric cancer patients, and it was positively correlated with a higher TNM stage and a lower 5-year survival rate. It acted as a sponge of *miR-483-3p*, upregulated the expression of cell-promoting factor cyclin-dependent kinase 6 (*CDK6*), and promoted the proliferation and migration of gastric cancer cells through the *circ-ZNF609/miR-483-3p/CDK6* axis (Wu et al., 2019). In interest, Liu et al. (Liu et al., 2019) had discovered different mechanisms of *circ-ZNF609* in gastric cancer, through binding to *miR-145-5p* and negatively regulating its expression. Knockdown of *circ-ZNF609* inhibited

cell proliferation and induced apoptosis, which could be partially reversed by *miR-145-5p* overexpression (Liu et al., 2019).

Glioma

Glioma is a primary brain tumor that is highly metastatic and aggressive (Weller et al., 2015; Chen et al., 2017). It is of great significance to determine the potential molecular mechanism of *circ-ZNF609* in glioma. Du et al. (Du et al., 2021) proved that *circ-ZNF609* was overexpressed in glioma tissues and cell lines and was significantly overexpressed in high-grade glioma than in low-grade glioma. Silencing *circ-ZNF609* could inhibit the proliferation and migration of glioma cells. In routine, it promoted the expression of polo-like kinase-1 (*PLK1*) by competitively binding to *miR-1224-3p*, and *circ-ZNF609* also promoted tumor growth *in vivo* (Du et al., 2021). Meanwhile, Tong et al. (Tong et al., 2019) found that *miR-134-5p* inhibited the expression of BTG antiproliferation factor 2 (*BTG-2*) and inhibited the proliferation and migration of glioma. *Circ-ZNF609* positively regulated the expression of *BTG-2* through competitively binding to *miR-134-5p*, leading to the proliferation and migration of glioma. It proposed a novel mechanism of *circ-ZNF609* in regulating the progression of glioma (Tong et al., 2019).

Hepatocellular Carcinoma

Liver cancer is the fourth leading cause of cancer deaths worldwide (Villanueva, 2019). Existing studies have demonstrated that circRNAs could promote the progress of HCC by regulating microRNAs (Zhang and Wang, 2021). *Circ-ZNF609* was highly expressed in HCC tissues and cell lines. Knockdown of *circ-ZNF609* could inhibit the proliferation, migration, and invasion of HCC and promote apoptosis (He et al., 2020). Adding SAG, an agonist of the Hedgehog signal pathway, could restore the phenotype caused by *circ-ZNF609* knockdown (He et al., 2020). Bioinformatics analysis and experiments validated that *circ-ZNF609* regulated the expressions of *miR-15a-5p/15b-5p* and GLI family zinc finger 2 (*GLI2*) and promoted the malignant phenotype of HCC through the Hedgehog pathway (He et al., 2020). Liao et al. (Liao et al., 2020) also proved that silencing *circ-ZNF609* could inhibit the proliferation of HCC and upregulate the expression of *RAP2C* (member of the RAS oncogene family) by acting as a sponge of *miR-342-3p*. The experiments *in vivo* showed that *circ-ZNF609* facilitated tumor growths, confirming the findings *in vitro*.[49]

Lung Cancer

Non-small cell lung cancer (NSCLC) is the most common type of lung cancer (Devesa et al., 2005), and circRNAs play a significant role in its pathogenesis and progression (Di et al., 2019; Huang et al., 2019). Fork head box protein M1 (*FOXM1*) is overexpressed in various cancers, which is a necessary transcription factor for cell proliferation (Liao et al., 2018). In NSCLC, it was targeted by miR-623 and *circ-ZNF609*. Knocking down *circ-ZNF609* inhibited cell viability, migration, and invasion and promoted apoptosis, and knocking down *miR-623* or overexpressed *FOXM1* could weaken these effects (Wang et al., 2021a). Lung adenocarcinoma (LUAD) is one of the histological subtypes of lung cancer with a poor prognosis (Devesa et al., 2005); *circ-ZNF609* was overexpressed in LUAD, acting as a sponge of *miR-1224-3p* to promote the cell proliferation of LUAD, which negatively regulated the expression of ETS variant transcription factor 1 (*ETV1*). They verified that *circ-ZNF609* promoted LUAD proliferation through the *miR-1224-3p/ETV1* axis (Zuo et al., 2020). In lung cancer, it was also found that FUS RNA binding protein could bind to the intron1 region of pre-mRNA of ZNF609, but not to exon1 and exon2. The specific binding may regulate the back-splicing of exon2, leading to upregulation of *circ-ZNF609* and promoting the malignant progression of lung cancer through the *miR-142-3p/GNB2* axis (Liu et al., 2021a). These studies provided different insights for understanding the value of *circ-ZNF609* in different histological subtypes of lung cancer, indicating that the pathogenic mechanism of *circ-ZNF609* in lung cancer was tissue specific.

Melanoma

Melanoma is a prevalent malignant skin cancer. Its incidence and mortality rates vary greatly worldwide. Once melanoma spreads, it will quickly become life-threatening (Schadendorf et al., 2018). As stated, *circ-ZNF609*-mediated DNA damage plays an important role in the development of melanoma. Knocking down *circ-ZNF609* could inhibit the proliferation, migration, and invasion of melanoma cell lines, reduce cell survival rate, and promote apoptosis (Liu et al., 2021b). Comet assays showed that the tail length was elevated and the expression level of γH2AX variant histone (*γH2AX*) was increased after *circ-ZNF609* depletion, suggesting that *circ-ZNF609* inhibited the DNA damage in melanoma (Liu et al., 2021b). *Circ-ZNF609* repressed DNA oxidative damage by acting as a sponge of *miR-138-5p*, which induced DNA oxidative damage by targeting sirtuin 7 (*SIRT7*). Adding *miR-138-5p* inhibitor or overexpression of *SIRT7* partially reversed the DNA damage phenotype caused by *circ-ZNF609* depletion, and *circ-ZNF609* depletion reduced the tumor size, tumor volume, and tumor weight through the *miR-138-5p/SIRT7* axis *in vivo* (Liu et al., 2021b). This study provided a new mechanism for the pathogenesis of DNA damage in melanoma, suggesting that circRNA-mediated DNA oxidative damage may be a valuable direction for melanoma biogenesis.

Nasopharyngeal Carcinoma

Nasopharyngeal carcinoma (NPC) is a common malignant tumor of the head and neck, and chemotherapy is an effective treatment method (Chen et al., 2019). However, since it is prone to lymph node metastasis and the degree of malignancy is high (Chua et al., 2016), it is of great significance to study the mechanism of occurrence and development. Pathological angiogenesis is a hallmark of cancer progression (Carmeliet and Jain, 2000), which is an important cause of the metastasis of NPC (Bao et al., 2018). The expression of vascular endothelial growth factor (VEGF) after the knockdown of *circ-ZNF609* in NPC cells was downregulated. The supernatant was added to treat human umbilical vein endothelial cells (HUVEC), and the proteins of

VEGF receptor-1 and VEGF receptor-2 in HUVECs are reduced. It could be observed that the total tube length was shortened, and the nodules were reduced when knocking down *circ-ZNF609* in HUVEC. These proved that the angiogenesis was reduced after knocking down *circ-ZNF609*. It negatively regulated the expression of *miR-145* and upregulated stathmin 1 (*STMN1*) to promote the proliferation, migration, and angiogenesis of NPC, forming a new regulatory mechanism for the pathological angiogenesis of NPC (Wang et al., 2021b). Zhu et al. (Zhu et al., 2019) found that *circ-ZNF609* promoted the growth and metastasis of NPC and exerted carcinogenic influence by competing with *miR-150-5p* which degraded *Sp1* expression. Liu et al. (Liu et al., 2021c) also proposed that *circ-ZNF609* was highly expressed in NPC tissues and cell lines, by binding to *miR-338-3p* to negatively regulate its expression, upregulating histidyl-tRNA synthetase (HARS) that promoted the proliferation, migration, invasion, and glycolysis of NPC, and xenograft experiments proved the result *in vitro*. The results of Li et al. (Li et al., 2020b) also showed that *circ-ZNF609* was overexpressed in NPC tissues and cell lines, knocking down it inhibited NPC cell proliferation and cell cycle transition, as well as accelerated apoptosis, and the carcinogenic effect was achieved through the *circ-ZNF609/miR-188/ELF2* axis. Their studies had shown that *circ-ZNF609* was overexpressed in NPC, as a molecular sponge of related microRNA and upregulated the expression of the target gene, achieving carcinogenic effects, and these suggest that *circ-ZNF609* may be a new therapeutic target for NPC. The molecular mechanism of *circ-ZNF609* in NPC had been inconsistently reached by different research teams, which may be caused by differences in patient samples. The mechanism of *circ-ZNF609* in NPC required a more rigorous study to reveal a clear conclusion.

Prostate Cancer

Prostate cancer is a common malignant tumor of the urinary system (Torre et al., 2015), and radiotherapy is the main treatment modality. However, the metastasis of advanced patients limits the application of radiotherapy (Mohler et al., 2010). It is of great significance to understand the mechanisms of radiological resistance. Even in the presence of oxygen and fully functional mitochondria, tumor cells increased glucose uptake and fermentation of glucose to lactate, and the process is called the Warburg effect. It is characterized by changes in glycolysis and metabolism, which can promote tumor metastasis (Liberti and Locasale, 2016). *Circ-ZNF609* was highly expressed in prostate cancer tissues and cells, and silencing it could repress cell viability, inhibit cell migration and invasion, and induce cell apoptosis (Du et al., 2020). *Circ-ZNF609* silencing decreased the glucose uptake and lactate product of tumor cells, and overexpression of *circ-ZNF609* could increase the radioresistance of cells. However, the radioresistance was significantly inhibited by the addition of glycolysis inhibitor 2-deoxy-D-glucose (2-DG), suggesting that *circ-ZNF609* promoted glycolysis to improve the radioresistance of cells (Du et al., 2020). Circ-ZNF609 acted as a molecular sponge of *miR-501-3p*, and 2-DG could significantly inhibit the promotion of glycolysis by anti-*miR-501-3p*. The *circ-ZNF609/miR-501-3p* axis was targeted to upregulate the expression of hexokinase 2 (*HK2*), a key enzyme of glycolysis, and then improved the radioresistance of tumor cells both *in vitro* and *in vivo* (Du et al., 2020). Jin et al. (Jin et al., 2019) proposed that silencing *circ-ZNF609* could restrain Yes1-associated transcriptional regulator (*YAP1*) and AMP-activated protein kinase (*AMPK*) signaling pathways by upregulating *miR-186-5p*, thereby inhibiting cell proliferation, migration, and invasion, and inducing apoptosis. In conclusion, *circ-ZNF609* could promote prostate cancer progression through multiple mechanisms, including regulated glycolysis and metabolism, promoting radioresistance and activating signaling pathways.

Renal Cell Carcinoma

Renal cell carcinoma (RCC) is a common tumor of the urinary system (Rini et al., 2009). Some ncRNAs have been proved to be involved in the biological process of kidney cancer, providing molecular targets for the treatment (Li et al., 2017; Wang et al., 2017; Shelar et al., 2018). Xiong et al. (Xiong et al., 2019) proved that *circ-ZNF609* represented a circular structure that was resistant to the digestion of RNase R. It was also overexpressed in renal cancer cell lines than in renal epithelial cells. By targeted binding to *miR-138-5p*, *circ-ZNF609* upregulated the expression of the transcription factor forkhead box P4 (*FOXP4*) and promoted the proliferation, migration, and invasion of renal cancer cells. Knocking down of *circ-ZNF609* inhibited the malignant phenotype in RCC (Xiong et al., 2019).

Rhabdomyosarcoma

RMS is a pediatric skeletal muscle malignancy that accounts for roughly 5% of all pediatric tumors (Egas-Bejar and Huh, 2014). Rhabdomyosarcoma in children is usually divided into two main histological subtypes, the embryonal rhabdomyosarcoma (ERMS) and the alveolar rhabdomyosarcoma (ARMS), and the latter has a generally worse prognosis (Egas-Bejar and Huh, 2014; Sun et al., 2015). Rossi et al. (Rossi et al., 2019) reported that *circ-ZNF609* was upregulated in biopsies from ERMS and ARMS. *Circ-ZNF609* knockdown induced a significant decrease in the p-*Akt* protein level, which modulated cell proliferation-related pathways and an alteration of the p-*Rb/Rb* ratio in an ERMS-derived cell line. The hypophosphorylated Rb protein could bind E2F transcription factor 1 (*E2F1*) to reduce the activation of S-phase transcription factors such as *TCF19* and *MCMs*, which caused a specific block of ERMS from the G1 to the S phase. Differently to ERMS, in the ARMS-derived cells, due to the lower *p53* that was involved in cell cycle arrest, ARMS does not undergo G1-S arrested after the *circ-ZNF609* knockdown, which means that *circ-ZNF609* knockdown was not enough to significantly inhibit ARMS cell proliferation (Rossi et al., 2019).

Circ-ZNF609 in Other Human Diseases

Similar to the function in human tumors, *circ-ZNF609* also acted as a sponge of microRNAs in nontumor diseases (**Figure 3**; **Table 2**). In nontumor diseases, the expression level of *circ-ZNF609* had not been verified in the human tissues. On accounting for cell lines and animal models, researchers found that *circ-ZNF609* promoted cell proliferation and induced poor phenotypes in most nontumorous diseases. However, in coronary

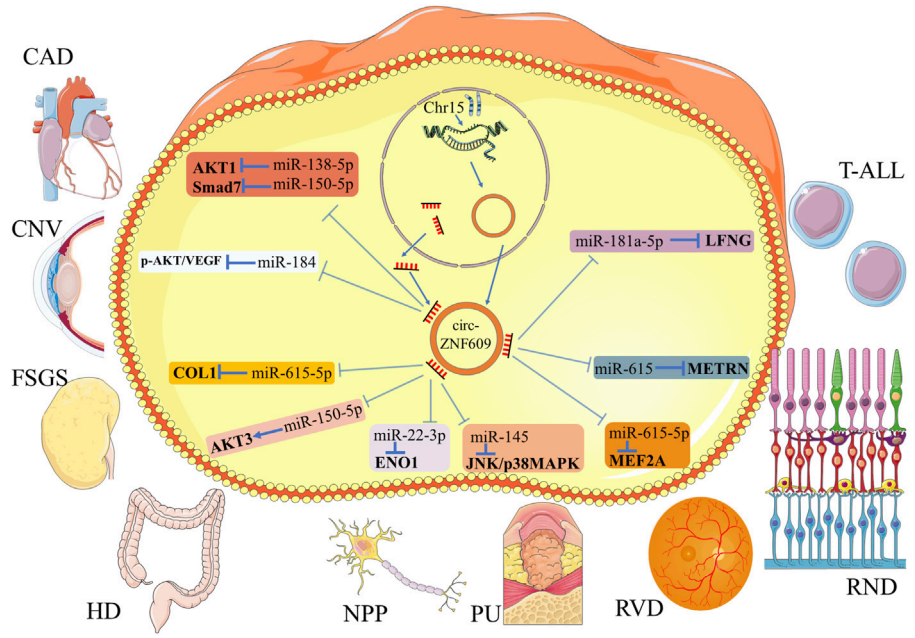

FIGURE 3 | Schematic diagram for the molecular mechanism of *circ-ZNF609* in nontumor diseases. *Circ-ZNF609* acts as a molecular sponge of specific miRNA to regulate the expression of targeted genes in nontumor diseases. T-shaped bars represent inhibition, and arrows represent promotion.

TABLE 2 | Mechanism of *circ-ZNF609* in other human diseases.

Diseases	Expression Change	Targeted miRNAs	Targeted genes	Diseases Progression	References
Coronary artery disease (CAD)	Downregulated	miR-138-5p[a] miR-150-5p[a]	AKT1[a] Smad7[a]	Inhibiting	Liang et al. (Liang et al., 2020)
Corneal neovascularization (CNV)	Upregulated	miR-184	p-AKT/VEGF	Promoting	Wu et al. (Wu et al., 2020)
Focal segmental glomerulosclerosis (FSGS)	Upregulated	miR-615-5p	COL1	Promoting	Cui et al. (Cui et al., 2020)
Hirschsprung's disease (HD)	Downregulated	miR-150-5p	AKT3	Inhibiting	Peng et al. (Peng et al., 2017)
Neuropathic pain (NPP)	Upregulated	miR-22-3p	ENO1	Promoting	Li et al. (Li et al., 2020c)
Pressure ulcer (PU)	Upregulated	miR-145	JNK/p38MAPK	Promoting	Ge and Gao (Ge and Gao, 2020)
Retinal neurodegeneration (RND)	Upregulated	miR-615	METRN	Promoting	Wang et al. (Wang et al., 2018b)
Retinal vascular dysfunction (RVD)	Upregulated	miR-615-5p	MEF2A	Promoting	Liu et al. (Liu et al., 2017)
T-cell acute lymphoblastic leukemia (T-ALL)	Upregulated	miR-181a-5p	LFNG	Promoting	Buratin et al. (Buratin et al., 2020)

[a]*Based on bioinformatics prediction and literature reports.*

heart disease and Hirschsprung's disease, it was downregulated, representing an opposite function as a protective regulator. Therefore, we summarized the role of *circ-ZNF609* in nontumorous diseases but not only in human cancers here.

Coronary Artery Disease

Coronary artery disease (CAD) is the major cause of mortality globally (Dagenais et al., 2020), and the inflammatory response theory has been widely recognized in its pathogenic mechanism (Hansson, 2005). It has been reported that circRNAs were involved in several cardiovascular pathological processes (Wang et al., 2016; Shen et al., 2019). Compared with normal populations, the expression of *circ-ZNF609* was downregulated in CAD patients. Logistic analysis suggested that a low *circ-ZNF609* level was an independent risk factor for CAD. Overexpression of *circ-ZNF609* in cells would cause the decrease of *IL-6* and *TNF-α* and an increase in *IL-10* expressions, suggesting its antiinflammatory effects, and could alleviate the development of CAD (Liang et al., 2020). Based on the bioinformatics prediction and the literature reports, researchers speculated that *circ-ZNF609* exerted a protective function in CAD by sponging microRNA and regulated the *miR-138-5p/AKT1* or *miR-150-5p/Smad7* axis to interrupter inflammation pathways.

Corneal Neovascularization

The cornea lacks blood vessels to ensure that light passes through the lens, and pathological corneal neovascularization derived from the corneal limbus which is filled with blood vessels can

affect the function of the transparent cornea and threaten vision (Feizi et al., 2017; Mobaraki et al., 2019). The study of corneal neovascularization by Wu et al. (Wu et al., 2020) suggested that in the rat corneal suture model, the overexpression of *circ-ZNF609* and a decrease of *miR-184* were observed in the corneal epithelia of rats after corneal suture surgery, and *circ-ZNF609* acted as a sponge of *miR-184* to regulate the *AKT/β-catenin/VEGF* signaling pathway and then promoted cell proliferation, migration *in vitro*, and angiogenesis *in vivo*.[84] Their study proved that inhibiting *circ-ZNF609* may be a new therapeutic method for the treatment of pathological corneal neovascularization. The role of *circ-ZNF609* in rat corneal neovascularization was different from that of human tumors; although there was no more cell line model to validate the finding, it could be validated in more animal models to ensure the conclusion.

Focal Segmental Glomerulosclerosis

Focal segmental glomerulosclerosis (FSGS) is the main cause of kidney disease worldwide, and it is a complex syndrome that arises after podocyte injury in general (Rosenberg and Kopp, 2017). In the mice model of FSGS, the expression of *circ-ZNF609* was increased in biopsies compared to normal control mice. The expression of *circ-ZNF609* was positively correlated with the degree of podocyte destruction and renal fibrosis, but *miR-615-5p* was negatively correlated with *circ-ZNF609* (Cui et al., 2020). In mechanism, it acted as a molecular sponge of *miR-615-5p* to downregulate the expression of podocyte biomarkers *WT1* and upregulate fibrotic proteins including *COL1*, promoting the progression of FSGS (Cui et al., 2020). The expression of *circ-ZNF609* in the kidney was limited not only to RCC but also to FSGS, indicating that the scope of research could be extended to other nontumor sites. This study suggested that *circ-ZNF609* might be a potential biomarker for the diagnosis of kidney disease.

Hirschsprung's Disease

Hirschsprung's disease (HSCR) is caused by a lack of enteric nerve cells in the variable part of the distal intestine, and infants with related genetic changes usually develop intestinal obstruction a few days after birth (Kenny et al., 2010). The expression of *circ-ZNF609* was downregulated in HSCR compared with normal colon tissues and inhibited the proliferation and migration of HSCR cells. In mechanism, it downregulated the expression of AKT serine/threonine kinase 3 (*AKT3*) through acting as a sponge of *miR-150-5p* and promoted disease progression (Peng et al., 2017). However, Rossi et al. (Rossi et al., 2019) found that the expressions of *miR-150-5p* and *AKT3* were not affected by the downregulation of *circ-ZNF609*; therefore, the mechanism of *circ-ZNF609*-regulated HSCR progression needs further study.

Neuropathic Pain

The widely accepted definition of neuropathic pain is the pain caused by a lesion or disease of the somatosensory system (Colloca et al., 2017). Due to the aging of the global population, the increasing incidence of cancer, and the consequences of chemotherapy, neuropathic pain may become more common (Colloca et al., 2017), and therefore finding its therapeutic targets has important clinical significance. The expression level of *miR-22-3p* was reduced in rat models with chronic constrictive injury and was involved in the progression of neuropathic pain, and *miR-22-3p* downregulation promoted neuropathic pain by targeting enolase 1 (*ENO1*) to regulate the expression of inflammatory factors (Li et al., 2020c). Li et al. (Li et al., 2020c) found that *circ-ZNF609* regulated the expression of inflammatory factors *TNF-α*, *IL-1*, and *IL-6* to promote neuropathic pain progression through the *miR-22-3p/ENO1* axis (Li et al., 2020c). Although it was inappropriate to quantify the neuropathic pain phenotype with the level of inflammatory factors, this paper provided a new molecular mechanism for *circ-ZNF609* in the regulation of inflammatory factors.

Pressure Ulcers

Pressure ulcers (PU) mostly occur in paralyzed and bedridden patients and are localized injuries to the skin and/or underlying tissues, usually over a bony prominence as a result of pressure combined with friction (Agrawal and Chauhan, 2012). PU are usually accompanied by skin oxidative damage, and drugs with antioxidant function are considered for treatment (Liu et al., 2018; Zhang et al., 2019b). In the PU model of HaCaT cells treated with H_2O_2, the expression of *circ-ZNF609* was promoted in the model, and silencing of the expression of *circ-ZNF609* alleviated oxidative stress damage including the viability loss, apoptosis, and ROS generation of HaCaT cells, through inhibiting the *JNK* and *p38MAPK* signaling pathways via acting as the sponge of *miR-145* (Ge and Gao, 2020). The study in the model of PU provided new evidence for *circ-ZNF609* in oxidative stress damage.

Retinal Neurodegeneration

Glaucoma is mainly manifested by visual field loss and irreversible blindness caused by progressively retinal neurodegenerative diseases, and the death of retinal ganglion cells (RGC) and high intraocular pressure are pathophysiological characteristics (Almasieh et al., 2012; Danesh-Meyer and Levin, 2015). In the rat model, *circ-ZNF609* was significantly upregulated in the degeneration of the optic nerve induced by high intraocular pressure, and silencing it could inhibit the proliferation of RGC and optic nerve damage caused by high intraocular pressure (Wang et al., 2018b). Their previous studies suggested that *circ-ZNF609* acted as a sponge of *miR-615* to promote the proliferation of vascular endothelial cells. *Circ-ZNF609* in RGC also acted as a sponge of *miR-615* and then upregulated mentoring glial cell differentiation regulator (*METRN*) expression, promoting cell proliferation (Wang et al., 2018b). This study of *circ-ZNF609* provided new insight into circRNAs in the growth of nerves, and it reflected the breadth of the role of circRNAs.

Retinal Vascular Dysfunction

Vascular dysfunction is a hallmark of pathological angiogenesis and contributes to the progression of various diseases (Puro et al., 2016), the expression of circRNAs is dysregulated in

cardiovascular disease that is accompanied by vascular dysfunction, and endothelial cell regulation plays an important role in it (Eelen et al., 2015; Aufiero et al., 2019). The retinal vascular system can be observed by noninvasive means, which can be used to investigate the mechanism of vascular dysfunction (Flammer et al., 2013). *Circ-ZNF609* promoted pathological angiogenesis and made endothelial cells more susceptible to oxidative stress and hypoxia (Liu et al., 2017; Wang et al., 2021b). Knocking down *circ-ZNF609* in the mouse model of oxygen-induced retinopathy did not affect the development of normal retinal vascular, while it reduced avascular area and reduced pathological retinal angiogenesis (Liu et al., 2017). The study revealed the mechanism of action for the *circ-ZNF609/miR-615-5p/MEF2A* axis in the mediation of vascular endothelial dysfunction, and since pathological angiogenesis is a hallmark of tumors, this study also verified that *circ-ZNF609* can cause tumors.

T-Cell Acute Lymphoblastic Leukemia

The expression level of circRNAs differs among normal blood cell types, but the expression in T-ALL is still unclear (Nicolet et al., 2018). RNA sequencing data from 25 T-ALL patients were analyzed and most circRNAs were found to be downregulated in expression in malignant T-ALL (Buratin et al., 2020). In particular, *circ-ZNF609* was overexpressed in immature T-ALL, knocking down *circ-ZNF609*-inhibited cell proliferation and survival compared with normal control (Buratin et al., 2020). Bioinformatics analysis suggested that *circ-ZNF609* was bound to *miR-181a-5p* in immature T-ALL, which by targeting O-fucosylpeptide 3-beta-N-acetylglucosaminyltransferase (*LFNG*) to promote leukemogenic potential through the Notch1 signaling pathway in T-ALL (Buratin et al., 2020). With only the predicted results of the bioinformatics analysis available here, researchers could verify the molecular mechanism of *circ-ZNF609* in T-ALL through more cell experiments and animal experiments.

CONCLUSION AND FUTURE PROSPECTS

The present review described the basic biological functions of *circ-ZNF609* and systematically concluded its differential expression and its underlying molecular mechanism in human diseases. We found that the expression of *circ-ZNF609* in various cancer tissues was higher than in adjacent normal tissues and dysregulation in nontumor diseases. When *circ-ZNF609* is overexpressed in tumor tissues, it could result in poor overall survival, and it positively correlated with lymph node metastasis and advanced TNM or clinical stage. Relevant research on *circ-ZNF609* helped us understand the pathogenesis of many diseases, and it was proved that *circ-ZNF609* might be an effective and promising biomarker for diagnosis.

CircRNAs not only exist in human tissues and blood cells but are also differentially expressed in the serum and exosomes, playing an important role in disease progression (Devaux, 2017; Vea et al., 2018; Kristensen et al., 2019; Wang et al., 2019). Therefore, researchers can use the circRNAs in the patient's body fluid as a noninvasive molecular marker. Emerging circRNAs have become potential therapeutic targets for human diseases, and *circ-ZNF609* is one of them. In particular, *circ-ZNF609* is an RNA that can be translated into a protein, giving it a broader role. Nowadays, the COVID-19 epidemic is serious, and the mRNA-based vaccine still has its limitations (Alameh et al., 2020; Corbett et al., 2020). The loop structure of *circ-ZNF609* prevents its degradation and confers stronger stability to it compared with linear mRNA (Xiao and Wilusz, 2019). It is a promising research direction to develop a circRNA-based vaccine, by integrating an antigen-encoding sequence of COVID-19 into *circ-ZNF609*. The internal ribosomal entry site of *circ-ZNF609* confers the translational function, making it possible to express the antigen of COVID-19. Qu et al. (Qu et al., 2022) reported a circRNA vaccine that elicited potent neutralizing antibodies and T-cell responses in an animal model (Qu et al., 2022; Szabó et al., 2022). The above studies indicated that *circ-ZNF609* might become an effective and safe molecular platform against the epidemic.

In human diseases, it exerts functions through the *circ-ZNF609*-miRNA-mRNA network, and *circ-ZNF609* knockdown or overexpression of miRNA will inhibit the malignant phenotype of cancers. Therefore, knocking down *circ-ZNF609* by precise RNA interference (RNAi) or knocking out by CRISPR/Cas9-mediated circRNA knockout (Yang et al., 2018), developing miRNA inhibitors, could serve as potential therapeutic strategies for treatments of multiple human diseases. In comparison with Qian et al. (Qian et al., 2021), we comprehensively discussed the underlying molecular mechanism of *circ-ZNF609* in multiple human diseases and expanded the types of the disease in detail. In addition, we discussed future research directions in *circ-ZNF609*-dysregulated diseases. The possible function of *circ-ZNF609* in the prevention of the COVID-19 epidemic was also explored. We hope this study could help reveal the far-reaching clinical significance of *circ-ZNF609*.

AUTHOR CONTRIBUTIONS

SBW and JJW wrote and revised the manuscript. ZYW and YYL helped to draft the manuscript. ZXG and YYL participated in the revision of the review. ZJW designed the project. All of the authors read and approved the final manuscript.

FUNDING

This research was supported by the National Natural Science Foundation of China (Grant Nos. 81270685 and 81771640), the Project of Nanjing Science and Technology Committee (No. 201605001), and the "333" Project of Jiangsu Province (No. BRA2018083).

REFERENCES

Agrawal, K., and Chauhan, N. (2012). Pressure Ulcers: Back to the Basics. *Indian J. Plast. Surg.* 45, 244–254. doi:10.4103/0970-0358.101287

Alameh, M.-G., Weissman, D., and Pardi, N. (2020). Messenger RNA-Based Vaccines against Infectious Diseases. *Curr. Top. Microbiol. Immunol.* doi:10.1007/82_2020_202

Almasieh, M., Wilson, A. M., Morquette, B., Cueva Vargas, J. L., and Di Polo, A. (2012). The Molecular Basis of Retinal Ganglion Cell Death in Glaucoma. *Prog. Retin. eye Res.* 31, 152–181. doi:10.1016/j.preteyeres.2011.11.002

Aufiero, S., Reckman, Y. J., Pinto, Y. M., and Creemers, E. E. (2019). Circular RNAs Open a New Chapter in Cardiovascular Biology. *Nat. Rev. Cardiol.* 16, 503–514. doi:10.1038/s41569-019-0185-2

Bao, L., You, B., Shi, S., Shan, Y., Zhang, Q., Yue, H., et al. (2018). Metastasis-associated miR-23a from Nasopharyngeal Carcinoma-Derived Exosomes Mediates Angiogenesis by Repressing a Novel Target Gene TSGA10. *Oncogene* 37, 2873–2889. doi:10.1038/s41388-018-0183-6

Buratin, A., Paganin, M., Gaffo, E., Dal Molin, A., Roels, J., Germano, G., et al. (2020). Large-scale Circular RNA Deregulation in T-ALL: Unlocking Unique Ectopic Expression of Molecular Subtypes. *Blood Adv.* 4, 5902–5914. doi:10.1182/bloodadvances.2020002337

Carmeliet, P., and Jain, R. K. (2000). Angiogenesis in Cancer and Other Diseases. *Nature* 407, 249–257. doi:10.1038/35025220

Chen, L.-L. (2020). The Expanding Regulatory Mechanisms and Cellular Functions of Circular RNAs. *Nat. Rev. Mol. Cell Biol.* 21, 475–490. doi:10.1038/s41580-020-0243-y

Chen, L.-L., and Yang, L. (2015). Regulation of circRNA Biogenesis. *RNA Biol.* 12, 381–388. doi:10.1080/15476286.2015.1020271

Chen, R., Smith-Cohn, M., Cohen, A. L., and Colman, H. (2017). Glioma Subclassifications and Their Clinical Significance. *Neurotherapeutics* 14, 284–297. doi:10.1007/s13311-017-0519-x

Chen, Y.-P., Chan, A. T. C., Le, Q.-T., Blanchard, P., Sun, Y., and Ma, J. (2019). Nasopharyngeal Carcinoma. *Lancet* 394, 64–80. doi:10.1016/S0140-6736(19)30956-0

Chua, M. L. K., Wee, J. T. S., Hui, E. P., and Chan, A. T. C. (2016). Nasopharyngeal Carcinoma. *Lancet* 387, 1012–1024. doi:10.1016/S0140-6736(15)00055-0

Cohen, P. A., Jhingran, A., Oaknin, A., and Denny, L. (2019). Cervical Cancer. *Lancet* 393, 169–182. doi:10.1016/S0140-6736(18)32470-X

Colloca, L., Ludman, T., Bouhassira, D., Baron, R., Dickenson, A. H., Yarnitsky, D., et al. (2017). Neuropathic Pain. *Nat. Rev. Dis. Prim.* 3, 17002. doi:10.1038/nrdp.2017.2

Corbett, K. S., Edwards, D. K., Leist, S. R., Abiona, O. M., Boyoglu-Barnum, S., Gillespie, R. A., et al. (2020). SARS-CoV-2 mRNA Vaccine Design Enabled by Prototype Pathogen Preparedness. *Nature* 586, 567–571. doi:10.1038/s41586-020-2622-0

Cui, X., Fu, J., Luan, J., Qi, H., Jiao, C., Ran, M., et al. (2020). CircZNF609 Is Involved in the Pathogenesis of Focal Segmental Glomerulosclerosis by Sponging miR-615-5p. *Biochem. Biophysical Res. Commun.* 531, 341–349. doi:10.1016/j.bbrc.2020.07.066

Dagenais, G. R., Leong, D. P., Rangarajan, S., Lanas, F., Lopez-Jaramillo, P., Gupta, R., et al. (2020). Variations in Common Diseases, Hospital Admissions, and Deaths in Middle-Aged Adults in 21 Countries from Five Continents (PURE): a Prospective Cohort Study. *Lancet* 395, 785–794. doi:10.1016/S0140-6736(19)32007-0

Danesh-Meyer, H. V., and Levin, L. A. (2015). Glaucoma as a Neurodegenerative Disease. *J. Neuro-Ophthalmology* 35, S22–S28. doi:10.1097/wno.0000000000000293

DeSantis, C. E., Ma, J., Goding Sauer, A., Newman, L. A., and Jemal, A. (2017). Breast Cancer Statistics, 2017, Racial Disparity in Mortality by State. *CA a cancer J. Clin.* 67, 439–448. doi:10.3322/caac.21412

Devaux, Y. (2017). Transcriptome of Blood Cells as a Reservoir of Cardiovascular Biomarkers. *Biochimica Biophysica Acta (BBA) - Mol. Cell Res.* 1864, 209–216. doi:10.1016/j.bbamcr.2016.11.005

Devesa, S. S., Bray, F., Vizcaino, A. P., and Parkin, D. M. (2005). International Lung Cancer Trends by Histologic Type: Male:Female Differences Diminishing and Adenocarcinoma Rates Rising. *Int. J. Cancer* 117, 294–299. doi:10.1002/ijc.21183

Di, X., Jin, X., Li, R., Zhao, M., and Wang, K. (2019). CircRNAs and Lung Cancer: Biomarkers and Master Regulators. *Life Sci.* 220, 177–185. doi:10.1016/j.lfs.2019.01.055

Ding, L., Wang, R., Shen, D., Cheng, S., Wang, H., Lu, Z., et al. (2021). Role of Noncoding RNA in Drug Resistance of Prostate Cancer. *Cell Death Dis.* 12. doi:10.1038/s41419-021-03854-x

Du, S., Li, H., Lu, F., Zhang, S., and Tang, J. (2021). Circular RNA ZNF609 Promotes the Malignant Progression of Glioma by Regulating miR-1224-3p/PLK1 Signaling. *J. Cancer* 12, 3354–3366. doi:10.7150/jca.54934

Du, S., Zhang, P., Ren, W., Yang, F., and Du, C. (2020). Circ-ZNF609 Accelerates the Radioresistance of Prostate Cancer Cells by Promoting the Glycolytic Metabolism through miR-501-3p/HK2 Axis. *Cmar* Vol. 12, 7487–7499. doi:10.2147/cmar.S257441

Eelen, G., de Zeeuw, P., Simons, M., and Carmeliet, P. (2015). Endothelial Cell Metabolism in Normal and Diseased Vasculature. *Circ. Res.* 116, 1231–1244. doi:10.1161/circresaha.116.302855

Egas-Bejar, D., and Huh, W. W. (2014). Rhabdomyosarcoma in Adolescent and Young Adult Patients: Current Perspectives. *Adolesc. Health Med. Ther.* 5, 115–125. doi:10.2147/AHMT.S44582

Feizi, S., Azari, A. A., and Safapour, S. (2017). Therapeutic Approaches for Corneal Neovascularization. *Eye Vis. (Lond)* 4, 28–10. doi:10.1186/s40662-017-0094-6

Flammer, J., Konieczka, K., Bruno, R. M., Virdis, A., Flammer, A. J., and Taddei, S. (2013). The Eye and the Heart. *Eur. heart J.* 34, 1270–1278. doi:10.1093/eurheartj/eht023

Ge, R., and Gao, G. (2020). Anti-antioxidant Impacts of circZNF609 Silence in HaCaT Cells through Regulating miR-145. *Artif. Cells, Nanomedicine, Biotechnol.* 48, 384–392. doi:10.1080/21691401.2019.1709863

Gu, Q., Hou, W., Shi, L., Liu, H., Zhu, Z., and Ye, W. (2021). Circular RNA ZNF609 Functions as a Competing Endogenous RNA in Regulating E2F Transcription Factor 6 through Competitively Binding to microRNA-197-3p to Promote the Progression of Cervical Cancer Progression. *Bioengineered* 12, 927–936. doi:10.1080/21655979.2021.1896116

Hansson, G. K. (2005). Inflammation, Atherosclerosis, and Coronary Artery Disease. *N. Engl. J. Med.* 352, 1685–1695. doi:10.1056/nejmra043430

Harbeck, N., and Gnant, M. (2017). Breast Cancer. *Lancet* 389, 1134–1150. doi:10.1016/s0140-6736(16)31891-8

He, Y., Huang, H., Jin, L., Zhang, F., Zeng, M., Wei, L., et al. (2020). CircZNF609 Enhances Hepatocellular Carcinoma Cell Proliferation, Metastasis, and Stemness by Activating the Hedgehog Pathway through the Regulation of miR-15a-5p/15b-5p and GLI2 Expressions. *Cell Death Dis.* 11, 358. doi:10.1038/s41419-020-2441-0

Ho-Xuan, H., Glažar, P., Latini, C., Heizler, K., Haase, J., Hett, R., et al. (2020). Comprehensive Analysis of Translation from Overexpressed Circular RNAs Reveals Pervasive Translation from Linear Transcripts. *Nucleic Acids Res.* 48, 10368–10382. doi:10.1093/nar/gkaa704

Ho-Xuan, H., Lehmann, G., Glazar, P., Gypas, F., Eichner, N., Heizler, K., et al. (2020). Gene Expression Signatures of a Preclinical Mouse Model during Colorectal Cancer Progression under Low-Dose Metronomic Chemotherapy. *Cancers* 13, 49. doi:10.3390/cancers13010049

Huang, X., Zhang, W., and Shao, Z. (2019). Prognostic and Diagnostic Significance of circRNAs Expression in Lung Cancer. *J. Cell. Physiology* 234, 18459–18465. doi:10.1002/jcp.28481

Jeck, W. R., Sorrentino, J. A., Wang, K., Slevin, M. K., Burd, C. E., Liu, J., et al. (2012). Circular RNAs Are Abundant, Conserved, and Associated with ALU Repeats. *Rna* 19, 141–157. doi:10.1261/rna.035667.112

Jin, C., Zhao, W., Zhang, Z., and Liu, W. (2019). Silencing Circular RNA circZNF609 Restrains Growth, Migration and Invasion by Up-Regulating microRNA-186-5p in Prostate Cancer. *Artif. Cells, Nanomedicine, Biotechnol.* 47, 3350–3358. doi:10.1080/21691401.2019.1648281

Kenny, S. E., Tam, P. K. H., and Garcia-Barcelo, M. (2010). Hirschsprung's Disease. *Seminars Pediatr. Surg.* 19, 194–200. doi:10.1053/j.sempedsurg.2010.03.004

Kim, E., Kim, Y. K., and Lee, S.-J. V. (2021). Emerging Functions of Circular RNA in Aging. *Trends Genet.* 37, 819–829. doi:10.1016/j.tig.2021.04.014

Kolakofsky, D. (1976). Isolation and Characterization of Sendai Virus DI-RNAs. *Cell* 8, 547–555. doi:10.1016/0092-8674(76)90223-3

Kristensen, L. S., Andersen, M. S., Stagsted, L. V. W., Ebbesen, K. K., Hansen, T. B., and Kjems, J. (2019). The Biogenesis, Biology and Characterization of Circular RNAs. *Nat. Rev. Genet.* 20, 675–691. doi:10.1038/s41576-019-0158-7

Legnini, I., Di Timoteo, G., Rossi, F., Morlando, M., Briganti, F., Sthandier, O., et al. (2017). *Circ-ZNF609* Is a Circular RNA that Can Be Translated and Functions in Myogenesis. *Mol. Cell* 66, 22–37. e29. doi:10.1016/j.molcel.2017.02.017

Li, J. K., Chen, C., Liu, J. Y., Shi, J. Z., Liu, S. P., Liu, B., et al. (2017). Long Noncoding RNA MRCCAT1 Promotes Metastasis of Clear Cell Renal Cell Carcinoma via Inhibiting NPR3 and Activating P38-MAPK Signaling. *Mol. Cancer* 16, 111–114. doi:10.1186/s12943-017-0681-0

Li, J., Sun, D., Pu, W., Wang, J., and Peng, Y. (2020). Circular RNAs in Cancer: Biogenesis, Function, and Clinical Significance. *Trends Cancer* 6, 319–336. doi:10.1016/j.trecan.2020.01.012

Li, L., Luo, Y., Zhang, Y., Wei, M., Zhang, M., Liu, H., et al. (2020). CircZNF609 Aggravates Neuropathic Pain via miR-22-3p/ENO1 axis in CCI Rat Models. *Gene* 763, 145069. doi:10.1016/j.gene.2020.145069

Li, M., Li, Y., and Yu, M. (2020). CircRNA ZNF609 Knockdown Suppresses Cell Growth via Modulating miR-188/ELF2 Axis in Nasopharyngeal Carcinoma. *Ott* Vol. 13, 2399–2409. doi:10.2147/ott.S234230

Li, Z., Huang, C., Bao, C., Chen, L., Lin, M., Wang, X., et al. (2015). Exon-intron Circular RNAs Regulate Transcription in the Nucleus. *Nat. Struct. Mol. Biol.* 22, 256–264. doi:10.1038/nsmb.2959

Liang, B., Li, M., Deng, Q., Wang, C., Rong, J., He, S., et al. (2020). CircRNA ZNF609 in Peripheral Blood Leukocytes Acts as a Protective Factor and a Potential Biomarker for Coronary Artery Disease. *Ann. Transl. Med.* 8, 741. doi:10.21037/atm-19-4728

Liao, G.-B., Li, X.-Z., Zeng, S., Liu, C., Yang, S.-M., Yang, L., et al. (2018). Regulation of the Master Regulator FOXM1 in Cancer. *Cell Commun. Signal* 16, 57. doi:10.1186/s12964-018-0266-6

Liao, X., Zhan, W., Tian, B., Luo, Y., Gu, F., and Li, R. (2020). Circular RNA ZNF609 Promoted Hepatocellular Carcinoma Progression by Upregulating PAP2C Expression via Sponging miR-342-3p. *Ott* Vol. 13, 7773–7783. doi:10.2147/OTT.S253936

Liberti, M. V., and Locasale, J. W. (2016). The Warburg Effect: How Does it Benefit Cancer Cells? *Trends Biochem. Sci.* 41, 211–218. doi:10.1016/j.tibs.2015.12.001

Liu, C., Yao, M.-D., Li, C.-P., Shan, K., Yang, H., Wang, J.-J., et al. (2017). Silencing of Circular RNA-Znf609 Ameliorates Vascular Endothelial Dysfunction. *Theranostics* 7, 2863–2877. doi:10.7150/thno.19353

Liu, J., Rybakina, E. G., Korneva, E. A., and Noda, M. (2018). Effects of Derinat on Ischemia-Reperfusion-Induced Pressure Ulcer Mouse Model. *J. Pharmacol. Sci.* 138, 123–130. doi:10.1016/j.jphs.2018.08.013

Liu, Q., Cui, W., Yang, C., and Du, L.-P. (2021). Circular RNA ZNF609 Drives Tumor Progression by Regulating the miR-138-5p/SIRT7 axis in Melanoma. *Aging* 13, 19822–19834. doi:10.18632/aging.203394

Liu, S., Yang, N., Jiang, X., Wang, J., Dong, J., and Gao, Y. (2021). FUS-induced Circular RNA ZNF609 Promotes Tumorigenesis and Progression via Sponging miR-142-3p in Lung Cancer. *J. Cell Physiol.* 236, 79–92. doi:10.1002/jcp.29481

Liu, Z., Pan, H. M., Xin, L., Zhang, Y., Zhang, W. M., Cao, P., et al. (2019). *Circ-ZNF609* Promotes Carcinogenesis of Gastric Cancer Cells by Inhibiting miRNA-145-5p Expression. *Eur. Rev. Med. Pharmacol. Sci.* 23, 9411–9417. doi:10.26355/eurrev_201911_19433

Liu, Z., Liu, F., Wang, F., Yang, X., and Guo, W. (2021). CircZNF609 Promotes Cell Proliferation, Migration, Invasion, and Glycolysis in Nasopharyngeal Carcinoma through Regulating HRAS via miR-338-3p. *Mol. Cell Biochem.* 476, 175–186. doi:10.1007/s11010-020-03894-5

Memczak, S., Jens, M., Elefsinioti, A., Torti, F., Krueger, J., Rybak, A., et al. (2013). Circular RNAs Are a Large Class of Animal RNAs with Regulatory Potency. *Nature* 495, 333–338. doi:10.1038/nature11928

Mobaraki, M., Abbasi, R., Omidian Vandchali, S., Ghaffari, M., Moztarzadeh, F., and Mozafari, M. (2019). Corneal Repair and Regeneration: Current Concepts and Future Directions. *Front. Bioeng. Biotechnol.* 7. doi:10.3389/fbioe.2019.00135

Mohler, J., Bahnson, R. R., Boston, B., Busby, J. E., D'Amico, A., Eastham, J. A., et al. (2010). Prostate Cancer. *J. Natl. Compr. Canc Netw.* 8, 162–200. doi:10.6004/jnccn.2010.0012

Nicolet, B. P., Engels, S., Aglialoro, F., van den Akker, E., von Lindern, M., and Wolkers, M. C. (2018). Circular RNA Expression in Human Hematopoietic Cells Is Widespread and Cell-type Specific. *Nucleic acids Res.* 46, 8168–8180. doi:10.1093/nar/gky721

Peng, L., Chen, G., Zhu, Z., Shen, Z., Du, C., Zang, R., et al. (2017). Circular RNA ZNF609 Functions as a Competitive Endogenous RNA to Regulate AKT3 Expression by Sponging miR-150-5p in Hirschsprung's Disease. *Oncotarget* 8, 808–818. doi:10.18632/oncotarget.13656

Puro, D. G., Kohmoto, R., Fujita, Y., Gardner, T. W., and Padovani-Claudio, D. A. (2016). Bioelectric Impact of Pathological Angiogenesis on Vascular Function. *Proc. Natl. Acad. Sci. U.S.A.* 113, 9934–9939. doi:10.1073/pnas.1604757113

Qian, Y., Li, Y., Li, R., Yang, T., Jia, R., and Ge, Y. Z. (2021). circ-ZNF609: A Potent circRNA in Human Cancers. *J. Cell Mol. Med.* 25, 10349–10361. doi:10.1111/jcmm.16996

Qu, L., Yi, Z., Shen, Y., Lin, L., Chen, F., Xu, Y., et al. (2022). Circular RNA Vaccines against SARS-CoV-2 and Emerging Variants. *Cell* S0092-8674, 00394. doi:10.1016/j.cell.2022.03.044

Rini, B. I., Campbell, S. C., and Escudier, B. (2009). Renal Cell Carcinoma. *Lancet* 373, 1119–1132. doi:10.1016/S0140-6736(09)60229-4

Rong, D., Lu, C., Zhang, B., Fu, K., Zhao, S., Tang, W., et al. (2019). CircPSMC3 Suppresses the Proliferation and Metastasis of Gastric Cancer by Acting as a Competitive Endogenous RNA through Sponging miR-296-5p. *Mol. Cancer* 18, 25. doi:10.1186/s12943-019-0958-6

Rosenberg, A. Z., and Kopp, J. B. (2017). Focal Segmental Glomerulosclerosis. *Clin. J. Am. Soc. Nephrol.*12, 502–517. doi:10.2215/cjn.05960616

Rossi, F., Legnini, I., Megiorni, F., Colantoni, A., Santini, T., Morlando, M., et al. (2019). *Circ-ZNF609* Regulates G1-S Progression in Rhabdomyosarcoma. *Oncogene* 38, 3843–3854. doi:10.1038/s41388-019-0699-4

Rybak-Wolf, A., Stottmeister, C., Glažar, P., Jens, M., Pino, N., Giusti, S., et al. (2015). Circular RNAs in the Mammalian Brain Are Highly Abundant, Conserved, and Dynamically Expressed. *Mol. Cell* 58, 870–885. doi:10.1016/j.molcel.2015.03.027

Salzman, J., Gawad, C., Wang, P. L., Lacayo, N., and Brown, P. O. (2012). Circular RNAs Are the Predominant Transcript Isoform from Hundreds of Human Genes in Diverse Cell Types. *PLoS One* 7, e30733. doi:10.1371/journal.pone.0030733

Sanger, H. L., Klotz, G., Riesner, D., Gross, H. J., and Kleinschmidt, A. K. (1976). Viroids Are Single-Stranded Covalently Closed Circular RNA Molecules Existing as Highly Base-Paired Rod-like Structures. *Proc. Natl. Acad. Sci. U.S.A.* 73, 3852–3856. doi:10.1073/pnas.73.11.3852

Schadendorf, D., van Akkooi, A. C. J., Berking, C., Griewank, K. G., Gutzmer, R., Hauschild, A., et al. (2018). Melanoma. *Lancet* 392, 971–984. doi:10.1016/S0140-6736(18)31559-9

Shelar, S., Shim, E.-H., Brinkley, G. J., Kundu, A., Carobbio, F., Poston, T., et al. (2018). Biochemical and Epigenetic Insights into L-2-Hydroxyglutarate, a Potential Therapeutic Target in Renal Cancer. *Clin. Cancer Res.* 24, 6433–6446. doi:10.1158/1078-0432.ccr-18-1727

Shen, L., Hu, Y., Lou, J., Yin, S., Wang, W., Wang, Y., et al. (2019). CircRNA-0044073 I-s U-pregulated in A-therosclerosis and I-ncreases the P-roliferation and I-nvasion of C-ells by T-argeting miR-107. *Mol. Med. Rep.* 19, 3923–3932. doi:10.3892/mmr.2019.10011

Shi, X., Wang, B., Feng, X., Xu, Y., Lu, K., and Sun, M. (2020). circRNAs and Exosomes: A Mysterious Frontier for Human Cancer. *Mol. Ther. - Nucleic Acids* 19, 384–392. doi:10.1016/j.omtn.2019.11.023

Shi, Y., Jia, X., and Xu, J. (2020). The New Function of circRNA: Translation. *Clin. Transl. Oncol.* 22, 2162–2169. doi:10.1007/s12094-020-02371-1

Sitarz, R., Skierucha, M., Mielko, J., Offerhaus, J., Maciejewski, R., and Polkowski, W. (2018). Gastric Cancer: Epidemiology, Prevention, Classification, and Treatment. *Cmar* Vol. 10, 239–248. doi:10.2147/CMAR.S149619

Sun, X., Guo, W., Shen, J. K., Mankin, H. J., Hornicek, F. J., and Duan, Z. (2015). *Rhabdomyosarcoma: Advances in Molecular and Cellular Biology. Sarcoma* 2015.

Suzuki, H., Zuo, Y., Wang, J., Zhang, M. Q., Malhotra, A., and Mayeda, A. (2006). Characterization of RNase R-Digested Cellular RNA Source that Consists of Lariat and Circular RNAs from Pre-mRNA Splicing. *Nucleic Acids Res.* 34, e63. doi:10.1093/nar/gkl151

Szabó, G. T., Mahiny, A. J., and Vlatkovic, I. (2022). COVID-19 mRNA Vaccines: Platforms and Current Developments. *Mol. Ther.* 30 (5), 1850–1868. doi:10.1016/j.ymthe.2022.02.016

Thomson, D. W., and Dinger, M. E. (2016). Endogenous microRNA Sponges: Evidence and Controversy. *Nat. Rev. Genet.* 17, 272–283. doi:10.1038/nrg.2016.20

Tong, H., Zhao, K., Wang, J., Xu, H., and Xiao, J. (2019). CircZNF609/miR-134-5p/BTG-2 axis Regulates Proliferation and Migration of Glioma Cell. *J. Pharm. Pharmacol.* 72, 68–75. doi:10.1111/jphp.13188

Torre, L. A., Bray, F., Siegel, R. L., Ferlay, J., Lortet-Tieulent, J., and Jemal, A. (2015). Global Cancer Statistics, 2012. *CA A Cancer J. Clin.* 65, 87–108. doi:10.3322/caac.21262

Vea, A., Llorente-Cortes, V., and de Gonzalo-Calvo, D. (2018). Circular RNAs in Blood. *Circ. RNAs*, 119–130. doi:10.1007/978-981-13-1426-1_10

Verduci, L., Tarcitano, E., Strano, S., Yarden, Y., and Blandino, G. (2021). CircRNAs: Role in Human Diseases and Potential Use as Biomarkers. *Cell Death Dis.* 12, 468. doi:10.1038/s41419-021-03743-3

Villanueva, A. (2019). Hepatocellular Carcinoma. *N. Engl. J. Med.* 380, 1450–1462. doi:10.1056/NEJMra1713263

Wang, F., Li, X., Jia, X., and Geng, L. (2021). CircRNA ZNF609 Knockdown Represses the Development of Non-small Cell Lung Cancer via miR-623/FOXM1 Axis. *Cmar* Vol. 13, 1029–1039. doi:10.2147/CMAR.S282162

Wang, J.-J., Liu, C., Shan, K., Liu, B.-H., Li, X.-M., Zhang, S.-J., et al. (2018). Circular RNA-Znf609 Regulates Retinal Neurodegeneration by Acting as miR-615 Sponge. *Theranostics* 8, 3408–3415. doi:10.7150/thno.25156

Wang, J., Lin, Y., Jiang, D. H., Yang, X., and He, X. G. (2021). CircRNA ZNF609 Promotes Angiogenesis in Nasopharyngeal Carcinoma by Regulating miR -145/STMN1 axis. *Kaohsiung J. Med. Sci.* 37, 686–698. doi:10.1002/kjm2.12381

Wang, K., Long, B., Liu, F., Wang, J.-X., Liu, C.-Y., Zhao, B., et al. (2016). A Circular RNA Protects the Heart from Pathological Hypertrophy and Heart Failure by Targeting miR-223. *Eur. Heart J.* 37, 2602–2611. doi:10.1093/eurheartj/ehv713

Wang, K., Sun, Y., Tao, W., Fei, X., and Chang, C. (2017). Androgen Receptor (AR) Promotes Clear Cell Renal Cell Carcinoma (ccRCC) Migration and Invasion via Altering the circHIAT1/miR-195-5p/29a-3p/29c-3p/CDC42 Signals. *Cancer Lett.* 394, 1–12. doi:10.1016/j.canlet.2016.12.036

Wang, S., Xue, X., Wang, R., Li, X., Li, Q., Wang, Y., et al. (2018). CircZNF609 Promotes Breast Cancer Cell Growth, Migration, and Invasion by Elevating p70S6K1 via Sponging miR-145-5p. *Cmar* Vol. 10, 3881–3890. doi:10.2147/CMAR.S174778

Wang, Y., Liu, J., Ma, J., Sun, T., Zhou, Q., Wang, W., et al. (2019). Exosomal circRNAs: Biogenesis, Effect and Application in Human Diseases. *Mol. Cancer* 18, 116–126. doi:10.1186/s12943-019-1041-z

Weller, M., Wick, W., Aldape, K., Brada, M., Berger, M., Pfister, S. M., et al. (2015). Glioma. *Nat. Rev. Dis. Prim.* 1, 15017. doi:10.1038/nrdp.2015.17

Wu, L., Xia, J., Yang, J., Shi, Y., Xia, H., Xiang, X., et al. (2018). *Circ-ZNF609* Promotes Migration of Colorectal Cancer by Inhibiting Gli1 Expression via microRNA-150. *J. buon* 23, 1343–1349.

Wu, P., Zhang, D., Geng, Y., Li, R., and Zhang, Y. (2020). Circular RNA-Znf609 Regulates Corneal Neovascularization by Acting as a Sponge of miR-184. *Exp. Eye Res.* 192, 107937. doi:10.1016/j.exer.2020.107937

Wu, W., Wei, N., Shao, G., Jiang, C., Zhang, S., and Wang, L. (2019). circZNF609 Promotes the Proliferation and Migration of Gastric Cancer by Sponging miR-483-3p and Regulating CDK6. *Ott* Vol. 12, 8197–8205. doi:10.2147/OTT.S193031

Xiao, M.-S., Ai, Y., and Wilusz, J. E. (2020). Biogenesis and Functions of Circular RNAs Come into Focus. *Trends Cell Biol.* 30, 226–240. doi:10.1016/j.tcb.2019.12.004

Xiao, M.-S., and Wilusz, J. E. (2019). An Improved Method for Circular RNA Purification Using RNase R that Efficiently Removes Linear RNAs Containing G-Quadruplexes or Structured 3′ Ends. *Nucleic Acids Res.* 47, 8755–8769. doi:10.1093/nar/gkz576

Xiong, Y., Zhang, J., and Song, C. (2019). CircRNA ZNF609 Functions as a Competitive Endogenous RNA to Regulate FOXP4 Expression by Sponging miR-138-5p in Renal Carcinoma. *J. Cell. Physiology* 234, 10646–10654. doi:10.1002/jcp.27744

Yang, J., Meng, X., Pan, J., Jiang, N., Zhou, C., Wu, Z., et al. (2018). CRISPR/Cas9-mediated Noncoding RNA Editing in Human Cancers. *RNA Biol.* 15 (1), 35–43. doi:10.1080/15476286.2017.1391443

Zhang, X.-y., and Zhang, P.-y. (2017). Gastric Cancer: Somatic Genetics as a Guide to Therapy. *J. Med. Genet.* 54, 305–312. doi:10.1136/jmedgenet-2016-104171

Zhang, X., Xue, H., Zhou, P., Liu, L., Yu, J., Dai, P., et al. (2019). RETRACTED: Angelica Polysaccharide Alleviates Oxidative Response Damage in HaCaT Cells through Up-Regulation of miR-126. *Exp. Mol. Pathology* 110, 104281. doi:10.1016/j.yexmp.2019.104281

Zhang, X., Zhao, Y., Kong, P., Han, M., and Li, B. (2019). Expression of circZNF609 Is Down-Regulated in Colorectal Cancer Tissue and Promotes Apoptosis in Colorectal Cancer Cells by Upregulating P53. *Med. Sci. Monit.* 25, 5977–5985. doi:10.12659/MSM.915926

Zhang, Y., and Wang, Y. (2021). Circular RNAs in Hepatocellular Carcinoma: Emerging Functions to Clinical Significances. *Front. Oncol.* 11. doi:10.3389/fonc.2021.667428

Zhang, Y., Zhang, X.-O., Chen, T., Xiang, J.-F., Yin, Q.-F., Xing, Y.-H., et al. (2013). Circular Intronic Long Noncoding RNAs. *Mol. Cell* 51, 792–806. doi:10.1016/j.molcel.2013.08.017

Zhu, L., Liu, Y., Yang, Y., Mao, X. M., and Yin, Z. D. (2019). CircRNA ZNF609 Promotes Growth and Metastasis of Nasopharyngeal Carcinoma by Competing with microRNA-150-5p. *Eur. Rev. Med. Pharmacol. Sci.* 23, 2817–2826. doi:10.26355/eurrev_201904_17558

Zuo, Y., Shen, W., Wang, C., Niu, N., and Pu, J. (2020). Circular RNA Circ-Znf609 Promotes Lung Adenocarcinoma Proliferation by Modulating miR-1224-3p/ETV1 Signaling. *Cmar* Vol. 12, 2471–2479. doi:10.2147/CMAR.S232260

Conflict of Interest: The authors declare that the research was conducted in the absence of any commercial or financial relationships that could be construed as a potential conflict of interest.

Publisher's Note: All claims expressed in this article are solely those of the authors and do not necessarily represent those of their affiliated organizations, or those of the publisher, the editors, and the reviewers. Any product that may be evaluated in this article, or claim that may be made by its manufacturer, is not guaranteed or endorsed by the publisher.

frontiers | Frontiers in Genetics

TYPE Original Research
PUBLISHED 14 October 2022
DOI 10.3389/fgene.2022.794621

OPEN ACCESS

EDITED BY
Deepanjan Paul,
Children's Hospital of Philadelphia,
United States

REVIEWED BY
Ehsan Nazemalhosseini-Mojarad,
Shahid Beheshti University of Medical Sciences, Iran
Deeksha Bhartiya,
Karolinska Institutet (KI), Sweden

*CORRESPONDENCE
Yongle Ju,
juyongle0757@163.com
Manzhao Ouyang,
ouyangmanzhao@163.com

†These authors have contributed equally to this work

SPECIALTY SECTION
This article was submitted to RNA, a section of the journal Frontiers in Genetics

RECEIVED 13 October 2021
ACCEPTED 20 September 2022
PUBLISHED 14 October 2022

CITATION
Liao T, Lu Y, Li W, Wang K, Zhang Y, Luo Z, Ju Y and Ouyang M (2022), Construction and validation of a glycolysis-related lncRNA signature for prognosis prediction in Stomach Adenocarcinoma. *Front. Genet.* 13:794621. doi: 10.3389/fgene.2022.794621

Construction and validation of a glycolysis-related lncRNA signature for prognosis prediction in Stomach Adenocarcinoma

Tianyou Liao[1†], Yan Lu[1†], Wangji Li[1,2†], Kang Wang[1,2], Yanxiang Zhang[1], Zhentao Luo[1], Yongle Ju[1,2*] and Manzhao Ouyang[1,2*]

[1]Department of Gastrointestinal Surgery, Shunde Hospital, Southern Medical University (The First People's Hospital of Shunde Foshan), Foshan, Guangdong, China, [2]The Second School of Clinical Medicine, Southern Medical University, Guangzhou, Guangdong, China

Background: Glycolysis is closely related to the occurrence and progression of gastric cancer (GC). Currently, there is no systematic study on using the glycolysis-related long non-coding RNA (lncRNA) as a model for predicting the survival time in patients with GC. Therefore, it was essential to develop a signature for predicting the survival based on glycolysis-related lncRNA in patients with GC.

Materials and methods: LncRNA expression profiles, containing 375 stomach adenocarcinoma (STAD) samples, were obtained from The Cancer Genome Atlas (TCGA) database. The co-expression network of lncRNA and glycolysis-related genes was used to identify the glycolysis-related lncRNAs. The Kaplan-Meier survival analysis and univariate Cox regression analysis were used to detect the glycolysis-related lncRNA with prognostic significance. Then, Bayesian Lasso-logistic and multivariate Cox regression analyses were performed to screen the glycolysis-related lncRNA with independent prognostic significance and to develop the risk model. Patients were assigned into the low- and high-risk cohorts according to their risk scores. A nomogram model was constructed based on clinical information and risk scores. Gene Set Enrichment Analysis (GSEA) was performed to visualize the functional and pathway enrichment analyses of the glycolysis-related lncRNA. Finally, the robustness of the results obtained was verified in an internal validation data set.

Abbreviations: GC, gastric cancer; lncRNA, long non-coding RNA; STAD, stomach adenocarcinoma; TCGA, The Cancer Genome Atlas; GSEA, Gene Set Enrichment Analysis; ROC, receiver operating characteristic; AUC, area under curve; OS, overall survival; GO, gene ontology; KEGG, Kyoto Encyclopedia of Genes and Genomes; C-index, index of concordance; CAMs, cell adhesion molecules; ECM, extracellular matrix; PDH, pyruvate dehydrogenase; NEAT1, lncRNA-nuclear paraspeckle assembly transcript 1; PCR, Polymerase Chain Reaction; SD, standard deviation; SE, standard error; HR, hazard ratio; CI, confidence intervals.

Results: Seven glycolysis-related lncRNAs (AL353804.1, AC010719.1, TNFRSF10A-AS1, AC005586.1, AL355574.1, AC009948.1, and AL161785.1) were obtained to construct a risk model for prognosis prediction in the STAD patients using Lasso regression and multivariate Cox regression analyses. The risk score was identified as an independent prognostic factor for the patients with STAD [HR = 1.315, 95% CI (1.056–1.130), $p < 0.001$] *via* multivariate Cox regression analysis. Receiver operating characteristic (ROC) curves were drawn and the area under curve (AUC) values of 1-, 3-, and 5-year overall survival (OS) were calculated to be 0.691, 0.717, and 0.723 respectively. Similar results were obtained in the validation data set. In addition, seven glycolysis-related lncRNAs were significantly enriched in the classical tumor processes and pathways including cell adhesion, positive regulation of vascular endothelial growth factor, leukocyte transendothelial migration, and JAK_STAT signaling pathway.

Conclusion: The prognostic prediction model constructed using seven glycolysis-related lncRNA could be used to predict the prognosis in patients with STAD, which might help clinicians in the clinical treatment for STAD.

KEYWORDS

glycolysis, lncRNA, prognostic model, stomach adenocarcinoma, the cancer genome atlas

Introduction

Gastric cancer, also known as stomach cancer, is a common malignant tumor of the digestive system. Its morbidity and mortality were ranked fifth and fourth, respectively, among the global malignant tumors. More than half of the new cases were reported in developing countries with poor medical and health conditions. (Sung et al., 2021). Due to difficulties in early detection and rapid progress, the 5-year overall survival rate of gastric cancer (GC) is about 25–30%. (Siegel et al., 2016). In recent years, with advancements in the diagnosis and treatment of GC, the survival rate of early-stage GC has been significantly improved but its prognosis in the patients with advanced GC is still very poor (Shen et al., 2013; Song et al., 2017; Selim et al., 2019). This has become a prominent public health issue, threatening the health of people worldwide, especially in China. Due to the poor overall prognosis and large differences in the term of prognosis among GC patients (Costa et al., 2018), it is difficult to assess its prognosis in clinical practices. Therefore, the establishment of an evaluation system with good diagnosis and prognosis screening is particularly important for the diagnosis and treatment of GC. At present, in addition to the TNM (tumor node metastasis) staging system, which is commonly used in clinical practices, many studies (Eom et al., 2015; Tonello et al., 2021; Zhang and Yu, 2021) have proposed the construction of new classification and prognosis-related prediction models. However, most of these models are based on the general data and clinical pathological data of patients, thereby having a certain lag in the evaluation of tumor prognosis as compared to molecular indicators, such as genes. In addition, these factors are not conducive to the quantitative expression of prediction results, leading to the lack of accuracy and effectiveness. With the advent of the era of precision medicine and the rapid development of gene sequencing technologies, the tumor prognosis prediction models often incorporate molecular indicators, such as genes, long non-coding RNAs (lncRNAs), and miRNAs, to improve the performance of the prediction models.

Changes in cellular metabolism are closely related to the occurrence and development of multiple tumors, one of the most prominent changes is glycolysis (Ganapathy-Kanniappan, 2018; Liu et al., 2019; Orang et al., 2019). The energy acquisition of cells is mainly derived from glycometabolism. Normal cells mainly produce ATP through oxidative phosphorylation under aerobic conditions, while in hypoxic conditions, cells obtain ATP *via* glycolysis. In 1924, Warburg proposed the "*Warburg effect*", demonstrating that the cancer tissues mainly obtain ATP through glycolysis; even in the presence of sufficient oxygen supply, they mainly use glycolysis to meet energy demand for their rapid growth. (Warburg, 1956). Aerobic glycolysis is the most basic metabolic change in the process of tumor malignancy, this phenomenon is widely present in various tumors (Chen et al., 2019; Weng et al., 2020; Zhang et al., 2020). Glycolysis promotes the proliferation of tumor cells, enhances invasiveness, and participates in tumor resistance. (Gatenby and Gillies, 2007; Akram, 2013). This phenomenon has also been found in GC (Liu et al., 2019) and indicates that aerobic glycolysis can lead to tumor progression and poor prognosis. (Gatenby and Gillies, 2004). Glycolysis can not only quickly supply energy and change the tumor microenvironment but also provides precursors or intermediates, such as nucleic acids, required for cell synthesis

(Yu et al., 2017; Hofmann, 2018), which is considered an optimized way for the oncocytic cells to respond to cellular stress. This makes the enzymes and signaling pathways related to glycometabolism potential targets for the treatment of tumors. (Gatenby and Gillies, 2007).

In the past few decades, people have made great advancements in studying the molecular mechanisms of GC (Carlomagno et al., 2017; Ye et al., 2020). However, there is still a lack of molecular markers in the treatment and prognosis assessment of GC. LncRNA, a type of RNA with ≥200 nucleotides length, has no functions on encoding the proteins. (Cabili et al., 2011). Recent studies have shown that the lncRNAs are widely distributed in the genome and participate in the regulation of chromatin modification, gene transcription, and other important physiological processes, which are closely related to the initiation and progression of the tumor, and can be used as a potential biomarker for the diagnosis and prognosis assessment of tumor (Ponting et al., 2009; Gómez-Maldonado et al., 2015). However, the mechanisms of action of glycolysis-related lncRNA in GC patients are still unclear. Furthermore, the potential values of glycolysis-related lncRNAs in the diagnosis, treatment and prognosis evaluation of GC are still needed to be explored. Therefore, a glycolysis-related lncRNA signature and a nomogram were constructed in this study to provide clinicians with a quantitative method for predicting the survival in GC patients. This might help clinicians to make accurate and personalized clinical decisions and prognostic assessments for the patients with GC.

Materials and methods

Sample data sets and data pre-processing

From the Cancer Genome Atlas (TCGA) database (https://portal.gdc.cancer.gov/), the RNA-seq data of 375 cases and clinical data of 443 cases in stomach adenocarcinoma (STAD) were obtained. In the TCGA official website, "transcriptome profiling" was selected in Data Category, "Gene Expression Quantification" was selected in Data Type, "RNA-Seq" was selected in Experimental Strategy, and "illumine" was selected in Platform. The inclusion criteria of this study were: 1) Pathological diagnosis was stomach adenocarcinoma; and 2) Patients had complete sequencing data and clinical information (gender, age, distant metastasis, lymphatic metastasis, primary tumor, TNM Stage, and survival status). In addition, when the clinical information of the patients was screened, those with a follow-up period of ≤30 days were excluded. After screening, a total of 337 STAD samples, having both the lncRNA expression and prognostic data, were included for the construction and verification of the prognostic model; among which, 296 STAD samples, having complete clinical and prognostic data, were selected to perform the univariate and multivariate Cox regression analysis.

Screening of lncRNA and identification of glycolysis-related LncRNA

First, the gene name data was used in the HUGO Gene Nomenclature Committee (HGNC, https://www.genenames.org) database to identify and isolate the lncRNA data from all the RNA-seq data sets to obtain lncRNA expression profiles. The total lncRNA expression data was normalized using log2 transformation. The glycolysis-related gene list was obtained from the Molecular Signatures Database (MSigDB) (https://www.gsea-msigdb.org/GSEA/msigdb). "Glycolysis" was used as a keyword to search for the glycolysis-related gene set, "REACTOME_GLYCOLYSIS", which was then downloaded. Then, the Pearson correlation analysis was performed to calculate the correlations between lncRNAs and glycolysis-related genes. The lncRNAs, having correlation coefficient |R (Siegel et al., 2016)| >0.3 and p-value < 0.001, were considered glycolysis-related lncRNAs. Subsequently, the co-expression network was drawn using Cytoscape (Version 3.7.1) to visualize the correlations.

Development and analysis of prognostic prediction model

First, a univariate Cox regression analysis was performed to evaluate the prognostic value of the identified glycolysis-related lncRNA. In univariate Cox regression analysis, all the glycolysis-related lncRNAs with a p-value < 0.05 were considered as related to the prognosis of STAD patients. The glycolysis-related lncRNAs with prognostic significance analysis were included to perform Lasso regression analysis. Then, the lncRNAs, which were obtained *via* Lasso regression analysis, were incorporated into a multivariate Cox regression model for the construction of a risk scoring model. The risk score for each patient was calculated using the following equation: Risk score = Coef lncRNA 1) × Expr lncRNA 1) + Coef lncRNA 2) × Expr lncRNA 2) + ... + Coef lncRNA (n) × Expr lncRNA (n). Coef value was the regression coefficient obtained through multivariate Cox regression analysis, and Expr lncRNA (n) was the expression of lncRNA (n). The patients were assigned into high- and low-risk cohorts according to the median value of risk score. Log-Rank (Mantel-Cox) test was used to compare the survival differences between the two cohorts. The survival program package in R 3.6.3 software was used to draw the survival curve of the model prognosis and compare the differences in survival between the two cohorts. SurvivalROC package in R software was used to draw the receiver operating characteristic (ROC) curve and the area under curve (AUC) value

was calculated to evaluate the sensitivity and specificity of the prognostic model.

Construction and analysis of nomogram graph

A nomogram graph was constructed to predict the survival time of patients with STAD. In order to verify the accuracy of the nomogram, the index of concordance (C-index) was calculated and calibration curves were drawn. The nomogram can provide a quantitative prediction method for clinicians and decision-makers in health-related departments. Therefore, a nomogram was constructed based on risk scores and clinicopathological information. In addition, the calibration curves for 1-, 3- and 5-year survival time were drawn concurrently. The closer the calibration curve is to the standard curve, the better the prediction model's performance. Then, the clinical data, including demographic data, pathological TNM stage, pathological tumor, node, metastasis stage and patient's risk score, were merged and those lacking accurate clinical data were deleted. In order to verify and compare the efficacy of the constructed prognostic signature with other clinical prognostic factors, a multivariate ROC curve was drawn. Furthermore, the AUCs of multiple factors, including age, gender, TNM stage, pathological grade and risk score, were calculated.

Gene Set Enrichment Analysis (GSEA) and correlation analysis

Although the usability of prognostic signature was tested for survival predictions, it was unclear how the function of glycolysis-related lncRNA would work. Therefore, the GSEA analysis, including Gene Ontology (GO) analysis and Kyoto Encyclopedia of Genes and Genomes (KEGG) pathways analysis, was performed to explore the functional enrichment of glycolysis-related lncRNAs. The top five enrichment analysis results of GO and KEGG were presented. All the RNA-seq data of patients with STAD were also assigned into the low- and high-risk cohorts according to the median value of risk score. In the first, the previously obtained risk score data and lncRNA expression data were integrated and converted into "cls" and "gct" file formats. Subsequently, these data files were imported into GSEA software (version 4.0.3) to explore significant differences in the functions of glycolysis-related lncRNA between the low- and high-risk groups. Furthermore, correlations between risk level and clinicopathological characteristics were calculated using Pearson's correlation coefficient analysis, where coefficient >0 indicated a positive correlation and coefficient <0 indicated a negative correlation.

Model verification

A total of 170 samples were randomly selected from 337 STAD samples having both the RNA-seq data of lncRNA and prognostic data to form an internal cross-validation data set, which was used to verify the constructed prediction model and evaluate its robustness. The Kaplan-Meier plots between the high- and low-risk groups, ROC curve of multiple factors including clinical information and risk score, and univariate and multivariable Cox regression analysis were performed using similar methods as described in above-mentioned section.

In addition, we performed 5-fold cross-validation to make the verification results more reliable. 337 STAD samples were divided into five cohorts where 80% of the data was used as training data and remaining 20% was used as a validation set, and then we repeat this five times so that every cohort serve as a validation set. The accuracy measures (AUC, confusion matrix, sensitivity, specificity) was reported.

This process was performed to identify consistency in the conclusions of training and verification cohorts to evaluate the robustness and reliability of the risk prognosis model.

Statistical analyses

Kaplan-Meier method was used to draw survival curve and Log-rank test was used to compare the survival curve between high-risk and low-risk cohorts. Cox regression analysis and Lasso regression analysis were performed to screen the glycolysis-related lncRNAs and clinical information that have a prognostic impact for the patients with STAD. The ROC curves were drawn to evaluate the performance of the prediction model. Univariate and multivariate Cox regression analyses were performed to recognize the predictors in clinical variables and risk scores, and then, the usability of the risk model as an independent prognostic indicator was assessed. Strawberry PERL (version 5.30.2.1) was used to process the data. All the statistical analyses in this study were performed using R software (version 4.0.2). The statistical test was two-sided, and $p < 0.05$ was considered statistically significant. The prediction with AUC >0.60 was considered to be an acceptable prediction, while the AUC >0.75 was considered to have a good predictive value.

Results

Co-expression network construction

The detailed flow chart for the prognostic predictive model construction in this study was shown in Supplementary Figure S1. A total of 14,142 lncRNAs in the TCGA-STAD data sets were extracted from the TCGA database and 72 glycolysis-related

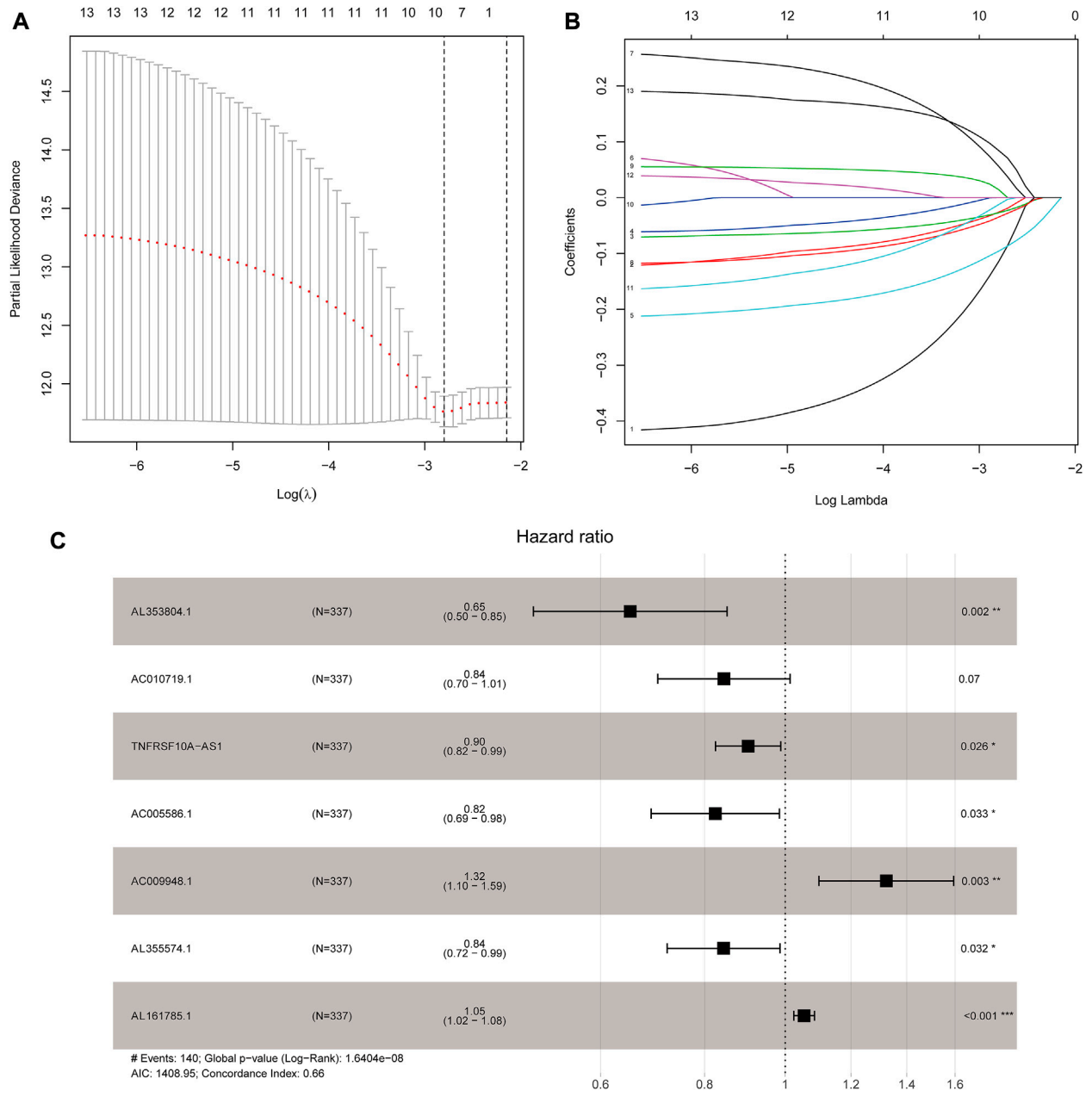

FIGURE 1
Development of the seven glycolysis-related lncRNAs signature. **(A)** Lasso coefficient values of nine glycolysis-related lncRNAs in stomach adenocarcinoma (STAD). The vertical dashed lines are at the optimal log(lambda) value. **(B)** Variables going to zero as we increase the penalty (lambda) in the objective function of the Lasso. **(C)** Results of the multivariate Cox proportional hazard model based on the nine variables; seven lncRNAs were screened to construct the signature.

genes were extracted from the GSEA-MSigDB database, among which, 70 genes were expressed in STAD (Supplementary Table S1). The co-expression network of glycolysis-related lncRNA was constructed to identify lncRNA related to glycolysis. Finally, a total of 870 lncRNAs were identified as glycolysis-related lncRNAs (|R (Siegel et al., 2016)|>0.3, and $p < 0.001$).

Construction of glycolysis-related lncRNA signature

Based on 870 glycolysis-related lncRNAs, univariate Cox regression analysis was used to screen the glycolysis-related lncRNAs having prognostic significance in the 337 cases of

TABLE 1 Multivariate Cox results of glycolysis-related lncRNAs in STAD.

lncRNA	Coefficient	HR	HR.95L	HR.95H	*p* Value
AL353804.1	−0.429	0.651	0.498	0.852	0.002
AC010719.1	−0.170	0.844	0.703	1.014	0.070
TNFRSF10A-AS1	−0.102	0.903	0.825	0.988	0.026
AC005586.1	−0.193	0.824	0.690	0.984	0.033
AC009948.1	0.280	1.323	1.098	1.594	0.003
AL355574.1	−0.170	0.843	0.721	0.986	0.032
AL161785.1	0.052	1.054	1.024	1.084	<0.001

TCGA-STAD data set. The univariate Cox regression analysis showed that there were 13 lncRNAs (AL353804.1, AC010719.1, TNFRSF10A-AS1, MAPKAPK5-AS1, AC005586.1, SREBF2-AS1, AC009948.1, AL355574.1, AL161785.1, AC084033.3. AP003392.1, AC037198.1, and AP001528.2), having significant prognostic value for STAD patients ($p < 0.05$, Supplementary Table S2). Subsequently, the Lasso regression analysis was used to avoid overfitting. After performing the Lasso regression, nine glycolysis-related lncRNAs were identified (Figure 1; Supplementary Table S3). Then, these lncRNAs were subjected to multivariate Cox regression analysis and a prognostic signature with seven glycolysis-related lncRNAs was developed. Among them, five lncRNAs (AL353804.1, AC010719.1, TNFRSF10A-AS1, AC005586.1, and AL355574.1) were identified as favorable prognostic factors, while the remaining two lncRNAs (AC009948.1 and AL161785.1) were presented as poor prognostic factors (Table 1). Subsequently, these seven lncRNAs were used to develop a glycolysis-related lncRNAs signature. Risk score = (-0.42868* AL353804.1) + (-0.16952* AC010719.1) + (-0.10245* TNFRSF10A-AS1) + (-0.19337* AC005586.1) + (0.279,944* AC009948.1) + (-0.17044* AL355574.1) + (0.052446* AL161785.1). In addition, a co-expression network of prognostic-related glycolytic lncRNAs was constructed (Figure 2). Simultaneously, a combined Sankey diagram was drawn based on 25 glycolysis-related genes, seven glycolysis-related lncRNAs and their risk conditions (Figure 3).

Glycolysis-related lncRNA signature for prognosis prediction in STAD

The risk score of the glycolysis-related lncRNA risk model was calculated using the above risk score formula (Table 2). Survival program package in R software was used to analyze survival differences based on the patient's risk score and the risk score curve, survival status map, and heat map based on the expression level of seven lncRNAs were drawn using the R programming language. Kaplan-Meier plot showed that the risk score was significantly correlated with overall survival (OS) of patients with STAD. As compared to the low-risk cohort, the OS of the high-risk cohort was significantly shorter ($p < 0.001$, Log-rank test) (Figure 4). With the increase in risk score, the number of patients' deaths in the high-risk cohort was significantly higher than that in the low-risk cohort, indicating the poor OS of STAD patients in the high-risk cohort (Figure 5). The above results showed that the risk score was significantly correlated with the OS of patients with STAD and exhibited a significant impact on the prognosis in STAD. It was suggested that the risk signature might better predict the survival and prognosis in STAD.

Clinical value and significance of the glycolysis-related lncRNA signatures

The risk score, lymph node status and pathological TNM stage were prognostic indicators identified by univariate Cox regression analysis. The Cox regression result of risk score are as follow: [HR = 1.315, 95% CI (1.056–1.130), $p < 0.001$], (Figure 6A). When the influence of other factors (gender, age, and tumor stage) was controlled and eliminated, the risk score was still identified as an independent prognostic indicator according to multivariate Cox regression analysis [HR = 1.092, 95% CI (1.054–1.131)), $p < 0.001$], (Table 2; Figure 6B). Subsequently, the survivalROC program package was used to draw the ROC curve of the risk model and evaluate its sensitivity and specificity. The results showed that the calculated AUC values of the prognostic signatures for 1-, 3-, and 5-year survival time were 0.691, 0.717, and 0.723, respectively (Figure 6C). Furthermore, the risk score, TNM stage, and age were used to construct a nomogram. As shown in Figure 7A, the risk score was the most important contributing factor to the 1-, 3-, and 5-year OS in STAD. The calculated C-index of the prediction model was 0.651 (95% CI: 1.056–1.135). The 5-year AUC of risk score was 0.703, which was higher than age (AUC = 0.571), gender (AUC = 0.540), TNM stage (AUC = 0.592), tumor stage (AUC = 0.561), node stage (AUC = 0.569), and distal metastasis stage (AUC = 0.521) (Figure 7B). The correlation analyses found that the level of risk score was not significantly correlated with age, gender, TNM staging, etc. (Table 3).

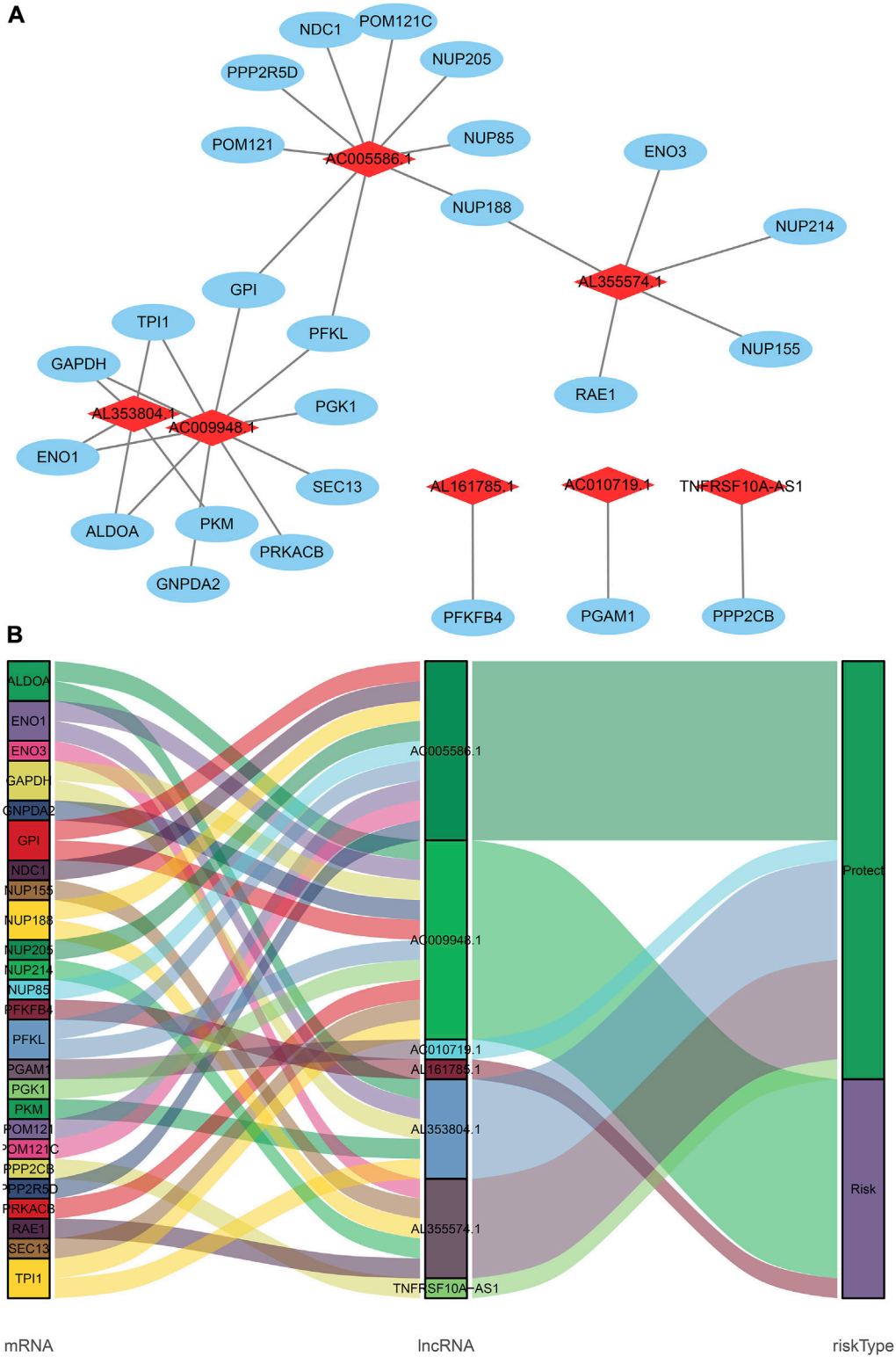

FIGURE 2
The coexpression network and Sankey diagram of prognostic glycolysis-related lncRNAs. **(A)** The coexpression network between prognostic glycolysis-related lncRNAs and glycolysis-related genes in STAD. Red diamond nodes represent prognostic glycolysis-related lncRNAs, and the sky-blue oval nodes represent glycolysis-related genes. The coexpression network was visualized using Cytoscape 3.7.1 software. **(B)** Sankey diagram showed the association between prognostic glycolysis-related lncRNAs, glycolysis--related genes, and risk types.

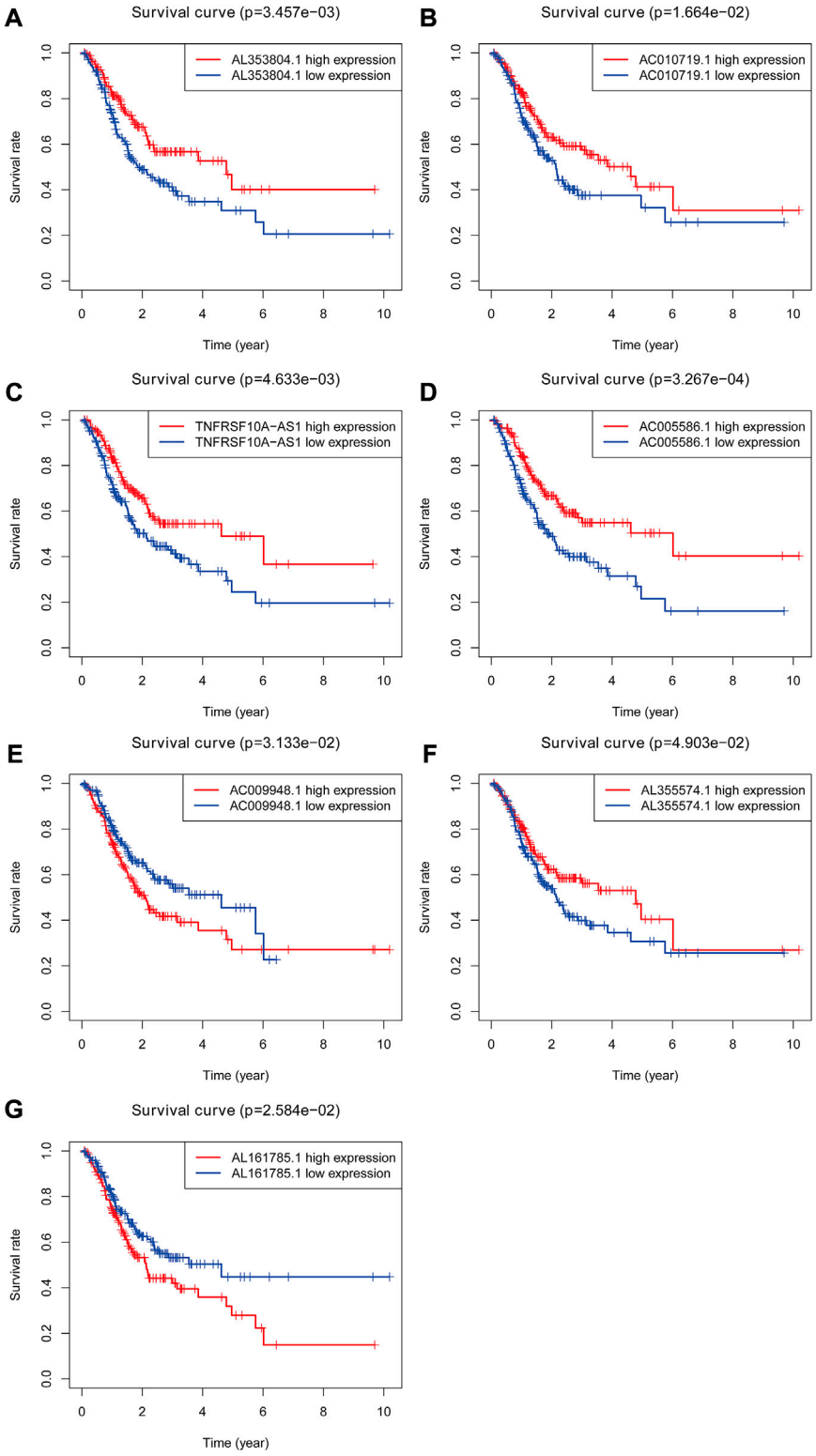

FIGURE 3
The Kaplan-Meier Survival curve of seven prognostic glycolysis-related lncRNAs. Two glycolysis-related lncRNAs (AC009948.1 and AL161785.1) were independent unfavorable factors. Five lncRNAs (AL353804.1, AC010719.1, TNFRSF10A-AS1, AC005586.1 and AL355574.1) were independent beneficial factors for STAD.

TABLE 2 Multivariate Cox regression based on clinical characteristics and risk scores in STAD.

lncRNA	B	SE	Z	HR	HR.95L	HR.95H	*p* Value
Age	0.027	0.010	2.753	1.027	1.008	1.047	0.006
Gender	0.277	0.201	1.374	1.319	0.889	1.956	0.169
Stage	0.256	0.211	1.215	1.292	0.855	1.952	0.224
T	0.088	0.154	0.573	1.092	0.808	1.476	0.567
M	0.243	0.429	0.566	1.275	0.550	2.955	0.571
N	0.147	0.117	1.257	1.159	0.921	1.458	0.209
Risk Score	0.088	0.018	4.905	1.092	1.054	1.131	<0.001

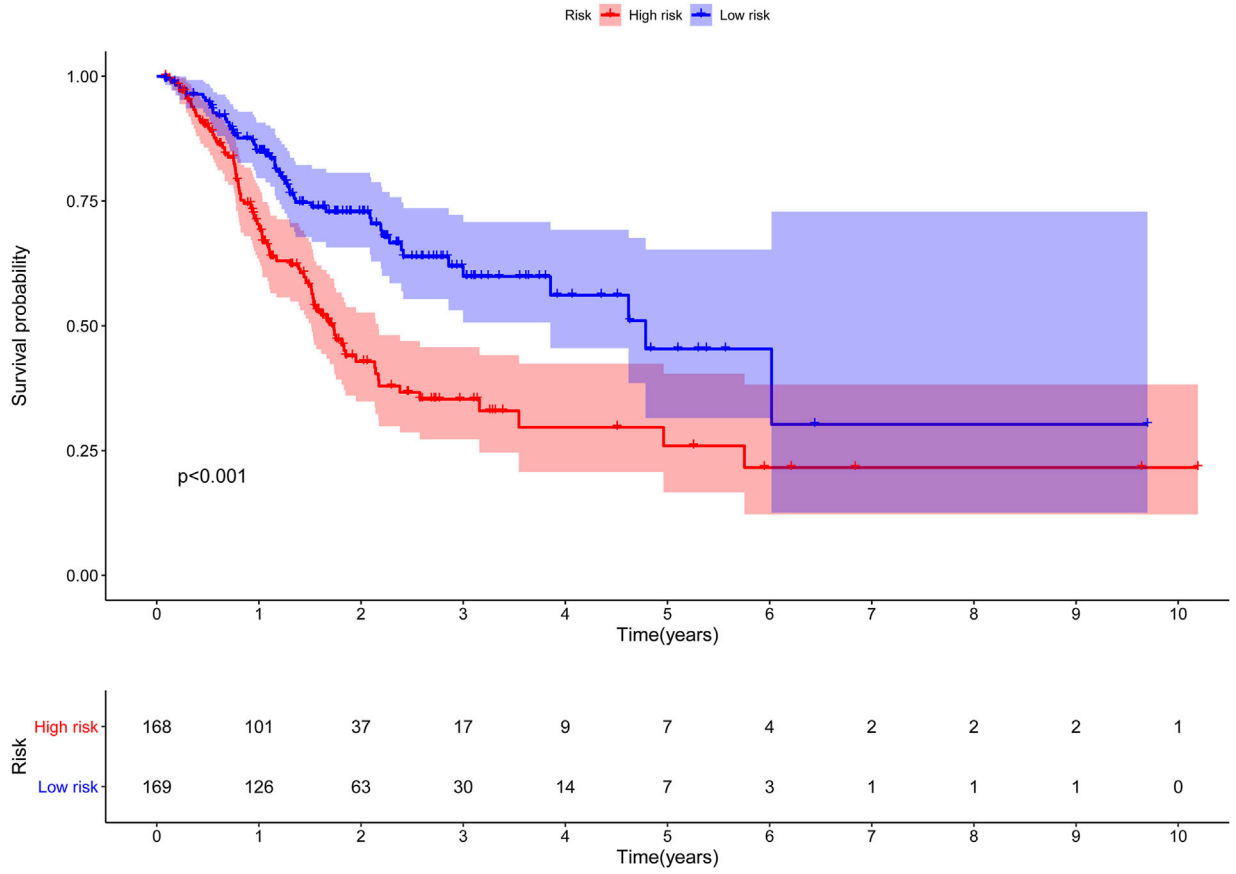

FIGURE 4
The Kaplan-Meier survival curve of risk score based on seven glycolysis-related lncRNAs.

GSEA analysis

In order to explore the functional differences in the glycolysis-related lncRNAs between the high- and low-risk groups, GO and KEGG enrichment analyses were performed using GSEA version 4.0.3, which are shown in Figures 8A,B. A total of 3009 GO entries and 95 KEGG pathways were obtained. In GO analysis, the enrichment results were mainly concentrated on the regulation of inositol phosphate biosynthetic process and vasculature development, activation of phospholipase C activity, positive regulation of vascular endothelial growth factor

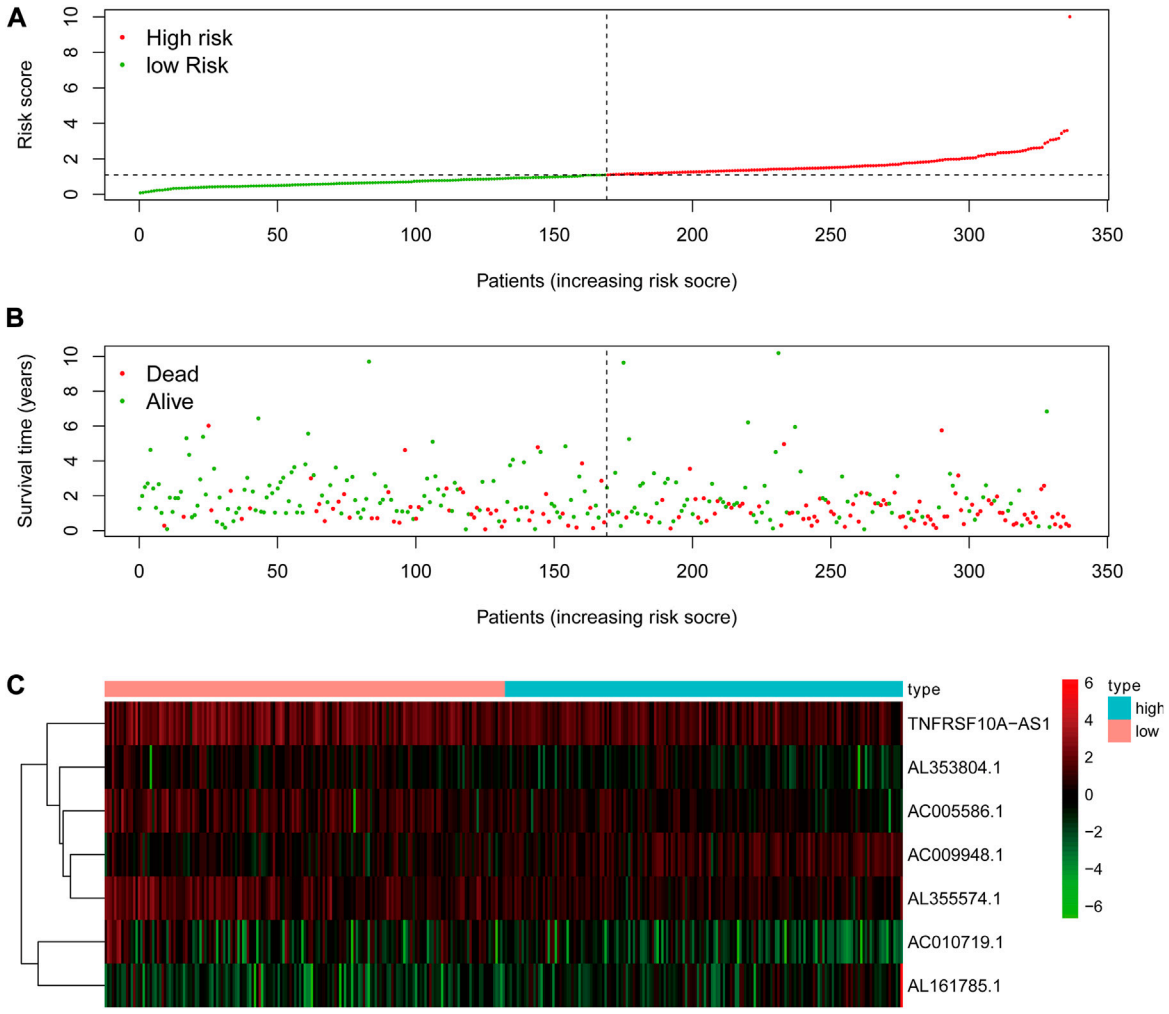

FIGURE 5
The analysis of glycolysis-related lncRNA signature for patients in STAD. **(A)** The risk score between the high-risk group and low-risk group. **(B)** The survival status of the high-risk group and the low-risk group in STAD patients. **(C)** Heat map of seven glycolysis-related lncRNAs' expression. The color from green to red reveals a rising tendency from low to high expression levels.

production, vascular endothelial growth factor production, etc. (Figure 8A). KEGG pathways analysis showed that the glycolysis-related lncRNAs were mainly involved in cell adhesion molecules (CAMs), extracellular matrix (ECM) receptor interaction, calcium signaling pathway, leukocyte transendothelial migration, and JAK_STAT signaling pathway (Figure 8B). In addition, it was also found that these enrichment results were related to important biological processes and functional pathways in the initiation and progression of the tumor. For instance, the regulation of vasculature development and vascular endothelial growth factor production, cell adhesion, leukocyte transendothelial migration, and JAK_STAT signaling pathway were closely related to the proliferation, invasion, and metastasis of tumor.

Verification in the internal verification set

The same Coef value was used to further verify the above results in the validation cohort (n = 170). Consistent with the results of the training cohort, the OS of high-risk patients was shorter than that of the low-risk STAD patients (p = 0.003) (Figure 9). The calculated AUC values of the risk model based on internal validation cohort for 1-, 3-, and 5-year survival times were 0.686, 0.699, and 0.730, respectively (Figure 8). The univariate and multivariate Cox regression analyses indicated that the risk score also was an independent predictor, affecting the prognosis of STAD ($p < 0.001$ and $p = 0.012$, respectively). In addition, the results of 5-fold cross-validation are shown in Figure 10, with similar results to the previous training dataset in most cohorts. The mean and standard deviation of the

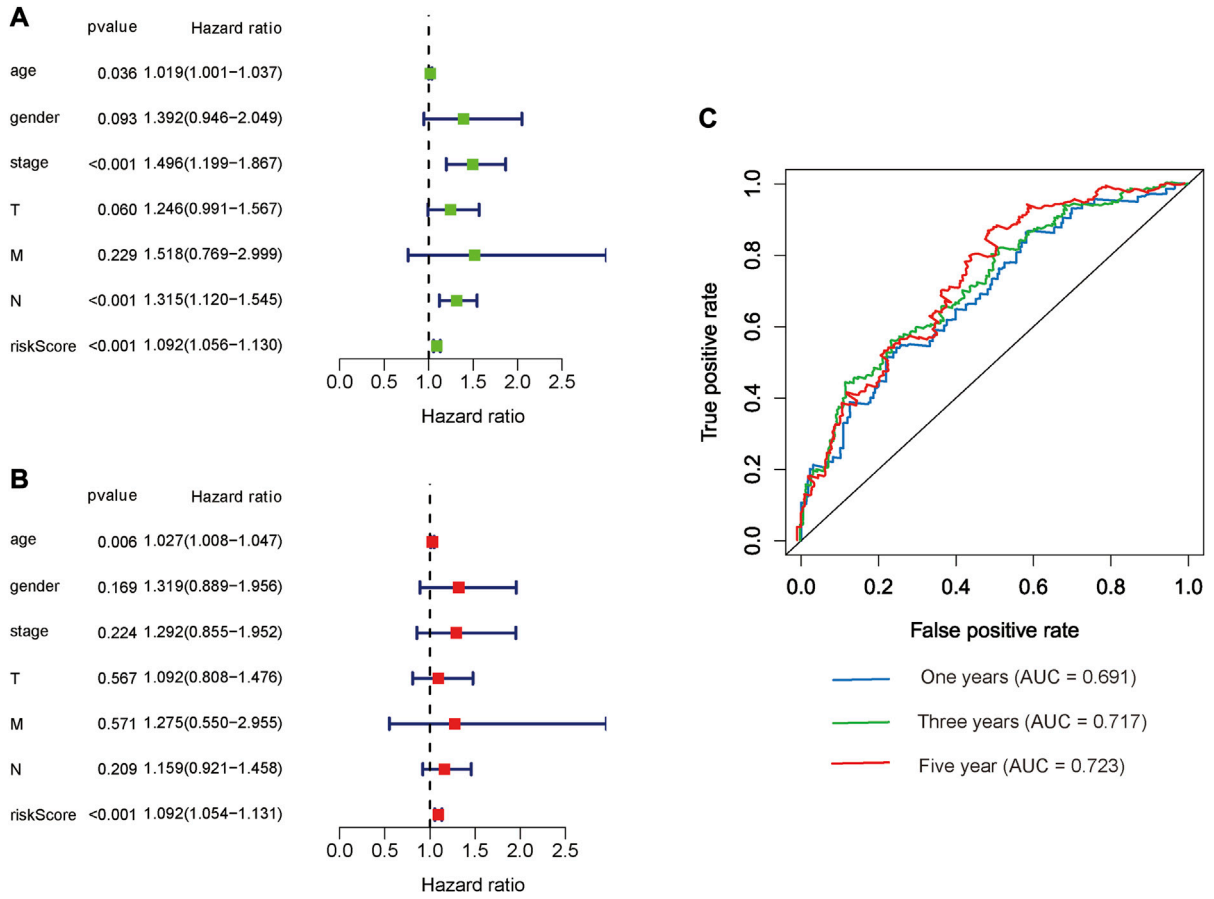

FIGURE 6
Prognostic indicators based on glycolysis-related lncRNAs showed great predictive performance. The forest plots for univariate **(A)** and multivariate **(B)** Cox regression analysis in STAD. **(C)** The areas under the ROC curve about 1-year, 3-year, and 5-year OS.

sensitivity and specificity in the cross-validated training dataset were 0.629 ± 0.012, 0.594 ± 0.010 respectively, and the sensitivity and specificity in the cross-validated training dataset were 0.625 ± 0.046, 0.594 ± 0.040 respectively.

Discussion

The occurrence and development of tumors are closely related to abnormal cellular metabolism. Changes in energy metabolism promote the growth and proliferation of tumor cells and have been considered as emerging cancer biomarkers (Hanahan and Weinberg, 2011; Yuan et al., 2016). In 1924, Warburg discovered the abnormalities between cancerous and normal cells and showed that even under aerobic conditions, the cancer cells could maintain a higher glycolysis rate than the neighboring normal tissues, known as the "*Warburg effect*" (Warburg, 1956; Gatenby and Gillies, 2004). This phenomenon has been widely found in various tumor tissues, including GC (Liu et al., 2019), indicating that aerobic glycolysis could lead to tumor progression and poor prognosis (Luo et al., 2020; Xia et al., 2021). LncRNA is a type of non-coding RNA molecules that regulates the growth, development, and survival of cancer cells and plays an important role in multiple aspects in the initiation and progression of tumors. Therefore, the lncRNAs are considered as a novel biomarker for tumor diagnosis and prognosis (Kong et al., 2016). Many previous studies have focused on the function of specific glycolysis-related genes or prognostic signature (Liu et al., 2019; Luo et al., 2020) but there is a lack of systematic studies on glycolysis-related lncRNA as a risk signature for predicting the survival time of patients with GC. Therefore, it is necessary to construct the glycolysis-related lncRNA risk signature for the prognosis prediction in STAD, which should fulfill the deficiency of the traditional TNM stage in predicting the individualized prognosis of patients.

In this study, a total of seven glycolysis-related lncRNAs (AL353804.1, AC010719.1, TNFRSF10A-AS1, AC005586.1, AL355574.1, AC009948.1, and AL161785.1) with prognostic

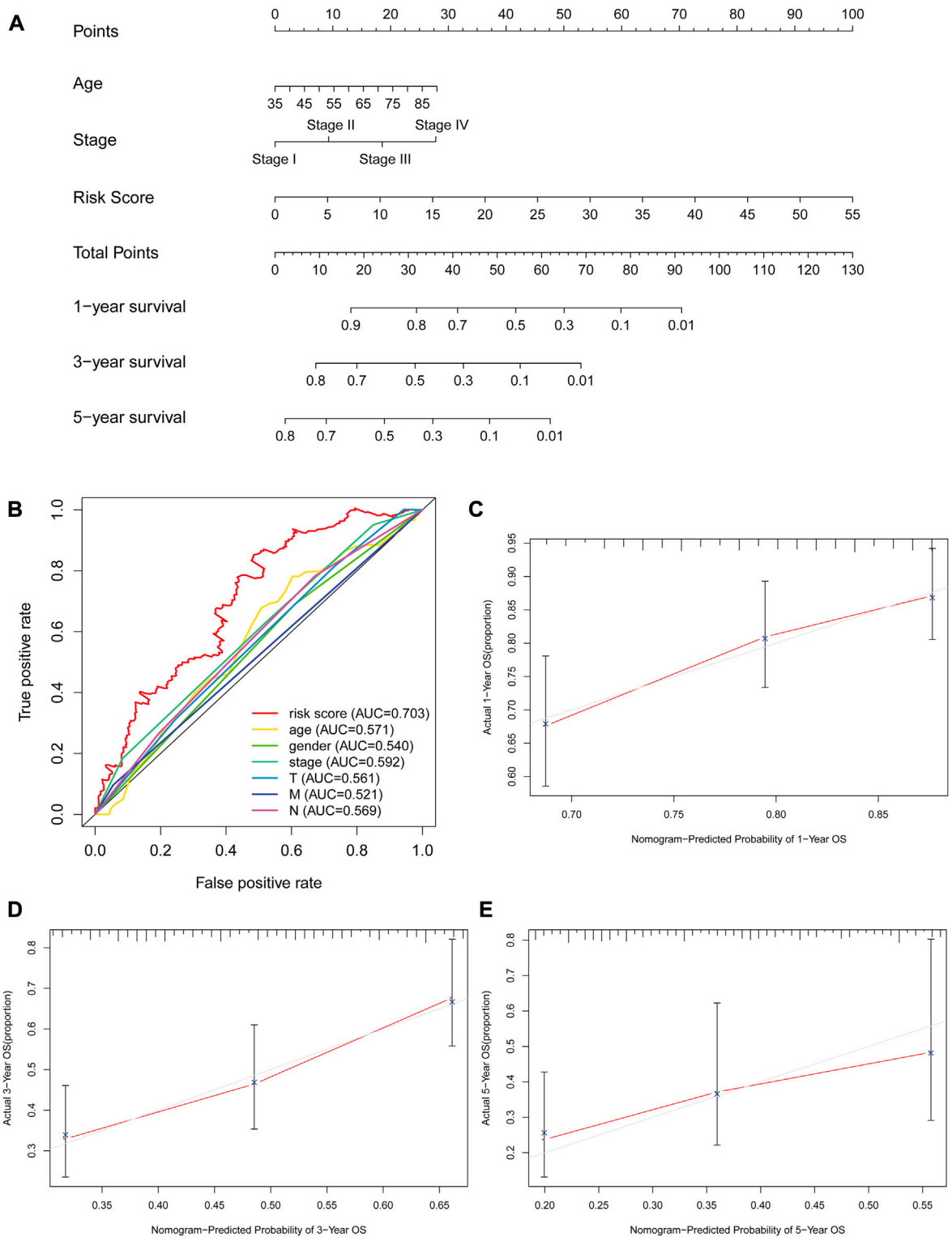

FIGURE 7
The evaluation of prognostic models based on seven glycolysis-related lncRNAs. **(A)** The nomogram of 1-, 3- and 5-year OS based on risk score, age, and TNM stage. **(B)** The ROC curves analysis based on risk score and the clinicopathologic parameters; **(C–E)** The calibration plots of 1-, 3- and 5-year OS for evaluating the concordance between the predicted and the standard OS for the prognosis model. The closer the calibration curve (red line) is to the standard curve (grey line), the better the prediction model's performance.

TABLE 3 Clinical influences of risk score signature for TCGA-STAD data.

Clinical	Group	*n*	Risk score		*t*	*P*
			Mean	SD		
Age	>60	194	1.35	3.613	0.354	0.724
	≤60	102	1.256	0.649		
Gender	0	110	1.066	0.636	-1.444	0.15
	1	186	1.466	3.681		
Stage	I-II	135	1.454	4.317	0.669	0.505
	III-IV	161	1.203	0.615		
T	1-2	74	1.781	5.806	0.915	0.363
	3-4	222	1.163	0.602		
M	0	277	1.314	3.042	-0.197	0.844
	1	19	1.362	0.688		
N	0	90	1.013	0.586	-1.734	0.084
	1-3	206	1.45	3.506		

univariate and multivariate Cox regression analyses showed that it was related to the prognosis in GC patients. These results suggested that the lncRNA TNFRSF10A-AS1 might be a common prognostic target for gastrointestinal tumors or multiple tumors and might be involved in various biological processes, such as autophagy and glycolysis. These findings also suggested that the TNFRSF10A-AS1 might participate in a variety of biological processes, affecting the prognosis of various tumors, and is worthy of further exploration in subsequent studies with good research potential. Fu et al. (FU et al., 2020) found that AC009948.1 was co-expressed with HSD11B2, which is related to the progression and prognosis of melanoma as demonstrated by mining the data of melanoma in TCGA. The GSEA analysis suggested that HSD11B2 was related to multiple cancer-related genes and pathways, including cytosolic DNA-sensing pathway, JAK_STAT signaling pathway, T-cell receptor signaling pathway, and Toll-like receptor signaling pathway. For the remaining five glycolysis-related lncRNAs (AL353804.1, AC010719.1,

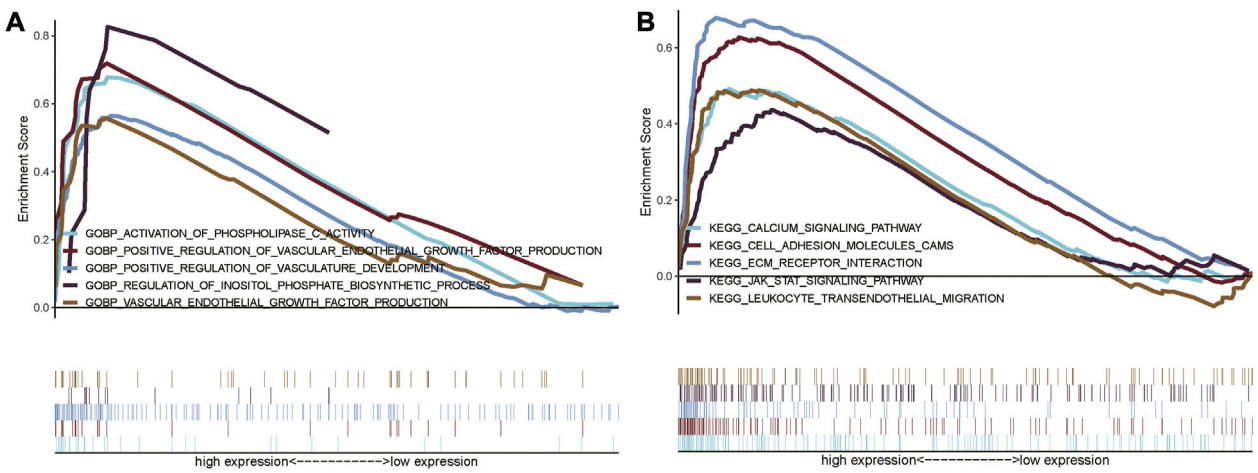

FIGURE 8
Gene set enrichment analysis showing the GO and KEGG enrichment between the high-risk and low-risk group. **(A)** GSEA for GO enrichment analysis; **(B)** GSEA for KEGG enrichment analysis.

significance in STAD were identified using Lasso and Cox regression analyses. Among them, the two glycolysis-related LncRNAs (TNFRSF10A-AS1 and AC009948.1) have been reported in previous studies (FU et al., 2020; Wei et al., 2020). In a study by Wei et al. (Xia et al., 2021), TNFRSF10A-AS1 was identified as an autophagy-related lncRNA associated with the poor prognosis of colorectal cancer, and along with other seven autophagy-related lncRNAs, it constructed a prognostic signature for colorectal cancer, which was used to predict the prognosis in colorectal cancer patients. TNFRSF10A-AS1 was identified as a lncRNA related to glycolysis in this study. The AC005586.1, AL355574.1, and AL161785.1), there were no published studies on their prognostic effects in cancers. Therefore, further studies are needed to explore the effects of these glycolysis-related lncRNAs on the prognosis of STAD patients.

Based on the risk signature, containing seven glycolysis-related lncRNAs, the prognosis of STAD could be significantly predicted. The AUC of 1-, 3- and 5-year OS were 0.691, 0.717, and 0.723 respectively. Similar results were obtained in the validation cohort, where the OS of the high-risk group was worser than that of the low-risk group, and the ROCs for 1-,

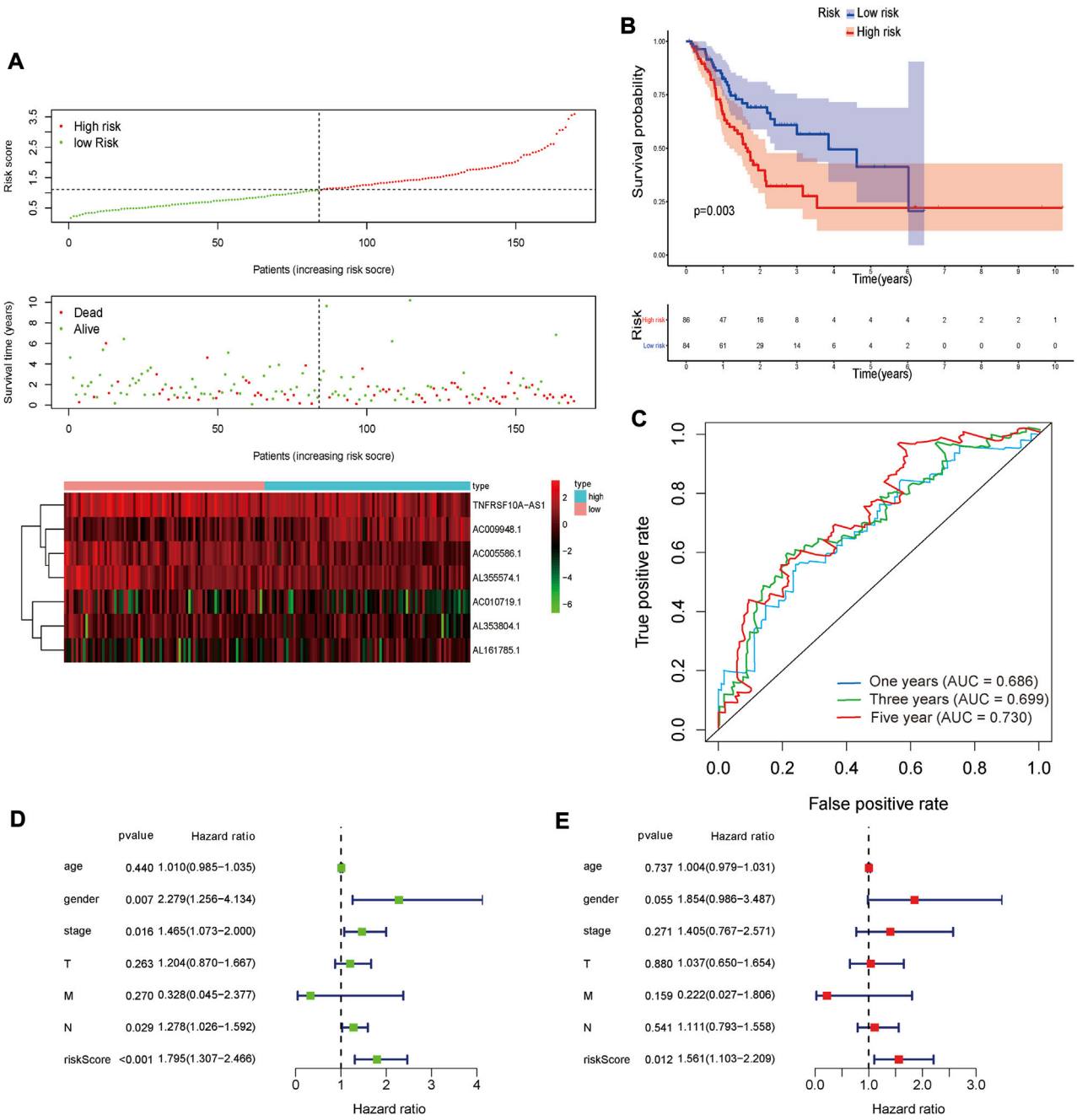

FIGURE 9
The result of validation cohort based on seven glycolysis-related lncRNAs in STAD. **(A)** The risk score, survival status and heat map of seven glycolysis-related lncRNAs between the high-risk and the low-risk group in validation cohort. **(B)** Kaplan-Meier survival curve of risk score in validation cohort. **(C)** The areas under the ROC curve about 1-, 3-, and 5-year in validation cohort. **(D,E)** The forest plots for univariate **(D)** and multivariate **(E)** Cox regression analysis in validation cohort.

3- and 5-year OS were 0.686, 0.699, and 0.730 respectively. Compared with other GC-related lncRNA signatures (Wang (Wang et al., 2020) LncSig' AUC = 0.589, Zhang (Zhang et al., 2019) LncSig' AUC = 0.536 and Han (Han et al., 2021) LncSig' AUC = 0.618), our glycolysis-related lncRNA signature performed better in prognosis prediction in TCGA-STAD datasets. These results indicated that this prognostic risk signature had a certain potential value for predicting prognosis in STAD patients. The risk score based on seven glycolysis-related lncRNAs could be used as independent

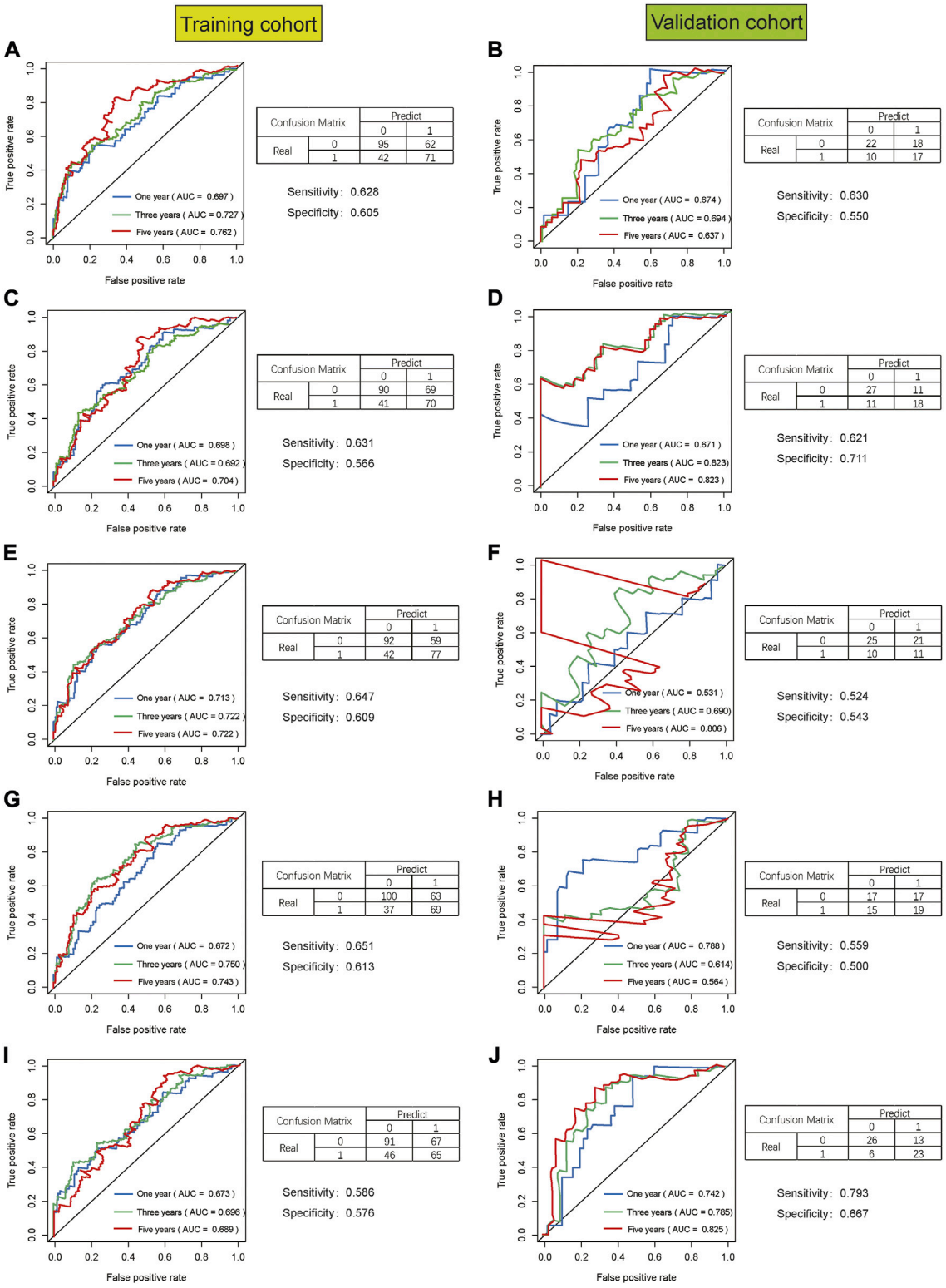

FIGURE 10
The result of 5-fold cross-validation based on seven glycolysis-related lncRNAs in STAD. AUC, confusion matrix, sensitivity and specificity were showed in each cross-validation cohort, results of training cohort on the left and validation cohort on the right in figure. **(A,B)**, **(C,D)**, **(E,F)**, **(G,H)**, **(I,J)** are the results from the first cross-validation to the fifth cross-validation.

prognostic indicators for the STAD patients through univariate and multivariate Cox regression analysis. Age and TNM stage were extracted from the training cohort to draw a concise nomogram, which was used to predict the prognosis of STAD patients. Besides, there was a good convergence between the calibration curve and standard curve. According to the results of the C-index, ROC, and calibration curve, the nomogram exhibited high discrimination and accuracy, which might become a novel potential predictive tool to provide individualized predictions in patients with GC.

Finally, although the usability of this signature in survival prediction was tested, the functions of glycolysis-related lncRNA were still unclear. Therefore, GSEA analysis was performed to explore functional differences between the high-risk and low-risk cohorts. The results of functional enrichment analysis showed that the most important pathways among these predicted glycolysis-related lncRNAs in KEGG analysis included cell adhesion, leukocyte transendothelial migration, JAK_STAT and other tumor-related classical pathways. These results could help explore and understand the mechanisms of glycolysis-related lncRNA in affecting the prognosis of STAD. Tumor invasion and metastasis are a continuous and complex process and the adhesion of tumor cells is closely related to the migration and metastasis of tumor cells. As compared to healthy tissues, tumor cells carry out glycolysis (*Warburg effect*) not only under hypoxic conditions but also in normoxic conditions, decreasing the extracellular pH (acidosis) due to increased glycolysis. As shown in a study by Hüsing et al. (Hüsing et al., 2021), after incubation at pH 6.6, the cell adhesion and migration abilities in AT1 prostate cancer cells increased by 75% and 100%, respectively, which increased lung metastases in rats. These results showed that the extracellular pH had an important effect on the migration and adhesion of tumor cells.

A previous study has shown that the JAK-STAT signal transduction pathway, widespread in humans, is related to glucose metabolism (Rastogi et al., 2007). JAK-STAT signal activation can reduce glucose metabolism by driving the expression of pyruvate dehydrogenase (PDH) kinase, which is also involved in the expression of multiple lncRNAs. The down-regulation of non-coding RNA ceruloplasmin (NRCP), identified as a highly expressed lncRNA in ovarian cancer, can lead to increased apoptosis, decreased cell proliferation, and inhibition of glycolysis (Rupaimoole et al., 2015). In addition, the lncRNA-nuclear paraspeckle assembly transcript 1 (NEAT1) is highly expressed in GC; the down-regulation of NEAT1 can inhibit the growth of GC cells and participate in the endogenous competition of miR-506/STAT3 to regulate the carbohydrate metabolism pathway in GC (Rupaimoole et al., 2015).

This study still had some limitations too. First of all, the data source of this study was single with not large sample size. Therefore, the results of the analyses might have certain deviations. Secondly, this study was a retrospective study with the inherent limitations of a retrospective study. Therefore, more prospective studies are needed to prove the predictive performance of this prognostic risk signature. Third, the validation data set of the prediction model was randomly selected as a part of the STAD samples and only internal cross-validation was carried out. We performed 5-fold cross-validation to further validate the predictive model due to lack of suitable external data for validation, but two cohorts with unsatisfactory results appeared in the validation dataset during 5-fold cross-validation (Figures: 10F and 10H). We compared the datasets in 10F and 10H with the other datasets of 10B, 10D, and 10J, respectively, and found that there were no significant differences in gender, age, tumor stage, etc. Thus, we supposed that the poor outcomes of 10F and 10H might be related to the small sample size. Therefore, further validation in other independent cohorts is necessary. Fourth, further experiments are needed to explore the potential mechanism of the lncRNAs included in the prediction model that has not been confirmed by functional experiments in the prognosis of STAD. Despite these limitations, our signature was the first prognostic risk signature based on glycolysis-related lncRNAs. In addition, the nomogram would provide clinicians with a quantitative method for predicting the survival time in STAD, which could be easily performed using Polymerase Chain Reaction (PCR) to distinguish the patients with poor prognosis from all the patients. In this way, the model might facilitate gastrointestinal oncologists to adopt a clinically individualized treatment plan. At the same time, the nomogram contained objective indicators, which could reduce differences among the observers and make the prediction of survival time more accurate.

Conclusion

In conclusion, a seven glycolysis-related lncRNA signature has been successfully developed and verified for predicting the survival time of STAD patients. This model was used to distinguish the patients with different risks and was identified as a significant independent factor for STAD. As compared to other common prognostic factors, this prognostic signature was proved to be better. These seven glycolysis-related lncRNAs and their risk signature might act as molecular biomarkers and therapeutic targets for STAD. In addition, the nomogram with high discrimination and accuracy might provide clinicians with a novel and quantitative tool to predict the survival time in STAD patients. This model might facilitate clinicians to adopt a clinically individualized treatment plan. However, a prospective, multi-center, large-scale study is required to confirm these results.

Data availability statement

The datasets presented in this study can be found in online repositories. The names of the repository/repositories and accession number(s) can be found in the article/ Supplementary Material.

Author contributions

Study concept and design: TL, YJ, and MO. Developed the methodologies: TL, YL, and KW. Contributed to the acquisition of data: YZ and ZL Performed the analysis and interpreted the data: YL, WL, and KW. Discussed the results and wrote the paper: TL, YL, and WL. Statistical analysis: YJ, YZ, and ZL. Corrected and revised manuscript: YJ and MO.

Funding

This work was supported by grants from the 2022 Guangdong Province Basic and Applied Basic Research Fund Project (No. 2022A1515012315); Southern Medical University Shunde Hospital Clinical Research Startup Program (No. CRSP2022009); the 2022 Beijing Science and Technology Medical Development Foundation (No. KC2021-JX-0186-94); the 2022 Wu Jieping Medical Foundation Clinical Research Special Fund Project (No. 320.6750.2021-22-31); Southern Medical University Shunde Hospital Scientific Research Initiative Project (No. SRSP2021035); the 2021 Special Innovation Project of Guangdong Provincial Department of Education (No. 2021KTSCX015); In-depth promotion of the innovation-driven assistance project in Foshan City (No. 2021043); The 2018 Foshan City Outstanding Young Medical Talent Training Project (No. 600009); 2020 Shunde District Competition Support Talent Project (no serial number); 2021 Foshan Engineering Technology Research Center Plan (no serial number); Guangdong Medical Science and Technology Research Fund Project (No. A2019302); National Natural Science Foundation of China, National Natural Science Youth Fund Project (No. 81802879); Southern Medical University Scientific Research Startup Plan (No. PY2018N110); and Foshan City 14th Five-Year Key Specialized Project (no serial number).

Conflict of interest

The authors declare that the research was conducted in the absence of any commercial or financial relationships that could be construed as a potential conflict of interest.

Publisher's note

Supplementary material

The Supplementary Material for this article can be found online at: https://www.frontiersin.org/articles/10.3389/fgene.2022.794621/full#supplementary-material

References

Akram, M. (2013). Mini-review on glycolysis and cancer. *J. Canc Educ.* 28 (3), 454–457. doi:10.1007/s13187-013-0486-9

Cabili, M. N., Trapnell, C., Goff, L., Koziol, M., Tazon-Vega, B., Regev, A., et al. (2011). Integrative annotation of human large intergenic noncoding RNAs reveals global properties and specific subclasses. *Genes Dev.* 25 (18), 1915–1927. doi:10.1101/gad.17446611

Carlomagno, N., Incollingo, P., Tammaro, V., Peluso, G., Rupealta, N., Chiacchio, G., et al. (2017). Diagnostic, predictive, prognostic, and therapeutic molecular biomarkers in third millennium: A breakthrough in gastric cancer. *Biomed. Res. Int.* 2017, 7869802. doi:10.1155/2017/7869802

Chen, F., Chen, J., Yang, L., Liu, J., Zhang, X., Zhang, Y., et al. (2019). Extracellular vesicle-packaged HIF-1α-stabilizing lncRNA from tumour-associated macrophages regulates aerobic glycolysis of breast cancer cells. *Nat. Cell Biol.* 21 (4), 498–510. doi:10.1038/s41556-019-0299-0

Costa, N. R., Gil da Costa, R. M., and Medeiros, R. (2018). A viral map of gastrointestinal cancers. *Life Sci.* 199, 188–200. doi:10.1016/j.lfs.2018.02.025

Eom, B. W., Ryu, K. W., Nam, B. H., Park, Y., Lee, H. J., Kim, M. C., et al. (2015). Survival nomogram for curatively resected Korean gastric cancer patients: Multicenter retrospective analysis with external validation. *PloS one* 10 (2), e0119671. doi:10.1371/journal.pone.0119671

Fu, H., Tang, Y., and Ding, Y. (2020). Analysis of HSD11B2 as a prognostic marker in Melanoma via TCGA data mining. *Res. Square* 7, 1–18.

Ganapathy-Kanniappan, S. (2018). Molecular intricacies of aerobic glycolysis in cancer: Current insights into the classic metabolic phenotype. *Crit. Rev. Biochem. Mol. Biol.* 53 (6), 667–682. doi:10.1080/10409238.2018.1556578

Gatenby, R. A., and Gillies, R. J. (2007). Glycolysis in cancer: A potential target for therapy. *Int. J. Biochem. Cell Biol.* 39 (7-8), 1358–1366. doi:10.1016/j.biocel.2007.03.021

Gatenby, R. A., and Gillies, R. J. (2004). Why do cancers have high aerobic glycolysis? *Nat. Rev. Cancer* 4 (11), 891–899. doi:10.1038/nrc1478

Gómez-Maldonado, L., Tiana, M., Roche, O., Prado-Cabrero, A., Jensen, L., Fernandez-Barral, A., et al. (2015). EFNA3 long noncoding RNAs induced by hypoxia promote metastatic dissemination. *Oncogene* 34 (20), 2609–2620. doi:10.1038/onc.2014.200

Han, C., Zhang, C., Wang, H., Li, K., and Zhao, L. (2021). Angiogenesis-related lncRNAs predict the prognosis signature of stomach adenocarcinoma. *BMC cancer* 21 (1), 1312. doi:10.1186/s12885-021-08987-y

Hanahan, D., and Weinberg, R. A. (2011). Hallmarks of cancer: The next generation. *Cell* 144 (5), 646–674. doi:10.1016/j.cell.2011.02.013

Hofmann, P. (2018). Cancer and exercise: Warburg hypothesis, tumour metabolism and high-intensity anaerobic exercise. *Sports (Basel)* 6 (1). doi:10.3390/sports6010010

Hüsing, T., Lange, L., Rauschner, M., Riemann, A., and Thews, O. (2021). Functional impact of acidosis-regulated MicroRNAs on the migration and adhesion of tumor cells. *Adv. Exp. Med. Biol.* 1269, 151–155. doi:10.1007/978-3-030-48238-1_24

Kong, X. Z., Hu, S. S., Sun, Z., Zuo, L. H., Kang, J., Zhu, Z. F., et al. (2016). Regulation of aerobic glycolysis by long non-coding RNAs in cancer. *Biochem. biophysical Res. Commun.* 479 (1), 28–32. doi:10.1016/j.bbrc.2016.09.007

Liu, Y., Zhang, Z., Wang, J., Chen, C., Tang, X., Zhu, J., et al. (2019). Metabolic reprogramming results in abnormal glycolysis in gastric cancer: A review. *Ott* Vol. 12, 1195–1204. doi:10.2147/ott.s189687

Luo, T., Du, Y., Duan, J., Liang, C., Chen, G., Jiang, K., et al. (2020). Development and validation of a scoring system based on 9 glycolysis-related genes for prognosis prediction in gastric cancer. *Technol. Cancer Res. Treat.* 19, 1533033820971670. doi:10.1177/1533033820971670

Orang, A. V., Petersen, J., McKinnon, R. A., and Michael, M. Z. (2019). Micromanaging aerobic respiration and glycolysis in cancer cells. *Mol. Metab.* 23, 98–126. doi:10.1016/j.molmet.2019.01.014

Ponting, C. P., Oliver, P. L., and Reik, W. (2009). Evolution and functions of long noncoding RNAs. *Cell* 136 (4), 629–641. doi:10.1016/j.cell.2009.02.006

Rastogi, S., Banerjee, S., Chellappan, S., and Simon, G. R. (2007). Glut-1 antibodies induce growth arrest and apoptosis in human cancer cell lines. *Cancer Lett.* 257 (2), 244–251. doi:10.1016/j.canlet.2007.07.021

Rupaimoole, R., Lee, J., Haemmerle, M., Ling, H., Previs, R. A., Pradeep, S., et al. (2015). Long noncoding RNA ceruloplasmin promotes cancer growth by altering glycolysis. *Cell Rep.* 13 (11), 2395–2402. doi:10.1016/j.celrep.2015.11.047

Selim, J. H., Shaheen, S., Sheu, W. C., and Hsueh, C. T. (2019). Targeted and novel therapy in advanced gastric cancer. *Exp. Hematol. Oncol.* 8, 25. doi:10.1186/s40164-019-0149-6

Shen, L., Shan, Y. S., Hu, H. M., Price, T. J., Sirohi, B., Yeh, K. H., et al. (2013). Management of gastric cancer in asia: Resource-stratified guidelines. *Lancet. Oncol.* 14 (12), e535–e547. doi:10.1016/s1470-2045(13)70436-4

Siegel, R. L., Miller, K. D., and Jemal, A. (2016). Cancer statistics, 2016. *CA a cancer J. Clin.* 66 (1), 7–30. doi:10.3322/caac.21332

Song, Z., Wu, Y., Yang, J., Yang, D., and Fang, X. (2017). Progress in the treatment of advanced gastric cancer. *Tumour Biol.* 39 (7), 1010428317714626. doi:10.1177/1010428317714626

Sung, H., Ferlay, J., Siegel, R. L., Laversanne, M., Soerjomataram, I., Jemal, A., et al. (2021). Global cancer statistics 2020: GLOBOCAN estimates of incidence and mortality worldwide for 36 cancers in 185 countries. *CA A Cancer J. Clin.* 71 (3), 209–249. doi:10.3322/caac.21660

Tonello, A. S., Capelli, G., Bao, Q. R., Marchet, A., Farinati, F., Pawlik, T. M., et al. (2021). A nomogram to predict overall survival and disease-free survival after curative-intent gastrectomy for gastric cancer. *Updat. Surg.* 73 (5), 1879–1890. doi:10.1007/s13304-021-01083-7

Wang, Y., Zhang, H., and Wang, J. (2020). Discovery of a novel three-long non-coding RNA signature for predicting the prognosis of patients with gastric cancer. *J. Gastrointest. Oncol.* 11 (4), 760–769. doi:10.21037/jgo-20-140

Warburg, O. (1956). On respiratory impairment in cancer cells. *Science* 124 (3215), 269–270. doi:10.1126/science.124.3215.269

Wei, J., Ge, X., Tang, Y., Qian, Y., Lu, W., Jiang, K., et al. (2020). An autophagy-related long noncoding RNA signature contributes to poor prognosis in colorectal cancer. *J. Oncol.* 2020, 4728947. doi:10.1155/2020/4728947

Weng, M. L., Chen, W. K., Chen, X. Y., Lu, H., Sun, Z. R., Yu, Q., et al. (2020). Fasting inhibits aerobic glycolysis and proliferation in colorectal cancer via the Fdft1-mediated AKT/mTOR/HIF1α pathway suppression. *Nat. Commun.* 11 (1), 1869. doi:10.1038/s41467-020-15795-8

Xia, R., Tang, H., Shen, J., Xu, S., Liang, Y., Zhang, Y., et al. (2021). Prognostic value of a novel glycolysis-related gene expression signature for gastrointestinal cancer in the Asian population. *Cancer Cell Int.* 21 (1), 154. doi:10.1186/s12935-021-01857-4

Ye, D. M., Xu, G., Ma, W., Li, Y., Luo, W., Xiao, Y., et al. (2020). Significant function and research progress of biomarkers in gastric cancer. *Oncol. Lett.* 19 (1), 17–29. doi:10.3892/ol.2019.11078

Yu, L., Chen, X., Sun, X., Wang, L., and Chen, S. (2017). The glycolytic switch in tumors: How many players are involved? *J. Cancer* 8 (17), 3430–3440. doi:10.7150/jca.21125

Yuan, L. W., Yamashita, H., and Seto, Y. (2016). Glucose metabolism in gastric cancer: The cutting-edge. *Wjg* 22 (6), 2046–2059. doi:10.3748/wjg.v22.i6.2046

Zhang, X., Zhang, W., Jiang, Y., Liu, K., Ran, L., and Song, F. (2019). Identification of functional lncRNAs in gastric cancer by integrative analysis of GEO and TCGA data. *J Cell. Biochem.* 120 (10), 17898–17911. doi:10.1002/jcb.29058

Zhang, Y., and Yu, C. (2021). Development and validation of a Surveillance, Epidemiology, and End Results (SEER)-based prognostic nomogram for predicting survival in elderly patients with gastric cancer after surgery. *J. Gastrointest. Oncol.* 12 (2), 278–296. doi:10.21037/jgo-20-536

Zhang, Z., Tan, X., Luo, J., Yao, H., Si, Z., and Tong, J. S. (2020). The miR-30a-5p/CLCF1 axis regulates sorafenib resistance and aerobic glycolysis in hepatocellular carcinoma. *Cell Death Dis.* 11 (10), 902. doi:10.1038/s41419-020-03123-3

Frontiers in Genetics

Highlights genetic and genomic inquiry relating to all domains of life

The most cited genetics and heredity journal, which advances our understanding of genes from humans to plants and other model organisms. It highlights developments in the function and variability of the genome, and the use of genomic tools.

Discover the latest Research Topics

See more →

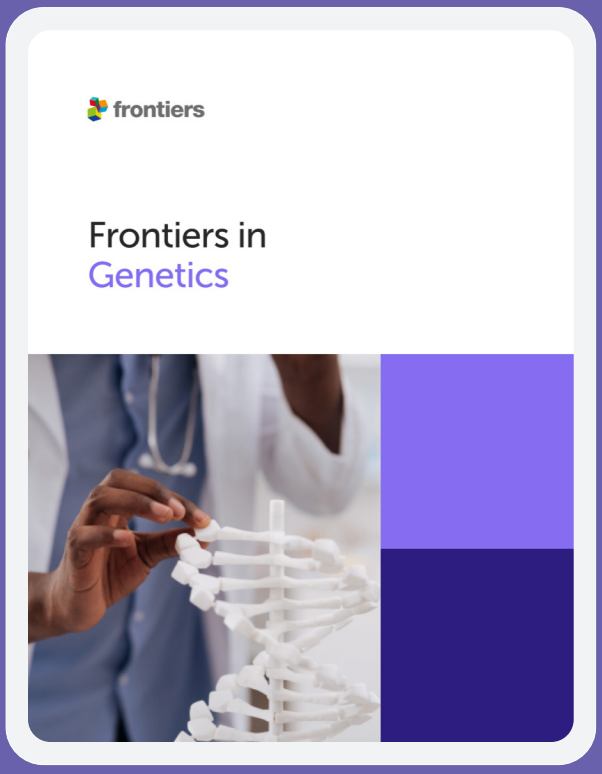

Frontiers

Avenue du Tribunal-Fédéral 34
1005 Lausanne, Switzerland
frontiersin.org

Contact us

+41 (0)21 510 17 00
frontiersin.org/about/contact